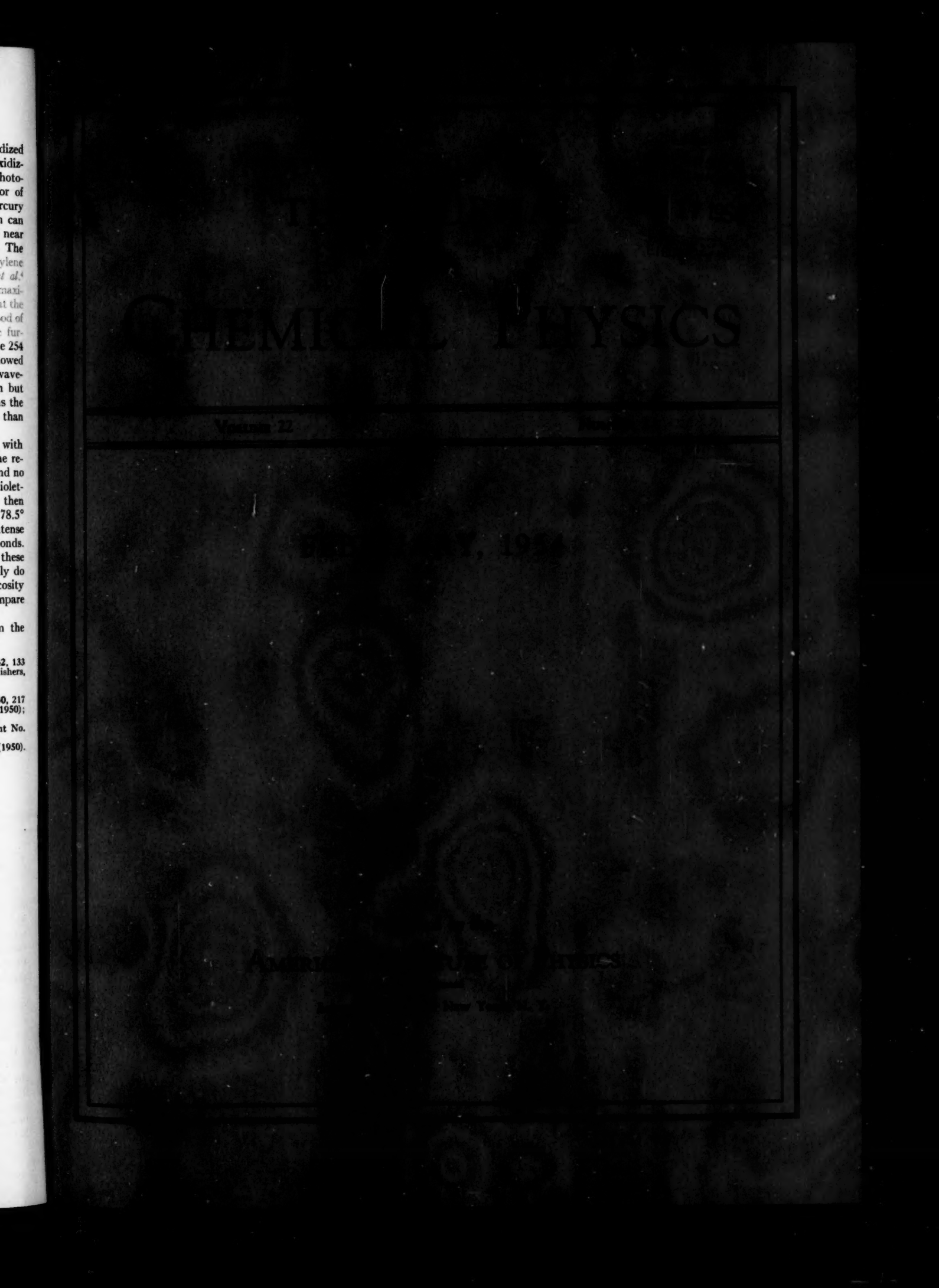
PHYSICS

THE JOURNAL
OF
CHEMICAL PHYSICS

VOLUME 22, NUMBER 2 FEBRUARY, 1954

The Heat of Sublimation of Graphite and the Composition of Carbon Vapor

GEORGE GLOCKLER*
Department of Chemistry, Duke University, Durham, North Carolina
(Received August 31, 1953)

The total vapor pressure of graphite is calculated as a function of temperature to the harmonic oscillator-rigid rotator approximation. It is assumed that three species (C_1, C_2, and C_3) are present in the gas. The C_1 atoms are most prominent in the mixture. C_3 molecules are relatively more abundant than C_2 diatoms. The heats of sublimation of the various carbon species are discussed.

SEVERAL investigations have recently been published[1,2] indicating that carbon vapor evaporating from a graphite surface contains C_3 molecules, besides the atomic and diatomic species. Earlier, Vaughan and Kistiakowsky[3] studied the problem of the heat of sublimation of carbon and involved in their calculations single atoms and diatomic molecules. They mentioned, however, that higher molecular weight species must also be taken into account in a complete discussion of the problem. Brewer, Gilles, and Jenkins[4] showed the presence of C_2 molecules and arrived at a value ($L_1=170$ kcal/mole) for the heat of sublimation of carbon.

Calculations have been made here, by the usual statistical methods to the rigid rotator-harmonic oscillator approximation, of the equilibrium vapor pressures of the three species mentioned above. It is shown that the composition of the vapor in equilibrium with a carbon surface involves a large fraction of C_3 molecules as found by Honig[1] and Chupka and Inghram.[2] The value of 170 kcal/mole for the heat of sublimation of carbon is assumed. It will be shown that it is the most satisfactory choice since lower values (124.3 or 141 kcal/mole) do not yield proper vapor pressure-temperature curves. The heat of formation of C_2 molecules was taken to be 139.7 kcal/mole, yielding a heat of sublimation of C_2 molecules, $L_2=200.5$ kcal/mole. This value is derived from bond energy-bond distance considerations.[5] The necessary molecular constants were taken from Herzberg.[6] The specific heat of graphite was estimated as shown in Table I.

The C_3 molecule was considered to be like the carbon frame of allene. However, the carbon-carbon distance is 1.29A to fit the bond energy discussed below. A linear molecule ($D_{\infty h}$) was assumed and three proper allene frequencies were chosen, corrected for the end masses being carbon atoms rather than CH_2-groups. The frequencies used were: $\omega_1=1071$, $\omega_2=353$, and $\omega_3=1980$

TABLE I. $\text{Log}P_1=F_1(T)-0.2186L_1\times T^{-1}+2.5\log T$ ($L_1=170.0$ kcal[a]).

°K	$C_p°$(Graphite) [b]	[c]	$\frac{1}{2.3R}\int_0^T\frac{dT}{T^2}\int_0^T C_p dt$ [d]	$-F_1(T)$ [e]	log P_1
1000	5.14	5.14	0.606		
1500	5.76	5.76	0.914		
2000	(6.00)	(5.95)	1.173	0.191	−10.520
2500	(6.10)	(5.89)	1.393	0.411	−6.781
3000	(6.20)	(5.74)	1.583	0.602	−4.296
3500	(6.30)	(5.64)	1.750	0.769	−2.526
4000	(6.40)	(5.60)	1.898	0.917	−1.202
4500	(6.50)	(5.65)	2.031	1.050	−0.175
5000	(6.60)	(5.76)	2.152	1.171	0.644
5500	(6.70)	(5.89)	2.264	1.284	1.311
6000	(6.80)	(6.00)	2.367	1.385	1.866

[a] Reference 4 and G. Glockler, J. Chem. Phys. **21**, 1224 (1953).
[b] Extrapolation: $Cp(E^-)=0.0002\ (T-2000)$; 2000–6000°K.
[c] Extrapolation made empirically. Based on behavior of several metals about their melting points (Al, Pb, Cd). The melting point of carbon was assumed to be ~3800°K.
[d] J. O. Clayton and W. F. Giauque, J. Am. Chem. Soc. **54**, 2610 (1932).
[e] $F_1(T)$ includes all constant factors and the double integral in column four.

* Visiting lecturer; on leave of absence from the State University of Iowa, Iowa City.
[1] R. Honig, Phys. Rev. **91**, 465 (1953).
[2] W. A. Chupka and M. C. Inghram, J. Phys. Chem. **21**, 1313 (1953).
[3] W. E. Vaughan and G. Kistiakowsky, Phys. Rev. **40**, 457 (1932).
[4] Brewer, Gilles, and Jenkins, J. Chem. Phys. **16**, 797 (1948).
[5] G. Glockler, J. Chem. Phys. **21**, 1242 (1953).
[6] G. Herzberg, *Molecular Spectra and Molecular Structure* (D. Van Nostrand Company, Inc., New York, 1950).

TABLE II.

$\log P_2 = F_2(T) - 0.2186 \times L_2 \times T^{-1} + 3.5 \log T - \log(1 - \exp(h\nu/kT))$,
$\log P_3 = F_3(T) - 0.2186 \times L_3 \times T^{-1} + 3.5 \log T - \sum_i \log(1 - \exp(h\nu_i/kT))$,
($L_1 = 170$; $L_2 = 200$; $L_3 = 212.3$ kcal).

°K	$-F_2(T)$	$\log P_2$	$-F_3(T)$	$\log P_3$	$\log P_{\text{total}}$
2000	1.848	−11.970	2.119	−12.130	−10.494
2500	2.288	−7.649	2.780	−7.529	−6.663
3000	2.669	−4.791	3.349	−4.483	−4.002
3500	3.003	−2.765	3.851	−2.325	−2.026
4000	3.299	−1.257	4.295	−0.718	−0.509
4500	3.565	−0.092	4.692	0.525	0.685
5000	3.807	0.831	5.057	1.510	1.639
5500	4.031	1.580	5.392	2.308	2.418
6000	4.236	2.199	5.701	2.969	3.065

cm^{-1}. The statistical weight of the ground state was taken to be five.

The heat of sublimation of C_3 molecules was estimated as follows: The work of Lummer[7] and of Benedict[7] indicates that the vapor pressure of carbon in an arc, burning under normal load, is one atmosphere at 4200°K. It is suggested that this measurement is satisfactory, while the work of Kohn and Guckel[8] on the heat of sublimation of carbon may not be correct. They used the results of Lummer[7] and Benedict[7] to establish one reference point of their vapor pressure curve. However in calculating the heat of sublimation of carbon they had to use a constant due to Henning.[9] If this constant had a somewhat different value and were more temperature dependent, the findings of Kohn and Guckel would of course be different. Their work needs careful attention, however, because they operated at high enough temperatures so that tarry impurities were of no significance. Brewer *et al.*[4] have pointed out that studies[10,11,12] made below 2600°K may be in error because of the presence of tars which would increase the apparent vapor pressure. Furthermore all work involving accommodation coefficients is inconclusive as Chupka and Inghram[2] have mentioned. Their work is free of such criticism because they measured relative abundances of given species and not total vapor pressure.

TABLE III. Heats of sublimation of graphite.

°K	L_μ	L_n	°K	L_μ	L_n
2000	173.1	160.3	4500	196.6	78.0
2500	178.7	129.9	5000	196.5	74.4
3000	186.9	102.4	5500	195.8	72.8
3500	192.7	88.2	6000	194.8	71.8
4000	195.2	81.0			

[7] E. Benedict, Ann. Physik **47**, 641 (1915).
[8] H. Kohn and M. Guckel, Z. Physik **27**, 305 (1924).
[9] F. Henning, Jahrb. Radioakt. u. Elektronik **16**, 1 (1919).
[10] Doeheard, Goldfinger, and Waelbroeck, J. Chem. Phys. **20**, 757 (1952).
[11] F. Waelbroeck, J. Chem. Phys. **20**, 757 (1952).
[12] P. Goldfinger, Compt. Rend. Soc. Chim. Phys. Jan (1952).

On the basis of these arguments the total pressure of all species present is taken to be one atmosphere at 4200°K. The equilibrium pressures of C_1 atoms and C_2 molecules were found to be 0.173 and 0.175 atmospheres at 4200°K from their respective vapor pressure curves. Hence C_3 molecules must be present to the extent of 0.652 atmosphere. This information allows a value of the heat of sublimation (L_3) of C_3 molecules to be calculated from their vapor pressure curves:

$$3C_s \rightarrow C_3(g); \quad L_3 = 212.3 \text{ kcal},$$

yielding a corresponding heat of formation from atoms (Qa)

$$3C(3P) \rightarrow C_3(^5\Sigma); \quad Qa = 2.969 \text{ kcal}.$$

The bond energy of the C=C bond in C_3 is therefore 148.5 kcal which is somewhat stronger than the C=C bond in the C_2 molecule (139.7 kcal), indicating that the four electrons on the end carbon atoms in C_3 are to some extent involved in the chemical binding. It is to be noted that even without the use of the work of Lummer[7] and Benedict[7] one would estimate that the C=C bond in C_3 would have a bond energy of at least 139 kcal as in C_2 molecules and the general findings would be the same.

TABLE IV. Composition of carbon vapor.[a]

°K	P_1	P_2	P_3	$\frac{\mu_1}{\mu_1} : \frac{\mu_2}{\mu_1} : \frac{\mu_3}{\mu_1}$
2000	3.022	0.107	0.074	1:0.04: 0.02
2500	1.654	0.224	0.296	1:0.14: 0.2
3000	5.058	1.620	3.288	1:0.3 : 0.7
3500	2.978	1.717	4.732	1:0.6 : 1.6
4000	0.063	0.055	0.192	1:0.9 : 3.1
4500	0.669	0.824	3.347	1:1.2 : 5.0
5000	4.406	6.781	32.32	1:1.5 : 7.3
5500	20.46	38.04	198.70	1:1.9 : 9.7
6000	73.52	158.02	930.00	1:2.1 :12.6

[a] Pressures in arbitrary units.

The results are shown in Tables I to IV and in Figs. 1 and 2. The lower values of the heat of sublimation ($L_1 = 124.3$ or 141.0 kcal) do not fit into the present picture at all. They yield a carbon vapor pressure greater than one atmosphere at 4200°K by considering C_1 and C_2 species only (Curves *A* and *B* of Fig. 1).

From the vapor pressures of the three species their mole fractions were calculated (Table IV). A study was made of the Clausius-Clapeyron equations of the individual species and their mixture. The following notation was used:

$L_{i\Delta T}$ = heat of sublimation of one mole of species i, derived from the temperature interval ΔT; $i = 1, 2, 3$; $\Delta T = T_j - T_k$. $L_{t\Delta T}$ = heat of sublimation of one mole of the mixture, derived from the temperature interval ΔT. $L_{\mu T}$ = heat of sublimation of one mole of the mixture at temperature T. L_{nT} = heat of sublimation of twelve grams of graphite at the temperature T.

μ_i = mole fraction of species i. n_i = moles of species i. P_{ij} = equilibrium partial pressure of species i (atmos) at the temperature T_j. P_t = total vapor pressure of the mixture. T = absolute temperature.

The following relations are then pertinent:

$$L_{t\Delta T}=\sum_i L_{i\Delta T}-\Delta T(T_j\cdot T_k)^{-1}\times F(P),$$

where

$$F(P)=45.743[\log\{(P_1P_2P_3)/P_t\}_j-\log\{(P_1P_2P_3)/P_t\}_k],$$

$$L_{i\Delta T}=\Delta T(T_jT_k)^{-1}[\log P_{ij}-\log P_{ik}],$$

$$L_{\mu T}=\mu_1L_{1T}+\mu_2L_{2T}+\mu_3L_{3T},$$

$$L_{nT}=n_1L_{1T}+n_2L_{2T}+n_3L_{3T},$$

$$12=12n_1+24n_2+36n_3,$$

$$n_i=\mu_i(\mu_1+2\mu_2+3\mu_3)^{-1}.$$

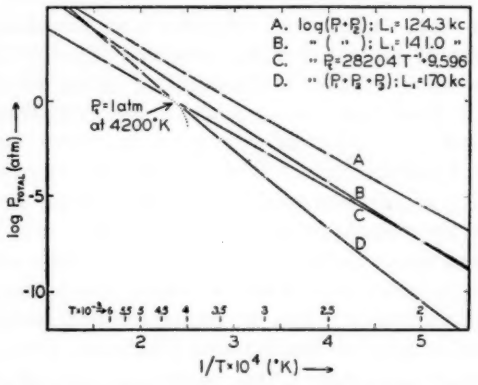

FIG. 1. Total vapor pressure of carbon. Curve C is from data given in I.C.T. III page 205. The point $P=1$ atm., $T=4200$°K is from reference 9.

These relations are shown in Fig. 2. There is also indicated the variation of $L_{i\Delta T}$ of the three species. From the total vapor pressure curve of the gas mixture only an apparent heat of sublimation ($L_{t\Delta T}$) can be derived. The relation between this pressure (P_t), the heats of sublimation at a given temperature of the three species considered, and their partial pressures, is rather complicated. The composition of the gas mixture must also be known and the specific heats of the three species must be ascertained in order to find the heats of sublimation at absolute zero.

From the vapor pressure curves of C_1 and C_2 molecules, the equilibrium constant (K) for the reaction

$$2C_1\rightleftarrows C_2;\quad K=P_2/P_1^2$$

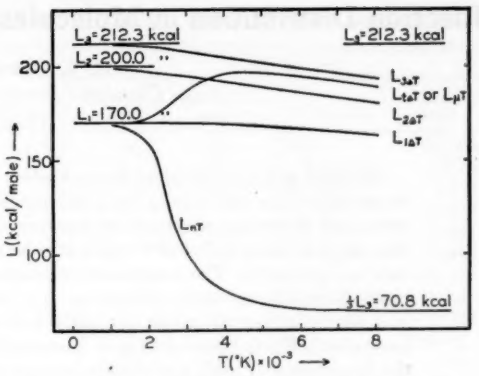

FIG. 2. Heats of sublimation of the gas mixture C_1, C_2, and C_3. The curves $L_{1\Delta T}$, $L_{2\Delta T}$, and $L_{3\Delta T}$ indicate the variation of these heats of sublimation with temperature. $L_{t\Delta T}$ or $L_{\mu T}$ is the heat of sublimation per mole of mixture. L_{nT} is the heat of sublimation per twelve grams of graphite.

can be obtained and compared with the calculations of Gordon.[13] Using his Eq. (5) with $D(C_2)=139$ kcal/mole yields results which compare satisfactorily with the present values: K(2000: 9.12, 9.07); (3000: 3.87, 3.80); (4000: 1.22, 1.14); (5000: −0.38, −0,46); and (6000: −1.46, −1.53). This agreement indicates that the rigid rotator-harmonic oscillator approximation used is sufficiently accurate for the present purpose.

The composition of carbon vapor is given by Chupka and Inghram[2] at 2450°K. They find $C_1^+:C_2^+:C_3^+=1.0:0.5:1.6$. The present calculations yield $C_1:C_2:C_3=1:0.1:0.2$ at 2500°K (Table IV). This difference should cause no great concern at this moment because on the one hand ionization cross sections are unknown as pointed out by Chupka and Inghram[1] and the present calculations are based on several assumptions. The heat of sublimation of C_1 is found by them to be $L_1=176\pm6$ kcal/mole; 170 kcal/mole was assumed here. The heat of sublimation of C_2 molecules was found from mass spectrometry to be 208 kcal/mole. Bond energy considerations indicate 200 kcal/mole as used in these calculations. The heat of sublimation of the C_3 species is given by Chupka and Inghram as 200 ± 10 kcal/mole, while the present considerations indicate 212.3 kcal/mole.

It is gratifying that the mass-spectrometric approach and the present thermodynamic calculations given such comparable results.

[13] A. R. Gordon, J. Chem. Phys. **5**, 350 (1937).

Electron Distribution in Molecules. IV. Phosphorus Magnetic Resonance Shifts*

H. S. GUTOWSKY AND D. W. MCCALL†
Noyes Chemical Laboratory, University of Illinois, Urbana, Illinois
(Received August 28, 1953)

Chemical shifts in the phosphorus nuclear magnetic resonance absorption have been measured in twenty compounds. The shifts arise from differences in the magnetic shielding of the phosphorus nuclei by electrons, and the values observed are interpreted qualitatively in terms of the molecular electronic structures. The range in shifts is 7×10^{-4} which is somewhat larger than observed for fluorine on which more extensive data are available. The phosphorus resonance shifts fall into two distinct groups one of which contains compounds with trivalent phosphorus and the other, pentavalent. The shifts in pentavalent compounds fall in a relatively narrow range, generally with greater nuclear magnetic shielding than in the trivalent. The resonance shifts between similar or homologous compounds can be accounted for by considering changes in the importance of ionic and double-bonded electronic structures.

INTRODUCTION

VARIATIONS in the location of a nuclear magnetic resonance with chemical constitution were first reported by Knight[1] for P^{31}. Although no details were given, his estimated magnitude of 0.01 percent for the effects is consistent with the measurements reported herein. Ramsey's[2] theoretical analysis ascribes the variations to magnetic shielding of nuclei by the molecular electrons, whose motions interact with the applied magnetic field. A change in electron distribution with chemical constitution changes the magnetic shielding of a nucleus and chemically shifts its resonance position. Thus, in principle, information about the electronic structures of molecules can be obtained from chemical shift data. Although detailed calculations have been made[2] only for H_2, data and semi-empirical analyses have been given for a large number of proton and fluorine chemical shifts in various types of compounds.[3–6]

If the chemical shifts are to be measured accurately, the resonance lines should be narrower than the shifts, and this usually requires that the sample be liquid to minimize internuclear magnetic dipole broadening. Also, as the resonances can be broadened by electric quadrupole interactions, the best nuclei for this type of experiment are those with spins of $\frac{1}{2}$, in which case the electric quadrupole moment is zero. Furthermore, the nuclei must exist in sufficient isotopic abundance and with a large enough magnetic moment to give measurable absorption. Fluorine and hydrogen nuclei are well suited for this type of experiment as evidenced by the results already obtained. Phosphorus has one stable isotope P^{31}, and it meets the requirements for shift measurements rather well as it has a spin of $\frac{1}{2}$ and a sizeable magnetic moment.

The main objective of this note is to summarize the phosphorus resonance shifts observed thus far and to discuss their utility in determining molecular differences in bond type. Some of the phosphorus resonance shifts we have observed were given in connection with the multiplet resonance lines arising from the electron coupling of nuclear spins.[7] Also, Dickinson[8] reported earlier the resonance shifts in PCl_3, PBr_3, and $POCl_3$ with respect to H_3PO_4 (aq.); our results agree with his within experimental error. In considering the phosphorus resonance shifts we encounter two factors not present in case of fluorine and hydrogen. First, phosphorus is multivalent and second, it has two stable valence states. Although these factors complicate any interpretation, one may be led to a better understanding of multivalent bond structures in the attempt.

EXPERIMENTAL METHOD

The experimental details were similar to these described earlier.[3,7] The resonances were observed at about 6365 gauss, using an rf bridge, 30 cps modulation, and oscilloscope display. The resonance shifts were measured at a fixed radio-frequency as the difference in applied field to center the resonance lines of the compound and the reference on the oscilloscope. The multiplet structures observed in many of the resonances were symmetrical and the center was used in determining the resonance shift, as is justified theoretically.[7] Usually a set of ten measurements was made by placing successively the sample and reference compound in the same coil. The order was reversed for half the measurements so any constant drift in frequency or field would cancel out. Statistical errors were the order of ±0.006 gauss, and systematic errors up to one percent may be present in addition.[3]

Compounds do not need to be extremely pure for chemical shift measurements, and commercial

* Supported by the U. S. Office of Naval Research.
† National Science Foundation Predoctoral Fellow.
[1] W. D. Knight, Phys. Rev. **76**, 1259 (1949).
[2] N. F. Ramsey, Phys. Rev. **78**, 699 (1950); **86**, 243 (1952).
[3] H. S. Gutowsky and C. J. Hoffman, J. Chem. Phys. **19**, 1259 (1951).
[4] Gutowsky, McCall, McGarvey, and Meyer, J. Am. Chem. Soc. **74**, 4809 (1952), I.
[5] L. H. Meyer and H. S. Gutowsky, J. Phys. Chem. **57**, 481 (1953), II.
[6] Meyer, Saika, and Gutowsky, J. Am. Chem. Soc. **75**, 4567 (1953), III.
[7] Gutowsky, McCall, and Slichter, J. Chem. Phys. **21**, 279 (1953).
[8] W. C. Dickinson, Phys. Rev. **81**, 717 (1951).

samples were used without further purification. The $Cl(CH_2)_3PCl_2$ and $C_2H_5OPOCl_2$ were kindly provided by Dr. D. R. Martin; the sources of the other samples have been given.[7] The shifts in PH_3 and PF_3 were measured in the liquids at about −90°C. Yellow phosphorus (P_4) and P_4S_3 were measured at room temperature in the solid state, the latter with a narrow band amplifier. The other compounds were liquid at room temperature and were measured as such.

In this paper we define the chemical shifts of P^{31} as $10^5\times(H_c-H_r)/H_r$ where H_c and H_r are the magnetic fields required for resonance in the sample and in a reference, respectively, at a fixed radio-frequency. Aqueous H_3PO_4 was chosen as an arbitrary reference, as it gives a strong, narrow resonance and is readily available. With this definition, more positive shifts correspond to greater magnetic shielding of the nucleus. The δ values used in discussions of fluorine[4,5] and proton[5,6] shifts are defined similarly, but the sign is reversed so that changes in δ correspond to changes in the charge on the atom.

RESULTS AND DISCUSSION

The phosphorus resonance shifts observed are given in Table I, with trivalent and pentavalent compounds listed separately. Before discussing individually several of the various types of compounds, some general observations will be given.

The pentavalent compounds, excluding HPF_6, have phosphorus shifts clustered in the narrow range from 2 to −3. In HPF_6, which has a higher shielding of 11.8, the structure is octahedral, sp^3d^2, while the other pentavalent compounds use sp^3d orbitals. In Ramsey's theory[2] the shielding increases with the electrostatic potential at the nucleus and is reduced by a second-order paramagnetism which arises in part from the lack of spherical symmetry introduced by the bonding electrons. The higher symmetry of the PF_6^- compared to the other compounds, as well as the contribution of the additional two electrons may account for the greater shielding of the phosphorus. Also, as we shall consider below, replacement of other atoms with fluorine increases the phosphorus shielding, and PF_6^- is unusual in the number of fluorines.

With the exception of P_4, PH_3, and P_4S_3, the trivalent phosphorus compounds have shielding values ranging from −9.7 to −22.2, considerably below the −3 lower limit of the pentavalent compounds. The bonding in the trivalent compounds is a combination of p^3 and sp^2, and the lower shielding most likely arises because there are fewer valence electrons and a less symmetrical electronic distribution than in the pentavalent compounds. In this connection it is of interest to note that the chlorine nuclear quadrupole coupling constants[9,10] demonstrate that the P−Cl bonds are considerably more covalent in PCl_5 than in PCl_3.

TABLE I. Chemical shifts[a] in the P^{31} magnetic resonance.

Trivalent compounds			Pentavalent compounds		
Formula	Chemical shift	Probable error	Formula	Chemical shift	Probable error
P_4 (in CS_2)	48.8	0.02	HPF_6	11.8[b,c]	
P_4	45.0	0.03	$F_2PO(OH)$	2.01[b]	0.01
PH_3	24.1[b]	0.03	$POClF_2$	1.48[b]	0.02
P_4S_3	11.4[c]		$POCl_2F$	0.00[b]	0.02
PF_3	−9.7[b]	0.05	H_3PO_4	0.00	reference
CH_3OPF_2	−11.1[b]	0.02	$HPO(OH)_2$	−0.45[b]	0.04
P_2I_4(in CS_2)	−17.0[c]		$POCl_3$	−0.54	0.04
PI_3	−17.8	0.04	$C_2H_5OPOCl_2$	−0.64	0.06
$Cl(CH_2)_3PCl_2$	−18.2	0.07	$H_2PO(OH)$	−1.38[b]	0.06
PCl_3	−21.5	0.09	$PSCl_3$	−3.08	0.05
PBr_3	−22.2	0.11			

[a] Referred to aqueous H_3PO_4; defined as $10^5\times(H_c-H_r)/H_r$ where H_c and H_r are the resonance magnetic fields for the sample compound and reference, respectively.
[b] The resonance exhibited multiplet structure; see reference 7 for details.
[c] The resonance was weak and the shift value is good only to ±1.0.

(*a*) PF_3, PCl_3, PBr_3, PI_3: In this homologous series the phosphorus shielding decreases in the order PF_3, PI_3, PCl_3, and PBr_3, with the iodide out of sequence and the fluoride shielded considerably more than the other halides. Similar trends have been noted in the proton shifts[5] in the methylene halides (CH_2X_2) and haloforms (CHX_3), and in the substituent effects[4] in benzene. The observed order reflects the presence of two opposing effects, ionic and double bond character. The P−X electronegativity difference increases on passing from PI_3 to PF_3, and the ionic bond character should increase accordingly. Also, fluorine and to a lesser extent chlorine and the larger halogens can form double bonds. So the observed shifts are compatible with the phosphorus shielding increasing as the double bond character is increased and decreasing as the ionic bond character is increased. Thus, for ionic character effects alone, the phosphorus shielding would decrease in the sequence I, Br, Cl, and F; the opposing double bond effect is greatest for F and the next for Cl, giving the observed sequence F, I, Cl, and Br. Moreover, the double bond character effect in PF_3 is very pronounced compared with the other halogens; this is consistent with the well-known chemical concept that first row atoms double bond most effectively.[11]

(*b*) $POCl_3$, $POCl_2F$, $POClF_3$, POF_3: In these compounds both the phosphorus and the fluorine[7] shielding increase with fluorine substitution. Pauling has proposed[12] structures for the phosphorus oxyhalides such as

(1a) (1b)

[9] R. Livingston, J. Phys. Chem. **57**, 496 (1953).
[10] D. W. McCall and H. S. Gutowsky, J. Chem. Phys. **21**, 1300 (1953).
[11] K. S. Pitzer, J. Am. Chem. Soc. **70**, 2140 (1948).
[12] L. Pauling, *The Nature of the Chemical Bond* (Cornell University Press, Ithaca, New York, 1948), second edition, p. 83.

However, in order to give the observed trend in the phosphorus shifts, there must be double bond structures of the type

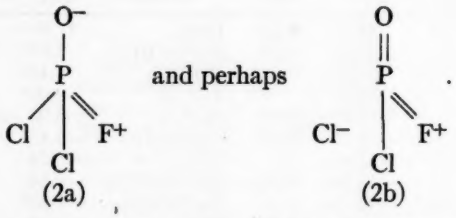

(2a) (2b)

The increase in phosphorus shielding with fluorine substitution again reflects the greater ease with which fluorine forms double bonds, compared to chlorine. The increase in the fluorine shielding upon continued substitution is analogous to that observed in the chlorofluoromethanes;[5] competition among the fluorines makes each P—F bond less double, *increasing* the fluorine shielding; but in the polyfluoro compound the P—F bonds still have more double bond character than P—Cl bonds. Although the effects of fluorine substitution are qualitatively the same in the tri- and pentavalent compounds, the magnitudes are considerably less in the latter.

(*c*) $POCl_3$, $PSCl_3$: The phosphorus shielding is higher in $POCl_3$ than in $PSCl_3$. If we consider the analysis above as valid, this provides a direct verification that oxygen forms double bonds more readily than does sulfur and that P=O structures are important in the oxyhalides, as expected.[11] By analogy with the trihalides, if the ionic forms (1*a*) were the most important in both $POCl_3$ and $PSCl_3$, the greater electronegativity difference in P—O would reduce the phosphorus shielding below that in the sulfide. The double bond structure (1*b*) must be the main structure in $POCl_3$ to account for the greater shielding observed in it.

(*d*) $H_2PO(OH)$, $HPO(OH)_2$, $PO(OH)_3$: The phosphorus shielding increases as hydrogens on the phosphorus are replaced by OH groups. This suggests the importance of structures like P—O—H and $P^-=OH^+$. Confirmation is provided by the shielding of the protons attached to the phosphorus,[7] which is greater in $HPO(OH)_2$ than in $H_2PO(OH)$. On the basis of the structures postulated, there should be a greater negative charge on the phosphorus in $HPO(OH)_2$ than in $H_2PO(OH)$, reducing the ionic character of the P—H bonds and increasing the proton shielding (i.e. decreasing the proton δ values[6]), as observed.

(*e*) F_3PO, $F_2PO(OH)$, $FPO(OH)_2$, $PO(OH)_3$: This set of compounds is similar to the hydrogen-hydroxyl series in (*d*) above and also the phosphorus oxyfluorochlorides in (*b*). The phosphorus resonance could be found only in $F_2PO(OH)$ and $PO(OH)_3$, with the phosphorus shielding greater in the fluorine derivative. Furthermore, the fluorine shielding increases with fluorine substitution. These trends are analogous to those in (*b*) and (*d*) and are explainable in the same manner, assuming $P^-=F^+$ electron distributions are relatively more important than $P^-=OH^+$.

(*f*) P_4; P_4S_3; PH_3: As remarked in the initial discussion, the phosphorus shifts are very large in these compounds, particularly in P_4. P_4 and P_4S_3 have abnormally small bond angles; the associated strain no doubt affects the bond hybridization and could be responsible for the observed effects. The high value in PH_3 could result from ionic forms P^-H^+, which increase the charge on the phosphorus and should increase its shielding. A sizeable chemical shift exists between $P_4(s)$ and P_4 (in CS_2) indicating there are significant intermolecular effects in the solid, as was evidenced earlier by relaxation of the infrared selection rules in the solid.[13]

In conclusion it is instructive to make an intercomparison of the influence of bond type upon the magnetic shielding of phosphorus, fluorine, and hydrogen nuclei. In the case of phosphorus we have seen that an increase in double bond character increases the nuclear shielding, while for fluorine the shielding is decreased.[5] In a double bond the charge distribution is $P^-=F^+$; the changes in net formal charge are opposite for the two nuclei, as are the associated chemical shifts. On the other hand an increase in ionic character decreases the phosphorus shielding while increasing that of fluorine; but again this is consistent with the opposite charges that ionic character places upon the two nuclei, P^+F^-. Hydrogen does not form double bonds, and its shielding decreases with an increase in ionic bond character, R^-H^+; however, there are appreciable bond hybridization effects as well.[5,6] The chemical shifts in the magnetic shielding of all three nuclei appear therefore to correspond qualitatively to what we might call differences in "electron density" about the nuclei.

ACKNOWLEDGMENT

We are indebted to Dr. Wayne E. White of Ozark-Mahoning Company, Mr. R. Mattair of Oldbury Electro-Chemical Company, and Professor Dr. R. Martin, who very kindly provided most of the compounds.

[13] H. S. Gutowsky and C. J. Hoffman, J. Am. Chem. Soc. **72**, 5751 (1950).

Modified Transition State Theory of Reaction Rates*

F. A. MATSEN
Departments of Chemistry and Physics, University of Texas, Austin 12, Texas
(Received September 8, 1953)

The specific reaction rate for chemical reactions is formulated in terms of the *total* transmission coefficient in the reaction coordinate and a modified transition state, which differs from the original transition state only in the treatment of the reaction coordinate. If the total transmission coefficient is factored into two partial transmission coefficients, the modified theory gives the transition state theory in both the classical and the quantum-mechanical-particle-in-a-box treatments. It is then shown that the momentum density in the virtual state over a symmetrical square barrier is that of a quantum-mechanical-particle-in-a-box at low momentum and that of a classical system at high momentum. Finally, the reaction rate transmission coefficient is calculated from the modified theory for an unsymmetric square barrier and shown to depend on the temperature, the activation energy, and the thermicity of the reaction.

I. DEVELOPMENT OF THE MODIFIED TRANSITION STATE THEORY

A CHEMICAL reaction may be represented by a flow of points (systems) over a potential energy hypersurface. On this surface are inscribed two hyperareas, one of which describes the reactants and the other the products. The rate of the reaction is essentially the product of a transmission coefficient between the two areas and a frequency factor, i.e., the number of systems which strike the reactant boundary in unit time. Both of these quantities are complicated functions of all momenta, quantized and unquantized, as well as of position coordinates.[1]

The multidimensional problem is reduced to a one-dimensional problem in the usual way by assuming that the reaction coordinate, X, and its conjugate momentum, p, can be separated from all other degrees of freedom.[2] It will then be assumed that there exists an intermediate called the "modified transition state" which is in equilibrium with the reactants in all degrees of freedom except the reaction coordinate. In this coordinate the intermediate is assumed to be in the reactant state; i.e., it moves as a free particle over a mean free path of length L at the energy of the reactant state. This distinguishes the modified transition state from the original transition state. The activation of the other degrees of freedom does not affect the activation energy since these are assumed to be in equilibrium with the reactants.

The number of systems which react per second is given by

$$R=\int \gamma(p_R)dv(p_R), \tag{1}$$

where $\gamma(p_R)$ is the total transmission coefficient and $dv(p_R)$ the number of systems with momentum p_R approaching the reactant boundary in unit time.† For the reaction

$$A+B\rightarrow D+E$$

it is given by

$$dv(p_R)=[AB\Gamma]\times[\exp(-p_R^2/2mkT)dp_RL/h][p_R/Lm]. \tag{2}$$

The first bracket gives the number of systems in the modified transition state. $\Gamma=Q_e^{\pm}/Q_AQ_B$ is the ratio of the partition function for the modified transition state without the reaction coordinate to that for the reactant state. The second bracket is proportional to the probability that a system in the modified reactant state will have momentum p_R, and the last bracket gives the frequency for traversing the mean free path L.

Since

$$R=k_rAB \tag{3}$$

$$k_r=(\Gamma/mh)\int_0^\infty \gamma(p_R)\exp(-p_R^2/2mkT)p_Rdp_R. \tag{4}$$

Equation (4) may be written in terms of the momentum p at the highest point E_R on the reaction coordinate. See Fig. 1. Now

$$p_R^2=p^2+2mE_R$$

and

$$p_Rdp_R=pdp.$$

If leakage through the barrier is neglected

$$\gamma(p_R)=0 \quad \text{for} \quad p_R<(2mE_R)^{\frac{1}{2}}$$

so that

$$k_r=(\Gamma/mh)\exp(-E_R/kT)\times\int_0^\infty \gamma(p)\exp(-p^2/2mkT)pdp, \tag{5}$$

where $\gamma(p)=\gamma(p_R)$. Equation (5) is the basic equation in the modified transition state theory.

* This research was supported in part by the United States Air Force under Contract No. AF 18(600)-430 monitored by the Office of Scientific Research.

[1] Eyring, Walter, and Kimball, *Quantum Chemistry* (John Wiley and Sons, Inc., New York, 1944).

[2] For a discussion of the separation of coordinates, see E. Wigner, Trans. Faraday Soc. **34**, 29 (1938).

† The statement "with momentum p_R" is to be taken to mean with momentum lying between p_R and p_R+dp_R.

II. DEVELOPMENT OF THE TRANSITION STATE THEORY

The transition state theory may be obtained from the modified theory as follows: The total transmission coefficient $\gamma(p)$ is broken down into the product of two partial transmission coefficients

$$\gamma(p)=\rho(p)\kappa(p). \tag{6}$$

The second of these $\kappa(p)$ may be taken to be the usual reaction rate transmission coefficient, the ratio of the number of systems which become products to the number which reach the top of the barrier. $\rho(p)$ is the ratio of the number of systems which reach the top of the barrier to the number which approach the barrier. It may be regarded as the density of momentum levels in the transition state normalized to the reactant state. Substitution of (6) in (5) and multiplication of the numerator and denominator by the arbitrary constant dq gives

$$k_r=\Gamma \exp(E_R kT)/(mdq) \times\int_0^\infty \rho(p)\kappa(p)\exp(-p^2/2mkt)pdpdq/h. \tag{7}$$

This is the basic equation of the original transition treatment. It is customarily obtained as follows:

$$R=\int \kappa(p)dv'(p), \tag{8}$$

where

$$dv'(p)=[AB\Gamma \exp(-E_R/kT] \times[\rho(p)\exp(p^2/2mkT)dpdq/h][p/mdq], \tag{9}$$

the number of particles per second, with momentum p in the forward direction and lying in the length dq of the transition state. The factors have the same meaning as in Eq. (2) except that reference is made to the transition state rather than to the modified transition state.

Integration of Eq. (8) together with Eq. (3) yields Eq. (7). Equation (7) may also be written

$$k_r=\langle[\kappa(p)p\rangle_{Av}\Gamma \exp(-E_R/kT)/mdq]Q_t(p)/2, \tag{10}$$

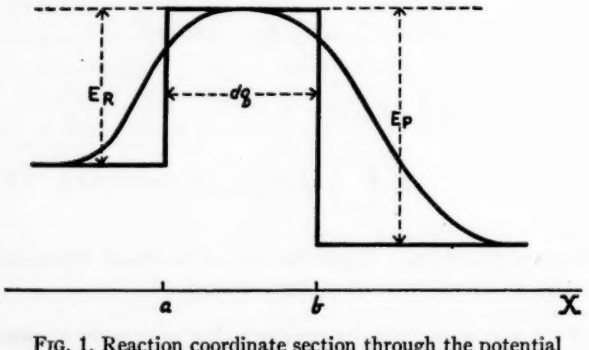

FIG. 1. Reaction coordinate section through the potential energy surface.

where

$$Q_t(p)=2\int_0^\infty \rho(p)\exp(-p^2/2mkt)dpdq/h,^3 \tag{11}$$

the translational partition function for the transition state and the bar denotes the average defined by the partition function.‡

In the early treatments, the following definition was made

$$\int\kappa(p)\rho(p)\exp(-p^2/2mkT)pdpdq/h =\kappa_A\int\rho(p)\exp(-p^2/2mkT)pdpdq/h. \tag{12}$$

κ_A may be called the mean transmission coefficient. Two quite different momentum density functions have been employed:

A. The classical momentum density:

$$\rho(p)=1. \tag{13}$$

Substitution in (7) or (10) yields directly

$$k_r=\kappa_A\Gamma\exp(-E_R/kT)kT/h. \tag{14}$$

This is the generalization of the results of Peltzer and Wigner[4] as given in Fowler.[5]

B. The momentum density for the quantum-mechanical-particle-in-a-box:

$$\rho(p)=(1/2)\delta(p-nh/2dq), \tag{15}$$

where δ is the Dirac delta function, which has the following properties.[6]

$$\delta(p-nh/2dq)=0 \quad \text{unless} \quad p=nh/2dq \tag{16}$$

$$\int_{p_{n-\frac{1}{2}}}^{p_{n+\frac{1}{2}}}\delta(p-nh/2dq)dpdq/h=1 \tag{17}$$

$$\int_{p_{n-\frac{1}{2}}}^{p_{n+\frac{1}{2}}}f(p)\delta(p-nh/2dq)dpdq/h=f(nh/2dq). \tag{18}$$

The factor $(1/2)$ in front of the delta function corrects the density from that of the quantum-mechanical-particle-in-a-box, for which the momentum may take both signs, to the density of the transition state for which the momentum takes only one sign.§

[3] It has been customary to associate the factor (1/2) with the average momentum rather than the partition function. See Glasstone, Laidler, and Eyring, *Theory of Rate Processes* (McGraw-Hill Book Company, Inc., New York, 1951).

‡ This follows from the definition of the average

$$\bar{X}=[\int\{\exp(-p^2/2mkT)\}X(p)dp]/Q.$$

[4] H. Peltzer and E. Wigner, Z. physik. Chem. **B15**, 445 (1932).

[5] R. H. Fowler, *Statistical Mechanics* (Macmillan Company, New York, 1936), second edition.

[6] E. C. Kemble, *Fundamental Principles of Quantum Mechanics* (McGraw-Hill Book Company, Inc., New York, 1937).

§ In the classical density the factor of (1/2) is introduced by integration over momentum from zero to infinity instead of from minus infinity to plus infinity.

Substitution of (15) in Eqs. (7) or (10) yields directly Eq. (14). This is the development used by Eyring in his original work.[7]

III. THE TRANSITION STATE AS A VIRTUAL STATE

In the previous section it was shown that a transition state in the reaction coordinate is obtained in the modified theory by breaking up the total transmission coefficients into two partial transmission coefficients. One of these defines the density of momentum levels in the transition state. It is of interest to calculate this function for several potential surfaces and compare the results with the density functions A and B which were assumed by earlier workers.

In transition state theory, the transition state is localized in a length dq of constant height E_R with the thermicity unspecified. These minimum specifications are met by the symmetrical square barrier. The effect of modifying the barrier will be discussed later.

The determination of the wave functions for this surface is straightforward.[8,9] The wave functions in the three regions of Fig. 1 are

$$\begin{aligned}\psi_R&=A\exp(ip_RX/\hbar)+B\exp(-ip_RX/\hbar),\\ \psi_T&=C\exp(ipX/\hbar)+D\exp(-ipX/\hbar),\\ \psi_P&=E\exp(ip_PX/\hbar).\end{aligned}\qquad(19)$$

At the boundaries the wave functions must be continuous, so that at a, $\psi_R=\psi_T$ and $d\psi_R/dX=d\psi_T/dX$ while at b, $\psi_T=\psi_P$ and $d\psi_T/dX=d\psi_T/dX$. These four boundary conditions give four relations among the five coefficients. The density of momentum levels, that is, the ratio of the number of systems on the top of the barrier to the number in the incident beam, is given by

$$\rho(p)=\frac{(|C|^2+|D|^2)p}{|A|^2p_R}.\qquad(20)$$

For the symmetric square barrier $p_R=p_P$, and

$$\rho(p)=\frac{\frac{1}{2}(p/p_R+p_R/p)}{1+(1/4)(p/p_R-p_R/p)^2\sin^2(pdq/\hbar)}.\qquad(21)$$

This momentum density has the following interesting properties: (1) For large values of the momentum it approaches the classical value of one. (2) At low values of the momentum it approaches the $(1/2)\delta(p-nh/2dq)$ of the quantum-mechanical-particle-in-a-box. This is borne out from an inspection of Fig. 2 and the fact that‖

$$\int_{p_{n-\frac{1}{2}}}^{p_{n+\frac{1}{2}}}\rho(p)dpdq/h=\tfrac{1}{2}.\qquad(22)$$

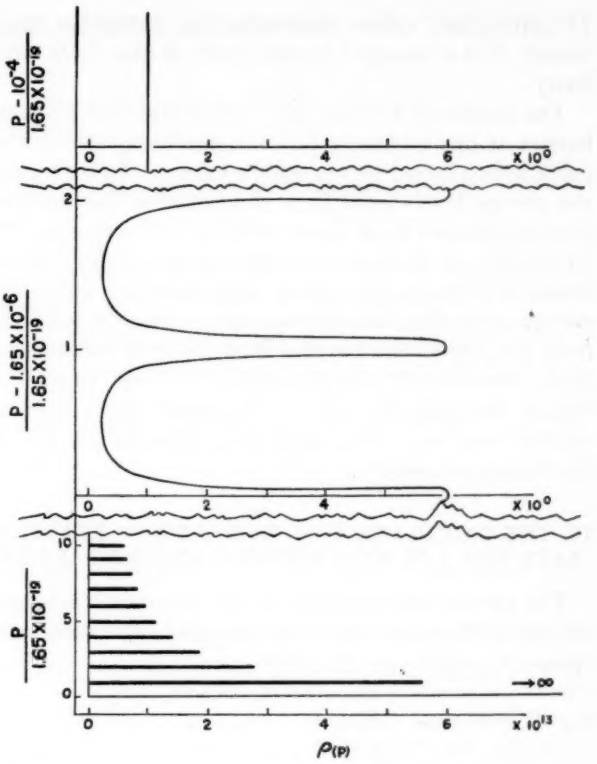

FIG. 2. The momentum density as a function of momentum over a symmetric square barrier.

(3) When p is averaged over one oscillation‖

$$\bar{\rho}(p)=\int_{p_{n-\frac{1}{2}}}^{p_{n+\frac{1}{2}}}\rho(p)dp/(h/2dq)=1\qquad(23)$$

the result required by both the classical and particle-in-a-box treatments. It follows then that $\bar{\kappa}(p)=\bar{\gamma}(p)$.¶ (4) The energy half-width of the bands is roughly equal to the uncertainty in the energy which one calculates from the lifetime τ of a system in the transition state[11].

$$\Delta E\cong p\Delta p/m\cong p_Rp^2h/\pi mdq(p_R+p)^2\qquad(24)$$

$$\Delta E=h/\tau\cong h/(mdq/pT)\cong 4p_Rp^2h/mdq(p_R+p)^2.\qquad(25)$$

It is concluded that the virtual state with a momentum level density obtained from a symmetric square barrier gives a satisfactory description of the transition state.

For the unsymmetrical square barrier[9]

$$\rho(p)=2pp_R(p^2+p_P^2)/[p^2(p_R^2+p_P^2)\cos^2(pdq/\hbar)+(p^2+p_Rp_P)^2\sin^2(pdq/\hbar)].\qquad(26)$$

Here the similarity to the classical and to the quantum-mechanical-particle-in-a-box is much less marked. While $\rho(p)$ has peaks at $p=nh/2dq$ as for the symmetrical barrier, it has in addition smaller peaks at $p=(n+\frac{1}{2})h/2dq$. Further, neither of the integrals (22 or

[7] H. Eyring, J. Chem. Phys. **3**, 107 (1937).
[8] D. Bohm, *Quantum Theory* (Prentice-Hall Inc., New York, 1951).
[9] J. O. Hirschfelder and E. P. Wigner, J. Chem. Phys. **7**, 616 (1939).

‖ For a finite dq it is not necessary to consider any variation except that of the sine term in carrying out the integration.

¶ It should be noted that $\bar{\kappa}(p)$ is not equal to T the transmission coefficient for a single edge.

23) gives the values demanded by transition state theory. For a rounded barrier there is also little similarity.

The similarity between the virtual state for a square barrier at low momenta and the quantum-mechanical-particle-in-a-box deserves some comment. In both cases the energy levels arise from constructive and destructive interference from waves reflected at the boundaries. In the box no particles can exist except at the discrete levels, whereas in the virtual state, particles possessing energy other than the discrete values are reflected away from the top of the barrier. This selective reflection is fairly common, occurring in interferometers, the scattering of electrons by gases (Ramsauer effect), many nuclear reactions, x-ray scattering from solids, and in the theory of metals.

IV. THE CALCULATION OF THE SPECIFIC REACTION RATE FOR THE UNSYMMETRIC SQUARE BARRIER

The specific reaction rate for the unsymmetric square barrier is calculated from the modified transition state theory by equation

$$k_r=(\Gamma/mh)\exp(-E_R/kT \times\int_0^\infty \gamma(p)\exp(-p^2/2mkT)pdp. \quad (5)$$

For this barrier

$$\gamma(p)=1/[p^2(p_R^2+p_P^2)\cos^2(dpq/\hbar) +(p^2+p_Rp_P)^2\sin^2(pdq/\hbar)]. \quad (27)$$

Since the other factors in the integrand vary slowly with p, it is permissible to replace $\gamma(p)$ by its average over one oscillation,

$$\bar{\gamma}(\rho)=\int_{p_{n-\frac{1}{2}}}^{p_{n+\frac{1}{2}}}\gamma(p)dp(h/2dq) =4pp_Rp_P/[p^2+p_Rp_P)(p_R+p_P)]. \quad (28)$$

For low momentum and high barrier $\bar{\gamma}(p)$ may be expanded in terms of $p^2/(E_RE_P)^{\frac{1}{2}}$. Equation (5) then yields

$$k_r=\Gamma\exp(-E_RkT)(kT/h)\kappa_A, \quad (29)$$

where

$$\kappa_A=\frac{(4kT)^{\frac{1}{2}}}{(E_R)^{\frac{1}{2}}+(E_P)^{\frac{1}{2}}}\left[1-\frac{9}{4}\left(\frac{kT}{E_RE_P}\right) +\frac{75}{32}\left(\frac{13}{5}+\frac{E_R+E_P}{(E_RE_P)^{\frac{1}{2}}}\right)\left(\frac{kT}{(E_RE_P)^{\frac{1}{2}}}\right)^2-\cdots\right]. \quad (30)$$

There are several points of interest in these results. The first is the kT/h factors out, just as in the Eyring theory. The factor kT/h has less significance here, however, and it is perhaps just as significant to treat the integral divided by mh as the frequency unit. The mean transmission coefficient κ_A is shown for a square barrier to have in general a value less than one, to increase with temperature and to decrease with increasing activation energy E_R and exothermicity, E_R-E_P. Rounding the barrier increases κ_A.[9] Further, preliminary calculations appear to indicate that rounding the barrier decreases the effect of temperature, activation energy and thermicity on the mean transmission coefficient.

It should perhaps be emphasized that the conclusions drawn here are only as valid as is a one-dimensional reaction rate theory.

THE JOURNAL OF CHEMICAL PHYSICS VOLUME 22, NUMBER 2 FEBRUARY, 1954

Transport Properties of Gases Obeying a Modified Buckingham (Exp-Six) Potential*

EDWARD A. MASON†
Naval Research Laboratory, Department of Chemistry, University of Wisconsin, Madison, Wisconsin
(Received July 10, 1953)

A large number of the Chapman and Cowling collision integrals have been calculated for gases obeying a modified Buckingham potential,

$$\varphi(r)=\frac{\epsilon}{1-6/\alpha}\left[\frac{6}{\alpha}e^{\alpha(1-r/r_m)}-\left(\frac{r_m}{r}\right)^6\right].$$

The results are tabulated over a large temperature range, kT/ϵ from 0 to 200, and for four values of the parameter α, 12, 13, 14, and 15. The treatment was entirely classical, and no corrections for quantum effects were made. The results should be applicable to most simple, nonpolar gases, and may be used to obtain information about intermolecular forces from the observed temperature dependence of gaseous transport properties.

The second approximation to the thermal diffusion ratio and the third approximation to the coefficient of ordinary diffusion have been derived according to the method of Chapman and Cowling.

Evaluation of the potential parameters for specific substances and applications of the results will be published later.

I. INTRODUCTION

THE influence of intermolecular forces on the transport properties of gases is well known, and information concerning intermolecular forces may be obtained from the temperature variation of gaseous transport coefficients by means of the theory developed by Enskog[1] and by Chapman.[2] Such information is useful in correlating other properties of gases, as well as properties of the liquid and solid states.

The theory of Enskog and Chapman depends on the following assumptions: (1) only binary collisions between molecules are important; (2) the binary collisions are elastic; (3) the intermolecular force field is spherically symmetric; (4) molecular collisions are adequately described by classical mechanics. Thus the theory applies strictly only to monatomic gases at moderate pressures and at temperatures high enough that quantum effects are negligible. The extent to which the theoretical relations do not apply when conditions (2) and (3) are not met is not yet known.[3] However, the theory has had success in correlating transport phenomena in polyatomic gases, so that these conditions may not be a severe limitation.[4]

In order to obtain specific information about intermolecular forces from transport phenomena, it is necessary to assume an analytical form for the intermolecular potential, calculate from this the Enskog-Chapman "collision integrals," or "temperature-dependent cross sections," as a function of temperature and the potential parameters, and evaluate the parameters for any specified gas by comparison with collision integrals derived from experimental measurements. If the theory is correct and the chosen potential form suitable, a single set of potential parameters should suffice to describe all the transport properties of the gas, as well as other properties, such as the equation of state. Except for very simple and physically unrealistic potential forms, the calculation of the collision integrals involves extensive numerical integrations.

The best intermolecular potential used to date for the study of transport phenomena is of the Lennard-Jones form, with a repulsion term varying as the inverse twelfth power of the distance of separation between centers of two molecules, and an attraction term varying as the inverse sixth power of the separation distance. The collision integrals for this potential have been evaluated independently by a number of workers,[5–8] and their results have been extensively compared with experiment.[9–14] The results obtained have not been entirely satisfactory, and the question arises whether this is primarily the fault of the theory or of an inadequate

* This work was supported in part by Contract N7onr-28511 with the U. S. Office of Naval Research.
† National Research Fellow, 1952–1953. Present address: Department of Chemistry, Pennsylvania State University, State College, Pennsylvania.

[1] D. Enskog, Physik. Z. **12**, 56, 533 (1911); Inaug. Diss. Upsala (1917).

[2] S. Chapman, Trans. Roy. Soc. (London) **A211**, 433 (1912); **A216**, 279 (1916); **A217**, 115 (1917).

[3] In the case of the thermal conductivity it is known that the the Enskog-Chapman theory fails badly when energy may be transported by means of the molecular internal degrees of freedom.

[4] S. Chapman and T. G. Cowling, *The Mathematical Theory of Non-Uniform Gases* (Cambridge University Press, Teddington, 1952), second edition, p. 7.

[5] T. Kihara and M. Kotani, Proc. Phys.-Math. Soc. Japan **25**, 602 (1943).

[6] J. de Boer and J. van Kranendonk, Physica **14**, 442 (1948).

[7] Hirschfelder, Bird, and Spotz, J. Chem. Phys. **16**, 968 (1948); 1343 (1949).

[8] J. S. Rowlinson, J. Chem. Phys. **17**, 101 (1949).

[9] (a) Hirschfelder, Bird, and Spotz, Chem. Revs. **44**, 205 (1949); Trans. Am. Soc. Mech. Engrs. **71**, 921 (1949); (b) Hirschfelder, Curtiss, Bird, and Spotz, *The Molecular Theory of Gases and Liquids* (John Wiley and Sons, Inc., New York, 1954), Chapter 8.

[10] K. E. Grew, Proc. Phys. Soc. (London) **62**, 655 (1949); K. E. Grew and T. L. Ibbs, *Thermal Diffusion in Gases* (Cambridge University Press, Teddington, England, 1952).

[11] E. R. S. Winter, Trans. Faraday Soc. **46**, 81 (1950).

[12] E. Whalley and W. G. Schneider, J. Chem. Phys. **20**, 657 (1952).

[13] B. N. Srivastava and M. P. Madan, Phil. Mag. **43**, 968 (1952); Proc. Phys. Soc. (London) **A66**, 277 (1953); J. Chem. Phys. **21**, 807 (1953).

[14] Amdur, Ross, and Mason, J. Chem. Phys. **20**, 1620 (1952).

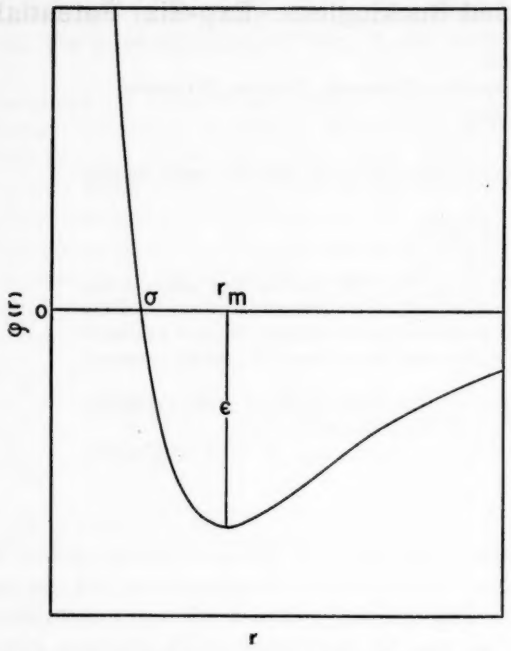

FIG. 1. A typical intermolecular potential energy curve.

potential form. That the Lennard-Jones (12–6) potential is not entirely adequate is shown by lack of complete agreement between theory and experiment even for the rare gases.

It is the purpose of the present article to describe calculations of the Enskog-Chapman collision integrals for a more realistic potential form than has been used previously. It is hoped that some light may be thrown on the reasons for the present lack of complete agreement between theory and experiment. The inverse sixth-power term in the Lennard-Jones (12–6) potential represents the leading term in the theoretical form for the dispersion energy, but the inverse twelfth power is only an empirical approximation to the repulsion energy, and is not expected to be accurate over a large range of separation distance. There is a considerable amount of theoretical and experimental evidence which indicates that the repulsion energy is more suitably described by an exponential form.[15–20] Accordingly we have chosen the form

$$\varphi(r)=\frac{\epsilon}{1-6/\alpha}\left[\frac{6}{\alpha}e^{\alpha(1-r/r_m)}-\left(\frac{r_m}{r}\right)^6\right], \qquad (1)$$

where $\varphi(r)$ is the potential energy of the molecules at separation distance r, $-\epsilon$ is the minimum potential energy, r_m is the value of r for which $\varphi(r)$ is a minimum, and α is an additional parameter which may be considered a measure of the steepness of the repulsion energy. The next higher term in the dispersion energy, a term varying as r^{-8} and representing the dipole-quadrupole energy, has not been included since the same effect as adding such a term may be achieved to a good approximation by a variation of the parameter α.

A typical potential energy curve is shown in Fig. 1. A more easily visualized measure of the steepness of the repulsion energy than α is the ratio σ/r_m, where σ is the value of r for which $\varphi(r)=0$. Table I gives σ/r_m as a function of α; included for comparison is σ/r_m for the Lennard-Jones (12–6) potential. A potential of the form of Eq. (1) was derived theoretically by Slater and Kirkwood[21] for the special case of helium, but its use as a semi-empirical form and its extensive application has been carried out mainly by Buckingham.[22] This potential has the defect that at a small separation distance, r_{max}, it has a spurious maximum, and approaches minus infinity as r approaches zero. Therefore Buckingham usually has used Eq. (1) only for $r>r_m$, and for $r<r_m$ has used another form in which the inverse sixth-power term of Eq. (1) was multiplied by another exponential term to prevent the potential from having a maximum. However, the maximum occurs at such high energies that it has little effect on ordinary thermal collisions, and we believe it is preferable to use Eq. (1) for $r>r_{max}$, and to set the potential equal to infinity for $r\leq r_{max}$. We have called this form a modified Buckingham potential, which might be referred to as the "Exp-Six" potential.

II. GENERAL FORMULAS

According to the theory of Enskog and Chapman, the transport phenomena depend on the intermolecular potential through collisions of single pairs of molecules, and the only feature of a collision which it is necessary to consider is the angle of deflection χ, through which the relative velocity vector of a pair of molecules under consideration is rotated by the collision. The angle χ is given by [23,24]

$$\chi(v,b)=\pi-2b\int_{r_c}^{\infty}[1-b^2/r^2-2\varphi(r)/\mu v^2]^{-\frac{1}{2}}dr/r^2, \qquad (2)$$

where v is the absolute value of the relative initial velocity of the pair of molecules, b, the collision param-

[15] C. Zener, Phys. Rev. **37**, 556 (1931).
[16] R. H. Fowler and E. A. Guggenheim, *Statistical Thermodynamics* (Cambridge University Press, Teddington, 1939), pp. 276–279, 291–294, give a summary of the evidence prior to 1939.
[17] R. A. Buckingham and J. Corner, Proc. Roy. Soc. (London) **A189**, 118 (1947); J. Corner, Trans. Faraday Soc. **44**, 914 (1948).
[18] I. Amdur, J. Chem. Phys. **17**, 844 (1949).
[19] J. L. Yntema and W. G. Schneider, J. Chem. Phys. **18**, 646 (1950).
[20] M. Kunimune, J. Chem. Phys. **18**, 754 (1950); Progr. Theoret. Phys. (Japan) **5**, 412 (1950).
[21] J. C. Slater, Phys. Rev. **32**, 349 (1928); J. C. Slater and J. G. Kirkwood, Phys. Rev. **37**, 682 (1931).
[22] R. A. Buckingham, Proc. Roy. Soc. (London) **A168**, 264 (1938); H. S. W. Massey and R. A. Buckingham, Proc. Roy. Soc. (London) **A168**, 378 (1938); **A169**, 205 (1938); Buckingham, Hamilton, and Massey, Proc. Roy. Soc. (London) **A179**, 103 (1941); R. A. Buckingham and R. A. Scriven, Proc. Phys. Soc. (London) **65**, 376 (1952).
[23] E. H. Kennard, *Kinetic Theory of Gases* (McGraw-Hill Book Company, Inc., New York, 1938), pp. 115–122.
[24] See reference (9b), Chapter 1.

eter, is the perpendicular distance between one of the molecules and the initial line of relative approach of the other, μ is the reduced mass of the colliding pair, and r_c is the distance of closest approach during the collision, given by

$$1-b^2/r_c^2-2\varphi(r_c)/\mu v^2=0. \quad (3)$$

The reduced velocity-dependent cross sections $S^{(l)}(K)$ are determined from χ by

$$S^{(l)}(K)=2\left[1-\frac{1}{2}\frac{1+(-1)^l}{1+l}\right]^{-1}\int_0^\infty (1-\cos^l\chi)\beta d\beta, \quad (4)$$

where we have introduced the reduced quantities $K=\mu v^2/2\epsilon$ and $\beta=b/r_m$. Finally, the reduced collision integrals, which directly determine the transport properties, are

$$\Omega^{(l,n)*}(T^*)=2[(n+1)!(T^*)^{n+2}]^{-1}\int_0^\infty e^{-K/T^*} \times K^{n+1}S^{(l)}(K)dK, \quad (5)$$

where $T^*=kT/\epsilon$, k is Boltzmann's constant, and T is the absolute temperature. The cross sections have been reduced by dividing by πr_m^2, and the collision integrals are just the $\Omega^{(l)}(n)$ of Chapman and Cowling,[25] divided by their values for rigid spheres of diameter r_m. Thus $S^{(l)}(K)$ and $\Omega^{(l,n)*}(T^*)$ are unity for rigid spheres.

The values of the transport coefficients may be expressed as infinite series, and higher approximations to the coefficients are obtained the more terms of the series that are taken. Fortunately, the convergence is rapid, and very few terms are needed. The coefficient of viscosity, η, of a pure gas is

$$\eta=\frac{5}{16}\left(\frac{MRT}{\pi}\right)^{\frac{1}{2}}\frac{f_\eta}{N_o r_m^2\Omega^{(2,2)*}(T^*)}, \quad (6)$$

where M is the molecular weight, R is the gas constant per mole, N_o is Avogadro's number, and f_η represents the infinite series, and is a complicated function of the collision integrals. The term f_η is nearly unity, and is a slowly varying function of T^*; in Appendix I the expression for the first three terms of f_η is given in terms of the collision integrals.

The coefficient of thermal conductivity, λ, of a pure gas is

$$\lambda=\frac{25}{32}\left(\frac{RT}{\pi M}\right)^{\frac{1}{2}}\frac{C_v}{N_o r_m^2}\frac{f_\lambda}{\Omega^{(2,2)*}(T^*)}, \quad (7)$$

where C_v is the molar heat capacity at constant volume of the gas, and f_λ is a term similar to f_η. The first three terms of f_λ are given in terms of the collision integrals in Appendix I. The formula (7) does not take account of the large amount of energy transported by the internal degrees of freedom of the molecules, and thus applies only to monatomic gases. An approximate correction for this extra energy transport may be made by multiplying the right-hand side of Eq. (7) by the "Eucken factor,"[26-28] which is usually taken to be $(9\gamma/10-1/2)$, where γ is the ratio of the constant-pressure heat capacity to the constant-volume heat capacity of the gas. No exact method for making this correction has yet been worked out.

The coefficient of mutual diffusion of a binary mixture of gases of types 1 and 2 is

$$D_{12}=\frac{3}{16}\left(\frac{M_1+M_2}{M_1M_2}\frac{2RT}{\pi}\right)^{\frac{1}{2}}\frac{f_D}{n(r_m)_{12}^2\Omega_{12}^{(1,1)*}(T^*)}, \quad (8)$$

where D_{12} is the mutual diffusion coefficient, M_1 and M_2 are the molecular weights of the species 1 and 2, and n is the total molecular density. The subscripts 1, 2 refer to an interaction between a molecule of type 1 and one of type 2. The term f_D is a very complicated function not only of T^*, but also of M_1, M_2, and the composition of the diffusing mixture. The dependence of D_{12} on the composition is entirely contained in this term, as well as the dependence of D_{12} on 1–1 and 2–2 molecular interactions. The third approximation to f_D is given in Appendix I. It seemed worthwhile to extend the expressions for the diffusion and thermal diffusion coefficients to one more approximation than has previously been used for a realistic intermolecular potential, inasmuch as there is evidence[29] that the lower approximations might differ from the limiting theoretical values by amounts greater than the error involved in determining the quantities experimentally. The expression for the self-diffusion coefficient, D_{11}, is obtained from Eq. (8) by setting $M_1=M_2$ and deleting the subscripts 1, 2.

The general expression for the thermal diffusion ratio is quite complicated, and for computational purposes is perhaps best expressed in the determinant notation of Chapman and Cowling. In this form, the expression for the mth approximation to the thermal diffusion ratio,

TABLE I. Ratio of the low velocity collision diameter, σ, to the position of the minimum, r_m.

α	σ/r_m
12	0.8761
13	0.8832
14	0.8891
15	0.8942
Lennard-Jones (12-6)	0.8909

[25] See reference 4, pp. 157, 160.

[26] A. Eucken, Physik. Z. 14, 324 (1913).
[27] See reference 4, pp. 237–240.
[28] See reference 9b, Chapter 7.
[29] See reference 4, pp. 169, 196.

$[k_T]_m$, of a binary mixture is

$$[k_T]_m=-\frac{5}{2}\frac{x_1\mathfrak{A}_{01}^{(m)}\left(\frac{M_1+M_2}{2M_1}\right)^{\frac{1}{2}}+x_2\mathfrak{A}_{0-1}^{(m)}\left(\frac{M_1+M_2}{2M_2}\right)^{\frac{1}{2}}}{\mathfrak{A}_{00}^{(m)}}, \tag{9}$$

where x_1 and x_2 are the mole fractions of the two components. $\mathfrak{A}^{(m)}$ is a determinant of $(2m+1)$ order, whose general term is a_{ij}, where i and j range from $-m$ to m. $\mathfrak{A}_{ij}^{(m)}$ is the minor of $\mathfrak{A}^{(m)}$ obtained by striking out the row and column containing a_{ij}. The elements a_{ij} are functions of the collision integrals $\Omega^{(l,s)*}$, the molecular weights of the component gases, and the composition of the mixture. The expressions for the a_{ij} for $m=2$ are given in Appendix I.

For binary mixtures of heavy isotopes, where the forces between the different molecular species are the same, Eq. (9) may be put into a simpler form by expanding the determinants in powers of the small quantity $(M_1-M_2)/(M_1+M_2)$, and keeping only the first power. To this order of approximation,

$$[k_T]_m=[k_T^*]_m\left(\frac{M_1-M_2}{M_1+M_2}\right)x_1x_2, \tag{10}$$

where $[k_T^*]_m$ is a reduced thermal diffusion ratio, and is a function of the reduced temperature alone. Since the expression for $[k_T^*]_m$ in terms of the collision integrals is complicated, it is placed in Appendix I. We prefer the function k_T^* to the more frequently encountered R_T, for reasons which are discussed in detail at the end of Appendix I. The two functions are very simply related: $R_T=(118/105)k_T^*$.

For mixtures of gases, the following three ratios of collision integrals occur frequently:

$$\begin{aligned} A^*&=\Omega_{12}^{(2,2)*}/\Omega_{12}^{(1,1)*},\\ B^*&=[5\Omega_{12}^{(1,2)*}-4\Omega_{12}^{(1,3)*}]/\Omega_{12}^{(1,1)*},\\ C^*&=\Omega_{12}^{(1,2)*}/\Omega_{12}^{(1,1)*}. \end{aligned} \tag{11}$$

These quantities are equal to unity for rigid spheres.

TABLE II. Conditions for orbiting.

α	K	β_0	y_0	y_1
12	0.4	1.7916	1.4468	0.9694
	$K_0=0.78101$	1.5835	1.1849	1.1849
13	0.4	1.7716	1.4353	0.9649
	0.8	1.5636	1.2098	1.1076
	$K_0=0.82691$	1.5530	1.1708	1.1708
14	0.4	1.7555	1.4253	0.9621
	0.8	1.5530	1.2209	1.0710
	$K_0=0.86809$	1.5281	1.1594	1.1594
15	0.4	1.7421	1.4166	0.9604
	0.8	1.5437	1.2248	1.0504
	$K_0=0.90530$	1.5075	1.1498	1.1498

III. NUMERICAL CALCULATIONS

The first step in the evaluation of the collision integrals is the calculation by numerical integration of the angle of deflection, χ, as a function of v, b, and the potential parameters. Equation (2) is inconvenient for numerical computations because the integrand becomes infinite at the lower limit of the integral. This singularity may be removed by substituting into Eq. (2) the value of b from Eq. (3), and making the change of variable $\sin\theta=r_c/r$, after which Eq. (2) may be rearranged into the form

$$\chi=\pi-\frac{2\beta}{y}\int_0^{\pi/2}\left[1-\frac{\sin^2\theta+\sin^4\theta}{K(1-6/\alpha)y^6}+\frac{(6/\alpha)e^{\alpha}}{K(1-6/\alpha)}\left(\frac{e^{-\alpha y}\sin^2\theta-e^{-\alpha y/\sin\theta}}{\cos^2\theta}\right)\right]^{-\frac{1}{2}}d\theta, \tag{12}$$

where y is the reduced distance of closest approach, r_c/r_m, and β is the reduced collision parameter, b/r_m, given by

$$\beta=y\left[1-\frac{1}{K(1-6/\alpha)}\left(\frac{6}{\alpha}e^{\alpha(1-y)}-\frac{1}{y^6}\right)\right]^{\frac{1}{2}}. \tag{13}$$

The integration in Eq. (12) was performed numerically, the integrand being evaluated at intervals of $\theta=\pi/60$ in cases where the integrand varied rapidly with θ, but otherwise at intervals of $\theta=\pi/20$ or $\pi/12$, depending on the behavior of the integrand. The integrand in Eq. (12) becomes indeterminate at $\theta=\pi/2$, but may be shown by L'Hospital's Rule to approach the limit

$$\left[1-\frac{2}{K(1-6/\alpha)y^6}+\frac{(6/\alpha)e^{\alpha(1-y)}}{K(1-6/\alpha)}\left(\frac{\alpha y}{2}-1\right)\right]^{-\frac{1}{2}}. \tag{14}$$

The numerical integration of Eq. (12) was sufficient to determine χ to a few ten-thousandths of a radian. Values of χ, together with the corresponding values of β, have been tabulated as a function of y and K for $\alpha=12$, 13, 14, and 15; the length of the tabulations prevented their publication in the present paper.[30] The tabulations cover thirteen values of K for each value of α, as in Table III, and an average of about 20 values of y for each K. The size of the intervals on y varies from 0.0050 to 0.40, depending on the behavior of χ, and was chosen so as to obtain an accuracy of 0.1 percent in the integration for $S^{(l)}(K)$.

The calculation of χ was complicated by the fact that for some collisions which occur at less than a certain critical energy, K_0, the molecules may "orbit" around each other for an indefinite number of revolutions, and χ consequently tends to minus infinity. Such orbiting collisions have been discussed in connection with the Lennard-Jones (12-6) potential,[7,14] and the same general behavior is observed with the present

[30] Multigraphed tables may be obtained from the author on request.

potential. For energies equal to or less than K_0, there is a critical value of beta, β_0, for which orbiting will occur. There are two values of the distance of closest approach, y, which corresponds to β_0; values of y between these two critical ones cannot occur physically. The larger y, designated as y_0, will cause the integrand of Eq. (12) to become infinite at the upper limit, so that the value of y_0 may be determined by numerical solution of the equation,

$$1-\frac{2}{K(1-6/\alpha)y_0^6}+\frac{(6/\alpha)e^{\alpha(1-y_0)}}{K(1-6/\alpha)}\left(\frac{\alpha y_0}{2}-1\right)=0, \quad (15)$$

which is obtained from Eqs. (12) and (14). The value of β_0 may be found by substituting the value of y_0 into Eq. (13) and solving. The smaller value of y, designated as y_1, also satisfies Eq. (13) with $\beta=\beta_0$, and may be calculated in this way. At $y=y_1$ the integrand of Eq. (12) becomes infinite for $\theta=\arcsin(y_1/y_0)$. Between $y=y_0$ and $y=y_1$ there are two values of y which give the same β when substituted into Eq. (13), but these values are without physical significance. Values of β_0, y_0, and y_1 for several values of K are given in Table II; y_0 and y_1 become equal at $K=K_0$.

For small values of χ, it is useful to have the asymptotic series, valid for large values of y:

$$\chi=-\frac{15\pi}{16}\left[\frac{1}{K(1-6/\alpha)y^6}\right]-\frac{585\pi}{1024}\left[\frac{1}{K(1-6/\alpha)y^6}\right]^2-\cdots$$
$$+\frac{(6/\alpha)e^{\alpha(1-y)}}{K(1-6/\alpha)}\left(\frac{\pi\alpha y}{2}\right)^{\frac{1}{2}}\left(1-\frac{1}{8\alpha y}+\frac{9}{32(\alpha y)^2}-\cdots\right), \quad (16)$$

which was obtained by the method of Amdur and Pearlman.[31]

To evaluate the cross sections $S^{(l)}(K)$ defined in Eq. (4), the integration variable was changed from β to y, and Eq. (4) transformed to

$$S^{(l)}(K)=\frac{2}{\left[1-\frac{1}{2}\frac{1+(-1)^l}{1+l}\right]}\int_{y_c}^{\infty}(1-\cos^l\chi)$$
$$\times\left[1-\frac{2}{K(1-6/\alpha)y^6}+\frac{(6/\alpha)e^{\alpha(1-y)}}{K(1-6/\alpha)}\left(\frac{\alpha y}{2}-1\right)\right]y\,dy, \quad (17)$$

where y is the value of y for which $\beta=0$, and represents the reduced distance of closest approach for a head-on collision. Most of the integration could then be carried out numerically, using the values of χ tabulated as a function of y for a given K and α. To avoid the necessity of calculating accurate values of y_c from Eq. (13), the numerical integration was started from a lower limit y_A which was slightly greater than y_c, and the integration from y_c to y_A executed as follows. Equations (12) and (13) were differentiated to form $(d\chi/d\beta)$ in terms of χ and β for the limit of $\beta\to 0$. Solution of the resulting differential equation then showed that χ varied linearly with β when β was near zero, so that the integration from y_c to y_A could be performed analytically. The equations obtained for these small contributions to the cross sections are:

$$A^{(1)}(K)=\beta_A^2-\frac{2\beta_A^2}{(\pi-\chi_A)^2}[1-\cos(\pi-\chi_A)]+\frac{2\beta_A^2}{\pi-\chi_A}\sin(\pi-\chi_A),$$

$$A^{(2)}(K)=\frac{3}{4}\beta_A^2+\frac{3}{8}\frac{\beta_A^2}{(\pi-\chi_A)^2}[1-\cos 2(\pi-\chi_A)]-\frac{3}{4}\frac{\beta_A^2}{\pi-\chi_A}\sin 2(\pi-\chi_A),$$

$$A^{(3)}(K)=\beta_A^2-\frac{1}{18}\frac{\beta_A^2}{(\pi-\chi_A)^2}[1-\cos 3(\pi-\chi_A)]-\frac{3}{2}\frac{\beta_A^2}{(\pi-\chi_A)^2}[1-\cos(\pi-\chi_A)]+\frac{1}{6}\frac{\beta_A^2}{\pi-\chi_A}\sin 3(\pi-\chi_A)+\frac{3}{2}\frac{\beta_A^2}{\pi-\chi_A}\sin(\pi-\chi_A), \quad (18)$$

$$A^{(4)}(K)=\frac{25}{32}\beta_A^2+\frac{5}{256}\frac{\beta_A^2}{(\pi-\chi_A)^2}[1-\cos 4(\pi-\chi_A)]+\frac{5}{16}\frac{\beta_A^2}{(\pi-\chi_A)^2}[1-\cos 2(\pi-\chi_A)]-\frac{5}{64}\frac{\beta_A^2}{\pi-\chi_A}\sin 4(\pi-\chi_A)-\frac{5}{8}\frac{\beta_A^2}{\pi-\chi_A}\sin 2(\pi-\chi_A),$$

where the $A^{(l)}(K)$ are the contributions to the $S^{(l)}(K)$ for the range y_c to y_A, and β_A and χ_A are the values of β and χ corresponding to y_A. The numerical integration of Eq. (17) when no orbiting occurred $(K>K_0)$ was carried out from y_A to y_E, where y_E was a large value of y, and the remainder of the integration, from y_E to infinity, carried out by substituting the small angle formula, Eq. (16), into Eq. (17), expanding $(1-\cos^l\chi)$,

[31] I. Amdur and H. Pearlman, J. Chem. Phys. 9, 503 (1941); I. Amdur, J. Chem. Phys. 15, 482 (1947).

and integrating analytically to yield:

$$\frac{1}{l}\left[1-\frac{1}{2}\frac{1+(-1)^l}{1+l}\right]F^{(l)}(K)$$
$$=\left(\frac{15\pi}{16}\right)^2 y_E^2\left[\frac{1}{10}\left(\frac{1}{K(1-6/\alpha)y_E{}^6}\right)^2-\frac{25}{512}\left(\frac{1}{K(1-6/\alpha)y_E{}^6}\right)^3\right]$$
$$-\left(\frac{15\pi}{16}\right)\frac{(6/\alpha)e^{\alpha(1-y_E)}}{K(1-6/\alpha)}\left(\frac{2\pi}{\alpha y_E{}^9}\right)^{\frac{1}{2}}$$
$$\times\left[1-\frac{37}{8\alpha y_E}+\frac{823}{32(\alpha y_E)^2}-\cdots\right], \quad (19)$$

where $F^{(l)}(K)$ is the contribution to $S^{(l)}(K)$ for the range y_E to infinity.

When K is equal to or less than the critical energy for orbiting, K_0, numerical integration of Eq. (17) cannot be carried out over the entire range from y_A to y_E because: (1) the region from y_1 to y_0 is physically inaccessible, and in fact χ is imaginary there; (2) the integrand oscillates violently near y_1 and y_0, where χ goes to minus infinity. For $K\leq K_0$ the integral from y_A to y_E was therefore broken up into four integrals: $B^{(l)}(K)$, $C^{(l)}(K)$, $D^{(l)}(K)$, and $E^{(l)}(K)$. The integral $B^{(l)}(K)$ extended from y_A to y_B, where y_B was slightly less than y_1, and was evaluated numerically. Similarly, the integral $E^{(l)}(K)$ extended from y_D, where y_D was slightly greater than y_0, to y_E, and was also evaluated numerically. The integrals $C^{(l)}(K)$ and $D^{(l)}(K)$, covering the regions y_B to y_1 and y_0 to y_D, respectively, were calculated by the method of Hirschfelder, Bird, and Spotz,[7] in which χ is represented near the regions of orbiting by equations of the form

$$\chi^2=\text{const}/(\beta^2-\beta_0{}^2), \quad (20)$$

and Eq. (4) is integrated analytically between the proper limits. The results of this integration are:

$$C^{(1)}(K)=(\beta_0{}^2-\beta_B{}^2)[1-\cos\chi_B+\chi_B\sin\chi_B-\chi_B{}^2Ci(-\chi_B)],$$
$$C^{(2)}(K)=\tfrac{3}{4}(\beta_0{}^2-\beta_B{}^2)[1-\cos2\chi_B+2\chi_B\sin2\chi_B-4\chi_B{}^2Ci(-2\chi_B)],$$
$$C^{(3)}(K)=\tfrac{1}{4}(\beta_0{}^2-\beta_B{}^2)[4-\cos3\chi_B-3\cos\chi_B+3\chi_B\sin3\chi_B+3\chi_B\sin\chi_B-9\chi_B{}^2Ci(-3\chi_B)-3\chi_B{}^2Ci(-\chi_B)], \quad (21)$$
$$C^{(4)}(K)=\tfrac{5}{32}(\beta_0{}^2-\beta_B{}^2)[5-\cos4\chi_B-4\cos2\chi_B+4\chi_B\sin4\chi_B+8\chi_B\sin2\chi_B-16\chi_B{}^2Ci(-4\chi_B)-16\chi_B{}^2Ci(-2\chi_B)],$$

where β_B and χ_B are the values of β and χ corresponding ing to y_B, and $Ci(-\chi_B)$ is the cosine integral, a tabulated function,[32] defined as follows:

$$Ci(z)=\int_\infty^z\frac{\cos t}{t}dt. \quad (21b)$$

The $D^{(l)}(K)$ are of the same form as the $C^{(l)}(K)$.

The cross sections $S^{(l)}(K)$ are not convenient to use directly, since they vary rapidly when K is small, and tend to infinity as K goes to zero. Kihara and Kotani have shown[5] that in the limit $K\to0$, the cross sections are independent of the potential energy of repulsion, and depend on the attraction energy alone. From this it is easy to show that the $S^{(l)}(K)$ are proportional to $[K(1-6/\alpha)]^{-\frac{1}{2}}$ for $K\to0$; we therefore define the functions $R^{(l)}(K)$:

$$R^{(l)}(K)=[K(1-6/\alpha)]^{\frac{1}{2}}S^{(l)}(K), \quad (22)$$

which are given in Table III, and plotted for $\alpha=12$ and 15 in Fig. 2 for the two most important cases, $l=1$ and 2. For comparison, the analogous functions for the Lennard-Jones (12–6) potential are also plotted. Since $R^{(l)}(0)$ is independent of the repulsion, the values given in the table for $l=1$ and 2 were taken directly from Kihara and Kotani.[5] For $l=3$ and 4, the values of $R^{(l)}(0)$ were obtained by extrapolation, a procedure which is permissible because these functions occur in the expressions for the transport properties only as correction terms.

For use in evaluating the collision integrals, the cross section functions were approximated by the following algebraic expressions:

$$R^{(l)}(K)=R^{(l)}(0)(1+a_1{}^{(l)}K^{\frac{1}{2}}+a_2{}^{(l)}K^{\frac{2}{3}}), \quad 0\leq K\leq0.8;$$
$$S^{(l)}(K)=a_3{}^{(l)}K^2+a_4{}^{(l)}K+a_5{}^{(l)}+a_6{}^{(l)}K^{-1}+a_7{}^{(l)}K^{-2}, \quad 0.8\leq K\leq2;$$
$$\left.\begin{aligned}S^{(l)}(K)&=a_8{}^{(l)}K+a_9{}^{(l)}+a_{10}{}^{(l)}K^{-1}+a_{11}{}^{(l)}K^{-2}\\ S^{(l)}(K)&=a_8{}^{(l)}+a_9{}^{(l)}K^{-1}+a_{10}{}^{(l)}K^{-2}+a_{11}{}^{(l)}K^{-3}, l\neq1\end{aligned}\right\} 2\leq K\leq10; \quad (23)$$
$$S^{(l)}(K)=a_{12}{}^{(l)}+a_{13}{}^{(l)}K^{-\frac{1}{3}}+a_{14}{}^{(l)}K^{-1}+a_{15}{}^{(l)}K^{-\frac{4}{3}}, \quad 10\leq K<\infty.$$

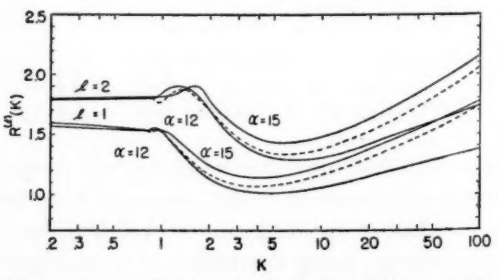

FIG. 2. The cross-section functions, $R^{(l)}(K)$. Solid lines: Exp-Six potential; broken lines: Lennard-Jones (12–6) potential.

[32] Federal Works Agency, Work Projects Administration for the City of New York, *Tables of Sine, Cosine, and Exponential Integrals* (1940), Vol. II; *Table of Sine and Cosine Integrals* (1942).

TABLE III. Cross-section functions, $R^{(l)}(K)$.

$K\backslash\alpha$	12	13	14	15
		$R^{(1)}(K)$		
0	1.5778	1.5778	1.5778	1.5778
0.4	1.5701	1.5588	1.5495	1.5490
0.78101	1.5327			
0.8		1.5280	1.5277	1.5275
1.0	1.5178	1.5297	1.5320	1.5282
1.2	1.4083	1.4392	1.4566	1.4811
1.6	1.2271	1.2714	1.3027	1.3282
2	1.1336	1.1743	1.2073	1.2350
3	1.0361	1.0805	1.1177	1.1509
4	1.0119	1.0613	1.1018	1.1366
5	1.0109	1.0626	1.1070	1.1443
10	1.0646	1.1297	1.1865	1.2356
20	1.1546	1.2401	1.3107	1.3769
50	1.2824	1.4032	1.5069	1.6000
100	1.3676	1.5226	1.6579	1.7811
		$R^{(2)}(K)$		
0	1.7865	1.7865	1.7865	1.7865
0.4	1.7923	1.7936	1.7985	1.7980
0.78101	1.7991			
0.8		1.8001	1.8060	1.8045
1.0	1.8357	1.7864	1.7959	1.7984
1.2	1.8941	1.8727	1.8627	1.8304
1.6	1.8344	1.8688	1.8826	1.8918
2	1.6929	1.7333	1.7587	1.7726
3	1.4442	1.4921	1.5288	1.5621
4	1.3418	1.3870	1.4305	1.4619
5	1.2986	1.3489	1.3918	1.4274
10	1.3051	1.3676	1.4200	1.4689
20	1.4141	1.4972	1.5605	1.6272
50	1.6063	1.7233	1.8294	1.9171
100	1.7599	1.9129	2.0461	2.1613
		$R^{(3)}(K)$		
0	(1.8236)	(1.8236)	(1.8236)	(1.8236)
0.4	1.8115	1.8005	1.7938	1.7987
0.78101	1.7831			
0.8		1.7749	1.7821	1.7745
1.0	1.7796	1.7833	1.7778	1.7797
1.2	1.6788	1.6930	1.7042	1.7285
1.6	1.6121	1.6333	1.6433	1.6595
2	1.5325	1.5665	1.5884	1.6151
3	1.3587	1.4012	1.4376	1.4692
4	1.2689	1.3167	1.3557	1.3934
5	1.2256	1.2776	1.3206	1.3574
10	1.2222	1.2875	1.3447	1.3893
20	1.3151	1.3993	1.4632	1.5363
50	1.4922	1.6047	1.7045	1.7928
100	1.6115	1.7641	1.8980	2.0141
		$R^{(4)}(K)$		
0	(1.9100)	(1.9100)	(1.9100)	(1.9100)
0.4	1.9335	1.9208	1.9225	1.9274
0.78101	1.9345			
0.8		1.9178	1.9221	1.9586
1.0	1.9330	1.9191	1.9065	1.9107
1.2	2.0278	1.9948	1.9907	1.9674
1.6	1.9600	1.9878	1.9770	1.9983
2	1.8895	1.9176	1.9300	1.9258
3	1.6584	1.7026	1.7363	1.7663
4	1.5197	1.5623	1.6045	1.6348
5	1.4433	1.4941	1.5328	1.5705
10	1.3868	1.4514	1.4987	1.5488
20	1.4838	1.5670	1.6252	1.6893
50	1.6931	1.8089	1.9105	1.9954
100	1.8636	2.0136	2.1450	2.2558

This curve-fitting procedure effectively permits the extrapolation of the $S^{(l)}(K)$ to infinite K, which is necessary because the potential energy function $\varphi(r)$ of Eq. (1) misbehaves for very small values of r by becoming negative.

The final integrations with respect to K to obtain the collision integrals defined in Eq. (5) could be carried out by replacing $S^{(l)}(K)$ in Eq. (5) by the algebraic expressions obtained from Eqs. (22) and (23). For $K>0.8$, the resulting integrals could be easily evaluated in terms of elementary functions and error integrals, which are tabulated functions. For $K<0.8$, the integrations were performed numerically for large T^*, where this region did not contribute greatly to the result, and for small T^* by means of incomplete gamma functions tabulated by Kotani.[33] In practice it turned out to be easier also to integrate numerically for $K>0.8$ when T^* was large. For numerical integrations, the algebraic expressions in Eq. (23) were used only as interpolation functions to obtain values of $S^{(l)}(K)$ at small intervals of K.

The collision integrals are not especially well suited to tabulation because their rapid variation for small T^* makes interpolation difficult unless the tabulations are made for small intervals of T^*. A more suitable function for tabulation is

$$Z^{(l,n)}(T^*)=[T^*(1-6/\alpha)]^{\frac{1}{2}}\Omega^{(l,n)^*}(T^*). \qquad (24)$$

This function varies relatively slowly with T^*, and unlike $\Omega^{(l,n)^*}(T^*)$ is finite and independent of the parameter α when $T^*=0$. The functions $Z^{(l,n)}(T^*)$ are tabulated in Table IV for T^* from 0 to 200. The inherent computational error is estimated to be of the order of 0.2 percent, except for very small T^*, where it may be as large as one percent. To maintain internal consistency, more figures are given in Table IV than is strictly justified by the estimated error. The reason for the lower estimated accuracy at small T^* is that the cross-section functions $R^{(l)}(K)$ seem to have an oscillatory behavior when K is small, but no attempt was made to follow this behavior in detail since many calculations at closely spaced values of K would have been necessary. The labor involved did not seem worth while, particularly since the neglect of quantum corrections at low K is probably a much more serious error.

IV. ADDITIONAL TABULATIONS

In Table V are presented the functions, f, which give the higher approximations to the transport coefficients for pure gases; the superscripts indicate that these are the third approximations rather than the exact values. The function f_D for a pure gas refers to the coefficient of self-diffusion.

The second approximation to the reduced thermal diffusion ratio for a binary mixture of heavy isotopes, $[k_T^*]_2$, is given in Table VI as a function of T^*, and plotted in Fig. 3 for $\alpha=12$ and 15. For comparison, the

[33] M. Kotani, Proc. Phys.-Math. Soc. Japan **24**, 76 (1942).

TABLE IV. Collision integral functions.

$Z^{(l,s)}(T^*) = [T^*(1-6/\alpha)]^{\frac{1}{2}}\Omega^{(l,s)*}(T^*), \quad T^* = kT/\epsilon.$

$\alpha=12$ T^*	$Z^{(1,1)}$	$Z^{(1,2)}$	$Z^{(1,3)}$	$Z^{(1,4)}$	$Z^{(1,5)}$	$Z^{(2,2)}$
0	1.1870	1.0551	0.9672	0.9027	0.8572	1.1178
0.1	1.1911	1.0523	0.9584	0.8883	0.8320	1.1079
0.2	1.1662	1.0142	0.9025	0.8113	0.7338	1.0704
0.3	1.1243	0.9515	0.8232	0.7239	0.6475	1.0161
0.4	1.0750	0.8900	0.7597	0.6667	0.6005	0.9641
0.5	1.0282	0.8402	0.7160	0.6328	0.5764	0.9194
0.6	0.9873	0.8025	0.6870	0.6131	0.5643	0.8828
0.7	0.9530	0.7745	0.6679	0.6019	0.5589	0.8536
0.8	0.9248	0.7538	0.6555	0.5959	0.5572	0.8305
0.9	0.9016	0.7387	0.6475	0.5930	0.5576	0.8125
1.0	0.8825	0.7272	0.6425	0.5923	0.5593	0.7985
1.2	0.8541	0.7130	0.6385	0.5942	0.5646	0.7793
1.4	0.8350	0.7058	0.6388	0.5985	0.5711	0.7684
1.6	0.8221	0.7028	0.6414	0.6039	0.5779	0.7625
1.8	0.8135	0.7025	0.6451	0.6096	0.5845	0.7601
2.0	0.8080	0.7037	0.6496	0.6155	0.5910	0.7600
2.5	0.8023	0.7104	0.6616	0.6296	0.6059	0.7654
3.0	0.8031	0.7195	0.6735	0.6425	0.6180	0.7746
3.5	0.8070	0.7288	0.6847	0.6541	0.6305	0.7853
4	0.8126	0.7382	0.6950	0.6644	0.6404	0.7963
5	0.8253	0.7556	0.7129	0.6819	0.6572	0.8174
6	0.8384	0.7709	0.7280	0.6962	0.6705	0.8364
7	0.8509	0.7842	0.7409	0.7081	0.6817	0.8533
8	0.8623	0.7961	0.7520	0.7185	0.6912	0.8680
9	0.8730	0.8067	0.7618	0.7272	0.6993	0.8813
10	0.8829	0.8160	0.7702	0.7351	0.7066	0.8929
12	0.9002	0.8322	0.7848	0.7485	0.7189	0.9133
14	0.9150	0.8457	0.7969	0.7594	0.7292	0.9301
16	0.9280	0.8572	0.8074	0.7690	0.7380	0.9444
18	0.9394	0.8674	0.8164	0.7773	0.7459	0.9568
20	0.9497	0.8762	0.8245	0.7846	0.7530	0.9680
25	0.9710	0.8951	0.8415	0.8007	0.7682	0.9910
30	0.9885	0.9103	0.8555	0.8138	0.7808	1.0094
35	1.0032	0.9232	0.8674	0.8253	0.7921	1.0250
40	1.0157	0.9346	0.8781	0.8355	0.8021	1.0385
45	1.0270	0.9446	0.8876	0.8450	0.8114	1.0508
50	1.0371	0.9538	0.8965	0.8535	0.8199	1.0614
60	1.0549	0.9701	0.9123	0.8691	0.8355	1.0807
70	1.0700	0.9846	0.9264	0.8827	0.8495	1.0978
80	1.0834	0.9973	0.9388	0.8957	0.8622	1.1129
90	1.0959	1.0091	0.9504	0.9074	0.8743	1.1265
100	1.1071	1.0201	0.9615	0.9184	0.8853	1.1391
200	1.1906	1.1038	1.0462	1.0049	0.9729	1.2356

$\alpha=12$ T^*	$Z^{(2,2)}$	$Z^{(2,3)}$	$Z^{(2,4)}$	$Z^{(2,5)}$	$Z^{(2,6)}$	$Z^{(4,4)}$
0	1.1947	1.0951	1.0221	0.9706	0.9193	1.0927
0.1	1.1983	1.1002	1.0291	0.9750	0.9323	1.1062
0.2	1.2098	1.1094	1.0401	0.9770	0.9188	1.1119
0.3	1.2065	1.0936	0.9978	0.9129	0.8381	1.0843
0.4	1.1799	1.0471	0.9367	0.8453	0.7711	1.0360
0.5	1.1421	0.9974	0.8835	0.7953	0.7280	0.9870
0.6	1.1028	0.9538	0.8428	0.7614	0.7017	0.9450
0.7	1.0667	0.9185	0.8133	0.7391	0.6862	0.9111
0.8	1.0352	0.8907	0.7923	0.7249	0.6775	0.8847
0.9	1.0084	0.8692	0.7775	0.7160	0.6731	0.8642
1.0	0.9859	0.8528	0.7673	0.7108	0.6716	0.8488
1.2	0.9520	0.8309	0.7561	0.7075	0.6736	0.8282
1.4	0.9290	0.8189	0.7525	0.7093	0.6790	0.8170
1.6	0.9137	0.8130	0.7531	0.7139	0.6860	0.8120
1.8	0.9039	0.8111	0.7560	0.7198	0.6936	0.8107
2.0	0.8978	0.8116	0.7604	0.7263	0.7014	0.8119
2.5	0.8930	0.8189	0.7742	0.7435	0.7202	0.8207
3.0	0.8963	0.8300	0.7891	0.7600	0.7374	0.8331
3.5	0.9033	0.8423	0.8035	0.7752	0.7529	0.8466
4	0.9122	0.8546	0.8171	0.7892	0.7668	0.8599
5	0.9313	0.8778	0.8415	0.8135	0.7906	0.8849
6	0.9503	0.8987	0.8623	0.8339	0.8105	0.9072
7	0.9681	0.9172	0.8806	0.8516	0.8275	0.9269
8	0.9845	0.9339	0.8967	0.8670	0.8424	0.9445
9	0.9995	0.9488	0.9110	0.8808	0.8559	0.9602
10	1.0133	0.9624	0.9241	0.8935	0.8678	0.9745

$Z^{(l,s)}(T^*) = [T^*(1-6/\alpha)]^{\frac{1}{2}}\Omega^{(l,s)*}(T^*), \quad T^* = kT/\epsilon.$

$\alpha=12$ T^*	$Z^{(2,2)}$	$Z^{(2,3)}$	$Z^{(2,4)}$	$Z^{(2,5)}$	$Z^{(2,6)}$	$Z^{(4,4)}$
12	1.0381	0.9862	0.9469	0.9153	0.8891	0.9998
14	1.0598	1.0068	0.9664	0.9341	0.9073	1.0213
16	1.0788	1.0248	0.9838	0.9508	0.9236	1.0404
18	1.0958	1.0409	0.9993	0.9658	0.9383	1.0575
20	1.1113	1.0557	1.0134	0.9796	0.9516	1.0731
25	1.1448	1.0875	1.0441	1.0095	0.9812	1.1070
30	1.1729	1.1145	1.0703	1.0352	1.0067	1.1357
35	1.1976	1.1382	1.0935	1.0582	1.0294	1.1608
40	1.2193	1.1593	1.1143	1.0787	1.0499	1.1832
45	1.2393	1.1786	1.1332	1.0976	1.0688	1.2041
50	1.2573	1.1962	1.1509	1.1152	1.0863	1.2228
60	1.2901	1.2283	1.1826	1.1469	1.1180	1.2572
70	1.3189	1.2571	1.2113	1.7156	1.1468	1.2878
80	1.3451	1.2828	1.2370	1.2014	1.1730	1.3157
90	1.3690	1.3068	1.2609	1.2257	1.1973	1.3413
100	1.3915	1.3292	1.2835	1.2481	1.2198	1.3649
200	1.5600	1.4988	1.4547	1.4208	1.3939	1.5470

$\alpha=13$ T^*	$Z^{(1,1)}$	$Z^{(1,2)}$	$Z^{(1,3)}$	$Z^{(1,4)}$	$Z^{(1,5)}$	$Z^{(2,2)}$
0	1.1870	1.0551	0.9672	0.9027	0.8572	1.1178
0.1	1.1813	1.0447	0.9528	0.8846	0.8305	1.1020
0.2	1.1618	1.0150	0.9084	0.8217	0.7479	1.0718
0.3	1.1275	0.9619	0.8389	0.7429	0.6681	1.0250
0.4	1.0851	0.9071	0.7807	0.6893	0.6236	0.9787
0.5	1.0436	0.8617	0.7400	0.6575	0.6011	0.9383
0.6	1.0068	0.8268	0.7129	0.6393	0.5904	0.9048
0.7	0.9756	0.8009	0.6953	0.6294	0.5862	0.8780
0.8	0.9498	0.7818	0.6841	0.6244	0.5855	0.8569
0.9	0.9285	0.7678	0.6772	0.6226	0.5871	0.8405
1.0	0.9112	0.7577	0.6732	0.6229	0.5897	0.8279
1.2	0.8854	0.7454	0.6710	0.6266	0.5970	0.8111
1.4	0.8684	0.7400	0.6729	0.6326	0.6052	0.8022
1.6	0.8573	0.7386	0.6770	0.6395	0.6136	0.7981
1.8	0.8503	0.7396	0.6823	0.6468	0.6219	0.7974
2.0	0.8461	0.7421	0.6881	0.6542	0.6299	0.7987
2.5	0.8436	0.7519	0.7032	0.6715	0.6483	0.8073
3.0	0.8472	0.7637	0.7181	0.6875	0.6643	0.8193
3.5	0.8535	0.7757	0.7320	0.7017	0.6785	0.8323
4	0.8614	0.7874	0.7446	0.7145	0.6910	0.8454
5	0.8782	0.8091	0.7671	0.7365	0.7121	0.8700
6	0.8950	0.8282	0.7862	0.7547	0.7296	0.8922
7	0.9107	0.8451	0.8024	0.7702	0.7441	0.9118
8	0.9253	0.8601	0.8166	0.7836	0.7568	0.9294
9	0.9389	0.8734	0.8292	0.7954	0.7678	0.9453
10	0.9514	0.8855	0.8404	0.8059	0.7777	0.9596
12	0.9736	0.9065	0.8599	0.8240	0.7948	0.9847
14	0.9927	0.9245	0.8765	0.8394	0.8094	1.0063
16	1.0096	0.9399	0.8907	0.8528	0.8223	1.0250
18	1.0247	0.9537	0.9034	0.8648	0.8337	1.0417
20	1.0384	0.9659	0.9147	0.8754	0.8440	1.0569
25	1.0674	0.9922	0.9392	0.8987	0.8664	1.0895
30	1.0913	1.0139	0.9596	0.9184	0.8855	1.1166
35	1.1118	1.0328	0.9775	0.9357	0.9027	1.1403
40	1.1296	1.0492	0.9933	0.9510	0.9179	1.1616
45	1.1456	1.0643	1.0076	0.9651	0.9318	1.1806
50	1.1602	1.0778	1.0208	0.9783	0.9447	1.1983
60	1.1861	1.1023	1.0447	1.0017	0.9682	1.2297
70	1.2087	1.1239	1.0659	1.0230	0.9894	1.2577
80	1.2287	1.1431	1.0849	1.0422	1.0089	1.2830
90	1.2469	1.1608	1.1025	1.0598	1.0267	1.3063
100	1.2639	1.1774	1.1193	1.0762	1.0434	1.3277
200	1.3892	1.3027	1.2456	1.2042	1.1723	1.4915

$\alpha=13$ T^*	$Z^{(2,2)}$	$Z^{(2,3)}$	$Z^{(2,4)}$	$Z^{(2,5)}$	$Z^{(2,6)}$	$Z^{(4,4)}$
0	1.1947	1.0951	1.0221	0.9706	0.9193	1.0927
0.1	1.1985	1.0994	1.0269	0.9709	0.9265	1.0986
0.2	1.2052	1.1090	1.0376	0.9783	0.9247	1.1116
0.3	1.2056	1.0977	1.0077	0.9278	0.8562	1.0944
0.4	1.1862	1.0602	0.9549	0.8664	0.7934	1.0526
0.5	1.1549	1.0164	0.9059	0.8190	0.7519	1.0076

TABLE IV.—*Continued.*

$Z^{(l,s)}(T^*) = [T^*(1-6/\alpha)]^{\frac{1}{2}}\Omega^{(l,s)*}(T^*), \quad T^* = kT/\epsilon.$

$\alpha=13$ T^*	$Z^{(2,2)}$	$Z^{(2,3)}$	$Z^{(2,4)}$	$Z^{(2,5)}$	$Z^{(2,6)}$	$Z^{(4,4)}$
0.6	1.1207	0.9766	0.8676	0.7866	0.7267	0.9681
0.7	1.0882	0.9436	0.8395	0.7653	0.7120	0.9360
0.8	1.0594	0.9175	0.8196	0.7519	0.7043	0.9110
0.9	1.0346	0.8972	0.8057	0.7439	0.7009	0.8917
1.0	1.0138	0.8820	0.7965	0.7398	0.7005	0.8775
1.2	0.9824	0.8618	0.7870	0.7382	0.7044	0.8590
1.4	0.9613	0.8514	0.7850	0.7418	0.7118	0.8499
1.6	0.9475	0.8471	0.7871	0.7481	0.7206	0.8466
1.8	0.9391	0.8465	0.7916	0.7557	0.7299	0.8469
2.0	0.9344	0.8484	0.7976	0.7638	0.7392	0.8496
2.5	0.9327	0.8590	0.8148	0.7844	0.7615	0.8617
3.0	0.9388	0.8731	0.8326	0.8040	0.7817	0.8771
3.5	0.9485	0.8880	0.8497	0.8219	0.7998	0.8931
4	0.9597	0.9027	0.8658	0.8381	0.8161	0.9087
5	0.9831	0.9303	0.8944	0.8668	0.8443	0.9378
6	1.0058	0.9548	0.9191	0.8911	0.8679	0.9637
7	1.0270	0.9769	0.9408	0.9121	0.8885	0.9867
8	1.0464	0.9964	0.9600	0.9309	0.9066	1.0072
9	1.0643	1.0143	0.9773	0.9477	0.9230	1.0257
10	1.0809	1.0306	0.9929	0.9628	0.9377	1.0425
12	1.1105	1.0592	1.0207	0.9898	0.9641	1.0725
14	1.1363	1.0843	1.0449	1.0133	0.9871	1.0984
16	1.1595	1.1064	1.0662	1.0342	1.0076	1.1216
18	1.1801	1.1264	1.0857	1.0530	1.0262	1.1422
20	1.1991	1.1448	1.1033	1.0704	1.0432	1.1611
25	1.2406	1.1847	1.1423	1.1085	1.0812	1.2027
30	1.2758	1.2187	1.1757	1.1416	1.1138	1.2382
35	1.3066	1.2486	1.2052	1.1709	1.1430	1.2694
40	1.3344	1.2757	1.2320	1.1975	1.1694	1.2974
45	1.3595	1.3004	1.2565	1.2217	1.1937	1.3230
50	1.3826	1.3232	1.2792	1.2444	1.2165	1.3466
60	1.4243	1.3644	1.3202	1.2854	1.2577	1.3896
70	1.4615	1.4015	1.3569	1.3224	1.2945	1.4280
80	1.4951	1.4348	1.3906	1.3559	1.3282	1.4628
90	1.5262	1.4656	1.4215	1.3869	1.3595	1.4948
100	1.5546	1.4942	1.4500	1.4161	1.3885	1.5248
200	1.7718	1.7128	1.6699	1.6376	1.6114	1.7518

$\alpha=14$ T^*	$Z^{(1,1)}$	$Z^{(1,2)}$	$Z^{(1,3)}$	$Z^{(1,4)}$	$Z^{(1,5)}$	$Z^{(3,3)}$
0	1.1870	1.0551	0.9672	0.9027	0.8572	1.1178
0.1	1.1727	1.0382	0.9481	0.8814	0.8287	1.0987
0.2	1.1575	1.0146	0.9115	0.8281	0.7571	1.0729
0.3	1.1286	0.9684	0.8497	0.7566	0.6836	1.0308
0.4	1.0914	0.9191	0.7963	0.7069	0.6420	0.9891
0.5	1.0542	0.8776	0.7585	0.6773	0.6214	0.9524
0.6	1.0208	0.8455	0.7336	0.6608	0.6121	0.9218
0.7	0.9924	0.8217	0.7176	0.6521	0.6091	0.8974
0.8	0.9688	0.8042	0.7076	0.6483	0.6096	0.8781
0.9	0.9495	0.7917	0.7018	0.6476	0.6121	0.8633
1.0	0.9337	0.7827	0.6989	0.6488	0.6157	0.8519
1.2	0.9106	0.7724	0.6984	0.6542	0.6246	0.8373
1.4	0.8956	0.7686	0.7019	0.6617	0.6342	0.8300
1.6	0.8863	0.7687	0.7074	0.6700	0.6440	0.8273
1.8	0.8808	0.7710	0.7139	0.6784	0.6534	0.8277
2.0	0.8780	0.7747	0.7208	0.6868	0.6625	0.8300
2.5	0.8784	0.7871	0.7385	0.7068	0.6836	0.8406
3.0	0.8843	0.8011	0.7557	0.7252	0.7022	0.8545
3.5	0.8928	0.8152	0.7716	0.7416	0.7188	0.8692
4	0.9025	0.8288	0.7863	0.7565	0.7335	0.8840
5	0.9228	0.8539	0.8125	0.7824	0.7587	0.9121
6	0.9426	0.8764	0.8349	0.8042	0.7796	0.9376
7	0.9612	0.8962	0.8543	0.8229	0.7974	0.9605
8	0.9784	0.9140	0.8715	0.8391	0.8129	0.9812
9	0.9944	0.9300	0.8867	0.8536	0.8266	0.9999
10	1.0092	0.9455	0.9005	0.8666	0.8390	1.0169
12	1.0358	0.9701	0.9245	0.8893	0.8606	1.0468
14	1.0588	0.9918	0.9450	0.9086	0.8792	1.0726
16	1.0794	1.0110	0.9629	0.9255	0.8956	1.0953
18	1.0978	1.0280	0.9789	0.9408	0.9101	1.1157
20	1.1143	1.0436	0.9931	0.9546	0.9235	1.1339
25	1.1501	1.0766	1.0244	0.9844	0.9526	1.1737

$Z^{(l,s)}(T^*) = [T^*(1-6/\alpha)]^{\frac{1}{2}}\Omega^{(l,s)*}(T^*), \quad T^* = kT/\epsilon.$

$\alpha=14$ T^*	$Z^{(1,1)}$	$Z^{(1,2)}$	$Z^{(1,3)}$	$Z^{(1,4)}$	$Z^{(1,5)}$	$Z^{(3,3)}$
30	1.1802	1.1044	1.0507	1.0097	0.9772	1.2070
35	1.2060	1.1281	1.0736	1.0320	0.9992	1.2359
40	1.2286	1.1494	1.0940	1.0520	1.0191	1.2615
45	1.2491	1.1685	1.1125	1.0703	1.0372	1.2848
50	1.2678	1.1862	1.1296	1.0871	1.0538	1.3063
60	1.3008	1.2176	1.1604	1.1179	1.0844	1.3446
70	1.3297	1.2455	1.1877	1.1450	1.1115	1.3789
80	1.3555	1.2708	1.2125	1.1699	1.1363	1.4095
90	1.3789	1.2938	1.2354	1.1926	1.1595	1.4377
100	1.4009	1.3150	1.2568	1.2141	1.1809	1.4637
200	1.5626	1.4758	1.4185	1.3768	1.3452	1.6611

$\alpha=14$ T^*	$Z^{(2,2)}$	$Z^{(2,3)}$	$Z^{(2,4)}$	$Z^{(2,5)}$	$Z^{(2,6)}$	$Z^{(4,4)}$
0	1.1947	1.0951	1.0221	0.9706	0.9193	1.0927
0.1	1.2017	1.1027	1.0301	0.9742	0.9296	1.0990
0.2	1.2090	1.1128	1.0416	0.9831	0.9309	1.1098
0.3	1.2109	1.1046	1.0168	0.9391	0.8695	1.0965
0.4	1.1947	1.0716	0.9690	0.8825	0.8109	1.0607
0.5	1.1670	1.0317	0.9235	0.8382	0.7718	1.0206
0.6	1.1359	0.9948	0.8878	0.8076	0.7481	0.9846
0.7	1.1060	0.9641	0.8615	0.7877	0.7346	0.9549
0.8	1.0794	0.9397	0.8428	0.7754	0.7277	0.9315
0.9	1.0564	0.9209	0.8300	0.7682	0.7249	0.9135
1.0	1.0370	0.9066	0.8215	0.7647	0.7250	0.9001
1.2	1.0078	0.8882	0.8132	0.7641	0.7299	0.8829
1.4	0.9885	0.8790	0.8122	0.7686	0.7380	0.8746
1.6	0.9761	0.8756	0.8151	0.7756	0.7476	0.8720
1.8	0.9688	0.8759	0.8205	0.7840	0.7580	0.8731
2.0	0.9649	0.8785	0.8271	0.7930	0.7683	0.8764
2.5	0.9651	0.8910	0.8464	0.8162	0.7937	0.8905
3.0	0.9729	0.9069	0.8666	0.8385	0.8172	0.9081
3.5	0.9844	0.9239	0.8862	0.8594	0.8384	0.9267
4	0.9973	0.9409	0.9048	0.8785	0.8575	0.9449
5	1.0244	0.9729	0.9384	0.9121	0.8908	0.9790
6	1.0507	1.0015	0.9765	0.9408	0.9188	1.0092
7	1.0755	1.0274	0.9882	0.9656	0.9428	1.0361
8	1.0982	1.0504	1.0154	0.9875	0.9639	1.0600
9	1.1192	1.0712	1.0357	1.0068	0.9827	1.0816
10	1.1385	1.0902	1.0539	1.0244	0.9996	1.1013
12	1.1731	1.1237	1.0859	1.0554	1.0293	1.1359
14	1.2034	1.1526	1.1136	1.0818	1.0550	1.1656
16	1.2302	1.1781	1.1379	1.1051	1.0777	1.1917
18	1.2540	1.2007	1.1596	1.1261	1.0980	1.2153
20	1.2758	1.2213	1.1792	1.1452	1.1168	1.2364
25	1.3229	1.2659	1.2222	1.1868	1.1576	1.2826
30	1.3622	1.3034	1.2583	1.2222	1.1925	1.3217
35	1.3963	1.3363	1.2902	1.2535	1.2231	1.3559
40	1.4266	1.3653	1.3185	1.2816	1.2510	1.3863
45	1.4543	1.3917	1.3445	1.3070	1.2766	1.4141
50	1.4793	1.4161	1.3684	1.3308	1.2999	1.4396
60	1.5239	1.4596	1.4115	1.3735	1.3427	1.4856
70	1.5636	1.4983	1.4497	1.4118	1.3806	1.5263
80	1.5990	1.5332	1.4846	1.4463	1.4156	1.5633
90	1.6314	1.5656	1.5165	1.4782	1.4474	1.5972
100	1.6612	1.5950	1.5461	1.5079	1.4771	1.6289
200	1.8858	1.8198	1.7713	1.7344	1.7043	1.8674

$\alpha=15$ T^*	$Z^{(1,1)}$	$Z^{(1,2)}$	$Z^{(1,3)}$	$Z^{(1,4)}$	$Z^{(1,5)}$	$Z^{(3,3)}$
0	1.1870	1.0551	0.9672	0.9027	0.8572	1.1178
0.1	1.1722	1.0378	0.9477	0.8810	0.8285	1.1007
0.2	1.1577	1.0163	0.9153	0.8343	0.7655	1.0765
0.3	1.1320	0.9750	0.8594	0.7687	0.6970	1.0392
0.4	1.0984	0.9300	0.8099	0.7221	0.6579	1.0012
0.5	1.0645	0.8916	0.7747	0.6944	0.6388	0.9672
0.6	1.0337	0.8618	0.7514	0.6792	0.6306	0.9387
0.7	1.0075	0.8397	0.7367	0.6715	0.6285	0.9158
0.8	0.9857	0.8235	0.7278	0.6687	0.6299	0.8978
0.9	0.9678	0.8121	0.7230	0.6687	0.6333	0.8840
1.0	0.9533	0.8040	0.7208	0.6707	0.6378	0.8735
1.2	0.9323	0.7954	0.7218	0.6777	0.6484	0.8605

TABLE IV.—*Continued.*

$\alpha=15$ T^*	$Z^{(1,1)}$	$Z^{(1,2)}$	$Z^{(1,3)}$	$Z^{(1,4)}$	$Z^{(1,5)}$	$Z^{(2,2)}$
1.4	0.9191	0.7931	0.7266	0.6867	0.6596	0.8548
1.6	0.9112	0.7944	0.7335	0.6964	0.6708	0.8535
1.8	0.9070	0.7979	0.7412	0.7063	0.6817	0.8554
2.0	0.9054	0.8028	0.7494	0.7159	0.6921	0.8593
2.5	0.9083	0.8179	0.7699	0.7389	0.7160	0.8734
3.0	0.9167	0.8344	0.7896	0.7597	0.7372	0.8903
3.5	0.9273	0.8507	0.8078	0.7783	0.7558	0.9077
4	0.9389	0.8662	0.8245	0.7953	0.7725	0.9245
5	0.9627	0.8951	0.8541	0.8245	0.8012	0.9558
6	0.9856	0.9203	0.8796	0.8494	0.8250	0.9836
7	1.0069	0.9430	0.9017	0.8708	0.8458	1.0086
8	1.0268	0.9632	0.9214	0.8895	0.8638	1.0308
9	1.0449	0.9816	0.9390	0.9063	0.8800	1.0514
10	1.0619	0.9981	0.9549	0.9216	0.8946	1.0699
12	1.0922	1.0277	0.9829	0.9483	0.9205	1.1032
14	1.1188	1.0530	1.0070	0.9715	0.9428	1.1321
16	1.1426	1.0756	1.0284	0.9921	0.9628	1.1579
18	1.1640	1.0957	1.0475	1.0104	0.9805	1.1812
20	1.1834	1.1140	1.0648	1.0273	0.9970	1.2026
25	1.2257	1.1537	1.1029	1.0642	1.0333	1.2494
30	1.2614	1.1872	1.1353	1.0957	1.0642	1.2897
35	1.2923	1.2167	1.1637	1.1234	1.0920	1.3254
40	1.3199	1.2429	1.1890	1.1486	1.1169	1.3574
45	1.3446	1.2666	1.2123	1.1718	1.1397	1.3869
50	1.3675	1.2886	1.2339	1.1929	1.1609	1.4141
60	1.4083	1.3280	1.2726	1.2316	1.1996	1.4631
70	1.4443	1.3630	1.3073	1.2660	1.2340	1.5072
80	1.4766	1.3945	1.3389	1.2974	1.2654	1.5471
90	1.5059	1.4235	1.3675	1.3267	1.2946	1.5837
100	1.5331	1.4505	1.3945	1.3534	1.3217	1.6180
200	1.7372	1.6538	1.5991	1.5596	1.5291	1.8773

$\alpha=15$ T^*	$Z^{(2,2)}$	$Z^{(2,3)}$	$Z^{(2,4)}$	$Z^{(2,5)}$	$Z^{(2,6)}$	$Z^{(4,4)}$
0	1.1947	1.0951	1.0221	0.9706	0.9193	1.0927
0.1	1.2016	1.1025	1.0306	0.9736	0.9290	1.1061
0.2	1.2081	1.1114	1.0403	0.9828	0.9325	1.1150
0.3	1.2107	1.1061	1.0211	0.9465	0.8796	1.1029
0.4	1.1978	1.0783	0.9791	0.8952	0.8252	1.0705

$\alpha=15$ T^*	$Z^{(2,2)}$	$Z^{(2,3)}$	$Z^{(2,4)}$	$Z^{(2,5)}$	$Z^{(2,6)}$	$Z^{(4,4)}$
0.5	1.1739	1.0426	0.9374	0.8536	0.7879	1.0333
0.6	1.1462	1.0088	0.9039	0.8247	0.7654	0.9996
0.7	1.1191	0.9803	0.8791	0.8060	0.7529	0.9718
0.8	1.0945	0.9575	0.8617	0.7946	0.7470	0.9499
0.9	1.0734	0.9400	0.8498	0.7883	0.7454	0.9331
1.0	1.0555	0.9268	0.8423	0.7858	0.7466	0.9209
1.2	1.0285	0.9102	0.8359	0.7872	0.7535	0.9057
1.4	1.0110	0.9027	0.8365	0.7936	0.7637	0.8992
1.6	1.0003	0.9009	0.8412	0.8024	0.7751	0.8982
1.8	0.9944	0.9027	0.8481	0.8124	0.7868	0.9007
2.0	0.9920	0.9067	0.8562	0.8227	0.7986	0.9054
2.5	0.9953	0.9223	0.8786	0.8488	0.8266	0.9222
3.0	1.0059	0.9409	0.9013	0.8734	0.8521	0.9419
3.5	1.0196	0.9602	0.9229	0.8960	0.8750	0.9622
4	1.0345	0.9790	0.9431	0.9169	0.8958	0.9819
5	1.0651	1.0139	0.9796	0.9533	0.9318	1.0187
6	1.0943	1.0452	1.0111	0.9844	0.9623	1.0514
7	1.1213	1.0733	1.0389	1.0115	0.9887	1.0805
8	1.1462	1.0985	1.0634	1.0356	1.0121	1.1064
9	1.1691	1.1212	1.0856	1.0570	1.0332	1.1300
10	1.1904	1.1421	1.1059	1.0766	1.0523	1.1515
12	1.2283	1.1791	1.1416	1.1115	1.0860	1.1895
14	1.2616	1.2111	1.1727	1.1416	1.1154	1.2225
16	1.2911	1.2397	1.2002	1.1683	1.1417	1.2518
18	1.3179	1.2655	1.2250	1.1925	1.1656	1.2781
20	1.3423	1.2887	1.2477	1.2148	1.1873	1.3020
25	1.3954	1.3399	1.2975	1.2634	1.2353	1.3544
30	1.4406	1.3835	1.3400	1.3054	1.2768	1.3992
35	1.4802	1.4219	1.3775	1.3425	1.3138	1.4382
40	1.5152	1.4561	1.4114	1.3759	1.3471	1.4737
45	1.5474	1.4874	1.4424	1.4067	1.3776	1.5057
50	1.5769	1.5163	1.4710	1.4352	1.4060	1.5353
60	1.6298	1.5684	1.5225	1.4865	1.4575	1.5889
70	1.6768	1.6150	1.5687	1.5326	1.5034	1.6365
80	1.7190	1.6569	1.6107	1.5747	1.5453	1.6797
90	1.7580	1.6952	1.6491	1.6132	1.5841	1.7194
100	1.7938	1.7312	1.6850	1.6489	1.6200	1.7562
200	2.0647	2.0026	1.9572	1.9227	1.8945	2.0351

function $[k_T^*]_1$ for the Lennard-Jones (12–6) potential, as calculated by the method of Chapman and Cowling, is also shown in Fig. 3. It is of interest to note that $[k_T^*]_2$ is always positive for $\alpha=15$, showing that there is no inversion temperature when the repulsive portion of the potential $\varphi(r)$ is steep enough.

Table VII gives the values of the ratios A^*, B^*, and C^* which occur in the expressions for the transport properties of mixtures. The dimensionless group $\rho D_{11}/\eta$, frequently encountered in kinetic theory, is given by $(6f_D/5f_\eta)A^*$.

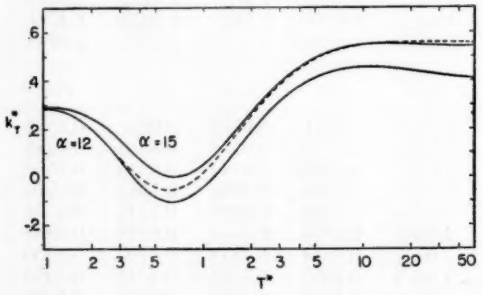

FIG. 3. The reduced thermal diffusion ratio, k_T^*, for isotopic thermal diffusion. Solid lines: second approximation for the Exp-Six potential; broken line: first approximation for the Lennard-Jones (12–6) potential.

Experimental viscosity results are often expressed by an equation of the form

$$\eta = cT^{s_\eta}, \tag{25}$$

where c and s_η are supposed to be constants for a particular gas. The temperature index, s_η, is seen to be given by

$$s_\eta = d\log\eta/d\log T. \tag{26}$$

The temperature index has the following physical significance: if the intermolecular potential were of the form $\varphi(r)=\text{const}/r^\nu$, then s_η would be constant and equal to $[\frac{1}{2}+2/(\nu-1)]$. We can investigate the behavior of s_η for the potential given by Eq. (1) by requiring that the values of η and $d\eta/dT$ determined from Eq. (25) agree with those from Eq. (6) at a given temperature. In this way we find that s_η is not a constant,

TABLE V. Functions for calculating the higher approximations to the transport coefficients.

T^*	$\alpha=12$	$\alpha=13$	$\alpha=14$	$\alpha=15$
	The function $f_\eta^{(3)}$			
0	1.0017	1.0017	1.0017	1.0017
0.1	1.0019	1.0018	1.0018	1.0018
0.2	1.0017	1.0021	1.0021	1.0020
0.3	1.0012	1.0014	1.0015	1.0016
0.4	1.0003	1.0005	1.0006	1.0008
0.5	1.0001	1.0001	1.0002	1.0003
0.6	1.0001	1.0000	1.0000	1.0001
0.7	1.0002	1.0001	1.0000	1.0000
0.8	1.0002	1.0001	1.0000	1.0000
0.9	1.0002	1.0001	1.0000	1.0000
1.0	1.0001	1.0001	1.0000	1.0000
1.2	1.0001	1.0001	1.0001	1.0001
1.4	1.0001	1.0002	1.0002	1.0003
1.6	1.0003	1.0004	1.0005	1.0007
1.8	1.0005	1.0007	1.0008	1.0010
2.0	1.0008	1.0011	1.0012	1.0015
2.5	1.0017	1.0020	1.0022	1.0026
3.0	1.0025	1.0029	1.0031	1.0035
3.5	1.0032	1.0036	1.0039	1.0043
4	1.0037	1.0042	1.0046	1.0050
5	1.0045	1.0050	1.0055	1.0058
6	1.0050	1.0055	1.0061	1.0064
7	1.0052	1.0058	1.0066	1.0067
8	1.0054	1.0060	1.0067	1.0070
9	1.0055	1.0061	1.0068	1.0071
10	1.0056	1.0062	1.0069	1.0072
12	1.0057	1.0062	1.0069	1.0073
14	1.0057	1.0063	1.0069	1.0073
16	1.0057	1.0063	1.0069	1.0073
18	1.0057	1.0064	1.0069	1.0073
20	1.0057	1.0064	1.0068	1.0073
25	1.0057	1.0064	1.0068	1.0073
30	1.0057	1.0065	1.0068	1.0074
35	1.0057	1.0065	1.0068	1.0074
40	1.0058	1.0066	1.0068	1.0075
45	1.0058	1.0067	1.0068	1.0075
50	1.0059	1.0068	1.0068	1.0075
60	1.0060	1.0069	1.0069	1.0077
70	1.0061	1.0071	1.0070	1.0078
80	1.0062	1.0072	1.0071	1.0079
90	1.0063	1.0073	1.0072	1.0080
100	1.0064	1.0074	1.0073	1.0082
200	1.0074	1.0084	1.0081	1.0091
	The function $f_\lambda^{(3)}$			
0	1.0027	1.0027	1.0027	1.0027
0.1	1.0029	1.0028	1.0029	1.0028
0.2	1.0027	1.0032	1.0033	1.0032
0.3	1.0020	1.0023	1.0025	1.0026
0.4	1.0006	1.0009	1.0011	1.0013
0.5	1.0002	1.0002	1.0003	1.0005
0.6	1.0002	1.0001	1.0001	1.0001
0.7	1.0003	1.0001	1.0000	1.0000
0.8	1.0003	1.0001	1.0000	1.0000
0.9	1.0003	1.0001	1.0000	1.0000
1.0	1.0002	1.0001	1.0000	1.0000
1.2	1.0002	1.0001	1.0001	1.0002
1.4	1.0002	1.0003	1.0004	1.0005
1.6	1.0004	1.0006	1.0008	1.0010
1.8	1.0008	1.0011	1.0013	1.0016
2.0	1.0013	1.0016	1.0019	1.0022
2.5	1.0026	1.0031	1.0034	1.0039
3.0	1.0038	1.0045	1.0048	1.0054
3.5	1.0049	1.0056	1.0060	1.0067
4	1.0058	1.0065	1.0071	1.0077
5	1.0070	1.0078	1.0035	1.0091
6	1.0077	1.0085	1.0094	1.0099
7	1.0081	1.0090	1.0105	1.0105
8	1.0085	1.0093	1.0104	1.0109
9	1.0087	1.0095	1.0106	1.0111
10	1.0088	1.0097	1.0107	1.0112
12	1.0089	1.0098	1.0109	1.0114
14	1.0089	1.0099	1.0108	1.0114
16	1.0089	1.0099	1.0108	1.0115
18	1.0088	1.0100	1.0108	1.0115
20	1.0089	1.0100	1.0107	1.0114
25	1.0089	1.0101	1.0106	1.0115
30	1.0089	1.0101	1.0106	1.0115
35	1.0090	1.0102	1.0106	1.0116
40	1.0090	1.0103	1.0106	1.0116
45	1.0091	1.0104	1.0106	1.0117
50	1.0092	1.0105	1.0107	1.0118
60	1.0093	1.0108	1.0108	1.0120
70	1.0096	1.0111	1.0109	1.0122
80	1.0097	1.0112	1.0110	1.0124
90	1.0099	1.0114	1.0113	1.0125
100	1.0101	1.0116	1.0114	1.0127
200	1.0115	1.0132	1.0127	1.0141
	The function $f_\lambda^{(3)}$			
0	1.0020	1.0020	1.0020	1.0020
0.1	1.0017	1.0017	1.0018	1.0018
0.2	1.0010	1.0012	1.0013	1.0014
0.3	1.0002	1.0004	1.0005	1.0006
0.4	1.0001	1.0001	1.0001	1.0002
0.5	1.0002	1.0001	1.0000	1.0000
0.6	1.0003	1.0001	1.0000	1.0000
0.7	1.0003	1.0001	1.0000	1.0000
0.8	1.0002	1.0001	1.0000	1.0000
0.9	1.0002	1.0001	1.0000	1.0000
1.0	1.0001	1.0000	1.0000	1.0001
1.2	1.0001	1.0001	1.0002	1.0003
1.4	1.0001	1.0003	1.0004	1.0006
1.6	1.0003	1.0005	1.0007	1.0009
1.8	1.0006	1.0008	1.0011	1.0013
2.0	1.0009	1.0012	1.0015	1.0017
2.5	1.0017	1.0020	1.0024	1.0028
3.0	1.0024	1.0028	1.0032	1.0037
3.5	1.0030	1.0035	1.0039	1.0044
4	1.0035	1.0041	1.0045	1.0050
5	1.0042	1.0049	1.0053	1.0059
6	1.0047	1.0053	1.0059	1.0064
7	1.0049	1.0057	1.0062	1.0068
8	1.0051	1.0059	1.0065	1.0070
9	1.0052	1.0060	1.0066	1.0072
10	1.0053	1.0061	1.0067	1.0073
12	1.0053	1.0061	1.0068	1.0074
14	1.0053	1.0062	1.0069	1.0075
16	1.0052	1.0061	1.0068	1.0075
18	1.0052	1.0061	1.0068	1.0075
20	1.0051	1.0060	1.0068	1.0075
25	1.0050	1.0059	1.0068	1.0075
30	1.0049	1.0058	1.0067	1.0075
35	1.0048	1.0058	1.0066	1.0075
40	1.0048	1.0058	1.0067	1.0075
45	1.0047	1.0058	1.0066	1.0075
50	1.0047	1.0058	1.0067	1.0076
60	1.0047	1.0058	1.0067	1.0077
70	1.0047	1.0058	1.0068	1.0077
80	1.0047	1.0059	1.0069	1.0078
90	1.0047	1.0059	1.0070	1.0079
100	1.0048	1.0060	1.0070	1.0081
200	1.0053	1.0067	1.0077	1.0088

but the following function of T^*:

$$s_\eta=\frac{9}{2}-\frac{4\Omega^{(2,3)*}}{\Omega^{(2,2)*}}+\frac{d\log f_\eta}{d\log T^*}, \tag{27}$$

where we have made use of the recursion relation

$$\frac{d\log\Omega^{(l,n)*}}{d\log T^*}=(n+2)\left(\frac{\Omega^{(l,n+1)*}}{\Omega^{(l,n)*}}-1\right). \tag{28}$$

TABLE VI. The reduced thermal diffusion ratio, $[k_T^*]_2$, for calculating isotopic thermal diffusion.

$$k_T = k_T^* \frac{M_1 - M_2}{M_1 + M_2} x_1 x_2$$

T^*	$\alpha=12$	$\alpha=13$	$\alpha=14$	$\alpha=15$
0	0.3133	0.3133	0.3133	0.3133
0.1	0.2844	0.2865	0.2887	0.2887
0.2	0.2047	0.2264	0.2401	0.2468
0.3	0.0738	0.1110	0.1369	0.1545
0.4	−0.0271	0.0157	0.0484	0.0727
0.5	−0.0829	−0.0389	−0.0037	0.0229
0.6	−0.1038	−0.0616	−0.0256	0.0020
0.7	−0.1031	−0.0623	−0.0270	0.0005
0.8	−0.0902	−0.0509	−0.0162	0.0105
0.9	−0.0690	−0.0317	0.0023	0.0287
1.0	−0.0456	−0.0088	0.0244	0.0498
1.2	0.0071	0.0419	0.0734	0.0981
1.4	0.0580	0.0923	0.1226	0.1466
1.6	0.1050	0.1386	0.1680	0.1911
1.8	0.1476	0.1797	0.2083	0.2310
2.0	0.1841	0.2161	0.2438	0.2665
2.5	0.2570	0.2883	0.3145	0.3380
3.0	0.3103	0.3404	0.3658	0.3890
3.5	0.3469	0.3786	0.4035	0.4270
4	0.3744	0.4060	0.4313	0.4544
5	0.4111	0.4437	0.4679	0.4931
6	0.4312	0.4643	0.4911	0.5134
7	0.4414	0.4778	0.5044	0.5283
8	0.4494	0.4858	0.5131	0.5358
9	0.4531	0.4889	0.5181	0.5427
10	0.4536	0.4911	0.5208	0.5446
12	0.4536	0.4917	0.5233	0.5494
14	0.4512	0.4919	0.5225	0.5495
16	0.4469	0.4887	0.5209	0.5496
18	0.4441	0.4866	0.5187	0.5485
20	0.4387	0.4826	0.5190	0.5479
25	0.4321	0.4764	0.5140	0.5452
30	0.4245	0.4713	0.5106	0.5427
35	0.4188	0.4681	0.5066	0.5429
40	0.4161	0.4648	0.5058	0.5426
45	0.4118	0.4641	0.5038	0.5426
50	0.4093	0.4616	0.5035	0.5429
60	0.4051	0.4598	0.5032	0.5443
70	0.4048	0.4590	0.5044	0.5460
80	0.4034	0.4583	0.5071	0.5474
90	0.4022	0.4584	0.5093	0.5505
100	0.4024	0.4586	0.5095	0.5534
200	0.4110	0.4703	0.5277	0.5727

Another common method of expressing experimental viscosity results is by the Sutherland equation,

$$\eta = \frac{c' T^{\frac{1}{2}}}{1 + S_\eta / T}, \tag{29}$$

where c' and S_η are supposed to be constants for a particular gas. This equation is based on the physical model of rigid spheres which have a weak attraction for one another. The physical significance of the Sutherland constant, S_η, is that it is proportional to the potential energy of two such spheres when in contact. We can find the dependence of S_η on T^* in the same way that the behavior of s_η was found; it is

$$\frac{S_\eta}{T} = \left[4\left(1 - \frac{\Omega^{(2,3)*}}{\Omega^{(2,2)*}}\right) + \frac{d \log f_\eta}{d \log T^*}\right] \Bigg/ \left[1 - 4\left(1 - \frac{\Omega^{(2,3)*}}{\Omega^{(2,2)*}}\right) + \frac{d \log f_\eta}{d \log T^*}\right]. \tag{30}$$

An entirely analogous result holds for the coefficient of thermal conductivity, λ. The expressions for s_λ and S_λ/T are the same as given in Eqs. (27) and (30), respectively, except that f_η is replaced by f_λ.

In a similar way, we can define a temperature index for self-diffusion,

$$s_D = d \log D_{11} / d \log T, \tag{31}$$

and a Sutherland constant for self-diffusion,

$$D_{11} = \frac{c'' T^{\frac{1}{2}}}{1 + S_D / T}. \tag{32}$$

If D_{11} in Eq. (31) is expressed at *constant density*, we find that the temperature index s_D is the following function of T^*:

$$s_D = \frac{7}{2} - \frac{3\Omega^{(1,2)*}}{\Omega^{(1,1)*}} + \frac{d \log f_D}{d \log T^*}. \tag{33}$$

For the Sutherland constant S_D/T we obtain

$$\frac{S_D}{T} = \left[3\left(1 - \frac{\Omega^{(1,2)*}}{\Omega^{(1,1)*}}\right) + \frac{d \log f_D}{d \log T^*}\right] \Bigg/ \left[1 - 3\left(1 - \frac{\Omega^{(1,2)*}}{\Omega^{(1,1)*}}\right) + \frac{d \log f_D}{d \log T^*}\right], \tag{34}$$

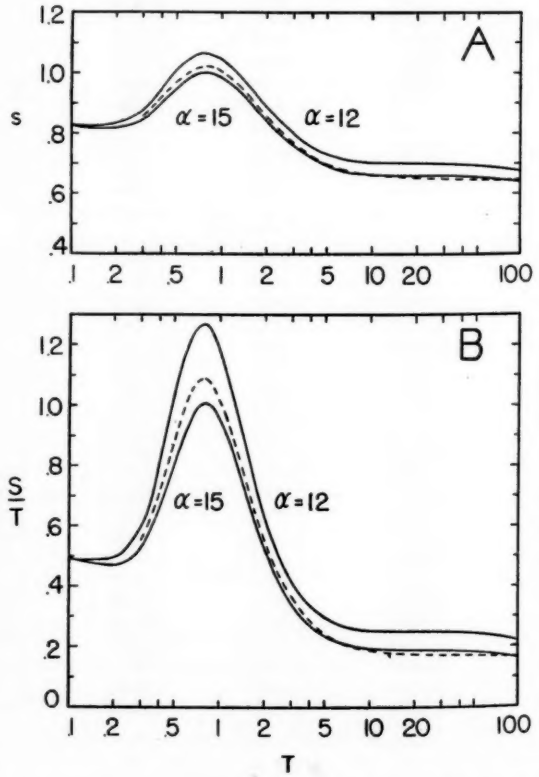

FIG. 4. A. Temperature indexes for viscosity and thermal conductivity; B. Sutherland constants for viscosity and thermal conductivity. Solid lines: Exp-Six potential; broken lines: Lennard-Jones (12–6) potential.

TABLE VII. Functions for calculating the transport properties of mixtures.

T^*	$\alpha=12$	$\alpha=13$	$\alpha=14$	$\alpha=15$
		The function A^*		
0	1.0065	1.0065	1.0065	1.0065
0.1	1.0060	1.0146	1.0247	1.0251
0.2	1.0374	1.0374	1.0445	1.0435
0.3	1.0731	1.0693	1.0729	1.0695
0.4	1.0976	1.0932	1.0946	1.0905
0.5	1.1108	1.1067	1.1070	1.1028
0.6	1.1170	1.1131	1.1128	1.1088
0.7	1.1193	1.1154	1.1145	1.1108
0.8	1.1194	1.1154	1.1142	1.1104
0.9	1.1185	1.1143	1.1126	1.1091
1.0	1.1173	1.1126	1.1106	1.1071
1.2	1.1146	1.1096	1.1067	1.1032
1.4	1.1126	1.1070	1.1037	1.1000
1.6	1.1114	1.1052	1.1013	1.0978
1.8	1.1111	1.1044	1.0999	1.0964
2.0	1.1111	1.1044	1.0990	1.0956
2.5	1.1130	1.1056	1.0987	1.0958
3.0	1.1161	1.1081	1.1002	1.0973
3.5	1.1193	1.1113	1.1026	1.0995
4	1.1226	1.1141	1.1050	1.1018
5	1.1284	1.1194	1.1101	1.1064
6	1.1335	1.1238	1.1147	1.1103
7	1.1377	1.1277	1.1189	1.1136
8	1.1417	1.1309	1.1224	1.1163
9	1.1494	1.1336	1.1255	1.1189
10	1.1477	1.1361	1.1281	1.1210
12	1.1532	1.1406	1.1326	1.1246
14	1.1583	1.1447	1.1366	1.1276
16	1.1625	1.1485	1.1397	1.1300
18	1.1665	1.1517	1.1423	1.1322
20	1.1702	1.1548	1.1449	1.1343
25	1.1790	1.1623	1.1502	1.1385
30	1.1865	1.1691	1.1542	1.1421
35	1.1938	1.1752	1.1578	1.1454
40	1.2005	1.1813	1.1612	1.1480
45	1.2067	1.1867	1.1643	1.1508
50	1.2123	1.1917	1.1668	1.1531
60	1.2230	1.2008	1.1715	1.1573
70	1.2326	1.2092	1.1759	1.1610
80	1.2416	1.2168	1.1796	1.1642
90	1.2492	1.2240	1.1831	1.1674
100	1.2569	1.2300	1.1858	1.1700
200	1.3103	1.2754	1.2068	1.1885
		The function B^*		
0	1.1851	1.1851	1.1851	1.1851
0.1	1.1988	1.1955	1.1926	1.1928
0.2	1.2528	1.2407	1.2328	1.2268
0.3	1.3028	1.2895	1.2788	1.2698
0.4	1.3127	1.3019	1.2922	1.2840
0.5	1.3003	1.2922	1.2844	1.2768
0.6	1.2808	1.2737	1.2668	1.2609
0.7	1.2601	1.2539	1.2476	1.2424
0.8	1.2403	1.2346	1.2289	1.2238
0.9	1.2239	1.2172	1.2125	1.2074
1.0	1.2079	1.2025	1.1973	1.1930
1.2	1.1837	1.1780	1.1733	1.1689
1.4	1.1662	1.1612	1.1561	1.1523
1.6	1.1536	1.1490	1.1440	1.1392
1.8	1.1458	1.1394	1.1347	1.1298
2.0	1.1387	1.1324	1.1279	1.1226
2.5	1.1288	1.1222	1.1174	1.1119
3.0	1.1250	1.1167	1.1113	1.1057
3.5	1.1217	1.1136	1.1084	1.1024
4	1.1211	1.1128	1.1067	1.1002
5	1.1225	1.1126	1.1048	1.1001
6	1.1242	1.1131	1.1059	1.0989

T^*	$\alpha=12$	$\alpha=13$	$\alpha=14$	$\alpha=15$
		The function B^*		
7	1.1252	1.1155	1.1067	1.1006
8	1.1278	1.1176	1.1079	1.1009
9	1.1298	1.1185	1.1094	1.1025
10	1.1317	1.1203	1.1103	1.1026
12	1.1351	1.1225	1.1127	1.1050
14	1.1376	1.1247	1.1135	1.1056
16	1.1384	1.1259	1.1149	1.1066
18	1.1405	1.1271	1.1153	1.1070
20	1.1404	1.1274	1.1178	1.1077
25	1.1426	1.1282	1.1176	1.1070
30	1.1426	1.1281	1.1178	1.1058
35	1.1427	1.1279	1.1162	1.1055
40	1.1427	1.1268	1.1159	1.1050
45	1.1418	1.1270	1.1148	1.1035
50	1.1407	1.1255	1.1142	1.1023
60	1.1388	1.1236	1.1119	1.1003
70	1.1378	1.1218	1.1106	1.0980
80	1.1365	1.1198	1.1096	1.0950
90	1.1350	1.1180	1.1077	1.0940
100	1.1331	1.1154	1.1049	1.0922
200	1.1206	1.1021	1.0911	1.0779
		The function C^*		
0	0.8889	0.8889	0.8889	0.8889
0.1	0.8835	0.8844	0.8853	0.8853
0.2	0.8697	0.8736	0.8765	0.8779
0.3	0.8463	0.8531	0.8581	0.8613
0.4	0.8279	0.8360	0.8421	0.8467
0.5	0.8172	0.8257	0.8325	0.8376
0.6	0.8128	0.8212	0.8283	0.8337
0.7	0.8127	0.8209	0.8280	0.8334
0.8	0.8151	0.8231	0.8301	0.8354
0.9	0.8193	0.8269	0.8338	0.8391
1.0	0.8240	0.8315	0.8383	0.8434
1.2	0.8348	0.8419	0.8482	0.8532
1.4	0.8453	0.8521	0.8582	0.8629
1.6	0.8549	0.8615	0.8673	0.8718
1.8	0.8636	0.8698	0.8753	0.8797
2.0	0.8709	0.8771	0.8823	0.8867
2.5	0.8855	0.8913	0.8961	0.9005
3.0	0.8959	0.9014	0.9059	0.9102
3.5	0.9031	0.9088	0.9131	0.9174
4	0.9084	0.9141	0.9183	0.9226
5	0.9155	0.9213	0.9253	0.9298
6	0.9195	0.9254	0.9298	0.9337
7	0.9216	0.9280	0.9324	0.9365
8	0.9232	0.9295	0.9342	0.9381
9	0.9241	0.9302	0.9352	0.9394
10	0.9242	0.9307	0.9359	0.9399
12	0.9245	0.9311	0.9366	0.9409
14	0.9243	0.9313	0.9367	0.9412
16	0.9237	0.9310	0.9366	0.9414
18	0.9234	0.9307	0.9364	0.9413
20	0.9226	0.9302	0.9366	0.9414
25	0.9218	0.9295	0.9361	0.9413
30	0.9209	0.9291	0.9358	0.9412
35	0.9203	0.9289	0.9354	0.9415
40	0.9202	0.9288	0.9355	0.9417
45	0.9198	0.9290	0.9355	0.9420
50	0.9197	0.9290	0.9356	0.9423
60	0.9196	0.9293	0.9360	0.9430
70	0.9202	0.9298	0.9367	0.9437
80	0.9205	0.9303	0.9375	0.9444
90	0.9208	0.9309	0.9383	0.9453
100	0.9214	0.9316	0.9387	0.9461
200	0.9271	0.9377	0.9445	0.9520

independent of whether D_{11} is expressed at constant density or constant pressure.

Values of the temperature indexes for viscosity, thermal conductivity, and self-diffusion were calculated from Eqs. (27) and (33) neglecting the terms involving f, and are given as a function of T^* in Table VIIIA.

The error introduced by neglecting the terms in f is in all cases less than one percent. In Fig. 4A is plotted s_η *vs* T^* for $\alpha=12$ and 15, together with the corresponding s_η for the Lennard-Jones (12–6) potential for comparison. Values of the Sutherland constants are given in Table VIIIB, and plotted in Fig. 4B for $\alpha=12$ and 15, and the Lennard-Jones (12–6) potential. The neglect of the terms involving f in the calculations of the Sutherland constants introduced an error of less than one percent.

Numerical values of the potential parameters of Eq. (1) for a particular gas may be calculated by comparison of the experimentally determined values of S/T or s with the theoretical values in Table VIII. Caution must be exercised if this procedure is used, however, because inconsistent results may be obtained unless the experimental quantities are calculated in the same way as the theoretical quantities were; that is, from both the temperature derivative and the numerical value of the transport coefficient at a given temperature.

TABLE VIIIA. Temperature indexes for viscosity, thermal conductivity, and self-diffusion.

	Index for η and λ				Index for D_{11}			
$T^*\backslash\alpha$	12	13	14	15	12	13	14	15
0	0.833	0.833	0.833	0.833	0.833	0.833	0.833	0.833
0.1	0.827	0.831	0.830	0.830	0.850	0.847	0.844	0.844
0.2	0.832	0.819	0.818	0.820	0.891	0.879	0.870	0.866
0.3	0.874	0.858	0.851	0.846	0.961	0.941	0.926	0.916
0.4	0.950	0.925	0.912	0.899	1.016	0.992	0.974	0.960
0.5	1.007	0.980	0.964	0.947	1.049	1.023	1.003	0.987
0.6	1.040	1.014	0.997	0.979	1.062	1.036	1.015	0.999
0.7	1.056	1.032	1.013	0.996	1.062	1.037	1.016	1.000
0.8	1.058	1.036	1.018	1.001	1.055	1.031	1.010	0.994
0.9	1.052	1.031	1.013	0.997	1.042	1.019	0.999	0.983
1.0	1.040	1.020	1.003	0.988	1.028	1.005	0.985	0.970
1.2	1.009	0.991	0.975	0.960	0.996	0.974	0.955	0.941
1.4	0.974	0.957	0.943	0.928	0.964	0.944	0.925	0.911
1.6	0.941	0.924	0.912	0.897	0.935	0.915	0.898	0.885
1.8	0.911	0.894	0.884	0.869	0.909	0.891	0.874	0.861
2.0	0.884	0.868	0.858	0.844	0.887	0.869	0.853	0.840
2.5	0.832	0.816	0.807	0.793	0.844	0.826	0.812	0.799
3.0	0.796	0.780	0.771	0.758	0.812	0.796	0.782	0.769
3.5	0.770	0.755	0.746	0.733	0.791	0.774	0.761	0.748
4	0.753	0.738	0.726	0.715	0.775	0.758	0.745	0.732
5	0.730	0.715	0.701	0.692	0.753	0.736	0.724	0.711
6	0.717	0.703	0.687	0.679	0.742	0.724	0.711	0.699
7	0.710	0.695	0.678	0.671	0.735	0.716	0.703	0.690
8	0.706	0.691	0.674	0.666	0.730	0.711	0.697	0.686
9	0.703	0.688	0.672	0.664	0.728	0.709	0.694	0.682
10	0.701	0.686	0.670	0.662	0.727	0.708	0.692	0.680
12	0.700	0.685	0.669	0.660	0.727	0.707	0.690	0.677
14	0.700	0.683	0.669	0.660	0.727	0.706	0.690	0.676
16	0.700	0.683	0.669	0.659	0.729	0.707	0.690	0.676
18	0.700	0.682	0.670	0.659	0.730	0.708	0.691	0.676
20	0.700	0.681	0.671	0.660	0.732	0.710	0.691	0.676
25	0.700	0.680	0.672	0.659	0.735	0.711	0.692	0.676
30	0.699	0.679	0.673	0.659	0.737	0.713	0.693	0.676
35	0.698	0.678	0.672	0.658	0.739	0.713	0.694	0.676
40	0.697	0.676	0.672	0.656	0.740	0.714	0.693	0.675
45	0.696	0.674	0.672	0.655	0.741	0.713	0.694	0.674
50	0.694	0.672	0.671	0.654	0.741	0.713	0.693	0.673
60	0.692	0.668	0.669	0.651	0.741	0.712	0.692	0.671
70	0.687	0.664	0.667	0.647	0.739	0.710	0.690	0.669
80	0.685	0.661	0.665	0.645	0.739	0.709	0.688	0.667
90	0.682	0.659	0.661	0.643	0.738	0.707	0.685	0.664
100	0.679	0.655	0.659	0.640	0.736	0.705	0.684	0.662
200	0.657	0.633	0.640	0.620	0.719	0.687	0.667	0.644

TABLE VIIIB. Sutherland constants for viscosity, thermal conductivity, and self-diffusion.

	S/T for η and λ				S/T for D_{11}			
$T^*\backslash\alpha$	12	13	14	15	12	13	14	15
0	0.500	0.500	0.500	0.500	0.500	0.500	0.500	0.500
0.1	0.487	0.494	0.491	0.492	0.537	0.531	0.525	0.524
0.2	0.497	0.469	0.467	0.471	0.642	0.611	0.588	0.578
0.3	0.598	0.558	0.541	0.528	0.856	0.788	0.742	0.713
0.4	0.819	0.739	0.701	0.664	1.067	0.969	0.900	0.852
0.5	1.028	0.922	0.865	0.810	1.215	1.096	1.010	0.950
0.6	1.176	1.059	0.988	0.921	1.281	1.157	1.063	0.996
0.7	1.251	1.135	1.054	0.985	1.283	1.161	1.066	0.999
0.8	1.264	1.154	1.073	1.003	1.246	1.131	1.040	0.975
0.9	1.233	1.133	1.054	0.989	1.184	1.080	0.994	0.933
1.0	1.174	1.084	1.012	0.952	1.118	1.022	0.942	0.886
1.2	1.036	0.965	0.904	0.852	0.983	0.902	0.836	0.787
1.4	0.901	0.843	0.796	0.750	0.866	0.797	0.740	0.699
1.6	0.788	0.736	0.700	0.660	0.771	0.710	0.661	0.625
1.8	0.697	0.651	0.622	0.584	0.693	0.641	0.597	0.565
2.0	0.623	0.583	0.558	0.524	0.632	0.584	0.545	0.515
2.5	0.497	0.462	0.443	0.415	0.524	0.484	0.453	0.426
3.0	0.420	0.389	0.372	0.349	0.454	0.420	0.393	0.369
3.5	0.370	0.343	0.326	0.304	0.410	0.376	0.353	0.329
4	0.338	0.312	0.292	0.273	0.379	0.347	0.324	0.303
5	0.298	0.274	0.252	0.238	0.339	0.309	0.289	0.267
6	0.277	0.254	0.230	0.219	0.318	0.288	0.267	0.248
7	0.266	0.242	0.218	0.207	0.307	0.276	0.254	0.235
8	0.259	0.236	0.211	0.200	0.299	0.268	0.246	0.228
9	0.255	0.231	0.207	0.196	0.295	0.265	0.241	0.222
10	0.251	0.229	0.204	0.194	0.294	0.262	0.238	0.220
12	0.250	0.227	0.203	0.191	0.293	0.261	0.235	0.215
14	0.250	0.224	0.203	0.191	0.294	0.260	0.234	0.214
16	0.250	0.224	0.204	0.189	0.297	0.261	0.235	0.214
18	0.250	0.222	0.205	0.189	0.299	0.262	0.235	0.214
20	0.250	0.221	0.206	0.189	0.302	0.265	0.235	0.214
25	0.250	0.220	0.208	0.189	0.306	0.268	0.237	0.214
30	0.249	0.218	0.209	0.188	0.311	0.270	0.239	0.214
35	0.248	0.216	0.208	0.187	0.314	0.271	0.240	0.213
40	0.245	0.214	0.208	0.185	0.315	0.272	0.240	0.212
45	0.244	0.211	0.208	0.184	0.317	0.271	0.240	0.211
50	0.241	0.208	0.206	0.182	0.317	0.271	0.239	0.209
60	0.237	0.202	0.203	0.177	0.318	0.269	0.237	0.206
70	0.231	0.197	0.200	0.173	0.315	0.267	0.234	0.203
80	0.227	0.192	0.197	0.169	0.313	0.264	0.231	0.200
90	0.222	0.189	0.192	0.167	0.312	0.261	0.227	0.196
100	0.218	0.184	0.190	0.162	0.308	0.258	0.225	0.193
200	0.186	0.154	0.163	0.137	0.280	0.230	0.200	0.168

ACKNOWLEDGMENTS

The author wishes to express his appreciation for the work done by Miss Elaine A. Petersen, who programmed and performed the calculations for χ and $\Omega^{(l,s)*}$ on the IBM Card Programmed Calculator at the University of Wisconsin Numerical Analysis Laboratory. For most of the other calculations he is indebted to the computing group of the Naval Research Laboratory, under the direction of Catherine Denton, and consisting of Judith Aronow, Lois Brittenham, Ying-Lan Wang, and Clarice Wruck. The author is particularly grateful to Dr. J. O. Hirschfelder for making the facilities of his laboratory available, and for his very helpful advice and criticism at all stages of the work. Thanks are also due to Dr. T. Kihara and Dr. C. F. Curtiss for helpful discussions, and to Mr. Raymond Solomon for help in checking some of the mathematical expressions.

APPENDIX I. HIGHER APPROXIMATIONS TO THE TRANSPORT COEFFICIENTS

The quantity f_η appearing in Eq. (6) is given by the series

$$f_\eta = 1+\gamma_1+\gamma_2+\cdots, \tag{35}$$

where

$$\gamma_1 = \frac{b_{12}^2}{b_{11}b_{22}-b_{12}^2},$$

$$\gamma_2 = \frac{b_{11}(b_{12}b_{23}-b_{22}b_{13})^2}{(b_{11}b_{22}-b_{12}^2)(b_{11}b_{22}b_{33}+2b_{12}b_{13}b_{23}-b_{11}b_{23}^2-b_{22}b_{13}^2-b_{33}b_{12}^2)};$$

and

$$b_{11}=4\Omega^{(2,2)*},$$

$$b_{12}=7\Omega^{(2,2)*}-8\Omega^{(2,3)*},$$

$$b_{13}=\frac{63}{8}\Omega^{(2,2)*}-18\Omega^{(2,3)*}+10\Omega^{(2,4)*},$$

$$b_{22}=\frac{301}{12}\Omega^{(2,2)*}-28\Omega^{(2,3)*}+20\Omega^{(2,4)*},$$

$$b_{23}=\frac{1365}{32}\Omega^{(2,2)*}-\frac{321}{4}\Omega^{(2,3)*}+\frac{125}{2}\Omega^{(2,4)*}-30\Omega^{(2,5)*},$$

$$b_{33}=\frac{25137}{256}\Omega^{(2,2)*}-\frac{1755}{8}\Omega^{(2,3)*}+\frac{1905}{8}\Omega^{(2,4)*}-135\Omega^{(2,5)*}+\frac{105}{2}\Omega^{(2,6)*}+12\Omega^{(4,4)*}.$$

The quantity f_λ appearing in Eq. (7) is given by the series

$$f_\lambda = 1+\delta_1+\delta_2+\cdots, \tag{36}$$

where

$$\delta_1 = \frac{a_{12}''^2}{a_{11}''a_{22}''-a_{12}''^2},$$

$$\delta_2 = \frac{a_{11}''(a_{12}''a_{23}''-a_{22}''a_{13}'')^2}{(a_{11}''a_{22}''-a_{12}''^2)(a_{11}''a_{22}''a_{33}''+2a_{12}''a_{13}''a_{23}''-a_{11}''a_{23}''^2-a_{22}''a_{13}''^2-a_{33}''a_{12}''^2)};$$

and

$$a_{11}''=b_{11},\quad a_{12}''=b_{12},\quad a_{13}''=b_{13},$$

$$a_{22}''=\frac{77}{4}\Omega^{(2,2)*}-28\Omega^{(2,3)*}+20\Omega^{(2,4)*},$$

$$a_{23}''=\frac{945}{32}\Omega^{(2,2)*}-\frac{261}{4}\Omega^{(2,3)*}+\frac{125}{2}\Omega^{(2,4)*}-30\Omega^{(2,5)*},$$

$$a_{33}''=\frac{14553}{256}\Omega^{(2,2)*}-\frac{1215}{8}\Omega^{(2,3)*}+\frac{1565}{8}\Omega^{(2,4)*}-135\Omega^{(2,5)*}+\frac{105}{2}\Omega^{(2,6)*}+4\Omega^{(4,4)*}.$$

The third approximation to the quantity f_D appearing in Eq. (8) is expressed in the determinant notation of Chapman and Cowling as

$$f_D^{(3)} = a_{00}\frac{\mathfrak{A}_{00}^{(2)}}{\mathfrak{A}^{(2)}}, \tag{37}$$

where $\mathfrak{A}^{(2)}$ is a fifth-order determinant whose general element is a_{ij}, with i and j ranging from -2 to 2. The term $\mathfrak{A}_{00}^{(2)}$ is the minor of $\mathfrak{A}^{(2)}$ obtained by deleting the row and column containing a_{00}. The elements a_{ij} are functions of the collision integrals, the molecular weights, and the relative concentrations of the gases in the diffusing mixture. In general, $a_{ij}=a_{ji}$; and if i, $j\neq 0$, a_{-i-j} has the same form as a_{ij} except that the subscripts 1 and 2, referring to the molecular species, are interchanged in the expression for a_{ij}. The a_{ij} necessary for the evaluation of Eq. (37) are as follows, where x_1 and x_2 are the mole fractions, and M_1 and M_2 the molecular weights of species 1 and 2, respectively:

$$a_{00}=8\frac{M_1M_2}{(M_1+M_2)^2}\Omega_{12}^{(1,1)*};$$

$$a_{01}=8\frac{(2M_1)^{\frac{1}{2}}M_2^2}{(M_1+M_2)^{5/2}}\left[\frac{5}{4}\Omega_{12}^{(1,1)*}-\frac{3}{2}\Omega_{12}^{(1,2)*}\right];$$

$$a_{02}=4\frac{(2M_1)^{\frac{1}{2}}M_2^3}{(M_1+M_2)^{7/2}}\left[\frac{35}{8}\Omega_{12}^{(1,1)*}-\frac{21}{2}\Omega_{12}^{(1,2)*}+6\Omega_{12}^{(1,3)*}\right];$$

$$a_{0-1}=-\left(\frac{M_1}{M_2}\right)^{\frac{1}{2}}a_{01};\quad a_{0-2}=-\left(\frac{M_1}{M_2}\right)^{5/2}a_{02};$$

$$a_{11}=a_{11}'+\frac{x_1}{x_2}a_{11}'',$$

$$a_{11}'=\frac{8M_2}{(M_1+M_2)^3}\left[\frac{5}{8}(6M_1^2+5M_2^2)\Omega_{12}^{(1,1)*}-\frac{15}{2}M_2^2\Omega_{12}^{(1,2)*}+6M_2^2\Omega_{12}^{(1,3)*}+2M_1M_2\Omega_{12}^{(2,2)*}\right],$$

$$a_{11}''=4\Omega_{11}^{(2,2)*}\left(\frac{2M_2}{M_1+M_2}\right)^{\frac{1}{2}}\left[\frac{(r_m)_{11}}{(r_m)_{12}}\right]^2;$$

$$a_{12}=a_{12}'+\frac{x_1}{x_2}a_{12}'',$$

$$a_{12}'=\frac{8M_2^2}{(M_1+M_2)^4}\left[\frac{35}{32}(12M_1^2+5M_2^2)\Omega_{12}^{(1,1)*}-\frac{63}{16}(4M_1^2+5M_2^2)\Omega_{12}^{(1,2)*}+\frac{57}{2}M_2^2\Omega_{12}^{(1,3)*}-15M_2^2\Omega_{12}^{(1,4)*}+7M_1M_2\Omega_{12}^{(2,2)*}-8M_1M_2\Omega_{12}^{(2,3)*}\right],$$

$$a_{12}''=\left(\frac{2M_2}{M_1+M_2}\right)^{\frac{1}{2}}[7\Omega_{11}^{(2,2)*}-8\Omega_{11}^{(2,3)*}]\left[\frac{(r_m)_{11}}{(r_m)_{12}}\right]^2;$$

$$a_{1-1}=-\frac{8(M_1M_2)^{\frac{1}{2}}}{(M_1+M_2)^3}\left[\frac{55}{8}\Omega_{12}^{(1,1)*}-\frac{15}{2}\Omega_{12}^{(1,2)*}+6\Omega_{12}^{(1,3)*}-2\Omega_{12}^{(2,2)*}\right]; \tag{38}$$

$$a_{1-2}=-\frac{8M_1^{5/2}M_2^{3/2}}{(M_1+M_2)^4}\left[\frac{595}{32}\Omega_{12}^{(1,1)*}-\frac{567}{16}\Omega_{12}^{(1,2)*}+\frac{57}{2}\Omega_{12}^{(1,3)*}-15\Omega_{12}^{(1,4)*}-7\Omega_{12}^{(2,2)*}+8\Omega_{12}^{(2,3)*}\right];$$

$$a_{22}=a_{22}'+\frac{x_1}{x_2}a_{22}'',$$

$$a_{22}'=\frac{8M_2}{(M_1+M_2)^5}\left[\frac{35}{128}(40M_1^4+168M_1^2M_2^2+35M_2^4)\times\Omega_{12}^{(1,1)*}-\frac{21M_2^2}{16}(84M_1^2+35M_2^2)\Omega_{12}^{(1,2)*}+\tfrac{3}{4}M_2^2(108M_1^2+133M_2^2)\Omega_{12}^{(1,3)*}-105M_2^4\Omega_{12}^{(1,4)*}+45M_2^4\Omega_{12}^{(1,5)*}+\frac{7}{2}M_1M_2(4M_1^2+7M_2^2)\Omega_{12}^{(2,2)*}-56M_1M_2^3\Omega_{12}^{(2,3)*}+40M_1M_2^3\Omega_{12}^{(2,4)*}+12M_1^2M_2^2\Omega_{12}^{(3,3)*}\right];$$

$$a_{22}''=\left(\frac{2M_2}{M_1+M_2}\right)^{\frac{1}{2}}\left[\frac{77}{4}\Omega_{11}^{(2,2)*}-28\Omega_{11}^{(2,3)*}+20\Omega_{11}^{(2,4)*}\right]\left[\frac{(r_m)_{11}}{(r_m)_{12}}\right]^2;$$

$$a_{2-2}=-\frac{8(M_1M_2)^{5/2}}{(M_1+M_2)^5}\left[\frac{8505}{128}\Omega_{12}^{(1,1)*}-\frac{2499}{16}\Omega_{12}^{(1,2)*}+\frac{723}{4}\Omega_{12}^{(1,3)*}-105\Omega_{12}^{(1,4)*}+45\Omega_{12}^{(1,5)*}-\frac{77}{2}\Omega_{12}^{(2,2)*}+56\Omega_{12}^{(2,3)*}-40\Omega_{12}^{(2,4)*}+12\Omega_{12}^{(3,3)*}\right].$$

The a_{ij}'' above are proportional to those defined in connection with the thermal conductivity, but now it is necessary to specify, by subscripts on the $\Omega^{(l,n)*}$, which molecular interaction is under consideration; for example, a_{11}'' refers to an interaction between two molecules of species 1, whereas a_{-1-1}'' refers to species 2. The above expression for the a_{ij} was calculated by the method of Chapman and Cowling.[34]

The expression for f_D may be considerably simplified for the cases of tracer diffusion and self-diffusion. For tracer diffusion where $x_1\rightarrow 0$, we obtain

$$f_D=\frac{1}{1-\Delta_1-\Delta_2-\cdots}, \tag{39}$$

where

$$\Delta_1=\frac{a_{01}^2}{a_{00}a_{11}'}=\frac{M_2^2(6C^*-5)^2}{30M_1^2+25M_2^2-12M_2^2B^*+16M_1M_2A^*},$$

$$\Delta_2=\frac{(a_{01}a_{12}'-a_{02}a_{11}')^2}{a_{00}a_{11}'(a_{11}'a_{22}'-a_{12}'^2)}.$$

The quantities A^*, B^*, and C^* are defined in Eq. (11). The result for $x_2\rightarrow 0$ is obtained from the above by changing the signs of all subscripts on the a_{ij}, or what has the same effect, interchanging M_1 and M_2. The expression for self-diffusion is obtained by setting $M_1=M_2$, $\Omega_{12}^{(l,n)*}=\Omega_{11}^{(l,n)*}=\Omega_{22}^{(l,n)*}$, and $(r_m)_{12}=(r_m)_{11}=(r_m)_{22}$.

The general expression for the thermal diffusion ratio given by Eq. (9) involves the a_{ij} defined above. For a binary mixture of heavy isotopes, the dimensionless quantity k_T^*, defined in Eq. (10) is given to a first approximation by

$$[k_T^*]_1=\frac{15}{2}\left(\frac{a_{0-1}}{a_{11}'a_{11}''}\right)[5\Omega^{(1,1)*}+2\Omega^{(2,2)*}]=\frac{15}{2}\frac{(6C^*-5)(2A^*+5)}{A^*(16A^*-12B^*+55)}, \tag{40}$$

and to a second approximation by

$$[k_T^*]_2=\frac{5}{2}[X_1-X_2Y_1-X_3Y_2], \tag{41}$$

where

$$X_1=\frac{3a_{0-1}a_{22}''-5a_{0-2}a_{12}''}{a_{11}''a_{22}''-a_{12}''^2},$$

$$X_2=\frac{a_{0-1}a_{22}'-a_{0-2}a_{12}'}{a_{11}'a_{22}'-a_{12}'^2},$$

$$X_3=\frac{a_{0-2}a_{11}'-a_{0-1}a_{12}'}{a_{11}'a_{22}'-a_{12}'^2},$$

$$Y_1=\frac{c_1a_{22}''-c_2a_{12}''}{a_{11}''a_{22}''-a_{12}''^2},$$

$$Y_2=\frac{c_2a_{22}''-c_3a_{12}''}{a_{11}''a_{22}''-a_{12}''^2},$$

[34] See reference 4, Chapter 9.

and

$$c_1=\frac{45}{8}\Omega^{(1,1)*}-\frac{45}{2}\Omega^{(1,2)*}+18\Omega^{(1,3)*},$$

$$c_2=\frac{1295}{64}\Omega^{(1,1)*}-\frac{1827}{32}\Omega^{(1,2)*}+\frac{285}{4}\Omega^{(1,3)*}-\frac{75}{2}\Omega^{(1,4)*},$$

$$c_3=\frac{7805}{512}\Omega^{(1,1)*}-\frac{5439}{64}\Omega^{(1,2)*}+\frac{2319}{16}\Omega^{(1,3)*}$$
$$-\frac{525}{4}\Omega^{(1,4)*}+\frac{225}{4}\Omega^{(1,5)*}-\frac{35}{8}\Omega^{(2,2)*}$$
$$-14\Omega^{(2,3)*}+10\Omega^{(2,4)*}+3\Omega^{(3,3)*}.$$

In the above expressions for k_T^* the a_{ij} are to be calculated as if $M_1=M_2$, inasmuch as the deviations from this equality have been explicitly allowed for in deriving Eq. (10). It is interesting to note that for rigid spheres $[k_T^*]_2$ is 8.8 percent larger than $[k_T^*]_1$.

The above expressions for the higher approximations to the transport coefficients were calculated by the method of Chapman and Cowling,[35] and their form depends on a particular approximation scheme for obtaining solutions to an infinite set of simultaneous equations. The scheme used by Chapman and Cowling is not unique, and indeed Kihara[36] has developed an alternative scheme and from it obtained the following second approximations to viscosity, thermal conductivity, and self-diffusion, and the first approximation to the thermal diffusion ratio for isotopic mixtures:

$$f_\eta^{(2)}=1+\frac{3}{49}\left[\frac{4\Omega^{(2,3)*}}{\Omega^{(2,2)*}}-\frac{7}{2}\right]^2, \tag{42}$$

$$f_\lambda^{(2)}=1+\frac{2}{21}\left[\frac{4\Omega^{(2,3)*}}{\Omega^{(2,2)*}}-\frac{7}{2}\right]^2, \tag{43}$$

$$f_D^{(2)}=1+\frac{(6C^2-5)^2}{16A^*+40}, \tag{44}$$

$$[k_T^*]_1=\frac{15}{16}\frac{(6C^*-5)}{A^*}. \tag{45}$$

Kihara's expressions are considerably simpler than the corresponding Chapman and Cowling expressions, and are known to be more accurate for the special case of a Lorentzian gas (a binary mixture in which one component has a much smaller molecular weight than the other, and collisions between molecules of the light component need not be considered). It is, therefore, of interest to compare the expressions of Kihara and of Chapman and Cowling for the more realistic potential given by Eq. (1), and to estimate their relative accuracy by comparison with the still higher approximations evaluated in the present paper.

TABLE IX. Comparison of the approximations of Chapman and Cowling (CC) and of Kihara (K) to the reduced thermal diffusion ratio for isotopes, k_T^*.

T^*	$[k_T^*]_1$ CC	$[k_T^*]_1$ K	$[k_T^*]_2$ CC
	$\alpha=12$		
0	0.3062	0.3104	0.3133
0.5	−0.0828	−0.0819	−0.0829
1	−0.0465	−0.0469	−0.0456
2	0.1860	0.1903	0.1841
10	0.4349	0.4455	0.4536
20	0.4197	0.4291	0.4387
100	0.3852	0.3942	0.4024
	$\alpha=15$		
0	0.3062	0.3104	0.3133
0.5	0.0217	0.0216	0.0229
1	0.0505	0.0511	0.0498
2	0.2668	0.2739	0.2665
10	0.5189	0.5348	0.5446
20	0.5204	0.5357	0.5479
100	0.5253	0.5422	0.5534

The two methods yield answers for the potential of Eq. (1) which are appreciably different only for the case of the thermal diffusion ratio; some selected values for isotopes are given in Table IX. The over-all accuracy of Kihara's expression seems to be somewhat better. In view of this and of their greater simplicity (fewer different collision integrals are required), Kihara's expressions for the second approximation to viscosity and thermal conducivity and the first approximation to the thermal diffusion ratio would seem to be definitely preferable to Chapman and Cowling's corresponding expressions. It is for this reason that we have avoided expressing our results for isotopic thermal diffusion in terms of the usual quantity R_T, defined as the ratio of k_T to the *first* approximation to k_T for rigid spheres. Since the first approximations to k_T for rigid spheres according to Chapman and Cowling and to Kihara are different, R_T involves an uncertain numerical factor, and the quantity k_T^* defined in Eq. (10) seems preferable from a theoretical standpoint.

APPENDIX II. COMPARISON WITH AMDUR'S SEMICLASSICAL CALCULATION OF $S^{(1)}(K)$

Amdur has devised an approximate method[37] for the calculation of gaseous transport properties which is capable of handling very complicated intermolecular potential functions with relatively little computation, and has applied his method to the calculation of the transport properties of the rare gases at low temperatures. The procedure, however, involves assump-

[35] See reference 4, Chapter 7.

[36] T. Kihara, *Imperfect Gases* (originally published in Japanese in 1949, and translated into English by the U. S. Air Force), Secs. 23, 26, 27, 31, 32; "Virial Coefficients and Models of Molecules in Gases," University of Wisconsin Report OOR-7, June 5, 1953 (unpublished).

[37] I. Amdur, J. Chem. Phys. **15**, 482 (1947); **16**, 190 (1948); **17**, 100 (1949).

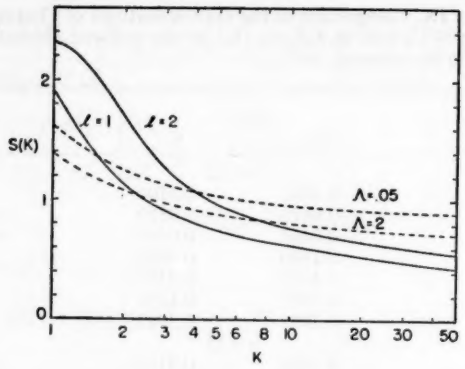

FIG. 5. Comparison of exact and approximate calculations of the reduced cross sections, $S(K)$, for the Exp-Six potential. Solid lines: calculated by numerical integration; broken lines: calculated by Amdur's approximation scheme.

tions which require further justification,[38] so that it is of interest to provide a test of the assumptions by comparing the results of the present calculations with those obtained by applying Amdur's method to the same intermolecular potential.

In the approximate procedure the transport cross sections are not calculated directly, but instead the total classical collision cross section is first obtained, and the transport cross sections are then assumed to be in the same ratio to the total collision cross section as in the case for rigid spheres. The total collision cross section is infinite if calculated by completely classical means, so a semiclassical approximation is used, in which only scattering through angles greater than a certain critical angle, χ_c, is considered. The total collision cross section, $S(K)$, is then given by

$$S(K)=\pi b_c^2, \tag{46}$$

where b_c is that value of the collision parameter which, for a given value of the energy K, will produce a deflection equal to χ_c. The velocity-dependent cross sections for viscosity and diffusion are then taken to be two-thirds and one-half, respectively, of $S(K)$, as for rigid spheres. The collision integrals are obtained from the cross sections by essentially the same procedure as used in the present paper.

[38] H. S. W. Massey and E. H. S. Burhop, *Electronic and Ionic Impact Phenomena* (Oxford University Press, London, 1952), pp. 381–382, 385.

Amdur's method was applied to the potential given in Eq. (1) to calculate approximate values of the velocity-dependent transport cross sections for comparison with the accurate values obtained in this paper by direct means. The critical scattering angle was taken to be[39]

$$\chi_c=\frac{\Lambda}{2yK^{\frac{1}{2}}}, \tag{47}$$

where Λ is the dimensionless group $h/[r_m(2\mu\epsilon)^{\frac{1}{2}}]$, h is Planck's constant, and the other quantities are as previously defined. Following Amdur, χ_c was represented by Eq. (16) with the second term neglected; use of this equation restricts the range of the results to $K>1$. The results are expressed in reduced form, $S^*(K)=S(K)/(\pi r_m^2)$. According to the approximation, $S^*(K)=S^{(1)}(K)$ for all values of l; however for $K>1$, it is actually found that $S^{(2)}(K)$ is always larger than $S^{(1)}(K)$, by as much as 49 percent. In Fig. 5, $S^*(K)$ is shown for $\Lambda=0.05$ and 2, where the potential parameter $\alpha=12$. The small value of Λ corresponds to a heavy gas with strong intermolecular attraction, such as xenon; the large value to a light gas with weak attraction, such as hydrogen. Also shown for comparison are $S^{(1)}(K)$ and $S^{(2)}(K)$ for $\alpha=12$. The results for other values of α are quite similar. It is seen that although $S^*(K)$ does not change rapidly enough with K, it may be nearly correct over a small range of K. This fact would account for Amdur's numerical results on the rare gases (except helium), where he found fair agreement between calculated and experimental values of the viscosity, but the calculated temperature variation was too small. The calculated values of the self-diffusion coefficients of neon and argon were, however, rather too small,[40,41] as might be expected since $S^{(1)}(K)$ is really smaller than $S^{(2)}(K)$. The agreement for helium was somewhat better, but this was perhaps due in part to the use of a potential which is no longer considered very accurate.[42]

The approximation scheme is thus seen to give results which are valid over a limited range, and hence may still prove useful because of its ability to handle very complicated potential functions.

[39] H. S. W. Massey and C. B. O. Mohr, Proc. Roy. Soc. (London) **A141**, 434 (1933).
[40] E. B. Winn, Phys. Rev. **80**, 1024 (1950).
[41] F. Hutchinson, J. Chem. Phys. **17**, 1081 (1949).
[42] See reference 36, p. 378.

Second Virial Coefficients of Gases Obeying a Modified Buckingham (Exp–Six) Potential*

WILLIAM E. RICE† AND JOSEPH O. HIRSCHFELDER
Naval Research Laboratory, Department of Chemistry, University of Wisconsin, Madison, Wisconsin
(Received July 10, 1953)

The second virial coefficient has been calculated for gases obeying a modified Buckingham potential, (Exp-Six),

$$\varphi(r)=\frac{\epsilon}{1-6/\alpha}\left[\frac{6}{\alpha}e^{\alpha(1-r/r_m)}-\left(\frac{r_m}{r}\right)^6\right].$$

The results are tabulated over the temperature range kT/ϵ from 0.40 to 400, and for seven values of the parameter α, from 12 to 15. The treatment was entirely classical, and no corrections for quantum effects were made.

A separate paper will present the evaluation of the parameters for specific substances and applications of the results, together with applications of the calculated transport properties given in the preceding paper.

I. INTRODUCTION

THE equation of state of any gas may be written in virial form,

$$\frac{PV}{RT}=1+\frac{B(T)}{V}+\frac{C(T)}{V^2}+\cdots, \tag{1}$$

where $B(T)$ is called the second virial coefficient. According to classical statistical mechanics, the second virial coefficient for molecules with central forces is directly related to the energy of interaction between pairs of molecules, $\varphi(r)$, by the integral

$$B(T)=-\frac{2\pi N}{3kT}\int_0^\infty r^3\frac{d\varphi(r)}{dr}e^{-\varphi(r)/kT}dr. \tag{2}$$

Up to the present time, the second virial coefficient has been evaluated[1] for Lennard-Jones type potentials, and, in a few special cases, for potentials containing an exponential repulsion term. The Buckingham potential is more reasonable from a theoretical standpoint than is a potential having an inverse-power repulsion, and is more flexible since it contains three parameters instead of two. Therefore, we have compiled a complete table, of the second virial coefficient using the Buckingham potential.

We have taken the Buckingham potential in the following modified form (which we shall henceforth refer to as "Exp-Six"):

$$\varphi(r)=\frac{\epsilon}{1-6/\alpha}\left[\frac{6}{\alpha}e^{\alpha(1-r/r_m)}-\left(\frac{r_m}{r}\right)^6\right], \quad r\geq r_{\max}, \tag{3}$$

$$\varphi(r)=\infty, \quad r<r_{\max}. \tag{4}$$

The constants ϵ, r_m, and α characterize the molecular interaction. Here ϵ is the maximum energy of attraction; r_m is the separation at the energy minimum; and α is a measure of the steepness of the repulsive potential. Figure 1 shows the behavior of $\varphi(r)$. The position of zero potential is σ; its value as a function of α is given in Table II. The function defined in Eq. (3) would pass through a maximum at $r_{\max}$ and then approach $-\infty$ as $r\to 0$. The location and height of the maximum for each α is given in Table II. Fortunately the height of the maximum is so large for all practical cases that very little error is produced by the anomalous behavior of our modified Buckingham potential in the neighborhood of

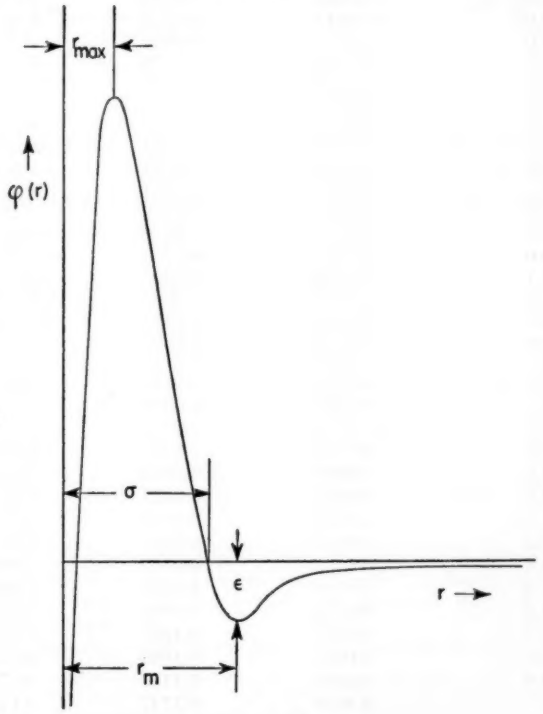

FIG. 1. The Buckingham potential,

$$\varphi(r)=\frac{\epsilon}{1-6/\alpha}\left[\frac{6}{\alpha}e^{\alpha(1-r/r_m)}-\left(\frac{r_m}{r}\right)^6\right],$$

as a function of intermolecular separation. The magnitude of $\varphi(r_{\max})$ relative to ϵ is much reduced in the figure.

* This work was supported by Contract N7onr-28511 with the U. S. Office of Naval Research.

† Present address: Experiment Incorporated, Richmond, Virginia.

[1] An extensive table of second virial coefficients for the Lennard-Jones (12–6) potential is given by R. B. Bird and E. L. Spotz, University of Wisconsin CM–599 (1950).

TABLE I. The second virial coefficient for the modified Buckingham potential.

$$B(T) = b_0 B^*(\alpha, T^*)$$
$$T^* = kT/\epsilon$$
$$b_0 = \tfrac{2}{3}\pi N \sigma_m^3$$

T^* \ α	12.0	12.5	13.0	13.5	14.0	14.5	15.0
0.40	−10.347	−10.052	−9.787	−9.548	−9.332	−9.134	−8.953
0.45	−8.060	−7.826	−7.616	−7.427	−7.256	−7.099	−6.956
0.50	−6.536	−6.342	−6.168	−6.012	−5.871	−5.741	−5.623
0.55	−5.455	−5.290	−5.141	−5.008	−4.887	−4.777	−4.676
0.60	−4.653	−4.508	−4.378	−4.262	−4.157	−4.061	−3.973
0.65	−4.035	−3.906	−3.791	−3.688	−3.595	−3.509	−3.431
0.70	−3.546	−3.430	−3.326	−3.233	−3.149	−3.072	−3.002
0.75	−3.149	−3.043	−2.949	−2.864	−2.788	−2.718	−2.654
0.80	−2.822	−2.725	−2.638	−2.560	−2.490	−2.425	−2.366
0.85	−2.547	−2.457	−2.377	−2.304	−2.239	−2.179	−2.125
0.90	−2.313	−2.229	−2.154	−2.087	−2.026	−1.970	−1.919
0.95	−2.111	−2.033	−1.963	−1.899	−1.842	−1.790	−1.742
1.00	−1.9362	−1.8623	−1.7960	−1.7363	−1.6823	−1.6330	−1.5877
1.05	−1.7827	−1.7127	−1.6499	−1.5934	−1.5422	−1.4955	−1.4526
1.10	−1.6470	−1.5805	−1.5208	−1.4671	−1.4184	−1.3740	−1.3332
1.15	−1.5263	−1.4628	−1.4059	−1.3546	−1.3082	−1.2658	−1.2269
1.20	−1.4181	−1.3574	−1.3029	−1.2539	−1.2095	−1.1689	−1.1316
1.25	−1.3208	−1.2625	−1.2103	−1.1632	−1.1206	−1.0816	−1.0459
1.30	−1.2327	−1.1767	−1.1264	−1.0812	−1.0401	−1.0027	−0.9682
1.35	−1.1526	−1.0986	−1.0502	−1.0066	−0.9670	−0.9309	−0.8976
1.40	−1.0795	−1.0274	−0.9806	−0.9385	−0.9002	−0.8653	−0.8332
1.45	−1.0125	−0.9621	−0.9168	−0.8761	−0.8391	−0.8052	−0.7742
1.50	−0.9509	−0.9020	−0.8582	−0.8187	−0.7828	−0.7500	−0.7199
1.55	−0.8941	−0.8467	−0.8041	−0.7657	−0.7309	−0.6990	−0.6698
1.60	−0.8416	−0.7954	−0.7541	−0.7168	−0.6829	−0.6519	−0.6234
1.65	−0.7928	−0.7479	−0.7076	−0.6713	−0.6383	−0.6082	−0.5804
1.70	−0.7475	−0.7037	−0.6645	−0.6291	−0.5969	−0.5675	−0.5404
1.75	−0.7052	−0.6625	−0.6242	−0.5897	−0.5583	−0.5296	−0.5031
1.80	−0.6657	−0.6240	−0.5866	−0.5529	−0.5222	−0.4941	−0.4683
1.85	−0.6287	−0.5880	−0.5514	−0.5184	−0.4884	−0.4609	−0.4357
1.90	−0.5940	−0.5542	−0.5184	−0.4861	−0.4567	−0.4298	−0.4050
1.95	−0.5614	−0.5224	−0.4873	−0.4557	−0.4269	−0.4005	−0.3763
2.0	−0.5307	−0.4924	−0.4581	−0.4271	−0.3988	−0.3730	−0.3492
2.1	−0.4744	−0.4376	−0.4045	−0.3746	−0.3474	−0.3224	−0.2995
2.2	−0.4241	−0.3885	−0.3565	−0.3276	−0.3013	−0.2772	−0.2550
2.3	−0.3788	−0.3443	−0.3134	−0.2854	−0.2600	−0.2366	−0.2151
2.4	−0.3379	−0.3045	−0.2744	−0.2473	−0.2225	−0.1999	−0.1789
2.5	−0.3007	−0.2683	−0.2391	−0.2127	−0.1886	−0.1665	−0.1461
2.6	−0.2669	−0.2353	−0.2068	−0.1811	−0.1577	−0.1361	−0.1163
2.7	−0.2359	−0.2051	−0.1774	−0.1523	−0.1294	−0.1083	−0.0889
2.8	−0.2075	−0.1774	−0.1503	−0.1258	−0.1034	−0.0828	−0.0638
2.9	−0.1813	−0.1519	−0.1254	−0.1014	−0.0795	−0.0593	−0.0407
3.0	−0.1572	−0.1283	−0.1024	−0.0789	−0.0574	−0.0377	−0.0194
3.1	−0.1348	−0.1066	−0.0811	−0.0580	−0.0370	−0.0176	0.0003
3.2	−0.1141	−0.0863	−0.0614	−0.0387	−0.0180	0.0010	0.0186
3.3	−0.0948	−0.0675	−0.0430	−0.0207	−0.0004	0.0184	0.0357
3.4	−0.0768	−0.0500	−0.0258	−0.0039	0.0161	0.0345	0.0516
3.5	−0.0600	−0.0336	−0.0098	0.0117	0.0314	0.0496	0.0664
3.6	−0.0442	−0.0183	0.0051	0.0264	0.0458	0.0637	0.0803
3.7	−0.0295	−0.0039	0.0192	0.0401	0.0593	0.0770	0.0933
3.8	−0.0156	0.0096	0.0324	0.0530	0.0719	0.0894	0.1055
3.9	−0.0026	0.0223	0.0448	0.0652	0.0838	0.1011	0.1170
4.0	0.0097	0.0343	0.0564	0.0766	0.0951	0.1121	0.1279
4.1	0.0212	0.0455	0.0674	0.0874	0.1056	0.1225	0.1381
4.2	0.0322	0.0562	0.0779	0.0976	0.1156	0.1323	0.1477
4.3	0.0425	0.0663	0.0877	0.1072	0.1250	0.1415	0.1568
4.4	0.0523	0.0758	0.0970	0.1163	0.1340	0.1503	0.1655
4.5	0.0616	0.0848	0.1058	0.1249	0.1425	0.1586	0.1736
4.6	0.0704	0.0934	0.1142	0.1331	0.1505	0.1665	0.1814
4.7	0.0787	0.1016	0.1222	0.1409	0.1581	0.1740	0.1888
4.8	0.0867	0.1093	0.1297	0.1483	0.1654	0.1811	0.1958
4.9	0.0943	0.1167	0.1369	0.1554	0.1723	0.1879	0.2025
5.	0.1015	0.1237	0.1438	0.1621	0.1789	0.1944	0.2088
6.	0.1581	0.1788	0.1976	0.2147	0.2305	0.2451	0.2586
7.	0.1955	0.2152	0.2331	0.2495	0.2645	0.2785	0.2916
8.	0.2215	0.2406	0.2578	0.2736	0.2882	0.3017	0.3144
9.	0.2403	0.2587	0.2755	0.2909	0.3051	0.3183	0.3307
10.	0.2540	0.2721	0.2885	0.3036	0.3175	0.3305	0.3427
20.	0.2937	0.3102	0.3252	0.3392	0.3522	0.3643	0.3758

TABLE I.—*Continued.*

$B(T)=b_0B^*(\alpha,T^*)$
$T^*=kT/\epsilon$
$b_0=\frac{2}{3}\pi N\sigma_m^3$

T^* \ α	12.0	12.5	13.0	13.5	14.0	14.5	15.0
30.	0.2904	0.3065	0.3213	0.3350	0.3478	0.3598	0.3712
40.	0.2811	0.2971	0.3118	0.3254	0.3381	0.3502	0.3616
50.	0.2712	0.2872	0.3018	0.3154	0.3282	0.3402	0.3517
60.	0.2619	0.2778	0.2924	0.3060	0.3188	0.3308	0.3423
70.	0.2534	0.2692	0.2838	0.2974	0.3101	0.3222	0.3337
80.	0.2456	0.2614	0.2759	0.2895	0.3023	0.3144	0.3259
90.	0.2385	0.2543	0.2688	0.2824	0.2951	0.3073	0.3188
100.	0.2320	0.2477	0.2623	0.2758	0.2886	0.3007	0.3123
200.	0.1877	0.2034	0.2177	0.2312	0.2438	0.2560	0.2676
300.	0.1624	0.1780	0.1921	0.2053	0.2178	0.2298	0.2413
400.	0.1444	0.1600	0.1740	0.1870	0.1994	0.2113	0.2228
0.78125	−2.937	−2.837	−2.748	−2.668	−2.595	−2.528	−2.468
1.5625	−0.8806	−0.8335	−0.7912	−0.7531	−0.7185	−0.6869	−0.6578
3.125	−0.1295	−0.1014	−0.0760	−0.0531	−0.0321	−0.0128	−0.0050
6.25	0.1688	0.1893	0.2078	0.2247	0.2403	0.2547	0.2681
12.5	0.2753	0.2927	0.3085	0.3230	0.3365	0.3491	0.3610
25.	0.2935	0.3098	0.3247	0.3385	0.3513	0.3634	0.3748

$r_{\max}$. The original Buckingham potential corresponds to the use of Eq. (3) for all separations. Instead of our modification [Eq. (4)] to avoid the anomalous behavior for small separations, Buckingham and Corner[2] use Eq. (3) for separations larger than r_m, that is $r_m\leq r\leq\infty$ and the following expression for separations less than r_m:

$$\varphi(r)=\frac{\epsilon}{1-6/\alpha}\left\{\frac{6}{\alpha}e^{\alpha(1-r/r_m)}-\left(\frac{r_m}{r}\right)^6\times\exp\left[-4\left(\frac{r_m}{r}-1\right)^3\right]\right\}. \quad (5)$$

This relation makes the potential unduly complicated. We have found that the effect of the maximum in the potential manifests itself only for very high temperatures and for small values of the parameter α.

It is convenient to introduce the following reduced quantities:

$$r^*=r/r_m, \quad (6)$$

$$\varphi^*(r^*)=\frac{\varphi(r)}{\epsilon}=\frac{1}{1-6/\alpha}\left\{\frac{6}{\alpha}\exp[\alpha(1-r^*)]-\frac{1}{r^{*6}}\right\},$$

$$r_{\max}{}^*\leq r^*\leq\infty, \quad (7)$$

$$\varphi^*(r^*)=\infty, \quad 0\leq r^*<r_{\max}, \quad (8)$$

$$T^*=kT/\epsilon, \quad (9)$$

$$B^*(\alpha,T^*)=B(T)/b_0, \quad b_0=\tfrac{2}{3}\pi N_0r_m{}^3. \quad (10)$$

In terms of (Exp-Six) potential, values of $B^*(\alpha,T^*)$ are given in Table I for the range $0.40\leq T^*\leq 400$ and $12.0\leq\alpha\leq 15.0$.

[2] R. A. Buckingham and J. Corner, Proc. Roy. Soc. (London) **A189**, 118 (1947). According to private correspondence Buckingham and Corner were primarily concerned with interpreting high-energy molecular beam scattering which is sensitive to the potential energy for small separations.

II. GENERAL FORMULAS

The integral for the second virial coefficient in reduced form is

$$B^*(\alpha,T^*)=-\frac{1}{T^*}\int_0^\infty r^{*3}\frac{d\varphi^*(r^*)}{dr^*}\times\exp(-\varphi^*(r^*)/T^*)dr^*. \quad (11)$$

Following the procedure of Buckingham and Corner,[2] we have divided the range of integration into two regions of r^* separated by the arbitrarily chosen value of the separation, $M(\alpha)$;

$$B^*(\alpha,T^*)=-\frac{1}{T^*}\int_0^{M(\alpha)} r^{*3}\frac{d\varphi^*(r^*)}{dr^*}\times\exp(-\varphi^*(r^*)/T^*)dr^*-\frac{1}{T^*}\int_{M(\alpha)}^\infty r^{*3}\times\frac{d\varphi^*(r^*)}{dr^*}\exp(-\varphi^*(r^*)/T^*)dr^*. \quad (12)$$

TABLE II. Reduced separation $\sigma^*=\sigma/r_m$ at which the Buckingham potential is zero, location ($r_{\max}{}^*$) and the height of the maximum, and separation κ taken as the lower limit of the numerical integration.

α	$\sigma^*=\sigma/r_m$	$r_{\max}{}^*$	$\varphi^*(r_{\max}{}^*)$	κ
12.0	0.8761 0051	0.3024 7469	1705.4129	
12.5	0.8798 2937	0.2730 3685	3518.3635	
13.0	0.8831 9813	0.2469 7188	7110.0863	0.2784
13.5	0.8862 7341	0.2238 1785	1 4114.558	0.3186
14.0	0.8891 0396	0.2031 8787	2 7585.192	0.3442
14.5	0.8917 2672	0.1847 5586	5 3170.123	0.3620
15.0	0.8941 7037	0.1682 4550	10 1221.60	0.3844

Since $M(\alpha)$ is taken to be almost equal to $\sigma^*(\alpha)$, the two regions of integration correspond roughly to a separation between the large separation where the energy of attraction is dominant from the small separations where the energy of repulsion prevails. Different sorts of mathematical techniques are used to evaluate the integrals in the two regions. We shall employ the symbol $-K(\alpha,T^*)$ for the integral from zero to $M(\alpha)$ in Eq. (12), and $\Gamma(\alpha,T^*)$ for the integral from $M(\alpha)$ to ∞. Then,

$$B^*(\alpha,T^*)=-K(\alpha,T^*)+\Gamma(\alpha,T^*). \tag{13}$$

In the range $M(\alpha)\leq r^*\leq\infty$, $|\varphi^*(r^*)|\leq 1$ and T^* varies from 0.40 to 400, the exponential function, $\exp(-\varphi^*(r^*)/T^*)$, can be expanded in powers of the argument and the series converges rapidly. This expansion is used in evaluating $\Gamma(\alpha,T^*)$ and permits the removal of the reduced temperature from under the integral sign:

$$\Gamma(\alpha,T^*)=-\frac{1}{T^*}\sum_{n=0}^{\infty}\frac{1}{n!}\left(-\frac{1}{T^*}\right)^n J_n(\alpha), \tag{14}$$

where

$$J_n(\alpha)=\int_{M(\alpha)}^{\infty} r^{*3}\frac{d\varphi^*(r^*)}{dr^*}[\varphi^*(r^*)]^n dr^*. \tag{15}$$

For $12.0\leq\alpha\leq 15.0$, the expansion converges sufficiently rapidly for the present purposes when $M(\alpha)$ is the largest integer multiple of 0.005 less than $\sigma^*(\alpha)$. This choice of M is convenient in preliminary hand computations because it avoided interpolation in the numerical tables of the exponential function. The coefficients $J_n(\alpha)$ have alternating signs so that Eq. (14) can be rewritten in the form:

$$\Gamma(\alpha,T^*)=-\sum_{n=0}^{\infty}\frac{|J_n(\alpha)|}{n!}(T^*)^{-n-1}. \tag{16}$$

It is in the range of integration of $K(\alpha,T^*)$ that our modification of the Buckingham potential enters into the calculations. $K(\alpha,T^*)$ may be rewritten as

$$K(\alpha,T^*)=-3\int_0^{M(\alpha)} r^{*2}[1-\exp(-\varphi^*(r^*)/T^*)]dr^* +M^3[1-\exp(-\varphi^*(M)/T^*)]. \tag{17}$$

TABLE III. Error of the sixteen-strip integration of $K(\alpha,T^*)$, the small-separation part of the integral in the second virial coefficient, $B^*(\alpha,T^*)$.

T^* \ α	12.0		15.0	
	B^*	Error	B^*	Error
400.	0.1444	8.7×10^{-7}		
12.5			0.3610	0.000057
6.25	0.1688	0.00013	0.2681	0.00023
3.125	−0.1295	0.00025	0.0050	0.00045
1.5625	−0.8806	0.00029	−0.6578	0.00057
0.78125	−2.937	0.00019	−2.468	0.00050
0.390625		0.000016		0.000022
0.40	−10.347		−8.953	

Setting the potential equal to ∞ for separations smaller than r_{max}^*,

$$K(\alpha,T^*)=-3\int_0^{r_{max}^*} r^{*2}dr^* -3\int_{r_{max}^*}^{M(\alpha)} r^{*2}[1-\exp(-\varphi^*(r^*)/T^*)]dr^* +M^3[1-\exp(-\varphi^*(M)/T^*)]. \tag{18}$$

III. NUMERICAL INTEGRATIONS

In evaluating $K(\alpha,T^*)$, it is certainly satisfactory to ignore the quantity $\exp[-\varphi^*(r^*)/T^*]$ in the integrand for separations smaller than r_1^*, where this exponential function is equal to 4×10^{-7} for $T^*=400$. For $13.0\leq\alpha\leq15.0$, the function actually is this small for certain separations, $r_1^*(\alpha)$. In actual practice, the lower limit of numerical integration of the complete integrand was $\kappa(\alpha)$, which is a separation smaller than $r_1^*(\alpha)$ such that $(M-\kappa)$ is an integer multiple of 0.0032. This value of κ was chosen so as to facilitate preliminary hand computations. For $\alpha=12.0$ and 12.5, the complete integrand was used for the entire range between r_{max}^* and M, so that κ and r_{max}^* are the same. The separations κ are given as a function of α in Table II. Having introduced $\kappa(\alpha)$, in order to shorten the range of numerical integration, we may write:

$$K(\alpha,T^*)=-\kappa^3+M^3[1-\exp(-\varphi^*(M)/T^*)] -3\int_{\kappa(\alpha)}^{M(\alpha)} r^{*2}[1-\exp(-\varphi^*(r^*)/T^*)]dr^*. \tag{19}$$

The eight-strip Newton-Cotes quadrature formula of the closed type was used to evaluate the integral appearing in $K(\alpha,T^*)$ in the following temperature ranges.

$12.5\leq T^*\leq400$

Sixteen integration strips covering the range of separations from $\kappa(\alpha)$ to $M(\alpha)$ were taken for $T^*=400$, 200, 100, 50, 25, and 12.5. The error arising in the course of this integration was estimated by repeating the integration with strips of half the usual width. The errors for several pairs of values of α and T^* both within and out of this temperature range are shown in Table III. The error taken to be maximum for the present temperature range is 6×10^{-5}.

$1.5625\leq T^*\leq8$

Thirty-two strips were taken for $T^*=8$, 6.25, 4, 3.125, 2, and 1.5625. The exponential function in the integrand was neglected through the first 16 strips, with no error resulting except at $T^*=8$, where the maximum error (at $\alpha=12.0$) was 6×10^{-8} out of a total B^* value of 0.2215.

TABLE IV. Interpolated values of the reduced second virial coefficient for $\alpha=12.0$, obtained by a curve-fit from the values at several sets of known points.

T^* \ Set	6.25 to 200.	3.125 to 50.	2. to 25.	1.5625 to 12.5	1. to 8.	0.78125 to 6.25	0.390625 to 3.125
20.	0.293578*	0.293594	0.294351	0.286059	(cf. 0.29378**)		
10.	0.254128	0.254024*	0.253981	0.254050	0.253128		
7.	0.195410	0.195521*	0.195530*	0.195522	0.195552	0.194388	
5.	0.104235	0.101484	0.101453*	0.101467*	0.101441	0.101659	
3.5		−0.060005	−0.059967	−0.059975*	−0.059968*	−0.059992	
2.5		−0.299797	−0.300806	−0.300738	−0.300763*	−0.300719*	−0.294767
1.75			−0.704730	−0.705212	−0.705178	−0.705204*	−0.705825
1.2			−1.40624	−1.41693	−1.41830	−1.41804	−1.41714*

$0.80 \leq T^* \leq 1.50$

Thirty-two strips were taken for $T^*=0.80$ to 1.50 by steps of 0.10. The exponential in the integrand was neglected in the first 24 strips, with a maximum resulting error, at $T^*=1.50$ and $\alpha=12.0$, of 3.5×10^{-5} out of $B^*=-0.9509$.

$0.40 \leq T^* \leq 0.75$

Sixteen strips were taken for $T^*=0.40$ to 0.75 by steps of 0.05. The exponential was neglected in the first 14 strips, with a maximum resulting error of 0.00033 for T^* slightly above the range (0.78125) and $\alpha=12.0$, where $B^*=-2.937$.

In the four temperature ranges, the errors in $K(\alpha,T^*)$ which are quoted above are maximum values, which are taken to be typical for the respective ranges in estimating the total error in $B^*(\alpha,T^*)$.

For the range of α mentioned above, and for all n, it was found that no significant error (less than one part in 10^7) is introduced in evaluating the coefficients $J_n(\alpha)$, by neglecting the repulsive part of the potential for separations larger than $\Lambda(\alpha)=M(\alpha)+2.48$. The integrand formed from the attractive potential alone is then integrated analytically and Eq. (15) becomes:

$$J_n(\alpha)=(-1)^n\frac{\Lambda^{-3-6n}}{n+\frac{1}{2}}+\int_{M(\alpha)}^{\Lambda(\alpha)} r^{*3}\frac{d\varphi^*(r^*)}{dr^*}[\varphi^*(r^*)]^n dr^*. \quad (20)$$

The eight-strip Newton-Cotes quadrature formula of the closed type was used to evaluate the integral in $J_n(\alpha)$. Beginning at $M(\alpha)$, 32 strips of width 0.005, then 32 strips of width 0.01, and finally 40 strips of width 0.05 were taken. The greatest error for any set of eight strips was 5.4×10^{-7} in the first eight strips for $\alpha=12.0$ and $n=0$, out of a total $J_0(12.0)=0.9657716$. This error was taken to be typical for $J_0(\alpha)$; the errors for other values of n were too small to be apparent in the eight-digit arithmetic employed in these calculations. The corresponding error in B^* is $5.4\times10^{-7}(T^*)^{-1}$.

$K(\alpha,T^*)$ and $J_n(\alpha)$ having been computed for various arguments, it was necessary only to perform a summation to obtain $B^*(\alpha,T^*)$, which was to be tabulated. $\Gamma(\alpha,T^*)$ was evaluated up to $n=10$. For $T^*=0.390625$ and $\alpha=12.0$ the tenth term in Γ was larger than for any other set of parameters, being 2.4×10^{-4}. A rough extrapolation indicated the eleventh term to be about 5×10^{-5}. For $T^*=0.78125$ and $\alpha=12.0$, the tenth term was 1.2×10^{-7}. Thus, the largest errors in B^* introduced by cutting off the summation at $n=10$ are found in the lowest temperature range, where they are an order of magnitude smaller than the errors in $K(\alpha,T^*)$. The errors arising from the numerical integration employed in evaluating $J_n(\alpha)$ are likewise smaller than the errors in the K function, even where the former errors are at their largest.

IV. INTERPOLATIONS

The numerical integrations described above afforded values of $B^*(\alpha,T^*)$ for $T^*=0.40$ to 0.75 by steps of 0.05, 0.78125, 0.80, to 1.50 by steps of 0.10, 1.5625, 2, 3.125, 4, 6.25, 8, 12.5, 25, 50, 100, 200, and 400. For other values of T^*, various interpolation schemes were used to determine B^*, with the aim of producing a more complete table, in which an uncertainty of about one part per thousand was desired.

The values of B^* for $T^*=300$ were found by linear interpolation, with $\log_{10}T^*$ being considered the argument of the function B^*. The corresponding error for the Lennard-Jones (12−6) potential was 0.067 percent; a slightly greater computational error would be expected for the present potential, because of the greater curvature of B^* as a function of T^* in this temperature range.

The values of B^* for $T^*=90$, 80, 70, 60, 40, 30, and 20 were interpolated by Everett's method, with argument $\log_{10}T^*$. The corresponding error in $B^*(20)$ for the (12−6) potential was 0.014 percent and the largest of the other errors was 0.0056 percent for $T^*=70$. The resulting $B^*(20)$ values were averaged with those found by a curve-fitting method described below.

The values of B^* for T^* in the range 1.60 to 20 were found by fitting the formula,

$$B^*=\sum_{i=-3}^{3} k_i(T^*)^i, \quad (21)$$

to several sets of known points in the range $T^*=0.78125$ to 200, excluding the evenly-spaced points between 0.80

and 1.50. For $\alpha=12.0$, the coefficients k_i were computed for several sets of known points, as indicated in Table IV. The interpolated values obtained from various sets of starting points are compared in the table (* indicates that the interpolated point is in an interval adjacent to the middle point of the range of known points; ** indicates the $B^*(20)$ computed by Everett's method). The discrepancies for $\alpha=15.0$ were found to be about the same as those for $\alpha=12.0$ shown in the table. Following a scrutiny of Table IV, it was decided to use the known set $T^*=3.125$ to 50 for interpolating B^* for $T^*=7$ to 20. The known set 1.5625 to 12.5 was employed for interpolating in the range 3.2 to 6.0, and the known set 0.78125 to 6.25 for interpolating in the range 1.60 to 3.1. The B^* value obtained in this way should be accurate to one in the fourth decimal place.

The values of B^* for $T^*=0.85$ to 1.55 by steps of 0.10 were found by curve-fitting the formula,

$$B^*=\sum_{i=-2}^{2} k_i(T^*)^i, \tag{22}$$

to the five points in each of the two known ranges: $T^*=0.8$ to 1.2 by steps of 0.1, and $T^*=1.2$, 1.3, 1.4, 1.5, and 1.5625; and interpolating the unknown points within these ranges. When the formula was fitted to all possible five-point ranges including $T^*=0.95$ and 1.25, for the extreme values of α, each of the unknown points was an interior point of four different ranges. The discrepancies among the four calculated values of B^* for each of these pairs of values of α and T^* were at most 3×10^{-6}. At higher temperatures, the error of interpolation was less (6×10^{-7} discrepancy between two interpolated values of B^* for $T^*=1.45$), whereas for $T^*=0.85$, the low-temperature boundary of the range, the greatest discrepancy among three interpolated values was 1×10^{-4}.

To summarize the computational errors present in the final values of $B^*(\alpha,T^*)$: For $0.40\leq T^*\leq 0.75$, the error (which arises in K) is 0.0003; for $0.80\leq T^*\leq 400$, the sum of the interpolation errors and the errors in $K(\alpha,T^*)$ may be as great as 0.0002; except that, at $T^*=300$, the larger error of interpolation may raise the total uncertainty to 0.0003.

ACKNOWLEDGMENTS

The authors gratefully acknowledge the assistance of Elaine A. Petersen, who programmed and performed all of the calculations on the IBM Card Programmed Calculator at the University of Wisconsin Numerical Analysis Laboratory.

In the course of investigations to determine the most efficient method of computing the second virial coefficient, the authors were given invaluable aid by the computing staff of the University of Wisconsin Naval Research Laboratory, including Catherine Denton, Judith Aronow, Lois Brittenham, Ying-Lan Wang, and Clarice Wruck.

Substituted Methanes. XVIII.* Vibrational Spectra of $C^{13}H_3I$

RICHARD B. BERNSTEIN,† *Department of Chemistry,*

AND

FORREST F. CLEVELAND AND FRED L. VOELZ, *Spectroscopy Laboratory,‡ Department of Physics, Illinois Institute of Technology, Chicago 16, Illinois*

(Received August 13, 1953)

Raman (liquid) and infrared (liquid and gas, with KBr and NaCl prisms) spectra have been obtained for two mixtures of $C^{13}H_3I$ (9.3 and 61 atom percent) and $C^{12}H_3I$, and from these the vibrational spectrum of $C^{13}H_3I$ has been deduced. In the Raman spectrum, only $\nu_3(a_1)$—the C−I stretching frequency—could be resolved from the $C^{12}H_3I$ lines; the isotopic shift was -17.7 ± 0.5 cm^{-1}. In the infrared spectrum (gas), five isotopic shifts were obtained; they were: $\nu_1(a_1)-10\pm3$, $\nu_2(a_1)-5.5\pm1.0$, $\nu_3(a_1)-16.1\pm1.0$, $\nu_5(e)-4.4\pm0.8$, and $\nu_6(e)-3.7\pm0.3$ cm^{-1}. For the remaining fundamental, $\nu_4(e)$, the shift was obtained by use of the Redlich-Teller product rule; the value was -9.4 ± 2.3 cm^{-1}. Analysis of the perpendicular bands yielded, with the aid of microwave data, values of the rotational constants, Coriolis interaction constants, and band origins for the $\nu_6(e)$, $\nu_5(e)$, and $\nu_4(e)$ bands of $C^{12}H_3I$ and $C^{13}H_3I$, though the values for the $\nu_4(e)$ band of $C^{13}H_3I$ are incomplete and are only estimated values since the sub-bands were not resolved in this case.

ORDINARY $C^{12}H_3I$ has been investigated many times,[1] but the vibration-rotational spectrum of $C^{13}H_3I$ apparently has not been studied. In fact, no C^{13} molecule of more than three atoms seems to have been studied in any great detail.

EXPERIMENTAL

After preliminary experiments and measurements with a sample containing only 9.3 atom percent C^{13}, a sample of enriched methyl iodide containing 61 atom percent C^{13} was obtained from the Eastman Kodak Company, Rochester, New York. The former sample was prepared from $BaC^{13}O_3$ (Eastman Kodak Company) by conversion to $C^{13}O_2$, reduction with lithium aluminum hydride to $C^{13}H_3OH$, and treatment with HI to give $C^{13}H_3I$, with an overall yield of 75 percent.[2] Both samples were vacuum distilled before use.

The Raman spectrograms of the liquid were obtained with the high-dispersion camera (E-614) of the Hilger E-612 spectrograph by use of previously described[3] techniques. A special small Raman tube of 0.4-ml capacity was used, with a plane mirror at the rear end (outside the Raman tube) to increase the amount of scattered light. Exposures up to 25 hr at 30°C were made, with excitation by Hg 4358A.

The infrared spectral records were obtained for both liquid and gas with a Perkin-Elmer Model 21 double-beam spectrophotometer (NaCl optics) and a Beckman IR-2 spectrophotometer (KBr optics). The liquid cell lengths were 0.12 and 0.11 mm, respectively. The gas cells for both were 10 cm in length and pressures up to 22 cm Hg were employed.

RAMAN SPECTRAL DATA

Comparison of the Raman spectrograms for normal methyl iodide with those for the 61 percent C^{13}-enriched sample showed only one Raman line attributable to $C^{13}H_3I$ that was clearly resolved from the lines of the normal compound; this was the C−I stretching frequency $\nu_3(a_1)$. Figure 1 shows a microphotometer (Leeds and Northrup) tracing for this region of the plate. The Raman displacements for the C^{12} and C^{13} lines were 525.1 and 507.4 cm^{-1}, respectively. The average deviation for 10 measurements on three plates was 0.2 cm^{-1}; the maximum deviation was 0.4 cm^{-1}. The isotopic shift in $\nu_3(a_1)$ was -17.7 ± 0.5 cm^{-1}.

INFRARED SPECTRAL DATA

The Parallel Bands

Resolution of the C^{13} bands from those of the normal molecule as not accomplished for the liquid. Examination of the records obtained for a CS_2 solution indicated a broadening of the $\nu_3(a_1)$ band, but no quantitative estimate for the isotopic shift was possible.

The $\nu_3(a_1)$ Band

Figure 2 shows a comparison of the infrared transmission curves obtained with the Beckman instrument for gaseous samples of the C^{13}-enriched (curve *B*) and the normal (curve *A*) methyl iodide in the region 490–555 cm^{-1}. Measurements for the normal methyl iodide yielded 522.1*P*, 533.4*Q*, and 544.4*R* cm^{-1} (the *P*, *Q*, and *R* branches of the band), while for $C^{13}H_3I$ the corresponding values were 507.6*P*, 517.3*Q* (average of *P* and *R*), and 527.0*R*. The isotopic shift was -16.1 ± 1.0

* For previous papers of this series, see J. Chem. Phys. **18**, 346, 1073, 1076, 1081 (1950); **19**, 119, 784, 1561 (1951); **20**, 454, 1949, 1979 (1952); **21**, 158, 189, 242, 930, 1778, 1781 (1953); J. Opt. Soc. Am. **43**, 1061 (1953).

† Present address: Department of Chemistry, University of Michigan, Ann Arbor, Michigan.

‡ Publication No. 93.

[1] Fenlon, Cleveland, and Meister, J. Chem. Phys. **19**, 1561 (1951), and the other references given there; I. L. Mador and R. S. Quinn, J. Chem. Phys. **20**, 1837 (1952).

[2] Cox, Turner, and Warne, J. Chem. Soc. 3167 (1950).

[3] F. F. Cleveland, J. Chem. Phys. **11**, 1, 227 (1943).

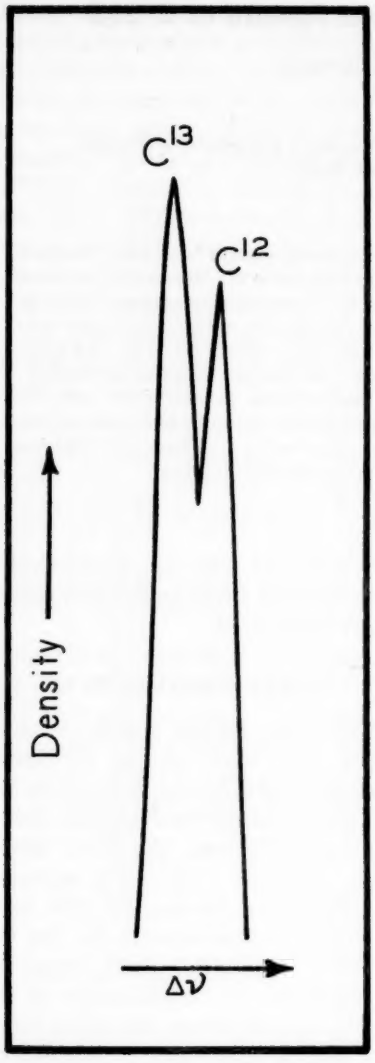

FIG. 1. Microphotometer tracing of the $\nu_3(a_1)$ Raman band for the mixture containing 61 percent $C^{13}H_3I$.

cm^{-1}, which is to be compared with the value -17.7 ± 0.5 cm^{-1} obtained from the Raman spectral data for the liquid.

TABLE I. Isotopic frequencies (vacuum corrected) for the fundamentals $\nu_2(a_1)$ and $\nu_1(a_1)$

Fundamental	Investigation		P	Branch Q	R
$\nu_2(a_1)$	Bennett, Meyer[a]		1240	1251.4	1263
	Lagemann, Nielsen[b]		(1238)[c,d]	1251.4	(1262)[c]
	Present results	C^{12}	1239	1252.5	1263
		C^{13}	(1238)	1247	(1259)
$\nu_1(a_1)$	Bennett, Meyer		2959	(2969.8)	2980
	Lagemann, Nielsen		...	2969.0	...
	Present results	C^{12}	2962	...	2978
		C^{13}	...	...	2968

[a] Reference 4.
[b] Reference 5.
[c] Estimated from the tracings of LN, reference 5.
[d] Parentheses enclose uncertain values.

The $\nu_2(a_1)$ Band

The data obtained for the fundamentals $\nu_2(a_1)$ and $\nu_1(a_1)$ are listed in Table I. The band ν_2, which appeared (Fig. 3) as a *PQR* structure, showed a *Q*-branch shift of -5.5 ± 1.0 cm^{-1} for the 61 percent C^{13} sample. With the 9.3 percent sample, the only evidence of the isotopic shift was a loss of the resolution between the *Q* and *R* branches, caused by the superposition of the C^{13} *R* branch between the C^{12} *Q* and *R* branches.

The $\nu_1(a_1)$ Band

The band $\nu_1(a_1)$ appeared as a *PR* doublet. For the 61 percent sample, the C^{13} *R* branch was observed between the *P* and *R* branches of the C^{12} band. The isotopic shift was estimated to be -10 ± 3 cm^{-1}.

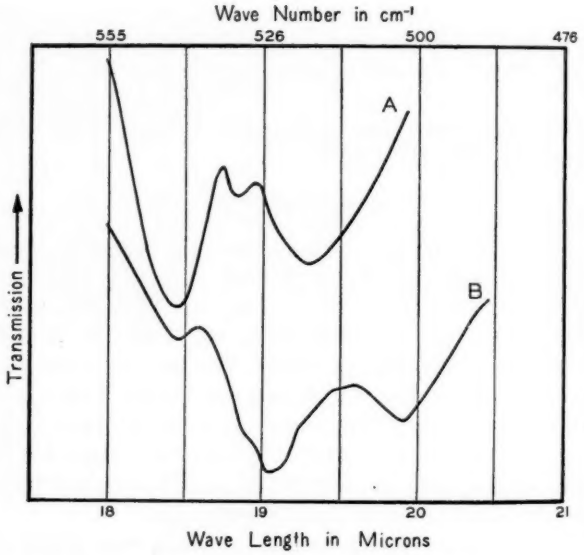

FIG. 2. Infrared absorption of gaseous CH_3I in the region of the $\nu_3(a_1)$ fundamental: (A) normal CH_3I, (B) 61 percent C^{13} enriched sample.

The Perpendicular Bands

The $\nu_6(e)$ Band

For the two perpendicular bands $\nu_6(e)$ and $\nu_5(e)$, resolution of the *Q* branch maxima for the $C^{13}H_3I$ molecule was attained. The transmission curves for $\nu_6(e)$ are shown in Fig. 4. The lower curve (C) shows the absorption arising from $C^{13}H_3I$ after the lines due to the normal CH_3I were removed.

High resolution infrared data obtained with grating instruments are available for the normal CH_3I.[4,5] The wave numbers obtained in the present investigation for the normal sample agreed with the grating data to within ± 1 cm^{-1}. Numerous lines of water vapor and

[4] W. H. Bennett and C. F. Meyer, Phys. Rev. **32**, 888 (1928).
[5] R. T. Lagemann and H. H. Nielsen, J. Chem. Phys. **10**, 668 (1942).

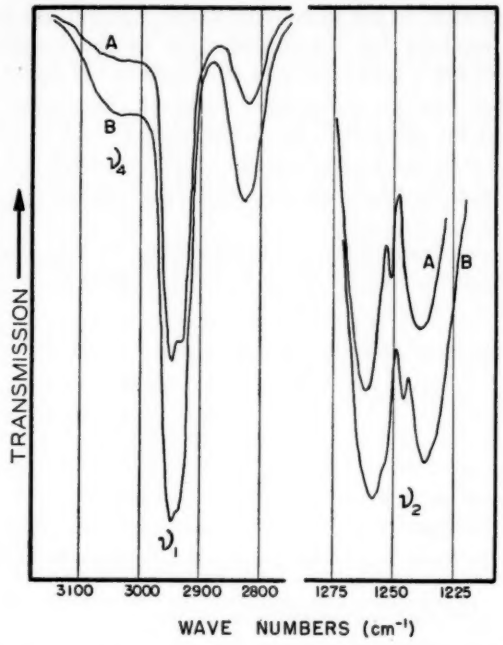

FIG. 3. Infrared absorption of gaseous CH_3I in the regions of the $\nu_2(a_1)$1250 cm^{-1}, $\nu_1(a_1)$2970 cm^{-1}, and $\nu_4(e)$3060 cm^{-1} fundamentals: (A) normal CH_3I, (B) 61 percent C^{13} enriched sample.

ammonia which covered the region 800–1800 cm^{-1} were used to establish and check the calibration of the wave number cam. Because of the proximity of the C^{13} lines to the C^{12} lines, it was found possible to determine the C^{12} wave numbers—by interpolation between the known C^{12} wave numbers—with an accuracy greater than that ordinarily obtainable with the instrument used. Interpolations over very small ranges were required.

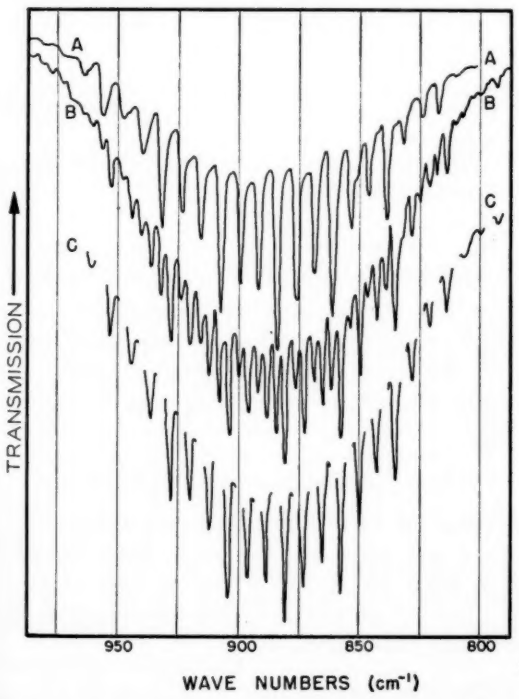

FIG. 4. Infrared absorption of gaseous CH_3I in the region of the $\nu_3(e)$ fundamental: (A) normal CH_3I, (B) 61 percent C^{13} enriched sample, (C) the deduced absorption for $C^{13}H_3I$ alone.

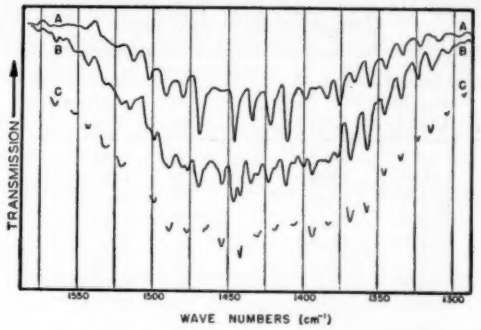

FIG. 5. Infrared absorption of gaseous CH_3I in the region of the $\nu_5(e)$ fundamental: (A) normal CH_3I, (B) 61 percent C^{13} enriched sample, (C) the deduced absorption for $C^{13}H_3I$ alone.

For $\nu_6(e)$, smoothed data of *BM*[4], corrected to vacuum, were used for the interpolation, since for this band *LN*[5] list only five values and these differ from those of *BM* by an average of +0.3 cm^{-1}. The wave numbers thus obtained for $C^{13}H_3I$, together with the wave numbers of *BM* for $C^{12}H_3I$, are given in Table II.

The $\nu_5(e)$ Band

The wave numbers for the $\nu_5(e)$ band (Fig. 5) of $C^{13}H_3I$ were likewise obtained by interpolation between the known wave numbers for the $C^{12}H_3I$. For this, smoothed data of *LN*[5] were used because of their greater resolution. The values obtained are listed in Table III.

The $\nu_4(e)$ Band

As may be seen from Fig. 3, the *Q* branches of the various sub-bands were not resolved in the present work for either $C^{12}H_3I$ or $C^{13}H_3I$. Nor was it possible to measure an isotopic shift for this band.

TABLE II. Positions of maximum absorption in the Q branches of the $\nu_6(e)$ band.[a]

Negative branch ($\Delta K=-1$)			Positive branch ($\Delta K=+1$)		
	ν_{vac} (cm^{-1})			ν_{vac} (cm^{-1})	
K	$C^{12}H_3I$	$C^{13}H_3I$	K	$C^{12}H_3I$	$C^{13}H_3I$
9	(818.2)[b]	814.3	0	884.9	881.2
8	(825.4)	821.3	1	892.6	889.0
7	832.3	828.7	2	900.5	896.5
6	839.8	836.0	3	908.3	904.7
5	847.4	843.4	4	916.1	912.8
4	854.7	851.0	5	924.1	920.4
3	862.2	858.4	6	932.3	928.2
2	869.5	866.2	7	940.3	936.7
1	877.3	873.7	8	948.7	945.0
			9	(956.8)	953.2

[a] ν_{vac} = wave number corrected to vacuum; K = quantum number; ΔK = change in the quantum number during the transition.
[b] Values in parentheses were calculated from the formula of BM, reference 4; all other $C^{12}H_3I$ values are from their data.

TABLE III. Positions of maximum absorption in the Q branches of the $\nu_5(e)$ band.

Negative branch ($\Delta K=-1$) ν_{vac} (cm^{-1})			Positive branch ($\Delta K=+1$) ν_{vac} (cm^{-1})		
K	$C^{12}H_3I$	$C^{13}H_3I$	K	$C^{12}H_3I$	$C^{13}H_3I$
13	...	1294	0	1445.6	1440.9
12	1312[a]	1304	1	1457.4	1453.5
11	1324[a]	1315	2	1469.6	1464.1
10	1336[a]	(1324)[b]	3	1480.9	1477.2
9	1347[a]	(1336)	4	1492.7	1490.1
8	1357[a]	(1347)	5	1504.4	1499.8
7	1368[a]	(1357)	6	1517.4	...[c]
6	1378[a]	(1369)	7	1528[a]	1524
5	1386.8	1382.6	8	1538[a]	1535
4	1398.5	1393.3	9	1549[a]	1545
3	1409.5	1404.7	10	...	1554
2	1421.7	1417.0	11	...	1567
1	1433.5	1429.3			

[a] Present results.
[b] The five values in parentheses are uncertain because of incomplete resolution of the C^{12} from the C^{13} sub-bands in this region for the mixture.
[c] This sub-band was not observed; the calculated value was 1512.4 cm^{-1}.

ROTATIONAL ANALYSIS OF THE PERPENDICULAR BANDS

For the doubly degenerate fundamentals, the energy of the lower state is[6]

$$W_L=W_0+[B_0J(J+1)+(A_0-B_0)K^2]hc \qquad (1)$$

and that of the upper state for Q branch transitions ($\Delta K=\pm1$, $\Delta J=0$) is

$$W_U=W_1+[B_1J(J+1)+(A_1-B_1)(K\pm1)^2 \mp 2A_1\zeta(K\pm1)]hc; \qquad (2)$$

W_0 is the zero-point energy for the lower state for which all vibrational quantum numbers are zero; W_1 is the vibrational energy of the upper state for which one of the vibrational quantum numbers v_4, v_5, or v_6 is equal to 1; B_0, A_0, B_1, and A_1 are rotational constants ($A_v=h/8\pi^2c(I_A)_v$, $B_v=h/8\pi^2c(I_B)_v$; I_A and I_B=moments of inertia parallel and perpendicular, respectively, to the symmetry axis); J and K are quantum numbers for the initial state in the transition; h is Planck's constant, c is the velocity of light; and ζ is the Coriolis interaction constant; the upper sign is used for $\Delta K=+1$, the lower sign for $\Delta K=-1$. It must be remembered that the rotational constants and ζ are not the same for the different degenerate fundamentals.

The wave numbers ν_m corresponding to the positions of maximum absorption in the Q branches of the sub-bands are therefore given by

$$\nu_m^{sub}=\nu_0+A_1(1-2\zeta)-B_1\pm 2[A_1(1-\zeta)-B_1]K +[(A_1-B_1)-(A_0-B_0)]K^2 +(B_1-B_0)J_m(J_m+1), \qquad (3)$$

where $\nu_0=(W_1-W_0)/hc$ is the origin of the band, J_m is the value of J for the transition of maximum absorption, the upper sign is for $\Delta K=+1$ (positive branch), and the lower sign is for $\Delta K=-1$ (negative branch).

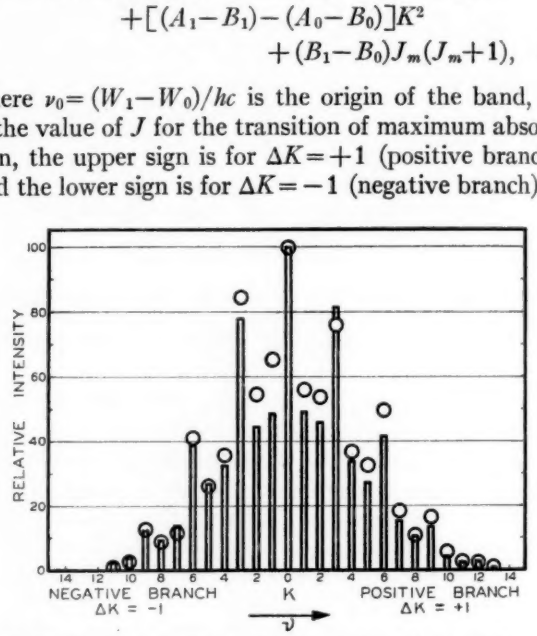

FIG. 6. Maximum intensities in the Q-branch sub-bands of the $\nu_6(e)$ band of $C^{12}H_3I$ (circles, observed; bars, calculated values).

The values of J_m for the various sub-bands can be found from the relation[7]

$$I_{KJ}=C'C''A_{KJ}g_{KJ}\nu S_f \times\exp\{-[B_0J(J+1)+(A_0-B_0)K^2]hc/kT\}, \qquad (4)$$

where I_{KJ} is the intensity of absorption for a given transition; C' is a constant of proportionality; C'' is a constant independent of J and K but depending on the particular vibrational transition; A_{KJ} for $\Delta J=0$ is given by

$$A_{KJ}=[(J+1\pm K)(J\mp K)]/[J(J+1)]$$

(upper sign for $\Delta K=+1$, lower sign for $\Delta K=-1$, and for $K=0$ and $\Delta K=+1$, the value given by this expression must be multiplied by 2); $g_{KJ}=2J+1$ for $K=0$, $2(2J+1)$ for $K\neq0$; ν is the wave number; S_f is a nuclear spin factor given by

$$S_f=(2I+1)(4I^2+4I+3)/3$$

(for K divisible by 3, including $K=0$)

TABLE IV. Calculated and observed values of the maximum intensities in the Q branches of the sub-bands of $\nu_6(e)$ for $C^{12}H_3I$.

Negative branch ($\Delta K=-1$)				Positive branch ($\Delta K=+1$)			
K	J_m	$(I_m)_{calc}$	$(I_m)_{obs}$	K	J_m	$(I_m)_{calc}$	$(I_m)_{obs}$
...	...	...	...	0	20	**100**	100
1	20	48.5	65.1	1	20	49.4	56.0
2	21	44.7	54.5	2	21	46.0	53.6
3	20	**77.8**	84.2	3	21	**81.2**	75.8
4	21	32.5	35.6	4	21	34.0	36.6
5	21	26.9	25.2	5	21	27.2	32.7
6	21	**38.4**	40.9	6	22	**41.6**	49.8
7	22	13.7	11.2	7	22	15.1	18.3
8	22	9.3	8.8	8	22	10.4	10.4
9	23	**12.2**	12.4	9	23	**13.6**	16.3
10	23	3.7	2.1	10	24	4.2	5.7
11	24	2.2	0.2	11	24	2.6	2.5
...	...	...	...	12	26	**2.9**	1.5
...	...	...	...	13	26	0.8	0.6

[6] See G. Herzberg, *Infrared and Raman Spectra of Polyatomic Molecules* (D. Van Nostrand Company, Inc., New York, 1945), first edition, Vol. 1, pp. 400 and 403.

[7] See reference 6, pp. 28, 421, 422, 426.

or

$$S_f=(2I+1)(4I^2+4I)/3 \quad \text{(for } K \text{ not divisible by 3)}$$

($I=\frac{1}{2}$ = nuclear spin of H); k is the Boltzmann constant, and T is the absolute temperature. Values of J_m, the corresponding calculated values of I_m, and the present observed values of I_m for the $\nu_6(e)$ band of $C^{12}H_3I$ are given in Table IV and are shown graphically in Fig. 6. To measure I_m, an envelope corresponding to the P, R branch background was drawn through the bases of the Q branches. This was assumed to be the 100 percent line, from which optical densities and the corresponding relative intensities were computed. The alternating intensities (strong, weak, weak; ...) arise from the nuclear spins of the three identical H atoms. The general correspondence between observed and calculated intensities is good; exact agreement is not to be expected because of superposition of the weaker P and R branch lines on the Q branch lines.

TABLE V. Molecular constants for $C^{12}H_3I$ and $C^{13}H_3I$.

Fundamental	Quantity	$C^{12}H_3I$	$C^{13}H_3I$
$\nu_6(e)$	B_1	0.24925	0.2362
	A_1	5.1203	5.1035
	ζ	0.199	0.198
	ν_0	882.5[a]	879.0[a]
$\nu_5(e)$	B_1	0.25171	0.2372
	A_1	5.1040	5.0894
	ζ	/−0.208	−0.216
	ν_0	1437.8	1434.1
$\nu_4(e)$	B_1	0.24772	
	A_1	5.0527	
	ζ	0.054	(0.041)[b]
	ν_0	3062.2	(3052.8)[c]

[a] If Lagemann and Nielsen's data had been used for $\nu_6(e)$, each of these values of ν_0 would have been increased by 0.3 cm^{-1}; the other constants would not have been affected.
[b] Obtained by ζ-sum rule.
[c] Obtained by use of the Redlich-Teller product rule.

The calculated values of I_m for the $\nu_4(e)$ and $\nu_5(e)$ bands of $C^{12}H_3I$, and for the three bands of $C^{13}H_3I$, differ very little from those given in Table IV, and the corresponding values of J_m show practically no change.

For $C^{12}H_3I$, values of B_1 were obtained from the relation $\nu_{J=J_m}-\nu_{J=0}=(B_1-B_0)J_m(J_m+1)$. The values of $\nu_{J=J_m}$ and $\nu_{J=0}$ were determined by measurement of enlargements of the published grating records of LN^5, and B_0 was obtained from microwave work.[8] For $C^{13}H_3I$, B_1 could not be obtained in this manner since no grating records were available.

An accurate value of A_0 is not available. The best one can do is to use the precise microwave values for B_0 together with the sum rule of Johnston and Dennison[9] to obtain the values 5.09 and 5.07 cm^{-1} as the A_0 values for $C^{12}H_3I$ and $C^{13}H_3I$, respectively. Herzberg has pointed out[10] that the accuracy of rotational constants obtained from this equation is limited, since the dependence of the moments of inertia on the vibrational frequency is neglected and the sum rule holds exactly only for strictly harmonic vibrations. If, despite this, we use these values of A_0, with the values of B_1, B_0, and J_m obtained as indicated above and the observed wave numbers, in Eq. (3), the molecular constants given in Table V are obtained.[11]

An attempt to determine all of the constants for $C^{12}H_3I$ by the method of least squares alone yielded values of B_1-B_0 whose signs were inconsistent with the values determined from the grating records of LN^5. Also, comparison of the results for $C^{12}H_3I$ and $C^{13}H_3I$ indicates discrepancies in sign for B_1-B_0 for the latter compound. These discrepancies arise from the difficulty in determining *two* small constants for $C^{13}H_3I$ by the least square method. While an error in sign for B_1-B_0 does not affect the other constants too greatly, nevertheless the values given in Table V for $C^{13}H_3I$ are probably not as reliable as those for $C^{12}H_3I$.

TABLE VI. Fundamentals for gaseous $C^{12}H_3I$ and the isotopic shifts for $C^{13}H_3I$.

Fundamental	$\nu_{vac}C^{12}H_3I$	$\nu(C^{12}H_3I)-\nu(C^{13}H_3I)$
$\nu_1(a_1)$	2969.0[a]	10±3 cm^{-1}
$\nu_2(a_1)$	1251.4[a]	5.5±1.0
$\nu_3(a_1)$	{533.4	16.1±1.0
	{525.1[b]	17.7±0.5
$\nu_4(e)$	3062.2[c]	9.4±2.3[d]
$\nu_5(e)$	1437.8[c]	4.4±0.8
$\nu_6(e)$	882.5[c]	3.7±0.3

[a] Lagemann and Nielsen value, corrected to vacuum.
[b] Raman value for the liquid state.
[c] These are the ν_0 values from Table V.
[d] Calculated from the Redlich-Teller product rule.

ISOTOPIC SHIFTS

The observed isotopic shifts in the $\nu_6(e)$ and $\nu_5(e)$ fundamentals were −3.7 and −4.4 cm^{-1}, respectively. The shift in $\nu_4(e)$ could not be measured, but was estimated from the Redlich-Teller product rule to be −9.4 cm^{-1}. The observed shifts for all the fundamentals are summarized in Table VI.

ACKNOWLEDGMENTS

This research has been aided by the U. S. Atomic Energy Commission; the Office of Ordnance Research, U. S. Army; and the Research Corporation. The authors appreciate the assistance of Mr. James E. Lamport in the early stages of this investigation. Thanks are due also to Dr. G. Herzberg for helpful correspondence relative to this work.

[8] Gordy, Simmons, and Smith, Phys. Rev. **74**, 243 (1948).
[9] M. Johnston and D. M. Dennison, Phys. Rev. **48**, 868 (1935).
[10] Reference 6, p. 436.
[11] The ν_0 values differ appreciably from those given in Table 85 of Herzberg's book (reference 6, page 315). Upon inquiry Dr. Herzberg has informed us that an error in sign has occurred in the computation of his table and that $+2A_1\zeta$ should be added to the values of ν_4, ν_5, and ν_6 given in that table.

Influence of Solvent upon the Energy Difference between Rotational Isomers

AKIYOSHI WADA
Department of Chemistry, Faculty of Science, Tokyo University, Bunkyo-ku, Tokyo, Japan
(Received July 9, 1953)

The energy difference between the rotational isomers of the *gauche*- and *trans*-forms of 1,2-dichloroethane in various solutions have been calculated by use of a modified Onsager's reaction field. The following assumptions have been employed in the calculation: first, the cavity of the solute molecule is spheroidal; second, the dipole moment of the molecule is composed of two point dipoles which are placed at the foci of the spheroidal cavity, the focal distance being taken as equal to the distance between the contact points of the carbon and chlorine atoms in the dichloroethane molecule. The change of energy difference between rotational isomers by solvents thus computed has been found to be in close agreement with the experimental observations, that is, those obtained by infrared absorption measurements as well as dipole moment.

1. INTRODUCTION

A MOLECULE which consists of rotational isomers is known to have various isomeric ratios in solution, since the relative energies of these isomers are greatly affected by the medium. 1,2-dichloroethane, for instance has two rotational isomers, namely the *trans*- and *gauche*-forms;[1] and the energy difference between them decreases when dissolved in solution, resulting in an increase in the amount of *gauche*-isomer and a decrease in *trans*-isomer. This phenomenon is due to the fact that the highly polar *gauche*-form which corresponds to a higher energy in vacuum than the nonpolar *trans*-form is stabilized in solution by the action of a high reaction field induced in the surrounding medium. This decrease of energy δE has been calculated by taking Onsager's field[2] as the reaction field,[3] that is,

$$\delta E=\Delta E_{\text{gas}}-\Delta E_{\text{soln}}=\tfrac{1}{2}r\mu^2=\frac{\epsilon-1}{2\epsilon+1}\cdot\frac{\mu^2}{a^3}, \qquad (1)$$

where ΔE_{gas} or ΔE_{soln} are the energy difference between the *gauche*- and *trans*-forms referred to the gaseous state and to the solution, respectively, μ the dipole moment of the *gauche*-form in the gaseous state, and a the radius of the cavity of the solute molecule.

The δE computed by Eq. (1) seemed to agree well with that observed; however, μ in Eq. (1) should not represent the moment in the gaseous state, but that of the solution. According to Onsager and Böttcher[2] the μ^2 of Eq. (1) must be written as Eq. (2) in the solution,

$$\mu^2=\frac{{\mu_{\text{gas}}}^2}{1-r\alpha}, \qquad (2)$$

where α is the polarizability of the molecule. When this formula is examined, it will be found that there is no coincidence with the experiment as shown by curve B in Figs. 1 and 2. Obviously this disagreement, in spite of closer approximation, seems due to the defect of the model. The cavity is considered as a sphere and the dipole is placed at its center. In fact, the dipole is localized at the two C—Cl bonds of dichloroethane molecule, and it may be more reasonable to consider the cavity as being spheroidal rather than spherical. In this paper it will be shown that the refinement of these two points brings about satisfactory results for estimating the reaction field.

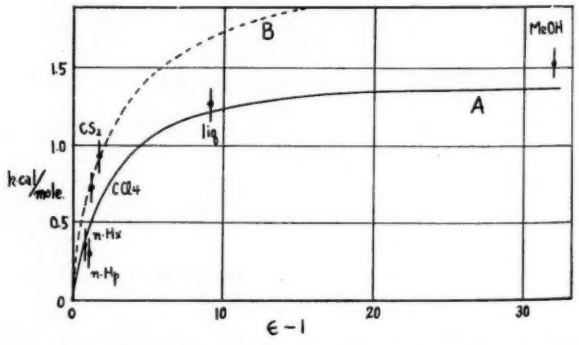

FIG. 1. The relation between the dielectric constant of solvent and δE of 1,2-dichloroethane. Curve A: The calculated values by the new model. Curve B: The calculated values by Onsager's spherical model.

2. THE CALCULATION OF REACTION FIELD AND THE ENERGY DECREASE

As stated above, the two-point dipoles are assumed to be located at the contact points of the carbon and chlorine atoms, and the dipoles are assumed to be in the direction of the C—Cl bonds.

As for the shape of the cavity, a prolate form of spheroid is assumed because of its resemblance to the real molecule, the circumference of the cavity being plastered by a continuous medium of dielectric constant ϵ. The line connecting the two dipoles is taken as the symmetry axis, that is, the z axis of the spheroid,

[1] Mizushima, Morino, Watanabe, Shimanouchi, and Yamaguchi, J. Chem. Phys. **17**, 591 (1949); J. Powling and H. J. Bernstein, J. Am. Chem. Soc. **73**, 1815 (1951).
[2] L. Onsager, J. Am. Chem. Soc. **58**, 1486 (1936); C. F. J. Böttcher, *Theory of Electrical Polarization* (Elsevier Publishing Company, Houston, 1952), Chapter V.
[3] Mizushima, Morino, Watanabe, and Shimanouchi, J. Chem. Phys. **17**, 663 (1949). S. Mizushima and Y. Morino, J. Chem. Phys. **18**, 1516 (1950); H. Frohlich, *Theory of Dielectrics* (Oxford University Press, London, 1949), p. 36.

and the positions of the dipoles are taken as the foci. The geometry of this model is shown in Fig. 3.

The polarizability of the whole molecule, $\alpha=3P_E/4\pi N$, is divided into two equal parts and placed at the same points as the two dipoles. Here P_E is the electronic polarization of this molecule and is computed from the index of refraction extrapolated to infinite wavelength. It is also assumed that these localized polarizabilities are isotropic.

On the basis of this model the reaction field at the focus is obtained by calculations, using the dielectric constant ϵ, the eccentricity of the spheroid e, and the distance between the dipoles $2c$. This reaction field has its origin in one dipole located at the focus itself and one at the other focus. (Also, the field induced by a dipole consists of the two components: the field parallel to the z axis due to the perpendicular component of the dipole.) Accordingly, the reaction field at a focus consists of the following four components:

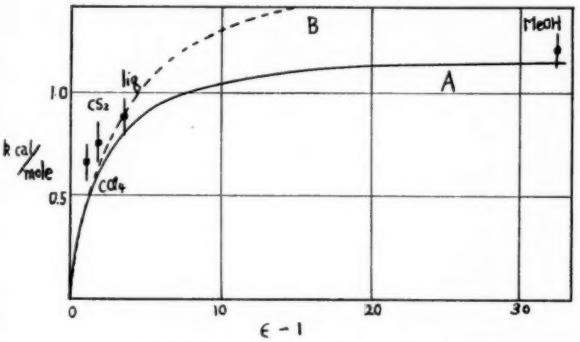

FIG. 2. The relation between the dielectric constant of solvent and δE of 1,2-dibromoethane. Curve A: The calculated values by the new model. Curve B: The calculated values by Onsager's spherical model.

$$r_\perp\mu_\perp=\mu_\perp\cdot\frac{(\epsilon-1)}{8c^3}\sum_{n=1}^{\infty}(2n+1)\{n(n+1)\}^2\cdot\left\{\epsilon\frac{P_n'(v_0)}{Q_n'(v_0)}-\frac{\dot{P}_n'(v_0)}{\dot{Q}_n'(v_0)}\right\}^{-1},\quad(3a)$$

$$r_\perp'\mu_\perp=\mu_\perp\cdot\frac{(\epsilon-1)}{8c^3}\left[\sum_{n=1}^{\infty}(4n-1)\{2n\cdot(2n-1)\}^2\cdot\left\{\epsilon\frac{P_{2n-1}'(v_0)}{Q_{2n-1}'(v_0)}-\frac{\dot{P}_{2n-1}'(v_0)}{\dot{Q}_{2n-1}'(v_0)}\right\}^{-1}-\sum_{n=1}^{\infty}(4n+1)\times\{2n(2n+1)\}^2\cdot\left\{\epsilon\frac{P_{2n}'(v_0)}{Q_{2n}'(v_0)}-\frac{\dot{P}_{2n}'(v_0)}{\dot{Q}_{2n}(v_0)}\right\}^{-1}\right],\quad(3b)$$

$$r_{\shortparallel}\mu_{\shortparallel}=\mu_{\shortparallel}\cdot\frac{(\epsilon-1)}{4c^3}\sum_{n=1}^{\infty}(2n+1)\{2n(2n+1)\}\times\left\{\epsilon\frac{P_n(v_0)}{Q_n(v_0)}-\frac{\dot{P}_n(v_0)}{\dot{Q}_n(v_0)}\right\}^{-1},\quad(3c)$$

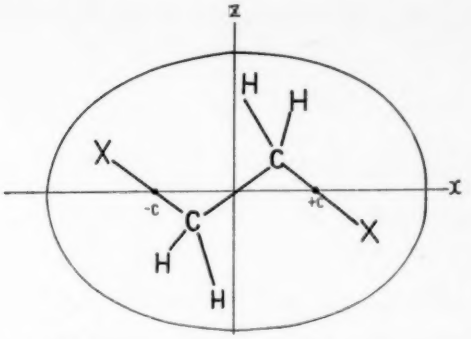

FIG. 3. The geometry of the model. The positions of the two foci are shown by $+c$ and $-c$, respectively.

$$r_{\shortparallel}'\mu_{\shortparallel}=\mu_{\shortparallel}\cdot\frac{(\epsilon-1)}{4c^3}\left[\sum_{n=1}^{\infty}(4n-1)\{2n(2n-1)\}\times\left\{\epsilon\cdot\frac{P_{2n-1}(v_0)}{Q_{2n-1}(v_0)}-\frac{\dot{P}_{2n-1}(v_0)}{\dot{Q}_{2n-1}(v_0)}\right\}^{-1}-\sum_{n=1}^{\infty}(4n+1)\times\{2n(2n+1)\}\cdot\left\{\epsilon\frac{P_{2n}(v_0)}{Q_{2n}(v_0)}-\frac{\dot{P}_{2n}(v_0)}{\dot{Q}_{2n}(v_0)}\right\}^{-1}\right].\quad(3d)$$

The derivation of these formulas are given in the appendix. Here the subscripts $\shortparallel$ and $\perp$ denote the components parallel and perpendicular to the z axis, respectively, $r\mu$ the reaction field at the position of the focus where the dipole is placed, and $r'\mu$ the field at the other focus.

Now, let the angle between the perpendicular component of two dipoles at each focus be θ as shown in Fig. 4, the total energy of the molecule is given by

$$E=E_0+2\left\{\frac{1}{2}\mu_{\shortparallel}^2(r_{\shortparallel}+r_{\shortparallel}')+\frac{1}{2}\mu_\perp^2(r_\perp+r_\perp'\cos\theta)\right\},\quad(4)$$

where E_0 is the energy due to the effect other than the reaction field. The components of the dipole moment $\mu_{\shortparallel}$ and $\mu_\perp$ in Eq. (4) are related to those in the gaseous state, $\mu_{\shortparallel\text{gas}}$ and $\mu_{\perp\text{gas}}$.

$$\mu_{\shortparallel}^2=\frac{\mu_{\shortparallel\text{gas}}^2}{1-(r_{\shortparallel}-r_{\shortparallel}')\alpha},\quad\mu_\perp^2=\frac{\mu_{\perp\text{gas}}^2}{1-(r_\perp-r_\perp'\cos\theta)\alpha}.\quad(5)$$

In consequence, the energy difference between the two molecular forms A and B in which the dipoles

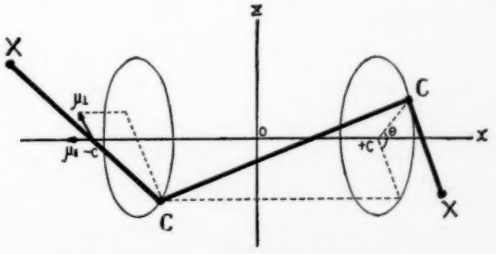

FIG. 4. The angle relation of the model.

components $\mu_\perp$ have the angles θ_A and θ_B, respectively, is written as

$$\Delta E=(E_{0A}+E_{rA})-(E_{0B}+E_{rB})=\Delta E_0+\Delta E_r, \quad (6)$$

where E_{rA} and E_{rB} correspond to the second term of Eq. (4). Therefore, the final expression for the energy decrease which occurs in the transfer from the medium of dielectric constant ϵ_1 to the medium of ϵ_2, is given by

$$\delta E=\Delta E(\epsilon_1)-\Delta E(\epsilon_2)=\Delta E_r(\epsilon_1)-\Delta E_r(\epsilon_2). \quad (7)$$

Here E_0 is assumed independent of ϵ.

Now the reaction field in the gaseous state is zero because $\epsilon_{gas}\simeq 1$. It follows that for the decrease of energy difference by the transfer from the gaseous state to the solution of dielectric constant ϵ_s, Eq. (7) is simply reduced to

$$\delta E=-\Delta E_r(\epsilon_s). \quad (8)$$

3. COMPARISON WITH THE EXPERIMENTAL RESULTS

In comparison of this theory with the experimental results, it seems proper to use the data of dichloroethane because it has been investigated in detail.

To obtain the parameters μ, e, and c for the calculation, the following experimental data are employed. The C−Cl bond moment in gaseous state μ(C−Cl) is taken as $1.56D$: this value was obtained from the observed moment of the *gauche* form μ_G in the gaseous state $2.55D$, assuming C−C−Cl=110° and θ *gauche* =44°.* The dipole-dipole distances are also taken as 2.52A and 2.27A in the *trans*- and *gauche*-forms, respectively, the covalent radii of carbon being assumed as 0.77A, together with θ *gauche*=44° and θ *trans*=180°. From the electronic polarization of this molecule, $P_E=21.0$ cm³, the polarizability located at each focus, $\alpha/2$, is estimated as 4.2×10^{-24} cm³.

TABLE I. The decrease of energy difference.

Solvent	$\delta E=\Delta E_{gas}-\Delta E_{soln}$ δE_{obs} cal/mole	δE_{calc} cal/mole
1,2-dichloroethane		
n-hexane	350	390
n-heptane	290	440
carbon tetrachloride	720	480
carbon disulfide	910	660
pure liquid	1270	1220
methyl alcohol	1530	1340
1,2-dibromoethane		
carbon tetrachloride	690	480
carbon disulfide	770	620
pure liquid	900	780
methyl alcohol	1170	1100

* The value of θ *gauche* is obtained by the model in which the central azimuthal angle of the two C−Cl bonds around the C−C axis is tentatively assumed as 60°.

TABLE II. Energy difference of the *gauche*- and *trans*-isomers in various solutions. $\Delta E=E_G-E_T$.

Solvent	ϵ	ΔE cal/mole	Method	Ref. No.	Mean
1,2-dichloroethane					
gas	1	1320	IR	a	
gas	1	1030	IR	b	
gas	1	1210	R and IR	c	1270±100
gas	1	1400	H	d	
gas	1	1480	IR(D)	e	
gas	1	1210	D.C.	f	
n-hexane	1.9	920	D.C.	g	920±100
n-heptane	2.0	980	D.C.	h	980±100
carbon tetrachloride	2.2	510	IR	i	510±100
carbon disulfide	2.7	360	IR	i	360±100
carbon disulfide	2.7	530	D.C.	h	
pure liquid	10.0	0	R and IR	i,j,k	0
methyl alcohol	33.0	−260	IR	i	−260±100
1,2-dibromoethane					
gas	1	1450	IR	l	
gas	1	1400	D.C.	l	
gas	1	1770	IR	m	1650±100
gas	1	2000	IR(D)	e	
carbon tetrachloride	2.2	960	IR	i	960±100
carbon disulfide	2.7	880	IR	i	880±100
pure liquid	4.8	740	R	k	
pure liquid	4.8	760	IR	b	750±100
pure liquid	4.8	730	IR	i	
methyl alcohol	33.0	480	IR	i	480±100

[a] H. J. Bernstein, J. Chem. Phys. **17**, 256 (1949).
[b] Morino, Mizushima, Kuratni, and Katayama, J. Chem. Phys. **18**, 754 (1950).
[c] Watanabe, Mizushima, and Mashiko, Sci. Papers Inst. Phys. Chem. Research (Tokyo) **40**, 425 (1950).
[d] W. D. Gwinn and K. S. Pitzer, J. Chem. Phys. **16**, 303 (1943).
[e] J. Powling and H. J. Bernstein, J. Am. Chem. Soc. **73**, 1815 (1951).
[f] Watanabe, Mizushima, and Morino, Sci. Papers Inst. Phys. Chem. Research (Tokyo) **39**, 401 (1941).
[g] Mizushima, Morino, and Higasi, Sci. Papers Inst. Phys. Chem. Research (Tokyo) **25**, 153 (1934).
[h] A. E. Stearn and C. P. Smyth, J. Am. Chem. Soc. **56**, 1667 (1934).
[i] K. Kuratani, Repts. Inst. Sci. Technol. (Tokyo Univ.) **6**, 221 (1952), **7**, 11 (1953).
[j] H. Gerding and P. C. Meermann, Rec. trav. chim. **61**, 523 (1942).
[k] Rank, Kagarise, and Axford, J. Chem. Phys. **17**, 1354 (1949).
[l] Shimanouchi, Turuta, and Mizushima, Sci. Papers Inst. Phys. Chem. Research (Tokyo) **42**, 117 (1944).
[m] H. J. Bernstein, J. Chem. Phys. **18**, 897 (1950).
IR: Infrared absorption spectrum, R: Raman spectrum, D.C.: dielectric constant, H: Heat capacity, and IR(D): Infrared absorption spectrum in dilute solution.
The ΔE from the dipole moment data is calculated by its temperature dependence. The details of the method are contained in a paper which will be published in the near future by I. Miyagawa.

Next, the eccentricity e of the spheroid is related to its volume v and the distance $2c$ between the two foci by

$$\frac{1-e^2}{e^3}=\frac{3v}{4\pi c^3}. \quad (9)$$

The volume v is given by the simple relation, $v=M/Nd$: from the density d of the liquid, molecular weight M of the molecule, and Avogadro number N. For dichloroethane, the density 1.24, and the molecular weight 98.97 give the values of $e=0.38$ and 0.35 for the *trans*- and the *gauche*-forms, respectively.

The calculated values of the decrease of the energy difference by the solvents are listed in Table I. The experimental values of δE are estimated from the values of the ΔE_{gas} and ΔE_{soln} obtained by the Raman and infrared spectra and dipole moment measurements which are shown in Table II.

For 1,2-dibromoethane the δE is calculated similarly by the use of the parameters, $\mu(C-Br)_{gas}=1.22D$ from the experimental result of $\mu_G=2.00D$,[4] $\alpha/2=5.3\times10^{-24}$ cm^3, and $e=0.38$ and 0.35 for the *trans*- and the *gauche*-forms, respectively. These results are also shown in Tables I and II.

4. DISCUSSION

As for the electrostatic energy of the dipole molecule in the solution, Bell[5] calculated only the field energy and obtained too small a value. The idea of the reaction field was proposed by Onsager, and his model proved to be a reasonable one for the explanation of the dielectric behavior of the polar liquids. This theory gave higher electrostatic energy than Bell's and showed that the reaction field gave the main contribution to such energy.

The Onsager's theory was refined by Fujishiro,[6] by Abbott and Bolton,[7] and by Food and Dekker,[8] the shape of cavity and the position of dipole being taken into consideration. Their results showed, in general, close agreement with the observed for the dielectric constant of the pure liquid.

On the other hand the case of rotational isomers in solution affords another example that the reaction field has an appreciable influence upon its character. However, for the explanation of solvent effect of molecules which have rotational isomers, these one dipole models are not satisfactory, as pointed out in Sec. 1. In contrast to them our two localized dipole model appears to be a better one for the experimental result, as shown in Figs. 1 and 2.

The above calculation includes some rough assumptions that the molecular volume as well as the C−Cl bond moment of the *gauche*- and the *trans*-forms are considered to be the same, because unfortunately we could not obtain these values by experiments. But a slight change of the molecular volume was found to have no significant effect on the result.

It has been well known that such molecules as dichloroethane show abnormal dipole moment and abnormal dependence of temperature in benzene and toluene solutions; and Mizushima *et al.*,[9] have suggested that it may be due to the affinity between the hydrogen atoms of benzene ring and halogen atoms in dichloroethane. This interesting phenomenon, which we may call "benzene effect," will not be discussed here, for it appears evident that this has no relation to the reaction field problem.

[4] Watanabe, Miyagawa, and Morino, Repts. Inst. Radiation Chem. (Tokyo Univ.) **3**, 25 (1948).
[5] R. P. Bell, Trans. Faraday Soc. **27**, 797 (1931).
[6] R. Fujishiro, J. Chem. Soc. (Japan) **65**, 352 (1943).
[7] J. A. Abbott and H. C. Bolton, Trans. Faraday Soc. **48**, 422 (1952).
[8] D. G. Food and A. J. Dekker, J. Chem. Phys. **20**, 1030 (1952).
[9] Mizushima, Morino, and Higashi, Sci. Papers Inst. Phys. Chem. Research (Tokyo) **25**, 153 (1934).

The author is grateful to Professor Y. Morino for his guidance, and to Mr. I. Miyagawa for his kind advice. Needless to say, the author is forever indebted to his father, the late Dr. Koroku Wada, for his constant encouragement.

APPENDIX

The Calculation of the Reaction Field

The reaction field induced in the medium surrounding the spheroidal cavity will be derived by the use of the model stated above. For this problem the spheroidal coordinates, v, w, and φ, would be convenient; according to them the Cartesian coordinates are represented by

$$x=c\cdot[(v^2-1)(1-w)^2]^{\frac{1}{2}}\cos\varphi,$$
$$y=c\cdot[(v^2-1)(1-w)^2]^{\frac{1}{2}}\sin\varphi, \qquad \text{(A1)}$$

and

$$z=c\cdot vw,$$

where c is the distance of a focus from the center of the spheroid. Now, the reciprocal of the distance R between the two points $P(x,y,z)$ and $P_1(x_1,y_1,z_1)$ is expanded in the series of spherical harmonics[10] as follows:

$$\frac{1}{R}=\frac{1}{[(x-x_1)^2+(y-y_1)^2+(z-z_1)^2]^{\frac{1}{2}}}$$
$$=\frac{1}{c}\cdot\sum_{n=0}^{\infty}[(2n+1)P_n(w)P_n(w_1)Q_n(v)P_n(v_1)]$$
$$+2\sum_{m=1}^{n}(-1)^m\left\{\frac{(n-m)!}{(n+m)!}\right\}(2n+1)$$
$$\times P_n^m(w)P_n^m(w_1)Q_n^m(v)P_n^m(v_1)\cos m(\varphi-\varphi_1), \qquad \text{(A2)}$$

where P_n^m and Q_n^m are, respectively, the first and second kind of spherical harmonics of the nth order and mth degree. By differentiating Eq. (A2) partially by x_1, multiplying by μ_x, and then putting $x_1=0$, $y_1=0$, and $z_1=c$; that is, $v_1=1$, $w_1=1$, and $\varphi=0$, the potential at the point P due to the dipole μ_x which is placed at the focus $x=c$ is written in terms of spherical harmonics as follows:

$$V_0=\mu_x\cdot\left\{\frac{\partial}{\partial x_1}\cdot\frac{1}{R}\right\}_{\substack{w_1=1\\ v_1=1\\ \varphi_1=0}}=\frac{\mu_x}{c^2}\sum_{n=1}^{\infty}\frac{(2n+1)}{2}$$
$$\times P_n'(w)Q_n'(v)\cos\varphi. \qquad \text{(A3)}$$

The reaction field will be derived from the dipole potential (A3) and the boundary conditions. In the first place, considering the fact that the potential in the cavity must be continuous at the origin, together with the fact that the dipole must have onefold symmetry about the z axis, the potential for the reaction field

[10] E. W. Hobson, *Spherical and Ellipsoidal Harmonics* (Cambridge University Press, Cambridge, 1931), p. 415.

inside the cavity may have the following form,

$$V_i=\sum_{n=1}^{\infty} A_n P_n'(w)P_n'(v)\cos\varphi. \tag{A4}$$

On the other hand, the potential outside the cavity may be expressed as Eq. (A5), referring to the condition that the potential must be zero at infinity,

$$V_e=\sum_{n=1}^{\infty} B_n P_n'(w)Q_n'(v)\cos\varphi. \tag{A5}$$

Two boundary conditions at the surface of the spheroid are as follows:

$$(V_0+V_i)_{v=v_0}=(V_e)_{v=v_0} \tag{A6}$$

and

$$\left\{\frac{\partial}{\partial v}(V_0+V_i)\right\}_{v=v_0}=\left(\frac{\partial V_e}{\partial v}\right)_{v=v_0}. \tag{A7}$$

The coefficients A_n's of Eq. (A4) are obtained by eliminating the B_n's:

$$A_n=-\frac{\mu}{c}\cdot\frac{(2n+1)}{2}\cdot(\epsilon-1)\Big/\left\{\epsilon\frac{P_n'(v_0)}{Q_n'(v_0)}-\frac{\dot{P}_n'(v_0)}{\dot{Q}_n'(v_0)}\right\}, \tag{A8}$$

where $v_0=1/e$, e being the eccentricity of the spheroid, and $\dot{P}_n'$ and $\dot{Q}_n'$ are, respectively, the first derivatives of P_n' and Q_n'.

Let $r_\perp\mu_\perp$ and $r_\perp'\mu_\perp$ be the reaction field at $z=c$ and $z=-c$, respectively, induced by a dipole placed at $z=c$ and perpendicular to the z axis: that is, $r_\perp\mu_\perp$ is the reaction field at the focus $z=c$ where the dipole is placed, and $r_\perp'\mu_\perp$ is that at the opposite focus, then finally

$$r_\perp\mu_\perp=\mu_\perp\cdot\frac{(\epsilon-1)}{8c^3}\sum_{n=1}^{\infty}(2n+1)\{n(n+1)\}^2\times\left\{\epsilon\frac{P_n'(v_0)}{Q_n'(v_0)}-\frac{\dot{P}_n'(v_0)}{\dot{Q}_n'(v_0)}\right\}^{-1}, \tag{A9}$$

and

$$r_\perp'\mu_\perp=\mu_\perp\cdot\frac{(\epsilon-1)}{8c^3}\left[\sum_{n=1}^{\infty}(4n-1)\{2n\cdot(2n-1)\}^2\cdot\left\{\epsilon\frac{P_{2n-1}'(v_0)}{Q_{2n-1}'(v_0)}-\frac{\dot{P}_{2n-1}'(v_0)}{\dot{Q}_{2n-1}'(v_0)}\right\}^{-1}-\sum_{n=1}^{\infty}(4n+1)\times\{2n\cdot(2n+1)\}^2\left\{\epsilon\frac{P_{2n}'(v_0)}{Q_{2n}'(v_0)}-\frac{\dot{P}_{2n}'(v_0)}{\dot{Q}_{2n}'(v_0)}\right\}^{-1}\right]. \tag{A10}$$

The parallel components of the reaction field induced by the perpendicular component of the dipole moment, $r_{\parallel}\mu_\perp$ and $r_{\parallel}'\mu_\perp$ are zero because of the symmetry of the spheroid about the z axis.

Similarly, the reaction field parallel to the z axis induced by the dipole component parallel to the z axis is obtained as

$$r_{\parallel}\mu_{\parallel}=\mu_{\parallel}\cdot\frac{(\epsilon-1)}{4c^3}\sum_{n=1}^{\infty}(2n+1)\{n(n+1)\}\times\left\{\epsilon\frac{P_n(v_0)}{Q_n(v_0)}-\frac{\dot{P}_n(v_0)}{\dot{Q}_n(v_0)}\right\}^{-1}, \tag{A11}$$

and

$$r_{\parallel}'\mu_{\parallel}=\mu_{\parallel}\cdot\frac{(\epsilon-1)}{4c^3}\left[\sum_{n=1}^{\infty}(4n-1)\{2n(2n-1)\}\times\left\{\epsilon\frac{P_{2n-1}(v_0)}{Q_{2n-1}(v_0)}-\frac{\dot{P}_{2n-1}(v_0)}{\dot{Q}_{2n-1}(v_0)}\right\}^{-1}-\sum_{n=1}^{\infty}(4n+1)\times\{2n(2n+1)\}\left\{\epsilon\frac{P_{2n}(v_0)}{Q_{2n}(v_0)}-\frac{\dot{P}_{2n}(v_0)}{\dot{Q}_{2n}(v_0)}\right\}^{-1}\right]. \tag{A12}$$

Their perpendicular components of the reaction field induced by the parallel component of the dipole moment, $r_\perp\mu_{\parallel}$ and $r_\perp'\mu_{\parallel}$ are also zero.

THE JOURNAL OF CHEMICAL PHYSICS VOLUME 22, NUMBER 2 FEBRUARY, 1954

The Vibrational Spectra and Structure of Solid Hydroxylamine and Deutero-Hydroxylamine*

R. E. NIGHTINGALE† AND E. L. WAGNER
Department of Chemistry, State College of Washington, Pullman, Washington
(Received May 28, 1953)

The infrared spectra of thin films of H_2NOH and D_2NOD were obtained at −78° and −190°C in the region 4000–500 cm^{-1}. Two distinct types of spectra resulted depending on whether the films were formed at −78° or at −190°C. The spectra obtained when the films were formed at −190°C were characterized by broad overlapping bands; those formed at −78°C gave much narrower bands, some of them splitting into two or more distinct components. The latter type spectrum is representative of the stable crystalline form at low temperature. This spectrum could not be correlated with the amine oxide form of hydroxylamine, $NH_3 \rightarrow O$. Satisfactory vibrational assignments could, however, be made for the model with symmetry of the point group C_s, H_2NOH. If *cis*- and *trans*-rotational isomers coexist in the solid, they must possess very nearly the same potential energy or at least a high potential barrier between them. The O−H stretching vibration in the solid is found at a very low frequency, 2867 cm^{-1}, indicating a very strong hydrogen-type bond with energy of about 13 kcal per mole.

I. INTRODUCTION

HYDROXYLAMINE is a relatively simple substance for which two different structures have been proposed to account for its properties. The first, and most commonly accepted configuration, is H_2NOH, where the HNO and the NOH angles are near to those in NH_3 and H_2O. This model has only one element of symmetry, i.e., a plane of symmetry through the N−O−H atoms and bisecting the HNH angle. It therefore would possess the symmetry of the point group C_s. Both the *cis*- and the *trans*-rotational isomers would have this symmetry. The second possible structure which has been considered is the amine oxide form, $H_3N \rightarrow O$, in which the hydrogen atoms and the oxygen atom are arranged tetrahedrally about the central nitrogen atom. This model has the symmetry of the point group C_{3v}. It has been proposed on the basis of chemical evidence,[1] but others[2] have interpreted the same type of data as evidence against the amine oxide form. Nevertheless, because it is still suggested as a possible tautomeric form in recent texts on inorganic chemistry[3] it would be desirable to settle this question definitely.

Neither the infrared spectrum nor the Raman spectrum of crystalline hydroxylamine has been reported.‡ A Raman spectrum has been reported for liquid hydroxylamine,[4] but only a mediocre spectrum resulted because of decomposition with the emission of gas bubbles. Raman spectra of a solution of hydroxylamine in water obtained by neutralizing hydroxylammonium chloride with sodium hydroxide, have also been reported.[5]

These Raman data, which are given in Table I, have been interpreted as arising from the C_s model of hydroxylamine although no detailed analyses have been made. No data of any kind have been reported on the deutero-compound, and unfortunately no crystal structure work has appeared on either compound.

In order to throw further light on the question of the structure of these molecules, the infrared spectra of thin films of crystalline H_2NOH and D_2NOD were studied at −78° and −190°C in the region 4000–500 cm^{-1}. The amine oxide model does not permit a satisfactory vibrational assignment to be made from our data, and consequently it must be ruled out as a possible structure for the hydroxylamine molecule in the crystal. The C_s model does allow a satisfactory vibrational

TABLE I. Raman studies on H_2NOH.

Medard[a] Liquid H_2NOH	Bernstein and Martin[b] 25 percent solution of H_2NOH
897 (6)	
921 (6) N−O stretch	906 (10) N−O stretch
1034 (0)	1042
1108 (1)	1120 (6)
...	1290 (0)
1311 (0)	1365 (1)
1605 (3)	
3259 (5)	3257 (1)
3306 (3)	

[a] See reference 4.
[b] See reference 5.

* Based on a thesis submitted by Richard E. Nightingale in partial fulfillment of the requirements for the Ph.D. degree at the State College of Washington.

† Present address: School of Chemistry, University of Minnesota, Minneapolis, Minnesota.

[1] F. Haber, Ber. deut. Chem. Ges. **29**, 2444 (1896).

[2] P. Baumgarten and H. Erbe, Ber. deut. chem. Ges. **72B**, 2603 (1938).

[3] N. V. Sidgwick, *The Chemical Elements and Their Compounds* (Oxford University Press, London, 1950), Vol. I, p. 681.

‡ After this manuscript was prepared an article appeared by P. A. Giguére and I. D. Liu [Can. J. Chem. **30**, 948 (1952)], in which the infrared spectrum of crystalline H_2NOH mulled in Nujol at room temperature was reported. Because of the reactive nature of H_2NOH and the fact that important bands are masked out by the Nujol, we feel that their spectrum does not give as true a picture of the solid as our low-temperature crystalline film spectra.

[4] L. Medard, Compt. rend. **199**, 421 (1934).

[5] H. J. Bernstein and W. H. Martin, Trans. Roy. Soc. Can. III, **31**, 95 (1937).

assignment to be made, although nothing can be concluded from this fact as to which of the two rotational isomers is most stable.

II. EXPERIMENTAL METHODS AND TECHNIQUES

Two separate methods were used for the preparation of free hydroxylamine and deutero-hydroxylamine.[6] The first method involved the neutralization of cp hydroxylammonium chloride with sodium butoxide and subsequent crystalization of the hydroxylamine at $-10°C$.[7] In the second method free hydroxylamine was

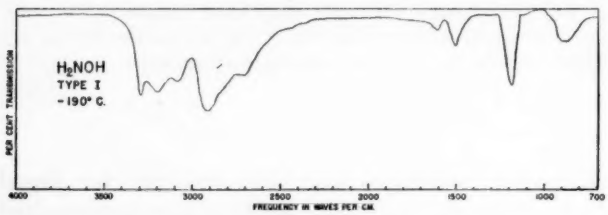

FIG. 1. Infrared spectrum of a "supercooled" film of hydroxylamine.

prepared by the thermal decomposition of the phosphate salt, tertiary hydroxylammonium phosphate, at reduced pressure.[8] After purification by vacuum sublimation the products from the two methods had the same appearance, the same melting points (33–33.5°C at 20 mm Hg pressure of dry nitrogen), and both gave identical spectra.

The hydroxlamine films were prepared by direct sublimation in a vacuum of less than 10^{-4} mm Hg onto the cooled rocksalt sample support of a low temperature infrared transmission cell. The cell is essentially the same as the one previously described[9] except that a means has been provided for introducing the vapors

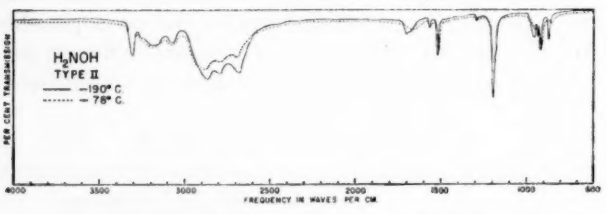

FIG. 2. Infrared spectra of the stable low-temperature form of hydroxylamine.

directly onto the sample support in the cell. The films were studied during formation by observing the interference patterns in a beam of light reflected from their surface. The film thickness was controlled by counting the number of times the color at the center of the film on the sample support went through red. The period of film formation was from one to two minutes, and the thickness were estimated to be 0.1–1.5 micron. Films were condensed at both $-190°$ and $-78°C$ using liquid nitrogen and dry ice as coolants. Those obtained at $-190°C$ were very transparent and nonscattering. Even the very thick films could be seen only by reflected light. The films obtained at $-78°C$ also showed interference colors by reflected light, but, in addition, they were slightly foggy when viewed by transmitted light, becoming more so with increasing thickness. The absorption spectra of these two types of films differed in some details. However, it was found that a film of the second type could be studied at $-190°C$ by forming the film at $-78°C$ and then cooling on down to $-190°C$. This did not result in any detectable change in the appearance of the original film.

The infrared spectra in the rocksalt region were taken on a Model 21 Perkin-Elmer infrared spectrometer. This is a double-beam instrument recording directly in percent transmission *versus* waves per centimeter. The spectra in the potassium bromide region were obtained on a modified Model 12C Perkin-Elmer Infrared Spectrometer. The modification consisted of enclosing the entire optical path in an air-tight housing so that it could be flushed out with dry nitrogen gas until the atmospheric water and CO_2 absorption bands were almost completely removed. Unfortunately, scattered radiation made the spectra below 500 cm^{-1} highly uncertain.

III. EXPERIMENTAL RESULTS

The spectrum obtained for a film of H_2NOH formed at $-190°C$ is shown in Fig. 1. Spectra resulting from films of H_2NOH and D_2NOD formed at $-78°C$ and then cooled on down to $-190°C$ are shown in Figs. 2 and 3. The observed frequencies of maximum absorption and their relative integrated band intensities for the two types of films are given in Table II. The intensities are based on the value of 100 for the strongest band in each spectrum. These were determined by measuring the area under the partitioned bands on the percent transmission *versus* waves per cm curves. Although a logarithmic plot of transmission should be used to calculate the integrated intensities, our method serves as a good approximation, and the errors involved are probably no greater than those introduced by the somewhat arbitrary partitioning of the overlapped bands. Admittedly, this method will cause the weak bands with small absorption to appear more intense than they actually are, and the strong bands with high absorption to appear less intense. In those cases where bands are greatly overlapped or where a band appears as a shoulder on a larger band, the estimated relative intensity can only be very approximate.

In general, the absorption bands of the first type of films (those formed at $-190°C$) are quite broad and apparently unresolved relative to those in the spectra of the type of film formed at $-78°C$. In addition, the

[6] R. E. Nightingale and E. L. Wagner, J. Am. Chem. Soc., 75, 4092 (1953).
[7] C. D. Hurd, *Inorganic Synthesis* (McGraw-Hill Book Company, Inc., New York, 1939), Vol. 1, p. 87.
[8] R. Uhlenhuth, Ann. Physik 311, 117 (1900).
[9] E. L. Wagner and D. F. Hornig, J. Chem. Phys. 18, 296 (1950).

bands at 1605 cm^{-1}, 1505 cm^{-1}, and 1185 cm^{-1} in H_2NOH and the corresponding bands in D_2NOD become quite sharp and split into two components in the second type of film. The broad band at 900 cm^{-1} in the Type I film of H_2NOH shows an indication of being composed of several overlapped bands. These actually become resolved into four separate peaks in the Type II spectra. The situation with D_2NOD in this region is a little different, since all but one band, that assigned to the N—O stretching mode, are shifted to lower frequencies and the bands become more distinctly separated. The relative intensity of the band at 2700 cm^{-1} is increased considerably in the Type II spectrum and other less pronounced differences, such as frequency shifts, occur between the two types of spectra.

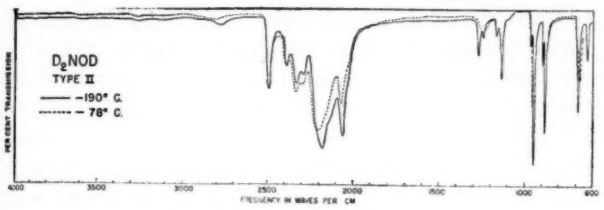

FIG. 3. Infrared spectra of the stable low-temperature form of deutero-hydroxylamine.

This phenomena, wherein different spectra are obtained for films formed at different temperatures, occurs quite commonly. A similar behavior has recently been reported by Malherbe and Bernstein[10] in forming films of 1,2-dichloroethane at low temperature. They found that when their films were formed at −150°C, the spectra showed characteristics of a true crystalline solid, as was evidenced by the absence of the *gauche*-bands. However, when the films were formed at −179°C, the infrared spectra were similar to that of the liquid, and bands resulting from the *gauche*- and *trans*-isomers of dichloroethane were formed. They concluded that a glassy solid was formed at −179°C and found a sudden transition to the normal crystalline state occurred at −150°±2°C when the films were allowed to warm gently. A similar interpretation may be given to the behavior of hydroxylamine when films are formed at low temperature. However, the possibility of there being more than one crystalline form in this temperature range also exists, as does the possibility that the molecules crystallize differently at the different rates of condensation. Until the infrared spectrum of the liquid is known and some information as to the crystal structure is available, this point will have to remain undecided. In any case, the stable crystalline from at both −78°C and −190°C gives a Type II spectrum as shown in Figs. 2 and 3. The interpretation of the low-temperature infrared spectrum of hydroxylamine will be based on this type of spectrum.

TABLE II. Infrared frequencies of the two types of spectra of H_2NOH and D_2NOD.

Type I Film at −190°C		Type II Films at −78°C		at −190°C	
H_2NOH	D_2NOD	H_2NOH	D_2NOD	H_2NOH	D_2NOD
3293 (33)	2480 (66)	3305 (17)	2490 (16)	3302 (18)	2494 (14)
	2380 (16)		2388 (8)	3245 (5)	2390 (8)
3195 (71)	2330 (81)	3180 (43)	2330 (41)	3173 (33)	2330 (28)
3080 (29)		3070 (27)	2290 (6)	3065 (20)	2290 (9)
2908 (100)	2200 (100)	2880 (100)	2195 (100)	2867 (100)	2175 (100)
		2800 (11)		2787 (29)	2145 (3)
2700 (53)	2060 (50)	2700 (36)	2060 (33)	2675 (71)	2056 (31)
				1697 (5)	1267 (4)
1605 (8)	1170 (5)	1670 (13)	1242 (6)	1675 (4)	1242 (2)
		1560 (4)	1158 (1)	1564 (2)	1165 (1)
1505 (15)	1125 (9)	1509 (5)	1130 (6)	1515 (7)	1132 (5)
		1286 (1)		1287 (1)	962 (1)
1185 (29)	940 (31)	1186 (19)	942 (15)	1191 (26)	942 (13)
		945 (11)	670 (10)	950 (8)	680 (9)
		928 (1)	890 (1)	932 (2)	891 (1)
900 (29)	880 (20)	904 (13)	874 (11)	912 (8)	867 (10)
		848 (6)		867 (4)	650 (2)

In addition to the spectra on the particular films shown, data were obtained on sixteen other H_2NOH films and on three other D_2NOD films. These varied in thickness from approximately 0.1 to 1.5 microns. There do not seem to be any outstanding changes in either intensity or peak frequency of any band in films of different thicknesses. However, in the case of H_2NOH, the band at 3185 cm^{-1} becomes relatively more intense and the band at 2688 cm^{-1} becomes less intense with the thicker films.

Spectra taken in the potassium bromide region at the lower frequencies are not shown. The data taken are somewhat uncertain, but there appears to be a broad band in the spectrum of H_2NOH extending from 500–570 cm^{-1} with its center at 535 cm^{-1}. The corresponding band in the spectrum of D_2NOD was expected at about 400 cm^{-1}, which was below the useful range of our spectrometer.

IV. DISCUSSION

The model for the hydroxylamine molecule which has the symmetry of point group C_s should give rise to six fundamental vibrational modes which are symmetric with respect to the plane of symmetry (A' modes) and three which are antisymmetric (A'' modes). These

[10] F. E. Malherbe and H. J. Bernstein, J. Chem. Phys. **19**, 1607 (1951).

modes include two N−H stretches, one O−H stretch, one N−O stretch, one HNH bend, one NOH bend, one NH_2 rock, one NH_2 wag, and a torsional oscillation about the N−O bond. All fundamentals, overtones, and combinations of these are allowed in both the infrared and Raman spectra provided the site symmetry is C_s.

On the other hand, the amine oxide model having the symmetry of point group C_{3v} should give three totally symmetric fundamental vibrational modes (A) and three doubly degenerate E modes. All these are again allowed in both the infrared and the Raman spectra if the site symmetry is actually C_{3v}.

Although there appears to be somewhat more than six fundamental frequencies in the observed spectra, one cannot definitely decide between these two structures on the basis of the number of observed bands alone, since in the spectra of crystalline substances intense combination and overtone bands may also appear, or bands may become duplicated several times depending on the number of molecules in the unit cell. However, if one compares the observed spectrum with that of a molecule similar to $H_3N{\rightarrow}O$, such as methyl chloride, H_3C-Cl,[11] it will be seen that a satisfactory vibrational assignment is not possible for this model. The lowest frequency to be expected is the one corresponding to the N^+-O^- stretch. The other fundamentals consist of one H_3N-O bend, two H_3N deformations of intermediate frequency, and two N−H stretches of high frequency. The N^+-O stretch has been observed at 1000 cm^{-1} in the Raman spectrum of crystalline H_3NOHCl[12] and one would expect the N^+-O^- stretch of $H_3N{\rightarrow}O$ to have a little higher frequency, certainly not lower. However, three strong bands are found in the spectrum of hydroxylamine below 1000 cm^{-1}. Moreover, there is some evidence for a torsional mode occurring with a frequency of 535 cm^{-1}. This certainly could not arise from the $H_3N{\rightarrow}O$ structure. Thus, it appears evident that the amine oxide model does not allow a satisfactory vibrational assignment to be made of our data.

TABLE III. Infrared vibrational assignments of H_2NOH and D_2NOD.

Frequency (cm^{-1})		Isotopic ratio		
H_2NOH	D_2NOD	$\frac{D_2NOD}{H_2NOH}$	Other molecules	Assignments
3302	2494	0.76	0.76[c]; 0.74[d]	$\nu_7(a'')$ Antisym. N−H stretch
3245	2390	0.74		
3173	2330	0.74	0.77[c]; 0.72[d]	$\nu_1(a')$ Sym. N−H stretch
3065	2290	0.75	0.76[c]	$2\nu_3(A')$
2867	2175	0.76	0.75[a]; 0.74[b]	$\nu_2(a')$ O−H stretch
2787	2145	0.77		
2675	2056	0.77	0.80[c]	$\nu_3+\nu_4(A')$
1697	1267	0.75		
1675	1242	0.74		$2\nu_6(A')$
1564	1165	0.75		
1515	1132	0.75	0.78[c]; 0.77[d]	$\nu_3(a')$ HNH bend
1287	962	0.75		
1191	942	0.79	0.81[a];	$\nu_4(a')$ O−H bend
950	680	0.72	0.72[c]	$\nu_8(a'')$ NH_2 wag
932	891	0.96		
912	876	0.96		$\nu_5(a')$ N−O stretch
867	630	0.73	0.73[c]	$\nu_6(a')$ NH_2 rock
535	(400)	(0.742)		$\nu^9(a'')$ torsion about N−O bond

[a] CH_3OH solid.
[b] CH_3OH vapor.
[c] H_2NCN solid.
[d] NH_3 solid.

The observed spectra can, however, be satisfactorily interpreted on the basis of the C_s model, H_2NOH. Our assignments are summarized in Table III. The observed peak frequencies for films of H_2NOH and D_2NOD formed at −78°C and then cooled to −190°C are given in the first two columns. The third column shows the ratio of the frequencies of a given vibrational mode of D_2NOD to that for the same mode of H_2NOH. For comparison the analogous ratio is listed in the next column for similar types of motion in other molecules. The comparison of these ratios was first suggested by Noether[13] as an empirical rule to aid in making vibrational assignments and has been amply supported by experimental data.[11]

1. Fundamental Frequencies

The absorption bands in the region above 2600 cm^{-1} arise from hydrogen stretching motions or from combination modes. Three hydrogen stretches are expected from the H_2NOH structure. At least six bands are observed in this region, with a corresponding number in the region above 2000 cm^{-1} in the spectrum of D_2NOD. The sharp band at 3302 cm^{-1} has been assigned to the fundamental ν_7 which originates in an antisymmetric N−H stretching motion. This frequency value may be compared to the corresponding modes in solid NH_3[14] and H_2NCN[15] which have the frequencies 3378 cm^{-1} and 3322 cm^{-1}, respectively. The corresponding band in the spectrum of D_2NOD occurs quite definitely at 2494 cm^{-1}, so that the isotope shift of 0.76 is quite close to that expected from Noether's rule.

The symmetric N−H stretching mode, ν_1, has been assigned the frequency 3173 cm^{-1} in H_2NOH and 2330 cm^{-1} in D_2NOD. The band at 3173 cm^{-1} may appear somewhat broad for a fundamental, but because its shape and intensity are to some degree temperature dependent, this may be due to lattice mode combinations which become less important at low temperature, or to intermolecular interactions. The alternative assignment in which ν_7 and ν_1 are interchanged does not give as good an agreement with the Teller-Redlich

[11] G. Herzberg, *Infrared and Raman Spectra of Polyatomic Molecules* (D. Van Nostrand Company, Inc., New York, 1945).

[12] R. Ananthakrishnan, Proc. Indian Acad. Sci. **5A**, 87 (1937).
[13] H. D. Noether, J. Chem. Phys. **11**, 97 (1943).
[14] F. P. Reding and D. F. Hornig, J. Chem. Phys. **19**, 594 (1951).
[15] G. D. Wagner, Jr., thesis, State College of Washington (1953).

product rule, although this assignment is not improbable. Perhaps Raman polarization measurements could settle this point.

The broad intense band at 2876 cm^{-1} does not fit any obvious combination or overtone, and besides, one would hesitate to assign the most intense band of the spectrum to an overtone or combination, even in crystalline substances. This band has been assigned to the O—H stretching mode, ν_2, in spite of the fact that it appears at a somewhat lower frequency than usually reported. The corresponding band occurs in the D_2NOD spectrum at 2175 cm^{-1}. There are actually very few analogous compounds which have been studied in the solid state under comparable circumstances, although it has recently been shown that such low O—H stretching frequencies are easily possible.[16] Water vapor has an absorption band at 3654 cm^{-1} which is attributed to the hydroxyl stretch. We find that in ice at liquid nitrogen temperature this band occurs at 3257 cm^{-1}. In methanol vapor the O—H stretch appears at 3680 cm^{-1}. In the solid at liquid nitrogen temperature we find it at 3220 cm^{-1}. Thus, our assignment of the O—H stretching mode which corresponds to a vapor to solid frequency shift of 790 cm^{-1} must indicate the existence of a particularly strong hydrogen-type bond with a bond energy which we estimate to be 12–13 kcal per mole. The corresponding O—D vibration in D_2NOD certainly occurs at 2175 cm^{-1}. Even in this case the deuteriun bond appears to have an energy of about 8 kcal per mole. On our scale, the deuteriun bond in D_2O at liquid nitrogen temperature is about 2–3 kcal per mole as estimated from our O—D vibrations in heavy ice at 2445 cm^{-1} and 2353 cm^{-1}.

The N—O stretching fundamental, ν_5, is found at 912 cm^{-1} with a weak component at 932 cm^{-1}. This band, as expected, shifts only a small amount to 876 cm^{-1} in the D_2NOD spectrum. A weak component is also found on the high-frequency side of this band at 891 cm^{-1}. Treating $H_2N—OH$ as a diatomic molecule, the calculated shift would be from 912 cm^{-1} to 873 cm^{-1}. Bernstein[17] has recently given another method for calculating the change in vibrational frequency due to change in mass. This method predicts a frequency shift of 42 cm^{-1} for the N—O stretch in going from H_2NOH at 912 cm^{-1} to 870 cm^{-1} in D_2NOD. The partially deuterated compounds, H_2NOD, HDNOD, and D_2NOH should absorb at 899 cm^{-1}, 884 cm^{-1}, and 883 cm^{-1}, respectively. The observed isotope shift of this band most certainly verifies the assignment.

The deformation fundamentals of highest frequency correspond to the HNH and the NOH bending modes. The band at 1515 cm^{-1} and its weaker component at 1564 cm^{-1} are believed to arise from the HNH bending fundamental ν_3. The corresponding bands in the spectrum of D_2NOD appear at 1132 cm^{-1} and 1165 cm^{-1}. These frequencies compare favorably with the values found in cyanamide[15] in which the bending motion is assigned the value 1572 cm^{-1} and the weak component is found at 1612 cm^{-1}.

The very sharp, intense band at 1191 cm^{-1} and the much weaker component at 1287 cm^{-1} are attributed to the fundamental ν_4, arising from the NOH bending motion. The corresponding bands in the spectrum of D_2NOD are found at 942 cm^{-1} and 962 cm^{-1}. The identification of absorption bands connected with the OH bending vibration has in the past been somewhat uncertain, the assignments ranging from 1050 cm^{-1} to 1615 cm^{-1}. The problem still has not been resolved, but most assignments are now made in the region from 1150 cm^{-1} to 1400 cm^{-1}. Smith and Creitz[18] have carried out infrared studies of the association of several alcohols in the liquid state. They demonstrated that in methanol, bands at 1020 cm^{-1}, 1072 cm^{-1}, and 1330 cm^{-1} are associated with the hydroxyl group, since they all move to higher frequencies as the liquid becomes more associated at higher concentration. In solid methanol at liquid nitrogen temperature we find an OH bend at 1130 cm^{-1} and the OD bend at 950 cm^{-1}. Further evidence that this band is associated with the OH rather than with an NH_2 deformation is given by comparison with the spectrum of solid cyanamide,[15] in which no corresponding band occurs. A Raman line in liquid hydroxylamine was found by Medard[4] at 1108 cm^{-1}. It is probable that this line also belongs to the OH bend and that it moves to 1191 cm^{-1} in the solid because of the stronger hydrogen bonding. This is further evidence for a very definite weakening of the OH bond suggested by the unusually low OH stretching frequency.

The antisymmetric wagging motion of the NH_2 group corresponding to the fundamental ν_8, is assigned the frequency 950 cm^{-1} in H_2NOH and 680 cm^{-1} in D_2NOD. The symmetric rocking fundamental ν_6, corresponding to a bending type motion similar to the wagging except that the NH_2 group swings as a unit back and forth in the symmetry plane of the molecule, is found at 867 cm^{-1} and 630 cm^{-1} in the undeuterated and deuterated compounds, respectively. The relative intensity of the wagging motion is about twice that of the rocking motion as expected. Both bands become sharper and more intense at lower temperature. Corresponding bands at approximately the same frequencies occur in cyanamide. Again Raman polarization measurements could establish which is the rocking and which is the wagging frequency.

There appears to be a broad band in the spectrum of H_2NOH in the KBr region of the spectrum extending from about 500–570 cm^{-1} with its center at about 535 cm^{-1}. Our data in this region are somewhat uncertain, so that the assignment of this band to the torsional mode, ν_9, is tentative only. The corresponding fundamental of D_2NOD, expected at about 400 cm^{-1} has not been observed.

[16] R. E. Rundle and M. Parasol, J. Chem. Phys. **20**, 1487 (1952). R. C. Lord and R. E. Merrifield, J. Chem. Phys. **21**, 166 (1953).
[17] H. J. Bernstein, Can. J. Chem. **29**, 284 (1951).
[18] F. A. Smith and E. C. Creitz, J. Research Natl. Bur. Standards, **46**, 145 (1951).

It is to be noted that many of the bands in the spectrum of hydroxylamine films formed at −78°C are split into two components. The average splitting observed is about 35 cm^{-1}. This is not at all unusual in the spectra of crystalline materials. It may arise from the coupling of the vibrations of different molecules in the unit cell, from combination modes with lattice vibrations, or from the coexistence of more than one form of the molecule. In the case of hydroxylamine, *cis*- and *trans*-isomers may exist in the solid. However, if they do exist they must have very nearly the same potential energy or else a very high barrier between them since no temperature effect indicating a change in the relative numbers of *cis*- and *trans*-molecules was observed.

2. Combinations and Overtones

There are a number of absorption maxima in the spectrum of solid hydroxylamine in addition to those assigned to the fundamental modes. Several of these can be assigned to reasonable combination and overtone modes of the internal vibrations of the molecule, but undoubtedly some are due to combinations with the lattice modes. The band at 3065 cm^{-1} is probably the overtone of the HNH bending mode, $2\nu_3$. The same overtone is found in the spectrum of cyanamide[15] but it occurs at a frequency slightly less than twice the value of the corresponding fundamental. In the case of hydroxylamine there may be a Fermi-type interaction between the overtone $2\nu_3$ and the very strong fundamental ν_2. This would shift the overtone to a higher frequency and the fundamental to a lower frequency. If we assume that the overtone borrows all of its intensity from the fundamental, a first-order perturbation calculation[9] yields for the unperturbed frequencies of the overtone and the fundamental the values 3032 cm^{-1} and 2900 cm^{-1}, respectively. This value for the overtone is much nearer to that expected.

Another strong band which occurs in the high-frequency region is the $(\nu_3+\nu_4)$ combination observed at 2675 cm^{-1} in H_2NOH and 2056 cm^{-1} in D_2NOD. This band must include as one of its components an OH frequency of some sort since it does not occur in other NH_2 compounds. Also the high value for the isotope shift indicates that ν_4 is one of its components.

The band at 1697 cm^{-1} with its weaker component at 1675 cm^{-1} is the most temperature dependent band in the spectrum. It changes from a single broad symmetrical band at −78°C centered at 1660 cm^{-1} to the sharper unsymmetrical doublet at −190°C. This behavior is more characteristic of a combination or overtone than of a fundamental. In many ways it behaves like a combination with the torsional mode. However, the data from the deutero-hydroxylamine spectrum are inconsistent with this type of assignment. We assign this band to the overtone of the NH_2 rock, $2\nu_6$. The fact that the overtone band is as intense as the fundamental is not at all unlikely in the spectra of crystalline substances since the number of transitions entering an overtone is enormously greater than in the case of a fundamental. It may also be noted that the fundamental ν_6 shifts to higher frequency on lowering the temperature just as does the overtone band.

3. The Isotope Product Ratios

The isotope product ratios are not as useful for hydroxylamine as might be desired because of the low symmetry. Nevertheless, some justification for our assignments can be obtained. The complete geometry of H_2NOH is not known, but we shall assume tetrahedral angles throughout, an N−H distance of 1.014A. This should be the symbol for Angstrom units = A from NH_3,[11] an O−H distance of 0.958A from H_2O,[11] and an N−O distance of 1.46A as found in both HONO and $(H_3NOH)^+$. These values will not be far in error and furthermore the results are probably not very sensitive to these parameters.

The product ratio for the six A' modes of hydroxylamine reduces to

$$\prod_{n=1}^{6}\left(\frac{\nu_n^i}{\nu_n}\right)=\left(\frac{m_H}{m_D}\right)^5\left(\frac{M^i}{M}\right)\left(\frac{I_z^i}{I_z}\right)^{\frac{1}{2}}=0.216,$$

where all quantities referring to the isotopic molecule, D_2NOD, are marked with the superscript i. The ν's are the normal modes of the symmetry type A', m_H and m_D are the masses of hydrogen and deuterium, M is the total mass of the molecule, and I_z is the moment of inertia about the z axis. The experimental value for this product ratio using the assignments of Table III is 0.229. Although this is 6 percent higher than the harmonic value, much of this difference is undoubtedly due to the effect of the strong hydrogen bonding.

The product ratio for the three A'' modes is

$$\prod_{n=6}^{9}\left(\frac{\nu_n^i}{\nu_n}\right)=\left(\frac{m_H}{m_D}\right)^2\left(\frac{M^i}{M}\right)^{\frac{1}{2}}\left(\frac{I_x^iI_y^i}{I_xI_y}\right)^{\frac{1}{2}}=0.411,$$

where the moments of inertia are again calculated from the assumed geometry of the molecule. Since the fundamental ν_9 has not been observed for D_2NOD, the experimental value of this product ratio could not be determined. However, the expected ratio for ν_9^i/ν_9 is calculated to be 0.742, which, if we use $\nu_9=535$ cm^{-1}, gives a value for the torsional frequency in D_2NOD of 400 cm^{-1}. This frequency is close to that predicted for ν_9^i in the normal coordinate treatment (429 cm^{-1}).§

The *cis*-structure for hydroxylamine is also possible. It was hoped that, by applying the product rule, one of the isomers might be favored over the other. However, the calculated values of I_z and I_z^i for the *cis*-configuration were so close to those for the *trans*-configuartion that the isotope product ratios were essentially equal. Therefore, one may conclude that, although the *trans*-form might be favored from the standpoint of bond repulsions, the infrared vibrational assignment can be fitted equally well to either isomer.

§ A complete normal coordinate treatment will be given in a separate communication.

The Dielectric Constant of Supercritical Steam*

JAMES K. FOGO,† SIDNEY W. BENSON, AND CHARLES S. COPELAND
Department of Chemistry, University of Southern California, Los Angeles 7, California
(Received September 8, 1953)

A description is given of the method used to measure the dielectric constant of steam at densities between 0.2 and 0.4 g/cc in the temperature range 377 to 395°C. Smoothed values of the dielectric constant are tabulated at 378, 383, 388, and 393°C for densities from 0.1 to 0.5 g/cc.

WHILE the dielectric constant of liquid water has been determined up to the critical temperature,[1] no studies appear to have been made in the supercritical region. Our own interest in this problem arose in connection with an investigation of the electrolytic conductance of NaCl in steam, when it became desirable to know the dielectric constants of steam at high pressures in the temperature range 375–400°C. We found that it was feasible to determine dielectric constants with the audio-frequency bridge already set up for resistance measurements, and accordingly the dielectric constant of supercritical steam was determined at various densities and temperatures.

EXPERIMENTAL

Apparatus

For the measurement of the dielectric constant and electrolytic conductivity of supercritical steam, and the electrolytic conductivity of NaCl in steam,[2] we required a capacitance-conductivity cell which could be used at temperatures above 374°C and at pressures up to 300 atmos. Full details are given elsewhere[3] of the construction of such a cell and of the pressure counterbalancing method developed to permit its use at high temperatures and pressures. Briefly, the cell consisted of two concentric platinum-iridium cylinders which formed the electrodes and which were insulated from each other by a synthetic sapphire separator. One cylinder formed the outer wall of the cell. The cell was so constructed that internal electrodes of various sizes could be used to give a replaceable capacitance or conductivity cell constant appropriate to the system investigated.

The audio-frequency parallel resistance-capacitance bridge circuit is shown in Fig. 1. The usual Wagner earth connection was omitted because of the practical necessity of operating with the outer electrode of the cell grounded. The bridge was well shielded from external influences, but was not completely shielded internally. As a consequence, there was a reproducible frequency dependence of the resistance balance and a reproducible resistance dependence of the capacitance balance. These aberrations were always small and due allowance was made for them in the calculation of the results.

The capacitors C_1 and C_2 (Fig. 1) were both equipped with precision drivers. The smaller capacitor, C_2, could be adjusted and read with about ten times the precision of C_1. These parallel capacitors were calibrated by direct substitution of a General Radio Company Type 722-D precision air capacitor. C_1 was found to be linear between 10 and 160 scale divisions (total range 0 to 180) with a capacitance of 6.58 mmf per division. C_2 was found to be linear between 1 and 15 revolutions (total range 0 to 15) with a capacitance of 8.00 mmf per revolution (total range 0 to 15) with a capacitance of 8.00 mmf per revolution.

The current generator for the bridge was a Hewlett-Packard Model 200B resistance-tuned oscillator. The output of this oscillator was continuously adjustable from 20 to 20 000 cps and zero to about 40 volts. Connection to the bridge was made with a coaxial cable.

The null detector used was a 3-inch oscilloscope without built-in amplifiers. Suitable high gain vertical and

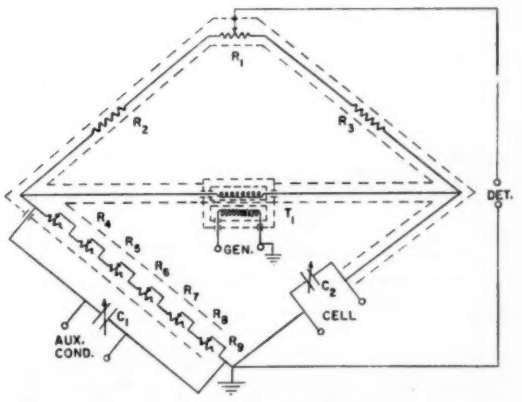

FIG. 1. The audio-frequency parallel resistance-capacitance circuit R_1, 3-ohm pot. IRC No. W-3. R_2, R_3 1000 ohms each, General Radio Company 500-H. R_4 through R_9, 0.1, 1, 10, 100, 1000, 1000 ohms per step decade resistors, General Radio Company 510-A through 510-F, respectively, C_1 and C_2. 1100 and 110 mmf, respectively, General Radio Company 848-B and 847-B. T_1 shielded transformer General Radio Company 578-A.

* This work was done under Contract No. N6onr238–11 between the U. S. Office of Naval Research and the University of Southern California and was presented in part at the XIIth International Congress of Pure and Applied Chemistry, New York, 1951.

† Present address, Union Oil Company of California Research Center, Brea, California.

[1] G. C. Akerlof and H. I. Oshry, J. Am. Chem. Soc. **72**, 2844 (1950). Values to 370°C are tabulated.

[2] Fogo, Benson, and Copeland, this issue.

[3] Fogo, Copeland, and Benson, Rev. Sci. Instr. **22**, 765 (1951).

horizontal amplifiers were constructed for use with the oscilloscope.

Connection between the bridge and the cell-pressure vessel assembly in the oven was made with a coaxial cable about a meter in length. Details of the electrical lead through the pressure vessel head and the cell-pressure vessel assembly are given in the paper cited under reference 2.

Measurements

The cell containing steam may be considered as electrically equivalent to a polarization capacitance, Cp, in series with a resistance, R_2, and with Cp and R_2 together in parallel with a dielectric-type capacitance, C_d. The impedance Z_2 of this circuit is given by the expression

$$\frac{1}{Z_2}=\frac{i\omega Cp}{i\omega CpR_2+1}+i\omega C_d, \tag{1}$$

where ω is 2π times the frequency.

The reference arm of the bridge, with a capacitance C_1 and a resistance R_1 in parallel has an impedance Z_1 given by the expression

$$\frac{1}{Z_1}=\frac{1}{R_1}+i\omega C_1. \tag{2}$$

It appears[4] that C_p may be represented by $C_p{}^0\omega^{-\frac{1}{2}}$. Then at infinite frequency, Eq. (1) becomes of the same form as Eq. (2) and we may identify R_2 with R_1 and C_d with C_1. Thus to obtain C_d it is necessary to determine C_1 at several frequencies and then by extrapolation to obtain the value of C_1 at infinite frequency.

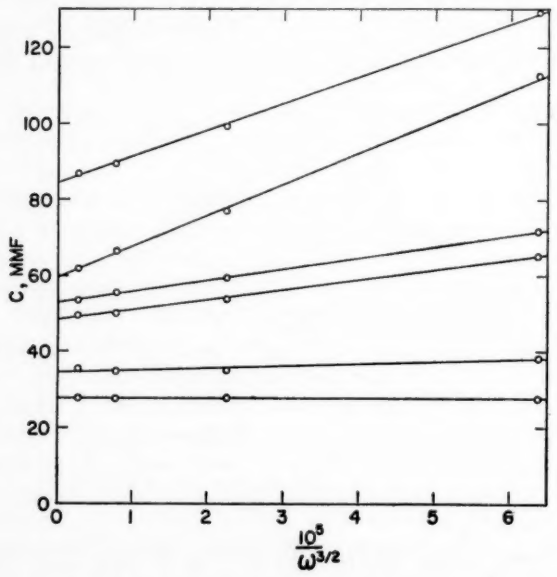

FIG. 2. Typical capacitance extrapolations to "infinite" frequency.

The dielectric-type capacitance C_d is defined by the equation

$$C_d=DC_r+c, \tag{3}$$

where D is the dielectric constant of the cell contents, C_r is the replaceable capacitance of the cell, and c is the lead capacitance (which includes all capacitances in the external circuit with the exception of C_r).

If, at a given temperature and pressure, we designate by $(C_1-c)^0$ the difference between the measured equivalent parallel capacitance C_1 of the cell circuit and the lead capacitance c, extrapolated to infinite frequency, then the dielectric constant of the cell contents is given by the equation

$$D=\frac{(C_1-c)^0}{C_r}. \tag{4}$$

Replaceable Capacitance

Measurements at 400, 1000, 2000, 4000, and 8000 cps were made of the equivalent parallel capacitance (C_1) when the bridge was connected to: (a) a nonreactive resistor; (b) the unfilled cell in parallel with the resistor; (c) the cell alone, filled with water[5] at known room temperature. For these measurements the cell was not mounted in the pressure vessel and short leads of negligible capacitance were used. The resistance of the cell filled with water was nearly the same as that of the resistor. The difference between measurements (a) and (b) at corresponding frequencies measured the total air capacitance of the cell. The difference between sets (a) and (c) at corresponding frequencies was plotted against the reciprocal of the 3/2 power of the frequency and extrapolated to infinite frequency. The difference between this extrapolated value and the air capacitance divided by the difference between the dielectric constants of water and air is the replaceable capacitance of the cell. The value found was 8.58 $\mu\mu$f. A calculation based on the coefficients of thermal expansion of the cell material indicated about a 0.3 percent increase in C_r from 25°C to 390°C.

Lead Capacitance

The unfilled and unsealed cell was mounted in the pressure vessel which was placed in the oven and connected to the bridge with the coaxial cable. The oven was heated to a desired temperature and nitrogen admitted to a desired pressure. In order to make it possible to balance the bridge, a 12 000-ohm nonreactive resistor was connected in parallel with the cell and lead. Measurements of the equivalent parallel capacitance were made at 400, 1000, 2000, 4000, and 8000 cps at several temperatures and pressures in the range 378–397°C and

[4] G. Jones and S. M. Christian, J. Am. Chem. Soc. **57**, 272 (1935).

[5] This water, as well as the water used subsequently, was distilled from a solution of potassium permanganate in distilled water. The specific conductances of the samples used ranged from 10^{-6} to 8.2×10^{-7} ohm^{-1} cm^{-1}.

TABLE I. Original results on the dielectric constant of steam.

Density g/cc	Temperature °C	Dielectric constant
0.2136	376.4	3.2_7
	382.5	3.2_1
0.2290	379.2	3.2_9
	384.9	3.2_9
	390.6	3.2_5
	395.6	3.2_5
0.2613	377.4	4.1_6
	383.5	4.1_6
	389.5	4.1_2
	395.6	4.0_5
0.2865	378.2	4.1_8
	383.6	4.1_8
	388.7	4.1_6
	393.6	4.1_2
0.3008	377.4	4.9_4
	382.5	4.8_9
	388.5	4.8_6
	393.6	4.8_3
0.3343	378.0	5.6_8
	383.5	5.6_2
	388.8	5.6_2
	393.6	5.6_1
0.3443	376.4	6.1_7
	382.6	6.1_3
	388.5	6.0_6
	392.6	5.9_3
0.4020	377.4	7.1_8
	383.2	7.0_9
	387.8	6.9_4
	393.2	6.9_4
0.5031	364.0	10.1_0[a]
	365.4	10.1_2[a]
	373.9	9.9_8

[a] Liquid phase.

230 to 275 atmos. The lead capacitance, for a given set of conditions, is given by the equation

$$c = C_1 - 1.05C_r, \tag{5}$$

where C_1 is the equivalent parallel capacitance and 1.05 is accurately enough the dielectric constant of nitrogen at the temperatures and pressures used.

The lead capacitance was found to be: practically independent of pressure; an accurately linear function of temperature at constant frequency; dependent upon frequency. Since all subsequent measurements with steam were made at the same frequencies already used, no frequency interpolations were ever necessary.

The Dielectric Constant of Steam

The dry, weighed cell was flushed with dry nitrogen and, while under a nitrogen tent, the desired amount of water was added from a hypodermic syringe. The cell was sealed and reweighed. The mean density of water in the cell was obtained from the weight of water added and the known cell volume.[6] The cell was mounted in the pressure vessel and the assembly heated. Values of the equivalent resistance and capacitance (C_1) were measured at several temperatures and at the selected frequencies previously mentioned. At temperature, just before measurements were made, the cell assembly was vigorously oscillated through 180° a number of times to insure thorough agitation of the cell contents. The oven was set in a horizontal position during the measurements since previous investigation had shown that in this position temperature gradients were minimized. Temperatures were measured with an iron-constantin thermocouple and a Leeds and Northrup direct reading potentiometer with automatic cold junction compensation. This potentiometer had been checked directly against the slide wire of an accurate potentiometer and the scale at all points was found to be in agreement with the standard table of iron-constantin electromotive forces. The thermocouple used was calibrated by comparison with a National Bureau of Standards certified Leeds and Northrup platinum-resistance thermometer.

After cooling, the cell was reweighed to verify that there had been no significant loss in weight. In general, the loss in weight of the cell did not amount to more than 4 mg or about 0.1 to 0.2 percent of the weight of water in the cell. Most of this loss is probably to be attributed to excessively thorough drying of the exterior of the cell.

From the values of the equivalent capacitance C_1 at different frequencies were subtracted the appropriate lead capacitances c. This difference was plotted against the reciprocal of the 3/2 power of the frequency and extrapolated to infinite frequency. A typical set of curves is shown in Fig. 2. From the extrapolated value of $(C_1 - c)$ the dielectric constant was obtained by means of Eq. (4).

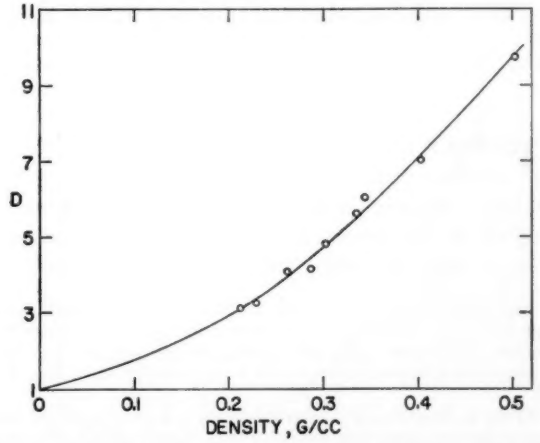

FIG. 3. The 388° isotherm of the dielectric constant of steam.

[6] The cell volume was determined at known room temperature from the weight of water required to fill the cell. It was estimated that the cell volume would increase 0.9 percent between 25 and 390°C. The volume was always redetermined after the cell had been dismantled for any reason. The volume was always close to 12 cc.

TABLE II. Dielectric constants of steam at various densities and temperatures.[a]

Density g/cc	Temperature, °C 378	383	388	393
0.10	1.85	1.84	1.83	1.82
0.15	2.36	2.33	2.31	2.29
0.20	2.97	2.94	2.91	2.89
0.23	3.43	3.39	3.36	3.33
0.26	3.97	3.93	3.89	3.85
0.29	4.58	4.53	4.49	4.45
0.32	5.26	5.21	5.17	5.13
0.34	5.75	5.70	5.65	5.60
0.36	6.25	6.19	6.13	6.07
0.38	6.76	6.69	6.62	6.55
0.40	7.27	7.19	7.12	7.05
0.45	8.58	8.49	8.40	8.31
0.50	9.94	9.83	9.72	9.61

[a] It is felt that the relative precision of the smoothed data warrants the use of three significant figures in order to show the temperature variation of the dielectric constant at constant density.

RESULTS

Table I gives the dielectric constant of steam at each of the experimental densities and temperatures. The results of 0.503 g/cc are of particular value in confirming the validity of the method used since the value at 364° can be compared directly with the value obtained by Akerlof and Oshry.[1] They report a dielectric constant of 10.7 for saturated water at 363.5°C (density=0.503 g/cc). In view of the experimental conditions, we consider our value of 10.1 to be in reasonably good agreement with the more precisely determined value of Akerlof and Oshry. The agreement obtained is taken as evidence that the method used is valid and not seriously affected by electrode polarization phenomena or other sources of error.

The dielectric constants of Table I were plotted against temperature at constant density, yielding very straight and parallel lines. The curves at 0.216 and 0.503 g/cc were extrapolated to 393°C parallel to the 0.229 and 0.402 g/cc curves, respectively. From the set of curves so obtained, interpolated values of the dielectric constant were found at 378, 383, 388, and 393°C. These values were plotted against density to give a set of four isotherms, one of which is shown in Fig. 3. The isotherms were drawn so as to pass smoothly through unity at zero density. The root-mean-square deviation of the points from the isotherms is about 2 percent. Dielectric constants obtained from the isotherms at selected densities are given in Table II.

The authors wish to express their thanks to the U.S. Office of Naval Research for its support of this work.

THE JOURNAL OF CHEMICAL PHYSICS VOLUME 22, NUMBER 2 FEBRUARY, 1954

The Electrical Conductivity of Supercritical Solutions of Sodium Chloride and Water*†

JAMES K. FOGO,‡ SIDNEY W. BENSON, AND CHARLES S. COPELAND
Department of Chemistry, University of Southern California, Los Angeles 7, California

(Received September 8, 1953)

A description is given of the method used to measure the electrical conductivity of NaCl in steam at steam densities between 0.2 and 0.4 g/cc. Values of the specific and equivalent conductances are tabulated at 378, 383, 388, and 393°C for various NaCl concentrations at different steam densities. Sodium chloride behaves as a weak electrolyte at all steam densities used. Estimates of the ion-pair dissociation constant K, based on Shedlovsky's method, indicate that K decreases from about 9×10^{-3} to 6×10^{-7} as the steam density decreases from 0.4 to 0.2 g/cc. Preliminary results for cesium chloride and hydrogen chloride in steam indicate that cesium chloride is comparable in strength with sodium chloride, but that hydrogen chloride is a much weaker electrolyte.

DESPITE the fact that it has been known for over seventy years that solvent vapors at high densities may dissolve relatively nonvolatile solutes, the study of the properties of such gaseous solutions represents a still virtually unexplored field.[1] Generally speaking, these solutions exist only at elevated pressures and usually at elevated temperatures. These conditions, particularly when steam is the solvent, present rather formidable experimental difficulties. The present paper gives our results on the electrolytic conductance of NaCl-steam solutions at temperatures above the critical temperature of water.

EXPERIMENTAL

Apparatus

Details of the construction of the conductivity cell and a discussion of the pressure counterbalancing method developed to permit its use at high tempera-

* This work was done under Contract No. N6onr238-11 between the U. S. Office of Naval Research and the University of Southern California and was presented in part at the XIIth International Congress of Pure and Applied Chemistry, New York, 1951.

† From a dissertation presented by Mr. Fogo in partial fullfilment of the requirements for the Ph.D. degree at the University of Southern California, 1954.

‡ Present address, Union Oil Company of California Research Center, Brea, California.

[1] The review article by H. S. Booth and R. M. Bidwell, Chem. Revs. 44, 477 (1949), covers the field in general. For the NaCl–H_2O system, see the papers by F. Spillner, Chem. Fabrik 13, 405 (1940); A. Olander and H. Liander, Acta Chem. Scandinavica 4, 1437 (1950); Copeland, Silverman, and Benson, J. Chem. Phys. 21, 12 (1953); Benson, Copeland, and Pearson, J. Chem. Phys. (to be published).

tures and pressures are given elsewhere.[2] The use of the cell is described and a description of the audio-frequency parallel resistance-capacitance bridge employed is given in another paper.[3]

The Cell Constant

The conductivity constant of the cell, defined as the product of specific conductance and measured resistance, was in all cases too small to measure with even the most dilute of the potassium chloride solutions used as secondary resistance standards. Instead, the cell constant was determined from measurements of the resistance of the cell when filled with dilute (about 10^{-4} M) hydrochloric acid solution. The specific conductance of the acid solution was obtained from the measured resistance of a Jones-type glass cell, of known conductivity constant, filled with the solution. All measurements were made at 25±0.01°C with a Leeds and Northrup Jones bridge[4] except in the one instance when the cell was fitted with a very large internal electrode for the measurement of the conductivity of steam. In this latter case, a sufficiently accurate cell constant was obtained from measurements made at room temperature with a bridge used to make our subsequent resistance measurements. Calculation based on the thermal coefficient of expansion of platinum-iridium indicated that about a 0.3 percent decrease in cell constant could be expected between 25 and 390°C. The cell constants were close to 0.01 cm^{-1} for the steam measurements and 0.09 cm^{-1} for the NaCl-steam measurements.

Preparation of Solutions

The water used in the preparation of solutions was obtained by distillation in an all-Pyrex glass still of a dilute solution of potassium permanganate in distilled water. The distillate was discarded until the specific conductance decreased to 10^{-6} ohm^{-1} cm^{-1} or less. Water so prepared was used immediately.

Solutions of sodium chloride in water were prepared on a weight basis. Dried, Baker's reagent grade sodium chloride was weighed into a small platinum boat on a microbalance. The boat and salt were then transferred into a dry 500-cc glass-stoppered Pyrex flask which was then weighed on an accurate kilogram balance before and after the introduction of 250 to 500 cc of the conductivity water described above. Five solutions were prepared, having different compositions between 3.6×10^{-5} and 1.1×10^{-2} mole NaCl/1000 g H_2O. The weights of salt and water were such that the compositions were known to ±0.5 percent or better. All solutions were stored in Pyrex flasks fitted with ground stoppers. Storage periods were kept as short as possible, particularly for the more dilute solutions.

[2] Fogo, Copeland, and Benson, Rev. Sci. Instr. **22**, 765 (1951).
[3] Fogo, Benson, and Copeland, J. Chem. Phys. (this issue).
[4] We are indebted to Prof. K. J. Mysels for permission to use this bridge.

Resistance Measurements

After temperature equilibrium had been established, the contents of the conductivity cell were agitated by vigorous oscillation of the oven through 180°. The oven was then set horizontally and resistance measurements were immediately made at 1000, 2000, 4000, and 8000 and again at 1000 cps. The total time required to take these measurements was about three minutes.

In no case was there found to be any significant dependence of resistance on frequency. The maximum variation among the five measurements of each set was about 0.2 percent. Because of this, and because the first observation at 1000 cps was made immediately after agitation of the cell contents, the initial resistances at 1000 cps have been used for calculation of specific conductances.

Resistance measurements were made with each of the five sodium chloride solutions at several different mean densities in the cell and at several temperatures in the range 377–395°C. In all, 100 measurements were made at 26 different composition-mean density combinations.

Examination of solubility data for NaCl in steam* indicated that at each density-composition combination and at each temperature only a single phase should have been present.

Resistance measurements with steam alone in the cell were made at eight different densities between 0.2 and 0.4 g/cc.

RESULTS

The specific conductance of steam at 1000 cps was plotted against temperature for each of the eight experimental densities. From these curves was obtained the necessary data to plot specific conductance-density isotherms, such as those shown in Fig. 1.

For each one of the 26 experiments made with NaCl solutions, the mean density of the steam in the cell was calculated from the cell volume and the weight and

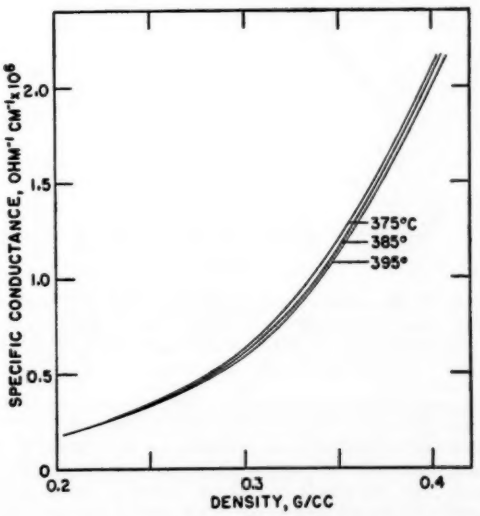

FIG. 1. The specific conductances of the steam used as solvent.

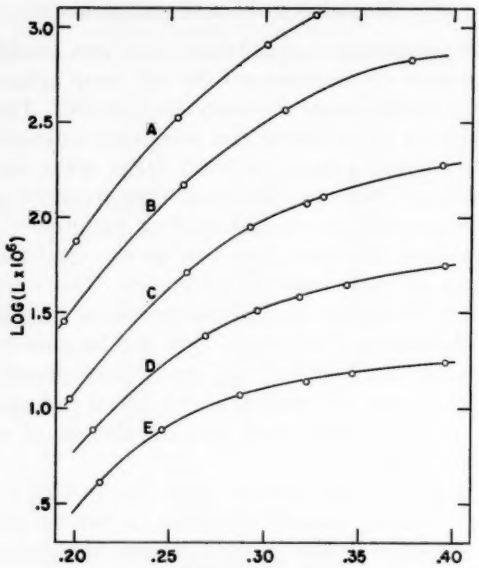

FIG. 2. The specific conductance of sodium chloride at constant composition as a function of the steam density. Molality$\times 10^5$: *A*, 1115; *B*, 246.1; *C*, 44.77; *D*, 11.96; *E*, 3.61.

composition of the solution in the cell.[5] The specific conductance of NaCl in the solution, hereafter designated by L, was obtained by subtraction of the specific conductance of steam from that of the solution.[6] The

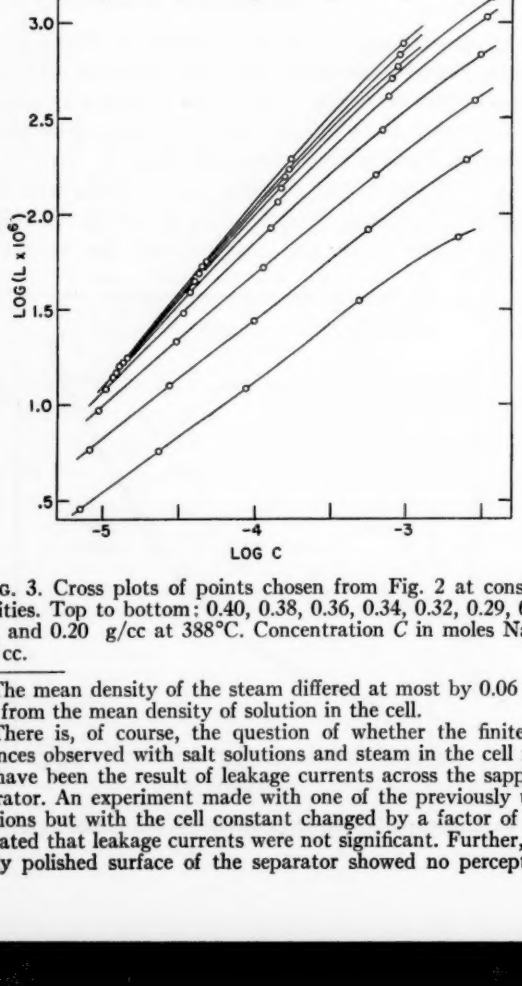

FIG. 3. Cross plots of points chosen from Fig. 2 at constant densities. Top to bottom: 0.40, 0.38, 0.36, 0.34, 0.32, 0.29, 0.26. 0.23, and 0.20 g/cc at 388°C. Concentration C in moles NaCl/1000 cc.

[5] The mean density of the steam differed at most by 0.06 percent from the mean density of solution in the cell.

[6] There is, of course, the question of whether the finite resistances observed with salt solutions and steam in the cell may not have been the result of leakage currents across the sapphire separator. An experiment made with one of the previously used solutions but with the cell constant changed by a factor of two indicated that leakage currents were not significant. Further, the highly polished surface of the separator showed no perceptible dulling, as would have been expected if it had been attacked by the solutions.

appropriate specific conductance of steam, at the temperature and steam density of the solution, was obtained by interpolation between curves such as those of Fig. 1. Log$L$ was then plotted against temperature for each of the 26 constant steam densities. From these curves were obtained values of log$L$ at 378, 383, 388, and 393°C.

We desired finally to obtain curves of equivalent conductance against the square root of the NaCl concentration (moles/1000 cc) at each of several constant steam densities and at the four selected temperatures. Such curves could not be obtained directly from the data at hand, since these data were the specific conductances of NaCl at 26 different steam densities and 26 different concentrations (moles/1000 cc) but at only five different compositions (moles/1000 g water). In order to eliminate the steam density as a variable, the following method of cross plotting was used.

For each of the five different compositions, and at each of the four selected temperatures, log$L$ was plotted against the steam density. The curves at 388°C are shown in Fig. 2. From such curves values of log$L$ were obtained at selected constant densities and at a fixed temperature. These values of log$L$ correspond to five different concentrations (moles/1000 cc) at each selected density and temperature. These values of log$L$ were then plotted against the logarithm of the concentration. The curves at 388°C are shown in Fig. 3. From such curves were obtained the values of log$L$ at constant steam density and temperature at a number of selected concentrations. From these data were calculated equivalent conductances of NaCl which were then plotted against the square root of the concentration for each of the several constant densities and temperatures. The isotherms at 388°C are shown in Fig. 4. Values of the equivalent conductance at different densities and concentrations, obtained from such isotherms, are given in Table I.

It is felt that little or no loss in accuracy resulted from the cross plotting. Large scales were used throughout. In the few instances where the experimental densities and temperatures were very close to the selected values, the equivalent conductance calculated directly from the original specific conductance of NaCl agreed to within less than one percent with the value read, or slightly interpolated, from isotherms such as those of Fig. 4. It may also be pointed out that while the curves of Fig. 3 need not have been used, such an omission would result in having at most five points for the plotting of the considerably curved equivalent conductance isotherms. Since the curves of Fig. 3 are only slightly curved, their use seems justified.

DISCUSSION

The curves of Fig. 4 indicate that NaCl in steam behaves as a weak electrolyte at all steam densities from 0.20 to 0.40 g/cc. It is also evident that the degree of

ionic association increases considerably as the steam density is lowered. These results are in qualitative agreement with the known behavior of strong electrolytes dissolved in solvents of low dielectric constant. In the present instance each steam density, of course, corresponds to a solvent of different dielectric constant.

It is interesting to note that at low concentrations the curves of Fig. 4 evidently cross, so that the limiting equivalent conductance of NaCl increases with decreasing steam density. This increase undoubtedly results from the increase in ionic mobilities as the steam density, and hence viscosity, is lowered.

The temperature dependency of the equivalent conductance is shown in Fig. 5. Since it is not obvious from Fig. 5, it may be pointed that the crossing of the several isotherms does not occur at the same concentration. Each pair of adjacent isotherms cross at slightly different concentrations: the higher the temperatures, the lower the concentration at the intersection. The inversion of the temperature coefficient of the equivalent conductance is analogous to that observed at relatively high temperatures for many electrolyte-liquid solvent systems.

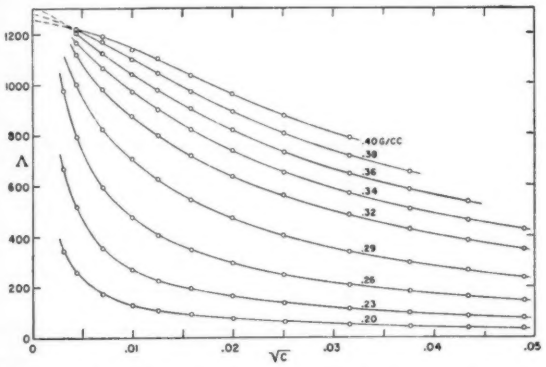

FIG. 4. The equivalent conductance of sodium chloride in steam at 388°C and various steam densities. Concentration C in moles NaCl/1000 cc.

It is of interest to attempt to estimate the values of the limiting equivalent conductance Λ^0 and the ion-pair dissociation constant K of NaCl in steam. To accomplish this, it was decided to use the method of Shedlovsky.[7] This requires that both the dielectric constant and viscosity of the solvent be known. The former we had already determined.[3] With regard to the latter, there appears to be no data available in the required density range. In order to obtain an estimate of the viscosity, the following procedure was used. The viscosities reported by Sigwart[8] for compressed water at 350, 360, and 370°C were plotted against density and in the density range 0.5 to 0.6 g/cc the course of the 388° isotherm was estimated by extrapolation at constant density of Sigwart's results. Up to about 0.1 g/cc the viscosity of steam was calculated by means of the equation obtained by Keyes.[9] The two branches of the isotherm were then connected across the intermediate density region. The completed isotherm indicates an increase in viscosity from about 3×10^{-4} poise to about 4.3×10^{-4} poise as the steam density is increased from 0.2 to 0.4 g/cc. If the basis on which the two branches of the curve were obtained is accepted, it is hard to

[7] T. Shedlovsky, J. Franklin Inst. **225**, 739 (1938).
[8] K. Sigwart, Forsch. Gebiete Ingenieurw. **7**, 125 (1936).
[9] F. G. Keyes, J. Am. Chem. Soc. **72**, 433 (1950).

TABLE I. Smoothed values of the equivalent conductance of sodium chloride in steam.

Steam density g/cc	Concentration $\times10^6$ mole/1000 cc	Equivalent conductance, ohm^{-1} cm^2 temperature, °C 378	383	388	393
0.4000	20.25	1174	1204	1219	1230
	64.00	1133	1160	1175	1188
	169.0	1057	1078	1086	1096
	400.0	943	954	958	960
	900.0	798	806	807	808
0.3800	20.25	1156	1190	1217	1226
	64.00	1097	1130	1148	1153
	169.0	1006	1025	1032	1036
	400.0	881	887	889	890
	900.0	731	734	736	735
0.3600	20.25	1140	1185	1203	1219
	64.00	1047	1090	1094	1103
	169.0	936	963	964	968
	400.0	799	816	816	816
	900.0	660	667	665	663
0.3400	20.25	1092	1140	1166	1191
	64.00	974	1011	1032	1038
	169.0	854	880	889	882
	400.0	719	738	736	726
	900.0	583	588	587	585
	1600	489	490	487	484
	2500	425	420	417	414
0.3200	20.25	1038	1096	1150	1136
	64.00	895	928	944	948
	169.0	767	782	787	783
	400.0	633	637	634	630
	900.0	501	500	497	492
	1600	414	410	406	400
	2500	351	347	340	332
0.2900	20.25	938	985	997	1005
	64.00	752	781	782	775
	169.0	608	616	614	604
	400.0	478	478	469	452
	900.0	369	364	353	335
	1600	296	292	283	268
	2500	246	240	232	221
0.2600	9.00	949	999	1008	1016
	36.00	667	672	661	646
	100.0	496	490	474	460
	256.0	372	361	347	329
	625.0	277	264	251	236
	1225	215	204	193	181
	2025	172.5	164.0	156.0	147.0
0.2300	9.00	725	716	685	652
	36.00	444	428	410	387
	100.0	306	286	269	252
	256.0	218	204	192	182
	625.0	158.0	149.5	139.5	132
	1225	120.5	114.0	104.5	97.5
	2025	96.0	89.5	82.5	76.5
0.2000	9.00	442	401	364	338
	36.00	240	220	202	186
	100.0	155	143	130	118
	256.0	108.5	100.5	91.0	83.5
	625.0	74.5	69.5	63.5	58.5
	1225	54.0	50.5	45.5	42.0
	2025	41.5	38.5	35.5	33.0

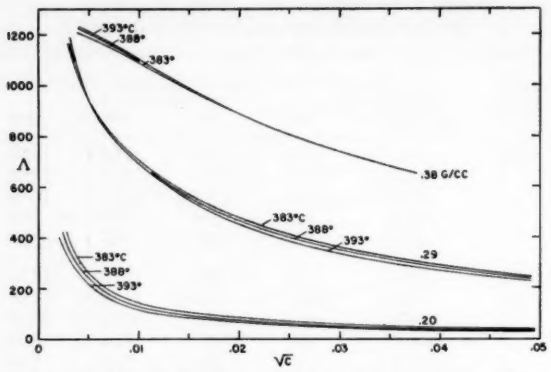

FIG. 5. Isotherms of the equivalent conductance of sodium chloride in steam at three steam densities.

imagine that the intermediate viscosities are in error by more than 10 percent.

Initial values of Λ^0 for the three highest steam densities were estimated from extrapolation of the appropriate curves of Fig. 4. The mean activity coefficients of NaCl were calculated from the Debye-Huckel limiting law equation and Shedlovsky plots were made. It was not possible to obtain straight lines over the entire concentration range. The final curves in the low concentration range are shown in Fig. 6.

To obtain estimates of Λ^0 at the lower densities, the final values of Λ^0 at the three highest densities were multiplied by the appropriate viscosity and the product Λ^0 was plotted against viscosity. From an extrapolation made to a viscosity of 3×10^{-4} poise (0.20 g/cc steam density) values of Λ^0 were obtained for steam densities from 0.20 to 0.34 g/cc. On the basis of our extrapolation, there is about a 20-percent decrease in the product Λ^0 from a steam density of 0.40 g/cc to one of 0.20 g/cc.

In the low concentration range the Shedlovsky plots were curved at all densities from 0.36 to 0.20 g/cc (Fig. 6). To obtain values of the ion-pair dissociation

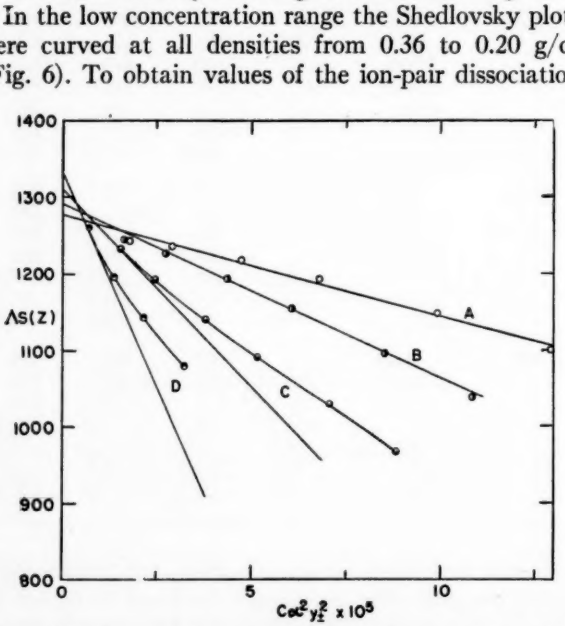

FIG. 6. Shedlovsky plots at low concentrations of sodium chloride in steam. Densities: *A*, 0.40; *B*, 0.38; *C*, 0.36; *D*, 0.34 g/cc. $S(Z)$ is Shedlovsky's function. C is the concentration in moles NaCl/1000 cc and α and y are the degree of dissociation and the mean activity coefficient, respectively, of the sodium chloride.

constant K, tangents were drawn from the selected value of Λ^0 to the curve, as shown in Fig. 6 for steam densities of 0.34 and 0.36 g/cc. Our present estimates of Λ^0 and K are given in Table II, together with the corresponding values of the effective ionic diameter a calculated from Bjerrum's equation.[10] While no great accuracy can be ascribed to the present values of Λ^0 and K, they are certainly indicative of the behavior of NaCl in steam. The values of the effective ionic diameter for the five highest densities are fairly constant and quite reasonable. The increase in the value at the lower densities most probably reflects the increasing inaccuracy of the data at the lower densities. Finally, on the basis of the equation developed by Fuoss and Kraus[11] for the prediction of the value of the dielectric constant below which triple ions are stable, it may be noted that, even if we assume the triple ions have twice the effective diameter of the ion-pairs (Table II), triple ions would be stable at all steam densities used.

We should like to mention that preliminary measurements were made of the conductance of cesium chloride and of hydrogen chloride in steam. The conductance of cesium chloride was determined at a steam density of 0.3256 ± 0.0005 g/cc and at cesium chloride concentrations from 12.26 to 728×10^{-6} moles/1000 cc. For hydrogen chloride, conductances were determined at a steam density of 0.3263 ± 0.0014 g/cc and at concentrations of 55.6, 245, and 758×10^{-6} moles/1000 cc and at a steam density of 0.3968 g/cc and a concentration of 67.3×10^{-6} moles/1000 cc. The results indicate that cesium chloride is very similar to sodium chloride in strength, but that hydrogen chloride is a much weaker electrolyte in steam than is sodium chloride. The equivalent conductance of hydrogen chloride at 388°C and a steam density of 0.3263 g/cc is about the same as that of sodium chloride at the same concentration and at a steam density of 0.20 g/cc (Fig. 4). The equivalent conductance at 0.3968 g/cc and at 388°C appears to fall about on the course of a 388° sodium chloride isotherm at a steam density of 0.25 g/cc.

TABLE II. Constants for sodium chloride in steam at 388°C.

Steam density g/cc	Λ_0 ohms^{-1} cm^2	K	cm$^a\times10^8$
0.40	1283	9.44×10^{-4}	3.92
0.38	1292	5.66×10^{-4}	3.95
0.36	1310	2.55×10^{-4}	3.83
0.34	1331	1.39×10^{-4}	3.92
0.32	1353	7.56×10^{-5}	4.06
0.29	1390	3.32×10^{-5}	4.38
0.26	1430	1.22×10^{-5}	4.67
0.23	1465	3.34×10^{-6}	4.88
0.20	1510	6.35×10^{-7}	4.96

The authors wish to express their thanks to the U. S. Office of Naval Research for their support of this work.

[10] H. S. Harned and B. B. Owen, *The Physical Chemistry of Electrolytic Solutions*, (Reinhold Publishing Corporation, New York, 1950), second edition, p. 190.

[11] R. M. Fuoss and C. A. Kraus, J. Am. Chem. Soc. **55**, 2387 (1933); **57**, 1 (1935).

The Infrared Spectra and Structure of LiOH, $LiOH \cdot H_2O$ and the Deuterium Species. Remark on Fundamental Frequency of OH^-*

LLEWELLYN H. JONES
Los Alamos Scientific Laboratory, University of California, Los Alamos, New Mexico
(Received August 6, 1953)

The infrared spectrum of a thin path of solid LiOH and $LiOH \cdot H_2O$ (undeuterated, partially deuterated, and completely deuterated) has been observed. The spectra indicate that both hydrogens from each water molecule are used to form strong hydrogen bonds in the hydrate. The results serve to substantiate the crystal structures previously determined by x-ray diffraction. For LiOH the absorption maximum occurs at 3678 ± 1 cm^{-1}; the fundamental frequency of OH^- in LiOH is 3839 ± 10 cm^{-1}. The spectrum of $LiOH \cdot HDO$ exhibits an anomaly in the bending frequency of HDO.

INTRODUCTION

THE crystal structure of lithium hydroxide monohydrate was studied with x-ray diffraction by R. Pepinsky.[1] He concluded that each lithium is at the center of a slightly distorted tetrahedron of oxygens (two hydroxyl and two water oxygens). Two such tetrahedra share an edge in a reflection plane (most likely through hydroxyl oxygens). Upper and lower corners of the paired tetrahedra are shared with tetrahedra in cells above and below, through water oxygens, resulting in unending chains of paired tetrahedra in the direction of the C axis. Oxygens of adjacent chains are separated by 2.68A, indicating strong hydrogen bonds linking chains together. The two hydroxyls within a tetrahedron are separated by 2.99A, indicating perhaps a weak hydrogen bond. Pepinsky shows that the most plausible structure is one in which each water molecule forms two strong hydrogen bonds with two different hydroxyl oxygens. If his conclusion is correct, the infrared spectrum should show a large decrease in the O—H stretching frequencies of the hydrate water.

The structure of LiOH was reported by Ernst.[2] It consists of layers of considerably distorted hydroxyl tetrahedra. Alternate layers have their tetrahedra completely filled with lithiums, but tetrahedra between these are completely empty. The closest approach of hydroxyl to hydroxyl is 3.05A, for four edges of a tetrahedron. Bonding between layers is very weak. The infrared spectrum of this substance should give a lower limit to the value of the vibrational frequency for the unperturbed $(OH)^-$ ion.

EXPERIMENTAL

A lithium mirror was formed by evaporating lithium in a vacuum onto a fluorite window. This disk was then placed in an evacuable absorption cell and exposed to CO_2-free water vapor (~17-mm pressure) until it was completely converted to $LiOH \cdot H_2O$, as determined by its spectrum. The H_2O can be completely removed by evacuation, leaving unhydrated LiOH. A similar experiment was performed using D_2O and later adding H_2O in order to observe the spectra of the partially and completely deuterated species.

To determine the amount of material in the path, a thin window was weighed on an Ainsworth Assay Balance (to 20 micrograms) empty, with LiOH, and with $LiOH \cdot H_2O$. As a further check, the sample was finally exposed to room air for several days and reweighed after complete conversion to Li_2CO_3.

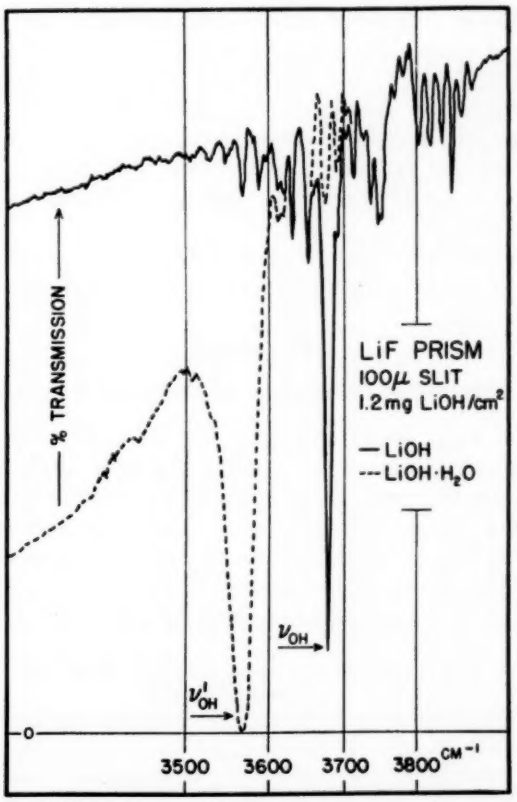

FIG. 1. Infrared spectrum of solid LiOH and $LiOH \cdot H_2O$ from 3300–3900 cm^{-1}. ν_{OH} = first harmonic of hydroxyl stretching vibration in LiOH. ν'_{OH} = first harmonic of hydroxyl stretching vibration in $LiOH \cdot H_2O$. Background includes absorption by water vapor.

* This work was sponsored by the U. S. Atomic Energy Commission.

[1] R. Pepinsky, Z. Krist., Abt. A., **102**, 119 (1940).
[2] Th. Ernst, Z. physik. Chem. (B) **20**, 65 (1933).

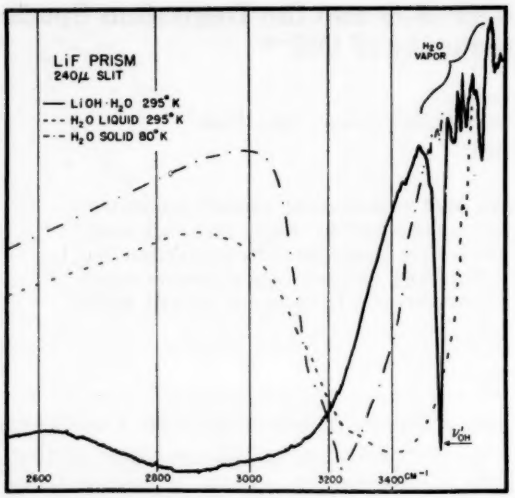

FIG. 2. Infrared spectrum of $LiOH \cdot H_2O$, H_2O liquid, and H_2O solid in region 2600–3800 cm^{-1}. Broad absorption by $LiOH \cdot H_2O$ from 2800–3200 cm^{-1} arises from H_2O stretching vibrations. ν'_{OH} = first harmonic of hydroxyl stretching vibration in $LiOH \cdot H_2O$.

RESULTS

Figure 1 shows the hydroxyl absorption bands of LiOH and $LiOH \cdot H_2O$. Figure 2 compares the spectrum of $LiOH \cdot H_2O$ with that of H_2O liquid and H_2O solid in the O—H stretching region. The spectra of the deuterated species are similar but displaced by the usual amount. In Fig. 3 are shown the H_2O bending vibration for the three isotopic species H_2O, HDO, and D_2O in partially deuterated lithium hydroxide monohydrate. The second harmonics of the OH^- vibration in unhydrated LiOH and LiOD were also observed with a LiF prism.

The results are tabulated in Table I, with the exception of the bending vibrations, which are tabulated in Table III.

DISCUSSION

1. Correlation of Spectra with Crystal Structure

The very broad and very low frequency for the stretching vibrations of hydrate water in $LiOH \cdot H_2O$ indicates that each water molecule uses both hydrogens in very strong hydrogen bonds. This is in agreement with the short O—O distance of 2.68A as discussed in the introduction. The formic acid dimer has a similar O—O distance, about 2.67A,[3] and a similarly low O—H stretching frequency at 3080 cm^{-1}.[4] The smallest O—O distance in ice is 2.76A,[5] indicating weaker hydrogen bonds than in the previous two substances. This is in agreement with the considerably higher stretching frequency of about 3250 cm^{-1} (see Fig. 2).

The very sharp O—H absorption band of unhydrated LiOH is decreased by 104 cm^{-1} and somewhat broadened in the monohydrate (Fig. 1). The OH—OH distance is in turn decreased from 3.05A to 2.99A. The decreased frequency probably arises from two sources: (1) a slight increase in association of hydroxyl with hydroxyl in the monohydrate, perhaps forming weak hydrogen bonds as:

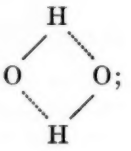

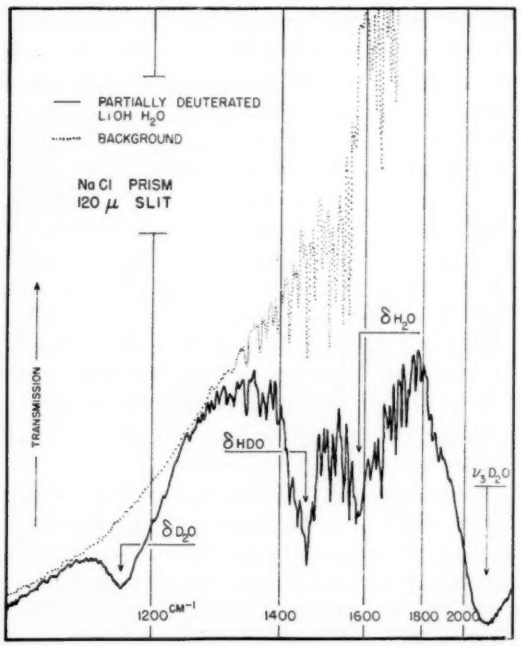

FIG. 3. Infrared spectrum of partially deuterated $LiOH \cdot H_2O$ from 1100–2200 cm^{-1}. δ_{H_2O} = bending vibration (ν_2) of H_2O. Background includes ν_2 of H_2O vapor.

(2) the hydrogen bonds from the water to the hydroxyl probably decrease the hydroxyl frequency somewhat.

2. Fundamental Frequencies for OH^- and OD^- and Comparison with OH and OH^+

In first approximation the term value of an anharmonic diatomic oscillator is given[6] by

$$G(v) = \omega_e(v+\tfrac{1}{2}) - \omega_e X_e(v+\tfrac{1}{2})^2, \qquad (1)$$

TABLE I. Observed infrared absorption bands in LiOH and $LiOH \cdot H_2O$.

	ν_{OH^-}	ν_{OD^-}	$2\nu_{OH^-}$	$2\nu_{OD^-}$	$\nu(H_2O)$[a]	$\nu(D_2O)$[a]
LiOH	3678±1	2708±1	7195±10	5330±10		
$LiOH \cdot H_2O$	3574±1	2632±1			3000	2200

[a] $\nu(H_2O)$ represents the frequency at the center of the broad absorption band arising from the stretching vibrations of H_2O.

[3] L. Pauling and L. O. Brockway, Proc. Nat. Acad. Sci. **20**, 336 (1934).

[4] L. G. Bonner and R. Hofstadter, J. Chem. Phys. **6**, 531 (1938).

[5] D. M. Dennison, Phys. Rev. **17**, 20 (1921); W. H. Bragg, Proc. Phys. Soc. (London) **34**, 98 (1922); W. H. Barnes, Proc. Roy. Soc. (London) **A125**, 670 (1929).

[6] G. Herzberg, *Spectra of Diatomic Molecules* (D. Van Nostrand Company, Inc., New York, 1950), p. 92.

TABLE II. Fundamental frequencies and anharmonic constants for hydroxyl groups in LiOH and LiOH·H_2O.

	$\omega_e(OH^-)$ cm^{-1}	$\omega_e(OD^-)$ cm^{-1}	$\omega_eX_e(OH^-)$ cm^{-1}	$\omega_eX_eOD(-)$ cm^{-1}	$\omega_e(OH^-)/\omega_e(OD^-)$	$[\mu_{OD}/\mu_{OH}]^{\frac{1}{2}}$[a]
LiOH	3839±10	2796±10	80.5±5	44.0±5	1.373±0.008	1.374
LiOH·H_2O	3735±10	2720±10	(80.5)[b]	(44.0)[b]	1.373±0.008	

[a] μ = reduced mass.
[b] The same values of ω_eX_e were assumed for LiOH·H_2O as were found for LiOH because the second harmonics for the hydrates were not observed.

TABLE III. Bending frequencies for H_2O, D_2O, and HDO in LiOH·H_2O, in the gas, and in the liquid.

	δ_{H_2O} cm^{-1}	δ_{D_2O} cm^{-1}	δ_{HDO} cm^{-1}	R_{H_2O}[a]	R_{D_2O}[a]	R_{HDO}[a]
LiOH·H_2O	1586±8	1167±3	1450±6	0.994±0.005	0.990±0.003	1.034±0.005
H_2O gas	1595.0	1178.7	1402			
H_2O liquid	1650±8	1212±3	1450±6	1.034±0.005	1.028±0.003	1.034±0.005

[a] $R_{H_2O} = \delta_{H_2O}/\delta_{H_2O}$ (gas).

where ω_e is the fundamental frequency for vibrations of infinitesimal amplitude and v is the quantum number of the vibration. ω_eX_e is the anharmonicity constant. Thus for the first harmonic transition $v=0\rightarrow v=1$

$$\nu_{0\rightarrow1}=G(1)-G(0)=\omega_e-2\omega_eX_e, \quad (2)$$

and for the second harmonic

$$\nu_{0\rightarrow2}=G(2)-G(0)=2\omega_e-6\omega_eX_e. \quad (3)$$

Substituting the observed values (Table I) of $\nu_{0\rightarrow1}(\nu_{OH})$ and $\nu_{0\rightarrow2}(2\nu_{OH})$ in Eqs. (2) and (3), we arrive at the results in Table II.

If the force constants in OD^- and OH^- are the same in similar surroundings, then the fundamental frequencies should be inversely proportional to the square root of the reduced masses. The agreement of the last two columns in Table II supports the usual assumption of similarity in force constants.

For the electronic ground state of the OH and OD molecules Herzberg[7] reports $\omega_e=3735.2$ and 2720.9 cm^{-1}, respectively, and $\omega_eX_e=82.81$ and 44.2 cm^{-1}, respectively. Thus, the calculated values of ω_eX_e for OH^- and OD^- are similar to those of the neutral molecules. The fundamental frequency for unperturbed OH^- is definitely greater than that for the neutral OH molecule which is, in turn, considerably greater than that reported for $(OH)^+$, 2955 cm^{-1}.[7] Though the frequency reported here for OH^- is not for the gas molecule, that for OH^- gas would be similar but greater since, on the average, it would be further from neighboring ions. Thus the ratio of fundamental frequencies and force constants is in the order $k_{OH^-}>k_{OH}>k_{(OH)^+}$.

It is interesting that the fundamental hydroxyl frequencies in hydrated LiOH and LiOD are practically identical with those of the neutral OH and OD molecules (see Table II and above paragraph). The close agreement suggests that the hydrogen bonds in the hydrate tend to completely neutralize the negative charge of the hydroxyl oxygens.

[7] G. Herzberg, *Spectra of Diatomic Molecules* (D. van Nostrand Company, Inc., New York, 1950), p. 560.

3. Anomaly in Bending Vibration of HDO

Of the two stretching vibrations of HDO, one is similar to ν_3 of D_2O and one to ν_3 of H_2O. Since the H_2O and D_2O absorption is so broad for LiOH·H_2O, the HDO does not change the spectrum appreciably on the O—H and O—D stretching regions. However, the bending vibrations of the three species yield three absorption bands as shown in Fig. 3. The results are tabulated in Table III along with the observed frequencies for gaseous[8] and liquid[9] H_2O, D_2O, and HDO.

As seen in Table III, the ratio of the H_2O bending vibration in LiOH·H_2O to that in H_2O gas is about the same for H_2O and D_2O, but considerably different for HDO. For liquid H_2O, D_2O, and HDO, the three corresponding ratios are similar. Thus in partially deuterated lithium hydroxide monohydrate there appears to be an anomaly in the frequency of the bending vibration of hydrate HDO.

With the instrument used there was detected no change in the hydroxide frequency of lithium hydroxide monohydrate, whether hydrated by H_2O, HDO, or D_2O. This makes it seem unlikely that there is any difference in the strength of the hydrogen bonds formed by H_2O, HDO, and D_2O. Thus, the anomaly in the HDO bending vibration of LiOH·HDO cannot be explained on this basis. It is hoped that further experiments will explain this result.

Bending frequencies were observed at 80° Kelvin, also. The bands were slightly narrower than at room temperature, but there was no appreciable frequency shift of the maximum.

Author's note.—After the above was submitted for publication, the author's attention was called to a paper, "The Spectra and Structure of NaOH and NaOD," presented by W. R. Busing of Yale University at the Ohio State Symposium on Molecular Structure and Spectroscopy, June, 1953.

[8] E. F. Barker and W. W. Sleator, J. Chem. Phys. **3**, 660 (1935); G. Herzberg, *Infrared and Raman Spectra* (D. van Nostrand Company, Inc., New York, 1947), p. 282.
[9] Values obtained in this laboratory by the author.

Occurrence of Natural $p-n$ Junctions in Lead Selenide*

ARTHUR E. GOLDBERG AND GEORGE R. MITCHELL
Chicago Midway Laboratories, Chicago, Illinois

(Received July 10, 1953)

Single crystals of PbSe were grown from melts in sealed quartz tubes. Except for a very narrow range of initial melt compositions, stoichiometric excesses of Pb or Se in the melt resulted in crystals that were wholly n or p type, respectively. Initial composition within the critical range yielded crystals showing both p and n regions.

The electrical resistivities were related to crystal compositions permitting the construction of the Pb-Se phase diagram in a narrow region about the compound PbSe. The invariant melting point for the system falls in the Se-rich region. This precludes the possibility of growing a crystal from a melt which is of stoichiometric composition throughout.

THE compounds lead sulfide (PbS), lead selenide (PbSe), and lead telluride (PbTe) offer an interesting series of semiconducting materials. The unusually high photoconductive sensitivities of specially treated thin films of these substances are well known. More recently these compounds have been prepared as single crystals[1] and their bulk properties studied. Very striking differences between the properties of thin films and the bulk materials have been reported.[2,3]

In this investigation single crystals of PbSe were grown from melts of precisely controlled compositions. The purest Pb and Se available commercially were used as starting materials. They were Pb (99.995 percent) and Se (99.92 percent). A combined chemical and spectrographic analysis of the selenium revealed the major impurity as Te (0.025 percent). Other impurities present were Fe (0.0025 percent), SiO_2 (0.0008 percent), and S (0.0006 percent).

The crystals were prepared by a method similar to that of W. D. Lawson.[1] A refinement of technique, manipulation of the vacuum-enclosed Se and Pb by means of magnetic gates, permitted quantitative introduction of these materials into the quartz reaction chamber. The resulting samples were shown to be single crystals by means of gentle sandblasting and by parallelism of cleavage planes. Back reflection Laue photographs of several samples also showed the materials to be single crystals. Figure 1 is of interest because it demonstrates the effectiveness of the sandblast etch in bringing out grain boundaries on polycrystalline PbSe.

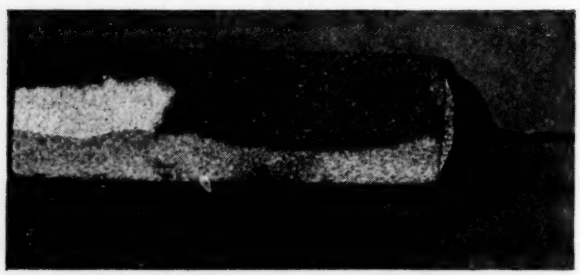

FIG. 1. A polycrystalline ingot of PbSe. Etching was accomplished by gentle sand-blasting.

RESULTS

It is found, in agreement with previous work,[1] that crystals grown from melts containing fairly large stoichiometric excesses of Pb or of Se exhibit conduction principally by electrons or by holes, respectively. The component in excess is largely rejected during crystal growth and appears as a separate phase at the top of the crystal. The Pb-Se phase diagram[4] identifies the Pb-rich residue as pure Pb and the Se-rich residue as $PbSe_2$. Rejection of the component in excess results in a melt which becomes progressively richer in this component during crystal growth; nevertheless, the resistivity of the resulting crystal is sensibly constant throughout its length. In the case of n-type crystals the resistivity varies from 3×10^{-3} to 2×10^{-3} ohm-cm as the melt composition varies from 50.1–52.5 atom percent Pb.

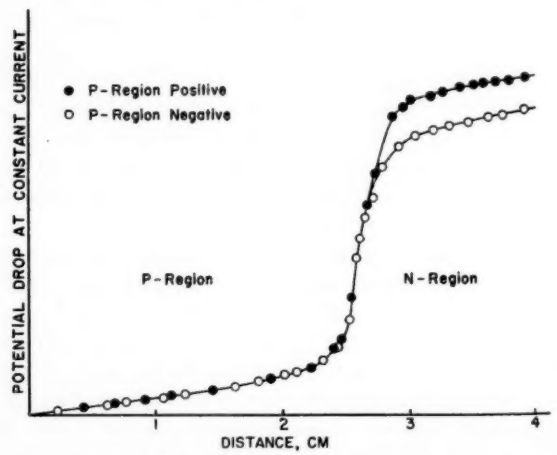

FIG. 2. Potential measurements on a single crystal of PbSe containing a natural p-n junction.

* This research was supported in whole by the United States Air Force under Contract No. AF 33(038)-25913, monitored by Wright Air Development Center.

[1] W. D. Lawson, J. Appl. Phys. **23**, 495 (1952).
[2] A. F. Gibson, Proc. Phys. Soc. (London) **65B**, 378 (1952).
[3] M. A. Clark and R. J. Cashman, Phys. Rev. **85**, 1043 (1952).
[4] *International Critical Tables* (McGraw-Hill Book Company, Inc., New York, 1928), Vol. IV, p. 27.

Crystals grown from melts with initial compositions in a narrow range near stoichiometry exhibit both p- and n-type regions. A small amount of Pb is observed on top of the crystal. Figure 2 shows the potential at constant current as measured by point probes along such a crystal in the direction of crystal growth. The splitting of the curves for the two directions of current has been shown to be the result of thermal effects rather than rectification. The resistivities in both the n and p regions are approximately 3×10^{-3} ohm-cm.

Figure 3 shows the position of the junction as a function of the initial composition of the melt. The precision of the results appears to be generally of the order ±0.01 atom percent. Because of possible systematic errors the position of the curve as plotted along the composition axis may be in error by several times this value. These errors could include systematic weighing errors and possible uncertainties in atomic weights. The dashed line represents a correction of the experimental results. The reasons for this correction are discussed in the following paragraphs.

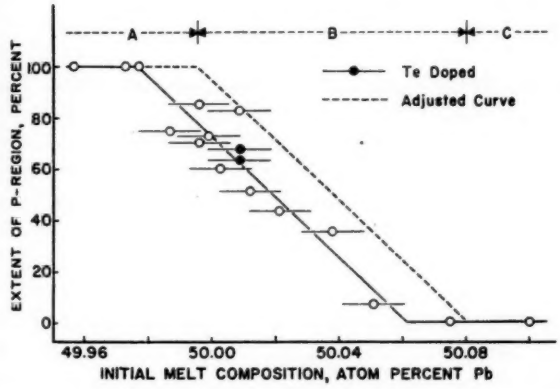

FIG. 3. Positions of naturally occurring p-n junctions in PbSe crystals as a function of initial melt composition.

With the aid of certain assumptions the results shown in Fig. 3 were used to construct the phase diagram for the Pb-Se system in a narrow region about the compound PbSe. The necessary assumptions were that each excess Se atom in the crystal behaves as a single ionized acceptor, and each excess Pb atom represents a singly ionized donor, at room temperature. Thus, the crystal composition may be inferred from a knowledge of carrier mobilities[5] and conductivities. The resulting diagram is shown in Fig. 4. The temperature scale is estimated from the gross phase diagram[4] and curves a-b and b-c are approximated by straight lines in this narrow region. The slope of curve a-b is unknown inasmuch as the phase diagram for this region has not been reported. The diagram is divided into the three regions A, B, and C which are related to those of Fig. 3. A crystal grown from a melt with an initial composition in region C is entirely n type and is accompanied by a

[5] C. A. Hogarth, Proc. Phys. Soc. (London) **64B**, 822 (1950).

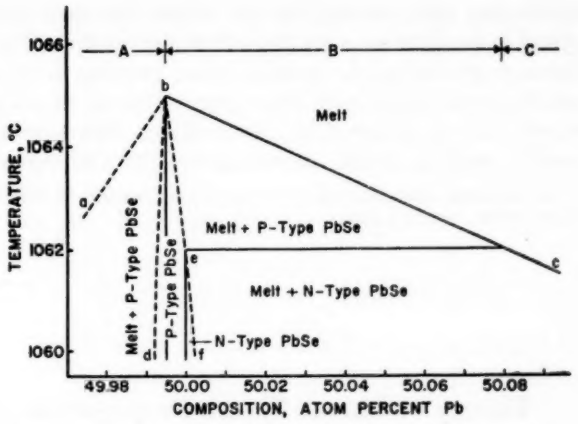

FIG. 4. Phase diagram for the Pb-Se system in the region of the compound PbSe.

final phase of Pb. The variation of composition and therefore resistivity along the direction of growth is defined by curve e-f. A melt of initial composition in region A yields a crystal wholly p type and of composition determined by curve $b-d$. A separate phase of $PbSe_2$ appears in this case. Finally, a crystal grown from a melt in region B exhibits an initial p region followed by the transition to the n region as given by curve b-e-f. This crystal also is accompanied by a final phase of Pb.

The p-n junction occurs at point e representing a stoichiometric crystal. The invariant melting point for the system, the point at which the melt and crystal are of identical composition, occurs at b. This crystal is p type and its composition, constant throughout, is approximately 0.005 atom percent from stoichiometry as inferred from conductivity measurements. The experimental curve of Fig. 3 has been translated so that the junction of regions A and B occurs at this composition.

The possibility has been considered that one or more impurities in the starting materials may segregate during crystal growth to produce the p-n junction.[6] In this connection the only known impurity present in sufficient quantity to warrant consideration is the Te contained in the Se. Two crystals were grown from melts containing additions of Te such as to increase its concentration fivefold. The initial melt composition was adjusted to make the atom percent Pb fall in region B, Fig. 3. The two points identified by solid circles represent the Te-doped samples. Within experimental error the resulting crystals exhibited p-n junctions with positions corresponding to the results with undoped samples.

CONCLUSIONS

This experiment has shown that the invariant melting point for the Pb-Se system in the region of the compound PbSe occurs in the Se-rich region (approximately 50.005 atomic percent Se). The invariant point

[6] R. H. McFee, J. Chem. Phys. **15**, 856 (1947).

defines the sole composition for which the melt and crystal in equilibrium are of identical composition. This situation precludes the possibility of growing from a melt in equilibrium with its vapor a crystal which is entirely of stoichiometric composition. Other compounds, notably Cu_2Sb, behave similarly.[7] Our experiments indicate that CdSb also exhibits this behavior. This phenomenon may be quite general and conceivably may present a serious obstacle to the development of some compounds as transistor materials.

The authors wish to thank Dr. F. F. Rieke for guidance and suggestions and Mr. F. Pizzarello for assistance with the measurements.

[7] M. Hansen, *Der Aufbau der Zweistofflegierungen* (Springer, Berlin, 1936), pp. 614–620.

THE JOURNAL OF CHEMICAL PHYSICS VOLUME 22, NUMBER 2 FEBRUARY, 1954

Theory of Linear Flame Propagation. Part I. Existence, Uniqueness, and Stability of the Steady State*

DAVID LAYZER
Harvard College Observatory and Forrestal Research Center, Princeton University, Princeton, New Jersey
(Received October 29, 1953)

It is shown that the equations governing the steady, adiabatic, one-dimensional propagation of single-reaction flames admit an infinity of solutions, only one of which, however, can be realized physically. The steady state is shown to be stable against small perturbations, and the possibility of reconciling this result with apparently contradictory experimental data is discussed.

1. INTRODUCTION

EXPERIMENTS suggest that every nondetonable mixture of explosive and inert gases can support a steady plane deflagration wave if the proportion of explosive gas in the mixture exceeds a certain limit, which, together with the speed and structure of the deflagration wave, is uniquely determined by the explosive, the diluent, the pressure, and the temperature. This paper seeks to provide the basis for a theoretical understanding of these phenomena.

Although it is generally agreed upon that the equations governing the structure of slow deflagration waves ought to possess one and only one steady state solution satisfying the appropriate boundary conditions, the usual flame equations[1] manifestly have no such solution whatever. Hirschfelder and Curtiss sought to overcome this difficulty by altering one of the boundary conditions; but in so doing they created a fresh difficulty in the shape of a flame-holder equipped with Maxwell demons.[2] We shall find that the original difficulty stems from a logical inconsistency in the usual formulation of the problem. After developing a self-consistent and unambiguous set of equations and boundary conditions for steady flame propagation (Sec. 2), we shall, in Sec. 3, investigate the multiplicity and physical significance of the solutions that satisfy the boundary conditions.

The stability of the steady state has been discussed previously by Lewis and von Elbe,[3] though without any definite results. These writers set out to establish relations between various parameters describing the overall structure of a perturbed deflagration wave. Since it is impossible to give definitions of such quantities as the flame width and "the percentage of excess enthalpy in the reaction zone" that are both precise and useful—at least in the general case of nonsteady propagation—the discussion was necessarily semiqualitative. Lewis and von Elbe held that under certain conditions the flame width will increase indefinitely in the course of time if it ever exceeds its steady-state value by an infinitesimal amount, but they were unable to deduce these conditions on theoretical grounds. In Sec. 4 of the present paper we shall develop a rather different approach to the problem of stability from that used by Lewis and von Elbe.

2. THE STEADY STATE AS AN APPROXIMATION TO REALITY

In a hypothetical steady state of flame propagation the temperature and chemical composition of the cold gas (i.e., the gas at an infinite distance ahead of the flame front) are constant in time. But in actual explosive mixtures the reaction rate remains finite as long as the temperature remains finite. Consequently, the flame equations can have no true steady-state solutions unless the cold gas is at zero temperature.

In practice, however, the temperature and chemical composition of the cold gas remain sensibly constant

* This work was supported in part by the U. S. Air Force Cambridge Research Center under Contract AF19(604)-146 with Harvard University.

[1] See, e.g., J. Corner, Proc. Roy. Soc. (London) **A198**, 388 (1949).

[2] J. O. Hirschfelder and C. F. Curtiss, *Third Symposium on Combustion and Flame and Explosion Phenomena* (Williams and Wilkins, Baltimore, 1949), p. 121.

[3] B. Lewis and G. von Elbe, *Combustion, Flames and Explosions of Gases* (Academic Press, Inc., New York, 1951), pp. 351, 369–371.

during time intervals appreciably greater than the characteristic time (flame width)/(flame speed), so that we may neglect the effects of chemical reaction in the cold gas. That is, we may represent all reaction rates by slightly incorrect expressions that vanish at the temperature of the cold gas, and, if need be, allow the boundary conditions to vary slowly with time. One can justify this procedure by showing that the solutions of the emended flame equations are insensitive to small changes in the reaction rates near the temperature of the cold gas.

3. FORMULATION OF THE FLAME EQUATIONS AND BOUNDARY CONDITIONS

We shall confine our attention to single-reaction flames, so that we may regard the gas as a mixture of two constituents, the reactant and the product. Assuming that there exists a steady state of linear flame propagation, we shall refer all physical quantities to a frame in which they depend upon the x coordinate alone.

By definition

$$m=\rho u; \tag{3.1}$$

$$\rho^{(1)}\equiv(1-\epsilon)\rho, \quad \rho^{(2)}\equiv\epsilon\rho; \tag{3.2}$$

$$m^{(1)}=\rho^{(1)}u^{(1)}\equiv(1-\Gamma)m, \quad m^{(2)}=\rho^{(2)}u^{(2)}\equiv\Gamma m, \tag{3.3}$$

where ρ, u, and m represent mass density, flow velocity, and mass flux, respectively, and the superscripts (1) and (2) refer, respectively, to the reactant and product constituents. By (3.1)–(3.3)

$$m(\epsilon-\Gamma)=\rho^{(2)}(u-u^{(2)})=-\rho^{(1)}(u-u^{(1)}), \tag{3.4}$$

so that

$$m(\epsilon-\Gamma)=D_{12}\rho\frac{d\epsilon}{dx} \tag{3.5}$$

if we neglect thermal diffusion and ignore the effects of both constituents' being, in general, mixtures rather than pure gases.

Altogether, seven variables enter into a description of steady flame propagation: p, ρ, T, ϵ, Γ, m, and the independent variable x. These are connected by Eq. (3.5), the equations of total mass, momentum, and energy balance, an equation of continuity for either the reactant or the product constituent, and an equation of state—six equations in all.

Conservation of mass.—The mass flux

$$m=\text{constant}. \tag{3.6}$$

Conservation of momentum.—The momentum flux

$$p+\rho u^2-\frac{4}{3}\frac{\eta}{}\frac{du}{dx}=p_0=\text{constant}. \tag{3.7}$$

We shall find that the flame width $L\approx\lambda/mc_p$, where λ is the thermal conductivity. Hence the contribution to the momentum flux arising from viscosity is of order $\eta u/L\approx\eta muc_p/\lambda\approx\rho u^2$ within the reaction zone: the viscosity term is of the same order of magnitude as the dynamic term in (3.7), and the ratio $(p_0-p)/p_0\approx M^2$, where M is the Mach number of the flow. When $M^2\ll1$ one may neglect the variation of pressure in calculating the functions T, ρ, ϵ, and Γ. Having found $\rho(x)$ and the constant m one can then use (3.7) to calculate $p(x)$.

Conservation of energy.—The energy flux

$$Q=-\lambda\frac{dT}{dx}+m\{(1-\Gamma)h^{(1)}+\Gamma h^{(2)}+\tfrac{1}{2}\rho u^2\}=Q_1=Q_2, \tag{3.8}$$

where h is specific enthalpy, and Q_1 and Q_2 stand for $Q(-\infty)$ and $Q(+\infty)$, respectively. (In the following, the subscripts 1 and 2 always have this meaning.) Assuming that each constituent obeys the perfect gas law we have

$$h^{(i)}=q^{(i)}+\int_{T_1}^{T}c_p^{(i)}dT. \tag{3.9}$$

By (3.8) and (3.9)

$$\frac{\lambda}{m}\frac{dT}{dx}=\int_{T_1}^{T}c_p dT-(\Gamma-\Gamma_1)q, \tag{3.10}$$

with the abbreviations

$$q\equiv q^{(1)}-q^{(2)}, \tag{3.11}$$

$$\int_{T_1}^{T}c_p dT\equiv(1-\Gamma)\int_{T_1}^{T}c_p^{(1)}dT+\Gamma\int_{T_1}^{T}c_p^{(2)}dT. \tag{3.12}$$

By (3.10)

$$\int_{T_1}^{T_2}c_p dT=(\Gamma_2-\Gamma_1)q. \tag{3.13}$$

Continuity.—

$$\frac{d(\Gamma m)}{dx}=\Psi(\epsilon,\rho,T), \tag{3.14}$$

where Ψ is the reaction rate and has dimensions $[ML^{-3}T^{-1}]$. In a steady state the reaction rate vanishes infinitely far ahead of the flame front and infinitely far behind it. Hence

$$\Psi(\epsilon_i,\rho_i,T_i)=0 \quad (i=1,2). \tag{3.15}$$

Perfect-gas equation.—

$$p=R_0\left(\frac{1-\epsilon}{\mu^{(1)}}+\frac{\epsilon}{\mu^{(2)}}\right)\rho T. \tag{3.16}$$

Ten constants of integration appear in the flame equations: p_0, $\rho_{1,2}$, $T_{1,2}$, $\epsilon_{1,2}$, and m. $\rho_{1,2}$ may be eliminated by means of (3.16). Further, since the gradients of all dependent variables vanish at $x=\pm\infty$ (3.5) shows that

$$\epsilon_1=\Gamma_1, \quad \epsilon_2=\Gamma_2. \tag{3.17}$$

T_1, p_0, and ϵ_1 (which measures the dilution of the unburnt gas) are initial data, and ϵ_2 and T_2 are determined by the simultaneous Eqs. (3.13) and (3.15$_2$). This leaves only m undetermined; m is an eigenvalue of the system of flame equations and boundary conditions.

We shall find it convenient to rewrite the flame equations in terms of new dependent variables. Let

$$\left.\begin{aligned} \theta &= \int_{T_1}^{T} c_p dT/q(\Gamma_2-\Gamma_1) \\ &= \int_{T_1}^{T} c_p dT \Big/ \int_{T_1}^{T_2} c_p dT; \\ \frac{\Gamma-\Gamma_1}{\Gamma_2-\Gamma_1} &\to \Gamma, \quad \frac{\epsilon-\epsilon_1}{\epsilon-\epsilon_2} \to \epsilon, \quad \frac{\Psi(\epsilon,\rho,T)}{\Gamma_2-\Gamma_1} \equiv \Phi(\epsilon,\theta). \end{aligned}\right\} \tag{3.18}$$

Then (3.5), (3.10), and (3.14) become

$$\frac{d\epsilon}{dx} = \frac{m}{D_{12}\rho}(\epsilon-\Gamma), \tag{3.19}$$

$$\frac{d\theta}{dx} = \frac{mc_p}{\lambda}(\theta-\Gamma), \tag{3.20}$$

$$\frac{d\Gamma}{dx} = \frac{\Phi}{m}; \tag{3.21}$$

and the new boundary conditions are

$$\left.\begin{aligned} \epsilon_1=\Gamma_1=\theta_1=0 \quad (x=-\infty) \\ \epsilon_2=\Gamma_2=\theta_2=1 \quad (x=+\infty) \end{aligned}\right\}. \tag{3.22}$$

4. VALIDITY OF A MACROSCOPIC DESCRIPTION

The equations of Sec. 3 embody a macroscopic description of flame propagation, and therefore depend upon a number of implicit assumptions. In this section we shall derive the conditions under which these assumptions are valid.

Thermal conduction, viscosity, and diffusion admit a macroscopic description if the molecular free path l is much smaller than the flame width L. L (like l) can be defined in three different ways:

$$\left.\begin{aligned} L_\epsilon &= \left(\frac{d\epsilon}{dx}\right)^{-1}_{\max} = \frac{1}{m}\left(\frac{D_{12}\rho}{\epsilon-\Gamma}\right)_{\min} > \frac{(D^{12}\rho)^*}{m}, \\ L_\theta &= \left(\frac{d\theta}{dx}\right)^{-1}_{\max} = \frac{1}{m}\left(\frac{\lambda}{c_p(\theta-\Gamma)}\right)_{\min} > \frac{1}{m}\left(\frac{\lambda}{c_p}\right)^*, \\ L_\Gamma &= \left(\frac{d\Gamma}{dx}\right)^{-1}_{\max} = \frac{m}{\Phi^*}, \end{aligned}\right\} \tag{4.1}$$

where the asterisk has an obvious meaning. Using either the first or the second definition we obtain

$$l/L<M, \tag{4.2}$$

since

$$\lambda \approx c_p\eta \approx c_p l\bar{c}\rho, \quad D_{12} \approx \eta/\rho \approx l\bar{c}.$$

According to (4.2) a macroscopic description of transport phenomena is valid within the flame itself if the flame speed is much smaller than the speed of sound in the flame.

Our description of heating by chemical reaction will be valid if the time of relaxation of the gas is much smaller than the characteristic time for flame propagation, i.e., if

$$l/\bar{c} \ll L/u.$$

By (4.2) this condition is equivalent to the condition $M^2 \ll 1$. Finally, one can show, using the third of the definitions (4.1), that fluctuations in the reaction rate are negligible provided that the flame width is much greater than the average distance between molecules.

We conclude that the flame equations of Sec. 3 are valid if they predict flame speeds much smaller than the speed of sound, which is also the condition that compressibility effects be negligible.

5. BENDIXSON'S THEORY

The points (0,0,0) and (1,1,1) in (ϵ,Γ,θ) space are singular points of the system (3.19–21). To investigate the run of integral curves in their vicinity we shall call upon Bendixson's theory of the singular points of ordinary first-order differential equations,[4] the pertinent results of which are summarized in the following three paragraphs.

B.1. Equations of the type

$$\frac{dx}{dy} = \frac{Ax+By+\cdots}{Cx+Dy+\cdots}$$

with

$$(A-D)^2+4BC>0.$$

(Here and in what follows "$\cdots$" stands for "higher-order terms.") If $AD-BC>0$ the origin of the (x,y)-plane is a nodal point: all integral curves that penetrate a fixed neighborhood of the origin terminate there with a definite slope. If $AD-BC<0$ the origin is a saddle point; four integral curves terminate there in two pairs of equal and opposite directions.

B.2. Equations of the type

$$x^m dy/dx = ay+bx+\cdots (m \text{ integral}).$$

We shall be concerned only with the region $x>0$. If $a<0$ one integral curve terminates in the origin, where it has a definite slope. If $a>0$ the origin is a nodal point. One can easily show that the last statement is valid even for nonintegral values of $m>1$ and for the equation

$$x^m dy/dx = ay+bx^{m-1}+\cdots (m>1).$$

[4] I. Bendixson, Acta Math. **24**, 3 (1900). For a partial account see also L. Bieberbach, *Theorie der Differentialgleichungen*, (Dover Publications, New York, 1944), Chap. I, Secs. 5, 6.

B.3. Reduction of equations to standard form by means of bilinear transformations. One example of Bendixson's general method is relevant. Consider the equation

$$y^m dy/dx = a(y-x+\cdots) \quad (m>1).$$

One can show that there is a unique solution having the asymptotic form $x=y^m/ma+\cdots$. To investigate the multiplicity of solutions having the asymptotic form $x=y+\cdots$ set $y-x=xz$. After some reductions one obtains, in place of the original equation,

$$x^m dz/dx = az - x^{m-1} + \cdots.$$

It follows from B.2 that for integral curves in the region $x>0$, the origin of the (x,z) plane is a nodal point or a saddle point according as a is $>$ or <0. If $a>0$, then, in the (x,y) plane, every integral curve that penetrates the wedge-shaped neighborhood bounded by the lines $x=y$, $x=\epsilon$ (for some sufficiently small value of ϵ), and the solution $x=y^m/ma+\cdots$, terminates in the origin with slope unity. If $a<0$ only one integral curve terminates in the origin.

6. APPLICATION TO THE FLAME EQUATIONS

Eliminating x from (3.19–21) we obtain

$$\frac{d\Gamma}{d\theta} = \frac{\lambda}{m^2 c_p}\frac{\Phi(\epsilon,\theta)}{\theta-\Gamma}, \tag{6.1}$$

$$\frac{d\epsilon}{d\theta} = \frac{\lambda}{D_{12}\rho c_p}\frac{\epsilon-\Gamma}{\theta-\Gamma}, \tag{6.2}$$

$$\frac{d\Gamma}{d\epsilon} = \frac{D_{12}\rho}{m^2}\frac{\Phi(\epsilon,\theta)}{\epsilon-\Gamma}. \tag{6.3}$$

For the asymptotic form of $\Phi(\epsilon,\theta)$ we may assume without loss of generality

$$\Phi(\epsilon,\theta) \sim \begin{cases} \theta^r & (r>1;\ \epsilon,\theta \approx 0) \\ (1-\epsilon)^i & (i \geq 1;\ \epsilon,\theta \approx 1) \end{cases}. \tag{6.4}$$

(a) *(1,1,1)*. Let $\bar{\epsilon}=1-\epsilon$, $\bar{\theta}=1-\theta$, $\bar{\Gamma}=1-\Gamma$. In the neighborhood of (1,1,1) the equations

$$\frac{d\bar{\Gamma}}{d\bar{\theta}} = \alpha\frac{\bar{\epsilon}^i}{\bar{\Gamma}-\bar{\theta}}, \tag{6.5}$$

$$\frac{d\bar{\epsilon}}{d\bar{\theta}} = \beta\frac{\bar{\Gamma}-\bar{\epsilon}}{\bar{\Gamma}-\bar{\theta}}, \tag{6.6}$$

$$\frac{d\bar{\Gamma}}{d\bar{\epsilon}} = \gamma\frac{\bar{\epsilon}^i}{\bar{\Gamma}-\bar{\epsilon}}, \tag{6.7}$$

are approximately valid, where α, β, and γ are positive constants ($\gamma=\alpha/\beta$). The cases $i=1$ and $i>1$ must be distinguished.

(a.1) $i=1$. The origin of the $(\bar{\Gamma},\bar{\epsilon})$ plane is a saddle point (B.1). Of the two solutions of Eq. (6.7),

$$\bar{\Gamma} = k_\pm\bar{\epsilon} + \cdots, \quad k_\pm = \tfrac{1}{2}[1 \pm (1+4\gamma)^{\frac{1}{2}}],$$

the second is inadmissible, owing to the requirement $\bar{\Gamma}, \bar{\epsilon}>0$. Substituting the first solution in Eqs. (6.5, 6) we obtain

$$\frac{d\bar{\Gamma}}{d\bar{\theta}} = \frac{\alpha}{k_+}\frac{\Gamma}{\bar{\Gamma}-\bar{\theta}}, \quad \frac{d\bar{\epsilon}}{d\bar{\theta}} = \beta(k_+-1)\frac{\bar{\epsilon}}{k_+\bar{\epsilon}-\bar{\theta}}.$$

In both the $(\Gamma,\bar{\theta})$ plane and the $(\bar{\epsilon},\bar{\theta})$ plane there is a unique integral curve terminating in the origin (B.2). Hence, for every value of m one and only one integral curve issues from the point (1,1,1) in (ϵ,Γ,θ) space. In this respect, then, (1,1,1) resembles an ordinary point. The same conclusion may be drawn in the case

(a.2) $i>1$. Again there are just two solutions of (6.7) terminating in the origin of the $(\bar{\Gamma},\bar{\epsilon})$-plane (B.3):

$$\bar{\Gamma} = -\gamma\bar{\epsilon}^i/i + \cdots, \quad \bar{\Gamma} = \bar{\epsilon} + \gamma\bar{\epsilon}^i + \cdots.$$

The first is inadmissible. Substituting the second in Eqs. (6.5, 6) we obtain

$$\frac{d\bar{\Gamma}}{d\bar{\theta}} = \alpha\frac{\bar{\Gamma}^i}{\bar{\Gamma}-\bar{\theta}}, \quad \frac{d\bar{\epsilon}}{d\bar{\theta}} = \beta\gamma\frac{\bar{\epsilon}^i}{\bar{\epsilon}-\bar{\theta}}.$$

In both the $(\bar{\Gamma},\bar{\theta})$ plane and the $(\bar{\epsilon},\bar{\theta})$ plane there is a unique integral curve terminating in the origin (B.2).

(b) *(0,0,0)*. In the neighborhood of (0,0,0) the equations

$$\frac{d\Gamma}{d\theta} = a\frac{\theta^r}{\theta-\Gamma}, \tag{6.8}$$

$$\frac{d\epsilon}{d\theta} = b\frac{\epsilon-\Gamma}{\theta-\Gamma}, \tag{6.9}$$

$$\frac{d\Gamma}{d\epsilon} = c\frac{\theta^r}{\epsilon-\Gamma}, \tag{6.10}$$

are approximately valid, where a, b, and c are positive constants ($c=a/b$). The two solutions of (6.8) are

$$\Gamma = \theta - a\theta^r + \cdots, \tag{6.11}$$

$$\Gamma = a\theta^r/r + \cdots. \tag{6.12}$$

According to B.3 there is a unique solution with the asymptotic form (6.12) and a continuously infinite set of solutions with the asymptotic form (6.11). Using B.1,2 one can show that for both types of solution the origin of the (ϵ,θ) plane and the origin of the (Γ,ϵ) plane are nodal points. We shall call solutions with the asymptotic form (6.12) r solutions, and those with the asymptotic form (6.11) c solutions. Our results may then be summed up as follows. For any given value of m the integral curves issuing from (0,0,0) and corre-

sponding to r solutions fill a certain region, $R(m)$, in (ϵ,Γ,θ) space, while those corresponding to c solutions generate a certain surface, $S(m)$, which forms part of the boundary of $R(m)$.

Now we have seen that for every value of m there is a unique integral curve issuing from (1,1,1). This curve terminates in (0,0,0) if (1,1,1) lies in $R(m)$ or on $S(m)$. For $m=0$ the integral curve emanating from (1,1,1) is the line $\epsilon=\theta=1$. Hence (1,1,1) lies outside $R(0)$. For $m=\infty$, on the other hand, the integral curve emanating from (1,1,1) is the line $\epsilon=\theta=\Gamma$, which represents an r solution. Hence (1,1,1) lies inside $R(\infty)$. There is evidently a unique value of m, m^*, for which (1,1,1) lies on $S(m)$. All values of $m>m^*$ correspond to integral curves that terminate in (0,0,0) and represent r solutions, all values of $m<m^*$ correspond to integral curves that do not terminate in (0,0,0), and m^* itself corresponds to an integral curve that terminates in (0,0,0) and represents a c solution. In short, the flame equations possess a continuous set of eigenvalues (∞,m^*) corresponding to r solutions, and a unique eigenvalue m^* corresponding to a c solution.

To interpret this result physically consider the energy equation written in the form

$$mc_p\frac{dT}{dx}=\frac{d}{dx}\left(\lambda\frac{dT}{dx}\right)+q\Psi. \tag{6.13}$$

It follows from (3.14) that the reaction term or the conduction term dominates the right-hand side of (6.13) at low temperatures according as (6.11) or (6.12) obtains. That is, r solutions describe flames in which chemical reaction produces the temperature gradient in front of the reaction zone, while c solutions describe flames that propagate by the conduction of heat from the reaction zone into the unburnt gas.

In practice the thermal contact between the explosive gas and its environment is usually efficient enough to prevent any systematic increase in the temperature of unburnt gas by chemical reaction alone, so that flames of the r variety cannot be realized physically. But even in rigorously adiabatic burning steady states of the r variety are violently unstable. For they can be destroyed by arbitrarily small perturbations of the steady-state temperature profile if these occur sufficiently far ahead of the reaction zone.

We conclude that while the equations governing slow deflagration waves admit a continuum of steady-state solutions, only one of these solutions represents true flame propagation; the others represent a kind of geometrical propagation that cannot be realized under ordinary experimental conditions.

7. CONDUCTION AND DIFFUSION

Let us examine more closely the asymptotic behavior of the c solution in the neighborhood of (0,0,0). Substituting (6.12) in (6.10) we obtain

$$\frac{d\Gamma}{d\epsilon}=\frac{rc}{a}\frac{\Gamma}{\epsilon-\Gamma}. \tag{7.1}$$

The asymptotic solution of this equation depends upon the magnitude of (r/b):

$$\left.\begin{array}{ll}\Gamma\sim(1-r/b)\epsilon & (r<b)\\ \epsilon\sim-\Gamma\ln\Gamma & (r=b)\\ \Gamma\sim\epsilon^{r/b} & (r>b)\end{array}\right\}. \tag{7.2}$$

Now in general

$$b=\left(\frac{\lambda}{D_{12}c_p\rho}\right)_1\approx 1, \tag{7.3}$$

and since $r>1$, $r/b>1$. To interpret this result physically, consider the diffusion equation written in the form

$$m\frac{d\epsilon}{dx}=\Psi+\frac{d}{dx}\left(D_{12}\rho\frac{d\epsilon}{dx}\right). \tag{7.4}$$

It follows from (7.2) and (3.14) that the diffusion term dominates the right-hand side of (7.4) at small values of ϵ if $r/b\geq 1$, while if $r/b<1$ the effects of diffusion and chemical reaction are comparable, the relative importance of diffusion decreasing with r/b. From our previous remarks we infer that in actual flames the dilution of unburnt gas by reaction products in the conduction zone occurs by diffusion rather than chemical reaction.

Having established the existence of a unique physically significant steady state, we shall now inquire into its stability.

8. FORMULATION OF APPROXIMATE TIME-DEPENDENT FLAME EQUATIONS

We shall employ the subscript notation for partial derivatives.

Conservation of mass.

$$\rho_t+m_x=0. \tag{8.1}$$

Conservation of momentum.

$$m_t+p_x=0, \tag{8.2}$$

with neglect of terms of order M^2.

Continuity.

$$(\epsilon,\rho)_t+(\Gamma m)_x=\Psi(\epsilon,\rho,T). \tag{8.3}$$

With the help of (8.1) and the diffusion Eq. (3.5) we obtain from (8.3)

$$\rho\epsilon_t=-m\epsilon_x+\Psi+(D_{12}\rho\epsilon_x)_x,$$

or, in terms of the variables defined by (3.18)

$$\rho\epsilon_t=-m\epsilon_x+\Phi+(D_{12}\rho\epsilon_x)_x. \tag{8.4}$$

Conservation of energy.

$$0=(\rho\epsilon)_t+Q_x\equiv(\rho h-p)_t+Q_x=(\rho h)_t+Q_x$$
$$=\left[\rho\left((1-\epsilon)\int_{T_1}^{T}c_p^{(1)}dT+\epsilon\int_{T_1}^{T}c_p^{(2)}dT+q^{(1)}-\epsilon q\right)\right]_t+Q_x,$$

with neglect of terms of order M^2. Using (8.3) and (3.8) we can write the last equation in the form

$$\left(\rho\int_{T_1}^{T}c_p'dT\right)_t=-\left(m\int_{T_1}^{T}c_pdT\right)_x+q\Psi+(\lambda T_x)_x, \quad (8.5)$$

where

$$\int_{T_1}^{T}c_p'dT\equiv(1-\epsilon)\int_{T_1}^{T}c_p^{(1)}dT+\epsilon\int_{T_1}^{T}c_p^{(2)}dT \quad [\text{cf. (3.12)}]. \quad (8.6)$$

Now in general—though not always—the reactant and product constituents of an explosive gas have rather different molecular weights, specific heats, self-diffusion coefficients, and thermal conductivities. This circumstance materially complicates the flame equations, but can evidently have no qualitative bearing on the question of stability. For the sake of simplicity we shall therefore set

$$\mu^{(1)}=\mu^{(2)}, \quad c_p^{(1)}=c_p^{(2)}=c_p=c_p'.$$

In addition, we shall set

$$D_{12}\rho=\lambda/c_p=\kappa,$$

which is consistent with our other approximations.[5] The equation of state now becomes

$$p=R\rho T, \quad (8.7)$$

while (8.4) and (8.5) become

$$\rho\epsilon_t=-m\epsilon_x+\Phi+(\kappa\epsilon_x)_x, \quad (8.8)$$
$$\rho\theta_t=-m\theta_x+\Phi+(\kappa\theta_x)_x, \quad (8.9)$$

with the help of (8.1). If we confine our attention to unsteady states that arise when the steady state is subjected to a finite perturbation, the boundary conditions are, as before,

$$\left.\begin{aligned}\epsilon_1=\theta_1=0 \quad (x=-\infty)\\ \epsilon_2=\theta_2=1 \quad (x=+\infty)\end{aligned}\right\}. \quad (8.10)$$

9. EVOLUTION OF NONSTEADY STATES; STABILITY OF THE STEADY STATE

By (8.8–10) the quantity $z=\epsilon-\theta$ satisfies the linear equation

$$\rho z_t=-mz_x+(\kappa z_x)_x \quad (9.1)$$

and the boundary conditions

$$z_1=z_2=0. \quad (9.2)$$

In the steady state $z=0$. Consider a nonsteady state in which $z\neq0$ initially. The last two equations show that z tends to zero everywhere as t tends to infinity.[6]

Now suppose that initially the flame variables, including z, differ infinitesimally from their steady-state values. Then either the perturbation δz remains comparable to the other perturbations, in which case the steady state is certainly stable; or else δz ultimately becomes and remains negligible in comparison with the other perturbations. We may therefore assume, without loss of generality, that $z=0$ to begin with.

Some further simplifications are possible. One may regard the most general perturbation of, say, the temperature profile as an overall distortion of the steady-state profile on which are superimposed small-amplitude ripples whose characteristic wavelengths are much smaller than the flame width. It is easy to show from the energy equation that the ripples tend to be damped out by conduction much in the same way as if they overlay a state of uniform temperature. Similarly, ripples in the concentration profile tend to be damped out by diffusion, while ripples in the pressure, density, and mass-flux profiles propagate out of the flame in the form of sound waves. We may therefore confine our attention to perturbations whose characteristic wavelengths are of order L (the flame width), and whose characteristic frequencies are of order u/L. Under these circumstances we may regard the pressure as constant in time as well as in space. For the variable part of the pressure is of order M^2 as compared with the total pressure, and since the frequency associated with perturbations of the pressure is the same as those associated with perturbations of the temperature and density, p_t/p is of order M^2 as compared with T_t/T and ρ_t/ρ. Hence, by (8.7),

$$\delta\rho/\rho=-\delta T/T \quad (9.3)$$

for either spatial or temporal variations.

We are now in a position to discuss the most essential features of time-dependent behavior. Consider the aggregate of reference frames $\mathfrak{F}(x)$ defined, at a fixed instant t_0 (which, for the sake of neatness, we shall not indicate explicitly in the notation), in the following way: (a) In $\mathfrak{F}(x)$ $\theta_t(x)=\rho_t(x)=0$; (b) the origins of all the frames coincide. We shall denote by $w(x;x')$ the velocity of $\mathfrak{F}(x)$ relative to $\mathfrak{F}(x')$, and by $f(x;x')$ the value of a

[5] The approximations made in this paragraph are discussed more fully in Part II.

[6] Since

$$p_1(x)z_x+p_2(x)z_{xx}=\left(\frac{d\xi}{dx}\right)^2p_2(x)z_{\xi\xi},$$

where

$$d\xi=dx\cdot\exp\left[-\int^x(p_1/p_2)dx\right],$$

the equation

$$z_t=p_1(x)z_x+p_2(x)z_{xx}$$

describes linear heat conduction in a medium of variable conductivity if $p_2(x)>0$ for all x.

function $f(\xi)$ at the point x, as measured in the frame $\mathfrak{F}(x')$. From these definitions it follows that

$$w(x;x')=-w(x';x);$$
$$w(x;x'')-w(x';x'')=w(x;x'); \quad (9.4)$$
$$\theta_t(x';x)=w(x;x')\theta_{x'}(x'); \quad \rho_t(x';x)=w(x;x')\rho_{x'}(x'). \quad (9.5)$$

By (8.1) and (9.5)

$$m(x;x)=m(-\infty;x)-\int_{-\infty}^{x}\rho_t(x';x)dx'$$
$$=m(-\infty;x)-\int_{-\infty}^{x}w(x;x')\rho_{x'}(x')dx'.$$

Hence

$$\frac{dm(x;x)}{dx}=\frac{dm(-\infty;x)}{dx}-\frac{w(x+dx;x)}{dx}\int_{-\infty}^{x}\rho_{x'}(x')dx',$$

by (9.4), so that

$$\frac{dm(x;x)}{dx}=-\rho(x)\frac{dw(x)}{dx}, \quad (9.6)$$

$w(x)$ being the local velocity of the density and temperature profiles in an arbitrary frame of reference. But by (8.9)

$$m(x;x)=\frac{\Phi(\epsilon,\theta)+(\kappa\theta_x)_x}{\theta_x}, \quad (9.7)$$

where, according to the previous discussion, we may set $\Phi(\epsilon,\theta)=\Phi(\theta,\theta)$, so that Φ depends on θ in exactly the same way as it does in the steady state.

Equations (9.6) and (9.7) describe the evolution of flame structure in a very perspicuous way. For the purpose of analysis, however, we shall find it convenient to have the same information in more compact form. By (9.7)

$$m_t(x;x)=-\frac{\Phi}{\theta_x}\frac{\theta_{xt}(x;x)}{\theta_x}$$
$$+\frac{\kappa\theta_{xx}}{\theta_x}\left(\frac{\theta_{xxt}(x;x)}{\theta_{xx}}-\frac{\theta_{xt}(x;x)}{\theta_x}\right)+\kappa_\theta\theta_x\frac{\theta_{xt}(x;x)}{\theta_x},$$

and by (9.5)

$$\theta_{xt}(x;x)=-w_x(x)\theta_x, \quad \theta_{xxt}(x;x)=-w_{xx}(x)\theta_x-2w_x(x)\theta_{xx}.$$

Hence

$$m_t(x;x)=w_x\left(\frac{\Phi-(\kappa\theta_x)_x}{\theta_x}\right)-\kappa w_{xx}$$

or, with the help of (9.6)

$$\rho m_t(x;x)=-m_x\left(\frac{\Phi-(\kappa\theta_x)_x}{\theta_x}\right)+\rho\kappa(m/\rho)_{xx}. \quad (9.8)$$

As we have already noted, equations of this form describe linear heat flow in media of variable conductivity. Consequently $m(x;x)$ tends to a constant. But (9.6) shows that m is constant only in a steady state, and according to the uniqueness theorem there is only one steady state for flames that propagate by conduction. It follows that $m(x;x)\to m^*$, and the steady state is stable.

Let us examine the physical basis of this result in more detail. Consider a small region of the steady flame centered on the plane $x=x^*$ that divides the conduction zone $[(\kappa\theta_x)_x>\Phi]$ from the reaction zone $[(\kappa\theta_x)_x<\Phi]$.[7] A perturbation that increases the steepness of the temperature profile in this region causes m to become greater than m^* in the left-hand portion of the region, where conduction predominates, and less than m^* in the right-hand portion, where chemical reaction predominates [(9.8)]. As a result, the temperature profile tends to expand [(9.9)]. Similarly, if the perturbed temperature profile is less steep than the steady-state profile in this region, it tends to contract. This spring-like resistance to distortion in the neighborhood of $x=x^*$ has a counterpart in the behavior of the local-mass-flux profile. One can show from (9.6) and (9.8) that if the perturbed temperature profile does not coincide with the steady-state profile in the neighborhood of $x=x^*$, then the perturbed local-mass-flux profile intersects the unperturbed profile at a point whose x coordinate coincides with x^* to the first order, and there is a couple tending to reduce the angle of intersection.

Regions of the flame in which either conduction or chemical reaction predominates throughout do not possess the kind of stability described above. In fact, one can always alter the steady-state temperature profile in such a way that the local mass flux assumes any given constant value close to m^* in any small region not containing the plane $x=x^*$. And, according to (9.8), $m(x;x)$ would remain different from m^* in such a region were it not that the structure of the flame as a whole influences the structure of its parts. By virtue of the diffusion term in (9.8) the mass-flux profile tends to become progressively flatter; i.e., it resists bending. It is the combined effects of this resistance to bending and the couple exerted in the neighborhood of $x=x^*$ that cause the perturbed profile to approximate more and more closely the straight line $m(x;x)=m^*$.

10. INTERPRETATION OF INFLAMMABILITY LIMITS

We have found that arbitrarily dilute mixtures of explosive and inert gases can support stable steady deflagration waves, whereas in practice definite limits of inflammability are observed. Now it is conceivable that departures from linear adiabatic flow, arising from the presence of walls, are responsible for the experimental instability phenomena; but this explanation

[7] The distinction drawn here between a conduction zone and a reaction zone is evidently more natural and more useful than the traditional distinction, based on the sign of θ_{xx}, between a preheating zone and a reaction zone.

seems unlikely, because experimental workers always take pains to minimize precisely these effects when they determine inflammability limits. We are therefore driven to the conclusion that—if the theory is correct—theoretical stability does not necessarily carry with it practical stability, and conversely, criteria for practical stability depend upon the experimental conditions as well as the structure of the theoretical steady deflagration wave. In short, we must anticipate that perturbations of flame structure do not bear a constant relation to the fluctuations of temperature and concentration that produce them, but increase systematically with increasing dilution, if the magnitude of the fluctuations remains fixed. In Part II, where a quantitative description of flame structure in the steady state is set forth, we shall find that this expectation is, in fact, fulfilled.

It is a fairly serious objection to the above views that inflammability limits apparently admit of precise experimental determination. One can argue, of course, that the experiments are for the most part conducted under standardized conditions; but the question can best be settled by further experiments. One aspect, at least, of the theory should be rather easy to test. The theory predicts that a deflagration wave propagating in a mixture of systematically variable dilution will exhibit perturbations of increasing amplitude when it passes through a region of increasing dilution. If, on the other hand, one were to observe that a deflagration wave does not respond more violently to external disturbances in regions of relatively high dilution than it does in regions of relatively low dilution, but merely recovers more slowly from their effects, then true instability in the usual theoretical sense (departures from the steady state proportional to e^{-nt}, n passing through the value 0) would be indicated.

It is a pleasure to record my indebtedness to Professor John A. Wheeler, not only for calling my attention to the problems of flame propagation in the first place, but for the stimulating interest he has taken in the progress of this work.

THE JOURNAL OF CHEMICAL PHYSICS VOLUME 22, NUMBER 2 FEBRUARY, 1954

Theory of Linear Flame Propagation. Part II. Structure of the Steady State*

DAVID LAYZER
Harvard College Observatory and Forrestal Research Center, Princeton University, Princeton, New Jersey
(Received October 29, 1953)

A quantitative approximate theory of flame structure in the steady state, including formulas for the determination of flame speeds, is set forth. The theory predicts that in a first approximation, the sensitivity of a steady deflagration wave to external perturbations depends upon the shape of the temperature profile, but not upon the speed or width of the wave, or the pressure. It is shown that the sensitivity increases with increasing dilution of the explosive mixture, in agreement with the explanation of inflammability limits suggested in Part I.

THE class of single-reaction flames, though neither very extensive nor of very great interest to the student of chemical kinetics, lends itself admirably, by virtue of its simplicity, to a study of the essential physical aspects of flame propagation. In Part I we discussed the existence, uniqueness, and stability of the steady deflagration wave. Here we shall develop a quantitative analytical description of flame structure, which includes formulas for the approximate determination of flame speeds. This will enable us to evaluate the influence of flame structure on stability.

The problem of calculating the speed of a single-reaction deflagration wave as a function of the parameters that specify the medium in which it propagates has already claimed the attention of several writers. Boys and Corner[1] have published an approximation method, later generalized by Corner,[2] based on an iterative solution of the flame equations. A much simpler method has been suggested by Adams,[3] which yields the flame width as well as the flame speed. Some of Adams's approximations are rather drastic, however, and seem difficult to justify, especially in the case of second-order flames. The method described below seeks to combine the virtues of accuracy and simplicity.

According to Part I, Sec. 2, the flame equations can be

* This work was supported in part by the Air Force Cambridge Research Center under Contract AF19(604)-146 with Harvard University.

[1] S. F. Boys and J. Corner, Proc. Roy. Soc. (London) **A197**, 90 (1949).
[2] J. Corner, Proc. Roy. Soc. (London) **A198**, 388 (1949).
[3] Described by Henkel, Spaulding, and Hirschfelder, *Third Symposium on Combustion and Flame and Explosion Phenomena* (Williams and Wilkins, Baltimore, 1949), p. 127.

written in the form

$$\frac{d\theta}{dx}=\frac{mc_p}{\lambda}(\theta-\Gamma), \tag{1}$$

$$\frac{d\Gamma}{d\theta}=\frac{\lambda}{m^2c_p}\frac{\Phi(\epsilon,\theta)}{\theta-\Gamma}, \tag{2}$$

$$\frac{d\epsilon}{d\theta}=\frac{\lambda}{D_{12}\rho c_p}\frac{\epsilon-\Gamma}{\theta-\Gamma}, \tag{3}$$

with the boundary conditions

$$\epsilon_1=\theta_1=\Gamma_1=0; \quad \epsilon_2=\theta_2=\Gamma_2=1. \tag{4}$$

As our first approximation, we shall set

$$\frac{\lambda}{D_{12}\rho c_p}=1. \tag{5}$$

Then (3) has the solution

$$\epsilon=\theta, \tag{6}$$

and our original set of three coupled equations reduces to a pair of uncoupled equations. The justification of the approximation (5) is as follows.

In the case of a pure gas we may with good accuracy represent the thermal conductivity by Eucken's formula, and the self-diffusion coefficient by the formula of Maxwell and Stefan (or, alternatively, Meyer's formula, corrected for the persistence of velocity),

$$\lambda=\tfrac{1}{4}(9-5/\gamma)c_p\eta, \quad D=1.34\eta/\rho.$$

Hence,

$$\frac{\lambda}{Dc_p\rho}=1.68-0.931\gamma. \tag{7}$$

Now γ, the ratio of specific heats, does not in general vary greatly over a typical range of flame temperatures (300–3000°K), and for typical values of γ the right-hand side of (7) is not very different from 1. (The value of γ appropriate to molecular oxygen, nitrogen, or nitric oxide, for example, varies between 1.4 and 1.3, the corresponding values of $\lambda/Dc_p\rho$ being 1.02 and 0.96.) In a mixture of gases the quantity $\lambda/D_{12}c_p\rho$ varies between

$$\frac{\lambda_{11}}{D_{11}c_p^{(1)}\rho^{(1)}}\cdot\frac{D_{11}}{D_{12}}\approx\frac{D_{11}}{D_{12}}$$

and

$$\frac{\lambda_{22}}{D_{22}c_p^{(2)}\rho^{(2)}}\cdot\frac{D_{22}}{D_{12}}\approx\frac{D_{22}}{D_{12}},$$

that is, between a value less than unity and a value greater than unity, since the value of D_{12} is intermediate between the values of D_{11} and D_{22}.

We shall assume that the reaction rate Φ has the form

$$\Phi(\epsilon,\theta)=(1-\epsilon)_i\varphi(\theta)=(1-\theta)^i\varphi(\theta), \quad i=1 \text{ or } 2^i. \tag{8}$$

We may then replace (2) by

$$\frac{d\Gamma}{d\theta}=A\frac{(1-\theta)^if(\theta)}{\theta-\Gamma}, \tag{9}$$

where

$$A=\frac{\lambda_2\varphi(1)}{m^2c_{p2}} \tag{10}$$

and

$$f(\theta)=(\lambda\varphi(\theta)/c_p)/(\lambda_2\varphi(1)/c_{p2}), \tag{11}$$

so that

$$f(1)=1. \tag{12}$$

By virtue of the boundary conditions, the numerical value of the constant A is uniquely determined by the function $f(\theta)$. To find the functional $A[f(\theta)]$ we shall first determine the function $A(n)=A[\theta^n]$, and then set up an approximate correspondence between the class of arbitrary normalized functions $f(\theta)$ and the much narrower class of functions θ^n.

With $f(\theta)=\theta^n$, Eq. (9) becomes

$$\frac{d\Gamma^{(n)}}{d\theta}=A\frac{(1-\theta)^i\theta^n}{\theta-\Gamma^{(n)}}. \tag{13}$$

Multiplying through by $(\theta-\Gamma)$ and integrating by parts we obtain

$$A(n;i)=\frac{\tfrac{1}{2}-\int_0^1\Gamma^{(n)}d\theta}{\int_0^1(1-\theta)^i\theta^nd\theta}. \tag{14}$$

Now by (13), $\Gamma^{(n)}(\theta)$ is given by

$$\Gamma^{(n)}(\theta)=A\int_0^\theta(1-\theta)^i\theta^{n-1}d\theta, \tag{15}$$

provided that the right-hand side of this equation is much smaller than θ. From (15) and (14) it follows that $\Gamma^{(n)}(\theta)\to0$ as $n\to\infty$ for every value of θ less than unity. Hence, $\int_0^1\Gamma^{(n)}d\theta\to0$ as $n\to\infty$, and by (14)

$$A(n;1)=\tfrac{1}{2}n^2+a_1n+a_0+a_{-1}n^{-1}+\cdots,$$

$$A(n;2)=\tfrac{1}{4}n^3+b_2n^2+b_1n+\cdots.$$

To determine the unknown coefficients in these expansions, Robert Goerss and I, using an IBM card-programmed electronic calculator and following the usual procedure of trial and error, have computed values of $A_i(n)$ to three significant figures for $2\leq n\leq10$, $i=1,2$. Theseco mputed values, which are listed in Table I, may be adequately represented by the formulas

$$\left.\begin{aligned}A(n;1)&=\tfrac{1}{2}n^2+\tfrac{1}{5}n-\tfrac{3}{5}+\tfrac{2}{5}n^{-1}\\A(n;2)&=\tfrac{1}{4}n^3+\tfrac{1}{2}n^2-\tfrac{3}{4}n+1-\tfrac{1}{2}n^{-1}\end{aligned}\right\}. \tag{16}$$

We have now to find a way of assigning effective values of n to arbitrary normalized functions $f(\theta)$. According to (14), $f(\theta)$ and θ^n correspond to the same value of A if and only if

$$\frac{\frac{1}{2}-\int_0^1 \Gamma^{(n)}d\theta}{\int_0^1 (1-\theta)^i\theta^n d\theta}=\frac{\frac{1}{2}-\int_0^1 \Gamma d\theta}{\int_0^1 (1-\theta)^i f(\theta)d\theta}.$$

Now for moderate and large values of n the numerator of the expression on the right is less sensitive to small variations of n than the denominator. This suggests that to a good approximation n is given by the equation

$$\int_0^1 (1-\theta)^i\theta^n d\theta=\int_0^1 (1-\theta)^i f(\theta)d\theta\equiv J_i \qquad (17)$$

or,

$$n+\tfrac{3}{2}=\left(\tfrac{1}{4}+\frac{1}{J_1}\right)^{\frac{1}{2}} \qquad (i=1), \qquad (18)$$

$$n+2=\left[\frac{2}{J_2}+\left(\frac{2}{J_2}+\cdots\right)^{\frac{1}{2}}\right]^{\frac{1}{2}} \qquad (i=2). \qquad (19)$$

In agreement with our previous approximations we may approximate $\Gamma(\theta)$ by $\Gamma^{(n)}(\theta)$. Now even $\Gamma^{(n)}$ is a rather complicated function of θ. It turns out, however, that except in the immediate vicinity of $\Gamma=1$, $\Gamma^{(n)}$ is adequately represented by the monomial θ^N if N is chosen in such a way that (14) is satisfied. Setting

$$\Gamma^{(n)}(\theta)=\theta^{N(n;\,i)} \qquad (20)$$

and using (14) and (16), one obtains

$$\left.\begin{aligned} N(n;1)&=0.77n+0.35+\cdots\\ N(n;2)&=0.5n+0.25+0.9n^{-1}+\cdots\end{aligned}\right\}. \qquad (21)$$

Finally, with the help of (20), we can solve Eq. (1), which may be written in the form

$$\frac{d\theta}{d\xi}=\theta-\theta^N, \qquad (22)$$

where

$$d\xi=(mc_p/\lambda)dx. \qquad (23)$$

The solution of (22) is

$$\theta=\frac{e^{\xi}}{(1+e^{(N-1)\xi})^{1/N-1}}. \qquad (24)$$

This completes our approximate solution of the flame equations.

According to Eq. (9.7), Part I, the local mass flux is given by

$$m(x;x)=\frac{\Phi(\epsilon,\theta)+(\kappa\theta_x)_x}{\theta_x}.$$

Table I.

n	$A(n;1)$	$A(n;2)$
2	2.01	3.18
3	4.66	9.89
4	8.32	22.0
5	13.0	41.0
6	18.6[5]	68.4
7	25.3	106.
8	33.0	155.
9	41.7	217.
10	51.4	293[5]

In terms of dimensionless variables

$$\frac{m(x;x)}{m^*}\approx\frac{A(1-\epsilon)^i\theta^n}{\theta_\xi}+\frac{\theta_{\xi\xi}}{\theta_\xi}, \qquad (25)$$

the left-hand side being equal to unity in the steady state. Let θ^* be the temperature at which the heating effects of conduction and chemical reaction are precisely equal in the steady state. Then by (25)

$$\frac{A(1-\theta^*)^i\theta^{*n}}{\theta_\xi{}^*}\approx\tfrac{1}{2}. \qquad (26)$$

In this equation we may replace $\theta_\xi{}^*$ by θ^* if $\Gamma^{(n)}(\theta^*)\ll\theta^*$, that is, according to (15), if

$$\left.\begin{aligned} &\frac{A(n;1)}{n+1}\left(1-\theta^*+\frac{1}{n+1}\right)\theta^{*n-1}\ll 1 \quad (i=1)\\ &\frac{A(n;2)}{n+1}\left[(1-\theta^*)^2+\frac{1}{n}-\frac{\theta^{*2}}{n+2}\right]\theta^{*n-1}\ll 1 \quad (i=2)\end{aligned}\right\}. \qquad (27)$$

(27) and (26), with θ^* in place of $\theta_\xi{}^*$, are consistent if n is sufficiently large and if $1-\theta^*\gg 1/n$. With $\theta_\xi{}^*=\theta^*=1-y/n$ (26) becomes, if n is large,

$$\tfrac{1}{2}=\frac{A(n;i)}{n^i}y^i(1-y/n)^{n-1}\approx\begin{cases}\frac{1}{2}nye^{-y} & (i=1),\\ \frac{1}{4}ny^2e^{-y} & (i=2).\end{cases}$$

The appropriate solutions are

$$\begin{aligned} y&=\log n+\log\log n+\cdots && (i=1),\\ y&=\log(n/2)+2\log\log(n/2)+\cdots && (i=2);\end{aligned}$$

$$\theta^*\approx 1-\frac{\log n}{n} \qquad (i=1,2). \qquad (28)$$

With increasing n, the reaction zone is compressed into a narrower and narrower range of temperature.

We are now in a position to examine the effect of fluctuations of temperature and concentration upon flame structure in the region where the heating effects of conduction and chemical reaction are comparable. By (25) and (28),

$$\frac{\delta m}{m}\approx\tfrac{1}{2}\left(\frac{-i}{1-\epsilon^*}\delta\epsilon+\frac{n}{\theta^*}\delta\theta\right)=-\frac{in}{2\log n}\delta\epsilon+\frac{n}{2}\delta\theta. \qquad (29)$$

Equation (29) shows that for any given fluctuations, $\delta\theta$ and $\delta\epsilon$, $\delta m/m$ increases indefinitely with n. Now we have seen in Part I, Sec. 4, that the region where conduction and reaction have comparable heating effects plays a dominant role in the evolution of a nonsteady flame, in that changes that occur there in the value of the local mass flux propagate outward into the conduction and reaction zones. Thus, fluctuations in the value of $m(x;x)$ in the "intermediate zone" give rise to pulsations of the flame as a whole; and large, irregular fluctuations give rise to large, irregular pulsations. Accordingly, if we were to examine a series of flames corresponding to increasing values of the parameter n, and subject to the same external perturbations, we should expect to find the most marked departures from steadiness in the flames corresponding to the greatest values of n.

We have now to inquire how the parameter n depends on the primary data of the problem. Suppose, for the sake of definiteness, that the reaction rate has the form

$$\Psi = B[\rho(1-\epsilon)]^i \exp[-E/R(T-T_1)],$$

and let us assume, in order to avoid irrelevant complications, that the specific heat of the mixture is constant throughout the flame, and that the reactant and product molecules have equal molecular weights. Then $\theta=(T-T_1)/(T_2-T_1)$ and

$$\Psi \sim T^{-i}(1-\epsilon)^i \exp[-E/R(T-T_1)]$$

$$\sim (1-\epsilon)^i(\theta+r)^{-i}\exp\left[-\alpha\left(\frac{1}{\theta}-1\right)\right],$$

where $\alpha=E/R(T_2-T_1)$, $r=T_1/(T_2-T_1)$. The parameter n is defined by

$$\int_0^1 (1-\theta)^i(\theta+r)^{-i}\exp\left[-\alpha\left(\frac{1}{\theta}-1\right)\right]d\theta$$

$$= \begin{cases} \dfrac{1}{(n+1)(n+2)} & (i=1), \\ \dfrac{2}{(n+1)(n+2)(n+3)} & (i=2), \end{cases}$$

whence it is clear that

$$\frac{\partial n}{\partial \alpha} > 0 \quad (E,\ T_1 \text{ fixed}).$$

From our previous discussion, it follows that the structure of a steady deflagration wave becomes increasingly sensitive to external perturbations as α increases. Since α increases with increasing dilution, this prediction of the theory is in qualitative agreement with experiment if the interpretation of experimental instability phenomena suggested in Part I is correct. The theory also predicts that the sensitivity of a flame to external perturbations is independent of the pressure, at least in a first approximation, and here too—with the same proviso as before—the theory agrees with experiment.[4]

[4] See Lewis and von Elbe, *Combustion, Flames and Explosions of Gases* (Academic Press, Inc., New York, 1951), p. 761.

THE JOURNAL OF CHEMICAL PHYSICS VOLUME 22, NUMBER 2 FEBRUARY, 1954

The Thermodynamic Properties of Gaseous Titanium*

HARWOOD G. KOLSKY, *Los Alamos Scientific Laboratory, University of California, Los Alamos, New Mexico*

AND

PAUL W. GILLES, *Department of Chemistry, University of Kansas, Lawrence, Kansas*

(Received October 1, 1953)

Tables of the thermodynamics properties of titanium considered as an ideal monatomic gas were calculated using the Los Alamos Scientific Laboratory IBM 701 Computer for a temperature range 0 to 8000°K.

IN an earlier paper[1] one of the authors participated in the calculation of a table of the thermodynamic properties of titanium considered as an ideal monatomic gas in the temperature range 0 to 5000°K. At that time the tables were stopped at 5000°K and several blank places were left because of the very tedious calculations required to proceed further. The recent appearance of high-speed digital computers on the scene has made it possible to perform such calculations in much shorter time and with much less human effort.

Table I from 0 to 8000°K was computed on the IBM 701 Calculator at the Los Alamos Scientific Laboratory.

* This work was supported by the U. S. Atomic Energy Commission.

[1] P. W. Gilles and Q. D. Wheatley, J. Chem. Phys. **19**, 129 (1951).

TABLE I. The thermodynamic properties of gasesous titanium.

T deg K	$-(F_T^0-H_0^0)/T$ cal/deg mole	$H_T^0-H_0^0$ cal/mole	S_T^0 cal/deg mole	C_p^0 cal/deg mole
10	18.8884	49.6798	23.8563	4.96798
20	22.3320	99.3628	27.3001	4.97000
30	24.3471	149.234	29.3215	5.02099
40	25.7816	200.216	30.7870	5.19654
50	26.9049	253.472	31.9742	5.46304
60	27.8367	309.517	32.9953	5.74307
70	28.6395	368.218	33.8997	5.98968
80	29.3487	429.148	34.7130	6.18802
90	29.9864	491.819	35.4510	6.33868
100	30.5670	555.781	36.1248	6.44708
110	31.1008	620.641	36.7429	6.51938
120	31.5950	686.067	37.3122	6.56135
130	32.0553	751.784	37.8382	6.57826
140	32.4860	817.565	38.3257	6.57488
150	32.8906	883.229	38.7787	6.55548
160	33.2719	948.634	39.2008	6.52378
170	33.6324	1013.67	39.5951	6.48299
180	33.9741	1078.27	39.9644	6.43575
190	34.2986	1142.37	40.3110	6.38425
200	34.6074	1205.95	40.6371	6.33023
225	35.3193	1362.48	41.3747	6.19224
250	35.9578	1515.61	42.0202	6.05972
275	36.5354	1665.56	42.5920	5.93872
298.16	37.0247	1801.92	43.0681	5.83861
300	37.0619	1812.66	43.1040	5.83116
325	37.5447	1957.23	43.5669	5.73689
350	37.9902	2099.60	43.9890	5.65484
375	38.4032	2240.06	44.3766	5.58361
400	38.7879	2378.86	44.7350	5.52176
425	39.1476	2516.22	45.0681	5.46798
450	39.4853	2652.32	45.3793	5.42108
475	39.8033	2787.32	45.6712	5.38006
500	40.1036	2921.36	45.9463	5.34406
550	40.6582	3187.01	46.4527	5.28431
600	41.1605	3450.01	46.9104	5.23733
650	41.6191	3710.90	47.3281	5.19998
700	42.0408	3970.13	47.7123	5.17011
750	42.4309	4228.02	48.0682	5.14629
800	42.7937	4484.84	48.3997	5.12758
850	43.1327	4740.85	48.7101	5.11344
900	43.4507	4996.26	49.0021	5.10356
950	43.7502	5251.27	49.2778	5.09783
1000	44.0332	5506.11	49.5392	5.09625
1050	44.3014	5760.97	49.7879	5.09886
1100	44.5562	6016.07	50.0253	5.10572
1150	44.7990	6271.61	50.2525	5.11689
1200	45.0308	6527.83	50.4706	5.13239
1250	45.2526	6784.92	50.6805	5.15221
1300	45.4653	7043.12	50.8830	5.17630
1350	45.6696	7302.62	51.0789	5.20457
1400	45.8662	7563.64	51.2687	5.23687
1450	46.0557	7826.38	51.4531	5.27304
1500	46.2386	8091.01	51.6325	5.31289
1550	46.4154	8357.72	51.8074	5.35620
1600	46.5866	8626.68	51.9782	5.40273
1650	46.7525	8898.04	52.1452	5.45225
1700	46.9136	9171.95	52.3087	5.50453
1750	47.0700	9448.54	52.4691	5.55930
1800	47.2222	9727.92	52.6265	5.61636
1850	47.3703	10010.2	52.7812	5.67546
1900	47.5147	10295.5	52.9333	5.73641
2000	47.7931	10875.4	53.2308	5.86303
2100	48.0590	11468.3	53.5200	5.99481
2200	48.3137	12074.5	53.8020	6.13059
2300	48.5583	12694.5	54.0776	6.26943
2400	48.7939	13328.5	54.3474	6.41057
2500	49.0214	13976.7	54.6120	6.55346
2600	49.2414	14639.2	54.8718	6.69761
2700	49.4547	15316.2	55.1273	6.84266
2800	49.6618	16007.8	55.3788	6.98829
2900	49.8632	16713.9	55.6265	7.13418
3000	50.0594	17434.6	55.8709	7.28006
3200	50.4376	18919.7	56.3500	7.57056
3400	50.7992	20462.6	56.8176	7.85720
3600	51.1463	22062.1	57.2746	8.13723
3800	51.4807	23716.8	57.7219	8.40776
4000	51.8038	25424.4	58.1598	8.66606
4200	52.1167	27182.3	58.5886	8.90968
4400	52.4240	28987.2	59.0083	9.13666
4600	52.7158	20835.7	59.4192	9.34556
4800	53.0035	32724.2	59.8210	9.53549
5000	53.2841	34648.6	60.2138	9.70608
5200	53.5581	36605.3	60.5975	9.85746
5400	53.8257	38590.4	60.9720	9.99008
5600	54.0875	40600.1	61.3375	10.1047
5800	54.3437	42631.1	61.6938	10.2022
6000	54.5945	44680.0	62.0411	10.2838
6200	54.8402	46743.6	62.3794	10.3505
6400	55.0810	48819.2	62.7089	10.4033
6600	55.3170	50904.1	63.0297	10.4435
6800	55.5485	52995.9	63.3419	10.4720
7000	55.7755	55092.2	63.6457	10.4898
7200	55.9982	57191.1	63.9414	10.4977
7400	56.2168	59290.7	64.2290	10.4967
7600	56.4314	61389.2	64.5088	10.4873
7800	56.6420	63485.1	64.7810	10.4703
8000	56.8488	65576.9	65.0458	10.4464

The problem code was prepared using "Dual Coding"[2] which is a system for automatically performing arithmetic operations in "floating decimal" (i.e., the numbers used are in the form $A\times10^B$). It also contains various common functions such as exp, ln, sin. Eight significant figures are carried in all calculational steps. The 701 required an average of twelve seconds to calculate and print the tabular values for one temperature.

The constants used in the calculation are identical to those used in reference 1. Only six nonrounding errors were found in the previous table, none of any consequence.

[2] S. Schlesinger, "Dual Coding System," Los Alamos Scientific Laboratory Report LA-1573 (1953).

Wavelength Shifts in the near Ultraviolet Spectra of Fluorinated Benzenes

H. SPONER*
Department of Physics, Duke University, Durham, North Carolina
(Received June 30, 1953)

Results on wavelength shifts of the 0,0 bands in the near ultraviolet absorption spectra of a number of fluorinated benzenes are presented, and a brief discussion in terms of the inductive effect and the migration effect is added.

IT has been observed that the electronic transition which occurs in benzene at 2600A shifts toward longer wavelengths upon substitution. This shift has been the subject of many studies and was discussed, usually together with the intensity of the absorption spectra, in its dependence upon the resonance interaction between ring and substituent (migration effect, mesomeric effect) and upon the polarity of the ring-substituent bond (inductive effect).[1] In general, the results on intensities[1b,1c,2] have been more satisfactory than those on wavelength shifts.

We have made in our laboratory some interesting observations on wavelength shifts in the spectra of fluorinated benzenes. The most unusual result was obtained for 1,3,5-trifluorobenzene.[3] Unlike the cases of other substitutions studied spectroscopically, in which the spectrum of the trisubstituted derivative shifts further to the red as compared to that of the mono-derivative (see for example 1,3,5-trichlorobenzene[4] in Table I), the spectrum of 1,3,5-trifluorobenzene shifts toward the violet as compared to the fluorobenzene spectrum. In fact, it even lies at shorter wavelengths than the benzene spectrum. Although the analysis has been carried through only partially so far, it can be said that the calculated position of the 0,0 band is probably at 38 527 cm^{-1}. This means that introduction of two more fluorine atoms in the 3 and 5 positions over-compensates the small red shift for fluorobenzene, causing a total shift of 708 cm^{-1} to the violet with respect to the 0,0 band in fluorobenzene. We believe this to be the first example of this type. The spectrum has the intensity and the appearance characteristic of a transition forbidden by symmetry, as is to be expected for the first absorption of a symmetrical trisubstituted benzene molecule and as has been found to be the case for 1,3,5-trimethylbenzene and 1,3,5-trichlorobenzene.

Subsequent investigation of the near ultraviolet spectrum of 1,3,5-tris-trifluoromethylbenzene[5] gave as probable position of the nonobservable 0,0 band 38 100 cm^{-1}, that is, it is shifted towards shorter wavelengths not only with respect to benzotrifluoride, but also with respect to benzene (Table I).

Another interesting example offers the series fluorobenzene, *p*-difluorobenzene,[6] 1,2,4-trifluorobenzene,[7] where the 0,0 band of the *p*-diderivative moves toward the red and that of the 1,2,4-triderivative shifts a little back toward the position of the 0,0 band of the mono-derivative. The corresponding transitions in chlorinated benzenes, added for comparison in Table I, show a continued red shift from the mono- to the trisubstituted compounds.

The observations on the shifts suggest that they are the result of the combined action of two effects. In the first effect, the fluorine because of its large electron affinity attracts σ electrons from the ring (inductive effect), in the second effect, charge from the non-bonding $2p\pi$ electrons of the substituent can migrate into the ring (migration effect).† Because of the very high ionization potential of the fluorine atom, the second effect is very small. The effects are opposite in sign. They will not only influence the charge of the fluorinated carbons, but also the charge of the whole frame in which the mobile π electrons travel. If the migration effect predominates, the negative charge added to the ring will decrease the potential field in which the π electrons move; if, on the other hand, the effect resulting from the electron affinity is greater, the ring potential increases.‡ Thus, in the first case the absorption spectrum will show a red shift and in the second case a blue shift. In multiple substitutions, the arrangements producing the smallest migration effect will give the largest blue shift. In the trisubstituted fluorobenzenes this is,

* Guggenheim Fellow, at present at Institute for Mechanics and Math. Phys., University of Uppsala, Sweden.

[1] (a) K. F. Herzfeld, Chem. Revs. **41**, 233 (1947); (b) A. L. Sklar, J. Chem. Phys. **7**, 984 (1939); *ibid.* **10**, 135 (1942); (c) Th. Förster, Z. Naturforsch. **2a**, 149 (1947); (d) F. A. Matsen, J. Am. Chem. Soc. **72**, 5243 (1950); (e) W. W. Robertson and F. A. Matsen, J. Am. Chem. Soc. **72**, 5252 (1950).

[2] John R. Platt, J. Chem. Phys. **19**, 263 (1951).

[3] M. L. N. Sastri, Ph.D. dissertation, Duke University, 1951.

[4] H. Sponer and M. D. Hall, V. Henri Memorial Vol. Contributions à l'Etude de la Structure Moléculaire, Desoer 1947–1948, p. 211.

[5] C. D. Cooper and F. W. Noegel, J. Chem. Phys. **20**, 1903 (1952).

[6] C. D. Cooper, Phys. Rev. **91**, 241 (A) (1953). The solution spectrum was taken by A. Wenzel and H. P. Stephenson at our laboratory.

[7] Vapor and solution spectra were first obtained by H. P. Stephenson and are now being studied in more detail by K. N. Rao in our laboratory.

† The π electrons can also be attracted in the inductive effect, but the migrational effect is considered more important for them.

‡ The views presented here lie somewhat along the lines recently put forward by C. A. Coulson [Proc. Phys. Soc. (London) **65**, 933 (1952)] in his treatment of alkyl shifts in absorption spectra of azulenes. See also Pullman, Mayot, and Berthier, J. Chem. Phys. **18**, 257 (1950) and H. C. Longuet-Higgins and R. G. Snowden, Jr., J. Chem. Soc. **1952**, 1404.

for example, the case for the 1,3,5-arrangement, but in the 1,2,4-compound the migrational effect outweighs the inductive effect. The chlorobenzenes will always give a red shift, as not only is the electron affinity of the Cl atom smaller than that of the F atom, but it also has a much smaller ionization potential, which will increase the migrational effect.

Förster has given a semi-empirical formula for the wavelength shift in substituted benzene spectra. It consists of two terms

$$\Delta\nu=\nu_0-\nu=nB+(n(3-n)/2+3p)C. \qquad (1)$$

Here ν_0 and ν are the 0,0 bands of benzene and the substituted benzene in wave numbers, n is the number of substituents, p is the number of pairs in *para*-position, and B and C are constants characteristic of the particular substituent. The number in the large bracket, called here μ, represents a geometrical property of the molecule. The same number is important for the intensity increase of the electronic transition in question over the intensity of the unsubstituted parent molecule, benzene, that is $I-I_0=\mu A$. Here I_0 is the "vibrational" contribution to the intensity (taken as the benzene value), I is the total intensity and A is another constant characteristic of the substituent. The ratios of μ numbers in substituted benzenes C_6H_5S: *o*-$C_6H_4S_2$: *m*-$C_6H_4S_2$: *p*-$C_6H_4S_2$: 1,2,4-$C_6H_3S_3$: 1,3,5-$C_6H_3S_3$=1:1:1:4:3:0 correspond then roughly to the ratios of the observed intensities I[1b,1c,2] (f values). It was found possible to express the observed shifts in the spectra of the fluorinated benzenes by a Förster formula, if a negative value is chosen for B. The negative B might indicate the importance of the large electronegativity of the fluorine atom. The best fit of the fluoro-series is obtained for B values between -100 and -130 and corresponding C values between 380 and 410, all in wave numbers. The shifts of the corresponding chloro-series (all to the red) may be represented with B and C values of about 845 and 170 cm^{-1}, respectively. Because of scarcity of material in the fluoromethyl-series no similar representation is possible for the shifts in this series and for the shifts in the fluorinated benzotrifluorides.

TABLE I. Positions of 0,0 bands (vapor) and intensities in the near ultraviolet spectra of some fluorinated and chlorinated benzenes.

Molecule	0,0 band cm^{-1}	Intensity $f\times10^3$
Benzene C_6H_6	38 089 calc	1.6
Fluorobenzene C_6H_5F	37 819[a]	8.9
m-difluorobenzene	37 909[b]	9.6
p-difluorobenzene $C_6H_4F_2$	36 843[a]	22.4
1,2,4-trifluorobenzene	37 123[f]	19.2
1,3,5-trifluorobenzene $C_6H_3F_3$	38 527[g] calc	~2.0
1,2,4,5-tetrafluorobenzene $C_6H_2F_4$	36 605/12[e]	
Benzotrifluoride $C_6H_5CF_3$	37 819[d]	7.1
1,4-bis-trifluoromethylbenzene $C_6H_4(CF_3)_2$	37 460[g]	12.0
1,3,5-tris-trifluoromethylbenzene $C_6H_4(CF_3)_3$	~38 100[g] calc	2.1
m-fluorobenzotrifluoride	37 355[e]	(14.7)
p-fluorobenzotrifluoride $C_6H_4FCF_3$	37 866[e]	(2.4)
2,5-difluorobenzotrifluoride $C_6H_3F_2CF_3$	36 800 sol[f]	27.0
Perfluorotoluene $C_6F_5CF_3$	37 700 sol[f]	21.0
Chlorobenzene C_6H_5Cl	37 052[g]	3.0
o-dichlorobenzene	36 265[h]	4.0
m-dichlorobenzene $C_6H_4Cl_2$	36 186[h]	4.1
p-dichlorobenzene	35 743[h]	~6.8
1,2,4-trichlorobenzene	35 108[i]	~6.0
1,3,5-trichlorobenzene $C_6H_3Cl_3$	35 498[i] calc	2.1

[a] S. H. Wollman, J. Chem. Phys. **14**, 123 (1946).
[b] V. Ramakrishna Rao and H. Sponer, Phys. Rev. **87**, 213(A) (1952).
[c] Results of K. N. Rao in our laboratory.
[d] H. Sponer and D. S. Lowe, J. Opt. Soc. Am. **39**, 840 (1949).
[e] W. T. Cave and H. W. Thompson, Disc. Faraday Soc. **9**, 35 (1950).
[f] H. B. Klevens and Lois J. Zimring, J. chim. phys. **49**, 377 (1952).
[g] H. Sponer and S. H. Wollman, J. Chem. Phys. **9**, 816 (1941).
[h] H. Sponer, Revs. Modern Phys. **14**, 224 (1942).
[i] Hedwig Kohn and H. Sponer, J. Opt. Soc. Am. **39**, 75 (1949).

It is perhaps not superfluous to add to this discussion that all known near ultraviolet spectra of fluorinated benzenes in the vapor phase show discrete structure with sharp or rather sharp bands. The difference of appearance of the spectra of 1,3,5-trifluorobenzene and 1,3,5-trichlorobenzene is particularly striking.

Acknowledgment is made to Dr. J. Rud Nielsen (University of Oklahoma), Dr. D. C. Smith, and Mrs. N. B. Moran (Naval Research Laboratory), for kindly supplying us with samples of 1,3,5- and 1,2,4-trifluorobenzene, and 1,2,4,5-tetrafluorobenzene; and to Dr. L. Bigelow (Duke University) for the *meta*- and *para*-difluorobenzene samples. It was a pleasure to have stimulating discussions with Dr. Platt on the subject of wavelength shifts.

THE JOURNAL OF CHEMICAL PHYSICS VOLUME 22, NUMBER 2 FEBRUARY, 1954

The Relation between Energy Levels of Substituent Groups and Electron Migration Effects in Some Monosubstituted Benzenes

SABURO NAGAKURA AND JIRO TANAKA
Institute of Science and Technology, University of Tokyo, Tokyo, Japan
(Received September 10, 1953)

Determinations of the highest occupied (H_B, H_S) and the lowest vacant levels (V_B, V_S) were made with benzene and some substituent groups using experimental knowledge of their ionization potentials and their near ultraviolet absorption spectra. On the basis of the relative height of these levels, monosubstituted benzenes can be classified into following three groups: (1) $|V_S-H_B|<|V_B-H_S|$ for *meta*-directing molecules: (2) $|V_S-H_B|>|V_B-H_S|$ for *ortho-*, *para*-directing molecules: (3) $|V_S-H_B|\approx|V_B-H_S|$ for styrene. By the aid of a simple quantum-mechanical treatment, it becomes sure that in the case of (1) the interaction between levels V_S and H_B is predominant and the migrating electron flows out of benzene into the substituent: on the other hand in the case of (2) the interaction between levels V_B and H_S is the stronger and the migrating electron moves in the reverse direction: and finally, in the case of (3), both interactions referred to in the foregoing should be taken into account with almost equal importance.

Furthermore, it was shown that the difference in the ionization potential between the *meta-* and the *ortho-*, *para*-directing monosubstituted benzenes can be interpreted by taking into consideration the interaction of H_B with H_S or V_S, and that the absorption bands in the wavelength region 2300~2600A, observed with *meta*-directing molecules, may be regarded as due to the transition between two levels which occur by the interaction between levels V_S and H_B.

INTRODUCTION

IT is well known that the monosubstituted benzenes may be classified into two different groups on the basis of the location on which the cationoid substitution takes place. One of them is the *ortho-*, *para*-directing group and the other is the *meta*-directing one. Aniline and phenol are typical examples of the former, and nitrobenzene and benzoic acid those of the latter. Between these two groups there are some notable differences in their physico-chemical properties. For instance, from the consideration of dipole moments, it is deduced that in the *ortho-*, *para*-directing monosubstituted benzenes, migrating electrons flow out of the substituent groups into the benzene ring, while in the *meta*-directing ones they move in the opposite direction.[1] Furthermore the recent investigation on the ionization potential made by Morrison[2] shows that ionization potentials of *ortho-*, *para*-directing molecules, such as phenol, toluene, and chlorobenzene, are smaller than that of benzene, and that the reverse is the case for those of *meta*-directing ones, e.g. nitrobenzene and acetophenone.

Previously, electron migrations of these molecules have been treated qualitatively from the standpoint of resonance theory.[3] Furthermore, for the *ortho-*, *para*-directing molecules, several quantitative treatments have also been carried out by the use of the molecular orbital method.[4–6] However, it does not seem that any quantum-mechanical calculation has been made for the *meta*-directing molecule.

In this paper, it will be emphasized that the interactions between the highest occupied and the lowest vacant orbitals of benzene and the substituent group play an important rôle in the electron migration effect of the *meta*-directing molecule as well as the *ortho-*, *para*-directing one. Moreover, it will be seen that several differences in physico-chemical properties between two kinds of monosubstituted benzene molecules can be explained sufficiently well by the simple quantum-mechanical treatment by which the foregoing interactions are taken into consideration.

THE ESTIMATION OF ENERGY LEVELS FOR BENZENE AND FOR SOME SUBSTITUENT GROUPS

We will try to determine locations of molecular orbitals for benzene and some substituent groups. First of all, their highest occupied orbitals will be determined. From the standpoint of the molecular orbital theory, highest occupied orbitals may be regarded as equal to ionization potentials[7] to a first approximation. By the use of ionization potential data, therefore, they can easily be determined as shown in Fig. 1 where they are designated by H_B and H_S for benzene and the substituent group, respectively.

Secondly, the lowest vacant orbital can be estimated approximately by the combination of the highest occupied level mentioned in the foregoing and experimental knowledge about the electronic absorption spectra. As an example, this procedure will be explained with benzene. Its highest occupied π level can be determined as -9.24 ev from its ionization potential value obtained

[1] C. A. Coulson, *Valence* (Oxford University Press, London, 1952), p. 248.
[2] J. D. Morrison, J. Chem. Phys. **19**, 1305 (1951); J. D. Morrison and A. J. C. Nicholson, **20**, 1021 (1952).
[3] L. Pauling, *The Nature of the Chemical Bond* (Cornell University Press, Ithaca, 1940), p. 150.
[4] A. L. Sklar, J. Chem. Phys. **7**, 984 (1939).
[5] K. F. Herzfeld, Chem. Revs. **41**, 233 (1947).
[6] F. A. Matsen, J. Am. Chem. Soc. **72**, 5243 (1950).
[7] R. S. Mulliken, Report on Molecular Orbital Theory, 1947–1948 and 1948–1949 U. S. Office of Naval Research Reports of the Physics Department Spectroscopic Laboratory of the University of Chicago.

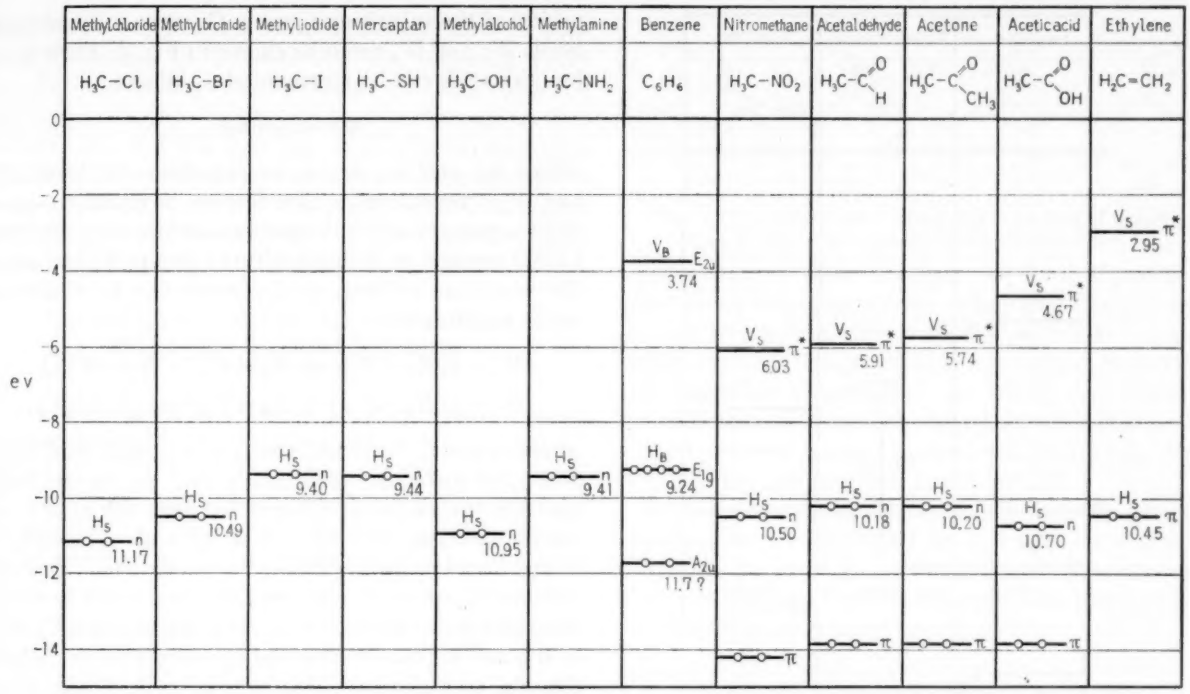

FIG. 1. Energy-level diagrams of benzene and some substituent groups. Ionization potential data are obtained from the following references. Benzene—references 2 and 8; ethylene—W. C. Price and W. T. Tutte, Proc. Roy. Soc. (London) **A174**, 207 (1940); nitromethane—private communication from Dr. Morrison; acetaldehyde—A. D. Walsh, Proc. Roy. Soc. (London) **A185**, 176 (1946); acetone—A. B. F. Duncan, J. Chem. Phys. **3**, 131 (1935); acetic acid, methyl amine, methyl alcohol—reference 2; methyl chloride, methyl bromide, methyl iodide—W. C. Price, J. Chem. Phys. **4**, 539 (1936); mercaptan—Price, Teegan, and Walsh, Proc. Roy. Soc. (London) **A201**, 600 (1951).

by Price and Wood,[8] and the mean value of six absorption bands corresponding to the transition $E_{1g} \rightarrow E_{2u}$ was estimated by Roothaan and Mulliken as 5.5 ev.[9] Then it may be concluded that its lowest vacant energy level V_B lies at -3.74 ev. For the carbonyl group the ionization potential (10.18 ev) should correspond to the energy value of the nonbonding electron in the oxygen atom,[10] and the absorption spectra corresponding to the $n \rightarrow \pi^*$ transition appears in 2880A (4.27 ev),[11] so its lowest vacant π^* level V_S can be estimated as -5.91 ev.

In the same way, we can determine energy levels for other substituent groups, such as nitro and carboxyl groups. In these cases it is estimated that the absorption spectra corresponding to the $n \rightarrow \pi^*$ transitions appear at 2800A[12] and 2050A[13] for nitro and carboxyl groups, respectively. Energy level-diagrams obtained thus with benzene and several substituent groups are shown in Fig. 1, where the level labeled by π represents the bonding π orbital. It may be estimated by the aid of the absorption spectrum corresponding to the $\pi \rightarrow \pi^*$ transition.

THE RELATION BETWEEN ENERGY-LEVEL DIAGRAMS AND THE DIRECTION OF THE ELECTRON MIGRATION

According to the method adopted for *ortho-*, *para-*directing monosubstituted benzene molecules by Sklar,[4] the electron migration between two groups can be interpreted on the basis of the interaction between the vacant orbital of one group and the occupied orbital of another. Furthermore, as pointed out by Coulson,[14] in order that there may be an effective interaction between two energy levels, it is necessary that their energies be of comparable magnitude, their symmetry appropriate, and their electron clouds overlap one another as much as possible.

From the foregoing viewpoint, the most striking feature of the energy-level diagrams given in Fig. 1 is that in *meta*-directing molecules the energy difference between levels H_B and V_S is much smaller than that between levels V_B and H_S. In addition to this, much more overlapping may be expected between orbitals V_S and H_B than between V_B and H_S, because the oxygen atom, to which the orbital H_S belongs, is far from the benzene ring. Therefore, it seems probable

[8] W. C. Price and R. W. Wood, J. Chem. Phys. **3**, 439 (1935).
[9] C. C. J. Roothaan and R. S. Mulliken, J. Chem. Phys. **16**, 118 (1948).
[10] R. S. Mulliken, J. Chem. Phys. **3**, 564 (1935).
[11] Am. Petroleum Inst. Catalog of Ultraviolet Spectrograms, p. 96; H. L. McMurry, J. Chem. Phys. **9**, 231 (1941); H. Baba, J. Chem. Soc. Japan, **72**, 214 (1951).
[12] Am. Petroleum Inst. Catalog of Ultraviolet Spectrograms, p. 104. This band may probably be due to the $n \rightarrow \pi^*$ transition because its intensity is weak and it shows the blue shift character.
[13] H. Ley and B. Arends, Z. physik. Chem. **B17**, 177 (1932); S. Nagakura, Bull. Chem. Soc. Japan **25**, 164 (1952).
[14] See reference 1, p. 71.

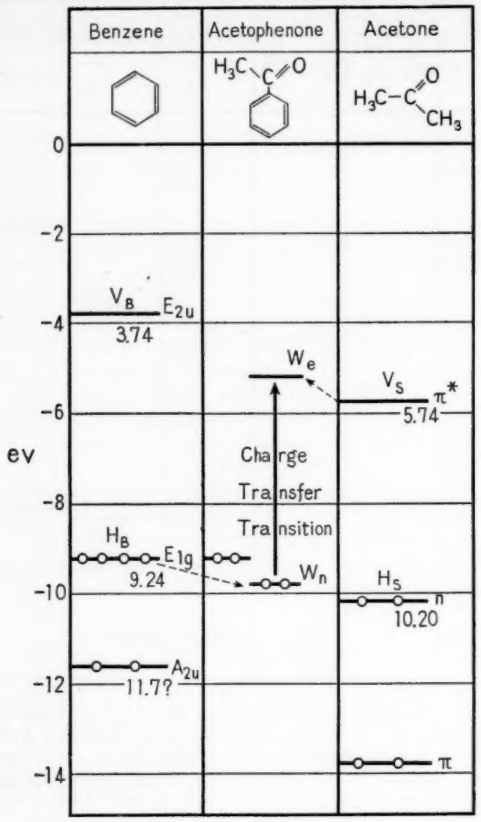

FIG. 2. New levels W_n and W_e caused by the interaction between levels H_B and V_S.

that for the *meta*-directing molecule, the interaction between levels H_B and V_S may be predominant and the π electron belonging to H_B migrates to V_S to some extent.

On the other hand, in *ortho*-, *para*-directing substituents, such as amino and hydroxyl groups, the lowest vacant orbital which can possess π character is $3p$. Its energy is probably so much greater[15] than that of H_B that no effective interaction occurs between them. In this case, therefore, we may expect that the interaction between levels H_S and V_B is overwhelming and the nonbonding π electron of the substituent migrates to the benzene ring. At any rate, it may be inferred from the foregoing qualitative consideration that the difference in the direction of the electron migration between *ortho*-, *para*-directing, and *meta*-directing monosubstituted benzene molecules can be interpreted on the basis of the interaction between the highest occupied and the lowest vacant orbitals of benzene and substituent groups. Then this problem will be treated somewhat more quantitatively by the following quantum-mechanical calculation.

For *meta*-directing molecules, the highest occupied orbital of benzene interacts with the lowest vacant orbital of the substituent group. Consequently two new levels W_n and W_e result as shown in Fig. 2. Their wave functions Ψ's can be represented as follows:

$$\Psi = a\varphi_B + b\varphi_S, \tag{1}$$

where φ_B and φ_S are wave functions for levels H_B and V_S, respectively. The former is equal to φ_1 in Sklar's paper[4] and the latter was obtained by applying LCAO method to each substituent group. By the aid of the variation method, energy levels can be evaluated easily as follows:[16]

$$\begin{aligned} W_n &= \tfrac{1}{2}[H_B + V_S - \{(H_B - V_S)^2 + 4c_b^2 c_s^2 \beta^2\}^{\frac{1}{2}}] \\ W_e &= \tfrac{1}{2}[H_B + V_S + \{(H_B - V_S)^2 + 4c_b^2 c_s^2 \beta^2\}^{\frac{1}{2}}], \end{aligned} \tag{2}$$

where c_b and c_s[17] are coefficients of π atomic orbitals χ_b and χ_s in molecular orbitals φ_B and φ_S, respectively, and β is the exchange integral between the above two atomic orbitals, provided that χ_b and χ_s belong to atoms b and s, by the linkage between which the substituent is attached to the benzene ring. If the exchange integral β is estimated as -3.00 ev, the numerical values of W_n and W_e can be obtained for nitrobenzene, benzaldehyde, acetophenone, and benzoic acid. These results are given in Table I, together with values of coefficients a, b, and c_s.

In the ground state, the level W_n is occupied by two electrons, so that π electron densities can be determined for several *meta*-directing molecules as shown in Fig. 3. Similar calculations can also be made for *ortho*-, *para*-directing molecules by considering the interaction between levels H_S and V_B. The results are given in Table I and Fig. 3.

It can be seen from Table I and Fig. 3 that π electrons migrate from the benzene ring to the substituent in the *meta*-directing molecule while in the *ortho*-, *para*-directing molecule, they flow in the reverse direction. Therefore, it may be said that the direction of the electron migration should be determined to a first approximation by the relative height of the highest occupied

TABLE I. Energy levels, coefficients a^*, b^*, and c_s for some monosubstituted benzene molecules.

	Nitrobenzene	Acetophenone	Benzaldehyde
W_n (ev)	−9.76	−9.82	−9.84
W_e (ev)	−6.33	−5.16	−5.31
a_n	0.912	0.936	0.931
b_n	0.388	0.343	0.365
c_s	0.71	0.89	0.89
	Benzoic acid	**Phenol**	**Aniline**
W_n (ev)	−9.56	−11.34	−9.74
W_e (ev)	−4.35	−3.35	−3.41
a_n	0.968	0.975	0.974
b_n	0.249	0.221	0.227
c_s	0.73	1.00	0.806

* These values are referred to the normal state.

[15] It is most probable that the $3p$ levels of oxygen and nitrogen atoms may be higher than -2 ev, although they cannot be determined definitely. See R. J. Thompson and A. B. F. Duncan, J. Chem. Phys. 14, 573 (1946).

[16] In this calculation, the overlap integral between φ_B and φ_S is neglected. Further, it is approximated that $\int \varphi_B H \varphi_B d\tau$ and $\int \varphi_S H \varphi_S d\tau$ are equal to H_B and V_S, respectively.

[17] c_b is equal to $(1/3)^{\frac{1}{2}}$.

and the lowest vacant orbitals of benzene and the substituent group. In this respect, the following point should be taken into consideration; *viz.*, in styrene the difference between V_B and H_S is almost equal to that between V_S and H_B (see Fig. 1). Therefore, one may expect it to be difficult to determine whether styrene is *ortho-*, *para*-directing or *meta*-directing. This surmise can probably be linked with the fact that its dipole moment is small.[18]

IONIZATION POTENTIALS OF SOME MONOSUBSTITUTED BENZENE MOLECULES

The experimental value of ionization potentials of some monosubstituted benzenes obtained by Morrison[2] are given in Table II. By a study of this table, it can be seen that ionization potentials of nitrobenzene, benzaldehyde, and acetophenone are larger than that of benzene, while the opposite tendency is observed with *ortho-*, *para*-directing monosubstituted benzenes such as phenol, toluene, and chlorobenzene, i.e., that the highest occupied level of the benzene ring (H_B) lowers in the case of the *meta*-directing monosubstituted benzene molecule, while it rises in the case of the *ortho-*, *para*-directing one. In order to explain this notable property, the two following reasons should be taken into consideration.[19] One of them is that interactions of the level H_B of benzene with those of the substituent may result in bonding or antibonding tendencies and it may become low or high (see Fig. 2). Another reason is that changes in the force field due to the electron migration, including the accumulation of net positive or negative charges on the benzene ring, may cause deviations of ionization potentials of monosubstituted benzene molecules from that of benzene. Here the first reason only will be treated in more detail.[20]

As apparently seen from Fig. 1, in the case of the *ortho-*, *para*-directing molecules the interaction between levels H_S and H_B probably will be predominant as

TABLE II. Values of ionization potentials for some monosubstituted benzene molecules.

Substance	Benzene	Phenol	Chloro-benzene	Bromo-benzene
I_p (ev)	9.52	9.03	9.42	9.41
Substance	Benzaldehyde	Acetophenone	Nitrobenzene	
I_p (ev)	9.82	9.77	10.15	
Substance	Iodobenzene	Styrene	Toluene	
I_p (ev)	9.10	8.86	9.23	

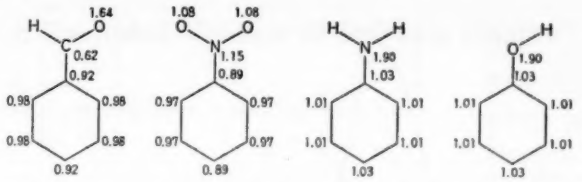

FIG. 3. Charge densities of some monosubstituted benzenes.

compared with those between the level H_B and the other levels belonging to the substituent. As the result of this interaction, the level H_B, which is certainly higher than H_S,[21] may rise, and it may be expected that the ionization potential of an *ortho-*, *para*-directing molecule becomes smaller than that of benzene. The same conclusion can be obtained with styrene, in which the level H_S probably lies just below H_B.

On the other hand, in the case of the *meta*-directing molecule the level H_B may be lowered by the interaction with the level V_S of the substituent as shown in Fig. 2.[22] This stabilization energy (ΔE) can easily be given by the following equation,

$$\Delta E = H_B - W_n = \tfrac{1}{2}[H_B - V_S + \{(H_B - V_S)^2 + 4c_b^2 c_s^2 \beta^2\}^{\frac{1}{2}}]. \quad (3)$$

Unfortunately, this quantity ΔE cannot be compared immediately with the increment of the ionization potential. As is well known, the highest occupied level of benzene is doubly degenerate and only one of them can interact with the level V_S. The other level cannot be altered by the substituent group; i.e., the doubly degenerate level splits into two levels. The energy difference between them, which is equal to ΔE, will probably be too small to detect them distinctly by the use of the electron impact method. Therefore, it seems probable that the observed ionization potential is equal to the average value of them. Thus, to a first approximation, $\frac{1}{2}\Delta E$ may be regarded as the difference in the ionization potential between benzene and the *meta*-directing molecule. The calculated values of $\frac{1}{2}\Delta E$ for some monosubstituted benzene molecules are shown in Table III together with corresponding observed values. The agreement between theoretical and observed values given in Table III may be satisfactory in view of uncertainties in the theoretical treatment.

NEAR ULTRAVIOLET ABSORPTION SPECTRA OF MONOSUBSTITUTED BENZENES

It is seen from Fig. 4 that *meta*-directing monosubstituted benzene molecules exhibit two absorption bands in the wavelength region from 2200A to 3000A. It seems certain that the longer wavelength one, which appears at 2600~2900A, corresponds to the benzene 2600A band. Another band, which appears at 2300

[18] This problem has been investigated by Mr. Nukasawa from the same point of view. Busseiron Kenkyu, July (1952) (in Japanese); J. Phys. Soc. Japan **8**, 132 (1953).

[19] R. S. Mulliken, J. Chem. Phys. **3**, 514 (1935).

[20] In this respect, it is to be noticed that the ionization potential of styrene, in which the effective electron migration seems to be negligible, is very much smaller than that of benzene. This fact seems to show that the second reason is not important, at least not in the case of styrene.

[21] The comparison must be made with the ionization potential values obtained by the same method, because the value obtained by the electron impact method is usually larger than that obtained by the far ultraviolet absorption spectrum.

[22] Although the level H_S of the *meta*-directing substituent lies near the level H_B, they cannot interact, because the orbital corresponding to the level H_S does not possess π-character.

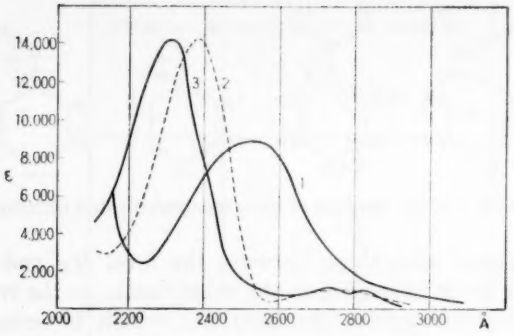

FIG. 4. Near ultraviolet absorption spectra of some monosubstituted benzenes (solvents; iso-octane or *n*-heptane).

1. Nitrobenzene, API (Am. Petroleum Inst. Catalog of Ultraviolet Spectrograms), p. 105.
2. Acetophenone, observed by the authors.
3. Benzoic acid, API (Am. Petroleum Inst. Catalog of Ultraviolet Spectrograms), p. 354.

~2600A, is very much stronger than the longer wavelength one, and its origin is not yet determined conclusively, although the possibility was suggested by Walsh[23] that the 2350A band of benzaldehyde may correspond to the benzene 1980A band. It may be especially difficult to interpret the 2600A band of nitrobenzene from the same point of view, because it is unusual to expect such a large shift of the wavelength as is observed in this case. Therefore, in this paper we will try to interpret the band from a different aspect, *viz.*, to show that it may be regarded as due to the transition between levels W_n and W_e which occur by the interaction between levels H_B and V_S as shown in Fig. 2.

Energy differences between levels W_n and W_e can easily be obtained by the use of Eq. (2) for *meta*-directing monosubstituted benzene molecules. Their values are shown in Table IV together with those of the oscillator strength f, which can be calculated by the following equation:

$$f=(4.704\times10^{-7})\nu\left(e\int\Psi_N\gamma\Psi_E d\tau\right)^2. \qquad (4)$$

In this table, the observed values of these two quantities are also given for the purpose of comparison. Although the present theoretical treatment is too simple to expect a satisfactory accordance between observed and calculated values, it is seen from the table that the wavelength and the intensity of the band can be explained semiquantitatively on the basis of the view that it occurs by a transition between levels W_n and W_e. At least, it may be said that the present theoretical treatment, in spite of its simplicity, can explain qualitatively the experimental results obtained until now.[24]

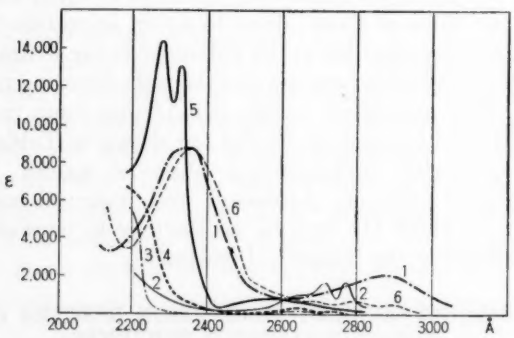

FIG. 5. Near ultraviolet absorption spectra of some monosubstituted benzenes (solvents; isooctane or *n*-heptane).

1. Aniline (Am. Petroleum Inst. Catalog of Ultraviolet Spectrograms), p. 106.
2. Phenol (Am. Petroleum Inst. Catalog of Ultraviolet Spectrograms), p. 99.
3. Chlorobenzene (Am. Petroleum Inst. Catalog of Ultraviolet Spectrograms), p. 300.
4. Bromobenzene (Am. Petroleum Inst. Catalog of Ultraviolet Spectrograms), p. 304.
5. Iodobenzene (Am. Petroleum Inst. Catalog of Ultraviolet Spectrograms), p. 308.
6. Thiophenol (Am. Petroleum Inst. Catalog of Ultraviolet Spectrograms), p. 427.

[23] A. D. Walsh, Trans. Faraday Soc. **42**, 62 (1946).

TABLE III. Values of $\frac{1}{2}\Delta E$ for some monosubstituted benzene molecules.

	Benzaldehyde	Acetophenone	Nitrobenzene
Difference of I_p between benzene and monosubstituted benzenes (ev)	0.30	0.25	0.63
$\frac{1}{2}\Delta E$ (ev)	0.30	0.29	0.26

TABLE IV. Calculated and observed values of the wavelength and the oscillator strength for the transition $W_n \rightarrow W_e$.

	Benzaldehyde	Acetophenone	Benzoic acid	Nitrobenzene
$h\nu$ (obs) (ev)	5.14	5.21	5.38	4.70
$h\nu$ (calc) (ev)	4.54	4.66	5.22	4.02
f (obs)	0.27	0.26	0.31	0.21
f (calc)	0.44	0.40	0.37	0.54

According to the mechanism mentioned in the foregoing, the light absorption causes the electron removal from benzene to the substituent for the *meta*-directing monosubstituted benzene molecule. Therefore, it is similar in the nature to the charge transfer absorption presented by Mulliken[25] and it may be regarded as the intramolecular charge transfer absorption.[26]

ACKNOWLEDGMENT

We wish to thank Professor S. Mizushima and Professor K. Higasi for their kind advice and encouragement throughout this investigation and Mr. Nukasawa for his helpful discussion. Our thanks are also due Dr. Morrison for his kindness in informing us of his unpublished ionization potential data.

[24] It may be possible to interpret the absorption bands in the 2300A region observed with aniline, thiophenol, and iodobenzene from the same point of view (see Fig. 5).

[25] R. S. Mulliken, J. Am. Chem. Soc. **74**, 811 (1952).

[26] McConnell *et al.* pointed out that the 2600A band of nitrobenzene may be the intramolecular charge transfer spectrum. See McConnell, Ham, and Platt, J. Chem. Phys. **21**, 66 (1953).

Critique of a Method of Treating the Effect of Excluded Volume in Polymer Chains*

ROBERT J. RUBIN
Applied Physics Laboratory, The Johns Hopkins University, Silver Spring, Maryland
(Received September 18, 1953)

The nature of an implicit assumption in a recent Fokker-Planck treatment of the excluded volume problem is indicated. This assumption makes the results of the treatment conditional. It is shown that if one can verify the assumption, one can dispense with the use of a Fokker-Planck equation.

INTRODUCTION

THE purpose of this note is to point out an implicit assumption in a recent treatment[1] of the excluded volume problem.[2] In addition, it will be shown that if one can verify the assumption made in HKU, one can dispense with the use of a Fokker-Planck equation and use the procedure of I. HKU consider a "molecule" consisting of a random walk of $N+1$ steps in which each step length has the same Gaussian probability distribution function (p.d.f.). They give the p.d.f. of finding steps at some point $\mathbf{R}$ when two specified steps of the random walk are at the origin and at $\mathbf{r}$. The calculated size of the "molecule" is completely determined by the form of this p.d.f., i.e., its dependence on N, $\mathbf{R}$, and $\mathbf{r}$.

We will first obtain an exact expression for the p.d.f. for finding intermediate steps in a small region ω around $\mathbf{R}$ when the first step is at the origin and the $N+1^{th}$ step is at $\mathbf{R}_N$. Then we will obtain the analogous p.d.f. for the restricted problem in which no intermediate steps can overlap. Comparison of these two p.d.f.'s should point up the nature of the implicit assumption in the HKU calculations.

STEP DENSITY

(a) No Intermediate Step Interaction

Consider a random walk of $N+1$ steps in which the first step is at the origin and the $N+1^{th}$ step is at $\mathbf{R}_N$. Let $P(\mathbf{R}_N,\mathbf{R})$ be the probability for this random walk that no intermediate step lies in a spherical region ω around $\mathbf{R}$, and let $P_0(\mathbf{R}_N)$ be the probability that the ends of the walk of $N+1$ steps are at 0 and $\mathbf{R}_N$. Then

$$P_\omega(\mathbf{R}_N,\mathbf{R})=[P_0(\mathbf{R}_N)-P(\mathbf{R}_N,\mathbf{R})]/P_0(\mathbf{R}_N) \quad (1)$$

is the p.d.f. for steps to be in the region ω around $\mathbf{R}$ when the ends are at 0 and $\mathbf{R}_N$ normalized to $P^0(\mathbf{R}_N)$.

For a random walk in which the step lengths have identical Gaussian distributions, the p.d.f., $P(\mathbf{R}_N,\mathbf{R})$, is

$$P(\mathbf{R}_N,\mathbf{R})=\left(\frac{3}{2\pi a^2}\right)^{3N/2}\int_{-\infty}^{\infty}\cdots^{3(N-1)}\int\prod_{i=1}^{N}\times\exp\left\{-\frac{3}{2a^2}(\mathbf{R}_i-\mathbf{R}_{i-1})^2\right\}\times\prod_{i=1}^{N-1}[1-\Delta(\mathbf{R}_i-\mathbf{R})]\prod_{i=1}^{N-1}d\mathbf{R}_i, \quad (2)$$

where

$$p(\mathbf{R}_i-\mathbf{R}_{i-1})=\left(\frac{3}{2\pi a^2}\right)\exp\left\{-\frac{3}{2a^2}(\mathbf{R}_i-\mathbf{R}_{i-1})^2\right\}$$

is the p.d.f. for the distance between the i^{th} and $i-1^{th}$ steps and

$$\Delta(\mathbf{R}_i-\mathbf{R})=\begin{cases}0, & \text{when } \mathbf{R}_i \text{ is outside the region } \omega,\\ 1, & \text{when } \mathbf{R}_i \text{ is inside the region } \omega.\end{cases}$$

In effect, the factor

$$\prod_{i=1}^{N-1}\{1-\Delta(\mathbf{R}_i-\mathbf{R})\}$$

gives zero weight to those random walk configurations for which steps enter the spherical region ω around $\mathbf{R}$. If the dimensions of the region ω are small compared to a, the characteristic length of a step in the walk, then the integrations in Eq. (2) can be performed. Operationally, one replaces $\Delta(\mathbf{R}_i-\mathbf{R})$ by $v_\omega\delta(\mathbf{R}_i-\mathbf{R})$ where v_ω is the volume of the spherical region ω and $\delta(\mathbf{R}_i-\mathbf{R})$ is the Dirac δ function. The result is

$$P(\mathbf{R}_N,\mathbf{R})=\left(\frac{3}{2\pi Na^2}\right)^{\frac{3}{2}}\exp\left\{-\frac{3\mathbf{R}_N^2}{2Na^2}\right\}-\frac{v_\omega}{a^3}\sum_{i=1}^{N-1}\left(\frac{3}{2\pi i}\right)^{\frac{3}{2}}\left(\frac{3}{2\pi(N-i)a^2}\right)^{\frac{3}{2}}\times\exp\left\{-\frac{3\mathbf{R}^2}{2a^2i}-\frac{3(\mathbf{R}_N-\mathbf{R})^2}{2a^2(N-i)}\right\}+\left(\frac{v_\omega}{a^3}\right)^2\times\sum_{i<j}\left(\frac{3}{2\pi i}\right)^{\frac{3}{2}}\left(\frac{3}{2\pi(j-i)}\right)^{\frac{3}{2}}\left(\frac{3}{2\pi(N-j)a^2}\right)^{\frac{3}{2}}\times\exp\left\{-\frac{3\mathbf{R}^2}{2a^2i}-\frac{3(\mathbf{R}_N-\mathbf{R})^2}{2a^2(N-j)}\right\}-\cdots. \quad (3)$$

* This work was supported by the Bureau of Ordnance, Department of the Navy under Contract NOrd-7386.

[1] Hermans, Klamkin, and Ullman, J. Chem. Phys. **20**, 1360 (1952). Hereafter this paper will be referred to as HKU. The same assumption is made in P. Debye and R. J. Rubin, Phys. Rev. **87**, 214 (1952). *Note added in proof.*—Two additional treatments of the excluded volume problem appeared after this paper was submitted for publication: F. T. Wall, J. Chem. Phys. **21**, 1914 (1953) and H. M. James, J. Chem. Phys. **21**, 1628 (1923). Wall's work differs only in detail from HKU. Part of James's work, although leading to different conclusions, involves the same assumption as that used by HKU and Wall. Thus the considerations of this note are pertinent to all three treatments.

[2] References to papers on the excluded volume problem may be found in R. J. Rubin, J. Chem. Phys. **20**, 1940 (1952). Hereafter this paper will be referred to as I.

Each of the series in Eq. (3) can be shown to be of order unity. Since it was assumed that $v_\omega \ll a^3$, one can neglect all but the first two terms of Eq. (3). If these two terms are inserted in Eq. (1), the HKU density is obtained,[3]

$$P_\omega(\mathbf{R}_N,\mathbf{R})=\frac{v_\omega}{a^3}\sum_{i=1}^{N-1}\left[\frac{3N}{2\pi i(N-i)}\right]^{\frac{3}{2}} \times\exp\left\{-\frac{3\mathbf{R}^2}{2a^2 i}-\frac{3(\mathbf{R}_N-\mathbf{R})^2}{2a^2(N-i)}+\frac{3\mathbf{R}_N{}^2}{2a^2 N}\right\}. \quad (4)$$

The approximations used to obtain Eq. (4) become exact in the limit $v_\omega/a^3 \to 0$. It should be emphasized that Eq. (4) gives the probability of finding steps near $\mathbf{R}$ when the first and last steps are at 0 and $\mathbf{R}_N$ and the intermediate steps do not interact with each other. This density is used by HKU to calculate the mean size of a polymer chain (from a Fokker-Planck equation) in which there is an excluded volume, v_ω, for every pair of steps in the chain, i.e., the intermediate steps do interact.

(b) Intermediate Step Interaction

Consider the restricted random walk of $N+1$ steps in which there is a region of excluded volume, ω, for every pair of intermediate steps. The analogous p.d.f.'s are denoted by primes: $P'(\mathbf{R}_N,\mathbf{R})$, $P_0'(\mathbf{R}_N)$, and $P_\omega'(\mathbf{R}_N,\mathbf{R})$. The expression for $P'(\mathbf{R}_N,\mathbf{R})$ is

$$P'(\mathbf{R}_N,\mathbf{R})=\left(\frac{3}{2\pi a^2}\right)^{3N/2}\int_{-\infty}^{\infty} 3(N-1)\int\cdots\int\prod_{i=1}^{N} \times\exp\left\{-\frac{3}{2a^2}(\mathbf{R}_i-\mathbf{R}_{i-1})^2\right\}\prod_{i=1}^{N-1}\{1-\Delta(\mathbf{R}_i-\mathbf{R})\} \times\prod_{i>j}\{1-\Delta(\mathbf{R}_i-\mathbf{R}_j)\}\prod_{i=1}^{N-1} d\mathbf{R}_i, \quad (5)$$

where the additional factor $\prod_{i>j}\{1-\Delta(\mathbf{R}_i-\mathbf{R}_j)\}$, also used in I, gives zero weight to random walk configurations which are excluded (i.e., configurations in which the distance between any two steps is less than b, the radius of the spherical region, ω).

Equation (5) may be expanded as before. Since we assume that $v_\omega \ll a^3$, we need only retain the first two terms to calculate $P_\omega'(\mathbf{R}_N,\mathbf{R})$. The expression for $P_\omega'(\mathbf{R}_N,\mathbf{R})$ is

$$P_\omega'(\mathbf{R}_N,\mathbf{R})=v_\omega\frac{\sum_{k=1}^{N-1}\left(\frac{3}{2\pi a^2}\right)^{3N/2}\int_{-\infty}^{\infty} 3(N-2)\int\cdots\int^{(k)}\prod_{i=1}^{N}{}^{(k)} \exp\left\{-\frac{3}{2a^2}(\mathbf{R}_i-\mathbf{R}_{i-1})^2\right\}\prod_{i>j}^{(k)}\{1-\Delta(\mathbf{R}_i-\mathbf{R}_j)\}\prod_{i=1}^{N-1}{}^{(k)} d\mathbf{R}_i}{\left(\frac{3}{2\pi a^2}\right)^{3N/2}\int_{-\infty}^{\infty} 3(N-1)\int\cdots\int\prod_{i=1}^{N} \exp\left\{-\frac{3}{2a^2}(\mathbf{R}_i-\mathbf{R}_{i-1})^2\right\}\prod_{i>j}\{1-\Delta(\mathbf{R}_i-\mathbf{R}_j)\}\prod_{i=1}^{N-1} d\mathbf{R}_i}, \quad (6)$$

where the superscript (k) is a summation index and also denotes the fact that $\mathbf{R}_k$ has been replaced by $\mathbf{R}$, following integration with respect to $\mathbf{R}_k$.

DISCUSSION

The assumption has been made in HKU that Eqs. (4) and (6) are the same. In order to verify the assumption, one would have to make estimates of the series obtained upon expanding $\prod_{i>j}^{(k)}\{1-(\mathbf{R}_i-\mathbf{R}_j)\}$ and integrating. Similar, but somewhat simpler, series were obtained in I. A difficulty encountered there was that one could not obtain the limiting value in which $N\to\infty$ and v_ω was fixed without actually summing the series in question.† The same difficulty is encountered in estimating Eq. (6). Therefore, one should preface the result of HKU with the remark that the unverified assumption has been made that $P_\omega(\mathbf{R}_N,\mathbf{R})=P_\omega'(\mathbf{R}_N,\mathbf{R})$.

Thus the method of HKU does not constitute a proof that the mean square distance between the ends of the chain $\langle R_N{}^2\rangle$ is proportional to N for $N\to\infty$. If $\langle R_N{}^2\rangle$ is, in fact, proportional to N for $N\to\infty$, then the method of HKU should give an approximate value for the proportionality constant.[4]

ACKNOWLEDGMENT

The author wishes to thank: Dr. B. A. Fleishman for helpful discussion; Mrs. Vera Rubin for comments on the manuscript; and Mrs. Carol Oberlin for typing the manuscript.

[3] Equation (4) agrees with Eq. (13) of HKU except for the two groups of terms $\sum_{j=1}^{P-1} g_j$ and $\sum_{j=t+1}^{N+1} k_j$ in HKU. These terms are absent in the present treatment because, for the sake of simplicity, we have considered the slightly less general problem in which the first and $N+1^{th}$ steps are fixed instead of the problem in which the p^{th} and t^{th} steps are fixed. The conclusions of this paper apply equally well to the full Eq. (13) of HKU. In any case, the two groups of terms do not contribute to the value of $\langle R_N{}^2\rangle$ obtained by HKU.

† *Note added in proof.*—This general difficulty is a manifestation of the theorem that in the limit of $N\to\infty$, the allowed paths form a set of measure zero in three dimensions. This Theorem (3) quoted in R. J. Rubin, J. Chem. Phys. **21**, 2073 (1953), is due to Dvorotzky, Erdös, and Kakutani, Szeged Egyetem Acta Univ. Szegediensis Acta Scientarium Mathematicarum **12**, 75 (1950).

[4] This observation was made by Dr. E. Montroll in commenting on the treatment of Debye and Rubin (see reference 2).

The Kinetics of Phase Transitions Involving Dimer Reactions*

H. L. Frisch and C. Willis
Department of Physics, Syracuse University, Syracuse, New York
(Received July 3, 1953)

Kinetic theory of phase transitions in which embryos of the new phase may grow or diminish by the acquisition or loss of monomer and dimer is presented. The error committed in neglecting the latter is shown to be negligible except in systems in which a large fraction of the old phase is present in the form of dimer.

I. INTRODUCTION

THE work of Volmer,[1] Becker and Döring,[2] Zeldovich,[3] and Frenkel[4] has led to an over-all satisfactory kinetic treatment of phase transitions in the steady state in one-component systems.[5] Reiss[6] has extended this theory to transitions in binary systems. A common assumption in these investigations is that, in view of the relatively low probability of a collision between two embryos of the newly formed phase, it can be assumed that embryos grow or diminish by the acquisition or loss of single molecules of the metastable or old phase.[2,6] If A_x denotes an embryo composed of x single molecules of the old phase ($x$mer), then the fundamental reaction is

$$A_{x-1}+A_1 \underset{\beta(x)}{\overset{\alpha(x-1)}{\rightleftarrows}} A_x, \tag{1a}$$

where $\alpha(x-1)$ is the probability per unit time of forming an $x$mer from a $(x-1)$mer and $\beta(x)$ is the probability per unit time of the decay of a $x$mer to a $(x-1)$mer and monomer. The purpose of this paper is to investigate the effect of considering reactions involving the addition or loss of dimer molecules, i.e.,

$$A_{x-2}+A_2 \underset{\eta(x)}{\overset{\zeta(x-2)}{\rightleftarrows}} A_x. \tag{1b}$$

This investigation gives us an estimate of the validity of the assumption embodied in Eq. (1a). In particular reaction (1b) gains in importance when there exists a strong tendency for the old phase to dimerize, so that at equilibrium a definite fraction k of the total molecules is present in the form of dimer. Such would be the case in considering the behavior of $NO_2-N_2O_4$. Possibly, the method used in this paper could be extended to the description of the nucleation of sulfur vapor. Without committing a serious error we can take for the steady-state concentrations of dimer and monomer their equilibrium values N_2 and N_1, respectively. More generally, if reactions of type

$$A_x+A_y \rightleftarrows A_{x+y}; \quad x,y>2 \tag{1c}$$

are considered, then the concentration of dimer will no longer be given by its equilibrium value; the kinetic equations of the phase transition become nonlinear. Since the concentration of dimer is considerably greater than trimer, tetramer, etc., we will be justified in neglecting reactions (1c). Work is in progress on the small perturbing influence on the phase transition when these reactions are not neglected. Formally the theory which will be developed applies to vapor-liquid transitions, but it may be extended to other phase changes by use of the methods of Kaischew and Stranski,[7] Becker and Döring,[2] Frenkel,[8] and Reiss.[6,9]

II. KINETICS INVOLVING DIMER REACTIONS

If $f(x)$ is the steady-state concentration of $x$mer, then the constant steady-state flow of embryos of any size J satisfies

$$J=\alpha(x-1)f(x-1)-\beta(x)f(x) -\eta(x)f(x)+\zeta(x-2)f(x-2), \tag{2}$$

where the constant concentrations of monomer and dimer are included in α and ζ, respectively. If "equilibrium," characterized by the vanishing of J, could be attained, the conditions imposed by detailed balancing[2,4] are, if $N(x)$ is the known[2,4] equilibrium concentration of $x$mer,

$$\beta(x)=\alpha(x-1)N(x-1)/N(x), \tag{3a}$$

$$\eta(x)=\zeta(x-2)N(x-2)/N(x), \tag{3b}$$

by virtue of Eqs. (1a) and (1b). The fact that this state does not occur, does not detract from the validity of Eqs. (3a) and (3b). Dividing both sides of Eq. (2) by

* This research was supported by the U. S. Air Force under Contract AF 18 (600)-459 monitored by the Office of Scientific Research, Hq. Air Research and Development Command, Post Office Box 1395, Baltimore, Maryland.

[1] M. Volmer, *Kinetik der Phasenbildung* (Edwards Bros., Inc., Ann Arbor, 1945).
[2] R. Becker and W. Döring, Ann. Physik **24**, 719 (1935).
[3] Zeldovich, J. Exp. Theoret. Phys. U.S.S.R. **12**, 525 (1942).
[4] J. Frenkel, *Kinetic Theory of Liquids* (Oxford University Press, London, 1946).
[5] F. J. M. Farley, Proc. Roy. Soc. (London) **212A**, 530 (1952).
[6] H. Reiss, J. Chem. Phys. **18**, 840 (1950).
[7] I. N. Stranski and R. Kaischew, Z. physik. Chem. **B26**, 317 (1934); Physik. Z. **36**, 393 (1935).
[8] J. Frenkel, J. Phys. U.S.S.R. **1**, 315 (1939).
[9] H. Reiss, J. Chem. Phys. **18**, 996 (1950).

$N(x)$ and setting $F(x)=f(x)/N(x)$, we obtain

$$\begin{aligned} J/N(x)&=\beta(x)[F(x-1)-F(x)] \\ &\quad+\eta(x)[F(x-2)-F(x-1)] \\ &=\beta(x)[F(x-1)-F(x)] \\ &\quad+\eta(x)[F(x-1)-F(x)] \\ &\quad+\eta(x)[F(x-2)-F(x-1)] \\ &=\xi(x)[F(x-1)-F(x)] \\ &\quad+\eta(x)[F(x-2)-F(x-1)] \end{aligned} \tag{4}$$

with $\xi(x)=\beta(x)+\eta(x)$. Equation (4) has to be solved for $F(x)$ under the boundary conditions that $F(x)\to 0$ as $x\to\infty$ and $F(1)=F(2)=1$. The substitution of

$$\begin{aligned} &G(x)=F(x-1)-F(x), \\ &G(2)=0 \end{aligned} \tag{5a}$$

into Eq. (4) reduces it to the linear first-order difference equation

$$J/N(x)=\xi(x)G(x)+\eta(x)G(x-1). \tag{5b}$$

Equations (5a) and (5b) are solved by iteration and give, respectively,

$$F(x)=1-\sum_{s=2}^{x} G(s)=1-\sum_{s=3}^{x} G(s) \tag{6a}$$

and

$$\begin{aligned} G(x)&=J/\xi(x)N(x)\Big[1-\eta(x)/\xi(x) \\ &\quad+\eta(x)\eta(x-1)/\xi(x)\xi(x-1) \\ &\quad-\cdots+(-1)^{x-3}\frac{\eta(x)\cdots\eta(4)}{\xi(x)\cdots\xi(4)}\Big] \\ &=J/\xi(x)N(x)[1-K(x)], \quad x\geqq 3, \end{aligned} \tag{6b}$$

$$G(2)=0$$

with

$$K(x)=\sum_{y=0}^{x-4}(-1)^{y}\frac{\eta(x)\eta(x-1)\cdots\eta(x-y)}{\xi(x)\xi(x-1)\cdots\xi(x-y)}.$$

Substituting Eq. (6b) into (6a) and allowing x to approach infinity, we find, since $F(x)\to 0$ as $x\to\infty$,

$$J=1\Big/\sum_{s=3}^{\infty}\frac{1-K(s)}{\xi(s)N(s)}, \tag{7a}$$

and

$$F(x)=1-J\sum_{s=3}^{x}\frac{1-K(s)}{\xi(s)N(s)}. \tag{7b}$$

When the restriction on the dimer concentration is lifted and is allowed to vanish, then J goes over smoothly into the flow of embryos $J_{\text{B.D.}}$ found by Becker and Döring[2] who neglected dimer reactions,

$$J_{\text{B.D.}}=1\Big/\sum_{s=2}^{\infty}\frac{1}{\beta(s)N(s)}. \tag{7c}$$

The "equilibrium" concentration appearing in Eqs. (7) is given by the "Boltzmann distribution"

$$N(x)=N\exp[-\Delta\Phi(x)/kT], \quad x>2, \tag{8a}$$

where N is the total number of polymers present at "equilibrium" ($\approx N_1$), and $\Delta\Phi(x)$ is the reversible work which must be expanded to form an $x$mer in the old phase. The rate constant $\beta(x)$ is, at least for spherical embryos, given to a first approximation by the Hertz-Knudsen relation and Eq. (3a),

$$\beta(x)\approx\mathfrak{N}p_1(2\pi RTM)^{-\frac{1}{2}}S_1\exp\left[-\frac{d\Delta\Phi(x)}{dx}\Big/kT\right], \tag{8b}$$

where $\mathfrak{N}$ is Avogadro's number, M the molecular weight of the monomer, S_1 the surface area of a monomer, and p_1 the partial pressure of monomer. The pressure $p_1=pN_1/N$ is generally taken to be the pressure p of the system. If $\beta(x)$ is given by Eq. (8b) then to be consistent $\eta(x)$ must satisfy to a first approximation

$$\eta(x)\approx\mathfrak{N}\cdot p_2(4\pi RTM)^{-\frac{1}{2}}S_2\exp\left[-2\frac{d\Delta\Phi(x)}{dx}\Big/kT\right], \tag{8c}$$

where

$$p_2=pN_2/N\approx pN_2/N_1.$$

III. DISCUSSION AND CONCLUSION

The exact expressions Eqs. (7) are extremely unwieldy to use because the indicated summations are laborious. If the critical embryo size $x=x^*$, i.e., when $d\Delta\Phi(x)/dx=0$, is sufficiently large then these summations may be replaced by integrations and these in turn approximately evaluated by the method of steepest descent.[4,5] For our purposes a sufficient approximation is given by the asymptotic estimate of Eqs. (7a) and (7c),

$$J\underset{a}{\sim}\xi(x^*)N(x^*)/[1-K(x^*)]\approx\xi(x^*)N(x^*) \tag{9a}$$

and

$$J_{\text{B.D.}}\underset{a}{\sim}\beta(x^*)N(x^*). \tag{9b}$$

Substituting Eqs. (8) into (9), we find for J

$$J\approx J_{\text{B.D.}}\xi(x^*)/\beta(x^*)=J_{\text{B.D.}}(1+2^{-\frac{1}{2}}B_{12}), \tag{10a}$$

where B_{12} is the surface fraction of dimer to monomer,

$$B_{12}=S_2N_2/S_1N_1. \tag{10b}$$

For most systems in which the old phase is pure monomer the expression $(1+2^{-\frac{1}{2}}B_{12})$ can be neglected in comparison with the exponential term, $\exp[-\Delta\Phi(x^*)/kT]$, in $J_{\text{B.D.}}$. If the old phase is a mixture of dimer and monomer present, say in the ratio $k:(1-k)$, then B_{12} is proportional to $k/(1-k)$. When $k<1$, the former conclusion holds. An appreciable effect due to dimer reactions is found only when $1-k$ is very nearly equal to zero.

The authors thank Professor P. G. Bergmann for helpful discussions.

Examination of Methods for Detecting OH*

T. M. SANDERS, JR.,† A. L. SCHAWLOW,‡ G. C. DOUSMANIS, AND C. H. TOWNES
Physics Department, Columbia University, New York, New York

(Received October 15, 1953)

The microwave spectrum of OH affords a new method of determining the abundance of OH in a low-pressure gas mixture. This method applied to the products of a discharge in H_2O shows that certain previous methods for detecting the presence of OH radicals in fact are not sensitive to OH, but to some other reactive components of a discharge in H_2O. OH radicals are obtained from a discharge in concentrations near 10 percent and with a lifetime of approximately $\frac{1}{3}$ sec.

SEVERAL methods for detecting the free hydroxyl radical OH have been reported in the past and used to study various properties of this radical. These include (1) measurement of intensity of the OH absorption spectrum in the ultraviolet region,[1] (2) measurement of temperature rise of a probe coated with KCl on which OH radicals are presumed to recombine,[2] and (3) determination of the amount of H_2O_2 condensed on a liquid air trap from gases containing OH, with the presumption that the H_2O_2 is formed from OH.[3]

A prolonged search was recently made[4] for the microwave absorption spectrum of OH in which tests (2) and (3) were used to assure us of the presence of OH in the absorption cell. After the microwave spectrum of OH was finally found,[4] it became apparent that these tests are quite misleading, and probably actually detect some other active molecule or atom rather than OH. Hence some detailed comparisons between the direct determination of OH abundance by its microwave absorption spectrum and detection methods (2) and (3) have been made. These are reported below.

Experiments reported here were carried out in the apparatus shown in Fig. 1. Water vapor flowed through an electrodeless discharge, and the resulting gas passed through the microwave absorption cell to a liquid nitrogen trap and then to pumps. A thermometer, previously coated with KCl, could be introduced into the side tube A, with the coated bulb in any position up to the tube B connecting the discharge tube and the absorption cell.

Papers[2] describing test (2) give evidence that KCl does not catalyze the reaction $H+H\rightarrow H_2$, and hence conclude that the observed rise in temperature of a thermometer (or thermocouple) coated with KCl and in contact with the products of an electrical discharge in H_2O is due to one of the reactions $H+OH\rightarrow H_2O$ or $OH+OH\rightarrow H_2O_2$. In either case the temperature rise should give an indication of the amount of OH present.

A detector of this type was made with a thermometer rather than a thermocouple in order to be certain that no metal surfaces were present. The thermometer was carefully cleaned and then coated with KCl by dipping it into a saturated KCl solution near 100°C. After the thermometer was removed from the solution and the surface water evaporated, a powdery KCl layer adhered to the glass. No thermometer subjected to this treatment alone showed any observable temperature rise when inserted into the apparatus. Two procedures for "activating" the thermometers were used. Some thermometers were sealed into the side tube and were heated under vacuum to about 200°C by the application of a flame to the outside surface of the glass. After such treatment not more than 50 percent of the thermometers proved to be sensitive. The second procedure used was to heat the thermometers in air over an air-rich bunsen burner flame. The fraction of thermometers sensitized by this procedure was somewhat greater than one-half. Qualitative results obtained with both methods of sensitization were the same. If a substantial amount of water vapor were allowed to accumulate in the vacuum system, the sensitive thermometer would generally become deactivated. Sensitivity could sometimes be restored by reapplication of the first activation procedure. Temperature rises measured on various thermometers varied from less than 1°C to greater than 80°C (offscale).

A point by point comparison of line intensity and thermometer temperature was made for various values of discharge current and pressure. Results for a fixed discharge current and varying pressure are shown in Fig. 2. Although there is presumably a maximum for I with increasing pressure, the particular discharge cur-

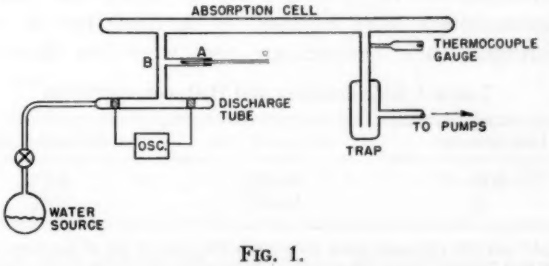

FIG. 1.

* This research has been aided by the U. S. Office of Naval Research and Signal Corps.

† RCA Fellow in Physics.

‡ Carbide and Carbon Chemical Corporation Postdoctoral Fellow in Physics.

[1] O. Oldenberg and F. F. Rieke, J. Chem. Phys. **6**, 439 (1938); **7**, 485 (1939).

[2] W. V. Smith, J. Chem. Phys. **11**, 110 (1943); H. S. Taylor and G. I. Lavin, J. Am. Chem. Soc. **52**, 1910 (1930).

[3] W. H. Rodebush and M. H. Wahl, J. Chem. Phys. **1**, 696 (1933).

[4] Sanders, Schawlow, Dousmanis, and Townes, Phys. Rev. **89**, 1158 (1953).

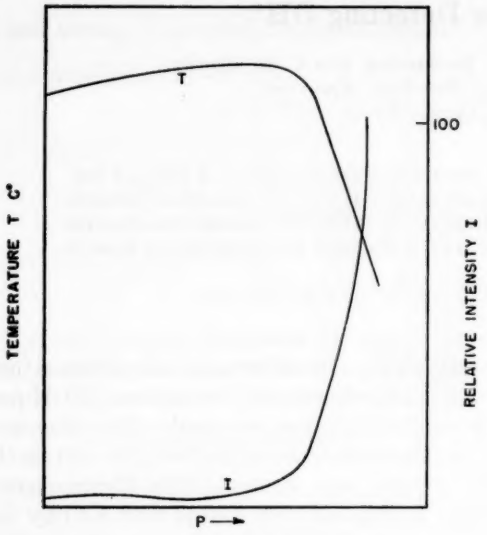

FIG. 2.

rent to which Fig. 2 applies was such that the pressure could not be increased to this maximum before the discharge changed character by suddenly jumping to the absorption cell. It is evident from Fig. 2 that the temperature rise decreases rather than increases with increasing abundance of OH radicals. It must hence be produced by some component of the gas other than OH. Under all discharge conditions used, the maximum temperature rise was reached at considerably higher excitation (lower pressure) than is the maximum intensity of the OH spectrum.

Further tests were made to find out if OH recombines on the KCl surface to an appreciable extent, and whether our KCl surfaces catalyzed the recombination of H atoms. To settle the first question, the coated thermometer bulb was inserted into the tube *B* directly in the path of the flowing gas to see if the observed abundance of OH decreased appreciably. This caused no more of a decrease in line intensity than that produced by a piece of clean Pyrex or an uncoated thermometer placed at the same point. On the other hand, a small strip of copper inserted into tube *B* in the same way caused a dramatic drop in intensity due to recombination of OH radicals on the copper.

Tests on the recombination of H atoms were somewhat less conclusive, but indicated that, in accordance with previous reports,[2] the observed temperature rises from a discharge in H_2O were probably not due to recombination of hydrogen atoms. When the coated thermometers were exposed to a discharge in wet hydrogen, their temperature rises were less than one quarter of those observed from a discharge in pure H_2O. However, in these hydrogen discharges, the Balmer series lines were not as prominent as in the discharges in H_2O.

TABLE I. Line intensity and H_2O_2 concentration.

Line intensity	H_2O_2 conc. (*A*)	H_2O_2 conc. (*B*)
100	14.6%	23%
2	14.4%	25%

(*A*) and (*B*) represent data taken with different choice of discharge current and pressure giving the stated line intensities. In (*B*) the liquid nitrogen trap, in addition to having different geometry, was closer to the output end of the absorption cell than in (*A*).

Method (3) for determining the abundance of free OH involves analyzing the condensate in the liquid air trap for H_2O_2. It is presumed that the wall reaction producing the H_2O_2, which is known not to be present in quantity in the vapor,[5,6] is $OH+OH \rightarrow H_2O_2$. This explanation for the formation of H_2O_2 has been questioned, however, by Geib.[7] To examine this test, the discharge was run continuously for periods of an hour or more under conditions which gave a substantial range in line intensity. The condensate from the trap shown in Fig. 1 (at the output end of the absorption cell) was titrated using the procedure of reference 3. The results of the comparison are given in Table I. It seems clear from this table that the H_2O_2 concentration does not measure the concentration of OH in the vapor.

In contrast to tests (2) and (3), test (1) is very direct, although it is still rather difficult to make quantitative measurement of absolute absorption intensity of OH lines in the ultraviolet region indicate abundances of OH radicals near $\frac{1}{10}$ percent in an H_2O discharge at 1.1 mm of Hg pressure.[1] Line widths and absolute intensities of microwave absorption can also be measured and used to determine the abundance of OH radicals.

From such measurements, the maximum abundance of OH radicals obtained during the above experiments was found to be between 3 and 30 percent at a discharge pressure of about 0.2 mm of Hg. Since this value for the abundance depends on an estimate of the dipole moment, this and other uncertainties prevent a more precise determination. The above result is not necessarily inconsistent with the abundance determined by ultraviolet absorption, since in the latter case a higher pressure and a pulsed dc discharge were used with current density considerably below that which was found to be optimum in the present experiments.

The lifetime of OH radicals in the microwave absorption cell of Fig. 1 was also determined as approximately $\frac{1}{3}$ sec in reasonable agreement with earlier results.[8] Further discussion of abundance and lifetime measurements will be published separately.

CONCLUSION

Of the three previously published tests for OH which are discussed above, only that involving the ultraviolet spectrum of OH seems consistent with results from the microwave spectrum. Tests (2) and (3) (at least as we have been able to reproduce and apply them) do not indicate the presence of OH at all, but of some other radical or atom. Conclusions[2,3] concerning kinetics and other properties of OH which have been made with the use of these indirect tests (2) and (3) should be reexamined.

[5] R. W. Campbell and W. H. Rodebush, J. Chem. Phys. 4, 293 (1936).
[6] A. A. Frost and O. Oldenberg, J. Chem. Phys. 4, 642 (1936).
[7] K. H. Geib, J. Chem. Phys. 4, 391 (1936).
[8] O. Oldenberg, J. Chem. Phys. 3, 266 (1935).

A Rectilinear Diameter Law of Mole Fractions for Binary Liquid-Vapor Coexistence Regions near the Critical Locus*

SIDNEY W. BENSON, PETER E. M. ALLEN, † AND CHARLES S. COPELAND
Chemistry Department, University of Southern California, Los Angeles 7, California

(Received September 2, 1953)

It has been found that in the neighborhood of the critical locus of many nonazeotropic binary, liquid-vapor systems at equilibrium, the sum of the mole fractions in the two phases of each of the two components (C,C') may with reasonable precision be represented by the relationship

$$X_v+X_l\equiv 2-(X_v'+X_l')=a\log P/P_0';$$

in which X_v and X_l are the mole fractions of the more volatile component (C) in vapor and liquid, respectively, which are in equilibrium at total pressure P at constant temperature, P_0' is the vapor pressure of the less volatile component C', and a is a constant for each isotherm. Between the critical temperatures of the two components a shows greater temperature dependence as the lower critical temperature is approached.

THE usual $P-x$ isotherm representing the coexistence surface of a binary gas-liquid system at equilibrium are closed curves of rather variable appearance. We have noted, however, for a number of systems that the sum of the mole fractions of a component in each phase is a linear function of the logarithm of the total pressure of the equilibrium system at constant temperature. Thus if X_v and X_l are the mole fractions of the component C of lower critical temperature in the vapor and liquid phases, respectively, and X_v' and X_l' are the corresponding mole fractions of the less volatile component C', then

$$X_v+X_l\equiv 2-(X_v'+X_l')=a\log\frac{P}{P_0'}, \qquad (1)$$

where a is a constant for a given isotherm, P is the total pressure, and P_0' is the vapor pressure of the pure component C' at that temperature. Quite obviously, Eq. (1) cannot be expected to hold for azeotropic systems.

When the data for a series of isotherms are plotted according to Eq. (1) it is found that the relation holds to within a few percent over most of the critical range of the binary system; that is, between the critical temperatures of the two components. In Figs. 1A and 2 are shown some typical isotherms for which Eq. (1) holds. Table I lists the values of a calculated from the isotherms of these and other systems. Except where annotation indicates otherwise, a has been obtained from the best straight line through all the points of a particular isotherm from the pure component axis (C') to the critical locus. The column headed by $100\Delta P/P$ gives the maximum deviation observed from the best rectilinear plot. It should be noted that, for those systems for which a point on the critical locus was available, the deviation of this point was in general not the maximum deviation. Cases where the deviation is systematic; that is, where the isotherm is visibly curved, are indicated by the letter (B) in the table.

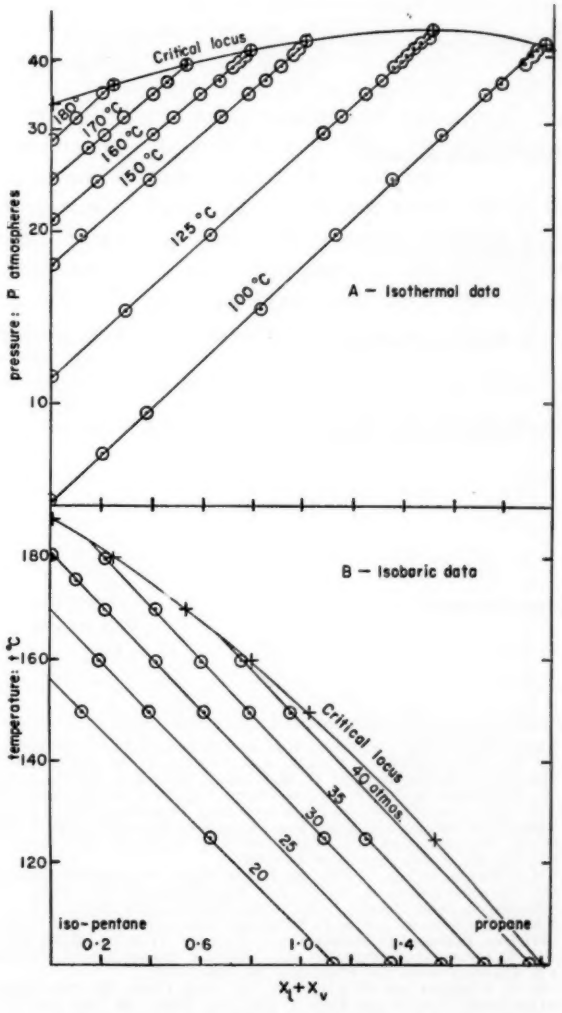

FIG. 1. A. Logarithmic plot of P against X_L+X_V.
B. $t-(X_L+X_V)$ plot (both for system iso-pentane-propane).

* This work was supported by the U. S. Office of Naval Research under Contract No. N6-onr-23811 with the University of Southern California.

† Post-Doctorate Research Associate at the University of Southern California.

TABLE I.

System*	Critical points* °C, atmospheres		T°C	a $\log_{10}$ (atmos) −°C units	$\frac{\Delta P}{P_{100}}\times 100$
propane-isopentane[a] (see Fig. 1)	96.85°C[i]	187.7°C[k]	180	2.58	1/2
	42.1 atmos[i]	32.9 atmos[k]	170	2.67	1
			160	2.67	1
			150	2.67	1
			125	2.53	2
			100	2.51	2
ethane-propylene[b]	32.4°C[j]	91.4°C[o]	80	4.03	2
	48.2 atmos[j]	45.4 atmos[o]	70	4.12	1/2
			60	4.03	1/2
			50	3.89	1/2
			40	3.96	1/2
			30	3.59	1/2
n-hexane-toluene[e]	234.8°C[k]	320.6°C[k]	280	4.72	1
	29.5 atmos[k]	48.7 atmos[k]	270	4.74	3/2
			260	4.88	5/2
			250	5.14	3
			240	5.71	3
			230(B)	15.20	6
ethane-benzene[d]	32.4°C[j]	289.5°C[p]	250[s]	1.24	1
	48.2 atmos[j]	48.7 atmos[p]	200[s]	1.01	3
			175[s]	0.94	1
			150[s]	1.04	10
			100[s]	1.22	5
			50[s]	2.14	2
carbon dioxide-propylene[c] (see Fig. 2)	31.04°C[l]	91.4°C[o]	70	2.40	1/2
	72.85 atoms[l]	45.4 atmos[o]	60	2.40	2
			50	2.42	3
			40	2.49	1
			30(B)	2.63	5
carbon dioxide-propane[f]	v.s.	96.85°C[i]	82.2	1.98	3
	v.s.	42.1 atmos[i]	60.0	2.09	5
			37.8	2.16	3
			26.7(B)	2.51	10
carbon dioxide-*n* butane[f]	v.s.	152.0°C[q]	93.3[t]	1.56	1
	v.s.	36.47 atmos[q]	71.1[t]	1.52	2
			48.9[t]	1.61	8
			26.7[t]	1.93	10
carbon dioxide-*n* pentane[f]	v.s.	297.6°C[h]	121.1[t]	1.24	1
	v.s.	33.0 atmos[h]	93.3[t]	1.04	2
			65.6[t]	1.04	8
			37.8[t]	1.31	10
carbon dioxide-sulfur dioxide[g]	v.s.	157.2°C[r]	130	2.21	1
		77.7 atmos[r]	120	2.05	2
			110	2.05	5/2
			100	2.03	3/2
			90	1.93	3
			80	1.89	1
			60(B)	1.66	7
			40(B)	...	...
oxygen-nitrogen[h]	−118.8°C[m]	−144.7°C[n]	−148	5.11	1/2
	49.3 atmos[n]	33.7 atmos[n]	−153	5.23	4
			−163	4.61	5/2
			−173(B)	3.94	9/2
			−182.5(B)	3.34	6

* The more volatile component is given first in each case. (B) signifies a systematic departure from linearity of that particular isotherm.

[a] F. C. Collins and W. E. Vaughn, Ind. Eng. Chem. **34**, 885 (1942).
[b] H. Lu, D. M. Newitt, and M. Ruhemann, Proc. Roy. Soc. (London) **A178**, 506 (1941).
[c] L. M. Watson and B. F. Dodge, Chem. Eng. Prog. Symposium Series, 48 No. 3, **71** (1952).
[d] W. B. Kay and T. D. Nevens, Chem. Eng. Prog. Symposium Series, 48 No. 3, 108 (1952).
[e] Haselden, Newitt, and Shah, Proc. Roy. Soc. (London) **A209**, 1 (1951).
[f] F. H. Poettman and D. L. Katz: Ind. Eng. Chem. **37**, 847 (1945).
[g] F. Caubet, Z. Physik. Chem. **40** (1902).
[h] B. F. Dodge and A. K. Dunbar, J. Am. Chem. Soc. **49**, 591 (1927).
[i] W. Drescher and G. G. Brown, Ind. Eng. Chem. **32**, 836 (1940).
[j] Beattie, Su, and Simard, J. Am. Chem. Soc. **61**, 924 (1939).
[k] A. F. O. Germann and S. F. Pickering, *International Critical Tables* **3**, 248 (1926).
[l] Michels, Blaisse, and Michels, Proc. Roy. Soc. (London) **A160**, 358 (1937).
[m] H. K. Omnes *et al.*, Proc. K. Akad. Wetens. Amsterdam **17**, 953 (1914).
[n] E. Cardoso, Arch. Sci. Phys. Nat. **39**, 400 (1915).
[o] W. E. Vaughan and N. R. Graves, Ind. Eng. Chem. **32**, 1252 (1940).
[p] Gornowski, Amick, and Hixson, Ind. Eng. Chem. **39**, 1348 (1947).
[q] Beattie, Sunard, and Su, J. Am. Chem. Soc. **61**, 24, (1939).
[r] E. Cardoso and R. Bell, J. Chim. Phys. **10**, 497 (1902).
[s] Calculated for points above 35 atmospheres below which there is a sharp breakdown.
[t] Calculated from points above 30 atmospheres.

If a of Eq. (1) is independent of temperature, then the temperature variation of Eq. (1) is accounted for by the term P_0'. For example, for the system carbon dioxide-propylene, between 40 and 70°C, a is virtually constant (Table I). In this range, $\log P_0'$ for propylene is a reasonably linear function of $1/T(°K^{-1})$ and so too is X_v+X_l at various constant pressures. When a is not independent of temperature, both a and P_0' will contribute to the temperature variation of X_v+X_l at constant pressure and no simple rule would be expected. However, X_v+X_l for the systems propane-isopentane, ethane-propylene, and n-hexane-toluene is a linear function of temperature at a number of different pressures. This is shown in Fig. 1B for the system propane-isopentane.

Below both critical temperatures of the components, if Eq. (1) applies, a would not be expected to be independent of temperature, for if it were, this would require the ratio of the vapor pressures of the two components to be independent of temperature. Equation (1) holds very well for the system oxygen-nitrogen below the critical temperature of nitrogen, and a shows a marked variation with temperature (Table I).

An interesting system to which Eq. (1) appears to be applicable, in the form that $X_v'+X_l'$ is a linear function of $\log P$, is the system NaCl-H_2O above the critical temperature of water. Using the data of Olander and Leander[1] at 380, 390, and 410°C, we find that $X_v'+X_l'$ is a linear function of $\log P$ from near the critical point of the solution to a mole fraction of NaCl in the liquid phase of 0.0932 (25 percent by weight NaCl), the limit of the data. The values of a vary from 0.99 at 380° to 0.86 at 410°C. Points corresponding to pressures near the critical pressure of the solution are above the 380° isotherm, above but close to the 390° isotherm, and below the 410° isotherm. Because of the great disparity in mole fractions of NaCl in the liquid and vapor phases at pressures much below the critical pressure of the solution, Eq. (1) is for all practical purposes the equation for the vapor pressure of the liquid solution at constant temperature. If we take the mole fraction of NaCl to be 0.206[2] in saturated liquid solution at 390°C, Eq. (1) predicts a vapor pressure of 155 atmos. The vapor pressure data of Keevil[2] give 150 atmos and Olander and Leander[1] report 163.6 atmos.

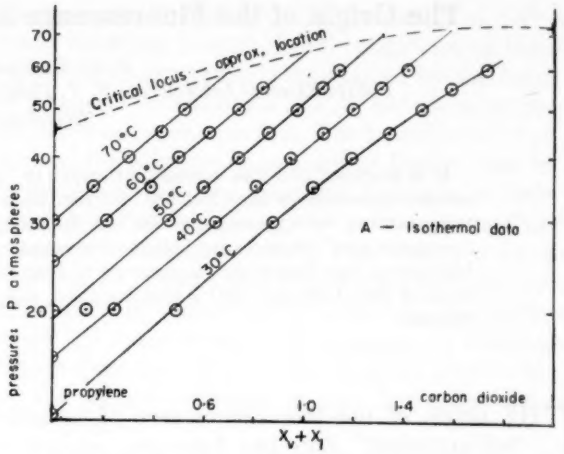

FIG. 2. Logarithmic plot of P against X_V+X_L for the system: propylene-carbon dioxide.

A system to which Eq. (1) is not applicable is the system hydrogen-propane.[3] This system appears to be unusual in that the critical pressures of mixtures can be of a different order of magnitude than the critical pressures of the components.

[1] A. Olander and H. Leander, Acta Chem. Scand. **4**, 1437 (1950). See also Copeland, Silverman, and Benson, J. Chem. Phys. **21**, 12 (1953).

[2] Interpolated from the data of N. B. Keevil, J. Am. Chem. Soc. **64**, 841 (1942).

[3] Burriss, Hsu, Reamer, and Sage, Ind. Eng. Chem. **45**, 210 (1953).

The Origin of the Fluorescence in Self-Activated ZnS, CdS, and ZnO

F. A. KRÖGER AND H. J. VINK
Philips Research Laboratories, N. V. Philips' Gloeilampenfabrieken, Eindhoven-Netherlands

(Received May 6, 1953)

It is proposed that the luminescent center in "self-activated" ZnS consists of a cation vacancy whose nearest surroundings have lost one electron. Such a center is consistent with the fact that at low firing temperatures, the appearance of the blue fluorescence of self-activated ZnS depends upon the presence of "promoter ions" (monovalent anions or trivalent cations) whereas, if the firing temperature be sufficiently high, some blue fluorescence is obtained without the presence of such promoter ions. The luminescence of reduced ZnS, CdS, and ZnO is also discussed, and is attributed to anion vacancies that have trapped one electron.

THE origin of the blue fluorescence of so-called "self-activated" ZnS has been the subject of many speculations. According to Schleede[1] it might lie in the simultaneous presence of the wurtzite and sphalerite structures. After later investigations had shown that this assumption was untenable, a comparison of ZnS with ZnO led to the assumption that the blue band of ZnS is due to an excess of zinc, the center being formed either by the zinc atoms placed interstitially[2] or by the sulfur vacancies arising from the incorporation of the extra zinc atoms at normal lattice sites.[3]

This assumption in turn was abandoned when it was observed that the appearance of the particular fluorescence depended on the presence of certain foreign ions like Al^{3+}, Ga^{3+}, Cl^-, Br^-, and I^- (hereafter called "promoting ions") rather than on the reducing power of the atmosphere.[4–6] Starting from the knowledge gained in the conductivity field (controlled valency, Verwey *et al.*[7]) it was assumed that the centers consist of Zn^+ ions formed according to the principle of charge compensation in a concentration equal to that of the promoting ions. It has been shown[5] that although the promoting ions aid in forming the centers, they do not actually belong to the centers. Such centers must then consist of Zn^+ ions present at sites far from their promoters. Under these conditions, however, Zn^+ represents a free electron. Now there are several reasons why free electrons cannot consitute the centers under consideration. In the first place if this were so, all free electrons should have the same effect, independent of the way in which they have been created; accordingly, each crystal of ZnS, irradiated sufficiently strongly in the fundamental absorption band, should become fluorescent in the blue because of the free electrons made in this way. In the second place, the fluorescence should disappear when free electrons originally present are trapped in some way or another, e.g., upon cooling to a sufficiently low temperature. Finally, products with blue fluorescence should show an appreciable electronic dark conductivity. None of these effects has, however, been observed. Therefore, this assumption, too, has to be discarded.

Bube[8] has shown recently that although the presence of promoting ions (monovalent anions and trivalent cations) is favorable for the appearance of the blue fluorescence, it is not indispensable; some blue fluorescence appears without them, provided the ZnS has been fired at a sufficiently high temperature. This has led Bube to the new assumption that the blue centers are due to cation vacancies, formed in chemical equilibrium at very high temperatures, the effect of the foreign promoting ions at lower temperatures consisting either in charge compensation or in specific chemical actions.

As shall be shown presently it is possible to define more precisely the model proposed by Bube, and thus to explain the high-temperature effects observed by Bube as well as the favorable effect of promoters, if it is assumed that the centers responsible for the blue fluorescence are cation vacancies that have lost one electron from their nearest surroundings (V_C^+). In the first place, V_C^+ is a configuration carrying an effective charge $-|e|$, and therefore will perturb neighboring sulfur ions in a way very similar to that of monovalent cations like silver. Accordingly, just as has been assumed for such ions (Klasens,[9] Leverenz[10]), it will cause local sulfur levels $S^{2-}(V_C^+)$ a little above the full S^{2-} band. Optical transitions between these local levels and the conduction band (or some excited level close to this band) correspond to the absorption and luminescence bands observed with "self-activated" ZnS,[4,*]

[1] A. Schleede, Angew. Chem. **48**, 277 (1935).
[2] A. Schleede, Angew. Chem. **50**, 908 (1937). F. Seitz, Trans. Faraday Soc. **35**, 74 (1939). J. Chem. Phys. **6**, 454 (1938). J. T. Randall, Trans. Faraday Soc. **35**, 8 (1939).
[3] J. T. Randall and M. H. F. Wilkins, Repts. Prog. Phys. **6**, 176 (1939).
[4] F. A. Kröger and J. E. Hellingman, J. Electrochem. Soc. **93**, 156 (1948). J. Electrochem. Soc. **95**, 68 (1949).
[5] F. A. Kröger and J. A. M. Dikhoff, Physica **16**, 297 (1950).
[6] N. Riehl and H. Ortmann, Doklady Akad. Nauk S. S. S. R. **66**, 613 (1949).
[7] Verwey, Haaijman, Romeijn, and van Oosterhout, Chem. Weekblad **44**, 705 (1946). Philips Research Repts. **5**, 173 (1950).
[8] R. H. Bube, Phys. Rev. **80**, 655 (1950); J. Chem. Phys. **20**, 708 (1952). R. H. Bube and S. Larach, J. Chem. Phys. **21**, 5 (1953).
[9] H. A. Klasens, J. Electrochem. Soc. **100**, 72 (1953); See also reference 5.
[10] H. W. Leverenz, *Introduction to Luminescence of Solids* (John Wiley and Sons Inc., New York, 1950), p. 197.
* The fact that Bube, Phys. Rev. **90**, 70 (1953), did not observe an absorption band connected with the centers of self-activation

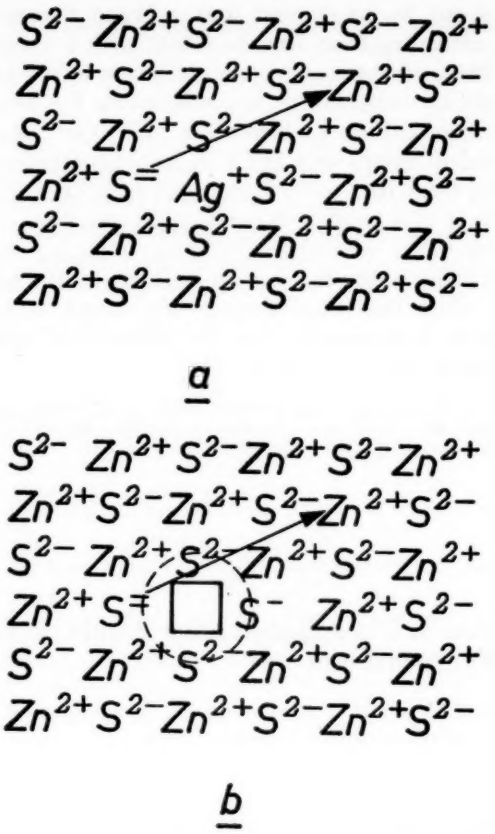

FIG. 1. Atomic picture of the centers in blue fluorescent ZnS
a: ZnS—Ag^+; b: ZnS—V_c^+.
The arrows indicate electronic transitions upon excitation. The dashed circle in b indicates the smearing-out of the missing negative charge over the four equivalent adjacent sulfur ions.

similarly as has been found with ZnS—Ag. Figure 1 shows a schematic drawing of the V_C^+ center and the Ag^+ center for comparison, clearly revealing the similarity between the two types of centers. In the second place, equivalence between the concentration of centers and that of promoting foreign ions as observed by Kröger and Hellingman[4] and Kröger and Dikhoff[5] is explained on the basis of the principle of compensation of charge (as was done for Zn^+ in a similar way).† A theory[11] deduced for CdS, but describing in principle the incorporation of ions of a valency deviating from that of the constituents of the base lattice in general, shows that the compensation of charge is effected in different ways, dependent upon the atmospheric conditions. Under reducing conditions, for instance, Cl^- is incorporated in CdS with the formation of Cd^+ ions; under oxidizing (=sulfurizing) conditions, on the other hand, electroneutrality is maintained by the formation of an equal concentration of V_C^+, and the same must be expected to occur with ZnS. The formation of V_C^+ centers in the absence of promoting foreign ions is also possible provided the Schottky constant of ionic disorder is sufficiently great; this will be the case at high temperatures as has actually been observed by Bube.

It will be obvious that equivalence between the concentrations of centers and of promoting ions holds only when the concentrations of promoters is considerably higher than that of V_C^+ centers which may be formed by the Schottky disorder in pure ZnS under the same conditions.

For the model of the blue centers now proposed, the centers and herewith both the fluorescence and the absorption caused by them must be expected to disappear upon reduction, contrary to what usually has been assumed. So far, this has not been verified with ZnS. It has been observed, however, for the corresponding case of CdS, in which a deep red fluorescence and an absorption in the yellow part of the spectrum caused by incorporation of gallium or chlorine was found to appear only after preparation in a sufficiently sulfurizing atmosphere.[11]

On the other hand, ZnS has been found to develop a green fluorescence band when prepared under strongly reducing conditions (zinc vapor).[12,13] It is likely that this band is identical in origin with that observed with reduced ZnO,[14] both being due to an amount of zinc present in excess above the stoichiometric composition.‡ The excess of zinc may be incorporated either in the interlattice (Zn_{is}) or at normal lattice sites with the formation of an equivalent amount of anion vacancies (V_A). In both cases, the deviation from stoichiometry causes the formation of a center containing primarily two electrons; *viz.*, Zn_{is} or V_A^{2-}. The energy necessary to liberate one electron out of the center is comparatively small, most of these first electrons being already free at room temperature (and thus giving rise to dark conductivity), leaving the ionized centers Zn_{is}^+ or V_A^- behind. The energy required to liberate a second electron from these centers is much greater;[15] the liberation may occur optically (photoconductivity), fluorescence

is due to the fact that the concentration of these centers is extremely low for the method of preparation used by this author.

† Although Bube (reference 8) observed the favorable effect of promoters, equivalence between the promoter (chlorine ions) content and the concentration of centers was not observed by him. It remains to be seen whether this was due to occluded $ZnCl_2$ or to the incorporation or chlorine ions in some other way not considered by us, such as, for instance, an associated complex of two Cl^- ions and one zinc vacancy (=$ZnCl_2$ molecule).

[11] Kröger, Vink, and van den Boomgaard, "Controlled Conductivity in CdS," Z. physik. Chem. (to be published).

[12] R. Ward, private communication, 1947.

[13] N. W. Smit and F. A. Kröger, J. Opt. Soc. Am. **39**, 661 (1949).

[14] A. Schleede and B. Bartels, Z. tech. Phys. **19**, 364 (1938).

‡ According to Thomsen, J. Chem. Phys. **18**, 770 (1950), the green band of ZnO should be due to the incorporation of sulfur. ZnO made from zinc which is free from sulfur, however, shows the same green emission, provided it has been prepared under reducing conditions. Therefore, sulfur cannot be essential for the formation of "green" centers. The effect of sulfur observed by Thomson can be regarded as being of a secondary nature, sulfur or a sulfide, causing a reduction of an oxide by the reactions $(1+2\delta)ZnO+\delta/2S_2 \rightarrow Zn_{(1+2\delta)}O+\delta SO_2$, $(1+2\delta)ZnO+\delta ZnS \rightarrow Zn_{(1+3\delta)}O+\delta SO_2$. [A. Schleede, Chem. Ber. Prüf-Nr. **15**, 487 (1942); F. A. Kröger and J. A. M. Dikhoff, J. Electrochem. Soc. **99**, 144 (1952).]

[15] D. C. Cronemeyer and M. A. Gilleo, Phys. Rev. **82**, 975 (1951).

being emitted upon recombination. This is in fact the model already suggested for ZnO—Zn by Mollwo and Stöckmann.[16] The corresponding band for reduced CdS has not been observed; it must be expected to lie in the infrared.[17]

Bands corresponding to the V_C^+ and V_A^- (or Zn_{is}) bands occur also with ZnO. The green V_A^- (or Zn_{is}) band appearing with reduced ZnO has already been mentioned in the foregoing. In addition ZnO may show bands in the yellow and red part of the spectrum, the origin of which has so far been unclear.[18] Experiments carried out by us showed that a broad fluorescence band, extending from 5000 to 8000A with a maximum at 6100A and appearing upon excitation by $\lambda = 3650$A at liquid air temperature, is promoted by the presence of trivalent cations such as Ga^{3+}, Al^{3+}, Gd^{3+}, and by monovalent anions such as Cl^- or Br^- in concentrations varying from 10^{-5} to 10^{-3} atom per mole ZnO. The intensity of this band is favored by preparation of the samples under oxidizing conditions; reducing atmospheres cause a decrease of the intensity of the orange band, while that of the green V_A^- band increases. Therefore, it is probable that the orange band must be ascribed to the V_C^+ centers.

[16] E. Mollwo and F. Stöckmann, Ann. Phys. **3**, 240 (1948). E. Mollwo, Z. physik. Chem. **198**, 258 (1951).
[17] See reference 11.
[18] E. Beutel and A. Kutzelnigg, Monatsh. Chem. **55**, 158 (1930); Sitzber. Akad. Wiss. Wien., Math. naturw. Kl. (IIf) **139**, 74 (1930). A. Kutzelnigg, Sitzber. Akad. Wiss. Wien., Math. naturw. Kl. (IIf) **142**, 728 (1933). J. Ewles, Phil. Mag. **45**, 957 (1923). E. Koerner, thesis, Greifswald (1930).

THE JOURNAL OF CHEMICAL PHYSICS VOLUME 22, NUMBER 2 FEBRUARY, 1954

Inter- and Intramolecular Energy Transfer Processes. 3. Phosphorescence Bands of Some Carcinogenic Aromatic Hydrocarbons

MARGARET M. MOODIE AND C. REID
Department of Chemistry, University of British Columbia, Vancouver, British Columbia, Canada

(Received August 28, 1953)

The triplet-singlet emission spectra of a number of carcinogenic hydrocarbons are recorded together with the corresponding spectra of their 1,3,5-trinitrobenzene complexes. A new explanation of the complex spectra is given, involving a radiationless transition from an ionic "charge transfer" state to a triplet state complex.

INTRODUCTION

IN rigid media many aromatic hydrocarbons, related substitution products, and heterocyclic compounds show emission from two different electronic levels.[1–4] The spectral position and the emission lifetime of 10^{-6} to 10^{-8} second usually identify the higher-energy luminescence as the result of a transition from the lowest excited singlet state to the ground state. The lower-energy emission band has a relatively long mean lifetime, in some cases several seconds. Paramagnetic measurements[3] and studies of the effects of heavy atomic weight substituents[5] have confirmed that the long-lived emission bands arise from the metastable triplet states of the molecule concerned. The position of the triplet emission bands[2,5] and lifetimes for the corresponding triplet states[5–8] have already been recorded in the literature for a large number of molecules. Here we shall record previously unreported phosphorescence band positions for some aromatic hydrocarbon molecules, notably the methyl derivatives of 1,2-benzanthracene and of benzo(*c*)phenanthrene.

[1] Lewis, Lipkin, and Magel, J. Am. Chem. Soc. **63**, 3005 (1941); **66**, 1579 (1944).
[2] G. N. Lewis and M. Kasha, J. Am. Chem. Soc. **66**, 2100 (1944); **67**, 994 (1945).
[3] G. N. Lewis and M. Calvin, J. Am. Chem. Soc. **67**, 1232 (1945).
[4] M. Kasha, Chem. Revs. **41**, 401 (1947).
[5] D. S. McClure, J. Chem. Phys. **17**, 905 (1949); **19**, 670 (1951).
[6] Dikun, Petrov, and Sveshnikov, Zhur. Eksptl. Teort. Fiz. **21**, 150 (1951) [Chem. Abstracts **45**, 8357 (1951)].
[7] M. D. Galanin, Doklady Akad. Nauk. **73**, 925 (1950) [Chem. Abstracts **45**, 6002 (1951)].
[8] B. A. Pyatnitskii, Izvest. Akad. Nauk. S. S. S. R. Ser. Fiz. **15**, 597 (1951) [Chem. Abstracts **46**, 8972 (1952)].

EXPERIMENTAL METHOD

Weighed portions of hydrocarbon were dissolved in a mixture of one part of isopentane and four of methyl cyclohexane which formed a clear glass when cooled in liquid nitrogen contained in an unsilvered Dewar vessel. The resulting systems were irradiated with monochromatic light from a General Electric AH6 mercury arc with suitable filters. The spectra were photographed using a Hilger E2 spectrograph on Eastman Kodak II F3 or sensitized IN plates. The plates were scanned with a densitometer. A mechanical phosphorescope, similar to those already described in the literature,[2,5] was used to obtain a phosphorescence spectrum completely free of short-lived fluorescence and scattered mercury arc light.

RESULTS

In Table I are given the values in cm^{-1} of the peaks of the highest energy phosphorescence band of the hydrocarbons and the position in A of the maxima of

TABLE I. Positions of emission band maxima for the long-lived phosphorescence bands of some hydrocarbons and for the short-lived emission from complexes of the hydrocarbons with 1,3,5-trinitrobenzene.

Hydrocarbon	Origin of phosphorescence band system cm^{-1}	Max λ of observed phosphorescence bands A	Max λ of T.N.B.—Complex emission bands A
1,2-benzanthracene	16 500	6060,6570,7250	5870,6250,6980
9,10-dimethyl-1,2-benzanth	15 500	6450,7150,7900	6250,6800,7600
10-ethyl-1,2-benzanthracene	16 370	6100,6590,7210	...
1′ methyl-1,2-benzanthracene	16 980	5890,6400,7040	5650,6150,6850
2′ methyl-1,2-benzanthracene	16 640	6010,6600,7220	5600,6100,6630
3′ methyl-1,2-benzanthracene	16 720	5980,6570,7220	5800,6260,7000
4′ methyl-1,2-benzanthracene	16 670	6000,6580,7230	6850,7700
3 methyl-1,2-benzanthracene	16 810	5950,6550,7150	6000,6630,7350
4 methyl-1,2-benzanthracene	16 980	5890,6530,7070	6450,7010
5 methyl-1,2-benzanthracene	16 650	5990,6500,7100	6350,7200
6 methyl-1,2-benzanthracene	16 530	6050,6560,7280	5600,6050,6550
7 methyl-1,2-benzanthracene	16 580	6030,6590,7200	6550,7170
8 methyl-1,2-benzanthracene	16 780	5960,6480,7110	5860,6350,7100
9 methyl-1,2-benzanthracene	16 260	6150,6790,7600	5950,6430,7100
10 methyl-1,2-benzanthracene	16 310	6130,6650,7500	7100,7750
benzo(*c*)phenanthrene	19 840	5040,5420	5150,5475
1 methyl benzo(*c*)phenanthracene	18 940	5280,5630	...
2 methyl benzo(*c*)phenanthracene	19 760	5060,5440	5230,5545
3 methyl benzo(*c*)phenanthracene	19 760	5060,5460	5280,5560
4 methyl benzo(*c*)phenanthracene	19 720	5070,5475	5370,5700
5 methyl benzo(*c*)phenanthracene	19 720	5070,5475	5180,5520
6 methyl benzo(*c*)phenanthracene	19 690	5080,5490	5260,5660
3,4,5,8,9,10-hexahydropyrene	19 800	5050,5100	
naphthacene[a]	19 600	5100,5550,6110	

[a] C. Reid, J. Chem. Phys. **20**, 1214 (1952).

each of the distinguishable bands. The dotted curves in Figs. 1 and 2 show the long-lived triplet emission spectra of a few of the compounds studied.

Previously it has been shown[9] that many addition compounds of aromatic nitro-compounds and hydrocarbons show a fluorescence similar in position but more strongly allowed than the phosphorescence of the hydrocarbon component. The 1,3,5-trinitrobenzene-hydrocarbon complexes were prepared as described elsewhere[9] and in Table I are recorded the positions in A of the emission peaks. The solid lines in Figs. 1 and 2 show the emission spectra of complexes of hydrocarbons with trinitrobenzene. It will be noted that the complex emission bands are somewhat broader than the hydrocarbon triplet bands. Thus, the band positions of the former, recorded in Table I, have a certain degree of uncertainty.

DISCUSSION

It will be seen that, in spite of a few deviations, the complex spectra are in general similar enough in position and intensity distribution to those of the parent hydrocarbon to be regarded as arising from the same, slightly perturbed, triplet level. This is in contrast to the complex absorption spectra[9] which show the characteristic appearance of "charge transfer" bands.[10] The triplet state is thus the result of a radiationless transfer of energy from the charge transfer state, approximately describable as R^+N^- (R=hydrocarbon, N=polynitro compound), to a state[3] RN in which the charge transfer electron has returned to the first excited level of the hydrocarbon. Since the first excited singlet state lies at higher energy than that of the charge transfer band it cannot be excited, whereas the triplet level is suitably placed for such excitation. Finally the excited electron returns to ground by the observed radiative transition.

Next we must explain why complex formation affects so markedly the lifetime of the triplet state. For hydrocarbons the triplet state lifetimes are several seconds and for the complexes approximately 5×10^{-4} second or less. This difference is much greater than can be accounted for by a simple atomic number effect. In the original paper dealing with this subject[9] a tentative explanation was given which is now considered to be unsatisfactory in the light of the following more reasonable discussion.

An examination of the reason why the aromatic hydrocarbon lifetimes are anomalously long when compared with the values calculated on the basis of the simplest spin-orbit coupling theory has been made by McClure.[11] The principal reason is the cancellation on symmetry grounds of spin-orbit coupling integrals involving two π electron states for all components of the spin-orbit coupling part of the Hamiltonian except those symmetric to reflections in the plane of the mole-

[9] C. Reid, J. Chem. Phys. **20**, 1212 (1952).

[10] For a discussion of charge-transfer spectra, see R. S. Mulliken, J. Chem. Phys. **19**, 514 (1951) and references contained therein.

[11] D. S. McClure, J. Chem. Phys. **20**, 682 (1952).

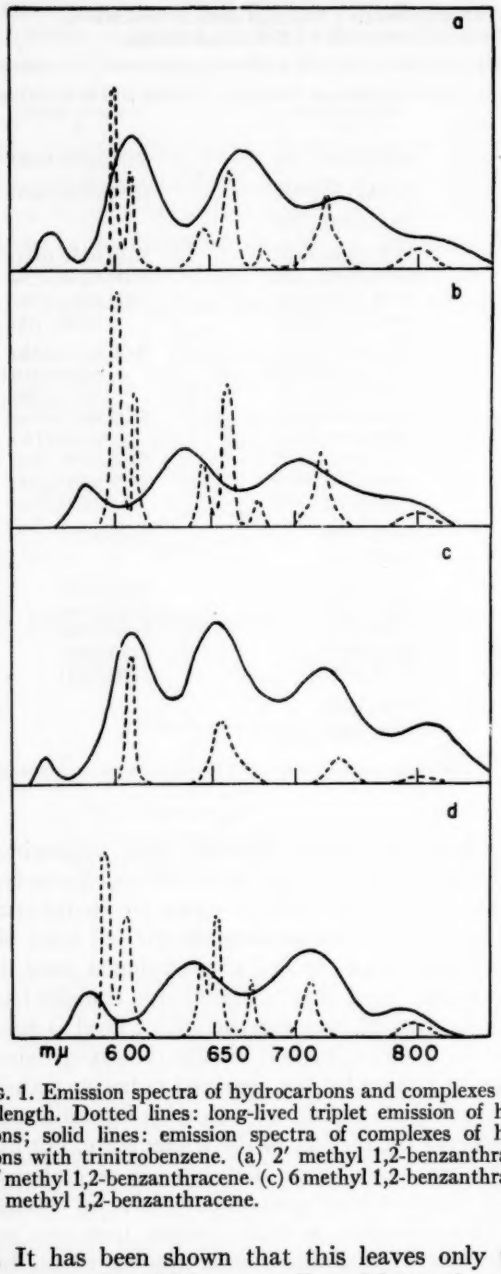

FIG. 1. Emission spectra of hydrocarbons and complexes *versus* wavelength. Dotted lines: long-lived triplet emission of hydrocarbons; solid lines: emission spectra of complexes of hydrocarbons with trinitrobenzene. (a) 2′ methyl 1,2-benzanthracene. (b) 3′ methyl 1,2-benzanthracene. (c) 6 methyl 1,2-benzanthracene. (d) 8 methyl 1,2-benzanthracene.

cule. It has been shown that this leaves only three center integrals, which are small, and integrals mixing π and σ states, which Mizushima and Koide[12] in a somewhat different treatment showed could account for the observed lifetimes.

Now "π complexes" of the kind which we are considering are complexes in which the two components form a "sandwich," the stability resulting from a shift of π electron density from the "donor" to the electron deficient "acceptor" molecule. An obvious consequence of this is severe distortion of the π orbitals of the hydrocarbon which now bulge on the trinitrobenzene side. Terms involving the X and Y components of the spin-orbit coupling terms in the Hamiltonian, previously zero, now appear and we may expect a lifetime similar to those of other oxygen or nitrogen containing aromatics. This is in fact what is observed.

[12] M. Mizushima and S. Koide, J. Chem. Phys. **20**, 765 (1952).

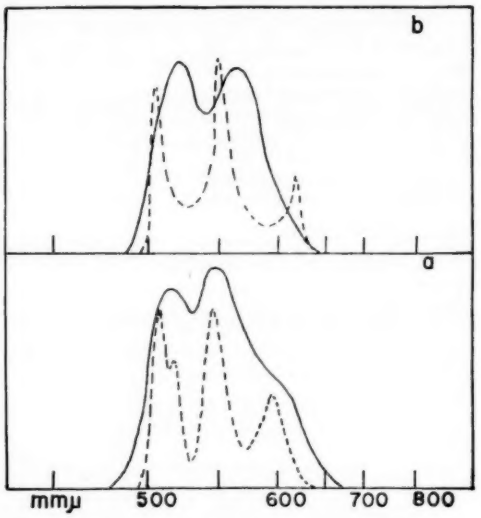

FIG. 2. Emission spectra of hydrocarbons and complexes *versus* wavelength. Dotted lines: long-lived triplet emission of hydrocarbons; solid lines: emission spectra of complexes of hydrocarbons with trinitrobenzene. (a) benzo(*c*)phenanthrene. (b) 6 methyl benzo. (*c*)phenanthrene.

TRIPLET LEVELS AND CARCINOGENESIS

This investigation was begun with the hope that it might be possible to correlate triplet state data with carcinogenic activity. Since no clear-cut correlations were in fact observed they are omitted from this paper but will be summarized elsewhere.

ACKNOWLEDGMENTS

One of us (M.M.M.) is indebted to the National Research Council of Canada for a studentship. The authors also wish to thank the National Research Council of Canada and the National Cancer Institute of Canada for grants in aid of research. Samples of 3,4,5,8, 9,10-hexahydropyrene and of 10-ethyl 1,2-benzanthracene were kindly furnished by Dr. R. N. Jones. Dr. M. S. Newman generously provided the mono-methyl derivatives of benzo(*c*)phenanthrene and of 1,2-benzanthracene.

Singlet-Triplet Absorption Bands in Some Halogen Substituted Aromatic Compounds*†

DONALD S. MCCLURE, NORMAN W. BLAKE,‡ AND PHILIP L. HANST§
Department of Chemistry and Chemical Engineering, University of California, Berkeley, California
(Received August 13, 1953)

Singlet-triplet absorption bands are reported for a number of halogen benzenes and naphthalenes. Combining the results with other data, the rates of radiationless triplet to ground state transitions are found. The effect of the atomic number of a substituted halogen atom on the absorption strength is shown to agree with a simple theory. It is also shown that the spectroscopic moments of substituents do not add vectorially for singlet-triplet transitions.

THIS note represents an extension of the work of Lewis and Kasha[1] who systematically looked for and identified singlet-triplet absorption bands (*ST* bands) in organic compounds. Reid has since found *ST* bands in pyridine[2] and ethylene.[3]

In our work, the *ST* bands were measured in liquid solutions at room temperature, and in solid glassy solutions at 77°K. Three principal problems are encountered in this work: (a) obtaining sufficiently pure compounds, (b) separating the *ST* band from the tail of the ordinary absorption band, (c) obtaining long enough path lengths. These problems arise, of course, because of the very weak absorptions (approximately from 0.0001 to 1 in molar extinction coefficient). Since $S-T$ absorption strength is expected to increase markedly with heavy atom substitution[4] it should be easier to identify $S-T$ absorption in, say, halogenated aromatics than in the unsubstituted ones. We were able to find the $S-T$ absorption in a series of halogen substituted benzenes and naphthalenes, as shown in Figs. 1 and 2. These spectra were obtained either with the Beckman spectrophotometer (the curves shown by dotted lines), or the Cary recording spectrophotometer (the curves shown by continuous lines). A 5- or 10-cm cell with 0.1 to 3.0 molar solutions was used. The sharp rise at the violet end of the spectra is the anti-Stokes singlet-singlet absorption leading to the first normal absorption band.

All of the solid compounds for which spectra are reported here were purified by several recrystallizations and vacuum sublimations. When further treatment (distillations and fractional recrystallization for liquids) did not change the spectra, we assumed that we had the correct $S-T$ absorption band, if it also had reasonable absorption strength and appeared at the correct wavelength. The latter quantity is determined by the fact that the beginning of the absorption must nearly coincide with the beginning of the long-lived emission band. This was verified in most of the cases, but it was not a very strict requirement for the halogen benzenes because of the diffuseness of the spectra.[5]

In order to get better resolution of the $S-T$ bands from the tail of the normal absorption, we tried some low-temperature absorption experiments. As the solubility of the compounds was reduced by the low temperatures, a path length of 100 cm was used. The solution (ether-isopentane-alcohol used as solvent) was frozen to a glass with liquid nitrogen. The freezing had to be done rapidly to prevent precipitation of the solute, but at the same time, this introduced strains which made the refractive index vary from point to point. For this and other reasons, we did not try to do accurate spectrophotometry on the solid solutions, but simply photographed the bands. In the case of the *p*-diiodobenzene bands shown in Fig. 2, we found it much easier at low temperatures to separate the $S-T$ absorption from the overlapping singlet bands, and noticed a considerable sharpening of the vibrational structure. This finding reinforced our belief that the continuous absorption found at room temperature actually is the $S-T$ absorption. The low-temperature spectra of *p*-dibromobenzene and of 2-iodonaphthalene showed an increase in the resolution of vibrational structure.

No $S-T$ bands were found for *p*-iodobiphenyl or for nitrobenzene, either at room temperature or 77°K. This is probably because these spectra are too diffuse to be separated from the normal absorption. There was faint absorption at the right place for toluene and naphthalene (using 10 cm of liquid in each case), but it was too weak and diffuse to be useful. $S-T$ absorption in chloro compounds is very weak, as seen in Fig. 2 for 2-chloronaphthalene. (This curve may partly represent impurity absorption). We found no bands attributable to $S-T$ absorption in *p*-dichlorobenzene at low or room temperature (contrary to Lewis and Kasha[1]). We did not investigate other chlorobenzenes.

The results of a comparison between the $S-T$ absorption strength and the emission lifetime have been presented elsewhere,[4] based on some of the data presented here. The lifetime τ is calculated from the

* Supported by the U. S. Office of Naval Research under Contract N6 ori 211 T.O. III.
† Presented at the Ohio State Spectroscopy Conference, June, 1953.
‡ Now at Experimental Station, E. I. duPont de Nemours and Company, Wilmington, Delaware.
§ Now at The Franklin Institute, Philadelphia, Pennsylvania.
[1] G. N. Lewis and M. Kasha, J. Am. Chem. Soc. **67**, 994 (1945).
[2] C. Reid, J. Chem. Phys. **18**, 1673 (1950).
[3] C. Reid, J. Chem. Phys. **18**, 1299 (1950).
[4] D. S. McClure, J. Chem. Phys. **17**, 905 (1949).
[5] D. S. McClure, thesis, University of California, Berkeley, 1948.

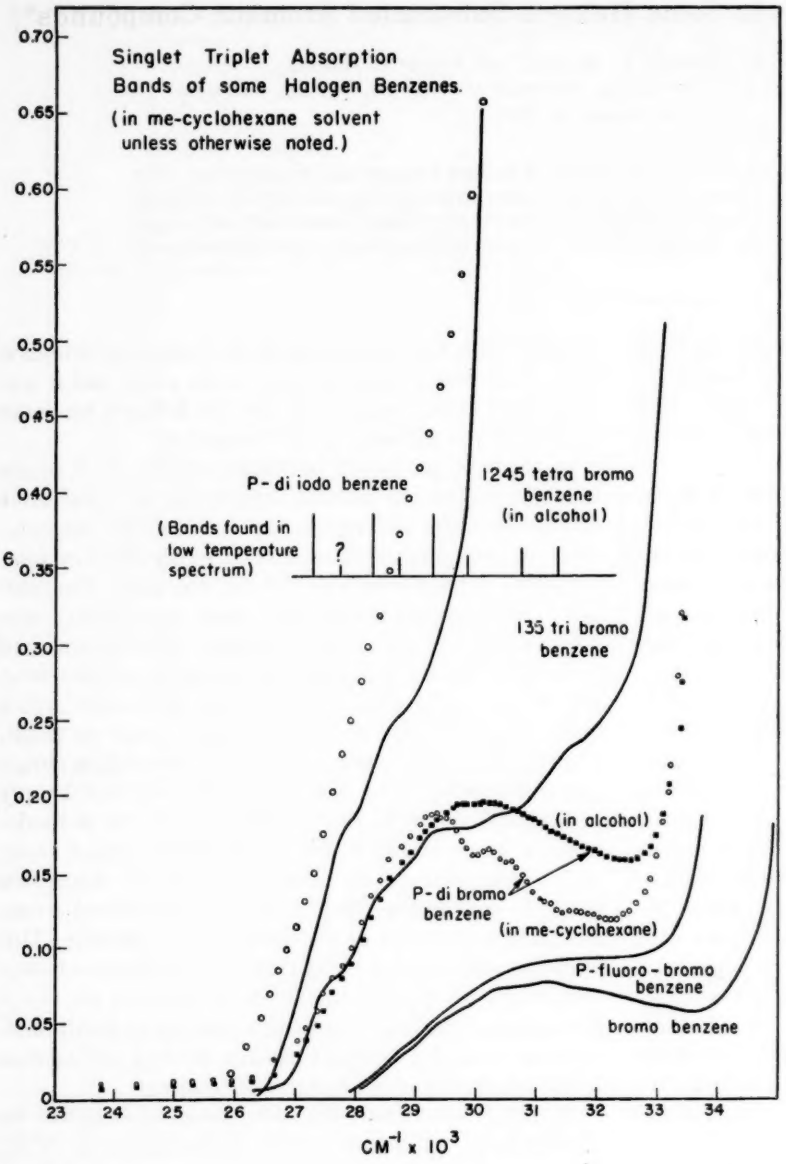

FIG. 1.

strength of the absorption band by the formula

$$\int \epsilon d\nu = \frac{10.41\times 10^8}{\bar{\nu}^2 \tau}$$

(see references 1 and 4). This is only approximately right when applied to molecular absorption, but the present data do not justify the use of a more accurate formula.|| The main reason for disagreements between emission lifetimes calculated from the absorption strength and the measured emission lifetimes is the occurrence of nonradiative processes.[6] For 1,3,5-tribromobenzene, the calculated lifetime is 0.0012 sec, while the measured lifetime is 0.00074 sec.[4] The absorption curve for 1,2,4,5-tetrabromobenzene is not sufficiently well resolved to justify an integration, but the absorption strength appears to be almost twice that of the tribromobenzene, judging by the resolved portion of this curve. This would bring the calculated lifetime to 0.0006 sec, in close agreement with the measured value of 0.00055 sec. It is interesting to compare the calculated radiative lifetimes to the measured ones, as is done in Table I. The reciprocal of the value in the first column should be the true radiative transition rate, while the reciprocal of the value in the second column should be the sum of the radiative and nonradiative transition rates. From these data, the values of the nonradiative transition rates from triplet to ground state, k_r, in the last column of the table have been calculated. They are rather rough

|| The accurate formula could be obtained from the work of D. L. Dexter, J. Chem. Phys. **21**, 836 (1953). One would simply determine the ratio of Q to $A(E)$, in that author's notation, from his Eqs. (14) and (11). A simplified version of this formula appears in reference 5.

[6] Gilmore, Gibson, and McClure, J. Chem. Phys. **20**, 629 (1952).

values, but at least illustrate that the nonradiative transition rates decrease markedly with increasing substitution. (From a very rough value of the quantum yield of triplet-singlet emission,[6] one finds for bromobenzene a k_r value of 33 000.) These values of k_r apply to the radiationless process taking place in a glassy solvent of E.P.A. (ether, isopentane, alcohol mixture) at 77°K. These rates must increase on passing to a liquid solution since the triplet-singlet luminescence efficiency goes down but the internal conversion from excited singlet to triplet should remain the same.[6] The effects of substitution on k_r seem to be the same for a series of chlorobenzenes. Monochlorbenzene has a triplet state lifetime of 0.004 sec, and a radiative quantum efficiency of only about three percent, leading to a k_r value of 2–300. The polychlorbenzenes have lifetimes on the order of 0.016 sec,[4] and we can assume that the increased triplet state lifetimes are caused by a reduction in the rate of the radiationless processes.

The atomic number effect on the absorption strength is illustrated in Fig. 2 for the 2-halogen naphthalenes and in Fig. 1 for *p*-diiodo and *p*-dibromobenzene. This, of course, is the same effect as has been observed for triplet state lifetimes.[4] The quantitative agreement with the simple theory is good for the naphthalenes. The bands were integrated up to the solid lines of Fig. 2. These lines are extrapolations of exponential curves fitted to the tail of the normal absorption in a region where $S-T$ absorption was not appreciable. The ratio of the integrated absorption strength for bromo to iodo is 1/5, while the square of the ratio of the atomic spin-orbit coupling parameters is 1/4.2. The ratio of integrated absorption strengths for *p*-dibromo to *p*-diiodobenzenes should be about the same, *viz.*, 1/4.2, but the integration under the poorly resolved iodo curve cannot be carried out with any accuracy.

There are two other effects of substituents worth considering, namely, the effect of added numbers of the same kind of heavy atom, and the effect of their relative positions. These will not be as simple as in singlet-singlet transitions because there is an intermediate state involved here. Spin-orbit interaction mixes the triplet state with the singlet intermediate state. It is probable that this mixing is simply proportional to the number of substituted atoms of the same kind, and the intensity of the transition would then be proportional to the square of this number. The dipole transition from the intermediate state is the next step in the complete transition. The spectroscopic moments of the heavy atoms would not add vectorially

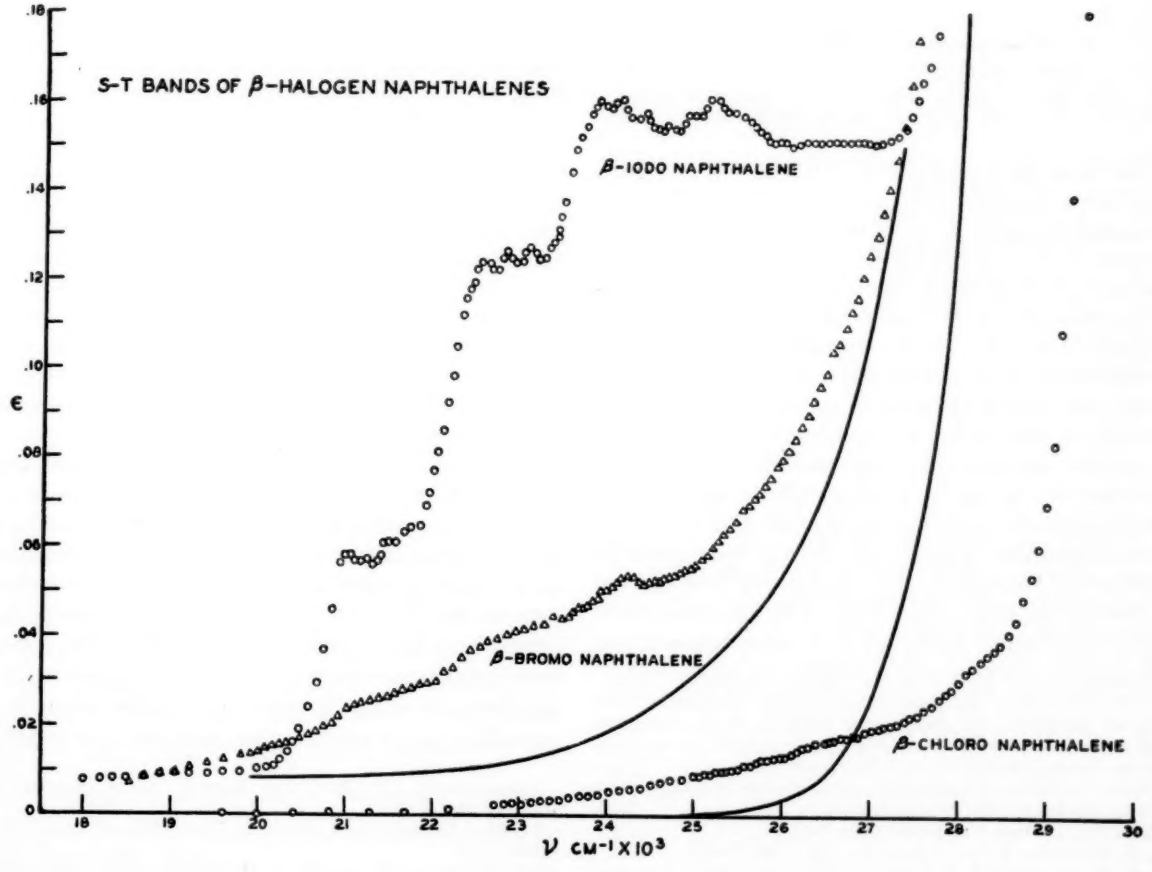

FIG. 2.

TABLE I. Comparison of triplet state lifetimes calculated from the strength of the $S-T$ absorption band to the measured values.[a]

Compound (a bromo-benzene)	calc	meas	k_r
mono-	0.0030	(0.0001)	10 000
para di-	0.0015	0.0003	2600
1,3,5 tri-	0.0012	0.00074	520
1,2,4,5 tetra-	(0.0006)	0.00055	100

[a] See reference 4.

in this step as Platt showed they do for the near ultraviolet spectra of substituted benzenes.[7] The reason for this is that the intermediate state is not derived from a trigonal wave function as are the $^1B_{1u}$ and $^1B_{2u}$ states of benzene, but its wave function must instead have two nodes cutting the molecular plane and one node in the molecular plane, *viz.*, a $^1E_{2u}$ state.[8] One can see with the aid of simple nodal diagrams of the partners in the E_{2u} state and the corresponding states of the substituted benzenes that the vector addition rule cannot apply.

Figure 1 shows that the absorption increases with the number of Br atoms substituted on the benzene ring, but does not do so as rapidly as expected. (The dibromo compound should have four times the absorption of the monobromo.) Not enough compounds were available for a complete study of the orientation effects. One can see, however, that the effect of the increased number of Br atoms on 1,3,5-tribromobenzene, compared to *p*-dibromobenzene is offset by a partial cancellation of the spectroscopic moments of the substituents.

[7] J. R. Platt, J. Chem. Phys. **19**, 263 (1951).

[8] M. Mizushima and S. Koide, J. Chem. Phys. **20**, 765 (1952).

THE JOURNAL OF CHEMICAL PHYSICS VOLUME 22, NUMBER 2 FEBRUARY, 1954

Adsorption Studies on Clay Minerals. IV. The System Montmorillonite-Cesium-Potassium*

JOSEPH A. FAUCHER† AND HENRY C. THOMAS
Sterling Chemistry Laboratory, Yale University, New Haven, Connecticut

(Received August 10, 1953)

The ion-exchange equilibria between a montmorillonite clay and potassium-cesium from chloride solutions have been studied by chromatographic and other methods. The results are summarized in terms of equilibrium constants and activity coefficients for the mixed clay phase. A tentative discussion is given of the rate of the exchange process, particularly as it affects the behavior of the chromatographic columns.

IT has long been recognized that the ion exchange equilibria between clay minerals and solutions of salts cannot be quantitatively described, even roughly, by a mass action expression in terms of stoichiometric concentrations only. When the complex character of the clay-ion combination is considered, this fact occasions no surprise. Looked upon as a solution of its ions, a wet montmorillonite is at the simplest a three-molar solution in which the anions are fixed in position and in which the motion of the cations is otherwise highly inhibited. The earliest attempts to describe the clay-solution equilibrium made use of a power law[1] without theoretical foundation. A partial application of the methods of thermodynamics appears first to have been made by Vanselow.[2] In this application the activity concept was used for the solution phase only. The experiments of Marshall and Gupta[3] indicated that this treatment was unsatisfactory. The most useful method for the description of experimental results is a purely formal procedure for calculating activity coefficients for the wet clay phase. By this means the experimental results are put into a form in which any regularities should be easily recognizable, and, if adequate theory becomes available, into a form susceptible of theoretical treatment. The method has been used with the resinous exchangers[4,5] and has recently been written out in more detail in a paper of this series.[6]

In our first study of this kind we have selected a system which we felt would be as simple as possible: the exchange adsorption on a montmorillonite of cesium and potassium from chloride solutions. To make possible a more rapid accumulation of data, the chromatographic method has been extensively used. The results so obtained have been checked by more direct batch experiments. In connection with the chromatographic work it has been necessary to make a tentative study of the rate of exchange reactions on clays and to consider the

* Contribution No. 1182 from the Sterling Chemistry Laboratory, Yale University. This paper is based on the dissertation submitted by Joseph A. Faucher to the Faculty of the Graduate School of Yale University in partial fulfillment of the requirements for the degree of Doctor of Philosophy.

† Present address: Physikalisches-Chemisches Institut, University of Innsbruck, Innsbruck, Austria.

[1] H. Jenny, J. Phys. Chem. **36**, 2219 (1932).

[2] A. P. Vanselow, J. Am. Chem. Soc. **54**, 1307 (1932).

[3] C. E. Marshall and R. S. Gupta, J. Soc. Chem. Ind. (London) **52**, 433T (1933).

[4] Argersinger, Davidson, and Bonner, Trans. Kansas Acad. Sci. **53**, 404 (1950).

[5] Sillén, Ekedahl, and Högfeldt, Acta Chem. Scand. **4**, 556 (1950).

[6] G. L. Gaines, Jr., and H. C. Thomas, J. Chem. Phys. **21**, 714 (1953).

various disturbing effects which influence the performance of a chromatographic column.

The clay used in this work was a montmorillonite from Chambers, Arizona, American Petroleum Institute, Reference Clay Mineral No. 23. Our sample is an exceptionally pure clay mineral: through the courtesy of the U. S. Geological Survey a physical examination of the material has been made which shows less than two percent of impurities, about half of which is quartz. X-ray examination failed to show the presence of any clay mineral other than montmorillonite. Chemical analysis[7] gave the results shown in Table I.

The formula of the material calculated by the method of Ross and Hendricks[8] is

$$(Al_{1.329}Fe^{III}_{0.216}Mg_{0.541}Fe^{II}_{0.076})(Si_{3.798}Al_{0.202})O_{10}(OH)_2 (Ca_{0.209}Na_{0.029}K_{0.023}).$$

In deducing this formula, the presence of 1.00 percent of quartz has been assumed and the titania and manganese oxide have been neglected (traces of pyrolusite are apparent in the clay). On the supposition that all the calcium, sodium, and potassium and no other ions are exchangeable, the exchange capacity according to the analysis is 1.32 meq. per gram of "backbone." (We define the "backbone" of the clay as the material left after ignition in air to constant weight less the weight of the exchangeable ions.) This value is in reasonable agreement with the capacity obtained in our chromatographic work, namely, 1.38 meq./g backbone.

The chromatographic methods have been described previously.[9] Traced cesium chloride solution was passed through a column of natural clay suspended on asbestos, the cesium form of the clay being quickly produced. Radioactive analysis of the effluent samples gave a typical breakthrough curve. The holdup volume was determined through the difference between the weight of the dry column and its weight saturated with solution. A potassium chloride solution of the same concentration as the initial cesium solution was then slowly passed through the column. Analysis of the effluent for radiocesium gave long, trailing curves, indicating that cesium is held more strongly than potassium. The isotherm was calculated in the usual fashion. Experiments were done at 0.01, 0.02, 0.04, 0.08, 0.20, and 0.40 molar. (All experiments reported in this paper were done at room temperature.) It was found impractical to go above 0.40M; at higher concentrations the cesium was eluted too rapidly to get accurate measurements. For example, at 0.40M c/c_0 dropped to 0.1 after only 25 ml had emerged from the column. Under these conditions the holdup volume, which is not too accurately known, becomes an important part of the computation.

To get an idea of the magnitude of the rate of the exchange reaction between clay and solution, nine two-gram samples of natural clay were weighed into centrifuge tubes. To each was added 40 ml of 0.0450M CsCl solution, traced with Cs 137. The tubes were shaken for a definite length of time and the clay separated by centrifuging for fifteen minutes, the supernatant liquid being then removed and counted. The tubes were analyzed in groups of three after separations at 15, 90, and 1080 minutes. The precision of the results was about 1 percent as expected from the character of the counting. The relative activities of the solutions were, respectively, 0.198, 0.154, 0.151. It is apparent that a matter of hours is required for the attainment of equilibrium. The results of this experiment are not inconsistent with the idea that diffusion in the solid is the rate-limiting factor. Although it would be most interesting to have more information of this type, we did not pursue the experiments further because of the large uncertainty in timing the separations and because of complete inability to assign a size parameter to the clay as dispersed in the solution.

During the course of this work many column experiments were made involving isotopic exchange of cesium with clay on asbestos. Generally it may be said that any single experiment at a definite flow rate can be entirely adequately described by a φ-function plot as described by Faucher, Southworth, and Thomas.[9] However, the constants necessary in these descriptions do not vary in a simple manner with the flow rate; no single mechanism is adequate to explain the results over the range of flow rates investigated, from 6.3 ml/min to 0.078 ml/min in a column 2.3 cm in inside diameter packed to a fractional free volume of 0.75–0.79. As the flow rates decreased from the highest value, the breakthrough curves gradually steepened, as would be expected if solid diffusion were the rate-determining factor. However, in the range 0.2–0.1 ml/min this behavior changes; on further decrease of the flow rate the curves become less steep. This effect is to be expected as we pass into the region in which longitudinal diffusion becomes of importance. In the transition region the behavior of the column is extremely complex. If one will content himself with a first approximation to the solid diffusion law and superimpose on this the effect of longitudinal diffusion, the mathematics are

TABLE I. Analysis of montmorillonite, Chambers, Arizona, API23.

SiO_2	51.43%	Na_2O	0.20
Al_2O_3	17.25	K_2O	0.24
Fe_2O_3	3.82	H_2O above 105–110°	9.75
FeO	0.12	H_2O below 105–110°	9.40
MgO	4.82	TiO_2	0.54
CaO	2.59	MnO	0.05
			100.21%

[7] This analysis was carried out by Ledoux and Company, Teaneck, New Jersey.

[8] C. S. Ross and S. B. Hendricks, U. S. Geological Survey, Professional Paper 205B, 1945.

[9] Faucher, Southworth, and Thomas, J. Chem. Phys. **20**, 157 (1952).

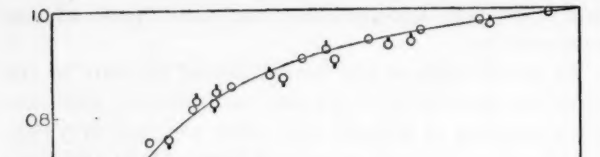

FIG. 1. Exchange adsorption isotherm for cesium-potassium montmorillonite. All concentrations refer to cesium. Circles without tails, chromatographic measurements; circles with tails up, batch experiments on cesium clay; circles with tails down, batch experiments on potassium clay.

available for the description.[10] For our purposes, however, we can be satisfied with a qualitative understanding of the column behavior. In the cases of interest to us, involving the exchange of different ions, the descriptions can be handled only by high-speed computing machines. In any case, for the exchange of different ions the nonequilibrium effects are of relatively less importance. In our results on the cesium-potassium system no corrections for the nonequilibrium behavior of the columns have been used. The size of these corrections is about the same as the uncertainty in the results of the batch experiments, and hence the corrections lose any significance.

At concentrations greater than 0.05M, with our Geiger-Müller counters, the natural radioactivity of potassium becomes of importance. Where necessary, measurements have been appropriately corrected for the presence of K^{40}.

In order to assess directly the reliability of the chromatographic results, points on the isothermal surface were determined by batch experiments. For this purpose pure cesium and pure potassium clays were required. These were prepared by shaking natural clay with repeated portions of CsCl or KCl solutions until the supernatant liquid no longer showed the presence of calcium. These preparations were washed with distilled water, dried for 24 hours at 60°, ground, and exposed to air at room temperature for a few days before storing. On ignition the cesium clay showed a total water content of 10.48 percent, the potassium clay, 11.76 percent. Chromatographic determination of the exchange capacity of the cesium clay gave 1.327 meq./g backbone, in good agreement with the value for the natural material. The potassium clay, on the other hand, gave 1.186 meq./g. This low value is evidence of potassium fixation and will be discussed in a little more detail below.

In the batch experiments about 1 g of clay was weighed into a centrifuge tube and a measured volume of traced CsCl solution was added. After shaking for several hours the suspension was centrifuged and the supernatant solution counted. With the cesium clay it was found necessary to use a mixed solution of cesium and potassium chlorides. Potassium chloride alone traced with Cs^{137} lost activity through adsorption on the walls of the vessels. Experiments were done with potassium clay at 0.01, 0.02, and 0.04M. When the data are plotted on relative coordinates (q/q_0 *vs* c/c_0) virtually identical curves were obtained at each concentration. For the cesium clay it was not found possible to get a wide spread of points on the isotherm by varying the ratio of clay to solution. Consequently, a number of mixed solutions were used to get a single isotherm at one total concentration, namely, 0.02M.

The results of all the experiments indicate that the total concentration of the salt in solution has no influence on the shape of the isotherm up to 0.4M. The isothermal surface can be simply represented by a single curve using the relative coordinates. This curve is given in Fig. 1 with a selection of points from the various experiments to illustrate the character of the agreement. A more useful summary of the results is given in Table II and in Fig. 2 in the form of the stoichiometric equilibrium "constant" $K_c = q(c_0-c)/c(q_0-q)$, as a function of q/q_0, the fraction of the exchange sites occupied by cesium. These numbers were obtained by computing values from data read from the isothermal curve drawn through the experimental points, plotting $\log K_c$ *vs* q/q_0, and arbitrarily drawing a smooth curve through these points. This somewhat devious procedure does no violence to the experimental results in the central region of the isotherm. Near the ends of the

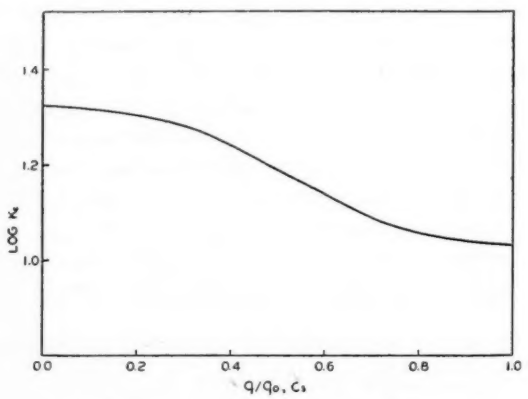

FIG. 2. Stoichiometric equilibrium constant. $K_c = q(c_0-c)/c(q_0-q)$.

[10] L. Lapidus and N. R. Amundson, J. Phys. Chem. **56**, 984 (1952).

isotherm the uncertainties are necessarily high, particularly at low values of q/q_0. The values of K_c in Table II reproduce the isotherm to well within the experimental uncertainty.

We have evaluated the thermodynamic equilibrium constant, and obtain $K=13.1$, through the use of the expression

$$\ln K=\int_0^1 \ln K_c d(q/q_0).$$

The simplifications and assumptions inherent in this calculation are apparent from an examination of Eq. (17) of the paper by Gaines and Thomas.[5] The above expression for $\ln K$ is exact only if the activity of water is constant in all the solutions. Since we have no knowledge of the values of the water contents of the various clays involved in the equilibria, it is not now possible to make a more exact calculation of the thermodynamic quantities.

On the same basis the activity coefficients of the mixed potassium and cesium clays have been evaluated. These are given in Fig. 3. Considerable deviations from ideality are apparent. It is of some interest to notice that cesium in a cesium-rich clay and potassium in a potassium-rich clay behave in nearly ideal fashion ($f\simeq 1$). The ion present in small amount behaves in the nonideal manner.

As mentioned above, the potassium clay prepared for the isotherm determinations exhibited an appreciably lower capacity than the cesium clay similarly prepared. The question immediately arises as to the effect, if any, of this change in capacity on the shape of the isotherm plotted in relative coordinates. The following experiments were carried out to investigate the possibility of

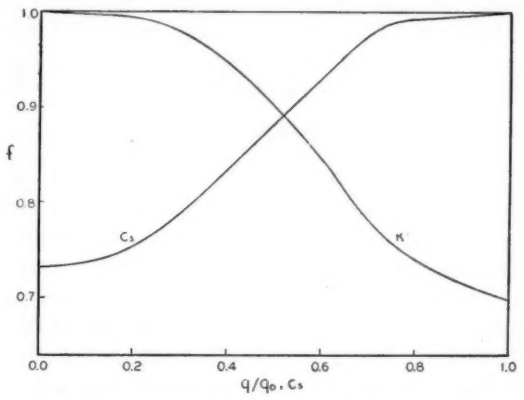

FIG. 3. Activity coefficients in mixed clay phase.

TABLE II. The stoichiometric equilibrium constant for cesium-potassium montmorillonite in chloride solutions at room temperature.

q/q_0, Cesium	K_c
0.00	(21.1)
0.10	20.75
0.20	20.2
0.30	19.1
0.40	17.5
0.50	15.6
0.60	13.9
0.70	12.25
0.80	11.4
0.90	11.0
1.00	(10.7)

an observable effect. With the natural mineral a column was prepared containing 4.698 g of clay and 5.0 g of asbestos in a tube 2.3 cm in diameter. The clay was converted to the cesium form and its capacity thereby shown to be 1.052 meq./g (1.379 meq./g backbone). The column was then eluted with 0.04M KCl at 0.2 ml/min. This speed was twice that used for previous potassium elutions; nevertheless, the isotherm calculated from the trailing boundary was identical with that previously obtained. The column was then dried, in a manner designed to fix part of the potassium, by passing through it air at 50–60°. The column was then placed in a vacuum desiccator for several days until constant weight was obtained. After wetting with more potassium chloride solution, the column was again saturated with 0.04M CsCl. The capacity of the clay as shown by this experiment was 1.253 meq./g backbone. Another elution with potassium chloride was carried out; the isotherm obtained was again identical with those obtained previously. Finally a new capacity determination with traced CsCl gave a value of 1.249 meq./g backbone. The complications of this experiment were great, and it is very difficult to estimate the accuracy of the results. We believe, however, that we may conservatively say that the decrease in capacity of 0.128 meq./g backbone produced an effect on the isotherm of less than 4 percent. It will be of interest to push these experiments further and determine if the fixation process can at all alter the exchange properties of a clay mineral as measured by the shape of the isotherm.

We wish again to express our indebtedness to the Department of Nuclear Engineering of Brookhaven National Laboratory for their continued support of this work.

The Microwave Spectra, Structure, and Dipole Moment of Stable Pentaborane

HENRY J. HROSTOWSKI* AND ROLLIE J. MYERS
Department of Chemistry and Chemical Engineering, University of California, Berkeley, California
(Received June 3, 1953)

The microwave spectra of several of the naturally occuring boron isotopic species of B_5H_9 and B_5D_9 have been observed. These data show that stable pentaborane consists of a tetragonal pyramid of boron atoms and has either C_4 or C_{4v} symmetry. The boron-boron distances are $B_1-B_2=1.687\pm0.005$ and $B_2-B_2=1.800\pm0.003$A. If C_{4v} symmetry and B_1-H_1 and B_2-H_2 distances equal to 1.22A are assumed, the following boron-hydrogen parameters are obtained: $B_2-H_3=1.35\pm0.02$A, $\angle B_1-B_2-H_2=136°10'\pm30'$ and $\angle B_1B_2B_2-B_2B_2H_3=196\pm2°$. Dipole moment values of 2.13 ± 0.04 and 2.16 ± 0.04 Debye units were measured for B_5H_9 and B_5D_9, respectively.

INTRODUCTION

SEVERAL structures have been proposed for stable pentaborane (B_5H_9). The earlier of these models[1,2] were based on the assumption that pentaborane would have a hydrocarbon-like structure of low symmetry. Recently, however, electron diffraction[3] and x-ray[4] workers have advanced an unusual pyramidal structure of C_{4v} symmetry. In a preliminary report[5] of the microwave spectra we have shown that stable pentaborane does indeed possess a C_4 axis and that the boron atoms form a tetragonal pyramid.

At first glance each new boron hydride structure has shown little relationship to the others. For this reason it is important to examine these molecules in detail and to derive an accurate structure for each member of the series. These molecules utilize their bonding electrons in a highly efficient manner and an explanation of their structures represents a test of modern chemical bonding theory.

In this paper we report the microwave spectra of naturally occurring boron isotopic species of B_5H_9 and B_5D_9. With these data we are able to confirm the over-all aspects of the new pyramidal structure for stable pentaborane and to determine accurate boron-boron distances. Our data also allow us, with certain assumptions, to calculate a detailed structure including the boron-hydrogen parameters.

EXPERIMENTAL TECHNIQUE

The microwave spectra were observed using the Stark modulated instrument that has been described previously,[6] and a sample of pentaborane that was obtained from Dr. A. E. Newkirk of the General Electric Company. This pentaborane was generally purified by distillation immediately before use.

In order to obtain maximum sensitivity the absorption spectra were observed in a wave guide cell cooled to 200°K. It was at first suspected that pentaborane decomposed in the wave guide system, but later evidence indicated that it is stable in a copper and glass system at temperatures up to 100°C. The absorption lines of pentaborane are broadened by the interaction of the electric quadrupole moments of the five boron atoms with the molecular rotation. This interaction is not very great, however, and the half widths of the observed absorptions were less than 2 mc/sec. The center of this multiplet pattern could be judged to better than ±0.2 mc/sec.

The deuterated pentaborane was prepared by the heterogeneous exchange of D_2 and B_5H_9 over a chromia-alumina catalyst. The exact procedure is described by Hrostowski and Pimentel.[7] The samples that were employed for the microwave work had 85–98 percent of the hydrogen replaced by deuterium. It was found that the lines due to the partially deuterated molecules were very weak and the most prominent absorptions were all present in the 98 percent sample. This behavior is to be expected for a random exchange of hydrogen atoms.

EXPERIMENTAL RESULTS

In the region between 28 000 and 29 200 mc/sec the 21 absorption lines listed in Table I were found for stable pentaborane. The strongest of these lines at 28 011.4 mc/sec had two first-order and two second-order Stark components. A slightly weaker line at 28 359.7 mc/sec had a similar Stark pattern. This Stark effect, with the selection rule $\Delta M_J=0$, is characteristic of $J=1$ to $J=2$ transitions for symmetric top molecules. Most of the other lines listed in Table I were observed to have two second order Stark components. A pattern of this type is consistent with their assignment as $J=1$ to $J=2$ transitions for slightly asymmetric top molecules.

In a previous report of the microwave spectra[5] we have shown that the observed lines are readily assigned if we assume that the boron atoms of stable pentaborane form a tetragonal pyramid. The two symmetric top lines

* Present address: Bell Telephone Laboratories, Murray Hill, New Jersey.

[1] S. H. Bauer and L. Pauling, J. Am. Chem. Soc. **58**, 2403 (1936).

[2] K. S. Pitzer, J. Am. Chem. Soc. **67**, 1126 (1945).

[3] K. Hedberg, M. E. Jones and V. Schomaker, Proc. Natl. Acad. Sci. U. S. **38**, 679 (1952).

[4] W. J. Dulmage and W. N. Lipscomb, Acta Cryst. **5**, 260 (1952).

[5] Hrostowski, Myers, and Pimentel, J. Chem. Phys. **20**, 518 (1952).

[6] R. J. Myers and W. D. Gwinn, J. Chem. Phys. **20**, 1420 (1952).

[7] H. J. Hrostowski and G. C. Pimentel (to be published).

arise from $B_5{}^{11}H_9$ and from $B_4{}^{11}B^{10}H_9$ with the B^{10} atom on the axis of symmetry. The other observed lines are assigned to the many boron isotopic species which do not possess a four fold axis of symmetry.

From the frequencies of the two symmetric top transitions a single moment of inertia ($I_a=I_b$) can be calculated for each of the two isotopic species with full symmetry. For each of the asymmetric top molecules three transitions are observed and three moments of inertia ($I_a\neq I_b$ and I_c) can be determined from these data. It can be shown, however, that if the boron atoms form a tetragonal pyramid that the moments of inertia of the various boron isotopic species can all be calculated using only five structural parameters. This assumes that rotation-vibration interaction can be neglected for isotopic boron substitutions in these molecules. These parameters will be those which are sufficient to place the boron atoms in the molecule, define the center of mass and determine the moments of inertia of a single isotopic species.

TABLE I. The $J=1$ to $J=2$ lines for B_5H_9.

Observed frequency[a] mc/sec	Calculated frequency[b] mc/sec	Assignment Transition	Molecule	
28 011.4±0.1	(28 011.4)	1–2	$B_5{}^{11}H_9$	C_{4v}
28 359.7±0.2[c]	(28 359.7)	1–2	$B_4{}^{11}B^{10}H_9$	C_{4v}
28 513.8±0.2	(28 513.8)	1_{11}–2_{21}		
28 359.7±0.2[c]	(28 359.7)	1_{10}–2_{20}	$B_4{}^{11}B^{10}H_9$	
28 187.1±0.2	(28 187.1)	1_{01}–2_{11}	C_s	
28 872	28 872.6	1_{11}–2_{21}	$B_3{}^{11}B_2{}^{10}H_9$	
28 715[d]	28 715	1_{10}–2_{20}	C_s	
28 537.7±0.2	28 537.6	1_{01}–2_{11}	B^{10} at apex	
29 024	29 024.5	1_{11}–2_{21}		
28 732	28 731	1_{10}–2_{20}	$B_3{}^{11}B_2{}^{10}H_9$	
28 364.5±0.5	28 365.0	1_{01}–2_{11}	C_{2v}	
28 694.0±0.5	28 694.5	1_{11}–2_{21}	$B_3{}^{11}B_2{}^{10}H_9$	
28 689.5±0.2	28 689.7	1_{10}–2_{20}	C_s	
28 686.5	28 685.0	1_{01}–2_{11}	B^{11} at apex	
	29 207	1_{11}–2_{21}	$B_2{}^{11}B_3{}^{10}H_9$	
29 045[e]	29 046	1_{10}–2_{20}	C_s	
28 870	28 868	1_{01}–2_{11}	B^{10} at apex	
29 057	29 057	1_{11}–2_{21}	$B_2{}^{11}B_3{}^{10}H_9$	
29 052	29 051	1_{10}–2_{20}	C_s	
29 045[e]	29 047	1_{01}–2_{11}	B^{11} at apex	
	29 393	1_{11}–2_{21}	$B_2{}^{11}B_3{}^{10}H_9$	
29 095	29 094	1_{10}–2_{20}	C_{2v}	
28 715[d]	29 718	1_{01}–2_{11}		
28 392	not assigned			
28 989	not assigned			
29 063	not assigned			

[a] Unless specified, ±1 mc/sec.
[b] Calculated using the parameters in Table III.
[c,d,e] These lines were not resolved.

In Table I we show a comparison between the observed frequencies and those calculated using only five parameters. The excellent agreement between the observed and calculated values for 18 transitions is strong evidence in favor of the assignments given in Table I. The five observed frequencies of the $B_5{}^{11}H_9$ and $B_4{}^{11}B^{10}H_9$ species were used to determine our five parameters and these in turn were used to determine the frequencies of the 13 remaining transitions. Making reference to Fig. 1, we have established the two unequal moments of inertia

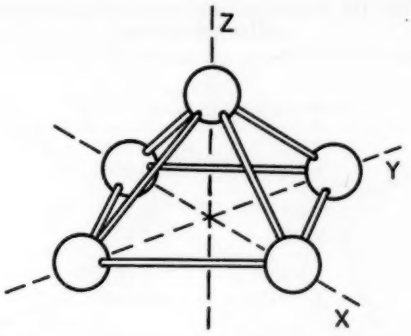

FIG. 1. The tetragonal boron pyramid of stable pentaborane.

of $B_5{}^{11}H_9$, the z and x (or y) coordinates of the apex and base borons respectively, and the sum of the z coordinates of the hydrogen atoms. The 1_{10}–2_{20} are the only transitions in Table I whose frequencies depend upon the moment of inertia about the axis of symmetry (I_c). Their dependence upon this parameter is not very great. For this reason the value obtained for I_c is much less accurate than that obtained for I_a (or I_b).

In Table II a similar, but not as extensive, series of lines is given for B_5D_9. It should be noted in particular that the two lines that were not resolved for $B_4{}^{11}B^{10}H_9$ are well resolved for $B_4{}^{11}B^{10}D_9$. Their occurrence at the same frequency was an accidental coincidence. We also include in Table II a list of $J=2$ to $J=3$ lines observed for B_5H_9. These lines were measured both to confirm the assignment and to obtain a better value for I_c. A summary of the rotational and structural parameters obtained from the microwave spectra of B_5H_9 and B_5D_9 is given in Table III.

A quantitative study of the Stark effect was made to establish the dipole moment of stable pentaborane. Both the first and second order components of the 1–2 line for $B_5{}^{11}H_9$ were measured and an average value of

TABLE II. Some observed lines for B_5D_9 and B_5H_9.

Observed frequency[a] mc/sec	Calculated frequency[b] mc/sec	Assignment Transition	Molecule	
20 845.4	(20 845.4)	1–2	$B_5{}^{11}D_9$	C_{4v}
21 051.8	(21 051.8)	1–2	$B_4{}^{11}B^{10}D_9$	C_{4v}
21 117.2	(21 117.2)	1_{11}–2_{21}	$B_4{}^{11}B^{10}D_9$	
21 032.1	(21 032.1)	1_{10}–2_{20}	C_s	
20 938.8	(20 938.8)	1_{01}–2_{11}		
21 329±1	21 329	1_{11}–2_{21}	$B_3{}^{11}B_2{}^{10}D_9$	
21 241±1	21 242	1_{10}–2_{20}	C_s	
21 146±1	21 147	1_{01}–2_{11}	B^{10} at apex	
	21 215	1_{11}–2_{21}	$B_2{}^{11}B_2{}^{10}D_9$	
21 211±1	21 212.5	1_{10}–2_{20}	C_s	
	21 210	1_{01}–2_{11}	B^{11} at apex	
42 017.3±0.1	(42 017.3)	2–3	$B_5{}^{11}H_9$	C_{4v}
42 5398	(42 539.8)	2–3	$B_4{}^{11}B^{10}H_9$	C_{4v}
42 776.1	(42 776.1)	2_{21}–3_{31}		
42 563.1	42 563.1	2_{20}–3_{30}	$B_4{}^{11}B^{10}H_9$	
42 525.3±0.4	42 525.6	2_{12}–3_{22}	C_s	
42 488.1	42 488.1	2_{02}–3_{12}		
42 286.5	(42 286.5)	2_{11}–3_{21}		

[a] Unless specified, ±0.2 mc/sec.
[b] Calculated using the parameters in Table III.

TABLE III. Rotational and structural parameters for stable pentaborane.

	B_5H_9 From 1–2 lines	B_5H_9 From 2–3 lines	B_5D_9 From 1–2 lines
I_a[a]	72.1773 ±0.0003	72.1769 ±0.0002	96.9895 ±0.0009
I_c[b]	104.3 ±1.3	103.3 ±0.2	134.6 ±3.5
z_B[c]	1.1074 ±0.0030	1.1075 ±0.0015	1.106 ±0.006
x_B	1.2742 ±0.0006	1.2747 ±0.0004	1.2710 ±0.0011
Σz_H	−1.08 ±0.18	−1.16 ±0.12	−1.11 ±0.25

[a] Moment of inertia about axis perpendicular to symmetry axis, calculated for $B_5{}^{11}H_9$ and $B_5{}^{11}D_9$ using I_a (atomic mass units $\times A^2$) $= \frac{505\,446.5}{a\ (\mathrm{mc/sec})}$.

[b] Moment of inertia about symmetry axis calculated for $B_5{}^{11}H_9$ and $B_5{}^{11}D_9$ using data obtained from the spectra of $B_4{}^{11}B^{10}H_9$ and $B_4{}^{11}B^{10}D_9$.

[c] Angstrom units, calculated using mass of $B^{11}=11.01284$, $B^{10}=10.01618$, $H=1.008130$, $D=2.014708$.

2.13±0.04 Debye was obtained. The second order components of the 1–2 line for $B_5{}^{11}D_9$ gave an average value of 2.16±0.04 Debye. This is a much larger value than expected for a hydride of boron.

THE STRUCTURE OF PENTABORANE

We learn from the microwave spectra of B_5H_9 and B_5D_9 that the boron atoms of pentaborane form a tetragonal pyramid and that the molecule itself has either C_4 or C_{4v} symmetry. In addition to this symmetry information we also obtain quite accurate values for the dimensions of the boron pyramid. We are left, therefore, with the problem of the placement of the hydrogen atoms.

One would normally expect that the structures of the boron hydrides, including pentaborane, can be considered as extensions of the diborane structure. It is now apparent, however, that a simple hydrocarbon-like extension is incorrect at least for B_5H_9 and $B_{10}H_{14}$. The infrared spectra of B_5H_9 and B_5D_9[7] indicate that the bonding of the hydrogen atoms in pentaborane is indeed similar to that of diborane[8] and that the molecule contains both regular B−H bonds and bridge type B−H−B bonds. Since pentaborane has a fourfold axis of symmetry, the most reasonable structure is one with four equivalent B−H bonds, four equivalent B−H−B bridge bonds and one B−H bonded hydrogen atom on the axis of symmetry. The x-ray[4] and electron diffraction[3] workers have chosen structures of C_{4v} symmetry which are consistent with our conclusions. Both of these groups place four bridge bonded hydrogen atoms considerably below the base of a tetragonal boron pyramid and four regularly bonded hydrogen atoms above this base. The rotational parameters given in Table III can be rearranged in order that we might compare quantitatively our results for B_5H_9 and B_5D_9 with the placement of the hydrogen atoms by electron diffraction. Our values of I_c can be utilized in Eq. (1) to yield values for $\sum x_H^2$.

$$I_c=\sum_i m_i(x_i^2+y_i^2)=2\sum_i m_i x_i^2 = 2m_H\sum x_H^2+2m_B\sum x_B^2. \quad (1)$$

I_a and I_c can also be combined in Eq. (2) to give values for $\sum z_H^2$. The results that we obtain are

$$I_a=\sum_i m_i(x_i^2+z_i^2)=\tfrac{1}{2}I_c+m_H\sum z_H^2+m_B\sum z_B^2, \quad (2)$$

15.75±0.10 and 15.75±0.88 for the $\sum x_H^2$ of B_5H_9 and B_5D_9 respectively. This can be compared with a calculated electron diffraction value[3] of 16.1±0.8. For the $\sum z_H^2$ we obtain 8.85±0.10 and 8.72±0.50 for B_5H_9 and B_5D_9, respectively. While the calculated electron diffraction value is 9.1±0.7. In addition, our value of $\sum z_H$ can be compared with a calculated electron diffraction value of +0.5±1.6.

The agreement that exists between the microwave and electron diffraction parameters appears to confirm the over-all placement of the hydrogen atoms of the electron diffraction model. Without the spectra of the partially deuterated species we cannot separate the contributions of the three kinds of hydrogen atoms nor can we differentiate between C_4 and C_{4v} symmetry. It would seem that the best thing to do at this time is to calculate a pentaborane structure of the type assumed by the electron diffraction and x-ray workers which is consistent with our more accurate but incomplete microwave data.

In Table IV we have calculated the two boron-boron distances using our boron coordinates determined for B_5H_9 and B_5D_9. We report the average of the two most accurate values obtained for each species with an uncertainty large enough to include both values. As in most microwave work we are determining only effective bond distances for the ground vibrational state. Because

TABLE IV. Structural parameters for stable pentaborane.

		Microwave		Elec. diff.[b]	X-ray[c]
B_1-B_2[a]		1.687 ±0.005		1.700 ±0.017	1.66 ±0.02
B_2-B_2		1.800 ±0.003		1.805 ±0.014	1.77 ±0.02
B_1-H_1 and B_2-H_2	(1.18)	(1.22)	(1.26)	1.234 ±0.066	1.21 and 1.20 ±0.05 ±0.07
B_2-H_3	1.39	1.35 ±0.02	1.31	1.359 ±0.077	1.35 ±0.04
$\angle B_1-B_2-H_2$	134°20′	136°10′ ±30′	138°0′	120° ±20°	115° ±5°
$\angle B_1B_2B_2-B_2B_2H_3$ (external dihedral)	192°	196° ±2°	200°	187° ±10°	190° ±5°

[a] The hydrogen and boron designations are those of Fig. 2.
[b] Reference 3.
[c] Reference 4.

[8] K. Hedberg and V. Schomaker, J. Am. Chem. Soc. 73, 1482 (1951).

of rotation-vibration interactions the equilibrium bond distances may differ from the effective values by an amount greater than our stated uncertainties. In order to calculate boron-hydrogen values we have assumed that the two regular B—H distances are equal (this was also assumed by electron diffraction workers) and we have taken the three successive values of 1.18, 1.22, and 1.26A. The resultant three sets of boron-hydrogen structural parameters are included in Table IV together with the electron diffraction and x-ray values.

The microwave and electron diffraction boron-boron distances are in excellent agreement while the x-ray values are appreciably smaller. It is probable that this discrepancy represents an actual contraction of pentaborane in the solid state. If this is the case we would also expect the x-ray boron-hydrogen parameters to differ appreciably from those for the gas state molecules.

We can also see from Table IV that the microwave results will agree with the electron diffraction and x-ray boron-hydrogen bond distances only if the two B—H bond angles are considerably larger than those determined by these methods. While no exact choice can be made, it would seem clear from these data that the best boron-hydrogen parameters are obtained with the regular B—H distances equal to 1.22A. This choice gives the most satisfactory agreement between the microwave and the diffraction results. A model for stable pentaborane based upon these parameters is given in Fig. 2.

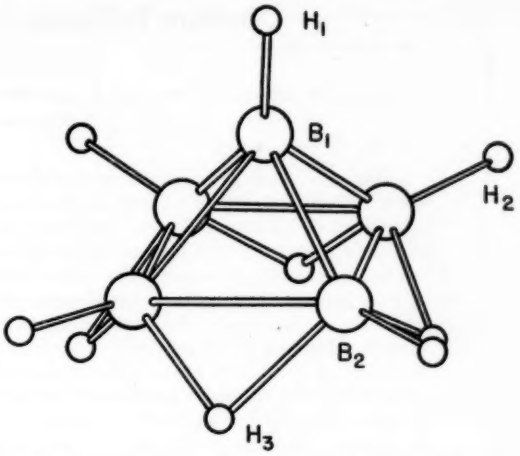

FIG. 2. A C_{4v} structure for stable pentaborane consistent with the microwave data.

DISCUSSION

If we take the B_1-H_1 and B_2-H_2 distances to be 1.22A, we find that our bond distances for the basal boron and hydrogen atoms of stable pentaborane are very close to the corresponding ones of diborane. These bond distances in diborane are[8] B—H=1.187 ±0.03, B—H (bridge)=1.334±0.027 and B—B=1.770 ±0.013A. This suggests that part of the bonding skeleton for pentaborane is closely related to that of diborane. Pitzer[2] has interpreted the bonding in diborane as hybrid s, p_x, and p_y boron orbitals with the bridge hydrogens contributing their electrons to p_z boron orbitals to form a "protonated double bond." Accordingly, we may think of the pentaborane structure as a four membered boron ring with strained s, p_x, and p_y hybrid bonds, again with the four bridge hydrogens contributing their electrons to four boron p_z orbitals.

In such a simplified picture the peripheral B—H bonds would lie in the plane of the four boron atoms and B—H—B bonds would be bent 90° below this plane. Our structural parameters for pentaborane place the B—H bonds 3° above the boron plane and the B—H—B bonds 57° down from this plane. This latter discrepancy may either be due to repulsive forces between the bridge hydrogen atoms ($H_3\cdots H_3$=1.8A) or to the influence of the apex boron atom.

The bonding between the apex and base boron atoms leads to a short B—B distance and is of a type not found in diborane. With the peripheral B—H bonds nearly in the boron plane the source of pentaborane's dipole moment must be found in the other bonds of the molecule. It is possible that the apex to base boron bonds involve considerable boron charge separation. It is also possible that the apex boron bonding utilizes some of the p_z base boron orbitals. In the latter case the bridge bonds will be left with a resultant positive charge. It would not seem probable, however, that p_z orbital interaction can entirely account for the bonding to the apex boron atom.

ACKNOWLEDGMENTS

We would like to thank Professor G. C. Pimentel and Professor W. D. Gwinn for continued help during this investigation. We are also indebted to Dr. A. E. Newkirk of the General Electric Company for our sample of pentaborane.

Sodium Diffusion in Sodium Tungsten Bronze*

J. F. SMITH AND G. C. DANIELSON
Institute for Atomic Research and Departments of Chemistry and Physics, Iowa State College, Ames, Iowa
(Received September 15, 1953)

Diffusivity has been measured in single crystals of the metallic sodium tungsten bronze, $Na_{0.78}WO_3$, at 664°C, 752°C, and 832°C. Concentration gradients were established by effusion of sodium from single crystals into a vacuum and were measured by determining the variation in the lattice constant. The diffusivities were calculated by a method which is based upon Fick's first law and which, to the author's knowledge, has not been used previously. The data obtained from several crystals held at constant temperature for varying periods of time gave a family of curves showing the sodium concentration as a function of depth with time as a parameter. From these curves the mass of sodium transferred through a plane parallel to the surface and at any particular depth could be obtained; this mass was plotted as a function of time. The slope of this curve divided by the concentration gradient, both evaluated at the same time and depth, was taken as the diffusivity for the corresponding concentration. The diffusivity of sodium in $Na_{0.78}WO_3$ was found to be represented by the equation $D=D_0\exp(-\Delta H/RT)$, where $D_0=0.87$ cm²/sec and $\Delta H=51.8$ kcal/mole. In order to calculate the diffusivity it was necessary to determine the coefficients of linear expansion. For $Na_{0.8}WO_3$ the length L at temperature T_c was found to be

$$L=L_0[1+(8.81\times10^{-6})T_c-(1.92\times10^{-9})T_c^2],$$

where L_0 is the length at 0°C and T_c is the temperature in degrees centigrade.

INTRODUCTION

SODIUM tungsten bronze is the name applied to the nonstoichiometric compound Na_xWO_3, where x has a value between zero and one. The structure of these remarkable compounds was shown to be perovskite by de Jong.[1] The changes in color and the linear dependence of the lattice constant upon concentration have been discussed by Hägg[2] and by Straumanis.[3] The anomalous electrical characteristics of these metals have been examined by Huibregste, Barker, and Danielson,[4] by Brown and Banks,[5] and by Gardner and Danielson.[6] The paramagnetic properties have been studied by Stubbin and Mellor[7] and by Kupka and Sienko.[8] However, the diffusion of sodium through this unusual metallic compound has not been investigated. Such diffusion should be interesting because the number of vacancies is large and variable and because coulomb forces are possibly responsible for the equilibrium configuration and the magnitude of the activation energies. This investigation was undertaken to study the process of sodium diffusion in this material.

CRYSTAL GROWTH

Single crystals of sodium tungsten bronze were grown from a melt of sodium orthotungstate, tungstic oxide, and tungsten metal.[3,9] When these materials were combined in an approximate mole ratio of 6.5:4:1, large crystals of Na_xWO_3 having $x=0.75$ were obtained. The sodium concentration was increased or decreased by increasing or decreasing the proportion of sodium orthotungstate. The crystals were usually grown in one thousand-gram batches which were heated to 1000°C in porcelain crucibles. After complete fusion the temperature was gradually lowered to about 600°C at which temperature the power to the heating furnace was shut off. Using cooling times of the order of two to three days, crystal faces were obtained which measured up to one-half centimeter on an edge. The crystals were normally obtained as an intergrown matrix of cubes from which individual crystals could be broken. The crystals were first treated with hot water in order to dissolve the excess sodium orthotungstate and then cleaned with an aqueous solution of hydrofluoric acid.

CONCENTRATION GRADIENTS

Concentration gradients were established in single crystals of the sodium tungsten bronze by a process of sodium effusion. To remove sodium from the crystals the samples were heated under reduced pressures of about 10^{-5} to 10^{-6} mm Hg. W. R. Savage[10] has recently made some preliminary measurements on the heat sublimation of sodium from the sodium tungsten bronze, which indicated that the heat of sublimation is a small value of the order of 10 kcal/mole. This value suggests that the diffusion process rather than sublimation is the rate-controlling process in effusion of the sodium.

After effusion the concentration gradients of sodium within the crystals were measured by a precision determination of the lattice parameter. The gradient

* Contribution No. 280 from the Institute for Atomic Research and the Departments of Chemistry and Physics, Iowa State College, Ames, Iowa. Work was performed in the Ames Laboratory of the U. S. Atomic Energy Commission.

[1] W. F. de Jong, Z. Krist. **81**, 314 (1932).
[2] G. Z. Hägg, Nature **135**, 874 (1935).
[3] M. E. Straumanis, J. Am. Chem. Soc. **71**, 679 (1949); **71**, 683 (1949).
[4] Huibregtse, Barker, and Danielson, Phys. Rev. **84**, 142 (1951).
[5] B. W. Brown and E. Banks, Phys. Rev. **84**, 609 (1951).
[6] W. R. Gardner and G. C. Danielson, Phys. Rev. (to be published.)
[7] P. M. Stubbin and D. P. Mellor, J. Proc. Roy. Soc. N. S. Wales **82**, 225 (1948).
[8] F. Kupka and M. J. Sienko, J. Chem. Phys. **18**, 1296 (1950).
[9] Brimm, Brantley, Lorenz, and Jellinek, J. Am. Chem. Soc. **73**, 5427 (1951).
[10] W. R. Savage, Iowa State College, private communication.

measurements were made on the following basis. For the region $0.3<x<1.0$, sodium tungsten bronze crystallizes in the cubic system with the perovskite structure[1-3] which is shown in Fig. 1. The crystals used in this determination were chosen with at least one well-developed (100) face, and the lattice parameter measurements were made on this face. By using unfiltered copper radiation and a Norelco x-ray diffractometer, it was possible to obtain nine (h00) reflections, five resulting from $K\beta$ and four from $K\alpha$. The calculated lattice parameters from the seven reflections of highest order were plotted against the function $\frac{1}{2}(\cos^2\theta/\sin\theta+\cos^2\theta/\theta)$ suggested by Nelson and Riley[11] rather than against $\cos^2\theta$ since such curves were more nearly linear as shown in Fig. 2. The reproducibility of a lattice parameter measurement in a homogeneous crystal was better than 0.01 percent as shown in Table I. The relationship between the lattice parameter and the sodium concentration has been studied by three different investigators,[3,9,12] and Vegard's law has been found to

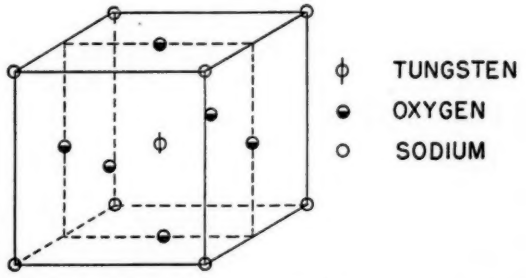

FIG. 1. Structure of cubic phase of NaW_xO_3. Lattice parameter in angstroms, $a_0=0.0820x+3.7845$. Cubic symmetry for range $0.3<x<1.0$.

hold. The equation by Banks

$$a_0=(0.0820x+3.7845)\text{A} \qquad (1)$$

was considered the most accurate and was used to relate the lattice parameter a_0 to the sodium concentration as defined by x in the formula Na_xWO_3. The lattice parameter was evaluated in true angstroms rather than kX units using $1\text{A}=1.00202\ kX$ units.

The concentration gradients were measured by taking a diffraction pattern of the surface of the crystal, machining from the crystal a measured increment, taking a diffraction pattern of the new surface, machining off another increment, and repeating the process until the initial sodium concentration was reached. The justification for using the diffraction patterns as representative of the surface lattice parameter is shown in Fig. 3. This figure shows the calculated intensity decline as a function of perpendicular depth from the surface for the two extremes of the seven reflections used in the lattice parameter extrapolation. Since the

[11] J. B. Nelson and D. P. Riley, Proc. Phys. Soc. (London) **57**, 160 (1945).

[12] E. Banks, *3rd Interim Report on Lattice*, Polytechnic Institute of Brooklyn, New York (July 6, 1951), Multigraphed, pp. 5–7.

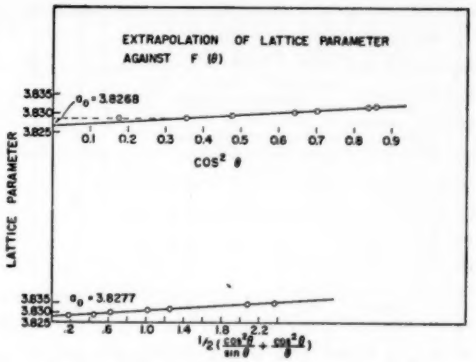

FIG. 2. Extrapolation to obtain precision lattice parameter.

increments machined from the crystals were of the order of 25×10^{-4} centimeters (1 mil) and since practically complete absorption of the x-rays takes place in this depth, the measured lattice parameter clearly corresponded to the sodium concentration of the removed increment. The high absorption of x-rays by tungsten is thus of considerable advantage in determining the sodium concentration of a thin surface layer by a lattice parameter determination.

DETERMINATION OF DIFFUSION COEFFICIENTS AND THEIR TEMPERATURE DEPENDENCE

The effusion apparatus was so designed that several crystals could be heated at the same temperature for varying periods of time. By using crystal samples of the same initial sodium concentration it was thus possible to obtain data from a given sample group heated at one particular temperature to plot a family of curves showing concentration as a function of depth from the surface with time as a parameter. The slope of the concentration-depth curves at any point yielded the concentration gradient $(\partial c/\partial x)$ at that point. From the concentration-depth curves, a second family of curves showing mass transfer against time with depth as a parameter could be obtained. The mass transfer values were determined from the concentration-depth curves by measuring the area between the initial concentration at $t=0$ and the final concentration at $t=t_1$ from infinite depth to some particular depth z_1. (Infinite depth in this case represented the region of constant sodium concentration.) The measured area represented the mass of sodium which had moved through unit cross sectional area at the depth $z=z_1$ during the time t_1 and corresponds to one point on the second family of curves.

TABLE I. Reproducibility of lattice parameter measurements.

No.	Increment in centimeters	Lattice parameter	Deviation from average
A	0.0×10^{-3}	3.8318	0×10^{-4}
B	2.0×10^{-3}	3.8314	-4×10^{-4}
C	1.8×10^{-3}	3.8319	$+1\times10^{-4}$
D	5.8×10^{-3}	3.8319	$+1\times10^{-4}$
E	9.9×10^{-3}	3.8320	$+2\times10^{-4}$
	Average	3.8318 ± 0.0001A	

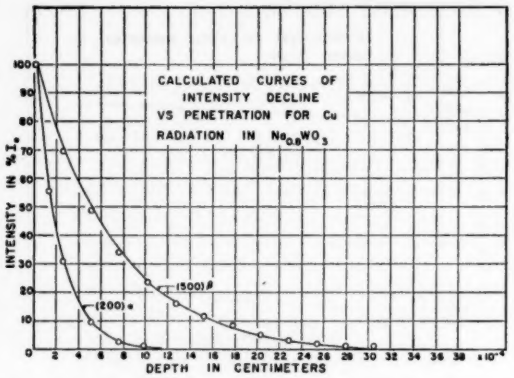

FIG. 3. Intensity decrease of incident x-radiation as a function of depth.

Fick's first law is normally written

$$dm = D(\partial c/\partial z)dt. \tag{2}$$

In this equation m is the mass transferred across a unit area, D is the diffusivity, c is the concentration, z is a space coordinate, and t is time. This can be rewritten as

$$D(c_1) = \frac{\left[\left(\frac{\partial m}{\partial t}\right)_{z=z_1}\right]_{t=t_1}}{\left[\left(\frac{\partial c}{\partial z}\right)_{t=t_1}\right]_{z=z_1}}, \tag{3}$$

where c_1 is the sodium concentration at a depth z_1 after a diffusion time t_1. This shows diffusivity values to be the ratio of two slopes. By measuring the slope in each of the two families of curves for the same time, $t=t_1$, and depth, $z=z_1$, one value of the diffusivity was determined. Additional values of the diffusivity are obtained by selecting different values for the parameters t and z. This correspondence in coordinates is shown by the subscripts in Eq. 3. The subscripts inside the brackets represent the parameter of the curve whose slope was measured. The subscripts outside the brackets represent the abscissa at the point of measurement. This takes into account the possible variation of the diffusivity with concentration since a particular combination of time and depth represent a particular concentration.

The range of change of sodium concentration used in calculating the diffusivities was kept to less than 10 percent of the original sodium concentration. The experimental diffusivities were then fitted to an Arrhenius-type equation:

$$D = D_0 \exp(-\Delta H/RT). \tag{4}$$

The symbols in the equation are: D_0 the frequency factor, ΔH the heat of activation, R the gas constant, and T the absolute temperature. C. Zener[13] has discussed the evaluation of the frequency factor,

$$D_0 = \nu_0 a_0^2 \exp(\Delta S/R). \tag{5}$$

The value should lie between 0.01 and 1 cm²/sec. In order to make a more accurate approximation of the frequency factor using Zener's approach, it would be necessary to know the Debye temperature to evaluate the characteristic frequency ν_0, and it would be necessary to know the melting point and the temperature dependence of one of the elastic constants in order to evaluate the entropy of activation, ΔS. As yet none of this information is available for sodium tungsten bronze. Only the lattice parameter, a_0, has been evaluated.

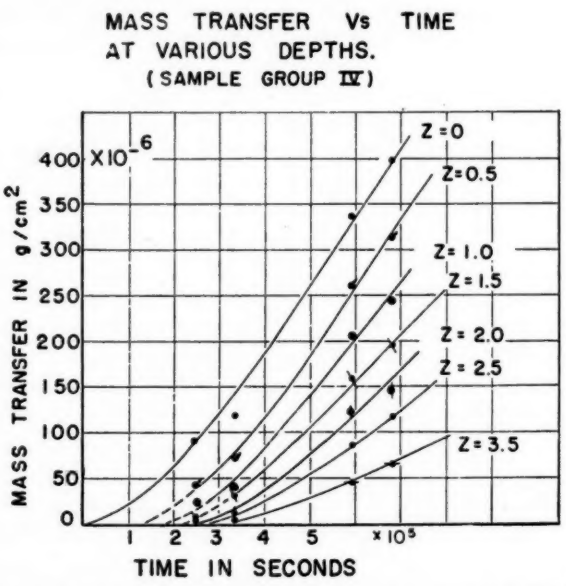

FIG. 5. Mass transfer *versus* time for sample group IV at 832°C.

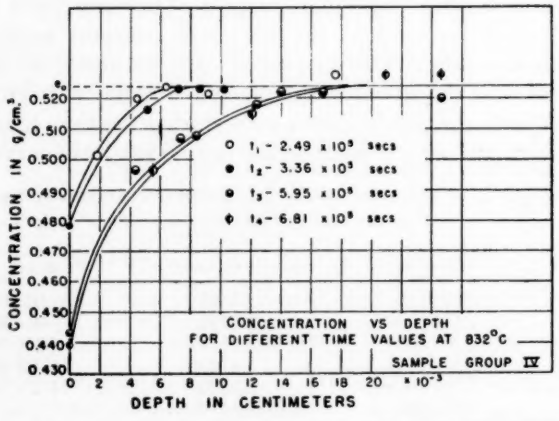
CONCENTRATION IN g/cm³
t_1 - 2.49 x10³ secs
t_2 - 3.36 x10³ secs
t_3 - 5.95 x10³ secs
t_4 - 6.81 x10³ secs
CONCENTRATION VS DEPTH
FOR DIFFERENT TIME VALUES AT 832°C
SAMPLE GROUP IV
DEPTH IN CENTIMETERS

FIG. 4. Concentration *versus* depth for sample group IV at 832°C.

EXPERIMENTAL RESULTS

The diffusivity of sodium in $Na_{0.78}WO_3$ was measured at 832°C, 752°C, and 664°C. The concentration-depth curves for 832°C are shown in Fig. 4. The validity of the shape of these curves was inferred from additional measurements made on other crystals with considerably

[13] C. Zener, J. Appl. Phys. **22**, 372 (1951).

greater ranges of change of sodium concentration. The mass transfer-time curves for 832°C are shown in Fig. 5. The points for the mass transfer-time curves were obtained by integrating the concentration-depth curves with a planimeter. The slopes of the two sets of curves were measured by the mirror technique.[14] The quantitative results are shown in Table II. The data were fitted to an Arrhenius-type equation, and the resulting temperature dependence of the diffusivity is shown in Fig. 6. The frequency factor D_0 was calculated to be 0.87 ± 0.04 cm²/sec., which is within the range predicted by Zener's theory. The activation energy ΔH was calculated to be 51.8 ± 0.7 kcal/mole.

LINEAR COEFFICIENT OF EXPANSION

Since the depth measurements on the crystals were made at room temperature, the true diffusivity was found by correcting for the lattice expansion occurring between room temperature and the temperature of diffusion. The expansion coefficients were obtained from lattice parameter measurements made with a high-temperature x-ray diffraction apparatus designed by P. Chiotti.[15] Measurements were made on $Na_{0.8}WO_3$ between room temperature and 750°C. The data were fitted to a parabolic expansion formula

$$L=L_0(1+\alpha T_c+\beta T_c^2). \qquad (6)$$

The expansion coefficients calculated by the method of least squares were

$$\alpha=8.81\times10^{-6} \text{ per } °C,$$
$$\beta=-1.92\times10^{-9} \text{ per } °C^2.$$

In the equation L is any linear length, L_0 is this length at 0°C, and T_c is the temperature in °C.

TABLE II. Temperature-corrected diffusivities, frequency factor, and activation energy for $Na_{0.78}WO_3$.

Temperature	Measured diffusivity	Correction factor for expansion	Corrected diffusivity
832°C	6.8×10^{-11} cm²/sec	1.0116	6.9×10^{-11} cm²/sec
752°C	6.8×10^{-12} cm²/sec	1.0107	6.9×10^{-12} cm²/sec
664°C	9.7×10^{-13} cm²/sec	1.0096	9.8×10^{-13} cm²/sec

Calculated quantities:
(1) Frequency factor: $D_0=0.87\pm0.04$ cm²/sec
(2) Activation energy: $\Delta H=51.8\pm0.7$ kcal/mole

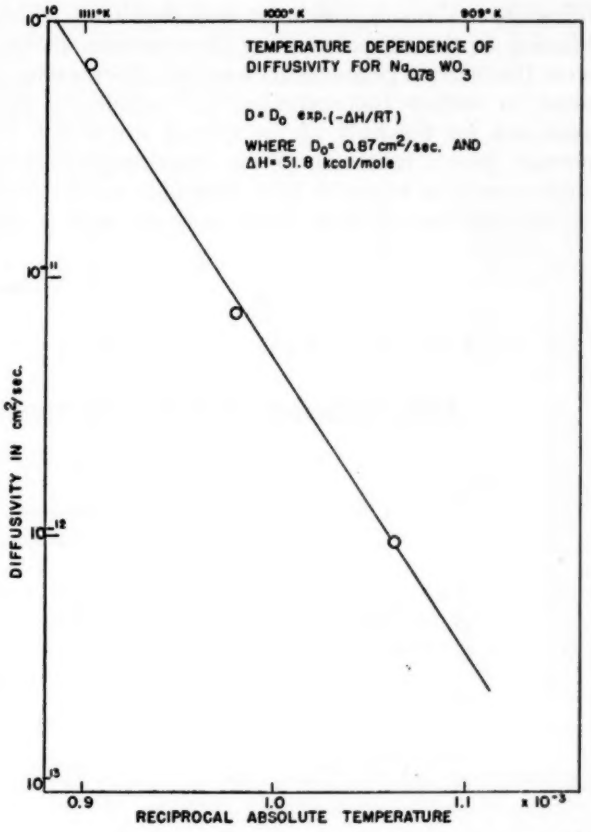
TEMPERATURE DEPENDENCE OF DIFFUSIVITY FOR $Na_{0.78}WO_3$
$D=D_0\ exp.(-\Delta H/RT)$
WHERE $D_0=0.87 cm^2/sec.$ AND $\Delta H=51.8$ kcal/mole
DIFFUSIVITY IN cm²/sec.
RECIPROCAL ABSOLUTE TEMPERATURE
x 10⁻³

FIG. 6. Temperature dependence of diffusivity for $Na_{0.78}WO_3$.

DISCUSSION

The retention of only two significant figures in the measured diffusivities results from several sources of error. The temperature was controlled to within ±3°C during the effusion period. A split-type furnace was used so that it could be preheated before being placed around the samples. This arrangement reduced the heating and cooling time for the sample crystals to the order of 15 minutes. Since the shortest effusion period was between three and four days, this represents an error in the time at equilibrium temperature of less than one part in a thousand. The increments which were machined from the crystals were measured to $\pm10^{-4}$ cm per increment. However, these errors were not cumulative since one of the two readings in measuring the depth of the increment represented the original crystal surface. The standard deviation for the lattice parameter measurements shown in Table I was ±0.0001A. This deviation represented a ±0.001 g/cm³ deviation in the sodium concentration. The precision in these measurements was masked by the empirical fit of the curves to the measured points. The planimeter used in integrating the concentration-depth curves was read to two parts in ten thousand, but the significant error was the personal error in tracing the curves. The measurements of the slopes of the curves could be made to two parts in a hundred, but again the more important error was the human error in judging the position at which the mirror was normal to the curve. Twenty-five measurements of the diffusivity at 832°C gave a standard deviation of $\pm0.5\times10^{-11}$ cm²/sec; six measurements at 752°C gave a standard deviation of $\pm0.7\times10^{-12}$ cm²/sec; and fifteen measurements at 664°C gave a standard deviation of $\pm0.8\times10^{-13}$ cm²/sec.

It is believed that the treatment of the data to yield

[14] A. G. Worthing and J. Geffner, *Treatment of Experimental Data* (John Wiley and Sons, Inc., New York, 1943), p. 89.
[15] P. Chiotti, Iowa State College (to be published).

diffusivity values is valid for any depth at which diffusion is the rate-controlling phenomenon. In the event that surface phenomenon was the rate-controlling factor in surface concentration, the validity of the treatment for the bulk of the crystal would not be affected since a flattening of the concentration-depth curves would be attended by a flattening of the mass transfer-time curves which would leave the ratio of the slopes undisturbed. However, in this experiment it is believed that there is no important surface phenomenon since diffusivity values calculated from surface points agree within experimental error with diffusivity values measured at points within the bulk of the crystal.

We wish to acknowledge the cooperation of Dr. H. A. Wilhelm in making possible this research and the assistance of Mr. Paul Sidles in growing the crystals.

THE JOURNAL OF CHEMICAL PHYSICS VOLUME 22, NUMBER 2 FEBRUARY, 1954

Determination of Some Carbon-Chlorine Bond Dissociation Energies

M. Szwarc, *College of Forestry, State University of New York, Syracuse, New York*
AND
J. Watson Taylor, *Chemistry Department, University of Manchester, Manchester, England*

(Received July 24, 1953)

An investigation of the pyrolyses of benzyl chloride and benzoyl chloride has been carried out by means of the "toluene carrier" technique. It is shown that the course of these reactions is analogous to that of the previously investigated pyrolyses of benzyl bromide and benzoyl bromide, i.e., the rate determining steps are

$$C_6H_5\cdot CH_2Cl \rightarrow C_6H_5\cdot CH_2\cdot + Cl$$

or

$$C_6H_5\cdot CO\cdot Cl \rightarrow C_6H_5\cdot CO + Cl.$$

From kinetic data we obtained the activation energies of the rate determining steps, and we identify these activation energies with the respective C—Cl bond dissociation energies. Thus we derive

$$D(C_6H_5\cdot CH_2-Cl) = 68 \text{ kcal/mole}$$

and

$$D(C_6H_5\cdot CO\cdot -Cl) = 73.2 \text{ kcal/mole}.$$

The consistency of these data with the respective C—Br bond dissociation energies is very satisfactory. For example, the heat of formation of the benzoyl radical, derived from the $D(C_6H_5\cdot CO-Cl)$, is 15.7 kcal/mole, and that calculated from the experimentally determined $D(C_6H_5\cdot CO-Br)$ is 15.6 kcal/mole.

DETERMINATION OF SOME CARBON-CHLORINE BOND DISSOCIATION ENERGIES

It has been shown in a series of publications by one of us[1–6] that the C—Br bond dissociation energies in suitable organic bromides can be determined by pyrolysing the compound in the presence of an excess of toluene. It was found that organic bromides which cannot be decomposed into olefines and hydrogen bromide, e.g., those which do not contain hydrogen atoms in α position to the C—Br bond, dissociate according to reaction (1):

$$R\cdot Br \rightarrow R + Br. \qquad (1)$$

The fragments produced react with toluene present in the system and abstract a hydrogen atom from the methyl group. Thus, benzyl radicals and molecules like $R\cdot H$ or $H\cdot Br$ are formed, e.g.,

$$C_6H_5\cdot CH_3 + Br \rightarrow C_6H_5\cdot CH_2\cdot + H\cdot Br. \qquad (2)$$

Since reaction (2) is much faster than reaction (1), the rate of formation of hydrogen bromide measures the rate of the initial dissociation (1).

We have now extended these investigations to organic chlorides, limiting our studies to the class of these organic chlorides for which the $D(C-Cl)$ is smaller than the C—H bond dissociation energy in toluene. This limitation is required by our experimental technique in which toluene is used as a carrier gas, and hence we cannot study the pyrolyses of compounds which decompose to a lesser extent than toluene. Benzyl chloride and benzoyl chloride seem to be suitable for such studies, and their behavior on pyrolysis is reported in the present communication.

EXPERIMENTAL

In the investigation of the pyrolysis of benzyl chloride, we followed closely the method used formerly in investigating the pyrolysis of benzyl bromide. The reader

[1] Szwarc, Ghosh, and Sehon, J. Chem. Phys. **18**, 1142 (1950).
[2] A. H. Sehon and M. Szwarc, Proc. Roy. Soc. (London) **A209**, 110 (1951).
[3] Leigh, Sehon, and Szwarc, Proc. Roy. Soc. (London) **A209**, 97 (1951).
[4] Ladacki, Leigh, and Szwarc, Proc. Roy. Soc. (London) **A214**, 273 (1952).
[5] M. Ladacki and M. Szwarc, Proc. Roy. Soc. (London) **A219**, 341 (1953).
[6] M. Szwarc and D. Williams, Proc. Roy. Soc. (London) **A219**, 353 (1953).

is referred, therefore, to a previous paper[1] for all the details of experimental technique.

Benzyl chloride used for pyrolyses has to be carefully purified by repeated distillation to remove traces of water and of hydrogen chloride. It appears that its decomposition takes place according to Eq. (3):

$$C_6H_5\cdot CH_2\cdot Cl \rightarrow C_6H_5\cdot CH_2\cdot + Cl. \qquad (3)$$

This conclusion follows from the fact that dibenzyl and hydrogen chloride were the products of the pyrolyses of benzyl chloride in the presence of an excess of toluene. Moreover, it was found that the molar ratio of dibenzyl to hydrogen chloride was close to the theoretically required value of unity (see Table I).

Table II summarizes the experimental results obtained in the pyrolysis of benzyl chloride. The percentages of decomposition and the first-order rate constants reported in this table are calculated on the basis of the amount of hydrogen chloride produced in the decomposition. Inspection of Table II shows that the first-order rate constants remain constant when the partial pressures of benzyl chloride are varied by a factor of six. Compare, e.g., runs 13 and 15, or runs 28 and 27. In the latter two runs the partial pressures of the compound are 0.05- and 0.30-mm Hg (the other variables remaining essentially constant), and the first-order rate constants interpolated to the temperature of 982°K (interpolation by 2° only) are 0.450 and 0.449 sec^{-1}, respectively. The variation of the partial pressure of toluene by a factor of three also leaves unaffected the magnitude of the rate constants, see e.g., runs 30 and 32. In these runs the partial pressures of toluene were 6.65- and 19.9-mm Hg, respectively, while the corresponding rate constants were 0.466 and 0.479 sec^{-1} (the latter value being obtained by interpolation of the results from 981°K to 982°K). Finally, it appears that the unimolecular rate constants are not affected by the variations in the time of contact, which was changed from about 0.3 sec to just above 1 sec.

TABLE I. Benzyl chloride.

T°K	Dibenzyl/HCl	mp of dibenzyl
956	0.96	51°C
960	0.93	49–51°C
988	0.99	45–49°C

The homogeneity of the reactions was checked by carrying out the pyrolysis in a reaction vessel packed with silica wool, the latter increasing the surface by a factor of eight. The corresponding runs are denoted in Table II by the letter *P*, and are marked in Fig. 1 by full points. It appears that there is a slight heterogeneity of the reaction amounting to about 9 percent of the total reaction.

The activation energy of the reaction was obtained in the usual way by plotting logs of first-order rate constants against the reciprocal of temperature. The plot, presented in Fig. 1, leads to a straight line corresponding to an activation energy of 68 kcal/mole and a frequency factor of 6.8×10^{14} sec^{-1}. The slight heterogeneity of this reaction may call for some correction of the activation energy. Maximum correction amounts to 2.1 kcal/mole, leading to an activation energy of 70 kcal/mole and a frequency factor 2.3×10^{15} sec^{-1}.

TABLE II. Benzyl chloride.

Run	T°K	P_{PhCH_2Cl} mm Hg	$P_{Toluene}$ mm Hg	Time of contact (sec)	Percent decomp.	k sec^{-1}
13	922	0.27	11.2	1.06	4.8	0.046
15	922	0.60	10.7	1.01	4.7	0.047
10	927	0.26	11.2	1.02	5.5	0.055
11	928	0.25	11.2	1.01	5.9	0.060
14	931	0.18	11.2	1.05	6.4	0.063
12	932	0.22	11.3	1.04	7.3	0.073
18	940	0.23	18.1	0.92	7.8	0.089
34*P*	943	0.66	10.3	1.02	17.5	0.188
9	945	0.21	11.3	1.01	11.6	0.122
37*P*	948	0.36	10.4	1.01	14.7	0.157
36*P*	950	0.27	10.5	1.02	18.5	0.200
16	956	0.22	10.8	1.02	15.8	0.169
17	960	0.21	10.7	1.01	17.8	0.195
28	980	0.05	9.95	0.32	12.8	0.425
32	981	0.17	19.9	0.885	33.7	0.465
30	982	0.15	6.65	1.08	39.5	0.466
27	984	0.30	10.1	0.326	14.4	0.479
29	984	0.10	6.70	1.09	40.9	0.485
31	984	0.20	20.3	0.90	36.0	0.497
19	987	0.22	11.1	0.98	40.6	0.533
20	989	0.22	11.1	0.97	42.1	0.562
21	990	0.23	10.9	0.96	43.1	0.585
24	1010	0.12	9.9	0.306	31.0	1.21
23	1015	0.13	10.0	0.307	34.7	1.39
22	1019	0.11	10.2	0.313	39.3	1.60
26	1019	0.12	10.2	0.311	41.3	1.71
25	1020	0.12	10.1	0.308	40.4	1.68

The investigation of the pyrolysis of benzoyl chloride was carried out in a manner very similar to that of the pyrolysis of benzoyl bromide, and the reader is again referred to a previous paper[4] for all the details of experimental technique. It was shown in this paper[4] that

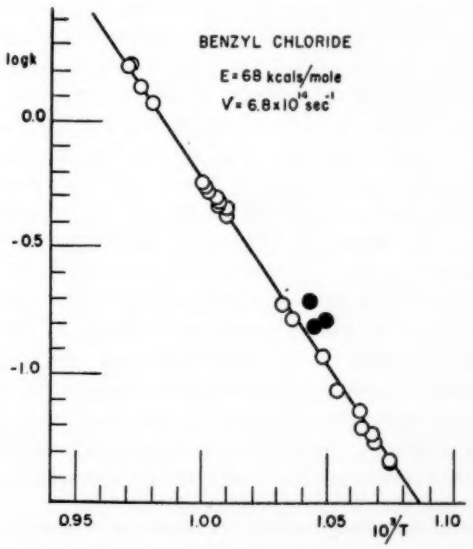

FIG. 1.

TABLE III. Stoichiometry of the decomposition of benzoyl chloride.

Run	CO millimoles	Benzoic acid millimoles	HCl total millimoles	HCl/(CO+*Ph*COOH)
13	0.358	0.308	0.584	0.88
28	0.490	0.094	0.583	1.00
29	0.450	0.264	0.615	0.86
30	0.437	0.443	0.818	0.93

benzoyl bromide decomposes according to Eq. (4).

$$C_6H_5\cdot CO\cdot Br \rightarrow C_6H_5\cdot CO + Br, \quad (4)$$

this reaction being followed by a rapid decomposition of the $C_6H_5\cdot CO$ radical, namely

$$C_6H_5\cdot CO \rightarrow C_6H_5 + CO. \quad (5)$$

Bromine atoms and phenyl radicals abstract hydrogen from toluene, and thus hydrogen bromide and benzene are formed.[7] One can use, therefore, the rate of formation of carbon monoxide, as well as the rate of formation of hydrogen bromide, as a measure of the rate of the initial dissociation (4). Technical reasons, explained fully in reference 4, make the rate of formation of carbon monoxide a more satisfactory measure for the rate of the initial dissociation (4) than the rate of formation of hydrogen bromide. We found that the same reasons applied to our case, and thus we measured the rate of the dissociation reaction

$$C_6H_5\cdot CO\cdot Cl \rightarrow C_6H_5\cdot CO\cdot + Cl \quad (6)$$

by the rate of formation of carbon monoxide [reaction (6) is followed by the rapid reaction (5)].

The correctness of the suggested mechanism for the decomposition of benzoyl bromide was proved in the following way. The number of moles of benzoyl bromide introduced into the reaction vessel is measured directly. If the assumed mechanism is correct, then the number of moles of carbon monoxide formed in the pyrolysis, together with the number of moles of benzoic acid formed by the hydrolysis of the undecomposed benzoyl bromide, should add up to the number of moles of benzoyl bromide introduced initially. The same should be true for the number of moles of hydrogen bromide formed in the pyrolysis and in the hydrolysis of the recovered benzoyl bromide. These stoichiometric equations were fully confirmed by special experiments (see reference 4). We applied the same checking technique in our present work; the results are given in Table III.

All the kinetic data obtained in the study of the pyrolysis of benzoyl chloride are summarized in Table IV. The percentages of decomposition and the first-order rate constants are calculated on the basis of the amount of carbon monoxide produced in the pyrolyses. Inspection of Table IV shows that the magnitude of the first-order rate constants is not affected by changes of partial pressure of benzoyl chloride, of partial pressure of toluene, or of time of contact. The partial pressure of benzoyl chloride was varied by a factor of nine (from 0.03- to 0.28-mm Hg, see e.g., runs 28, 29, 14). The partial pressure of toluene was varied by factor of three (from about 6.7-mm Hg to 21-mm Hg; see, e.g., runs 18, 17). The time of contact was increased from about 0.3 sec to about 1.0 sec. The homogeneity of the reaction was checked by increasing the surface of the reaction vessel by a factor of eight. A minute heterogeneity was observed amounting to about 6 percent of the total reaction (see runs 31*P* and 32*P* denoted by full points on Fig. 2).

The temperature dependence of the rate constants is illustrated in Fig. 2. The activation energy was found to be 73.6 kcal/mole corresponding to a very high frequency factor, namely 2.4×10^{15} sec^{-1}. The slight heterogeneity of this reaction may call for some correction of the activation energy. The maximum correction amounts to 1.3 kcal/mole, leading to an activation energy 74.9 kcal/mole and a frequency factor 12×10^{15} sec^{-1}.

DISCUSSION OF BOND DISSOCIATION ENERGIES

The stoichiometry and kinetics of the pyrolyses of benzyl chloride and of benzoyl chloride indicate that we measure the rates of decomposition of these compounds into radicals and chlorine atoms. The presence of dibenzyl[8] in the products of pyrolysis is particularly

TABLE IV. Benzoyl chloride.

Run	$T°K$	P_{PhCOCl} mm Hg	$P_{Toluene}$ mm Hg	Time of contact (sec)	Percent decomp.	k sec^{-1}
7	971	0.27	10.6	1.00	6.1	0.063
6	975	0.28	10.6	1.00	7.0	0.073
12	975	0.26	10.6	0.99	7.1	0.074
10	975	0.18	21.0	0.89	6.8	0.079
11	977	0.25	10.8	0.99	7.4	0.078
5	991	0.26	10.7	0.97	12.2	0.134
4	992	0.26	10.7	0.97	18.8	0.141
32*P*	995	0.27	10.8	0.98	19.5	0.222
31*P*	995	0.23	10.9	0.98	20.5	0.234
3	1004	0.25	10.6	0.945	19.6	0.231
2	1005	0.26	10.9	0.95	20.1	0.235
9	1008	0.09	10.7	0.98	22.1	0.256
8	1008	0.12	10.9	0.97	22.6	0.264
19	1027	0.14	6.6	1.01	38.3	0.476
21	1027	0.10	9.8	0.31	14.1	0.494
20	1028	0.10	9.9	0.31	14.9	0.526
15	1028	0.27	10.7	0.95	40.4	0.545
18	1029	0.14	6.7	1.02	41.2	0.521
17	1030	0.12	21.0	0.85	38.4	0.571
16	1031	0.12	21.0	0.85	38.1	0.566
14	1032	0.25	10.8	0.955	42.1	0.572
30	1034	0.10	10.9	0.91	43.7	0.633
29	1034	0.10	10.9	0.93	45.0	0.645
28	1036	0.03	11.0	0.94	49.0	0.715
24	1072	0.09	10.1	0.30	48.9	2.27
27	1072	0.10	10.0	0.29	49.3	2.35
25	1073	0.08	10.0	0.29	51.8	2.49
26	1074	0.10	10.1	0.29	50.8	2.43
23	1076	0.09	10.1	0.29	53.7	2.64
22	1080	0.10	10.0	0.29	56.7	2.91

[7] Part of the phenyl radicals recombine with benzyl radicals, present in the system as results of reactions, such as, e.g., reaction (2), and form diphenyl methane.

[8] Dibenzyl isolated from products of pyrolyses of benzoyl chloride is contaminated with diphenylmethane.

significant and demonstrates that the reaction indeed involves radicals. The only disturbing features of these decompositions are the high values of the frequency factors which amount to $10^{14}-10^{15}$ sec^{-1}.[9] Extensive studies of the pyrolyses of organic bromides showed that the frequency factors for reactions of the type

$$R\cdot Br \rightarrow R + Br$$

are of the order 10^{13} sec^{-1} (i.e., $1.10^{13}-5.10^{13}$ sec^{-1}). It is reasonable to expect that the frequency factors for reactions

$$R\cdot Cl \rightarrow R-Cl$$

would be somewhat higher; however, the values actually found seem to be excessively high. It appears that this problem should be left until more experimental data are available.

On the other hand, the activation energies determined in this work agree excellently with the values found in the studies of the corresponding organic bromides. If we assume that the recombination process

$$R + Cl \rightarrow R\cdot Cl$$

does not require any activation energy, then we have to conclude that the observed activation energies correspond to the respective bond dissociation energies, i.e.,

$$D(C_6H_5\cdot CH_2-Cl) = 68 \text{ kcal/mole},$$

and

$$D(C_6H_5\cdot CO\cdot -Cl) = 73.6 \text{ kcal/mole}.$$

Now, the difference between the $R-Cl$ bond dissociation energy and the $R-Br$ bond dissociation energy is given by the difference in the heats of formation of gaseous chlorine and bromine atoms less the difference in the heats of formation of the parent compounds, i.e.,

$$D(R-Cl)-D(R-Br) = \Delta H_f(Cl)-\Delta H_f(Br) + \Delta H_f(R\cdot Br)-\Delta H_f(R\cdot Cl).$$

Fortunately, we have reliable data for the heats of formation of benzoyl bromide and benzoyl chloride.[10] Using these thermochemical data we conclude

$$D(C_6H_5\cdot CO-Cl)-D(C_6H_5\cdot CO-Br) = 16.5 \text{ kcal/mole}.$$

On the other hand, the directly determined values are

$D(C_6H_5\cdot CO-Br) = 57.0$ kcal/mole, (see reference 4)

$D(C_6H_5\cdot CO-Cl) = 73.6$ kcal/mole, (this paper)

and the difference is 16.6 kcal/mole.[11] The agreement is better than expected.

The above calculations can be presented in a slightly modified form. Having values for bond dissociation energies, we may calculate the heats of formation of the respective radicals. For example, the heat of formation of the benzoyl radical is given by the equations

$$\Delta H_f(C_6H_5\cdot CO\cdot) = D(C_6H_5\cdot CO-Br) + \Delta H_f(C_6H_5\cdot CO\cdot Br)-\Delta H_f(Br),$$

$$\Delta H_f(C_6H_5\cdot CO) = D(C_6H_5\cdot CO-Cl) + \Delta H_f(C_6H_5\cdot CO\cdot Cl)-\Delta H_f(Cl).$$

Using the values for the heats of formation of benzoyl bromide and of benzoyl chloride from reference 10, we obtain the following values for the heat of formation of the benzoyl radical:

$\Delta H_f(C_6H_5\cdot CO) = -15.6$ kcal/mole, (see reference 4)

$\Delta H_f(C_6H_5\cdot CO) = -15.7$ kcal/mole.[12] (present paper)

We lack reliable data for the heat of formation of benzyl chloride, and thus we are unable to compare directly the consistency of our data for $D(C_6H_5\cdot CH_2-Cl)$ with the published value for $D(C_6H_5\cdot CH_2-Br)$. However, the review of available thermochemical data indicates that $D(R-Cl)-D(R-Br)$ for various radicals R is of the order 13–16 kcal/mole (see Table V). The directly determined values for $D(C_6H_5\cdot CH_2-Cl)$ and $D(C_6H_5\cdot CH_2-Br)$ are 68 kcal/mole (this paper)[13] and 50.5 kcal/mole (see reference 1). In view of the fact that the pyrolytic technique yields values for bond dissociation energies which are on the whole reliable within ± 2 kcal/mole, the agreement with the data quoted in Table V seems to be satisfactory.

One point deserves some further discussion. The kinetic data and the stoichiometry of the pyrolyses of benzoyl chloride or benzoyl bromide do not permit the distinction between the two possibilities of initial reac-

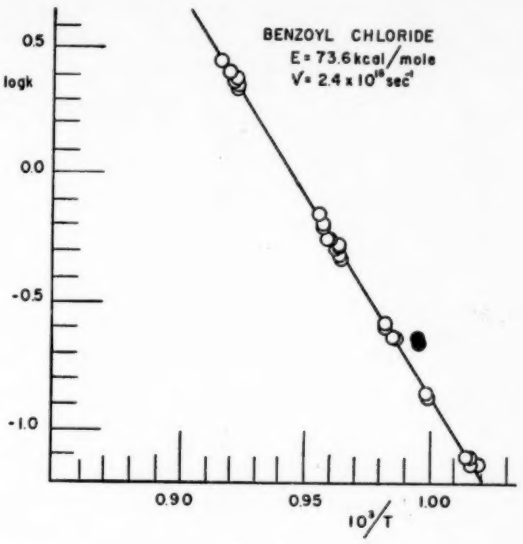

FIG. 2.

[9] Introducing the maximum correction for the activation energies increases the frequency factors to $2,3.10^{15}$ sec^{-1} and 12.10^{15} sec^{-1}, i.e., they are still higher!

[10] Carson, Pritchard, and Skinner, J. Chem. Soc. **1950**, 656.

[11] The maximum correction for the heterogeneity of the reaction raises this value to 17.9 kcal/mole.

[12] On introducing the maximum correction for the heterogeneity of the reaction, we arrive at $\Delta H_f(C_6H_5\cdot CO) = -14.4$ kcal/mole.

[13] On introducing the maximum correction for the activation energy, we arrive at the values $D(C_6H_5\cdot CH_2-Cl) = 70$ kcal/mole.

TABLE V.

R	$D(R-Cl)-D(R-Br)$ kcal/mole	Ref.
CH_3	13.3	8
C_2H_5	14.6	8
t-butyl	13.9	8
phenyl	15.4	9
acetyl	14.7	10
benzoyl	16.5	7

tions, namely (A):

$$C_6H_5\cdot CO\cdot Cl\rightarrow C_6H_5\cdot CO+Cl,$$

followed by the rapid reaction

$$C_6H_5\cdot CO\rightarrow C_6H_5+CO,$$

and (B):

$$C_6H_5\cdot CO\cdot Cl\rightarrow C_6H_5+CO\cdot Cl,$$

followed by the rapid reaction

$$CO\cdot Cl\rightarrow CO+Cl.$$

Such a distinction is possible, however, by comparison of the data obtained from the investigations of the pyrolyses of benzoyl chloride and benzoyl bromide. We have shown that, assuming the first alternative, i.e., the decomposition into a benzoyl radical and a halogen atom, we can derive values for the heat of formation of the benzoyl radical on the basis of either $D(C_6H_5\cdot CO-Cl)$ or $D(C_6H_5\cdot CO-Br)$. Both values agree well. On the other hand, assuming the second alternative, i.e., the decomposition into a phenyl radical and a $CO\cdot Cl$ (or $CO\cdot Br$) radical, it can be shown that

$$D(CO-Cl)-D(CO-Br)=-0.1 \text{ kcal/mole.}^{14}$$

Such a relation is unreasonable, and thus we have to conclude that the decompositions of benzoyl chloride and benzoyl bromide are initiated by the dissociation of these molecules into benzoyl radicals and halogen atoms.

Furthermore, a recent investigation of photosynthesis of phosgene by Burns and Dainton[15] lead these authors to the conclusion that $D(CO-Cl)=6.3$ kcal/mole. From this data we derive the value -3 kcal/mole for the heat of formation of $CO\cdot Cl$ radical, and finally a value of about 96 kcal/mole for the $Ph-CO\cdot Cl$ bond dissociation energy. This value shows that the process

$$Ph\cdot CO\cdot Cl\rightarrow Ph\cdot+CO\cdot Cl.$$

would have much too high an activation energy to account for the observed value for the decomposition of benzoyl chloride and must therefore be regarded as further evidence in favour of the process

$$Ph\cdot CO\cdot Cl\rightarrow PhCO+Cl.$$

[14] This conclusion is derived on the basis of thermochemical equations correlating the values of bond dissociation energies with the heats of formation of radicals. On introducing the correction for heterogeneity of the pyrolysis of benzoyl chloride, we arrive at the value of -2.2 kcal/mole for the difference $D(CO-Cl)-D(CO-Br)$. Such a value is still less plausible.

[15] W. G. Burns and F. S. Dainton, Trans. Faraday Soc. **48**, 39, 52 (1952).

The Near Infrared Spectrum and the Internuclear Distances of Nitrous Oxide*

A. E. Douglas and C. K. Møller†
Division of Physics, National Research Council, Ottawa, Canada
(Received October 16, 1953)

The near infrared spectra of $N_2{}^{14}O^{16}$ and $N^{15}N^{14}O^{16}$ have been investigated using a high-resolution grating spectrometer. The α's and hence the B_e values for both isotopic species have been determined. From the B_e values, the equilibrium N−N and N−O internuclear distances have been found to be 1.126A and 1.186A, respectively.

INTRODUCTION

In spite of the large number of investigations of the spectrum of N_2O, up to the present, accurate internuclear distances have remained unknown. The accurate B_0 values obtained from recent microwave investigations of a number of isotopes of N_2O have been used to calculate internuclear distances, but rather conflicting results have been obtained from different pairs of isotopes.[1] This lack of agreement is caused by the zero-point vibrations of the molecules. In order to calculate the correct equilibrium internuclear distances, it is necessary to obtain the B values of the vibrationless equilibrium states for at least two isotopic species. These B_e values can be obtained from an extrapolation of the rotational constants of the higher vibrational levels to the equilibrium state. Work along this line has already been done on $N_2{}^{14}O$ in the photographic infrared by Herzberg and Herzberg.[2] The present work has extended the investigation of $N_2{}^{14}O$ by analyzing a number of bands in the region from 4000 to 4700 cm^{-1}. In addition, a number of bands of $N^{15}N^{14}O^{16}$ in the same region have been measured. These investigations have provided sufficient information to allow us to determine B_e values for both isotopic molecules and hence to determine the equilibrium internuclear distances. The measurements have also provided additional information regarding the vibrational constants of the molecules.

EXPERIMENTAL

A mixture of 37-percent $N_2{}^{14}O^{16}$ and 63-percent $N^{15}N^{14}O^{16}$ was prepared by pyrolysis of Eastman ammonium nitrate in which the $N^{15}H_4N^{14}O_3{}^{16}$ content was 63 percent. According to Richardson and Wilson[3] (see also Friedman and Bigeleisen),[4] the pyrolysis of this isotope of ammonium nitrate yields only nitrous oxide with the heavy nitrogen in the end position. About $\frac{1}{2}$ liter of the gas was prepared and was examined in an absorption tube of 60 cm length and one-liter volume.

The spectrum of the gas was recorded with a grating spectrometer which has been described by Douglas and Sharma.[5] The technique for measuring the wavelengths of the lines was the same as that described in their paper, with high-order mercury lines and Fabry-Perot fringes being used as wavelength standards. All spectra were recorded at least twice, first with a 7000 and then with a 15 000 lines-per-inch grating in the spectrometer. The observed limit of resolution was about 0.12 cm^{-1}. The uncertainty in measurement of the relative positions of the lines in a band is believed to be not larger than 0.02 cm^{-1} for unblended lines. The uncertainty on the absolute wave number determination is larger but presumably not above 0.10 cm^{-1}.

The rotational structure of the $2\nu_3$, $2\nu_1+\nu_3$, $\nu_1+2\nu_2+\nu_3$, $2\nu_3+\nu_2-\nu_2$, and the $2\nu_1+\nu_3+\nu_2-\nu_2$ bands (following Herzberg's nomenclature[6]) have been measured both for the $N_2{}^{14}O^{16}$ and the $N^{15}N^{14}O^{16}$ molecules. In addition, the $4\nu_2+\nu_3$ and $\nu_1+\nu_2+\nu_3$ bands of $N_2{}^{14}O^{16}$ have been measured, using an 8-m absorption path and $\frac{1}{3}$-atm pressure. The wave numbers of the lines of the bands are given in Tables I and II.

ANALYSIS

The B values of both the upper and lower states of the bands can be obtained from the combination differences $\Delta_2F(J)$. In order to test the accuracy of the present work, the ground-state constants B_0 and D_0 were determined from the mean ground-state combination differences. Since the $4\nu_2+\nu_3$ band is quite weak and the lines of the R branch of the $2\nu_1+\nu_3$ bands appear to be slightly systematically shifted by the overlapping lines of the hot band, these bands have been omitted in the determination of the mean combination differences. For $N_2{}^{14}O$ the values obtained are $B_0=0.41898\pm0.00005$ cm^{-1} and $D_0=(0.18\pm0.02)\times10^{-6}$ cm^{-1}. These results agree well with the microwave values of $B_0=0.419014$ cm^{-1} and $D_0=0.19\times10^{-6}$ cm^{-1} (using the velocity of light $c=299790$). For $N^{15}N^{14}O^{16}$ our data give $B_0=0.40493\pm0.00010$ cm^{-1} and $D_0=(0.15\pm0.03)\times10^{-6}$ cm^{-1}, again in agreement with the microwave value of $B_0=0.404860$ cm^{-1} and the calculated value of $D_0=0.16\times10^{-6}$ cm^{-1}.

Though the B values of the bands may be obtained

* Contribution from the National Research Council of Canada.
† National Research Laboratories Postdoctorate Fellow.
[1] (a) Coles, Elyash, and Gorman, Phys. Rev. **72**, 973 (1947). (b) D. K. Coles and R. H. Hughes, Phys. Rev. **76**, 178 (1949). (c) S. J. Tetenbaum, Phys. Rev. **88**, 772 (1952).
[2] G. Herzberg and L. Herzberg, J. Chem. Phys. **18**, 1551 (1950).
[3] W. S. Richardson and E. Bright Wilson, Jr., J. Chem. Phys. **18**, 694 (1950).
[4] L. Friedman and J. Bigeleisen, J. Chem. Phys. **18**, 1325 (1950).
[5] A. E. Douglas and D. Sharma, J. Chem. Phys. **21**, 448 (1953).
[6] G. Herzberg, *Infrared and Raman Spectra* (D. Van Nostrand Company, Inc., New York, 1947).

from the combination differences, more accurate upper-state B values can be found by determining the difference $B'-B''$ from the combination sums and accepting the accurate microwave values of B''. A plot of $R(J-1)+P(J)$ plotted against J^2 will (neglecting a small term in $D'-D''$) give a line with a slope of $2(B'-B'')$ and an intercept of $2\nu_0$ (reference 6, page 391). In this way the upper state B values of all bands originating in the ground state were determined. For the hot bands the B values were determined from the combination differences $\Delta_2F(J)$. The B values and the positions of the band origins determined in this work are given in Table III.

The B values of a linear triatomic molecule such as N_2O are given by

$$B_{v_1v_2v_3}=B_e-\alpha_1(v_1+\tfrac{1}{2})-\alpha_2(v_2+1)-\alpha_3(v_3+\tfrac{1}{2}). \quad (1)$$

From this expression it follows that the difference between the upper- and lower-state B values $(B'-B'')$ of any band depends upon the values of the α's and the vibrational numbering of the band. Conversely, the α values can be determined from the differences $B'-B''$ of suitable bands. As discussed above, these differences in B values can be obtained accurately from the observed bands.

Equation (1) shows that $B_e=B_{000}+\frac{1}{2}(\alpha_1+2\alpha_2+\alpha_3)$. Hence, to determine B_e from the accurately known B_{000}, we require the sum $\alpha_1+2\alpha_2+\alpha_3$ rather than the individual α values. It also follows from Eq. (1) that the difference $B'-B''$ for the $\nu_1+2\nu_2+\nu_3$ band is just this sum $\alpha_1+2\alpha_2+\alpha_3$. Thus, insofar as Eq. (1) is valid, the simplest and most accurate way of determining B_e is to combine the sum $\alpha_1+2\alpha_2+\alpha_3$ found from the $\nu_1+2\nu_2+\nu_3$ band with the accurate microwave values of B_{000}. The values of B_e given in Table IV have been determined in this way. The remaining bands have been used to calculate the individual α values.

Only one band showing a Q branch was measured, namely the $\nu_1+\nu_2+\nu_3$ band of $N_2{}^{14}O^{16}$. This band corresponds to a $\Pi-\Sigma$ transition. As is well known, the molecular rotation splits the degeneracy of the Π level giving rise to the so-called l-type doubling. There are thus two effective B values for the Π level; the values

TABLE I. Wave numbers of the lines of $N_2{}^{14}O^{16}$ bands. (ν_{vac}, cm^{-1}).

	$2\nu_1+\nu_3$ $\nu_0=4730.86$		$2\nu_1+\nu_2+\nu_3-\nu_2$ $\nu_0=4730.46$		$\nu_1+2\nu_2+\nu_3$ $\nu_0=4630.31$		$4\nu_2+\nu_3$ $\nu_0=4491.65$	
J	$R(J)$	$P(J)$	$R(J)$	$P(J)$	$R(J)$	$P(J)$	$R(J)$	$P(J)$
0	4731.70							
1	32.50	4730.02						
2	33.28	29.17			4632.76	4628.61		
3	34.07	28.31			33.58	27.74	4494.90	
4	34.85	27.45	4734.42		34.35	26.86	95.77	4488.24
5	35.60	26.54	35.20	4726.14	35.14	25.98	96.62	87.38
6	36.34	25.64	35.94	25.22	35.91	25.12	97.43	86.60
7	37.07	24.73		24.31	36.68	24.27	98.20	85.73
8	37.78	23.78		23.38	37.44	23.35	99.03	84.86
9	38.49	22.83	38.10	22.44	38.18	22.44	4499.83	84.00
10	39.17	21.87		21.47	38.94	21.53	4500.63	83.11
11	39.85	20.89		20.48	39.67	20.60	01.45	82.24
12	40.49	19.89		19.49	40.42	19.67	02.22	81.37
13	41.13	18.90		18.49	41.10	18.71	02.99	80.48
14	41.77	17.88		17.51	41.81	17.79	03.79	79.63
15	42.39	16.85		16.48	42.51	16.82	04.56	78.74
16	42.99	15.81		15.43	43.19	15.85	05.35	77.83
17	43.58	14.76		14.38	43.86	14.86	06.13	76.93
18	44.14	13.70		13.34	44.55	13.88	06.88	76.04
19	44.70	12.60		12.28	45.23	12.90	07.64	75.16
20	45.26	11.51		11.18	45.88	11.90	08.40	74.23
21	45.78	10.41		10.10	46.53	10.88	09.13	73.29
22	46.32	09.27		08.92	47.16	09.86	09.91	72.39
23	46.85	08.12			47.79	08.84	10.67	71.47
24	47.32	06.97			48.41	07.82	11.37	70.55
25	47.74	05.80			49.02	06.77	12.12	69.59
26	48.26	04.59			49.65	05.70	12.88	68.71
27	48.70	03.43			50.22	04.63	13.60	67.75
28	49.15	02.24			50.80	03.57	14.30	66.82
29	49.58	4700.98			51.38	02.48	15.00	
30	49.99	4699.79			51.94	01.43	15.73	
31	50.38	98.50			52.48	4600.34		
32	50.77	97.26			53.05	4599.19		
33	51.14	95.99			53.59	98.09		
34	51.49	94.69			54.10	96.95		
35	51.84	93.23			54.62	95.82		
36	52.15	92.08			55.12	94.66		
37	52.47	90.76			55.66	93.55		
38	52.77	89.40			56.11	92.40		
39	53.06	88.07			56.63	91.20		
40	53.34	86.68			57.04			

TABLE I—*Continued.*

	$2\nu_3$ $\nu_0=4417.51$		$\nu_2+2\nu_3-\nu_2$ $\nu_0=4389.06$		$\nu_1+\nu_2+\nu_3$ $\nu_0=4062.09$		
J	$R(J)$	$P(J)$	$R(J)$	$P(J)$	$R(J)$	$Q(J)$	$P(J)$
0	4418.34				4062.93		
1	19.15	4416.68			63.72		
2	19.96	15.81			64.55		
3	20.73	14.96			65.33		
4	21.50	14.07	4393.04	4385.61	66.13		4058.77[a]
5	22.25	13.18		84.80	66.89		57.79[a]
6	23.00	12.28		83.84[a]	67.67		56.95[a]
7	23.72	11.35	95.27	82.88	68.43		56.03[a]
8	24.44	10.42	95.88[a]	81.93	69.18		55.10[a]
9	25.14	09.47	96.70	81.00	69.92		54.19[a]
10	25.82	08.51	97.36	79.99[a]	70.65		53.27
11	26.49	07.52	98.09[a]	79.05	71.37		52.34
12	27.15	06.54	98.70	78.07	72.06		51.38
13	27.79	05.55	99.22[a]	77.08	72.77		50.43
14	28.42	04.52	4399.99	76.00	73.45		49.45
15	29.03	03.49	4400.57	75.03	74.13	4061.12	48.48
16	29.64	02.44	01.34[a]	73.99	74.81	60.98	47.49
17	30.22	01.38	01.80	72.92	75.45	60.86	46.50
18	30.81	4400.31	02.42[a]	71.84[a]	76.12	60.70	45.49
19	31.37	4399.24	02.95	70.76	76.76	60.54	44.46
20	31.91	98.12	03.47[a]	69.62	77.38	60.39	43.46
21	32.45	97.01	04.03	68.52	78.01	60.20	42.41
22	32.97	95.90	04.51[a]	67.43	78.61	60.02	41.37
23	33.48	94.75	05.10		79.19	59.83	40.31
24	33.97	93.58	05.53[a]		79.79	59.63	39.24
25	34.43	92.46	06.04		80.38	59.46	38.17
26	34.90	91.27	06.52[a]		80.93	59.24	37.09
27	35.34	90.05	06.95		81.50	59.01	36.00
28	35.79	88.83	07.49[a]		82.05	58.77[a]	34.89
29	36.21	87.60	07.84		82.58	58.55[a]	33.76
30	36.62	86.39			83.11	58.29	32.65
31	37.01	85.14			83.64	58.04	31.52
32	37.39	83.87			84.15	57.79[a]	30.37
33	37.76	82.58			84.64	57.53	29.22
34	38.11	81.30			85.13	57.25	28.04
35	38.44	80.01			85.62	56.95[a]	26.88
36	38.77	78.68			86.08	56.66	25.70
37	39.08	77.35			86.52	56.36[a]	24.50
38		76.02			86.98	56.03[a]	23.27
39		74.63			87.43	55.75	22.07
40		73.29			87.85	55.42	20.85

[a] Blended lines.

differing by a constant q. One of the B values (B_d) can be determined from the Q branch and the other (B_c) from the P and R branches. The numbering of the P and R lines of the $\nu_1+\nu_2+\nu_3$ band is straightforward. Because the Q branch cannot be resolved close to the origin, it is more difficult to find the correct numbering here. By trying different numberings and plotting $Q(J-1)+Q(J)=2\nu_0+2(B'-B'')J^2$ against J^2, it was found that a straight line passing through $2\nu_0$ (already known from the P and R branches) was obtained for only one numbering. The Q branch thus numbered was then used to determine one of the effective B values of the Π state. It was found from the Q branch that $B_d=0.41489$ and from the P and R branches that $B_c=0.41403$ cm^{-1}. The difference between these two B values gives the l-type doubling constant for the 111 vibrational level:

$$q_{111}=0.86\times10^{-3}\text{ cm}^{-1}.$$

The band origins in this work may be used to calculate some of the vibrational constants of N_2O. It has been found by Herzberg and Herzberg[2] that Fermi resonances make it impossible to represent the bands satisfactorily by any set of vibrational constants. Because of this difficulty, we have not attempted to determine a set of vibrational constants, from our limited data. The vibrational constant x_{23}, however, should not be effected by Fermi resonances and may be determined from the wave number differences between the $2\nu_3$ and the $2\nu_3+\nu_2-\nu_2$ bands. It was found that $x_{23}=-14.2$ cm^{-1} for both $N^{15}N^{14}O$ and $N_2{}^{14}O$. This value is identical with that determined by Herzberg and Herzberg[2] from bands in the photographic infrared region.

DISCUSSION

From the values of B_e for the two isotopic molecules, we can obtain the moments of inertia and hence the equilibrium internuclear distances. The B_e values given in Table IV, and the fundamental constants of DuMond and Cohen[7] have been used in this calculation. The

[7] J. W. M. DuMond and E. R. Cohen, Phys. Rev. **82**, 555 (1951).

TABLE II. Wave numbers of lines of $N^{15}N^{14}O^{16}$ bands. (ν_{vac}, cm^{-1}).

	$2\nu_1+\nu_3$ $\nu_0=4679.98$		$2\nu_1+\nu_2+\nu_3-\nu_2$ $\nu_0=4680.55$		$\nu_1+2\nu_2+\nu_3$ $\nu_0=4585.79$		$2\nu_3$ $\nu_0=4373.73$		$\nu_3+2\nu_2-\nu_2$ $\nu_0=4345.34$	
J	$R(J)$	$P(J)$	$R(J)$	$P(J)$	$R(J)$	$P(J)$	$R(J)$	$P(J)$	$R(J)$	$P(J)$
0	4680.80						4374.61			
1	81.57	4679.17			4587.37	4584.45	75.30			
2	82.33	78.34			88.16	83.73	76.03	4371.87		
3	83.08	77.51			88.92	83.31	76.84	71.27		
4	83.84	76.67			89.64	82.54	77.57	70.43		
5	84.57	75.81			90.48	81.64	78.31	69.57	4349.97	
6	85.29	74.94			91.22	80.80	79.03	68.66	50.63[a]	
7	86.00	74.05			91.97	79.94	79.74	67.78	51.36	4339.40
8	86.69	73.15			92.68	79.09	80.41[a]	66.88	52.05	38.47
9	87.36	72.24			93.44	78.20	81.09	65.97	52.83[a]	
10	88.04	71.32			94.16[a]	77.31	81.75[a]	65.03	53.37	36.59
11	88.70	70.39		4670.93	94.85	76.43	82.40[a]	64.07		35.70
12	89.34	69.43		70.00	95.57[a]	75.52	83.03	63.11	54.68	34.88[a]
13	89.96	68.47		69.01	96.26	74.61	83.67	62.16	55.30	33.76
14	90.59	67.50		68.06	96.95[a]	73.69	84.25[a]	61.18		32.76
15	91.19	66.51		67.05	97.64	72.76	84.86	60.19	56.53	31.76
16	91.76	65.51		66.04	98.27	71.84	85.43[a]	59.17	57.13[a]	
17	92.34	64.49		65.02	98.95	70.88	85.99	58.14	57.68	
18	92.89	63.46		63.96	4599.61[a]	69.94	86.55	57.11	58.16[a]	
19	93.44	62.43		62.95	4600.26	68.99	87.10	56.05	58.74	
20	93.99	61.36		61.90	00.88[a]	68.03	87.62[a]	54.99		
21	94.52[a]	60.30		60.81	01.50	67.04	88.14	53.93	59.80	
22	95.03[a]	59.23		59.74	02.14[a]	66.06	88.64[a]	52.81		
23	95.54	58.14			02.73	65.08	89.12	51.74	60.83	
24	96.01[a]	57.02			03.34[a]	64.07	89.60	50.61		
25	96.49	55.90			03.92	63.07	90.05[a]	49.47	61.73	
26	96.95[a]	54.78			04.51[a]	62.05	90.51	48.31		
27	97.39[a]	53.64			05.07	61.02	90.94	47.18		
28	97.84	52.50			05.66[a]	59.99	91.28[a]	46.00		
29	98.27[a]	51.33[a]			06.20	58.94	91.78	44.81		
30	98.65[a]	50.15			06.78[a]	57.91	92.15	43.61		
31	99.07	48.96[a]			07.31	56.84	92.45[a]	42.38		
32	99.45	47.76[a]			07.83[a]	55.77	92.90	41.17		
33	4699.80[a]	46.53[a]			08.37	54.70	93.25	39.94		
34	4700.20	45.29			08.85[a]	53.61	93.60[a]	38.68		
35	00.55	44.04[a]			09.34	52.50	93.90	37.43		
36	00.91[a]	42.80[a]			09.85	51.40	94.21	36.13		
37	01.19	41.45[a]				50.31	94.51	34.83[a]		
38	01.49	40.27[a]				49.17	94.77	33.54		
39	01.80	38.97[a]				48.05	95.05	32.22		
40	02.22[a]	37.67[a]					95.30	30.80		

[a] Blended lines.

numerical equations giving the internuclear distances in Angstrom units are:

$$15.8490r^2_{N-N}+16.9013r_{N-N}r_{N-O}+16.9013r^2_{N-O}=(66.4394\pm0.0030)$$

$$16.6013r^2_{N-N}+17.7036r_{N-N}r_{N-O}+17.1152r^2_{N-O}=(68.7651\pm0.0040).$$

TABLE III. Band origins and rotational constants. (ν_{vac}, cm^{-1}).

Band	$N_2{}^{14}O^{16}$ ν_0	$N_2{}^{14}O^{16}$ $B'_{v_1v_2v_3}$	$N^{15}N^{14}O^{16}$ ν_0	$N^{15}N^{14}O^{16}$ $B'_{v_1v_2v_3}$
$\nu_1+\nu_2+\nu_3$	4062.09	0.41446		
$2\nu_3$	4417.51	0.41210_8	4373.73	0.39814_0
$4\nu_2+\nu_3$	4491.65	0.41724_1		
$\nu_1+2\nu_2+\nu_3$	4630.31	0.41468_1	4585.78	0.40070_9
$2\nu_1+\nu_3$	4730.86	0.41213_0	4679.98	0.39842_4
$2\nu_3+\nu_2-\nu_2$[a]	4389.06	0.412_4	4345.34	0.399_7
$2\nu_1+\nu_3+\nu_2-\nu_2$[b]	4730.46	0.412_6	4680.55	

[a] For the $2\nu_3+\nu_2-\nu_2$ bands of $N_2{}^{14}O^{16}$ and $N^{15}N^{14}O^{16}$, the values of B'' are 0.419_8 and 0.406_3, respectively.
[b] For the $2\nu_1+\nu_3+\nu_2-\nu_2$ band of $N_2{}^{14}O^{16}$, the value of B'' is 0.418_9.

Solving these equations gives

$$r_{N-N}=1.1257\pm0.0020\text{A}, \quad r_{N-O}=1.1863\pm0.0020\text{A}.$$

The large errors in the individual internuclear distances can be attributed to the fact that the coefficients of the two simultaneous equations giving the distances are quite similar. For any given value of one of the internuclear distances, the above equations fix the other with an error of much less than 0.001A.

It has been pointed out by Herzberg and Herzberg[2] that the B values of N_2O cannot be accurately represented by Eq. (1) because of Fermi resonance and possibly other types of interaction. One may then question whether the experimental accuracy in determining an apparent sum $\alpha_1+2\alpha_2+\alpha_3$ from the $\nu_1+2\nu_2+\nu_3$ band does indeed lead to an accurate value of B_e. It is certainly true that the $\nu_1+2\nu_2+\nu_3$ band is a member of the Fermi triad $2\nu_1+\nu_3$, $\nu_1+2\nu_2+\nu_3$ and $4\nu_2+\nu_3$, and probably gains some of its intensity from

TABLE IV. Rotational constants and rotation-vibration interaction constants.[a]

	$N_2^{14}O^{16}$			$N^{15}N^{14}O^{16}$	
	Microwave[b]	Herzberg and Herzberg[c]	This invest.	Microwave[b]	This invest.
B_{000}	0.419014 cm^{-1}	0.4191_{25} cm^{-1}	0.41898 cm^{-1}	0.404860 cm^{-1}	0.4049_3 cm^{-1}
D_{000}	0.19×10^{-6} cm^{-1}	0.19×10^{-6} cm^{-1}	0.18×10^{-6} cm^{-1}		0.15×10^{-6} cm^{-1}
α_1		$1.7_0\times10^{-3}$ cm^{-1}	1.72×10^{-3} cm^{-1}		1.54×10^{-3} cm^{-1}
α_2		$-0.2_2\times10^{-3}$ cm^{-1}	-0.42×10^{-3} cm^{-1}		-0.37×10^{-3} cm^{-1}
α_3		$3.3_9\times10^{-3}$ cm^{-1}	3.45×10^{-3} cm^{-1}		3.36×10^{-3} cm^{-1}
$\alpha_1+2\alpha_2+\alpha_3$		$4.6_5\times10^{-3}$ cm^{-1}	$4.33_3\times10^{-3}$ cm^{-1}		$4.15_1\times10^{-3}$ cm^{-1}
B_e		0.4214_5 cm^{-1}	0.42118_1[d] cm^{-1}		0.40693_6[d] cm^{-1}
I_e			$66.439_4\times10^{-40}$ g/cm^2		$68.765_1\times10^{-40}$ g/cm^2

[a] The last figure is printed in full size when the accuracy is well within one unit of the next to the last figure. If the accuracy is less, the last figure is a subscript.
[b] See reference 1.
[c] See reference 2.
[d] B_e has been calculated from the microwave B_0 and $\alpha_1+2\alpha_2+\alpha_3$.

the $2\nu_1+\nu_3$ band by this Fermi interaction. However, for $N_2{}^{14}O$ all three members of this triad have been measured and according to theory the value of $(B_{201}+B_{121}+B_{041})-3B_{000}=3(\alpha_1+2\alpha_2+\alpha_3)$ should not be perturbed. Our experimental value of $\alpha_1+2\alpha_2+\alpha_3$ determined from the complete triad agrees with that determined from the $\nu_1+2\nu_2+\nu_3$ band. This observation might perhaps have been predicted since the $\nu_1+2\nu_2+\nu_3$ band is the central member of a triad for which the perturbations in the B value should be less than for the other two members. Similarly, we should expect the sum $\alpha_1+2\alpha_2+\alpha_3$ for $N^{15}N^{14}O^{16}$ determined from the $\nu_1+2\nu_2+\nu_3$ band to be relatively free from Fermi perturbations. Therefore, though a detailed analysis of many bands would be necessary to make it absolutely certain that the α values given here are not influenced by some type of interaction which invalidates Eq. (1), the results appear to be quite reliable.

For the $\nu_1+\nu_2+\nu_3$ band, the mean value of the B' from the two component sets of levels is 0.41446 cm^{-1} while the value calculated from the B_{000} and the α values given in Table IV is 0.41425 cm^{-1}. This difference of 0.00021 seems to be beyond the experimental error and is probably caused by Fermi interaction of the $\nu_1+\nu_2+\nu_3$ level with the $3\nu_2+\nu_3$ level. Certainly the $3\nu_2+\nu_3$ and the $\nu_1+\nu_2+\nu_3$ levels lie close together and a Fermi type interaction is to be expected. The calculated B value of the $3\nu_2+\nu_3$ level is higher than that of the $\nu_1+\nu_2+\nu_3$ level and an interaction between the two could be the cause of the observed high B value of the latter.

According to Nielsen,[8] the q value of the ν_2 level is given approximately by the expression

$$q_{010}=\frac{2B_e^2}{\omega_2}\left(1+\frac{4\omega_2^2}{\omega_3^2-\omega_2^2}\right).$$

Using $B_e=0.421$ cm^{-1}, $\omega_2=596$ cm^{-1} and $\omega_3=2276$ cm^{-1}, this equation gives $q_{010}=0.77\times10^{-3}$ cm^{-1}. This value is in fair agreement with the observed value of $q_{111}=0.86\times10^{-3}$ cm^{-1}.

The values of α_1 and α_3 determined in this work agree quite well with those given in reference 2, but for α_2 the agreement is not good. There may be several reasons for this discrepancy, e.g., the Fermi resonance has been neglected in both cases and although this does not affect $\alpha_1+2\alpha_2+\alpha_3$ seriously, it may affect the separate α_i values, in particular α_1 and α_2. Furthermore, Herzberg and Herzberg base their α_2 value on measurements of bands with rather high quantum numbers v_1 and v_3, and, considering that α_2 is small compared to α_1 and α_3, it may very well be that the neglect of higher power terms in v_1 and v_2 in Eq. (1) may cause a relatively large error in α_2. It is, however, interesting to note that Herzberg and Herzberg's measurements of the $2\nu_1+4\nu_2+2\nu_3$ band give $\alpha_1+2\alpha_2+\alpha_3=0.00439$ cm^{-1} in fair agreement with the value determined here from the $\nu_1+2\nu_2+\nu_3$ band: 0.00433 cm^{-1}. It appears that the true value of α_2 could best be determined by a microwave measurement of the B value of the 010 level.‡

We wish to thank Dr. G. Herzberg for much helpful advice during the course of this work.

[8] H. H. Nielsen, Phys. Rev. **77**, 130 (1950).

‡ *Note added in proof.*—While this present paper was in press, a paper by H. W. Thompson and R. L. Williams (Proc. Roy. Soc. (London) **A220**, 435, 1953) appeared giving two values of α_2; -0.00026 and -0.00042 cm^{-1}. Their value of -0.00026 is not correct, since it is derived from the P and R branches only of a perpendicular band, and the l-type doubling has been neglected. If, however, their value of $\alpha_2=-0.00026$ is corrected by using $q=0.00086$, then one obtains $\alpha_2=-0.00069$ cm^{-1}.

The Librational Heat Capacity of Ice and of Heavy Ice[1]

R. W. BLUE
Phillips Petroleum Company, Research Division, Bartlesville, Oklahoma
(Received May 14, 1953)

Interpretation of the heat capacities of crystals is difficult when polyatomic molecules or ions are involved, owing to the variation with temperature of the translational heat capacity, arising from intermolecular vibrations, in the same regions in which rotational and vibrational heat capacities are also varying with temperature. It is shown how translational and rotational heat capacities may be studied separately in the case of ice where the heat capacities of both H_2O and D_2O have been measured. Moments of inertia are nearly doubled by substitution of D for H, while the molecular weight is increased by only ten percent. Thus the effect of isotopic substitution is relatively large on the rotational heat capacity as compared to the translational heat capacity.

AN important deterrent to interpretation of heat capacity of polyatomic crystals is that effects arising from molecular translation (intermolecular vibration) are much more obtrusive than in gases where the translational heat capacity is fully excited and constant above a very low temperature. In crystals the translational heat capacity appears to merge into the heat capacity of other forms of motion to the extent that rotational and vibrational effects cannot be distinguished.

The purpose of the present paper is to show how rotational and translational heat capacities can be studied separately in the case of ice where the heat capacities of both H_2O and D_2O have been measured. In a subsequent paper the same method will be applied to NH_4Cl and ND_4Cl. In both cases advantage is taken of the fact that moments of inertia are nearly doubled by substitution of D for H while the molecular and ionic weights are only slightly increased. The analysis leads to an approximate value for the librational frequency in each case in the temperature range below the transition region or, in the case of ice, below the melting region, i.e., the region in which forces restraining rotation are weakened.

By separating the rotational or librational heat capacity, one can also obtain a better understanding of translational effects in these relatively complicated crystals.

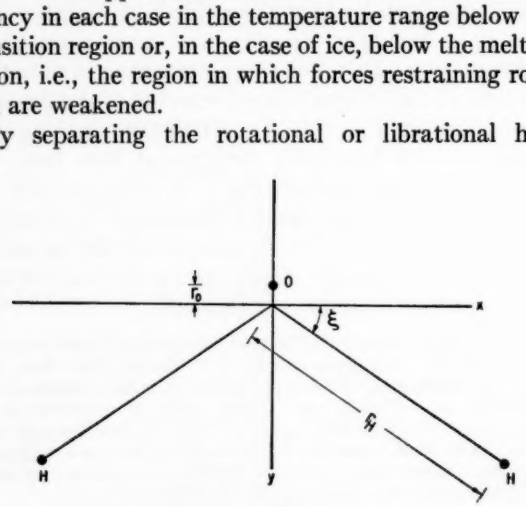

FIG. 1. The water molecule.

Lord, Ahlberg, and Andrews[2] have calculated the heat capacity of deutero benzene from that of benzene using the Debye formula for both librational and translational heat capacities. They were primarily interested in intramolecular vibrations, however, and did not seek the precision which we hope to attain in calculation of the librational frequencies.

LIBRATIONAL MOTION OF H_2O MOLECULES IN THE ICE CRYSTAL

As a first approximation, it is assumed that the motion of H_2O molecules in ice may be resolved into the following independent vibrations: (a) The translational vibration of the centers of gravity about the equilibrium positions; (b) the rotational oscillation or libration of the rigid molecules; and (c) the internal vibrations of the constituent nuclei of the molecules. It is further assumed that all librational frequencies are equal not only for each molecule, but for all molecules. As will be shown, these assumptions are only partially correct, but they are sufficiently good to serve as a starting point for analysis of the heat capacities and, superficially at least, are surprisingly close to the conditions existing in the crystal.

In the Pauling[3] model of ice, the H_2O molecules retain their identity and are not ionized; they are held together in an open structure largely by hydrogen bonds between the oxygen of each molecule and the hydrogens of two neighboring molecules. The water-vapor molecule may be incorporated into the tetrahedral arrangement of oxygens without appreciable distortion, and the hydrogens lie very nearly on the lines connecting the center of gravity of one molecule with the oxygens of two neighboring molecules. Thus, the rotational motion of the molecule results (at low amplitude) in motion of hydrogen perpendicular to the O—H line, and the motion is very similar to that of two pendulums moving in phase.

[1] Some of the material in this paper was presented at the Rochester Meeting of the American Chemical Society, April, 1938. Most of the calculations described in this paper were carried out while the author was a member of the staff of the Department of Chemistry, Massachusetts Institute of Technology, Cambridge, Massachusetts.

[2] Lord, Ahlberg, and Andrews, J. Chem. Phys. **5**, 649 (1937).
[3] Linus Pauling, J. Am. Chem. Soc. **57**, 2681 (1935).

For the sake of comparison of libration frequencies in ice and heavy ice three modes of libration may be considered involving rotational motion around each of the principal axes of inertia. Expressions for frequencies will then have the form:

$$\nu_x=\frac{1}{2\pi}\left\{\frac{k_H r_H^2 \sin^2\xi+\frac{1}{2}k_0 r_0^2}{I_A}\right\}^{\frac{1}{2}},$$

$$\nu_y=\frac{1}{2\pi}\left\{\frac{k_H r_H^2 \cos^2\xi}{I_B}\right\}^{\frac{1}{2}},$$

$$\nu_z=\frac{1}{2\pi}\left\{\frac{k_H r_H^2+\frac{1}{2}k_0 r_0^2}{I_C}\right\}^{\frac{1}{2}}.$$

Where k_H is a force constant such that for a rotational displacement through the angle, α, around the C axis, the restoring force on each hydrogen is $k_H r_H \alpha$.

k_0 is a corresponding force constant for oxygen displacements.

I_A, I_B, and I_C, are the principal moments of inertia of the H_2O molecule, and the other symbols have the significance indicated in Fig. 1.

In order to estimate the librational frequencies, it is necessary to make some assumptions about the origin of restoring forces. One might assume, for example, that all the restoring forces arise from stretching of hydrogen bonds, and that the hydrogen bond force constant is the same in both ice and heavy ice; or one might assume that restoring forces are proportional to displacements from the equilibrium positions and that the same force constants apply to oxygen displacements as to hydrogen displacements. Either set of assumptions leads to frequency expressions such that the average librational frequency for heavy ice is $2^{-\frac{1}{2}}$ times that for ordinary ice. A simpler assumption is that the numerators will be roughly equal for ice and heavy ice. The corresponding frequencies would then be inversely proportional to the square roots of the moments of inertia. This assumption has been used in the following discussion.

On this basis, and neglecting interactions between librators, the librational frequencies differ among themselves by less than 10 percent for ice and less than 20 percent for heavy ice. Thus, the librational heat capacity may be represented to a good approximation by an Einstein function for three degrees of freedom with a single value of θ_1. Similarly, the librational heat capacity of heavy ice may be represented by an Einstein function with a single value for θ_2 such that $(\theta_1/\theta_2)=(I_2/I_1)^{\frac{1}{2}}$ where I_1 is the average of the three moments of inertia of H_2O, $(I_A+I_B+I_C)/3$, and I_2 is the average of the three moments of inertia of D_2O.

This relationship provides a simple method of estimating the difference between the librational heat capacity of ice and that of heavy ice as may be seen by referring to Fig. 2. Here the librational heat capacity in units of $3R$ is plotted against $\log\theta_1/T$ so that the curve for heavy ice can be obtained from that for ice simply by moving the curve parallel to the axis of abscissas by $\frac{1}{2}\log 2$. (In the case of ice, the displacement along the $\log\theta/T$ axis is only $\frac{1}{2}\log 1.9$, since the moments of inertia[4] of D_2O are on the average 1.908 times as great as those of H_2O.) The difference between the two curves may be calculated readily using a table of values of the Einstein function,[5] and the difference is shown also in Fig. 2 plotted *vs* $\log\theta/T$.

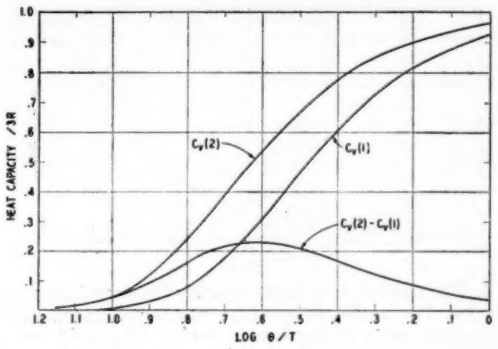

FIG. 2. The Einstein heat capacity function for two librators, characteristic temperatures for which differ by the square root of 2. The difference between the two curves is also shown.

The observed difference between the C_p's of ice[6] and heavy ice[4] may be compared with the difference calculated by the method of the preceding paragraph using $\theta_1=945°$ ($\nu=660$ cm^{-1}) without any corrrection for translational or vibrational (intra molecular) heat capacities, or for C_p-C_v. Since the isotope effect on these quantities is relatively slight as compared with the effect of librational heat capacities, a fair comparison with experimental data may be made without taking translation, vibration, and (C_p-C_v) into account.

In the region from 100° to 200°K the agreement with the Einstein function with a single θ is quite satisfactory (average deviation, 3 percent of the difference in heat capacity), since only one parameter, namely θ_1, was chosen in obtaining a fit with the data. The departure of observed points from the curve below 100°K may be attributed at least in part to translational effects, and the departure at temperatures above 200°K may be attributed to intramolecular vibrations, to small differences in C_p-C_v and to the change in the librational frequency with temperature. Each of these effects will now be discussed separately.

TRANSLATIONAL HEAT CAPACITIES OF ICE AND HEAVY ICE

No satisfactory formula is available for calculating the shift in translational heat capacity to be expected

[4] E. A. Long and J. D. Kemp, J. Am. Chem. Soc. **58**, 1829 (1936).

[5] An unpublished five-place table of values of the Einstein function compiled by Professor F. G. Keyes has been of great help in making these calculations.

[6] W. F. Giauque and J. W. Stout, J. Am. Chem. Soc. **58**, 1184 (1936).

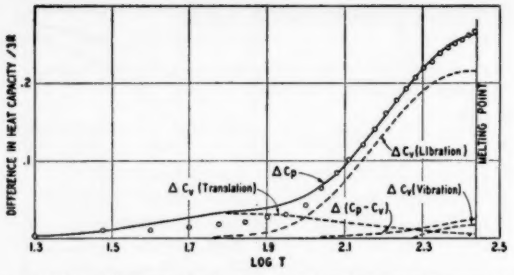

FIG. 3. The difference in heat capacity between heavy ice and ordinary ice. The broken lines represent the calculated values for the component parts of the heat capacity. The solid line is the sum of the broken lines and the points are obtained from the experimental work of Giauque and Stout and Long and Kemp.

from changing the molecular weight without changing the intermolecular forces. The Debye function does not apply strictly to a discontinuous medium, and the Debye θ does not correspond to any molecular vibration.[7] However, since the Debye function describes the translational heat capacity of monatomic substances fairly well, and since the Debye θ varies with the inverse half-power of the atomic weight,[8] an attempt has been made to calculate the difference between the translational heat capacity of heavy ice and that of ice from the Debye function.[9] The calculated curve is shown in Fig. 3 along with the curve for the calculated difference for vibrational heat capacity and the calculated dif ference in librational heat capacity which fits best when translation and vibration are taken into account. The appropriate Debye θ's for translation were obtained directly from the heat-capacity curves (in preference to the difference curve) in the following way: The librational heat capacity calculated from the Einstein function with $\theta=1040°$ ($\nu=723$ cm^{-1}) was subtracted from the observed C_p of ice and a Debye curve was fitted to the remainder as shown in Fig. 4. The Debye θ so obtained, 315°, was used in calculating the translational difference curve in Fig. 3.

The poor agreement between the Debye curve and the "residual" measured values in Fig. 4 may be attributed in part to failure of the Debye theory at the lower temperatures, and in part to interaction of translational motion with the zero-point libration of H_2O molecules in the crystal. The latter effect may be of appreciably different magnitude in the D_2O crystal owing to the much lower zero-point energy in this case as compared to the H_2O crystal.

HEAT CAPACITY OF INTRA-MOLECULAR VIBRATION

The only mode of internuclear vibration appreciably excited below the ice point is that of the bending motion in the water molecule which has the frequencies, 1595 cm^{-1}, in water vapor,[10] and 1179 cm^{-1} in D_2O vapor.[11] While these frequencies may not apply strictly to the molecules in the crystal (as indicated by the Raman spectra of ice[12]), they may be used to estimate the difference in vibrational heat capacity between H_2O and D_2O at the relatively low temperatures involved. The calculated difference is shown in Fig. 3, and is presented along with other kinds of heat capacity in Table I.

C_p—C_v

C_p-C_v for ice may be calculated from the formula

$$C_p-C_v=V_0T\alpha^2/\beta.$$

Where V_0 is the molal volume, T is the absolute temperature, α is the volume coefficient of thermal expansion, and β is the isothermal compressibility. Using the data given in *International Critical Tables* for −7°C, one obtains the value, 0.406 cal/deg mole for C_p-C_v in ice. No data are available at lower temperature, or for D_2O, but the formula given by Lord, Ahlberg, and Andrews,[2] $C_p-C_v=kC_v^2T$ (where k is a constant) may be used as an approximation for calculating the difference in (C_p-C_v) for D_2O and H_2O. Also, since C_p-C_v turns out to be a small fraction of the heat capacity, C_p may be used instead of C_v in the formula. Using the observed C_p's, and the value 0.406 cal/deg mole for C_p-C_v in ice at −7°C, one obtains the values shown in Fig. 3, and presented in Table I. The same value of k has been used for D_2O and H_2O although a more accurate calculation would probably require different k's owing to the large differences in zero-point energy in D_2O and H_2O.

COMPARISON OF HEAT-CAPACITY DATA WITH RAMAN DATA

Raman spectra of ice by Hibben and by Cross, Burnham, and Leighton[12] both show a strong sharp line at about 600 cm^{-1}, and this line is identified by the latter authors with librational motion. Since the value obtained from heat capacities is 660 cm^{-1} (723 cm^{-1}

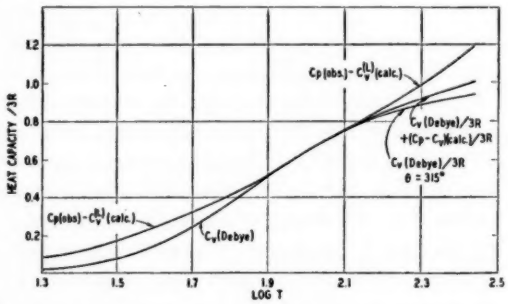

FIG. 4. Translational heat capacity of ice obtained from the experimental values by subtracting the librational heat capacity calculated from an Einstein function with $\theta=1040°$. This result is compared with a Debye function with $\theta=315°$ and with a Debye function to which the calculated values of C_p-C_v have been added.

[7] M. Blackman, Proc. Roy. Soc. (London) **A148**, 365; **A149**, 117 (1935).

[8] See, for example, A. Magnus, Z. physik. Chem., Bodenstein Festband, 273–82 (1931).

[9] J. A. Beattie, J. Math. and Phys. **6** (1926).

[10] E. K. Plyler and W. W. Sleator, Phys. Rev. **37**, 1493 (1931); H. H. Nielsen, Phys. Rev. **59**, 565 (1941).

[11] E. F. Barker and W. W. Sleator, J. Chem. Phys. **3**, 660 (1953).

[12] J. H. Hibben, J. Chem. Phys. **5**, 166 (1937); Cross, Burnham, and Leighton, J. Am. Chem. Soc. **59**, 1134 (1937).

TABLE I. Calculated and observed difference in heat capacity, $[C_p(D_2O)-C_p(H_2O)]/3R$.

T,°K	$\frac{\Delta C_v^{(L)}}{3R}$	$\frac{\Delta C_v^{(T)}}{3R}$	$\frac{\Delta C_v^{(V)}}{3R}$	$\frac{\Delta(C_p-C_v)}{3R}$	$\frac{\Delta C_p(\text{calc})}{3R}$	$\frac{\Delta C_p(\text{Exp})}{3R}$
20		0.003			0.003	0.007
30		0.010			0.010	0.010
40		0.020			0.020	0.010
50	0.000	0.027			0.027	0.014
60	0.001	0.032			0.033	0.017
80	0.007	0.030			0.037	0.027
100	0.028	0.026		0.000	0.054	0.042
120	0.060	0.022	0.000	0.001	0.082	0.084
160	0.138	0.015	0.001	0.006	0.160	0.160
200	0.192	0.010	0.005	0.013	0.220	0.219
240	0.212	0.008	0.015	0.020	0.255	0.250
270	0.214	0.006	0.017	0.025	0.262	0.266

when translation is also taken into account as in Fig. 3), it appears that the librational frequency is not a constant above about 200°K, but decreases with rising temperature, and the values observed in Raman spectra are those prevailing not far from the melting point. Observations of the Raman spectrum of ice at lower temperatures, and also of the Raman spectrum of heavy ice would be of assistance in elucidating this point. The rise of the observed heat capacity above calculated values near the melting point, as shown in Fig. 4, may well be associated with the rapidly changing librational frequency.

CONCLUSIONS

The close agreement of the calculated heat capacities with the experimental data is undoubtedly fortuitous. However, since only one parameter was chosen to obtain a fit with the librational heat capacity, which gives rise to the bulk of the difference between the heat capacities of ice and heavy ice, it seems reasonable that the model chosen for the system of librators is not very far from the true model. This means that the individual librators do not interfere very much with each other and that the spectrum of frequencies is not very broad. It appears also that interaction of libration with other degrees of freedom is not very important except in the low-frequency range.

At any rate, the heat capacity promises to be of value, along with the entropy, the dielectric constant, Raman and infrared spectra, and x-ray and neutron diffraction data, in the search for true models of crystals containing hydrogen.

Dielectric Properties of Hydrogen Halides. II. Hydrogen Chloride*

RICHARD W. SWENSON† AND ROBERT H. COLE
Metcalf Research Laboratory, Brown University, Providence, Rhode Island

(Received September 18, 1953)

Dielectric constant and loss measurements have been made for liquid and solid hydrogen chloride in the temperature range 63–190°K and frequency range 20 cps to 10^6 cps. The dielectric constants of the liquid and disordered solid phase stable above 99°K are described quite accurately by Onsager's equation. Below 99°K a slight dispersion with activation energy of 2.6 kcal/mole is found with dielectric constants in the range 3.7–4.3. Special precautions against sample inhomogeneity were necessary; these and various residual effects are discussed.

I. INTRODUCTION

THE dielectric properties of solid hydrogen chloride have been the subject of investigation by a number of workers and are of interest because of the evidence they can give concerning the nature of the two solid phases. Following Pauling's discussion[1] of free and hindered rotations, Cone, Dennison, and Kemp[2] reported an irregular variation of the dielectric constant, measured at 3 Mc/sec, from a value 11.1 at the melting point to 9.9 at the 99°K phase transition, below which a constant, low value of about 3 was found. Smyth and Hitchcock[3] found somewhat larger values at audio- and low radio-frequencies in the high-temperatures phase, and the possibility was thus suggested that the difference might be due to dielectric dispersion at radio-frequencies. Kanda[4] found intermediate behavior at a frequency of 1 Mc/sec, and attributed the decrease in dielectric constant below the melting point to increasing "crystallinity" of his sample.

Hettner and Pohlmann[5] found no evidence of dispersion in the high-temperature phase in the range 60 kc/sec to 10 Mc/sec, but their results were not in very good agreement with any of the other work. They did observe small but definite dispersion and loss in the low-temperature phase between 86 and 95°K, but it is not easy from their graphs to characterize the nature of the relaxation process very definitely. In the course of our work, Phillips[6] reported quite extensive measurements which gave evidence of dispersion at frequencies below 10 kc/sec; he suggested, however, that the effects might be a consequence of electrode polarization rather than a genuine relaxation process characteristic of the dielectric.

The values reported by the various workers are plotted in part in Fig. 1, and it is evident that no very definite conclusions can be drawn from them. None of the previous explanations of the discrepancies or of the general behavior seems very satisfactory, and the present investigation was undertaken to obtain a better knowledge of the true behavior.

On the basis of previous experience with solid hydrogen bromide,[7] it was clear that sample inhomogeneities could cause considerable error in the present problem where dielectric constants of order ten or more are involved. It is also clear, however, that not all of the differences shown in Fig. 1 can be attributed to this cause alone, as values reported for the liquid, for which no such effect should occur, are also in poor agreement. A rather detailed study with attention to various possible sources of error therefore seemed necessary if reliable results were to be obtained.

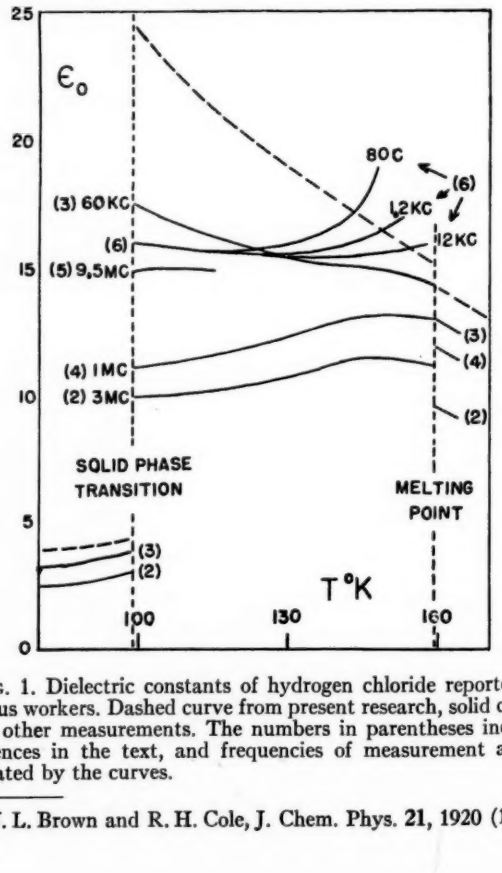

FIG. 1. Dielectric constants of hydrogen chloride reported by various workers. Dashed curve from present research, solid curves from other measurements. The numbers in parentheses indicate references in the text, and frequencies of measurement are as indicated by the curves.

* This paper is based on a thesis submitted by R. W. Swenson in partial fulfillment of the requirements for the Ph.D. degree.

† Now with the E. I. du Pont de Nemours and Company, Photoproducts Department, Parlin, New Jersey.

[1] L. Pauling, Phys. Rev. **36**, 430 (1930).

[2] Cone, Dennison, and Kemp, J. Am. Chem. Soc. **53**, 1273 (1931).

[3] C. P. Smyth and C. S. Hitchcock, J. Am. Chem. Soc. **55**, 1830 (1931).

[4] E. Kanda, Bull. Chem. Soc. Japan **12**, 473 (1937).

[5] E. Hettner and R. Pohlmann, Z. Physik **108**, 45 (1938).

[6] C. S. Phillips, J. phys. et radium **13**, 216 (1952).

[7] N. L. Brown and R. H. Cole, J. Chem. Phys. **21**, 1920 (1953).

In this investigation, it was found possible by suitable design and precautions to obtain reproducible dielectric constant values in the high-temperature solid phase, and a plausible explanation of the low-frequency dispersion can be advanced. Results from the low-temperature phase were not as reproducible, we believe because of crystalline anisotropy, but were sufficiently consistent to be significant.

II. EXPERIMENTAL

The general experimental procedure was in most respects an evolution from that devised for the earlier work on hydrogen bromide (reference 7, hereafter referred to as I). In particular, the details of electrical measurements and of temperature control and measurement were the same except for minor refinements which need not be described here.

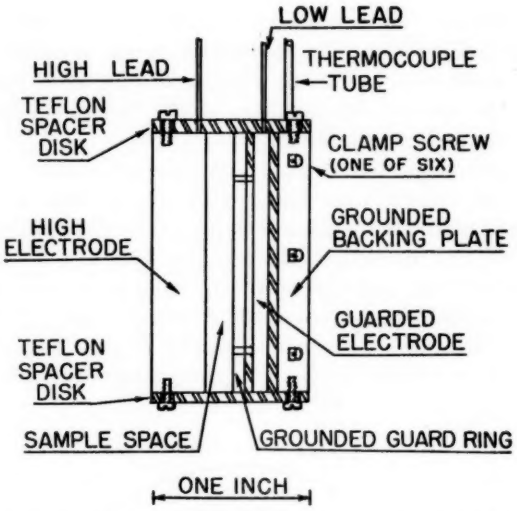

FIG. 2. Section of parallel plate condenser of cylindrical form. The guarded electrode is clamped between the solid backing plate and the rectangular guard ring and insulated from them by 5-mil Teflon gaskets. Grounded shielding of high and low electrode leads not shown.

The basic cell design embodied the principle previously employed of overcompensating lateral contraction of the solid between the measuring electrodes, this being accomplished by use of Teflon disks supporting the electrodes at a distance several times the electrode separation. The main difference between the present cell, shown in Fig. 2, and the designs of I is a more positive means of positioning the low-potential, guarded electrode in its confining guard ring by a sort of "sandwich" construction using a Teflon insulating gasket and backing. The electrode spacings of 1.5 and 3 mm resulted in geometric capacitances of approximately 2.8 and 1.5 $\mu\mu$f. With the Teflon disk spacers used, corresponding thermal expansion coefficients of the electrode gap were found from capacitance measurements to be 650 and 300×10^{-6} °C^{-1}. The former figure was large enough to make possible reproducible measurements of properly frozen solid samples, but the latter was not. Measurements using the larger spacing were useful, however, in confirming values for the liquid and in studying the low-frequency dispersion below the melting point.

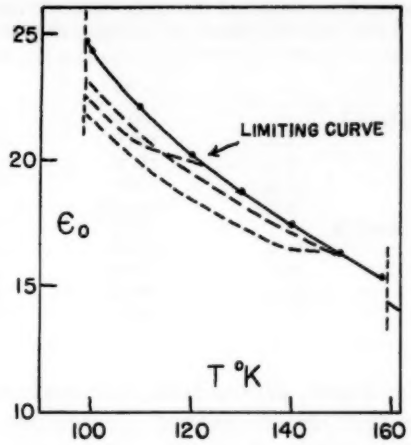

FIG. 3. Static dielectric constant data obtained in the present work. The uppermost solid curve is the reproducible limiting one; the lower irregular curves result from sample voids.

The starting material was compressed gas from the Mathiesen Company of better than 99-percent stated purity, the chief contaminant being acetylene. The gas admitted to the system, previously evacuated to 10^{-5} mm Hg, passed through two glass wool entrainment traps cooled in a CO_2-isopropanol slush to a distillation trap, and then was distilled into the cell assembly. Corrosion of the brass cell material by a liquid or solid was undetectable if the cell was thoroughly cleaned and pumped out after electropolishing, and the final colorless liquid in the cell had specific conductivity of 10^{-7} mho/cm or less in all cases.

The freezing process found to give reproducible samples most consistently was a fairly rapid one in which a brass block surrounding the cell was kept about thirty degrees below the melting point, and under these conditions the sample froze in less than five minutes. Much faster or slower freezing produced samples whose measured capacitances dropped erratically and usually quite abruptly. The nature of these failures is shown in the plot of Fig. 3 of apparent dielectric constants of a number of samples. The upper curve was substantially duplicated by data above 10 kc/sec for a number of samples and was never exceeded.

The deviations shown in Fig. 3 are of the sort encountered in I and are similarly explained as the result of imperfectly homogeneous samples. They are also of the same form as the curves of various earlier investigators shown in Fig. 1, although these latter curves show much larger differences, as would be expected for experimental arrangements making no allowance for thermal contraction of the dielectric. The failure to obtain satisfactory samples on all occasions in the present work is, we believe, to be attributed to the formation, as the

TABLE I. Interpolated values of the static dielectric constant for the liquid and solid phases of hydrogen chloride.

T(°K)	ϵ_0	T(°K)	ϵ_0
Solid phase I		130.0	18.7_5
62.4	3.7_2	140.0	17.4_5
70.0	3.7_8	150.0	16.3_0
80.0	3.8_8	158.9	15.2_5
90.0	4.0_6	Liquid	
Solid phase II		158.9	14.3_0
98.4	24.7_0	160.0	14.2_0
100.0	24.3_5	170.0	13.0_0
110.0	22.2_0	180.0	12.0_5
120.0	20.2_5	188.1	11.3_0

sample was frozen, of interfaces which opened up on further cooling despite over-all compression by the electrodes. In nearly all cases, successful samples were perfectly clear and colorless at the melting point but became cloudy and ultimately opaque at lower temperatures.

III. RESULTS

A. Liquid

Measurements of dielectric constant were made in four different runs using two different electrodes spacings. No dependence on frequency was observed in the range 1 kc/sec to 500 kc/sec, and the results were reproducible to within 1 percent. Interpolated average values are listed in Table I. Below 1 kc/sec, some dispersion was observed of the sort characteristic of electrode polarization effects.

The values obtained by us are somewhat higher than those of previous workers, particularly the earlier ones. The range of values at or near the melting point reported in the literature is from 8.85[8] to 13.1[3] as compared with our value of 14.3. Phillips[6] did not report numerical data, but a value of about 14 can be estimated from a graph in his paper.

It is not possible definitely to assign the differences between the various reported results to impurity, errors of measurement or calibration, or other causes. In the present work, considerable pains were taken to preclude contamination and eliminate residual or systematic errors. This, plus the excellent agreement of measurements with different samples and cell capacitances, gives us confidence in the accuracy of the results reported here.

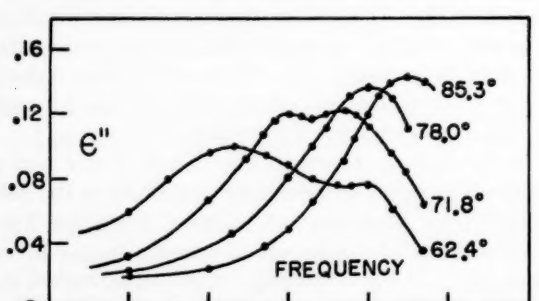

FIG. 4. Curves of dielectric loss ϵ'' *versus* frequency in the low-temperature phase at temperatures as indicated (°K).

[8] O. C. Schaefer and H. Schlundt, J. Phys. Chem. 13, 669 (1909).

B. The High-Temperature Solid Phase

As discussed in Sec. II, reproducible limiting dielectric constant values were obtained for this phase at frequencies above 10 kc/sec, with no evidence of frequency dependence in the range 10 kc/sec to 1 Mc/sec investigated. The reproducibility of data for five samples which exhibited no evidence of void formation was better than one percent, and interpolated values from these data are listed in Table I.

Below 10 kc/sec, and especially near the melting point, frequency-dependent dielectric-constant and loss values were observed, much as in the results reported by Phillips[6] (see Fig. 1). A fair correlation was found between the conductance of the solid sample and the magnitude of rise of apparent dielectric constant at low frequencies, but there was no correlation of either with the specific conductance of the liquid before or after the solid measurements.

It was suspected that, as Phillips conjectured, the observed effects were the result of electrode space-charge polarization effects set up by the solid state conductivity of the sample. To test this hypothesis, measurements were made near the melting point with the cell modification employing a 3- rather than 1.5-mm electrode separation, as one would expect less error from space-charge effects with the greater thickness of sample. Although the spacing was too great to prevent noticeable effects of void formation at lower temperatures, the measurements were adequate to show that the low-frequency polarization effects were not significantly different for samples of comparable specific conductance.

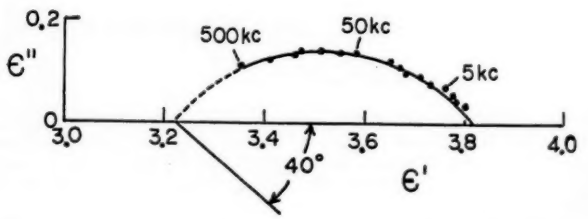

FIG. 5. Complex dielectric constant locus of solid HCl at 78.0°K.

From these results, it seems necessary to conclude that the observed effects were not a consequence of electrode processes, but rather a bulk property of the sample. On the other hand, this and other evidence shows definitely that the effects are not intrinsic properties of the crystalline solid. It was found that the deviations decreased with time at a given temperature, were markedly reduced on cooling and warming the sample, and were smaller for more slowly frozen samples. These observations are consistent with the

hypothesis that a form of interfacial polarization process at microcrystalline boundaries was responsible for the effects, and this is the best explanation we can offer of them.

C. The Low-Temperature Solid Phase

Measurements of dielectric constant and loss below 99°K were made only on samples which exhibited consistent behavior at higher temperatures. The results for different samples were, even so, somewhat variable, the measured values differing by as much as 20 percent.

While it is possible that some of the variability resulted from sample voids caused by the 4.5-percent density increase at the 99°K first-order phase transition, errors from this source would not be very large because

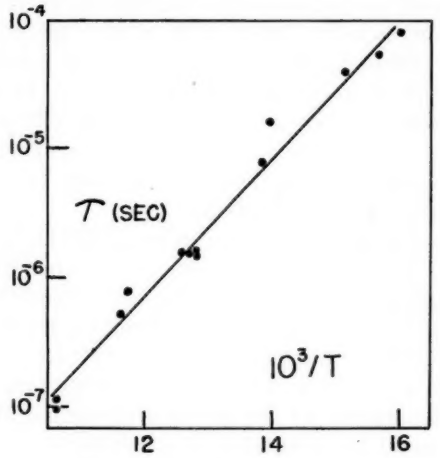

FIG. 6. Rate plot of relaxation time τ *versus* reciprocal of temperature from 63 to 90°K.

of the small value of the dielectric constant, which is less than 4.5. A more likely explanation is in terms of anisotropy of the dielectric constant and variability in the orientations of microcrystals composing the sample. Rough values of static dielectric constant are listed in Table I.

Despite the variability of absolute values, the frequency range of the small but definite dispersion and loss was quite reproducible. Typical curves of dielectric loss *versus* frequency are shown in Fig. 4. A curious feature of these curves is the appearance at temperatures below 78°K of an unmistakable hump or shoulder in a frequency range centered at about 100 kc/sec with no determinable temperature dependence. This was observed for every sample studied, and no instrumental error capable of producing the effect could be found.

Both the 100 kc/sec peak and the approximate character of the data make a detailed analysis of the form of the dispersion unwarranted. The complex plane plot in Fig. 5 of typical data at 78°K suggests that the temperature-dependent dispersion is described by the

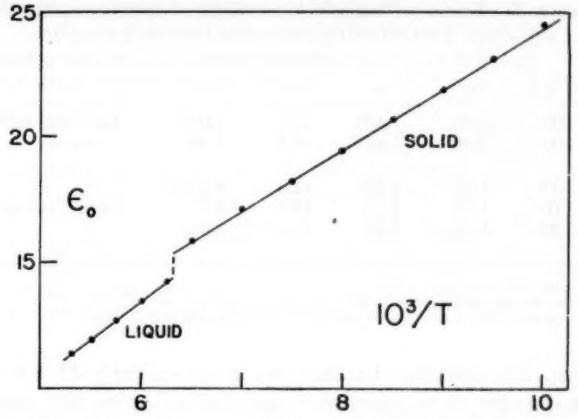

FIG. 7. Static dielectric constants of liquid and solid hydrogen chloride as a function of reciprocal absolute temperature.

circular arc function characteristic of hydrogen bromide (see paper I) and many solid dielectrics.[9]

The dependence of relaxation time, defined as $1/2\pi$ times the frequency of maximum loss ϵ'', on temperature is shown by the rate plot of Fig. 6, and is described by the equation

$$\tau(\text{sec}) = 1.01\times10^{-13}\exp(2620/RT). \qquad (1)$$

Estimates of the limiting values of dielectric constant at high frequency can be made only roughly because of the necessary extrapolation and variability of the data, but give a value of about 3.2 without any significant temperature dependence

IV. DISCUSSION

The experimental dielectric constants for both the liquid and the high-temperature solid phase exhibit a simple and regular temperature dependence, being very nearly linear functions of reciprocal absolute temperature as shown in Fig. 7. This is the behavior predicted by Onsager's theory for polar liquids[10] which can be written

$$\epsilon - n^2 = \frac{3\epsilon}{2\epsilon+n^2}\left(\frac{n^2+2}{3}\right)^2 \frac{4\pi N d}{M}\frac{\mu_0^2}{3kT}, \qquad (2)$$

where n is the refractive index, d the density, μ_0 the gas dipole moment, and N, M, k, T have their usual significance. Although n, d, and ϵ are all temperature-dependent, their variations in Eq. (2) have the effect in the present case of modifying the slope of ϵ *versus* $1/T$ and imparting only a slight curvature.

The numerical agreement of Eq. (2) with the measurements is quite remarkable, all things considered. The comparison is conveniently made by using (2) to calculate μ_0 from the measured values of ϵ and d and values of n^2 calculated from Hammer and Rollefson's[11] polarizability data with the Clausius-Mossotti expres-

[9] K. S. Cole and R. H. Cole, J. Chem. Phys. **9**, 341 (1941).
[10] L. Onsager, J. Am. Chem. Soc. **58**, 1486 (1936).
[11] C. F. Hammer, Ph.D. thesis, University of Wisconsin (1948).

TABLE II. Values of the dipole moment of hydrogen chloride calculated from dielectric data using Onsager's equation.

T(°K)	n^2	d	ϵ_0	μ_0	
100	2.09	1.48[a]	24.3	1.06D	Isotropic solid phase
107	2.08	1.47[b]	22.8	1.09	
160	1.89	1.26[c]	14.2	1.15D	
176	1.86	1.22	12.4	1.14	Liquid phase
188	1.83	1.19	11.3	1.15	

[a] See reference 13.
[b] F. Simon and C. von Simson, Z. Physik **21–22**, 168 (1924).
[c] Steele, McIntosh, and Archibald, Z. Physik **55**, 129 (1909).

sion. The calculated values are listed in Table II. Lack of density data precluded such calculations for solid HCl above 107°K, but it is clear that the results would not be greatly different.

The most reliable figure for the gas dipole moment is presumably the value 1.12 debyes obtained by Hammer and Rollefson[11] from careful infrared dispersion measurements. Although comparison of μ_0 is an optimistic fashion of testing Eq. (2), which involves μ_0^2, the agreement of the values in Table II with each other and with the gas value shows that Onsager's equation describes the measured values quite accurately.

The validity of the equation indicates that its basic assumptions are adequate approximations for both the liquid and high-temperature solid phases. As Kirkwood[12] has shown from a statistical mechanical treatment, major deviations from Onsager's result are to be expected as a consequence of short range intermolecular correlation, notably, hydrogen bonding, and lesser deviations can result from asymmetry of molecular shape. It is reasonable to conclude that hydrogen chloride behaves as a normal polar liquid in its dielectric properties without significant hydrogen bonding, in agreement with the usual conclusion from other physical properties. X-ray studies[13] of the solid phase stable above 100°K indicate a face-centered cubic structure of the halogens, and it is now commonly assumed that the molecular orientations are disordered above the 99°K phase transitions. The dielectric data are consistent with this conclusion and can be taken as evidence against appreciable net correlation of neighbors. The same situation was found for hydrogen bromide, as reported in I, and it seems quite clear that no special explanations of the disordered phases in either HCl or HBr are required.

The small values of dielectric constant below 99°K, and the fact that only the beginnings of significant dispersion are observed as the transition is approached, indicate that the anisotropic low-temperature phase is well ordered with much stronger intermolecular coordination than in the case of hydrogen bromide. The difficulty in attributing this difference wholly to the greater importance of dipole forces in hydrogen chloride has been discussed by Powles.[14] The observed dispersion occurs at considerably higher frequencies than does the principal dispersion in HBr, but the activation energy of 2.62 kcal/mole from the rate plot in Fig. 6 is not significantly different from the value 2.70 kcal/mole for HBr.

The estimated value of 3.2 for the dielectric constant at frequencies above the dispersion region is significantly larger than the value estimated for the square of the refractive index. Both values are approximate, the first because of uncertainties in extrapolation and the second because the density is not accurately known; but it seems quite definite that combined errors could not reasonably explain the difference. Whether the discrepancy is to be accounted for by a second relaxation dispersion, as in the case of HBr, or by a resonance dispersion cannot be decided from available information. It is tempting to assume the former and to explain the two dispersions as a consequence of relaxation of principal dielectric constants for different crystallographic arrangements, but this can only be regarded as a conjecture at the present.

The origin of the loss maximum at 100 kc/sec below 78°K is obscure. All attempts to account for it by instrumental or other experimental difficulties have failed, and we have no reason to doubt its reality. There are indications that at higher temperatures the peak becomes less sharp and may move to higher frequencies or be obliterated by the broader dispersion. This behavior could be attributed to a resonance dispersion, but the existence of such a dispersion at such extraordinarily low frequencies is a result we are unable to explain at present.

In summary, it can be said that special attention to insuring measurements of homogeneous samples has led to simple and readily interpreted results for the high-temperature solid phase of hydrogen chloride, and that the results for the low-temperature phase indicate only slight changes in order near the transition. The detailed interpretation of the low-temperature results may well require further experimental studies and correlation with a variety of other physical evidence, but the amount of characteristic and quite specific information obtainable from adequate studies of the dielectric properties is quite impressive.

ACKNOWLEDGMENT

One of us (RWS) is indebted to the Union Carbide and Carbon Corporation for a fellowship grant during 1952–53.

[11] J. G. Kirkwood, J. Chem. Phys. **7**, 911 (1939).
[12] G. Natta, Gazz. chim. ital. **63**, 423 (1933).
[13] J. G. Powles, Trans. Faraday Soc. **48**, 430 (1952).

The Infrared and Raman Spectra of Formaldehyde-d_1 Vapor*

D. W. DAVIDSON,† B. P. STOICHEFF,‡ AND H. J. BERNSTEIN
Division of Chemistry, National Research Council, Ottawa, Ontario, Canada

(Received August 17, 1953)

The infrared spectrum of HDCO vapor has been investigated in the region 2.5μ−25μ and all six fundamentals have been observed. Four of the fundamentals have also been observed in the Raman spectrum of the vapor.

The perpendicular component of an hybrid band at 3.5μ and the pure rotational Raman spectrum were resolved and analyzed. The rotational constant $(A-\bar{B})$ for the symmetric top approximation was found to be 5.47±0.03 cm^{-1}. This value, combined with the rotational constants of H_2CO obtained by Dieke and Kistiakowsky, yields approximate molecular dimensions for the ground state of formaldehyde.

THE infrared spectra of the symmetrical formaldehydes H_2CO and D_2CO were obtained by Nielsen[1] and Ebers and Nielsen.[2,3] In their work, only the rotational structure of the three perpendicular bands was resolved. Moreover, in both molecules the rotational analysis of these bands was complicated by the occurrence of strong Coriolis coupling between the two perpendicular bending vibrations and overlapping of the third perpendicular band by parallel bands. For the H_2CO molecule, much more accurate ground-state rotational constants are given by the high-resolution ultraviolet results of Dieke and Kistiakowsky[4] and by the recent microwave data of Lawrance and Strandberg.[5] Since spectroscopic data on H_2CO can fix only two of the three independent geometric parameters, it is necessary to have supplementary rotational data for an isotopic molecule.[6] In this connection the most useful isotopic molecule to investigate under conditions of low resolution is the monodeuterated form.

Formaldehyde-d_1 (HDCO) was recently made available and a study of the vibrational spectrum and the rotational structure of the perpendicular bands was undertaken. It was hoped that some of the perpendicular bands in HDCO would be free of such interference effects as observed in the infrared spectra of H_2CO and D_2CO, and that a reliable value of $A-\bar{B}$ (for the symmetric top approximation) would be forthcoming.

In the present investigation, both the infrared and Raman spectra of HDCO vapor were obtained. Although all of the fundamentals were observed in the infrared region, none of the bands showing perpendicular structure was found to be free from Coriolis or Fermi interaction; much the same difficulty as in the symmetrical formaldehydes was encountered in evaluating the rotational constant $A-\bar{B}$. However, an analysis of the perpendicular structure of the "CH stretching" band, which is least perturbed, was found possible.

The difficulties caused by polymerization of liquid formaldehyde have limited the earlier investigations of the Raman effect to aqueous solutions of H_2CO.[7] These difficulties were avoided, as outlined below, by a study of the gaseous state.

The vibrational Raman spectrum of HDCO vapor was of considerable assistance in the location of band centers, particularly for overtone and combination bands enhanced through Fermi resonance. Also, the pure rotational Raman spectrum afforded a more direct evaluation of $A-\bar{B}$ than the infrared band structure, since a perturbation of the vibrational ground level is unlikely; but the accuracy was limited by the available resolution.

EXPERIMENTAL DETAILS

The preparation of formaldehyde-d_1 has been described by Bannard, Morse, and Leitch.[8] It was made available as the *para*-polymer through the courtesy of Dr. L. C. Leitch. The mass spectrometric analysis (93 percent HDCO) was qualitatively confirmed by the absence of spectral evidence of H_2CO or D_2CO.

The infrared data were obtained with a model 12C Perkin-Elmer spectrometer. The prism used for wave numbers above 1900 cm^{-1} was LiF, between 1900 and 1500 cm^{-1} CaF_2, and below 1500 cm^{-1} NaCl. All wave numbers were corrected to vacuum. The infrared cell consisted of a Pyrex tube 8 cm long and 4 cm in diameter, with KBr windows sealed to the ends with benolite cement. The paraformaldehyde-d_1 was placed in the absorption cell which was then evacuated for several hours. The cell was placed in an oven of the type described by Bernstein[9] and slowly heated to 120–140°C. Enough HDCO was added to the cell to give a vapor pressure of *ca* 250 mm upon complete vaporization.

* Presented at the Symposium on Molecular Structure held at The Ohio State University, Columbus, Ohio, June, 1953.

† National Research Laboratories Post doctoral Research Fellow, Division of Chemistry, 1951–1953.

‡ National Research Laboratories Post doctoral Research Fellow, Division of Physics, 1951–1953.

[1] H. H. Nielsen, Phys. Rev. **46**, 117 (1934).

[2] E. S. Ebers and H. H. Nielsen, J. Chem. Phys. **5**, 822 (1937).

[3] E. S. Ebers and H. H. Nielsen, J. Chem. Phys. **6**, 311 (1938).

[4] G. H. Dieke and G. B. Kistiakowsky, Phys. Rev. **45**, 4 (1934).

[5] R. B. Lawrance and M. W. P. Strandberg, Phys. Rev. **83**, 363 (1951).

[6] A few microwave lines of the $H_2C^{13}O$ molecule have been reported [R. B. Lawrance, Phys. Rev. **78**, 347 (1950); "Molecular Microwave Spectra Tables" Natl. Bur. Standards (U. S.) Circ. 518, (1952)].

[7] K. W. F. Kohlrausch and F. Koppl, Z. physik. Chem. **B24**, 370 (1934).

[8] Bannard, Morse, and Leitch, Can. J. Chem. **31**, 351 (1953).

[9] H. J. Bernstein, J. Chem. Phys. **18**, 897 (1950).

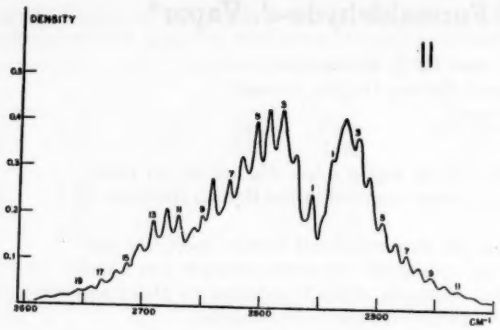

FIG. 1. Band ν_1. The equivalent slit width is indicated.

The ν_5, ν_6 band (see the following) was subsequently re-examined under the higher resolution of a double-pass spectrometer, with no appreciable change in the results.

In the Raman investigation, a Pyrex tube 1.2 meters long was used, having at the window end a diaphragm system of black glass. One gram of the paraformaldehyde was placed in the rear end of the Raman tube. The tube was evacuated and sealed. The temperature of the tube was slowly raised by means of a nichrome heating coil wound along the length of the tube. With the tube at a temperature of 130°C, as measured by a thermocouple, and the window kept at about 150° by an additional heater, the temperature of the paraformaldehyde was slowly raised to 120°C by means of a heated oil bath. Under these conditions the vapor pressure of the monomer was about one atmosphere. No polymerization at the walls was observed.

Formaldehyde has absorption bands in the region λ3600, and in order to prevent photodissociation by the intense mercury lines in this region, a solution of $NaNO_2$ was circulated in a Pyrex jacket surrounding the tube (see Appendix). The Raman tube was irradiated symmetrically along 70 cm of its length by means of four Toronto-type mercury lamps enclosed in a MgO-coated reflector. In this way it was possible to photograph the rotational and vibrational Raman spectra of HDCO excited by the Hg 4358 line. A three-prism spectrograph was used, having a camera aperture $f/5$ and a dispersion of 130 cm^{-1}/mm at λ4358. The Raman frequencies are based on one plate exposed for 40 hours using a 5-cm^{-1} slit. However, the appearance of the vibrational spectrum was confirmed by a second plate photographed with an $f/2.5$ camera in 12 hours.

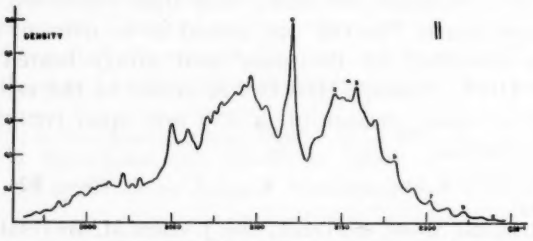

FIG. 2. Band ν_2.

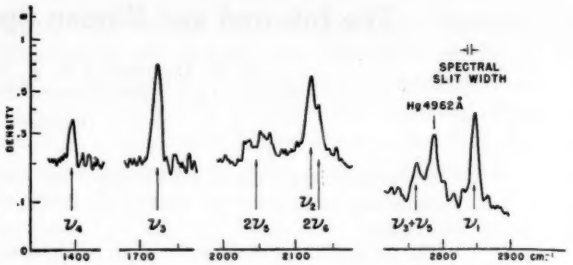

FIG. 3. The Raman spectrum of HDCO vapor.

During the course of this investigation the Raman spectrum of H_2CO vapor was also obtained in the manner described in the foregoing and the results are reported in the Appendix.

VIBRATIONAL SPECTRUM

HDCO belongs to the point group C_S and has five in-plane vibrations of type a', and one out-of-plane vibration of the type a''. All six fundamentals are infrared and Raman active. The a' type vibrations give rise to hybrid bands (although parallel or perpendicular features may predominate) and the a'' type vibration gives rise to a perpendicular band. All six fundamentals have been observed in the infrared and four have been observed in the Raman spectrum (see Table I). The strong bands at 2844 and 2120 cm^{-1} can be attributed to the CH and CD "stretching" vibrations and have pronounced perpendicular festures in absorption (see Figs. 1 and 2). These bands show up as narrow lines in the Raman spectrum (Fig. 3). The infrared bands at 1723 and 1400 cm^{-1} (Fig. 4) are almost entirely parallel in character with a $P-R$ peak separation of ~55 cm^{-1} in agreement with the value calculated by the method of Gerhard and Dennison[10] for unresolved parallel bands. They can be atrributed to the C=O stretching vibration

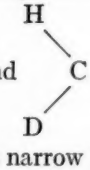

and C bending vibration, respectively, and appear as narrow bands in the Raman spectrum (Fig. 3). The remaining fundamentals ν_5 and ν_6 are strongly coupled with one another because of Coriolis interaction and

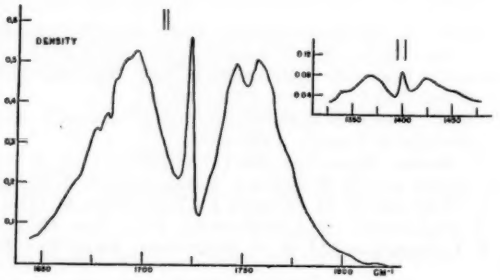

FIG. 4. Bands ν_3 and ν_4 (ν_4 is inset).

[10] S. L. Gerhard and D. M. Dennison, Phys. Rev. **43**, 197 (1933).

exhibit irregular fine structure spacing (Fig. 5). They were not observed in the Raman spectrum. The values finally chosen for ν_5 and ν_6 are based on Nielsen's treatment[11] of the effect of Coriolis interaction on rotational levels, and upon sum and product rules for isotopic homologs (see the following); they are less certain than the other frequencies.

Because of the low symmetry of HDCO and the closeness of summation bands to the fundamentals ν_1 and ν_2, Fermi resonance seems likely. Indeed, both ν_1 and ν_2 exhibit irregularities suggesting the presence of overtones or combination bands whose intensity has been enhanced possibly by Fermi resonance. The peak at 2758 cm^{-1} in the infrared spectrum corresponds to the weak band observed at 2760 cm^{-1} in the Raman spectrum and is probably $\nu_3+\nu_5$ rather than $2\nu_4$, since both ν_3 and ν_5 are each relatively strong, whereas ν_4 is a weak band.

The Raman band at 2133 cm^{-1} locates the center of the disturbance on the high-frequency side of ν_2 and is probably $2\nu_6$. The band at 2055 cm^{-1} in the infrared absorption spectrum is observed as a weak broad band

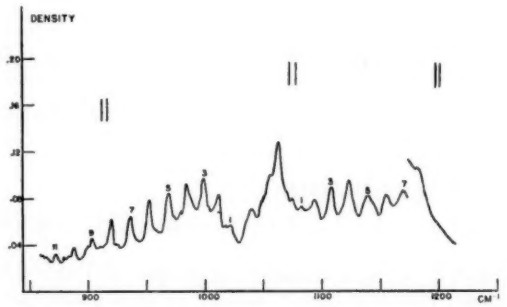

FIG. 5. The ν_5, ν_6 band.

~2045 cm^{-1} in the Raman spectrum and is probably $2\nu_5$. It is not clear why the band at 2045 cm^{-1} should be the only broad band observed in the Raman spectrum.

ROTATIONAL STRUCTURE

The perpendicular rotational structure has been analyzed in the ν_1 band and in the ν_5, ν_6 band. The inertial constant $A-\bar{B}$ for the ground state was also determined from the rotational Raman effect.

The ν_1 band (Fig. 1) has a well defined perpendicular component, superimposed on an unresolved parallel band contour in which the $P-R$ peak separation is about 55 cm^{-1}. The principal perpendicular sub-band frequencies are given in Table II. Although Fermi resonance with $\nu_3+\nu_5$ (see the foregoing) enhances the intensity of the perpendicular sub-bands on the low-frequency side, it appears to affect appreciably the frequencies of only two peaks. The remaining subbands may be fitted by the symmetric top approximation for the perpendicular bands ($\Delta K=\pm1$, $\Delta J=0$) with the usual formula[12] to which a term in K^3 has been added:

$$\nu_1^{\text{sub}}=\nu_1+(A'-\bar{B}')\pm2(A'-\bar{B}')K+[(A'-\bar{B}')-(A''-\bar{B}'')]K^2\mp4D_kK^3.$$

The notation follows Herzberg,[12] with $\bar{B}=(B+C)/2$. Although the term in K^3 was found to be of the right order of magnitude for a purely centrifugal effect, it must be regarded as including a number of other influences. In particular, for large K values, the asymmetry of the molecule produces a frequency shift in the same direction as centrifugal distortion.[13]

From the least squares treatment of the sub-band frequencies for $K\geq3$, excluding $K=8$ and 10, the foregoing equation becomes

$$\nu_1^{\text{sub}}=2849.6\pm10.922K-0.0085K^2\mp0.00093K^3.$$

TABLE I. Infrared and Raman bands of HDCO vapor.

Assignment	Infrared ν_{vac} (cm^{-1})	Raman $\Delta\nu_{\text{vac}}$ (cm^{-1})
$\nu_1(a')$	2844.1	2846.2 (s-sharp)
$\nu_3+\nu_5(A')$	2758	2761 (w-sharp)
$2\nu_6(A')$		2133 (w-sharp)
$\nu_2(a')$	2120.7	2120.3 (s-sharp)
$2\nu_5(A')$	2055	2045 (v.w-broad)
$\nu_3(a')$	1723.4	1723.2 (v.s-sharp)
$\nu_4(a')$	1400.0	1397.4 (m-sharp)
$\nu_5(a')$	1041	...
$\nu_6(a'')$	1074	...

TABLE II. Principal peaks in the ν_1 band.

Observed frequency	K	Calculated frequency ($\Delta K=+1$)	Observed frequency	K	Calculated frequency ($\Delta K=-1$)
(2851)	0	(2849.7)	(2843)	1	(2838.6)
2859.6	1	2860.5	2828.6	2	2827.7
2871.7	2	2871.4	2816.8	3	2816.8
2882.4	3	2882.2	2805.8	4	2805.8
2893.0	4	2893.0	2795.4	5	2794.9
2903.9	5	2903.8	2783.6	6	2783.9
2915.1	6	2914.6	2772.9	7	2773.0
2924.9	7	2925.3	2758.2		
2935.1	8	2935.9		8	2762.1
2945.2	9	2946.5	2750.7	9	2751.3
2956.6	10	2957.0	2743.1		
(2968.3)	11	2967.4		10	2740.3
			2730.0	11	2729.6
			2719.7	12	2718.9
			2708.5	13	2708.4
			2697.0	14	2697.7
			2686.7	15	2687.2
			2677.4	16	2676.5
			2665.4	17	2666.0
			2656.3	18	2655.7
			2646.0	19	2645.4

Average deviation, excluding parenthesized frequencies, ±0.48 cm^{-1}.

[11] H. H. Nielsen, J. Chem. Phys. **5**, 818 (1939).

[12] G. Herzberg, *Infrared and Raman Spectra of Polyatomic Molecules* (D. Van Nostrand Company, Inc., New York, 1945), p. 424.

[13] The actual asymmetric top levels may be obtained from the tables of King, Hainer, and Cross, J. Chem. Phys. **11**, 27 (1943); **12**, 210 (1944). For HDCO, the asymmetry parameter $\delta=(B-C)/(A-C)\approx0.032$ as compared with 0.019 for H_2CO and 0.054 for D_2CO.

The frequencies calculated from this equation are included in Table II. The band center occurs at $\nu_1 = 2844.1$ cm^{-1} and the rotational constant $A''-\bar{B}''$ is found to be 5.46_9 cm^{-1}.

The rotational structure of the ν_2 band is so strongly perturbed that it cannot be analyzed simply, although a K assignment, as shown in Fig. 2, is possible on the high frequency side. This band appears to have a stronger parallel component than ν_1, probably because the least inertial axis lies nearer to the CD bond by more than 10° than it does to the CH bond. The band center is taken to be the frequency of the strong Q branch ($\Delta K=0$, $\Delta J=0$) contributed by the parallel component.

The frequencies of the principal peaks in the ν_5, ν_6 Coriolis-coupled band (Fig. 5) are listed in Table III. To the extent that ν_5 is a perpendicular band, the general effect of the Coriolis interaction on the observed spectrum is the same as for the two perpendicular bending vibrations in H_2CO and D_2CO. In the symmetric top approximation as before, the sub-band frequencies in the ν_5, ν_6 band are given by the equation of Nielsen:[11]

$$\nu_{5,6}{}^{\text{sub}} = \frac{\nu_5+\nu_6}{2} + \xi^2 A' - (A''-\bar{B}'') \pm 2(A''-\bar{B}'')K \pm \left[\left(\frac{\nu_5-\nu_6}{2}\right)^2 + (2A'\xi K)^2\right]^{\frac{1}{2}} + [(A'-\bar{B}')-(A''-\bar{B}'')]K^2.$$

Here, K refers to the quantum number of the excited state and the first $\pm$ sign to $\Delta K=\pm 1$ transitions. The second $\pm$ sign distinguishes the two states which result from the rotational coupling between the ν_5 and ν_6 vibrational modes. The coupling parameter ξ is related to the geometry of the molecule.

This equation can be applied in the present case only to the outer sides of the band system, where the signs are either both positive or both negative. When the signs differ, the sub-band spacing is lesst han $2(A-\bar{B})$ and there is an overlap of the $+,-$ and $-,+$ combinations in the center region where the structure was not resolved. At the sides of the band, however, the spacing is greater than $2(A-\bar{B})$ and sub-bands corresponding to individual K values may be identified. At the outer extremity, as K gets large, the spacing approaches $2[(1+\xi)A-\bar{B}]=16$ cm^{-1}, from which $\xi\approx 0.4$. To find the "best" K assignment the combination differences

$$\Delta\nu^{\text{sub}} = \nu^{\text{sub}}(+,+) - \nu^{\text{sub}}(-,-)$$

were found for various choices of K, and the left-hand side of the following equation

$$\left[\frac{\Delta\nu^{\text{sub}}}{2} - 2K(A''-\bar{B}'')\right]^2 = \left(\frac{\nu_5-\nu_6}{2}\right)^2 + 4A'^2\xi^2K^2$$

plotted against K^2. The slope is known approximately from rough values of A' and ξ and the numbering scheme that agreed with this slope was chosen.

The last equation and the combination sum

$$\frac{\nu^{\text{sub}}(+,+)+\nu^{\text{sub}}(-,-)}{2} = \frac{\nu_5+\nu_6}{2} + \xi^2A' - (A''-\bar{B}'') + [(A'-\bar{B}')-(A''-\bar{B}'')]K^2 \quad (\text{for } K\geq 2)$$

were each subjected to a least squares treatment in K^2. This led to

$$\nu_{5,6}{}^{\text{sub}} = 1052.9 \pm 10.960K \pm (272.2+26.70K^2)^{\frac{1}{2}} - 0.0032K^2,$$

from which the calculated frequencies of Table III are obtained. The numerical values in this equation may be varied somewhat and still fit the observed frequencies almost as well. For example, the value of $A''-\bar{B}''$ used in the equation with $\Delta\nu^{\text{sub}}$ is assumed to be 5.480 cm^{-1} [14] and may be varied slightly to cause a small change in $\nu_5-\nu_6$. The above analysis yields values for ν_5 and ν_6 of 1040.8 and 1073.8 cm^{-1} (but fails to distinguish between them), and $\xi=0.394$. These quantities, especially ξ, are somewhat dependent upon the value assumed for A' (6.55 cm^{-1}, which arises from calculation of the molecular geometry and is probably correct within ± 0.05 cm^{-1}).

The reliability of the values of ν_5 and ν_6 resulting from this analysis is rather less than for the other fundamentals. This is also true of the Nielsen results for the Coriolis-coupled bands in H_2CO and particularly in D_2CO, where no rotational analysis was made.

Sum and product rules for isotopic species which make use of the known frequencies of the other two formaldehydes may be used to distinguish between ν_5 and ν_6 in HDCO. Both the Decius-Wilson[15] and Bern-

TABLE III. Principal peaks in the ν_5, ν_6 band.

K (emission nomenclature)[a]	Observed frequency	Calculated frequency $\Delta K=+1$ +state	Observed frequency	Calculated frequency $\Delta K=-1$ −state
	1062.2		1055.6	
	1073.9		1039.7	
1	1082.0	1081.1	(1021.5)	1024.6
2	1093.2	1094.3	1011.3	1011.5
3	1107.6	1108.4	998.2	997.3
4	1122.6	1123.1	983.5	982.6
5	1138.4	1138.3	968.4	967.4
6	1154.0	1153.7	951.6	951.9
7	1169.4	1169.2	935.8	936.3
8	(1183.4)	1184.9	919.4	920.5
9			(902.9)	904.6
10			(887.7)	888.7
11			(872.1)	872.7

[a] The K refers to the excited state.
Mean deviation (excluding parenthesized frequencies) is ± 0.63 cm^{-1}.

[14] This value was a preliminary one. Use of 5.470 cm^{-1} would have been more consistent, but would change the parameters only slightly.

[15] J. C. Decius and E. B. Wilson, Jr., J. Chem. Phys. **19**, 1409 (1951).

TABLE IV. Rotational Raman shifts for HDCO.

K	$\Delta\nu$(cm^{-1})[a]	$\Delta\nu/4(K+1)$
4	(110.0)	5.50
5	131.4	5.48
6	152.4	5.44
7	174.8	5.46
8	196.1	5.45
9	(217.4)	5.44
10	(239.2)	5.44

[a] The wave number shifts are the mean for Stokes and anti-Stokes lines, except the values in brackets which are for the Stokes' lines only.

stein-Pullin[16] sum rules predict a somewhat larger value for ν_6 than for ν_5. The Teller-Redlich product rule, applied to the H_2CO frequencies assigned by Nielsen, gives a similar result. For this reason, the assignment $\nu_6=1074$ cm^{-1} and $\nu_5=1041$ cm^{-1} is more probable than the reverse.[17]

The observed rotational Raman spectrum consists of a series of widely spaced lines extending to about 200 cm^{-1} on either side of the exciting line, superimposed on a strong continuum. The spectrum is satisfactorily explained by the accidentally symmetric top approximation with the intense lines corresponding to transitions $\Delta J=0$, $\Delta K=+2$. For this case, the wave number shifts from the exciting line are given by $\Delta\nu=4(A''-\bar{B}'')(K+1)$ where centrifugal and asymmetry effects are neglected, since the accuracy of measurement (±1 cm^{-1}) does not warrant such refinement. Seven Stokes and four anti-Stokes lines were used to evaluate $A''-\bar{B}''$, as indicated in Table IV. The average value is 5.46 ± 0.04 cm^{-1} which is in good agreement with the infrared value resulting from the ν_1 analysis (5.47 ± 0.03 cm^{-1}).

The continuum in the neighborhood of the exciting line is probably due to unresolved R and S branches ($\Delta J=+1, +2$, $\Delta K=0$), as well as to overexposure of the exciting line.

GEOMETRY OF THE FORMALDEHYDE MOLECULE

Dieke and Kistiakowsky[4] (D. and K.) evaluated the moments of inertia (of which only two are independent) for the ground state of H_2CO from an analysis of ultraviolet bands. Their results are in excellent agreement with the values obtained from recent microwave data.[5] Two independent moments of inertia, however, provide only two of the three relations required to determine completely the geometry of formaldehyde, that is, $r_{CH}{}^0$, $r_{CO}{}^0$ and the HCH angle θ. D. and K. originally assumed θ to be tetrahedral which leads to the $r_{CH}{}^0$ and $r_{CO}{}^0$ values given in the first line of Table V. The last column of the table gives the value of $(A''-\bar{B}'')$ for HDCO calculated from these dimensions. In a similar manner, several molecular models can be obtained by assuming a value for one of the dimensions and then calculating the other two from the D. and K. results. For example, the value of $r_{CO}=1.213$A, obtained from electron diffraction[18] of H_2CO, leads to the results shown in the second line of Table V. Since the HCH group in formaldehyde is rather similar to that in ethylene or ketene, it is not unreasonable to assume either a value of 1.071A for $r_{CH}{}^0$ (line 3 of the table) or 120° for θ (line 4). (The values of $r_{CH}{}^0$ and θ^0 in ethylene are 1.071A, 119°55′ [19] and in ketene[20] 1.075A, 122°, respectively.)

Since the axis of least moment of inertia in HDCO makes an angle of only about 5° with the C=O axis, the value of $(A''-\bar{B}'')$ is not very sensitive to changes in geometry. That is, an uncertainty in the value of $(A''-\bar{B}'')$ for HDCO (assuming errors in the D. and K. results to be negligible in comparison), leads to a rather large range of values for $r_{CH}{}^0$, $r_{CO}{}^0$, and θ^0. For the value $(A''-\bar{B}'')=5.47\pm0.03$ cm^{-1} obtained in this investigation the corresponding values of the geometric parameters are given in line 5 of Table V together with their accompanying uncertainties. Although the geometry is not fixed within very narrow limits, the present results suggest that the "equilibrium" value for the CH bond distance (1.12 ± 0.01A) given by Lawrance and Strandberg[5] is somewhat high.

We wish to express our thanks to Dr. L. C. Leitch for supplying the paraformaldehyde-d_1, and Dr. G. Herzberg and Dr. B. R. Chinmayanandam for helpful discussions.

APPENDIX

Four vibrational bands of H_2CO were found in the Raman spectrum of the vapor. They are identified as follows: $\nu_1(a_1)=2781.6$ cm^{-1} (sharp, strong); $\nu_2(a_1)=1742.3$ cm^{-1} (sharp, weak); $\nu_3(a_1)=1499.7$ cm^{-1} (sharp, medium); $\nu_4(b_1)=2866$ cm^{-1} (broad, weak). The frequencies are the average measurements from two plates, and are probably accurate to ±3 cm^{-1}. The accuracy of ν_1 is lower (±5 cm^{-1}) since this line is blended with the much weaker Hg 4962 line, and the error in the measurement of the broad band ν_4 is about ±10 cm^{-1}. The Raman frequencies are in good agree-

TABLE V. Ground state parameters of formaldehyde.

	Assumed	Calculated[a] $r_{CH}{}^0$(A)	$r_{CO}{}^0$(A)	θ^0	$(A''-\bar{B}'')_{CHDO}$
1.	$\theta=109°27'$	1.15	1.185		5.60
2.	$r_{CO}{}^0=1.213$A	1.097		118°39′	5.49$_9$
3.	$r_{CH}{}^0=1.071$A		1.225	123°26′	5.48$_2$
4.	$\theta^0=120°$	1.090	1.217		5.49$_2$
5.	$(A''-\bar{B}'')=5.47$	1.060	1.230	125°48′	
	±0.03 cm^{-1}	±0.038	∓0.017	$\mp7°0'$	

[a] From the assumed parameter and two of the Dieke and Kistiakowsky moments of inertia.

[16] H. J. Bernstein and A. D. E. Pullin, J. Chem. Phys. **21**, 2188 (1953).

[17] In the symmetrical formaldehydes, however, $\nu_5>\nu_6$.

[18] Stevenson, duValle, and Schomaker, J. Am. Chem. Soc. **61**, 2508 (1939).

[19] Reference 10, p. 439.

[20] H. R. Johnson and M. W. P. Strandberg, J. Chem. Phys. **20**, 687 (1952).

ment with the infrared values given by Ebers and Nielsen.[3] Also, the observation of only one strong Raman line in the 3000-cm^{-1} region establishes the frequency of ν_1, and confirms the earlier assignment of two strong infrared bands at 2780 and 2973 cm^{-1} as ν_1 and $2\nu_3$, respectively.

The Raman spectrum of H_2CO (unlike that of HDCO) was superimposed on an intense background which precluded the observation of all but the strongest Raman lines. This background is partly due to the fluorescence spectrum of H_2CO excited by the strong mercury lines in the region λ3650. In the initial attempt to photograph the H_2CO Raman spectrum the $NaNO_2$ filter was not used, and in this way the fluorescence spectrum was obtained superimposed on a strong continuum. It was not possible to quench the fluorescence spectrum completely even with a 1 cm thickness of saturated $NaNO_2$ filter solution.

THE JOURNAL OF CHEMICAL PHYSICS VOLUME 22, NUMBER 2 FEBRUARY, 1954

The Infrared Spectrum and Molecular Constants of DBr*†

FRED L. KELLER AND ALVIN H. NIELSEN
Department of Physics, The University of Tennessee, Knoxville, Tennessee

(Received September 15, 1953)

High-dispersion measurements have been made for the first time on the fundamental, first overtone, and second overtone infrared vibrational bands of DBr. Path lengths from 40 cm to 17 m were used with pressures ranging from 90 mm to 460 mm. The isotopic splitting of the rotation lines was measured and molecular constants determined for both isotopic species, DBr^{79} and DBr^{81}. The principal constants for DBr^{79} are $\omega_e=1885.33$ K, $x_e\omega_e=22.73$ K, $y_e\omega_e=-0.0106$ K, $B_e=4.290_8$ K, $\alpha_e=0.083_9$ K, $D_e=9.6_4\times10^{-5}$ K, $\beta=-2.2\times10^{-6}$ K. The principal constants for DBr^{81} are $\omega_e=1884.75$ K, $x_e\omega_e=22.72$ K, $y_e\omega_e=-0.0106$ K, $B_e=4.287_6$ K, $\alpha_e=0.083_8$ K, $D_e=9.5_9\times10^{-5}$ K, $\beta=-2.2\times10^{-6}$ K.

I. INTRODUCTION

THE infrared vibration-rotation bands of HBr have been examined by a number of investigators, notably Imes,[1] who observed the fundamental ($v=1-0$) band; Plyler and Barker,[2] who measured the fundamental and first overtone ($v=2-0$) bands; Naudé and Verleger,[3] who photographed several lines in the third overtone ($v=4-0$) band; and Thompson, Williams, and Callomon,[4] who very recently re-examined the fundamental band. Only the last two[3,4] achieved resolutions sufficient to permit detailed analyses to be made of the separate contributions of the isotopic molecules HBr^{79} and HBr^{81}. A search of the literature reveals no references to infrared measurements on the isotopic molecules DBr^{79} and DBr^{81}.

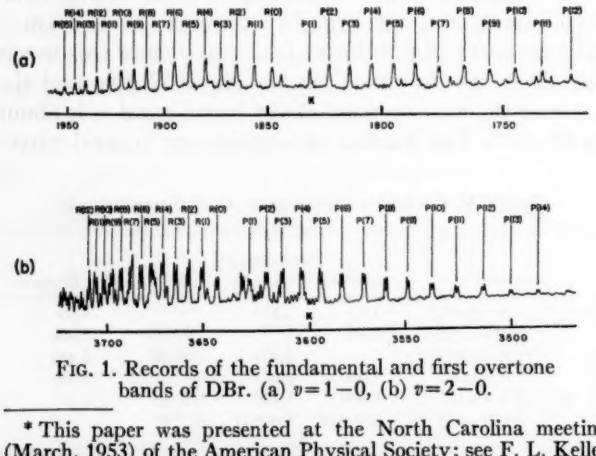

FIG. 1. Records of the fundamental and first overtone bands of DBr. (a) $v=1-0$, (b) $v=2-0$.

The present paper concerns recent high-dispersion measurements which have been made on the fundamental, first overtone, and second overtone vibration-rotation bands of DBr. The isotopic separation of the rotational lines has been measured and molecular constants determined for both isotopic species, DBr^{79} and DBr^{81}. These constants are shown to be in good agreement with the constants for HBr recently obtained by Thompson *et al.*[4]

II. EXPERIMENTAL DETAILS

All measurements on the DBr bands were made with The University of Tennessee automatically recording, high-dispersion, prism-grating spectrometer.[5] As the isotopic separation of DBr^{79} and DBr^{81} was quite small (about 0.5 K in the fundamental band), high resolving power was of particular importance in this investigation, necessitating the use of the narrowest possible slit widths.

A 7200 lines-per-inch echelette grating was used in conjunction with a Golay pneumatic detector for

* This paper was presented at the North Carolina meeting (March, 1953) of the American Physical Society; see F. L. Keller and A. H. Nielsen, Phys. Rev. **91**, 235(A) (1953).

† Submitted in partial fulfillment of the requirements for the degree of Master of Science in Physics at The University of Tennessee.

[1] E. S. Imes, Astrophys. J. **50**, 251 (1919).

[2] E. K. Plyler and E. F. Barker, Phys. Rev. **44**, 984 (1933).

[3] S. H. Naudé and H. Verleger, Proc. Phys. Soc. (London) **A63**, 470 (1950).

[4] Thompson, Williams, and Callomon, Acta Spectrochim. **5**, 313 (1952).

[5] A. H. Nielsen, J. Tenn. Acad. Sci. **22**, No. 4, 241 (1947).

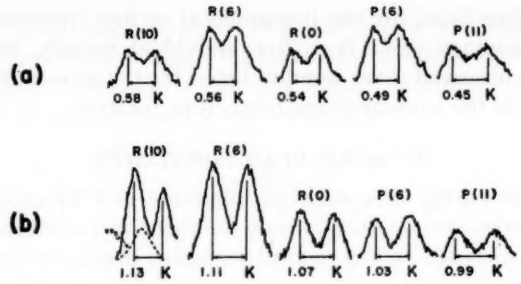

FIG. 2. Representative lines of the fundamental and first overtone bands of DBr, showing the isotopic splitting. (a) $v=1-0$, (b) $v=2-0$.

making measurements on the fundamental band. The absorption cell was a 40-cm glass cell with rocksalt windows and was used at pressures of 90–150 mm Hg. The slits included a spectral interval of 0.23 K.

For measurements on the first and second overtone bands, a 15 000 lines-per-inch echelette grating was used with a PbS photoconductive detector. To obtain sufficiently strong absorption for the weak overtone bands it was necessary to use a 60-cm multiple reflection cell constructed after a plan by White.[6] The cell was adjusted for 28 traversals resulting in a total absorption path of approximately 17 meters. In making observations on the first overtone band pressures of 220–460 mm Hg were used and the slits were adjusted to include a spectral interval of 0.5 K. For the second overtone band the pressure was 460-mm Hg and the slits included an interval of 0.8 K.

All the DBr bands observed in this investigation were overlapped by regions of strong atmospheric absorption. The fundamental and second overtone bands were overlapped by the 6.2μ and 1.8μ water vapor bands, respectively, while the first overtone band was overlapped by the 2.7μ water band. In addition, the first overtone coincided with the 2.69μ and 2.77μ CO_2 bands. The interference by atmospheric absorption was appreciably reduced by means of trays of P_2O_5 and Ascarite placed in the spectrometer. After the trays were inserted, the spectrometer was carefully sealed, flushed with dry N_2 gas, and allowed to dry for several days before records were made of the bands.

The gratings were calibrated by observing standard mercury lines in many orders. In addition, Benedict and Plyler[7] have recently reported very accurate wave numbers for the lines of the two CO_2 bands which overlap the DBr first overtone band. These interspersed CO_2 lines provided further internal checks on the line wave numbers reported in this investigation. All wave numbers given in this paper have been reduced to vacuum.

The sample of deuterium bromide was prepared by adding heavy water to PBr_3 in vacuum. The resulting gas was condensed in a cold trap and then fractionally distilled into the cell.

[6] J. U. White, J. Opt. Soc. Am. **32**, 285 (1942).
[7] W. S. Benedict and E. K. Plyler, J. Research Natl. Bur. Standards **46**, 246 (1952).

III. EXPERIMENTAL RESULTS

Records of the fundamental and first overtone bands of DBr are shown in Fig. 1. Because these records were made as preliminary runs in which the grating was turned at a much greater speed than was actually used for making measurements, the isotopic separation of the rotation lines is not clearly shown. The background CO_2 lines which were used as an aid in the calibration procedure may be seen on the record of the first overtone band. Figure 2 shows reproductions of representative lines of the fundamental and first overtone bands made at the normal speed for measurement. The isotopic splitting is clearly demonstrated and the two components are seen to be of approximately equal intensity. This is to be expected because the percent abundances of the stable isotopes, Br^{79} and Br^{81}, are 50.6 and 49.4, respectively.

The second overtone band (not shown) was also completely resolved into separate contributions from the two isotopic molecules; however, because of the limited amount of gas available, this band was extremely weak.

Tables I to VI inclusive give the wave numbers of the observed lines of DBr^{79} and DBr^{81} for each of the bands investigated. The line designations are given in column 1, the observed wave numbers in column 2, the wave

TABLE I. Wave numbers (vacuum) of the observed rotational lines in the $\sigma(1-0)$ band of DBr^{79}.

Line assignment	σ(obs)	σ(calc)	$\Delta\sigma$
$R(16)$	1956.96	1956.94	0.02
$R(15)$	1951.62	1951.56	0.06
$R(14)$	1946.03	1945.99	0.04
$R(13)$	1940.20	1940.22	−0.02
$R(12)$	1934.26	1934.26	0.00
$R(11)$	1928.05	1928.10	−0.05
$R(10)$	1921.75	1921.75	0.00
$R(9)$	1915.18	1915.21	−0.03
$R(8)$	1908.48	1908.49	−0.01
$R(7)$	1901.57	1901.58	−0.01
$R(6)$	1894.48	1894.48	0.00
$R(5)$	1887.20	1887.20	0.00
$R(4)$	1879.74	1879.75	−0.01
$R(3)$	1872.07	1872.11	−0.04
$R(2)$	1864.26	1864.30	−0.04
$R(1)$	1856.30	1856.31	−0.01
$R(0)$	1848.19	1848.15	0.04
$P(1)$	1831.31	1831.32	−0.01
$P(2)$	1822.69	1822.66	0.03
$P(3)$	1813.80	1813.83	−0.03
$P(4)$	1804.85	1804.85	0.00
$P(5)$	1795.74	1795.70	0.04
$P(6)$	1786.39	1786.40	−0.01
$P(7)$	1776.94	1776.95	−0.01
$P(8)$	1767.35	1767.34	0.01
$P(9)$	1757.60	1757.59	0.01
$P(10)$	1747.67	1747.69	−0.02
$P(11)$	1737.66	1737.65	0.01
$P(12)$	1727.43	1727.47	−0.04

TABLE II. Wave numbers (vacuum) of the observed rotational lines in the $\sigma(1-0)$ band of DBr^{81}.

Line assignment	σ(obs)	σ(calc)	$\Delta\sigma$
$R(16)$	1956.34	1956.34	0.00
$R(15)$	1951.00	1950.97	0.03
$R(14)$	1945.42	1945.40	0.02
$R(13)$	1939.58	1939.63	−0.05
$R(12)$	1933.63	1933.67	−0.04
$R(11)$	1927.51	1927.51	0.00
$R(10)$	1921.16	1921.17	−0.01
$R(9)$	1914.67	1914.63	0.04
$R(8)$	1907.87	1907.91	−0.04
$R(7)$	1900.99	1901.00	−0.01
$R(6)$	1893.89	1893.91	−0.02
$R(5)$	1886.65	1886.64	0.01
$R(4)$	1879.21	1879.19	0.02
$R(3)$	1871.55	1871.56	−0.01
$R(2)$	1863.74	1863.75	−0.01
$R(1)$	1855.76	1855.77	−0.01
$R(0)$	1847.63	1847.61	0.02
$P(1)$	1830.82	1830.80	0.02
$P(2)$	1822.17	1822.14	0.03
$P(3)$	1813.34	1813.33	0.01
$P(4)$	1804.35	1804.35	0.00
$P(5)$	1795.26	1795.21	0.05
$P(6)$	1785.93	1785.91	0.02
$P(7)$	1776.47	1776.47	0.00
$P(8)$	1766.87	1766.87	0.00
$P(9)$	1757.15	1757.12	0.03
$P(10)$	1747.22	1747.23	−0.01
$P(11)$	1737.18	1737.20	−0.02
$P(12)$	1727.01	1727.03	−0.02

numbers computed from the new constants in column 3, and the differences between observed and calculated wave numbers in column 4. Each observed wave number listed for the fundamental or first overtone is the average value from five individual records, while each observed wave number listed for the second overtone is the average value from three records.

TABLE III. Wave numbers (vacuum) of the observed rotational lines in the $\sigma(2-0)$ band of DBr^{79}.

Line assignment	σ(obs)	σ(calc)	$\Delta\sigma$
$R(13)$	3717.00	3716.98	0.02
$R(12)$	3713.34	3713.34	0.00
$R(11)$	3709.38	3709.35	0.03
$R(10)$	3704.99	3704.99	0.00
$R(9)$	3700.26	3700.29	−0.03
$R(8)$	3695.23	3695.23	0.00
$R(7)$	3689.84	3689.83	0.01
$R(6)$	3684.10	3684.07	0.03
$R(5)$	3677.96	3677.96	0.00
$R(4)$	3671.51	3671.51	0.00
$R(3)$	3664.69	3664.71	−0.02
$R(2)$	3657.56	3657.57	−0.01
$R(1)$	3650.11	3650.09	0.02
$R(0)$	3642.26	3642.26	0.00
$P(1)$	3625.59	3625.60	−0.01
$P(2)$	3616.75	3616.77	−0.02
$P(3)$	3607.64	3607.61	0.03
$P(4)$	3598.11	3598.12	−0.01
$P(5)$	3588.33	3588.31	0.02
$P(6)$	3578.21	3578.17	0.04
$P(7)$	3567.69	3567.71	−0.02
$P(8)$	3556.93	3556.93	0.00
$P(9)$	3545.89	3545.84	0.05
$P(10)$	3534.46	3534.44	0.02
$P(11)$	3522.74	3522.73	0.01
$P(12)$	3510.77	3510.72	0.05
$P(13)$	3498.33	3498.40	−0.07

IV. MOLECULAR CONSTANTS

The energy of a diatomic molecule in a vibrational state denoted by the quantum number v and a rotational state denoted by the quantum number J may be represented to a very good approximation by the equation

$$E/hc(\mathrm{K}) = E_e/hc + \omega_e(v+\tfrac{1}{2}) - x_e\omega_e(v+\tfrac{1}{2})^2 + y_e\omega_e(v+\tfrac{1}{2})^3 + B_vJ(J+1) - D_vJ^2(J+1)^2, \quad (1)$$

TABLE IV. Wave numbers (vacuum) of the observed rotational lines in the $\sigma(2-0)$ band of DBr^{81}.

Line assignment	σ(obs)	σ(calc)	$\Delta\sigma$
$R(14)$	3719.07	3719.13	−0.06
$R(13)$	3715.88	3715.85	0.03
$R(12)$	3712.16	3712.21	−0.05
$R(11)$	3708.25	3708.22	0.03
$R(10)$	3703.88	3703.87	0.01
$R(9)$	3699.15	3699.17	−0.02
$R(8)$	3694.12	3694.12	0.00
$R(7)$	3688.73	3688.72	0.01
$R(6)$	3682.97	3682.96	0.01
$R(5)$	3676.86	3676.86	0.00
$R(4)$	3670.40	3670.41	−0.01
$R(3)$	3663.60	3663.62	−0.02
$R(2)$	3656.48	3656.48	0.00
$R(1)$	3649.07	3649.00	0.07
$R(0)$	3641.21	3641.19	0.02
$P(1)$	3624.55	3624.54	0.01
$P(2)$	3615.72	3615.72	0.00
$P(3)$	3606.55	3606.56	−0.01
$P(4)$	3597.08	3597.08	0.00
$P(5)$	3587.27	3587.27	0.00
$P(6)$	3577.16	3577.14	0.02
$P(7)$	3566.66	3566.69	−0.03
$P(8)$	3555.88	3555.92	−0.04
$P(9)$	3544.89	3544.83	0.06
$P(10)$	3533.49	3533.44	0.05
$P(11)$	3521.76	3521.74	0.02
$P(12)$	3509.73	3509.73	0.00
$P(13)$	3497.39	3497.42	−0.03

where

$$\left.\begin{aligned} B_v &= B_e - \alpha_e(v+\tfrac{1}{2}) \\ \text{and} \quad D_v &= D_e + \beta_e(v+\tfrac{1}{2}). \end{aligned}\right\} \quad (2)$$

E_e is a constant energy term which is not affected by a change in v or J. The constant ω_e represents the harmonic vibrational wave number for infinitesimal amplitudes, and $x_e\omega_e$ and $y_e\omega_e$ represent the second and third power anharmonic vibrational constants, respectively. B_e is the equilibrium rotational constant, $h/8\pi^2cI_e$; D_e is the vibrationless centrifugal stretching constant; and finally, α_e and β_e are small constants which represent the vibration-rotation interaction energy. The wave numbers of the permitted spectral lines may be determined by using Eq. (1) with the Bohr frequency condition and the selection rules $\Delta v = 1, 2,$ etc.; $\Delta J = \pm 1$.

The wave numbers of the R and P lines in a vibration-rotation band in which the transition has been from the ground vibrational state to a higher vibrational state may be represented by the relations

$$\left.\begin{matrix} R(J-1) \\ P(J) \end{matrix}\right\} = \sigma(v'-0) \pm (B_{v'}+B_0)J + [(B_{v'}-B_0)-(D_{v'}-D_0)]J^2 \mp 2(D_{v'}+D_0)J^2-(D_{v'}-D_0)J^4, \quad J=1, 2, \cdots, \quad (4)$$

where

$$\sigma(v'-0)=\omega_e v'-x_e\omega_e(v'^2+v')+y_e\omega_e[(v'+\tfrac{1}{2})^3-\tfrac{1}{8}] \quad (5)$$

is the band center of the transition and the number designating the line is the J value of the ground vibrational state.

TABLE V. Wave numbers (vacuum) of the observed rotational lines in the $\sigma(3-0)$ band of DBr^{79}.

Line assignment	σ(obs)	σ(calc)	$\Delta\sigma$
$R(8)$	5435.64	5435.87	−0.23
$R(7)$	5431.85	5431.90	−0.05
$R(6)$	5427.42	5427.43	−0.01
$R(5)$	5422.32	5422.45	−0.13
$R(4)$	5416.98	5416.97	0.01
$R(3)$	5410.91	5410.98	−0.07
$R(2)$	5404.53	5404.50	0.03
$R(1)$	5397.63	5397.50	0.13
$R(0)$	5390.00	5390.01	−0.01
$P(1)$		5373.51	
$P(2)$	5364.60	5364.50	0.10
$P(3)$	5354.84	5354.99	−0.15
$P(4)$	5344.77	5344.98	−0.21
$P(5)$	5334.47	5334.47	0.00
$P(6)$	5323.52	5323.45	0.07
$P(7)$	5312.17	5311.93	0.24

The differences in the extra nuclear electric fields of isotopic molecules are usually negligible; therefore, if ρ is used to denote $(\mu/\mu^i)^{\frac{1}{2}}$, where μ represents the reduced mass of the lighter isotopic molecule and μ^i the reduced mass of the heavier molecule, the ratio of the values of each molecular constant for the two isotopic molecules is a simple power of ρ. The complete result is summarized in Table VII.

Rotational

Because the measurements on the fundamental and first overtone bands were much more accurate than those on the second overtone band, only the wave numbers of the fundamental and first overtone lines were used in computing the accurate values of the molecular constants of DBr. The determination of the rotational constants was accomplished by finding linear relationships involving the wave numbers of the P and R lines of each band such that the values of the fundamental constants emerged as intercepts and slopes of straight lines. The combination relations used in this analysis were

TABLE VI. Wave numbers (vacuum) of the observed rotational lines in the $\sigma(3-0)$ band of DBr^{81}.

Line assignment	σ(obs)	σ(calc)	$\Delta\sigma$
$R(8)$	5434.29	5434.41	−0.12
$R(7)$	5430.23	5430.44	−0.21
$R(6)$	5425.72	5425.97	−0.25
$R(5)$	5420.90	5420.99	−0.09
$R(4)$	5415.64	5415.51	0.13
$R(3)$	5409.56	5409.52	0.04
$R(2)$	5403.08	5403.04	0.04
$R(1)$	5396.07	5396.04	0.03
$R(0)$	5388.44	5388.55	−0.11
$P(1)$		5372.05	
$P(2)$	5363.06	5363.04	0.02
$P(3)$	5353.11	5353.53	−0.42
$P(4)$	5343.52	5343.52	0.00
$P(5)$	5332.91	5333.01	−0.10
$P(6)$	5322.05	5321.99	0.06
$P(7)$	5310.59	5310.47	0.12

$$\frac{[R(J-1)-P(J+1)]}{2(2J+1)} = (B_0-\tfrac{3}{2}D_0)-\tfrac{1}{2}D_0(2J+1)^2, \quad (6)$$

$$\frac{[R(J)-P(J)]}{2(2J+1)} = (B_{v'}-\tfrac{3}{2}D_{v'})-\tfrac{1}{2}D_{v'}(2J+1)^2, \quad (7)$$

and

$$\tfrac{1}{2}[R(J-1)+P(J)]+v'\beta_e J^4=\sigma(v'-0)-v'\alpha_e J^2. \quad (8)$$

The combination relation expressed by Eq. (6) was first applied to the data for the fundamental and first overtone bands of DBr^{79}. When the left side of Eq. (6) was plotted *versus* $(2J+1)^2$, as shown in Fig. 3, a straight line resulted which yielded the values of B_0 and D_0. Since both bands contributed to the values of B_0 and D_0, these ground vibrational state values of B and D should be the most accurately determined constants.

Next, Eq. (7) was applied in the same manner to each of the two DBr^{79} bands. The resulting plots, shown in Fig. 4, yielded the values of B_1, D_1, B_2, and D_2. With these values of B_v and D_v it was possible to use Eqs. (2) and (3) to determine B_e, D_e, and β_e. The value of β_e was then substituted into Eq. (8) and the left side of this equation, plus an appropriate constant times J^2,

TABLE VII. Mass dependence of the molecular constants.

Constant	Mass factor	Ratio
ω_e	$\mu^{-1/2}$	ρ
$x_e\omega_e$	μ^{-1}	ρ^2
$y_e\omega_e$	$\mu^{-3/2}$	ρ^3
B_e	μ^{-1}	ρ^2
α_e	$\mu^{-3/2}$	ρ^3
D_e	μ^{-2}	ρ^4
β_e	$\mu^{-5/2}$	ρ^5

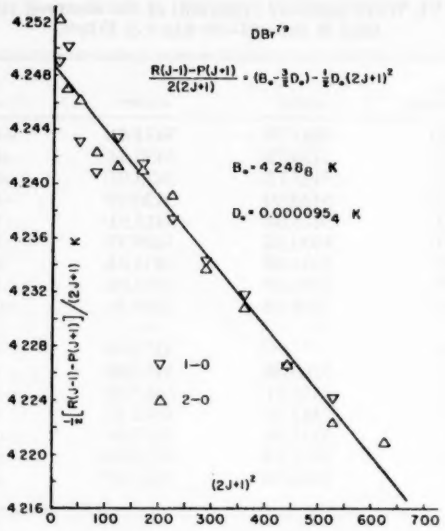

FIG. 3. Plot of $\frac{1}{2}[R(J-1)-P(J+1)]/(2J+1)$ *versus* $(2J+1)^2$ giving values of B_0 and D_0 for DBr^{79}.

was plotted *versus* J^2 for each of the DBr^{79} bands, as shown in Fig. 5. From these plots the values of $\sigma(1-0)$, $\sigma(2-0)$, and α_e were obtained.

The entire procedure outlined above was then repeated for the fundamental and first overtone bands of DBr^{81}. The rotational constants obtained for both of the isotopic molecules are listed in Table VIII. The band centers are given in Table IX.

If the atomic mass of deuterium given by Mattauch[8] is used with the masses of the bromine isotopes reported by Ogata,[9] the following values are obtained for the

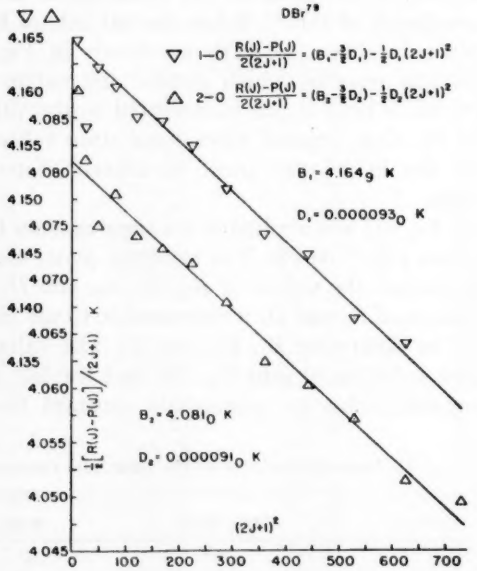

FIG. 4. Plots of $\frac{1}{2}[R(J)-P(J)]/(2J+1)$ *versus* $(2J+1)^2$ giving values of B_1, B_2, D_1, and D_2 for DBr^{79}.

[8] J. Mattauch, *Nuclear Physics Tables* (Interscience Publishers, Inc., New York, 1946), Table IV, p. 126.
[9] K. Ogata, Phys. Rev. **75**, 200 (1949).

reduced masses of DBr^{79} and DBr^{81}, and for ρ_{DBr}:

$$\mu_{DBr^{79}}=1.964582, \quad \mu_{DBr^{81}}=1.965789,$$
$$\text{and} \tag{9}$$
$$\rho_{DBr}=(\mu_{DBr^{79}}/\mu_{DBr^{81}})^{\frac{1}{2}}=0.9996929.$$

From Table VII it is seen that the ratio B_e^{79}/B_e^{81} should equal $1/(\rho_{DBr})^2$ or 1.00062. The experimental value of B_e^{79}/B_e^{81} is 1.000_7, which agrees within experimental error. The number of significant figures in the other rotational constants is too small to permit additional checks on the mass ratio.

The third and fifth columns of Table VIII give the values of the rotational constants of DBr which result when the reduced mass conversions of Table VII are applied to the HBr constants determined by Thompson *et al.*[4] The following values of μ and ρ were used in

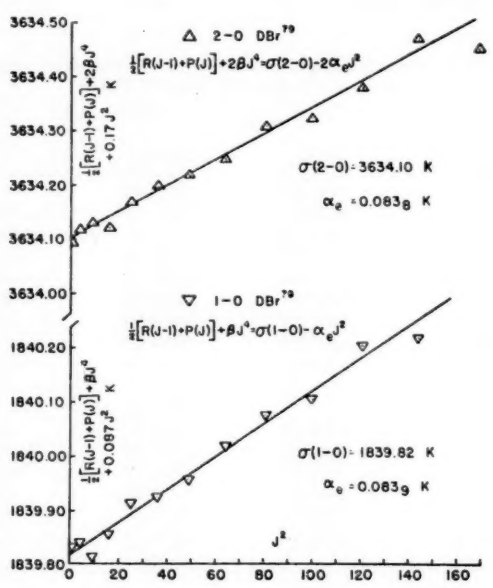

FIG. 5. Plots of $\frac{1}{2}[R(J-1)+P(J)]+v'\beta J^4$ *versus* J^2 giving values of $\sigma(1-0)$, $\sigma(2-0)$, and α_e for DBr^{79}.

applying the conversions:

$$\mu_{HBr^{81}}=0.9957282, \quad \mu_{HBr^{79}}=0.9954183,$$
$$\rho^{81}=\left[\frac{\mu_{HBr^{81}}}{\mu_{DBr^{81}}}\right]^{\frac{1}{2}}=0.7117083,$$
$$\text{and} \tag{10}$$
$$\rho^{79}=\left[\frac{\mu_{HBr^{79}}}{\mu_{DBr^{79}}}\right]^{\frac{1}{2}}=0.7118162.$$

The values obtained from the two investigations appear to be in quite good agreement.

When the values of the constants listed in Table VIII and the band centers listed in Table IX are substituted into Eq. (4), the following equations are obtained for the wave numbers of the lines of the fundamental and

TABLE VIII. Rotational constants (kaysers) of DBr^{79} and DBr^{81}.

Constant	DBr^{79} Observed	DBr^{79} Calc from HBr^{79}*	DBr^{81} Observed	DBr^{81} Calc from HBr^{81}*
B_e	4.290_8	4.291_1	4.287_6	4288_5
α_e	0.083_9	0.083_4	0.083_8	0.083_4
D_e	9.64×10^{-5}	$10.0_2\times10^{-5}$	$9.5_9\times10^{-5}$	$10.0_2\times10^{-5}$
β_e	-2.2×10^{-6}	-1.4×10^{-6}	-2.2×10^{-6}	-1.4×10^{-5}
I_e	$6.521_7\times10^{-40}$ g-cm^2		$6.526_5\times10^{-40}$ g-cm^2	
r_e	1.414_2A		1.414_4A	

* From 1−0 of HBr by Thompson *et al.*

first overtone bands, respectively:

DBr^{79} fundamental (1−0) band,

$$\left.\begin{matrix}R(J-1)\\P(J)\end{matrix}\right\}=1839.82\pm8.413_7J-0.0839J^2\mp0.000376_8J^3+0.000002_2J^4; \quad (11)$$

DBr^{81} fundamental (1−0) band,

$$\left.\begin{matrix}R(J-1)\\P(J)\end{matrix}\right\}=1839.29\pm8.407_4J-0.0838J^2\mp0.000374_2J^3+0.000002_2J^4; \quad (12)$$

DBr^{79} first overtone (2−0) band,

$$\left.\begin{matrix}R(J-1)\\P(J)\end{matrix}\right\}=3634.10\pm8.329_8J-0.1678J^2\mp0.000372_8J^3+0.000004_4J^4; \quad (13)$$

and DBr^{81} first overtone (2−0) band,

$$\left.\begin{matrix}R(J-1)\\P(J)\end{matrix}\right\}=3633.03\pm8.323_5J-0.1677J^2\mp0.000369J^3+0.000004_4J^4. \quad (14)$$

These equations were used to calculate the wave numbers listed in the third columns of Tables I–IV.

When combination relations were applied to the lines of the second overtone bands of DBr, the values of the constants obtained were found to be in agreement with those listed in Table VIII, within the accuracy of the measurements. The following equations result when the values of the constants are substituted into Eq. (4):

DBr^{79} second overtone (3−0) band,

$$\left.\begin{matrix}R(J-1)\\P(J)\end{matrix}\right\}=5382.01\pm8.250J-0.2517J^2; \quad (15)$$

TABLE IX. Vibrational constants (kaysers) of DBr^{79} and DBr^{81}.

Constant	DBr^{79}	DBr^{81}
$\sigma(1-0)$	1839.82	1839.29
$\sigma(2-0)$	3634.10	3633.03
ω_e	1885.32_7	1884.74_8
$x_e\omega_e$	22.73_2	22.71_8
$y_e\omega_e$	-0.010_6	-0.010_6

and DBr^{81} second overtone (3−0) band

$$\left.\begin{matrix}R(J-1)\\P(J)\end{matrix}\right\}=5380.55\pm8.250J-0.2517J^2. \quad (16)$$

The wave numbers of the lines calculated from these equations are given in the third columns of Tables V and VI.

Vibrational

The fundamental and first overtone band centers of DBr from this investigation were used with Naudé and Verleger's[3] third overtone (4−0) band centers of HBr to determine the vibrational constants ω_e, $x_e\omega_e$, and $y_e\omega_e$. Using these six band centers, together with Eq. (5) and the mass conversions of Table VII, it was possible to write six equations in terms of ω_e, $x_e\omega_e$, and $y_e\omega_e$ of DBr^{81}. The two equations from each band were then added and the resulting three equations were solved for the vibrational constants of DBr^{81}. The vibrational constants of DBr^{79} were obtained by applying mass conversions to the constants of DBr^{81}. The constants obtained in this manner are listed in Table IX.

TABLE X. Band centers (kaysers) of DBr and HBr.[a]

Molecule	Band center assignment	Wave numbers Observed	Calculated	Δ
DBr^{79}	$\sigma(1-0)$	1839.82	1839.83	−0.01
	$\sigma(2-0)$	3634.10	3634.10	0.00
	$\sigma(3-0)$	5382.01	5382.75	−0.74
DBr^{81}	$\sigma(1-0)$	1839.29	1839.28	0.01
	$\sigma(2-0)$	3633.03	3633.03	0.00
	$\sigma(3-0)$	5380.55	5381.18	−0.63
HBr^{79}	$\sigma(1-0)$	2558.76	2558.79	−0.03
	$\sigma(4-0)$	9694.50	9694.50	0.00
HBr^{81}	$\sigma(1-0)$	2558.40	2558.41	−0.01
	$\sigma(4-0)$	9693.15	9693.14	0.01

[a] Observed band centers of $\sigma(1-0)$ of HBr by Thompson, Williams, and Collomon; observed band centers of $\sigma(4-0)$ of HBr by Naudé and Verleger.

Finally, the mass conversions of Table VII were applied to the vibrational constants of DBr in such a manner as to yield values for the vibrational constants of HBr. All of the constants were then used to calculate the band centers of the 1−0, 2−0, and 3−0 bands of DBr, and the 1−0 and 4−0 bands of HBr. The observed and calculated band centers are listed in Table X. The agreement between the observed and calculated band centers of the 1−0 of HBr, which was not used in the determination of the vibrational constants, is seen to be very good. The difference of approximately 0.7 K between the observed and calculated band centers of the 3−0 of DBr is perhaps not unreasonable considering the sources of error affecting measurements on this band.

A Comparative Study of Accommodation Coefficients by the Temperature Jump and Low-Pressure Methods and Thermal Conductivities of He, Ne, and CO_2

LLOYD B. THOMAS AND RALPH C. GOLIKE
Chemical Laboratory, University of Missouri, Columbia, Missouri
(Received August 28, 1953)

The temperature jump and low pressure methods are used to determine the accommodation coefficients of He, Ne, and CO_2 on platinum under conditions as closely identical as compatible with the methods. Agreement is very close for He and for CO_2, giving values centering about 0.176 for He and 0.78 for CO_2. For Ne the results are ambiguous, giving good agreement with one sequence of preparation and giving temperature jump values 25 percent low with another. Variability is correlated with preparation history and variability with time is noted by both methods. Thermal conductivity values of He, Ne, and CO_2 are given and compared briefly with values in the literature.

INTRODUCTION

WE have previously, from this laboratory, expressed concern and discussed reasons for the wide variation in the published values of the thermal accommodation coefficients (A.C.), excluding those for presumably clean surfaces.[1,2] One quite possible contributing reason for this wide variation could be inability of the two prominent methods of determination of the A.C. to agree. Roughly two thirds of the A.C. values in the literature were obtained by the "free molecule" or low-pressure (L.P.) method, utilizing the pressure range in which the thermal conductivity is linear with pressure (usually below 0.05 mm but upper limit determined by filament diameter and the specific gas). The L.P. method is based on theory which becomes very accurate at sufficiently low pressure and if the experimental details are adequately handled seems to be without serious objection. The temperature jump (T.J.) method, which has contributed the other third of the A.C. values, utilizes measurements of thermal conductivity at a series of pressures over which this property of the gas is independent of pressure but, due to the pressure-dependent temperature discontinuity between filament and gas, the apparent conductivity of the cell diminishes as pressure decreases. Theory relating this temperature discontinuity to the A.C. seems to be precariously based. Kennard[3] has outlined the T.J. theory essentially as we and others have applied it and states, page 324, concerning it: "Furthermore, it must not be forgotten that our formula (238a), while probably the best available, is itself subject to some uncertainty." Modern work with the T.J. method begins with Dickins,[4] followed by Archer,[5] Gregory and coworkers,[6,7] and more recently by Grilly, Taylor, and Johnston.[8] All the work is on platinum. There are two or more published values by the T.J. method for He, CO, O_2, H_2, CO_2, and N_2O. Agreement is good (within ± 5 percent of the mean) for the first three, but, five A.C. values for H_2 range from 0.23 to 0.40, the three values for CO_2 are 0.45, 0.64, and 0.78, and the two values for N_2O are 0.61 and 0.76. Agreement of T.J. with L.P. values is good (± 5 percent) for CO and O_2, but the average T.J. value is 30 percent high for H_2, 25 percent low for CO_2, and 150 percent high for He compared to modern probable values by the L.P. method. The lack of agreement between methods for helium in particular (0.50,[4] and 0.53[8] by T.J. and a mean value around 0.2 by L.P.) suggests that the two methods might not yield the same A.C. value, especially since helium could hardly show complications due to its adsorption or to internal heat capacity which conceivably could alter the values obtained in the two pressure ranges. We have thought it important to make a careful comparison of the two methods on the same filament, in the same tube and vacuum system, with gas from the same reservoir and purification system—in short, under as near identical conditions as are consistent with the experimental procedures necessary. We have chosen He, Ne, and CO_2 on platinum for investigation and have devoted most of the work to helium.

EXPERIMENTAL

The tube used is shown in Fig. 1. The filament is of thermocouple grade platinum (Bishop), 0.01255 cm diam and 26.35 cm length, and is accurately located on the axis of a Pyrex tube of 0.398-cm internal radius (0.510-cm external radius) selected for uniformity and straightness. The tube is of an end heater type in which platinum blocks, carrying thermocouples and potential leads and tapered sharply to the point of filament attachment, are maintained in use at the filament temperature by heat flow along the tungsten supports from the platinum wire heaters wound in glass. Accurate centering, originally adjusted according to micrometer eyepiece readings, is maintained on filament

[1] L. B. Thomas and Olmer, J. Am. Chem. Soc. **65**, 1036 (1943).
[2] L. B. Thomas and R. E. Brown, J. Chem. Phys. **18**, 1367 (1950).
[3] E. H. Kennard, *Kinetic Theory of Gases* (McGraw-Hill Book Company, Inc., New York, 1938).
[4] Dickins, Proc. Roy. Soc. (London) **A143**, 517 (1933). (See Kennard (reference 3) for recalculation of Dickins values.)
[5] Archer, Phil. Mag. **25**, 129 (1938); Proc. Roy. Soc. (London) **A165**, 474 (1938).
[6] Gregory, Proc. Roy. Soc. (London) **A149**, 35 (1935).
[7] Gregory and Dock, Phil. Mag. **25**, 129 (1938).
[8] Grilly, Taylor, and Johnston, J. Chem. Phys. **14**, 435 (1946).

expansion by having the tip of the lower block and the center of the tungsten spring on a horizontal line. The heater circuits are powered by twin 6-volt transformers, with variable resistance in the secondaries, which in turn draw from a constant voltage transformer. The tube was maintained in a thermostat bath (kerosene) at 30°C for all A.C. measurements.

The vacuum system is all of Pyrex glass with mercury condensation pump, liquid air traps, and no stopcocks in the system as used during measurement. The gas admitting system, separated by a mercury cutoff, had several mercury seal stopcocks with "Apiezon N" grease. The purest available "Airco" gases in Pyrex flasks were used, and the helium and neon were admitted from standing over outgassed charcoal at liquid air temperature. A wide range McLeod gauge was used for the lower pressures and a cathetometer, sighting on mercury columns in the 25 mm. "U" tube leading to the condensation pump, was used at the higher pressures. The tube and system were frequently torched and baked to 450°C to promote at least moderately clean vacuum conditions.

Electrical measurements were taken with a Type K-2 potentiometer and standard resistance to at least four significant figures. A calibrated manganin fixed resistor with potential leads at 0.02-ohm intervals was used in series with the filament which was brought to the desired temperatures by adjustment of the current together with the block temperatures until the filament showed the same resistance as that selected on the standard. Under this "balanced" condition the filament temperature is constant over its entire length and there are no end losses. The "balancing" operation requires from 15 to 45 minutes, being the more tedious in vacuum and low pressure. The temperature coefficient of resistance of the filament (0.00388) and the voltage-temperature scale of the Pt; Pt, 10-percent Rh thermocouples were very carefully determined against N.B.S. calibrated thermometers. The power loss in vacuum (radiation loss) was determined. It follows very closely the Stefan-Boltzmann law with emissivity linear with absolute temperature, given by $e=1.72\times10^{-4}T$ or $e=0.047$ at 0°C. The L.P. runs were taken with pressures below 0.05 mm for He and below 0.03 mm for Ne and CO_2. The T.J. runs were taken with five pressures in the range 1 cm to 12 cm. The vacuum preparation and time elapsed thereafter were found to affect the resulting A.C. values by both methods. These will be specified in the discussion of results. Most of the runs were taken on the day following bake out which allows sufficient time for the A.C. to reach a steady condition.

THEORETICAL TREATMENT OF DATA

The L.P. method needs no elaboration here. To obtain the A.C. values we have simply subtracted the power loss in vacuum (radiation only) from that in gas, reduced to unit ΔT and P and divided by the quantity

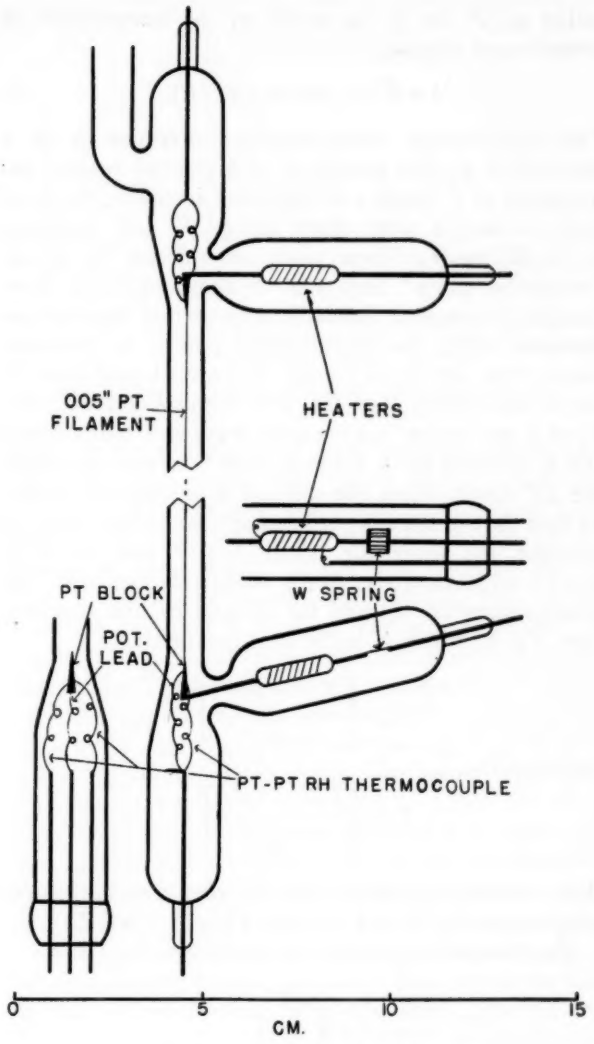

FIG. 1.

$(C_v/R+\frac{1}{2})(R/2\pi MT)^{\frac{1}{2}}$ (filament area). With pressure in mm at bath temperature 303.1°K and filament surface 1.039 cm² this expression gives 0.02893 (watt) for He, 0.012885 for Ne, and 0.017479 for CO_2.

The T.J. method as applied here is modified somewhat but follows Kennard[3] in the main and uses his symbols where feasible. Applying the Poisson T.J. expression to the Fourier heat conduction equation one finds for Q, the total heat conducted in a cylindrical cell with filament radius r_1, filament surface A, inner wall radius r_2, temperatures of filament and wall T_f and T_w:

$$Q=\frac{A\bar{K}(T_f-T_w)}{r_1 \ln r_2/r_1+g_1+r_1g_2/r_2}. \quad (1)$$

$\bar{K}$ is the effective thermal conductivity of the gas assuming that it behaves as a homogeneous medium and g_1 and g_2 are the temperature-jump distances at filament and wall. Dividing Q by A and ΔT, i.e., (T_f-T_w), neglecting the last term in the denominator, substi-

tuting g_1'/P for g_1 in which g_1' is independent of pressure one obtains:

$$\Lambda=\bar{K}/(r_1 \ln r_2/r_1+g_1'/P). \tag{2}$$

The experimental measurements determine Λ as a function of P. The reciprocal of Λ plotted against the reciprocal of P yields a straight line according to (2) of form $y=mx+b$ with slope $m=g_1'/\bar{K}$ and intercept $b=(r_1/\bar{K})\ln r_2/r_1$. These plots are referred to as the "reciprocal plots" and Fig. 3 shows five of them (atypical examples). Actually, with certain reservations discussed later, the experimental points, at pressures above 2 cm, are linear enough to warrant confidence in the formal theory thus far. The thermal conductivity, K, of a gas varies in a complex way with temperature and $\bar{K}$ above is the K value at some temperature within the ΔT range. From the data of Johnston and Grilly[9] we find that in the range of interest for helium (and we presume the same for neon) $K\propto T^{\frac{1}{2}}$ and for CO_2, $K\propto T^{\frac{3}{4}}$ approximately. With these relations and the Fourier equation we find for He and Ne the temperature, $T_{\bar{K}}$, at which $\bar{K}$ is the heat conductivity

$$T_{\bar{K}}=\left[\frac{T_f^{1.5}-T_w^{1.5}}{1.5\Delta T}\right]^2$$

and for CO_2

$$T_{\bar{K}}=\left[\frac{T_f^{2.5}-T_w^{2.5}}{2.5\Delta T}\right]^{\frac{4}{3}}.$$

Both of these expressions give $T_{\bar{K}}$ very close to the mid-temperature of T_f and T_w, i.e., $T_{\bar{K}}=T_w+\Delta T/2$.

The Poisson expression assumed above is

$$T_f-T_e=-g_1\left(\frac{dT}{dr}\right)_{r=r_1 \text{ or } T=T_e} \tag{3}$$

in which T_e, (Kennard's T_K) is the temperature in the gas at the filament surface assuming that the temperature gradient continues in regular functional relation to r, as established out in the gas, right up to $r=r_1$. Combining the kinetic-molecular and heat flow aspects, the heat conducted from unit area of filament per second is

$$-Kr_e\left(\frac{dT}{dr}\right)_{r_e}$$
$$=a\left[\frac{n\bar{c}}{4}\left(\frac{C_v+\frac{1}{2}R}{N}\right)(T_f-T_e)-\tfrac{1}{2}Kr_e\left(\frac{dT}{dr}\right)_{r_e}\right], \tag{4}$$

in which "a" is the A.C., "n" is the number of molecules per cm^3, "$\bar{c}$" is the average speed, "N" is the Avogadro number, and "C_v" and "R" are the usual molar quantities. Equation (4) is, as we see it, an attempt to set up the Knudsen A.C. in a more complicated situation than the L.P. case. As in the L.P. case, Eq. (4) equates observed heat flow to the A.C. multiplied into the possible heat that could be taken by the incoming molecules if they were to attain the energy characteristic of T_f. It makes a statement of the energy of incoming molecules (for difference calculation purposes), which is rendered applicable thru assumptions of the T.J. method as stated. The merit of the T.J. method depends upon its ability to give the Knudsen A.C. We do not see the desirability of defining a second "Maxwell-Knudsen A.C." as suggested in reference 9, unless it may serve some purpose in an engineering sense as a heat transfer coefficient with no direct fundamental significance or unless it is merely to identify it as having come from the T.J. method. It is to be noted in Eq. (4) that K, dT/dr, n, $\bar{c}$, and C_v all are to be taken at T_e. Equation (4) leads to

$$\frac{2-a}{a}=\frac{g_1'}{Kr_e}\left(\frac{C_v}{R}+\frac{1}{2}\right)\left(\frac{2R}{\pi MT_e}\right)^{\frac{1}{2}}$$
$$=m\frac{\bar{K}}{Kr_e}\left(\frac{C_v}{R}+\frac{1}{2}\right)\left(\frac{2R}{\pi MT_e}\right)^{\frac{1}{2}}.$$

For He and Ne:

$$\frac{2-a}{a}=\frac{m\left(T_w+\frac{\Delta T_e}{2}\right)^{\frac{1}{2}}}{T_w+\Delta T_e}\left(\frac{8R}{\pi M}\right)^{\frac{1}{2}}=\beta m. \tag{5}$$

For a typical helium run ΔT_e, i.e., (T_e-T_w) varies from 87 percent (at 10 cm) to 40 percent (at 1 cm) of ΔT, i.e., (T_f-T_w). It appears, if the A.C. is constant and the above substantially correct, that the reciprocal plots should not be quite straight, but that the slope, m, should diminish at lower pressures, i.e., to the right on the reciprocal plots. However, we have emphasized the slopes toward the left of the plots and have used ΔT rather than ΔT_e in the calculation of β. For helium, β varies from 0.5422 to 0.4797 as ΔT goes from 11.22° to 68.39°. For neon, only "M" is changed and the approximation of ΔT for ΔT_e is better. For calculation of C_v in β for CO_2 we have used a four-constant expression.[10] The expression corresponding to Eq. (5) for CO_2 is

$$\frac{2-a}{a}=\frac{m\left(T_w+\frac{\Delta T_e}{2}\right)^{\frac{3}{4}}}{(T_w+\Delta T_e)^2}\cdot\left(\frac{2R}{\pi M}\right)^{\frac{1}{2}}\left(\frac{C_v}{R}+\frac{1}{2}\right)=\beta m \tag{6}$$

and the substitution of ΔT for ΔT_e is still less objectionable. After calculating each β value and determining "m" from the reciprocal plots the A.C. is obtained from:

$$a=\frac{2}{\beta m+1}. \tag{7}$$

[9] H. L. Johnston and E. R. Grilly, J. Chem. Phys. 14, 233 (1946).

[10] S. Glasstone, *Thermodynamics for Chemists* (D. Van Nostrand Company, Inc., New York), p. 503.

For the A.C. calculations the temperature drop across the glass envelope is neglected.

EXPERIMENTAL RESULTS AND DISCUSSION

With helium we have taken seventeen sets of data at each of six values of ΔT from 6° to 180° by the L.P. method and fifteen sets using five pressures at each of five values of ΔT from 11.22° to 68.39° by the T.J. method. The resulting A.C. values at each of the three ΔT values common to both methods are given in the order taken in Table I. Runs 1 to 6 are regarded as trial runs for which vacuum conditions and filament preparation were not carefully controlled. Run 13 was started as soon as feasible following extended flashing of the filament to clean the surface (partially). A.C. measurements were taken from 20 to 990 minutes after flashing, at $\Delta T = 50.4$, by the L.P. method. Curve *A* of Fig. 2 shows that the A.C. values rise during the first part of the period and hold a steady apparently limiting value after about 400 minutes. This behavior is typical and has been observed numerous times with helium and neon on both platinum and tungsten. Run 6 shows A.C. values over twice those normally observed in a well kept vacuum system. In this case the filament had been exposed to air in the system for days and the A.C. determinations were made without any attempt other than evacuation—no torching or flashing—to clean up the filament or system. Run 15 by the T.J. method was made without a waiting period following extended

TABLE I. Accomodation coefficients of helium by two methods.

Run	Type	$\Delta T = 11.22°$	$\Delta T = 21.40°$	$\Delta T = 50.4°$
1	L.P.	0.255	0.265	0.233
2	L.P.	0.233	0.211	0.194
3	L.P.	0.243	0.208	0.202
4	L.P.	0.253	0.217	0.221
5	L.P.	0.156	0.151	0.146
6	L.P.	0.431	0.422	0.412
7*	L.P.	0.191	0.191	0.188
8	L.P.	0.224	0.218	0.210
9	L.P.	0.291	0.284	0.245
10*	L.P.	0.172	0.164	0.169
11*	L.P.	0.174	0.175	0.177
12*	L.P.	0.191	0.183	0.183
13	(L.P. time run; A.C. from 0.136 to 0.183, 1000 min, $\Delta T = 50.4$)			
14	T.J.	0.154	0.151	0.144
15	T.J.	0.117	0.118	0.120
16	T.J.	0.158	0.159	0.161
17	T.J.	0.171	0.166	0.164
18*	T.J.	0.170	0.163	0.160
19	L.P.	0.186	0.186	0.181
20	L.P.	0.186	0.178	0.175
21*	L.P.	0.186	0.178	0.176
22*	L.P.	0.170	0.175	0.168
23	T.J.	0.155	0.159	0.173
24*	T.J.	0.196	0.197	0.195
25	T.J.	0.186	0.183	0.187
26*	T.J.	0.167	0.166	0.164
27*	T.J.	0.190	0.190	0.185
28	T.J.	0.149	0.141	0.144
29	T.J.	0.146	0.146	0.149
30	T.J.	0.163	0.162	0.163
31*	T.J.	0.185	0.181	0.180
32*	T.J.	0.160	0.163	0.163
33*	L.P.	0.152	0.151	0.155
Av. by LP (excluding No. 1 to 6 and 9)		*0.183*	*0.180*	*0.178*
Av. by TJ (excluding No. 15)		*0.167*	*0.166*	*0.167*
*Av. of LP**		*0.1766* (±0.009)	*0.1739* (±0.009)	*0.1737* (±0.008)
*Av. of TJ**		*0.1780* (±0.012)	*0.1766* (±0.013)	*0.1745* (±0.012)

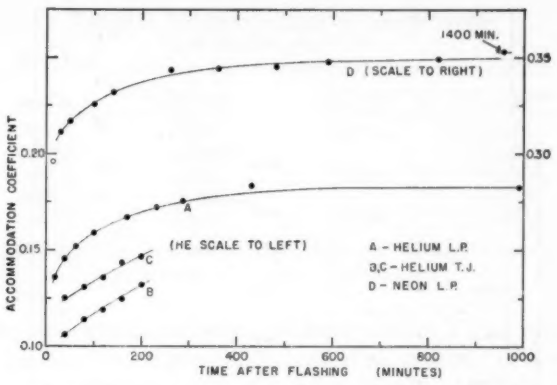

FIG. 2. Change of accommodation coefficient with time.

torching and flashing. The lower pressure points, taken first, show abnormally high values of $1/\Lambda$ which gives the reciprocal plots large slopes and a concave (upward) shape. Run 28 is of similar nature and will be considered in some detail since it demonstrates (for the first time to our knowledge) distinct time effects observed by the T.J. method. The reciprocal plots are shown in Fig. 3, and the points numbered were taken in that order. The points below 0.3 in abscissas, taken in the latter part of the run after the A.C. had stabilized, serve to fix the straight lines and give values of $\bar{K}$ at the $1/P = 0$ intercepts which are consistent with other runs. The approach in succession of the points to the lines demonstrates an increase of the A.C. with time. The individual A.C. values indicated by the points are shown as time runs in Curve B, Fig. 2 (points 1 to 5) and Curve C, Fig. 2 (points 6 to 10). (Between points 5 and 6 there is a break in continuity with admission of new gas for the higher pressure.) The rate of increase of the A.C. with time is of the same order as that observed by the L.P. method although the gas pressure in the latter is about 0.1 percent of those used in the T.J. runs. The discussion so far indicates that low values of the A.C. are encountered under the cleaner conditions of vacuum system and filament and high values under lax conditions. It is obvious that this factor must be controlled to obtain reproducibility within either method. Difficulty with this filament surface condition is the greatest source of uncertainty in the comparison of the two methods, with helium and neon at least.

Comparison of A.C. values in Table I taken by the two methods (except 1–6, 9, and 15 which are considered atypical) shows the average A.C. by the T.J. method to be 7.6 percent below that of the L.P. method. More reliable comparison of the methods can be obtained by selection of runs on the basis of preparation history together with the quality of the reciprocal plots in the case of the T.J. runs. The starred runs were selected on these bases only, without regard to resulting A.C. values. They were prepared by baking, flashing, filling with gas one day, then were left to stand 12 hours at least until the A.C. according to our experience, should

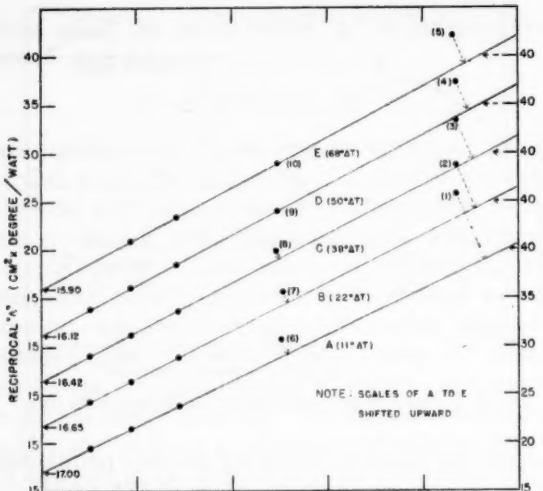

FIG. 3. Reciprocal plots for run 28.

stabilize. Comparison of starred values gives 0.1747 ±0.0095 by the L.P. and 0.1764±0.012 by the T.J. method. The deviation from the mean in each case is due largely to real differences in the A.C. prevailing rather than uncertainty in the determinations. The mean deviations within each run at different ΔT are ±0.0025 for the L.P. and ±0.0015 for the T.J. and over half of these is due probably to a real change of the A.C. with ΔT. Indications are that the accuracy by either method is at least tenfold better than the observed variation attributed to surface condition in the most carefully controlled starred runs. We conclude that the two methods agree very well applied to helium. The A.C. values of 0.50[4] and 0.53[9] by the T.J. method cannot be attributed to failure of the T.J. method to agree with the L.P. method.

For neon, results by the two methods are set forth in the order taken at the common ΔT values and also at $\Delta T = 180°$ for the L.P. runs in Table II. Run 5 is a time run and is plotted in detail in Curve D, Fig. 2. After five hours the A.C. has almost reached the stable value 0.353 which holds for the next 12 hours. Run 5 was followed as quickly as possible by T.J. Run 6 at the same

TABLE II. Accommodation coefficients of neon by two methods.

Run	Type	ΔT =11.22°	ΔT =21.40°	ΔT =50.4°	ΔT =180.4°
1	T.J.	0.326	0.318	0.315	
2	L.P.	0.468	0.456	0.445	0.431
3	T.J.	0.326	0.330	0.322	
4	L.P.	0.416	0.392	0.387	0.305
5	L.P. (Time run; A.C. from 0.296 to 0.353 in 1500 min; ΔT=21.4°)				
6	T.J. (Follows 5 immediately; A.C. 0.368; ΔT=21.4°)				
7	T.J.	0.337	0.330	0.326	
8	L.P.	0.454	0.448	0.433	0.333
Av. 2, 4, 8 by L.P.		*0.446*	*0.432*	*0.422*	
Av. 1, 3, 7 by T.J.		*0.330*	*0.326*	*0.321*	

ΔT. This gave an A.C. 0.368 which may be considered very good agreement. The other runs consist of three pairs of T.J. followed by L.P. runs. The gas samples for the L.P. runs were trapped from the last highest pressure part of the T.J. run just preceding, a procedure which was not followed with helium but which we hoped would give closely comparable surface conditions. The temperature jump runs gave excellent reciprocal plots (16 in all), showing a slight decrease in slope to the right as predicted earlier from theory and as observed in the later helium runs when the filament had aged long enough in the system to give stable A.C. values. These T.J. neon runs show good self-consistency, averaging about 0.326 (neglecting small real differences with ΔT). The L.P. runs average 0.433 which is 33 percent higher than the T.J. average. There are no T.J. values for neon in the literature. The L.P. A.C. values found here are lower than others in the literature (0.75, 0.65, 0.70, 0.57,[1] 0.55,[2] 0.54). Even so, information in Runs 4 and 8 for $\Delta T = 180.4°$ indicates by the large drop in the A.C. for the 130° increase in the ΔT that there is loosely adsorbed gas on the platinum at the lower ΔT values. We are inclined to credit the finding of Runs 5 and 6

TABLE III. Accommodation coefficients of CO_2 by two methods.

Run	Type	ΔT =11.22°	ΔT =21.40°	ΔT =37.7°	ΔT =50.4°	ΔT =68.4°
1	L.P.	0.781	0.786	none	0.771	none[a]
2	T.J.	x	x	0.77	0.81	0.82
3	T.J.	x	x	0.79	0.80	0.75
4	T.J.	x	x	0.79	0.78	0.77

[a] (L.P. A.C. values are 0.729 at ΔT97.6°; and 0.687 at ΔT180.4°). Av. values: T.J. 0.787 ±0.017; L.P. 0.779 ±0.006.

and attribute the disagreement in the other runs to consistent failure to reproduce the same surface condition from the T.J. to L.P. runs rather than to failure of the T.J. method in this case. It might be added that neon has been in other instances markedly difficult in the variability of its A.C.

For carbon dioxide the results are presented in Table III. Since variation of the A.C. with time is not displayed by CO_2 and the L.P. values agreed well with previous work in this laboratory, Run 1 was the only one made by this method. Difficulty was experienced getting satisfactory reciprocal plots by the T.J. method at low ΔT—in the cases of poorly defined slopes we have marked "x" in Table III. No distinct trend of the A.C. with ΔT is noted in the table so simply averaging values for each method gives 0.787±0.017 by the T.J. and 0.779±0.006 by the L.P. method. Agreement is considered excellent and it is also in very good agreement with 0.78[4] by T.J. and 0.807 by L.P. (Knudsen) and 0.76[1] by L.P. but is disturbingly off from the 0.63[8] and 0.45[5] by T.J. In both reference 8 and 5 the ΔT used was in the range we have tried and omitted. Our average of the six values omitted is about 0.65. Al-

though speculative, it appears that in the case of CO_2 adsorption may increase to such an extent at low ΔT and the relatively high pressure of the T.J. method, that it may cause a reversal of the usual effect and actually lower the A.C. Archer[5] has treated his data differently than that outlined by Kennard[3] and others and has used a different type of reciprocal plot. We have treated the data of his Table III by our method and find agreement with his thermal conductivity value but a rather poor reciprocal plot which can be interpreted to yield A.C. values 0.42 to 0.51 at 24.2°C filament temperature. However, it is definitely in disagreement with our 0.787 value. In summary, very good agreement by the two methods was found for CO_2 using the T.J. method with ΔT at least 37.7° but that at lower ΔT by the T.J. method an apparent instability in the A.C. appears.

THERMAL CONDUCTIVITIES OF He, Ne, AND CO_2

As a product of the A.C. studies, the thermal conductivities of the gases have been obtained from the intercepts, b, of the reciprocal plots. Considering the care taken in the measurements involved, the advantages of the type of tube used, and the extensive repetition, these results could be among the best in accuracy. They are limited to the single bath temperature but are unusually extensive with respect to range of ΔT and in the case of helium in the number of repeated runs. Results are shown in Table IV. Only those runs for which the reciprocal plots are satisfactory for definite location of the intercept are included in calculating the average value of "b." The subtraction of 0.138 from "b" corrects for the resistance to heat flow in the glass envelope—K (in calories) is taken as 0.0027.

TABLE IV. Thermal conductivities of He, Ne, and CO_2.

	ΔT	$T_{\bar{K}}$	No. of trials included	$\bar{K}\times10^4$ (Calories)
Helium	11.22	308.7	10	3.7078±0.53%
	21.4	313.8	10	3.7509±0.28%
	37.7	322.0	9	3.8106±0.18%
	50.4	328.3	9	3.8799±0.50%
	68.4	337.3	7	3.9425±0.44%
Neon	11.22	308.7	3	1.199 ±0.20%
	21.4	313.8	3	1.2119±0.21%
	37.7	322.0	3	1.2362±0.18%
	50.4	328.3	3	1.2532±0.25%
	68.4	337.3	3	1.2800±0.23%
Carbon dioxide	21.4	313.8	2	0.4184±0.19%
	37.7	322.0	2	0.4331±0.1%
	50.4	328.3	3	0.4451±0.07%
	68.4	337.3	3	0.4640±0.04%

TABLE V. Interpolated thermal conductivities of He, Ne, and CO_2.

T	$K_{He}\times10^4$	$K_{Ne}\times10^4$	$K_{CO_2}\times10^4$
310°K	3.718	1.2016	0.4117
310°K	3.674[a]	...	0.4175[a]
320°K	3.801	1.2304	0.4290
320°K	3.746[a]	...	0.4371[a]
330°K	3.883	1.2580	0.4483

[a] K values given in Table IX, J. and G., reference 9.

The ΔT of measurement, the temperature $T_{\bar{K}}$ at which $\bar{K}$ applies, the number of reciprocal plots used to get the average intercept, the $\bar{K}$ values obtained with the mean deviations are given in the table. To obtain values of K for comparison with others the $\bar{K}$ values were plotted against $T_{\bar{K}}$ and K values applicable at 310°, 320°, and 330°K were read from the graphs. These are shown in Table V together with values from J. and G. Selecting the K values at 310°K as most accurate (since they are associated with smallest ΔT and hence smallest error in assigning the temperature to the $\bar{K}$ observed) and comparing with the J. and G. results at 310°K, our "K" for helium is 1.2 percent greater and for CO_2 is 1.4 percent smaller than these. On the plausible assumption that our values would keep the same percentage deviation from J. and G. at the ice point, our values show remarkable agreement with Kannuluik and Martin[11] (deviation from J. and G.+1.2 percent for He and −1.5 percent for CO_2) and are in excellent agreement with the mean of the closely grouped values of K. and M., Weber, and Eucken (given in J. and G. Table X) which average +1.17 percent deivation from J. and G. for He and −1.4 percent for CO_2. Perhaps this independent check on these thermal conductivities summarized in J. and G., Table X, may be taken as an indication that J. and G., while expanding the breadth of thermal conductivity measurements may not have attained the absolute accuracy of the other investigators mentioned, at least with He and CO_2. Assuming that our K_{He}/K_{Ne} ratio at 310°K would remain the same at 0°C, and borrowing the K. and M. value for He at 0°C ($K=3.43\times10^{-4}$), we obtain 1.1085×10^{-4} for Ne at 0°C. This is 0.3 percent below that of K. and M. and 0.4 percent above Weber's later value (1927), which again is unusually close agreement for thermal conductivity values.

We wish to express our appreciation for the support given this investigation by the Office of Ordnance Research and by the U. S. Office of Naval Research.

[11] Kannuluik and Martin, Proc. Roy. Soc. (London) **A144**, 496 (1934).

The Vibrational Spectrum and the Specific Heat of Germanium and Silicon*

YÜ-CHANG HSIEH
Department of Physics, Vanderbilt University, Nashville, Tennessee
(Received August 13, 1953)

The vibrational spectra of Ge and Si have been constructed by computation of 174 characteristic frequencies in 29 directions by Born's lattice theory as elaborated by Smith. Two approximations have been considered, involving (a) the interaction between each atom and its first neighbors only, and (b) the interaction between the atom and its first neighbors, and the central force interaction between the atom and its second neighbors. The specific heats of Ge and of Si at low temperatures are calculated from the spectra. The theory indicates a minimum of the Debye characteristic temperature in qualitative agreement with the experiments, but fails to give quantitative agreement.

I. INTRODUCTION

SUBSTANCES with diamond structure such as diamond, germanium, silicon, and grey tin show that the variations of the Debye characteristic temperature can be very large. Such substances are good test cases for the lattice theory developed by Born and von Kármán.[1] The details of the general theory have been worked out by Smith[2], who has calculated the frequency spectrum of diamond by two different approximations, taking into account (a) the interaction between each atom and its first neighbors only, and (b) the interaction between each atom and its first neighbors, and the central-force interaction between the atom and its second neighbors. With an adjustment of the elastic constants of diamond measured by Bhagavantam and Bhimasenachar,[3] the frequency spectrum obtained from the case (b) could give specific heat values in good agreement with experiments. The present calculation follows exactly the method used by Smith. Both the case (a) and the case (b) have been considered.

TABLE I. Frequencies of vibration of Ge under the action of first-neighbor forces only.

			(units of ω_j are 10^{13} sec^{-1})					
p_x	p_y	p_z	ω_1	ω_2	ω_3	ω_4	ω_5	ω_6
8	4	0	6.402	6.402	4.924	4.924	2.739	2.739
8	2	2	6.488	6.364	5.120	4.720	2.826	2.531
8	2	0	6.402	6.402	4.924	4.924	2.739	2.739
8	0	0	6.402	6.402	4.924	4.924	2.739	2.739
7	3	1	6.483	6.398	5.241	4.586	2.750	2.543
7	1	1	6.449	6.414	5.346	4.463	2.712	2.627
6	6	0	6.488	6.364	5.120	4.720	2.826	2.531
6	4	2	6.581	6.473	5.378	4.423	2.567	2.275
6	4	0	6.541	6.406	5.392	4.407	2.732	2.388
6	2	2	6.554	6.495	5.522	4.243	2.511	2.352
6	2	0	6.531	6.471	5.666	4.049	2.574	2.416
6	0	0	6.503	6.503	5.790	3.869	2.491	2.491
5	5	1	6.590	6.450	5.399	4.398	2.625	2.252
5	3	3	6.651	6.592	5.377	4.425	2.244	2.063
5	3	1	6.642	6.541	5.757	3.919	2.390	2.091
5	1	1	6.609	6.605	6.048	3.451	2.206	2.194
4	4	4	6.689	6.689	5.373	4.430	1.937	1.937
4	4	2	6.689	6.623	5.636	4.090	2.151	1.937
4	4	0	6.689	6.534	5.858	3.765	2.409	1.937
4	2	2	6.715	6.703	6.043	3.461	1.887	1.846
4	2	0	6.745	6.658	6.249	3.073	2.041	1.730
4	0	0	6.714	6.714	6.434	2.665	1.847	1.847
3	3	3	6.733	6.733	5.871	3.746	1.778	1.778
3	3	1	6.786	6.707	6.228	3.115	1.873	1.549
3	1	1	6.805	6.777	6.603	2.213	1.602	1.480
2	2	2	6.833	6.833	6.458	2.606	1.341	1.341
2	2	0	6.884	6.831	6.649	2.069	1.352	1.048
2	0	0	6.895	6.895	6.830	1.359	0.973	0.973
1	1	1	6.927	6.927	6.835	1.332	0.716	0.716

II. VIBRATIONAL SPECTRUM OF GERMANIUM

According to the lattice theory (by the notation of Smith), the force constants between the atoms and the elastic constants of the crystal are related by the equations

$$C_{11}=(1/2a)(\alpha+8\mu),$$
$$C_{12}=(1/2a)(2\beta-\alpha-4\lambda-4\mu+8\tau), \quad (1)$$
$$C_{44}=(1/2a)(\alpha-\beta^2/\alpha+4\lambda+4\mu),$$

where α and β are the force constants between an atom and its first neighbors; λ, μ, τ are the force constants between the atom and its second neighbors; and 2a is the lattice constant. As a first approximation, if $\lambda=\mu=\tau=0$, the elastic constants should satisfy the condition

$$4C_{11}(C_{11}-C_{44})/(C_{11}+C_{12})^2=1. \quad (2)$$

In the case of germanium, the elastic constants measured by Bond[4] and his collaborators, using 5.35 as the specific gravity, are

$C_{11}=1.298\times10^{12}$, $C_{12}=0.488\times10^{12}$, $C_{44}=0.673\times10^{12}$ dynes/cm^2. The germanium atom has a mass

$$m=1.205\times10^{-22}\text{ g},$$

and the lattice constant calculated from this mass and

* The preliminary calculation on the Ge case was done at Purdue University and has been reported at the American Physical Society Chicago meeting in 1951 [Phys. Rev. **85**, 730 (1952)]. Part of the work since then was done while the author was at Hampton Institute, Hampton, Virginia.

[1] M. Born and T. von Kármán, Physik Z. **13**, 297 (1912); **14**, 15 (1913). M. Born, Repts. Progr. in Phys. (London) **9**, 294 (1942). M. Born and G. H. Begbie, Proc. Roy. Soc. (London) **A188**, 179 (1947).

[2] H. M. J. Smith, Trans. Roy. Soc. (London) **A241**, 105 (1948).

[3] S. Bhagavantam and J. Bhimasenachar, Proc. Roy. Soc. (London) **A187**, 381 (1946).

[4] Bond, Mason, McSkimin, Olson, and Teal, Phys. Rev. **78**, 176 (1950).

the specific gravity is

$$2a=5.649\times10^{-8}\text{ cm}.$$

The left side of Eq. (2) has the value 1.017, which shows that the first approximation should be fairly good.

A. First Approximation

With $\lambda=\mu=\tau=0$, the average values of α and β, from the three Eqs. (1) are given by

$$\alpha=7.307\times10^{4},\quad \beta=5.046\times10^{4}\text{ dynes/cm}.$$

The numerical values of the characteristic frequencies of vibration ω_j in the twenty-nine directions chosen (Eqs. (3.11) and (3.13) of Smith's paper) are given in Table I.

TABLE II. Frequencies of vibration of Ge under the action of first- and central second-neighbor forces.

			(units of ω_j are 10^{13} sec^{-1})					
p_x	p_y	p_z	ω_1	ω_2	ω_3	ω_4	ω_5	ω_6
8	4	0	6.776	6.776	5.142	5.142	2.717	2.717
8	2	2	6.891	6.723	5.351	4.907	2.784	2.546
8	2	0	6.784	6.784	5.121	5.121	2.736	2.736
8	0	0	6.792	6.792	5.101	5.101	2.755	2.755
7	3	1	6.907	6.731	5.497	4.757	2.715	2.550
7	1	1	6.846	6.794	5.582	4.607	2.707	2.642
6	6	0	6.891	6.723	5.351	4.907	2.784	2.546
6	4	2	7.006	6.890	5.602	4.603	2.462	2.265
6	4	0	6.949	6.770	5.656	4.573	2.683	2.394
6	2	2	6.968	6.879	5.794	4.374	2.482	2.364
6	2	0	6.934	6.864	5.945	4.168	2.556	2.424
6	0	0	6.907	6.907	6.072	3.958	2.503	2.503
5	5	1	7.010	6.825	5.657	4.553	2.579	2.265
5	3	3	7.081	7.048	5.702	4.446	2.126	2.074
5	3	1	7.065	6.942	6.050	4.028	2.359	2.102
5	1	1	7.030	7.020	6.373	3.523	2.201	2.199
4	4	4	7.125	7.125	5.607	4.539	1.948	1.948
4	4	2	7.125	7.041	5.905	4.192	2.139	1.948
4	4	0	7.125	6.923	6.170	3.873	2.366	1.948
4	2	2	7.148	7.138	6.367	3.523	1.899	1.841
4	2	0	7.146	7.126	6.604	3.130	2.008	1.752
4	0	0	7.151	7.151	6.815	2.697	1.849	1.849
3	3	3	7.176	7.176	6.163	3.813	1.787	1.787
3	3	1	7.240	7.143	6.573	3.183	1.837	1.564
3	1	1	7.275	7.257	6.954	2.384	1.482	1.403
2	2	2	7.292	7.292	6.843	2.627	1.346	1.346
2	2	0	7.352	7.286	7.071	2.085	1.342	1.055
2	0	0	7.363	7.363	7.284	1.365	0.972	0.972
1	1	1	7.401	7.401	7.289	1.334	0.718	0.718

One obtains the frequency spectrum by dividing the range of the values of ω into equal intervals

$$d\omega=0.6\times10^{13}\text{ sec}^{-1},$$

and counting the number of frequencies in each interval. Three histograms each shifted 0.2×10^{13} sec^{-1} from the other two were plotted and smoothed out. The vibrational spectrum was thus obtained as shown in Fig. 1. The characteristics of the spectrum are given in Table III.

B. Second Approximation

One obtains a second approximation to the frequency distribution by considering the second-neighbor forces

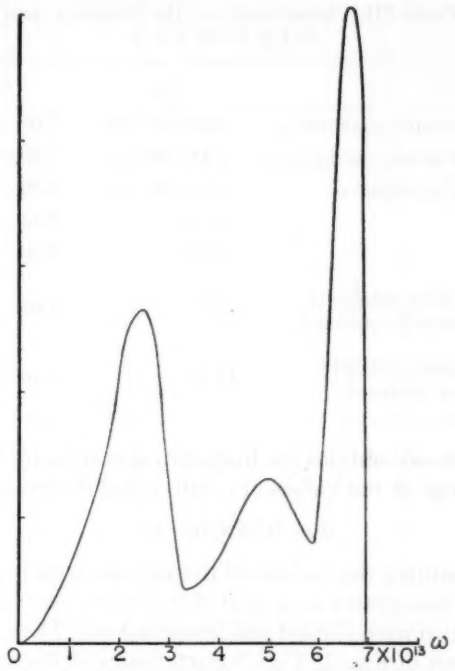

FIG. 1. Frequency spectrum of Ge (first-neighbor forces only).

to be central, i.e., $\lambda=0$, $\mu=\tau$. The three force constants α, β, and μ are, from Eqs. (1),

$$\alpha=8.348\times10^{4},$$
$$\beta=5.807\times10^{4},$$
$$\mu=-0.127\times10^{4}\text{ dynes/cm}.$$

For this case the characteristic frequencies are given in Table II.

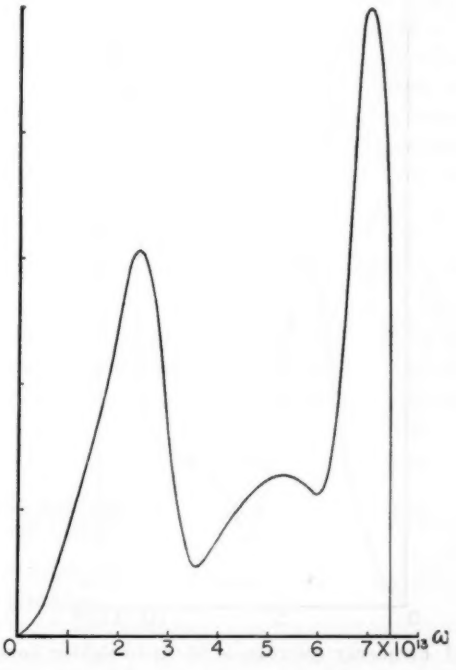

FIG. 2. Frequency spectrum of Ge (first- and central second-neighbor forces).

TABLE III. Characteristics of the frequency spectra in Fig. 1 and Fig. 2.

	Fig. 1	Fig. 2
Freq. of main maximum ω_1	6.65×10^{13} sec^{-1}	7.00×10^{13} sec^{-1}
Freq. of second maximum ω_2	2.45×10^{13} sec^{-1}	2.40×10^{13} sec^{-1}
Freq. of minimum ω_3	3.35×10^{13} sec^{-1}	3.50×10^{13} sec^{-1}
ω_1/ω_2	2.71	2.92
ω_1/ω_3	1.99	2.00
Ht. of main maximum / Ht. of second maximum	1.92	1.63
Ht. of main maximum / Ht. of minimum	12.70	9.26

Again one obtains the frequency spectrum by dividing the range of the values of ω into equal intervals

$$d\omega=0.75\times10^{13}\ \text{sec}^{-1},$$

and counting the number of frequencies in each interval. Three histograms each shifted 0.25×10^{13} sec^{-1} from the other two were plotted and smoothed out. The spectrum is shown in Fig. 2. The characteristics of the spectrum are given in Table III together with that of Fig. 1 for comparison.

III. VIBRATIONAL SPECTRUM OF SILICON

The elastic constants of silicon measured by McSkimin[5] and his collaborators are

$$C_{11}=1.6740\times10^{12},$$
$$C_{12}=0.6523\times10^{12},$$
$$C_{44}=0.7957\times10^{12}\ \text{dynes/cm}^2,$$

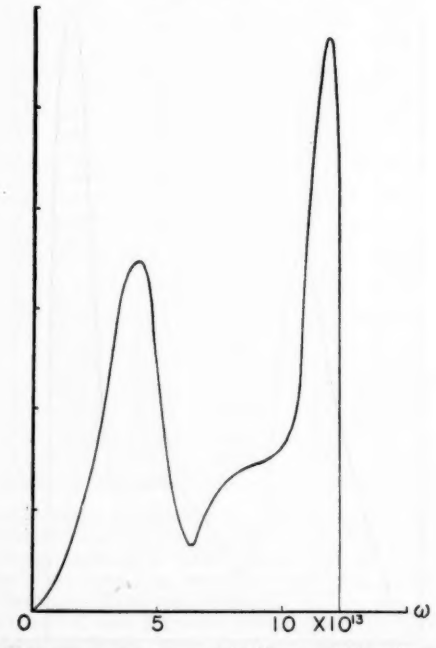

FIG. 3. Frequency spectrum of Si (first-neighbor forces only).

[5] McSkimin, Bond, Buehler, and Teal, Phys. Rev. **83**, 1080 (1951).

with density

$$\rho=2.331\ \text{g/cc}.$$

The mass of the silicon atom is

$$m=0.4658\times10^{-22}\ \text{g},$$

and the lattice constant calculated from m and ρ is

$$2a=5.427\times10^{-8}\ \text{cm}.$$

The left side of Eq. (2) now gives 1.087. The first approximation is therefore not expected to be so good as in the case of germanium.

TABLE IV. Frequencies of vibration of Si under the action of first-neighbor forces only.

			(units of ω_j are 10^{13} sec^{-1})					
p_x	p_y	p_z	ω_1	ω_2	ω_3	ω_4	ω_5	ω_6
8	4	0	11.442	11.442	8.754	8.754	4.728	4.728
8	2	2	11.584	11.378	9.117	8.376	4.880	4.368
8	2	0	11.442	11.442	8.754	8.754	4.728	4.728
8	0	0	11.442	11.442	8.754	8.754	4.728	4.728
7	3	1	11.575	11.434	9.331	8.136	4.748	4.392
7	1	1	11.520	11.460	9.506	7.931	4.680	4.536
6	6	0	11.584	11.378	9.117	8.376	4.880	4.368
6	4	2	11.751	11.605	9.558	7.869	4.314	3.897
6	4	0	11.672	11.447	9.600	7.817	4.716	4.127
6	2	2	11.695	11.594	9.838	7.516	4.343	4.062
6	2	0	11.651	11.558	10.078	7.191	4.437	4.186
6	0	0	11.608	11.608	10.294	6.878	4.306	4.306
5	5	1	11.755	11.518	9.627	7.784	4.541	3.887
5	3	3	11.857	11.817	9.746	7.635	3.692	3.562
5	3	1	11.839	11.672	10.251	6.942	4.128	3.622
5	1	1	11.785	11.777	10.758	6.127	3.818	3.794
4	4	4	11.921	11.921	9.623	7.789	3.343	3.343
4	4	2	11.921	11.808	10.054	7.225	3.721	3.343
4	4	0	11.921	11.657	10.428	6.674	4.171	3.343
4	2	2	11.961	11.941	10.759	6.125	3.271	3.195
4	2	0	12.006	11.874	11.115	5.453	3.506	3.022
4	0	0	11.960	11.960	11.438	4.738	3.198	3.198
3	3	3	11.994	11.994	10.463	6.619	3.070	3.070
3	3	1	12.086	11.948	11.084	5.516	3.244	2.684
3	1	1	12.112	12.065	11.739	3.934	2.777	2.564
2	2	2	12.162	12.162	11.489	4.613	2.317	2.317
2	2	0	12.248	12.157	11.825	3.667	2.344	1.809
2	0	0	12.265	12.265	12.143	2.415	1.688	1.688
1	1	1	12.318	12.318	12.145	2.405	1.238	1.238

A. First Approximation

For the first approximation, the average values of α and of β obtained from the Eqs. (1) are

$$\alpha=8.925\times10^4,\quad \beta=6.322\times10^4\ \text{dynes/cm}.$$

The characteristic frequencies obtained with this set of values are given in Table IV.

With the same method used as in the germanium case, with 1.5×10^{13} sec^{-1} as the interval for the construction of the histograms, the frequency spectrum was constructed as shown in Fig. 3. The characteristics of the spectrum are given in Table VI.

B. Second Approximation

In this case the three force constants are

$$\alpha=15.353\times10^4,$$
$$\beta=11.013\times10^4,$$
$$\mu=-0.784\times10^4\ \text{dynes/cm}.$$

The characteristic frequencies are given in Table V.

With the same procedure as in the first approximation, the frequency spectrum was constructed as shown in Fig. 4. The characteristics of the spectrum are given in Table VI together with that of the first-approximation spectrum.

IV. SPECIFIC HEATS OF GERMANIUM AND SILICON

When the frequency distribution $N(\nu)(\omega=2\pi\nu)$ is known, the specific heat per mole of the crystal can be

TABLE V. Frequencies of vibration of Si under the action of first- and central second-neighbor forces.

			(units of ω_j are 10^{13} sec^{-1})					
p_x	p_y	p_z	ω_1	ω_2	ω_3	ω_4	ω_5	ω_6
8	4	0	14.479	14.479	10.567	10.567	4.515	4.515
8	2	2	14.845	14.296	11.033	9.942	4.508	4.477
8	2	0	14.538	14.538	10.407	10.407	4.695	4.695
8	0	0	14.593	14.593	10.243	10.243	4.879	4.879
7	3	1	14.792	14.424	11.359	9.624	4.434	4.379
7	1	1	14.727	14.563	11.456	9.156	4.674	4.630
6	6	0	14.845	14.296	11.033	9.942	4.508	4.477
6	4	2	15.084	14.738	11.566	9.068	3.879	3.786
6	4	0	15.256	13.999	11.951	9.177	4.267	4.161
6	2	2	15.035	14.741	12.037	8.647	4.176	4.050
6	2	0	14.929	14.724	12.387	8.208	4.325	4.199
6	0	0	14.874	14.874	12.622	7.643	4.411	4.411
5	5	1	15.146	14.549	11.777	9.098	4.074	4.010
5	3	3	15.323	15.208	11.802	8.640	3.668	3.588
5	3	1	15.281	14.891	12.674	7.882	3.872	3.656
5	1	1	15.183	15.135	13.425	6.740	3.864	3.751
4	4	4	15.438	15.438	11.558	8.733	3.450	3.450
4	4	2	15.438	15.185	12.283	8.110	3.586	3.450
4	4	0	15.438	14.820	12.990	7.596	3.742	3.450
4	2	2	15.474	15.462	13.407	6.674	3.338	3.128
4	2	0	15.574	15.292	14.036	5.942	3.350	3.064
4	0	0	15.487	15.487	14.547	5.016	3.222	3.222
3	3	3	15.563	15.563	12.878	7.204	3.158	3.158
3	3	1	15.726	15.433	13.963	5.964	3.096	2.768
3	1	1	15.801	15.759	14.921	4.382	2.578	2.408
2	2	2	15.854	15.854	14.621	4.794	2.366	2.366
2	2	0	16.008	15.809	15.251	3.809	2.251	1.867
2	0	0	16.029	16.029	15.802	2.469	1.674	1.674
1	1	1	16.129	16.129	15.818	2.367	1.255	1.255

calculated from the equations

$$C_v=\int_0^\infty kN(\nu)E(h\nu/kT)d\nu, \quad \int_0^\infty N(\nu)d\nu=3N, \quad (3)$$

where N is Avogadro's number and $E(x)=3Rx^2e^x/(e^x-1)^2$ is the Einstein function, which has been tabulated.[6] Both integrals in Eqs. (3) are calculated numerically by the trapezoidal method. The results are given in Tables VII and VIII.

The values of the Debye characteristic temperature at different temperatures derived by Debye's theory from the calculated specific heat are also given in Table VII and Table VIII. The specific heat curves are plotted in Figs. 5 and 6. The circles in Fig. 5 are the experimental data of Hill and Parkinson[7] and the tri-

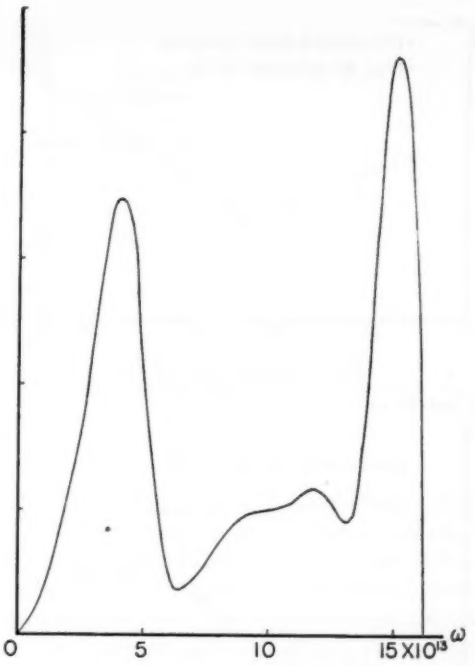

FIG. 4. Frequency spectrum of Si (first- and central second-neighbor forces).

angles are those measured by Estermann and Weertman.[8] The circles in Fig. 6 are the experimental data of Pearlman and Keesom.[9]

V. DISCUSSION

The frequency spectra were obtained by a smoothing of the hundred and seventy-four discrete characteristic frequencies. When different frequency intervals are used in construction of the histograms, different frequency spectra will necessarily result. Although all of them must have the same form, some differences will occur and will lead to somewhat different values of the specific heats. One way of getting a more accurate frequency spectrum would be to calculate the characteristic frequencies in more directions than the twenty-

TABLE VI. Characteristics of the frequency spectra in Fig. 3 and Fig. 4.

	Fig. 3	Fig. 4
Freq. of main maximum ω_1	11.7×10^{13} sec^{-1}	15.1×10^{13} sec^{-1}
Freq. of second maximum ω_2	4.2×10^{13} sec^{-1}	4.0×10^{13} sec^{-1}
Freq. of minimum ω_3	6.3×10^{13} sec^{-1}	6.3×10^{13} sec^{-1}
ω_1/ω_2	2.79	3.78
ω_1/ω_3	1.86	2.40
Ht. of main maximum / Ht. of second maximum	1.64	1.33
Ht. of main maximum / Ht. of minimum	8.91	13.53

[6] Landolt-Börnstein, *Phys.-Chem. Table* (Julius Springer, Berlin, 1927), fifth edition, first supplement, p. 702.
[7] R. W. Hill and D. H. Parkinson, Phil. Mag. **43**, 309 (1952).
[8] I. Estermann and J. R. Weertman, J. Chem. Phys. **20**, 972 (1952).
[9] N. Pearlman and P. H. Keesom, Phys. Rev. **88**, 398 (1952).

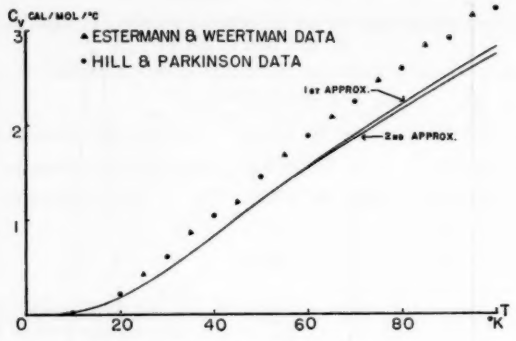

FIG. 5. Specific heat of Ge.

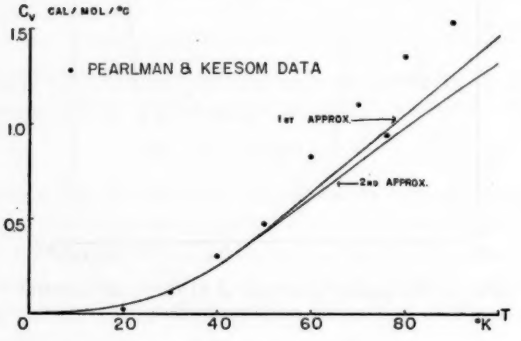

FIG. 6. Specific heat of Si.

nine used in the calculation. But such a procedure would greatly increase the labor by necessitating numerical solution of sixth-order algebraic equations. In the numerical integration for the specific heat, if the whole frequency spectrum is effective, i.e., at higher temperatures, the error introduced by using the continuous spectrum should be small; at low temperatures where only a small portion of the frequency spectrum is effective, the results calculated from the continuous spectrum must necessarily become inaccurate. On the other hand, if the hundred seventy-four discrete frequencies, each with the same statistical weight, are used to calculate the specific heat, the results at low temperatures might be more reasonable than those obtained from the continuous spectrum. The specific heats and the corresponding Debye characteristic temperatures calculated from the discrete spectra are given in Tables IX and X.

The calculation shows now that in the case of both Ge and Si, the first approximation and the second approximation give practically the same results at low temperatures. The Debye characteristic temperature Θ_0 for Ge and for Si at 0°K—calculated from the elastic constants given above, by the modified Hopf and Lechner method[9]—are 375°K for Ge[10] and 669°K for Si. The value for Si, calculated by Pearlman and Keesom,[9] using estimated elastic constants at 0°K is 653°K. Plots of Θ/Θ_0 against T/Θ_0 for both Ge and Si are shown in Fig. 7, together with the experimental data of Pearlman and Keesom on Si and Hill and Parkinson on Ge. The two curves are very close to each other and so are the two sets of experimental data. As mentioned before, the theoretical curves have been calculated from the discrete frequency spectra. They indicate the existence of a minimum of the Debye characteristic temperature in each case, as found experimentally, but deviate quantitatively from the data by about 10 percent. On the other hand, calculations based on the continuous spectra at low temperatures fail to show the minima.

In Eqs. (1) there are five force constants related to the three elastic constants C_{11}, C_{12}, and C_{44}. In the present calculation, as well as in the calculation on diamond by Smith, only two approximations have been considered. The first approximation leads to Eq. (2), whereas the second approximation gives three equations to determine the three force constants α, β, and μ. However, in Smith's calculation another relationship was used, namely, the equation for the frequency-shift of the first-order Raman line. In fact, that is the condition used by Smith to determine the value of α. The value μ was then determined from the first equation of Eqs. (1). It turned out to be positive. Smith adjusted the elastic constant C_{44} to 5.0×10^{12} dynes/cm^2, although the experimental value was 4.3×10^{12}. The difference between them amounts to 14 percent. If one does not use the Raman shift equation, the three force constants calculated from the adjusted elastic constants would be

$$\alpha=0.203\times10^6,$$
$$\beta=0.137\times10^6,$$
$$\mu=-0.0169\times10^6 \text{ dynes/cm},$$

which are altogether different from the set of values

TABLE VII. Specific heat of Ge.

	1st approx.		2nd approx.	
T°K	C_v cal/mole/°C	Θ°K	C_v cal/mole/°C	Θ°K
10	0.027	258	0.027	257
20	0.17	280	0.18	274
30	0.45	299	0.47	296
40	0.81	322	0.82	320
50	1.18	344	1.18	345
75	2.05	391	2.00	397
100	2.81	421	2.74	430
150	3.98	445	3.87	462

TABLE VIII. Specific heat of Si.

	1st approx.		2nd approx.	
T°K	C_v cal/mole/°C	Θ°K	C_v cal/mole/°C	Θ°K
20	0.042	448	0.042	446
30	0.12	472	0.12	472
40	0.25	491	0.25	493
50	0.43	510	0.41	516
75	0.95	567	0.89	582
100	1.47	623	1.32	654
150	2.42	704	2.04	784
200	3.23	748	2.68	873

[10] N. Pearlman, "Low Temperature Atomic Heat of Silicon, Germanium and Silver," Ph. D. thesis, Purdue University (1952).

0.157×10^6, 0.104×10^6, and 0.0226×10^6 used in Smith's calculation. The value of μ even has a different sign. It seems that a check on the force constants used by Smith still depends upon more accurate experimental data on the elastic constants of diamond.

In the present calculation, no Raman shifts are available and Eqs. (1) are the only relationships for the determination of the force constants. The experimental error of the elastic constants is less than 1 percent. Under the assumptions used in the theory, the force constants calculated should also be accurate to 1 percent. In both cases the value of μ is negative.

The main difference between the frequency spectrum obtained from the first approximation and that from the second approximation is the upper limit of the frequency. Since Ge satisfies Eq. (2) more closely than Si, the difference between the frequency limits in the two approximations is smaller in the Ge case than in the Si case. In the case of diamond, the first-order Raman shift determines the upper limit, but no such information can be used for Ge and Si. Although there are large differences in the frequency limits between the two approximations, the specific heat curves deduced from them are still close together. However, the second approximation curves agree less satisfactorily with the experiments than the first approximation curves. In view of the accuracy of the experimental elastic constants, the discrepancies between the theoretical and experimental specific heats may mean that the second-neighbor forces are not central or that more distant neighbors also exert appreciable forces, as suggested by Born.[11] The consideration of more distant neighbors would introduce more force constants, which would make the calculation practically impossible. Acceptance of noncentral second-neighbor forces would necessitate other assumptions about the force constants λ, μ, and τ in order that they might be determined together with α and β from the three elastic constants.

TABLE IX. Specific heat of Ge calculated from discrete spectrum.

	1st approx.		2nd approx.	
T°K	C_v cal/mole/°C	Θ°K	C_v cal/mole/°C	Θ°K
10	0.012	335	0.012	335
15	0.057	314	0.057	312
20	0.14	299	0.14	298
30	0.41	311	0.41	311
40	0.75	332	0.75	332
50	1.10	355	1.09	357

TABLE X. Specific heat of Si calculated from discrete spectrum.

	1st approx.		2nd approx.	
T°K	C_v cal/mole/°C	Θ°K	C_v cal/mole/°C	Θ°K
20	0.022	551	0.022	554
30	0.089	521	0.089	521
40	0.21	523	0.21	522
50	0.37	536	0.37	535
75	0.86	590	0.85	593
100	1.35	649	1.28	663

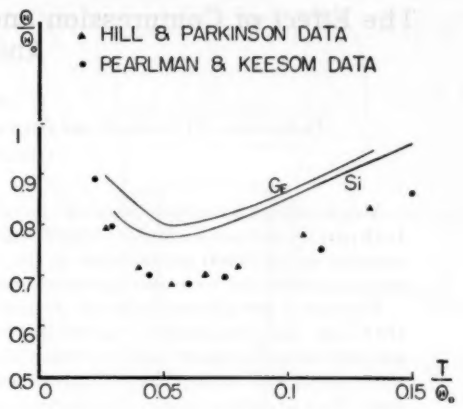

FIG. 7.

Another question is whether the use of the elastic constants at 0°K would improve the agreement between the theory and the experiment. The elastic constants of Si at 0°K estimated by Pearlman and Keesom[9] are $C_{11}=1.689\times10^{12}$, $C_{12}=0.6532\times10^{12}$, $C_{44}=0.8005\times10^{12}$. They show less than 1 percent difference from the values used in the present calculation. Within the accuracy of the present method, it seems unlikely that a 1-percent change of the elastic constants would give a much closer agreement between the theory and the experiment.

A recent experiment on diamond[12] shows that besides a flat minimum, there exists a sharp maximum at 60°K in the Debye characteristic temperature against temperature curve. In both the Ge and Si cases, experiments show only the minimum. More experimental data are needed to show whether there also exists a maximum at still lower temperatures. The accuracy of the present calculation, as well as that of Smith, could not give any reliable information at such temperatures.

The author wishes to express his thanks to Dr. K. Lark-Horovitz for his encouragement in this work. Thanks are also due Dr. P. H. Keesom and Dr. N. Pearlman for their valuable discussions, for communicating their experimental results on Si before publication, and for their unpublished results on Ge.

[11] M. Born, Nature **157**, 582 (1946).
[12] Warren DeSorbo, J. Chem. Phys. **21**, 876 (1953).

The Effect of Compression and of Hydrostatic Pressure on the Diffusion Anisotropy in Zinc*

T. Liu and H. G. Drickamer
Department of Chemistry and Chemical Engineering, University of Illinois, Urbana, Illinois
(Received September 10, 1953)

Measurements have been made on the rate of self-diffusion in single crystals of zinc along the directions both parallel and perpendicular to the *C* axis. The effects of compression by an applied force and hydrostatic pressure up to 10 000 atmospheres on the rate of diffusion were studied. The self-diffusion coefficients of polycrystalline zinc were also measured under both atmospheric pressure and compression.

The rate of self-diffusion in single crystals of zinc was found always to be larger in the direction parallel to the *C* axis, while the enthalpy of activation was found always to be smaller in this direction. Both compression and hydrostatic pressure tend to reduce the rate of self-diffusion, the greater effect being observed in the direction parallel to the *C* axis. Compression perpendicular to the direction of diffusion gave essentially the same effect as compression in the direction of diffusion. The enthalpy of activation was found to be increased 30 percent by the application of a pressure of 8000 atmospheres and to be decreased slightly by compression. The anisotropy in the rate of diffusion was found to decrease with increased hydrostatic pressure. The self-diffusion coefficients of polycrystalline zinc were found to be intermediate between the values observed in the two directions (parallel and perpendicular to the *C* axis) in single crystals and to be closer in magnitude to the values observed in the direction perpendicular to the *C* axis.

In order to understand the effect of molecular arrangement on diffusion, measurements have been made of the self-diffusion coefficient in single crystals of zinc parallel and perpendicular to the *C* axis. The effects of compression along one axis and of hydrostatic pressure to 10 000 atmospheres on the rate of diffusion have been studied. Self-diffusion coefficients for polycrystalline zinc were also measured under atmospheric pressure and uniaxial compression.

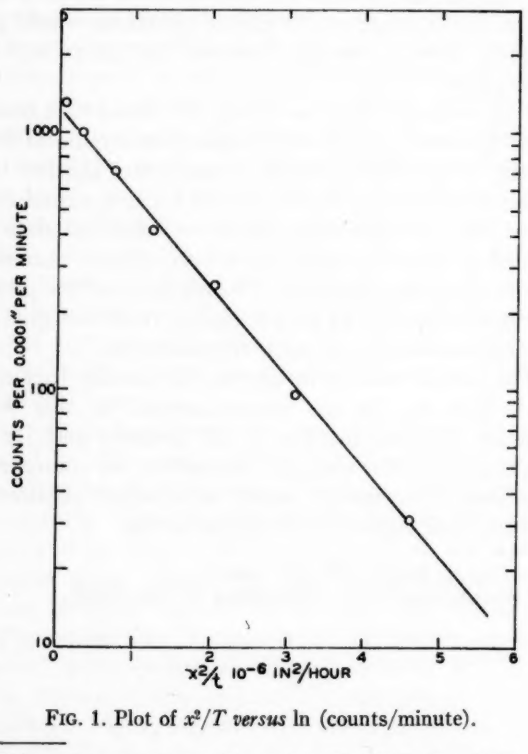

FIG. 1. Plot of x^2/T *versus* ln (counts/minute).

EXPERIMENTAL PROCEDURE

A. Growth, Preparation, and Analysis of Crystals

The single crystals were grown from 99.99-percent Zn in a Bridgman-type furnace. The orientation was determined by the method described by Gwathmey.[1] The crystals were cooled to liquid-air temperature and cleaved along the basal plane. For diffusion perpendicular to the *C* axis, the pieces were sawed with a jeweler's saw and polished with 0000 emery paper. In all cases the faces used for diffusion were carefully electropolished. Any strains due to cleaving or cutting were very evident after the electropolishing. All strained crystals were discarded. The Zn^{65} was obtained from the Oak Ridge National Laboratory as $ZnCl_2$ in acid solution. All surfaces of the crystal, except that used for diffusion were coated with polyvinyl plastic. The Zn^{65} was plated on this face from a 0.1*N* solution to a thickness not exceeding 0.0008 inch.

After the diffusion the crystals were gripped in a special chuck modified for each crystal and sanded perpendicular to the direction of diffusion on 0000 emery paper. The sandings were collected on a circle 2 cm in diameter on the paper. The crystal was micrometered to 0.0001 inch after each slice. The average slice thickness was 0.001 inch and was kept within 20 percent for all slices. The papers were counted with carefully reproducible geometry using a Geiger-Muller tube and a Nuclear Instrument Company Model-161 scalar. The results were reduced to a common thickness.

The equation for diffusion from an instantaneous source is

$$C=Q(\pi Dt)^{-\frac{1}{2}}\exp\left(-\frac{Dt}{4x^2}\right), \quad (1)$$

* This work was supported in part by the U. S. Atomic Energy Commission.

[1] A. T. Gwathmey and A. F. Benton, J. Phys. Chem. 44, 35 (1940).

so a plot of $\ln C$ *vs* t/x^2 gives a slope of $-D/4$. Figure 1 shows a typical plot for a good run.

B. Diffusion Apparatus

The atmospheric pressure diffusion measurements were made in a ceramic furnace, the crystals being immersed in silicone grease.

Compression was applied to the crystals in the apparatus shown in Fig. 2. Weights were added to the pan to give the compressive load desired. The crystals were protected by silicone grease. Runs were discarded if any sign of permanent deformation could be observed or measured. This condition set the upper temperature limit for these runs. Diffusion measurements were made (on different crystals) both in the direction of and perpendicular to the applied force.

The apparatus for obtaining hydrostatic pressure has been described previously.[2] The pressures could either

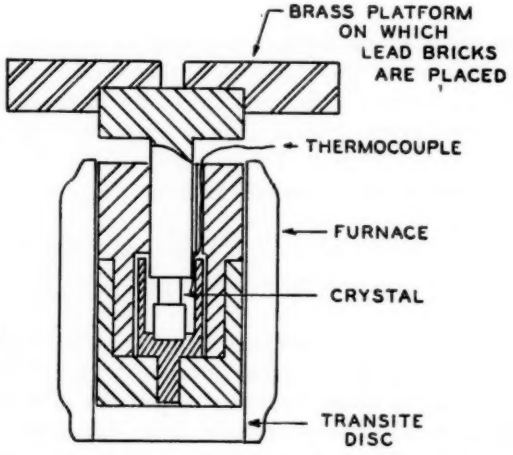

FIG. 2. Apparatus for measurement of diffusion in single crystals with applied force.

be measured directly by a manganin gauge or by calibration of the low-pressure end of the intensifier against the manganin gauge. The accuracy of measurement was better than 1 percent, but on the long high-pressure runs (above 8000 atmos) fluctuations of up to 150 atmospheres occurred as a result of the effect of room temperature on the expansion of the low-pressure oil.

The bomb for diffusion was held in a heated bath at about 120°. The interior of the bomb is shown in Fig. 3. There were two electrical windings and two thermocouples. With this arrangement the temperature could be held uniform to ±3°C over a range of $1\frac{1}{2}$ cm at the middle of the bomb. The crystals were kept in this area, sitting on a steel plug. The thermocouples had some error due to the electrical seals. They were calibrated against a traversing couple at atmospheric pressure. This gave somewhat irregular results at the highest temperatures due to incipient boiling of the liquid on the

[2] R. C. Koeller and H. G. Drickamer, J. Chem. Phys. **21**, 267 (1953).

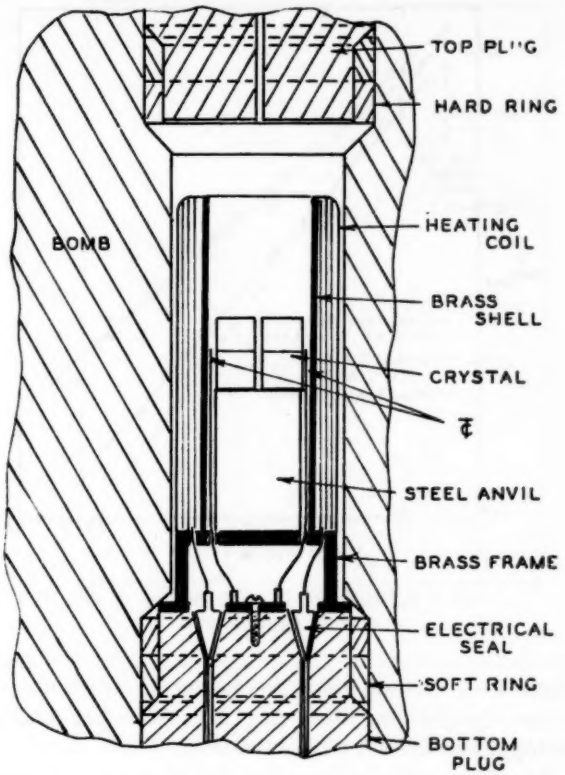

FIG. 3. Arrangement inside bomb for high-pressure diffusion measurements.

coil. The absolute temperature was established from the 307°C isotherm runs which were made down to 20 atmospheres and the results (both parallel and perpendicular to the C axis) extrapolated to atmospheric pressure. Both smooth curves gave a temperature of exactly 307°, so this was taken as a fixed point in the calibration. In the actual high-pressure runs Dow Corning DC200 silicone fluid (2 centipoise viscosity grade)† was used in the bomb. The technique qualitatively resembled that described by Nachtrieb, *et al.*[3]

For pressures below 2000 atmospheres a handpump and Bourdon Gauge calibrated against a dead weight gauge were employed.

Theory

On rather general grounds[4–6] one can write the equation for D in the form

$$D=\frac{\nu d_i^2}{6}\exp(\Delta S/R)\exp(-\Delta H/RT)$$
$$=\frac{\nu d_i^2}{6}\exp(-\Delta F/RT), \qquad (2)$$

† This fluid was recommended to us for high-temperature high-pressure work by A. W. Lawson of the University of Chicago.

[3] Nachtrieb, Weil, Catalano, and Lawson, J. Chem. Phys. **20**, 1189 (1952).

[4] C. A. Wert, J. Appl. Phys. **21**, 1196 (1950).

[5] C. A. Wert and C. Zener, Phys. Rev. **76**, 1169 (1949).

[6] C. Zener, J. Appl. Phys. **22**, 372 (1951).

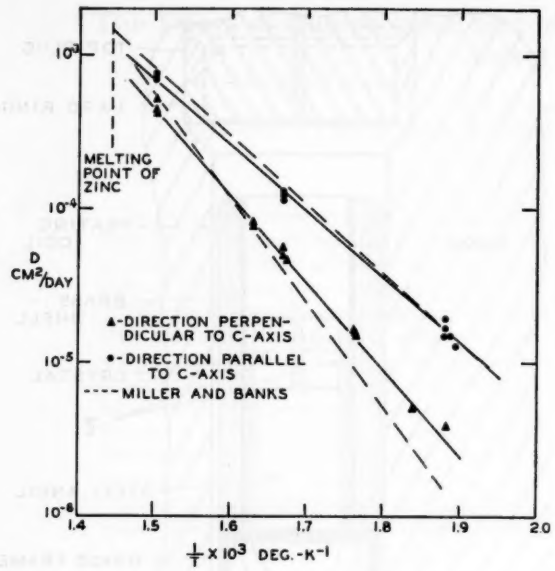

FIG. 4. Self-diffusion in single crystals of zinc without applied force.

where ν=a characteristic frequency, d_i=distance between equilibrium sites, ΔF, ΔS, ΔH=free energy, entropy, and enthalpy of activation.

An additional quantity, the activation volume can be defined by the equation

$$\Delta V^{\ddagger}=\left(\frac{\partial \Delta F}{\partial p}\right)_T \tag{4}$$

$$\Delta V^{\ddagger}=-RT\left[\frac{\partial \ln D}{\partial p}-\frac{\partial \ln \nu}{\partial p}-\frac{\partial \ln d_i^2}{\partial p}\right]_T. \tag{5}$$

For an anisotropic crystal it is convenient to define an activation length in terms of the activation volume

$$\Delta l^{\ddagger}=(\Delta V^{\ddagger}/N_0)^{\frac{1}{3}}. \tag{6}$$

Although a quantitative interpretation of this quantity is not possible, it is useful in discussing the effect of hydrostatic pressure.

TABLE I. Self-diffusion in single crystal of zinc under atmospheric pressure in the direction parallel to the C axis.

T°C	D 10^{-5} cm²/day
255	1.29
257	1.51
258.5	1.92
258.5	1.52
258.5	1.66
326	12.8
326	11.7
326	12.0
393	73.3
393	68.1
393	69.3

TABLE II. Self-diffusion in single crystal of zinc under atmospheric pressure in the direction perpendicular to the C axis.

T°C	D 10^{-5} cm²/day
258	0.38
271	0.50
295	1.53
295	1.59
325	4.57
326	4.80
326	5.59
341	7.71
341	7.94
393	41.0
393	50.5
393	42.0

Results

The self-diffusion coefficients of zinc obtained experimentally are tabulated in Tables I through X. Graphs of these results can be found in Figs. 4 through 11.

The self-diffusion coefficient of single crystals of zinc was measured in the direction both parallel and perpendicular to the C axis under the following conditions:

(1) *Atmospheric pressure over a temperature range of 253–393*°C.—The data (Tables I and II, Fig. 4) can be represented by the following equations:

$$D_{\parallel}=1840\exp(-19\,600/RT)\ \text{cm}^2/\text{day}; \tag{7}$$

$$D_{\perp}=1.38\times10^5\exp(-25\,900/RT)\ \text{cm}^2/\text{day}. \tag{8}$$

The uncertainty of the activation enthalpies is estimated to be ±500 calories per gram atom for both directions.

(2) *Diffusion under compression with the direction of diffusion parallel to the direction of the force applied.*—Runs with a stress of approximately 500 psi were carried out over the temperature range 243–332°C, and runs with a stress of about 950 psi were made between 225 and 253°C. (Higher temperatures were used but the

TABLE III. Self-diffusion in single crystal of zinc under compression with both diffusion and compression in the direction parallel to the C axis.

T°C	D 10^{-5} cm²/day	Stress psi
250	0.70	475
260	1.06	475
267.5	1.29	475
295	3.06	475
296.5	3.26	475
326	6.10	475
327	5.61	475
329	6.39	475
222	0.238	920
232	0.290	920
254	0.468	920
255	0.701	920
256	0.685	920
256.5	0.581	920
256.5	0.614	920

TABLE IV. Self-diffusion in single crystal of zinc under compression with diffusion in the direction perpendicular to the C axis and compression in the direction of diffusion.

T°C	D 10^{-5} cm²/day	Stress psi
267.5	0.405	515
274	0.585	515
292	1.18	515
293.5	1.40	515
325	3.78	515
329	4.39	515
231	0.117	1000
233	0.129	1000

samples were deformed permanently.) The results, given by Tables III and IV and Fig. 5, fit the equations:

for 475 psi,

$$D_{\parallel}=184\exp(-17\,700/RT)\ \text{cm}^2/\text{day}; \quad (9)$$

for 515 psi,

$$D_{\perp}=3.92\times10^{4}\exp(-24\,600/RT)\ \text{cm}^2/\text{day}; \quad (10)$$

for 920 psi,

$$D_{\parallel}=21.2\exp(-15\,800/RT)\ \text{cm}^2/\text{day}. \quad (11)$$

The uncertainty of the enthalpy of activations is estimated to be ±500, 800, and 1500 calories per gram atom for the above three equations, respectively.

(3) *Diffusion under applied force, with the direction of diffusion perpendicular to the direction of the force applied.*—The force applied was in the neighborhood of 500 psi, and the temperature range was 250–335°C. The results are listed in Tables V and VI. The diffusion coefficients were corrected to a stress of 475 and 515 psi for the direction (of diffusion) parallel and perpendicular to the C axis, respectively. The data are compared with the results obtained with the direction of diffusion parallel to the direction of the applied force in Fig. 6. One can see that Eqs. (9) and (10) also fit these data.

(4) *Diffusion under hydrostatic pressure.*—Two series of experiments were done, *viz.*, a 307°C isotherm and an 8000 atmosphere isobar. The results are shown in Tables VII and VIII, and Figs. 7 and 8. The data for

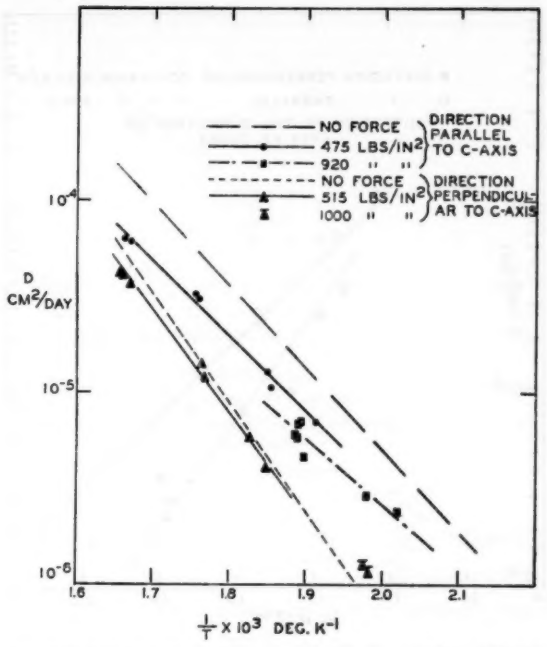

FIG. 5. Self-diffusion in single crystals of zinc with applied force in the direction of diffusion.

the isobar can be represented by the following equations:

$$D_{\parallel}=4.8\times10^{4}\exp(-25\,000/RT)\ \text{cm}^2/\text{day}, \quad (12)$$

$$D_{\perp}=1.8\times10^{7}\exp(-32\,000/PT)\ \text{cm}^2/\text{day}. \quad (13)$$

The uncertainty of activation enthalpy in Eq. (12) is ±1500-cal/g atom and in Eq. (13) is ±800-cal/g atom.

The self-diffusion coefficients of polycrystalline zinc with an average grain size of 0.05 mm were measured under atmospheric pressure from 250 to 375°C and under an applied stress of 470 psi over the temperature range of 250–330°C. The results are shown in Tables IX, X, and Fig. 9 and fit the following equations:
for atmospheric pressure,

$$D=3.6\times10^{4}\exp(-23\,800/RT)\ \text{cm}^2/\text{day}; \quad (14)$$

under applied force,

$$D=2.9\times10^{4}\exp(-23\,000/RT)\ \text{cm}^2/\text{day}; \quad (15)$$

the uncertainty in ΔH is 500-cal/g-atom in each case.

TABLE V. Self-diffusion in single crystal of zinc under compression with diffusion in the direction parallel to the C axis and compression perpendicular to the C axis.

T°C	D 10^{-5} cm²/day	Stress psi	D475 psi 10^{-5} cm²/day
257.5	0.732	702	0.970
258	0.865	539	0.938
265	0.858	475	0.858
291	2.39	490	2.60
293	2.55	639	2.57
320	6.85	450	6.65
326	7.70	416	6.98
344	13.3	365	10.4

TABLE VI. Self-diffusion in single crystal of zinc under compression with diffusion in the direction perpendicular to the C axis and compression parallel to the C axis.

T°C	D 10^{-5} cm²/day	Stress psi	D515 psi 10^{-5} cm²/day
254	0.382	528	0.379
256	0.242	418	0.240
257	0.287	467	0.287
285	0.844	486	0.841
302	1.07	505	1.07
318	2.96	373	2.76
329	3.82	398	3.57

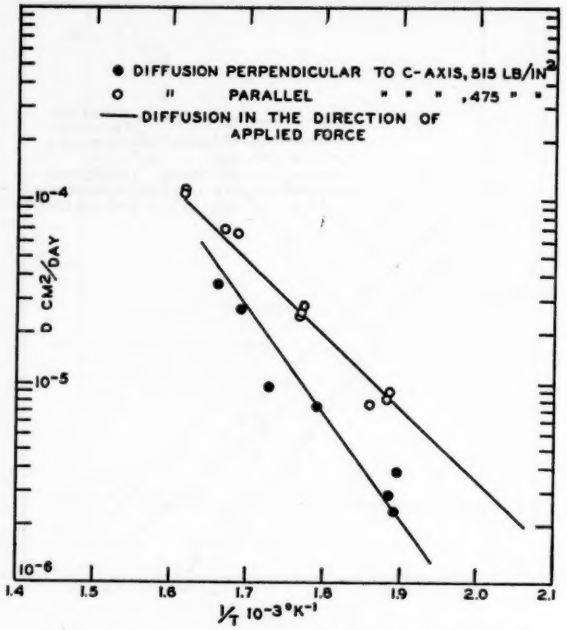

FIG. 6. Self-diffusion in single crystals of zinc with applied force perpendicular to the direction of diffusion.

The enthalpy of activation and D_0's for all the isobars measured are summarized in Table XI, which also includes all the entropies, free energies, and volumes of activation at 307°C. The enthalpy of activation and D_0 for each isobar were obtained from the empirical equation $D=D_0\exp(-H/PT)$ which fits the experimental data. The entropy and free energy at 307°C for each condition were calculated from Eqs. (2) and (3). The activation volumes were obtained by using Eq. (5). Besides those quantities, the activation lengths defined by Eq. (6) are also listed in Table XI.

The data required for the calculations, besides the experimental figures, include the lattice constants, coefficients of linear thermal expansion, linear compressibilities, elastic constants, thermal vibration frequency, and the relationship between melting point and pressure for single crystals of zinc. The lattice constants at 25°C and the thermal vibration frequency were taken from *Metal Reference Book*.[7] At higher temperatures, the coefficients of linear expansion given by Birch[8] were used to calculate the lattice constants. The linear compressibilities at 307°C, required for the calculation of lattice constants under hydrostatic pressure were obtained from Bridgman's[9] data at 30 and 75°C. assuming the constants vary linearly with temperature. The data of Wert and Tyndall[10] on elastic constants were used for calculating the lattice constants under applied force. The vibration frequencies under pressures were calculated using Lindemann's relation:

$$\nu=\nu_1(Tm/Tm_1)^{\frac{1}{2}}(V_1/V)^{\frac{1}{6}}, \tag{16}$$

where the subscript 1 refers to the values under atmospheric pressure and Tm is the melting point. The melting point was assumed to vary linearly with pressure according to the value of $\Delta P/\Delta T$ given by Birch.[8]

TABLE VII. Self-diffusion in single crystal of zinc under hydrostatic pressure at 307°C.

P atmospheres	$D_{\parallel}$	$D_{\perp}$
	10^{-5} cm²/day	
1	7.20	2.25
700	5.77	1.97
	5.68	2.20
2000	4.16	2.14
	4.23	1.90
5000	2.57	1.68
	2.64	
8000	1.90	1.60
	1.80	1.40
10 000	1.66	1.32
		1.24

TABLE VIII. Self-diffusion in single crystal of zinc under 8000 atmospheres.

T°C	$D_{\parallel}$	$D_{\perp}$
	10^{-5} cm²/day	
274	0.520	0.204
	0.585	0.234
287		0.458
		0.439
		0.470
307	1.90	1.40
	1.80	1.60
327	4.52	3.75
	4.40	3.83

The interpretation of ΔS and ΔF as directional quantities is somewhat anomalous. Therefore, these quantities are merely tabulated, and our discussion of results is mainly concerned with ΔH and $\Delta V^{\ddagger}$.

DIFFUSION UNDER ATMOSPHERIC PRESSURE

The results are shown in Fig. 4. Also shown in Fig. 4 are the results of Miller and Banks.[11,12] The agreement in the direction parallel to the C axis is very good, but in the direction perpendicular to the C axis, their values do not agree with our results too well. In fact, these authors did not measure $D_{\perp}$ directly; they obtained the curve by measuring the rates of diffusion of

[7] C. J. Smithel, *Metal Reference Book* (Butterworth Scientific Publications, London, 1949).
[8] F. Birch, "Handbook of physical constants," Geol. Soc. Am. Special Paper No. 36, 1942.
[9] P. W. Bridgman, Proc. Am. Acad. Arts Sci. **60**, 305 (1923).
[10] C. A. Wert and E. P. T. Tyndall, J. Appl. Phys. **20**, 587 (1949).
[11] F. R. Banks, Phys. Rev. **59**, 3761 (1941).
[12] P. H. Miller and F. R. Banks, Phys. Rev. **61**, 648 (1942).

several variously oriented crystals and calculating the values of $D_\perp$. Most of their samples used for this calculation had the value $\theta<45°$, and the temperature range of their measurement was only 67°C. Besides, the consistency of their data was poor. Therfore, the lack of agreement is not surprising.

The diffusion in the direction perpendicular to the C axis has a larger value of $D_0(1.38\times10^5$ cm²/day as compared to 1840 cm²/day for the direction parallel to the C axis) and also a higher enthalpy of activation (25 900 cal/g-atom as compared to 19 600 cal/g-atom for the parallel direction).

An attempt was made to calculate the activation entropies from Eq. (11) using the elastic constants given by Wert and Tyndall.[10] Unfortunately, the uncertainty of extrapolating their data to 0°K is too

TABLE IX. Self-diffusion in polycrystalline zinc (average grain size 0.2 mm) under atmospheric pressure.

T°C	D 10^{-5} cm²/day
243	0.286
243	0.312
291	2.25
291	2.34
325	6.6
325	7.0
365.5	23.6
365.5	24.1

TABLE X. Self-diffusion in polycrystalline zinc (average grain size 0.2 mm) under a compressive stress of 470 psi.

T°C	D 10^{-5} cm²/day
238	0.18
239	0.20
295	1.86
298	2.02
306	2.72
308	2.98
329	5.81

large (ten-fold) to give any significance, although the experimental results, which are consistent with the assumption of vacancy mechanism, do fall in the middle of the possible range while the ring mechanism fails. The ratios between $\Delta S_\perp$ and $\Delta S_{||}$ calculated on the vacancy mechanism using the extreme values are in good agreement with the observed value.

THE EFFECT OF COMPRESSION ON DIFFUSION

The diffusion coefficients are found to decrease with applied force (Fig. 5) in the directions both parallel and perpendicular to the C axis, when the direction of the force is parallel to the direction of diffusion. In Fig. 6, the points represent the diffusion coefficients with an applied force perpendicular to the direction of diffusion. Comparing these points with the curves giving the

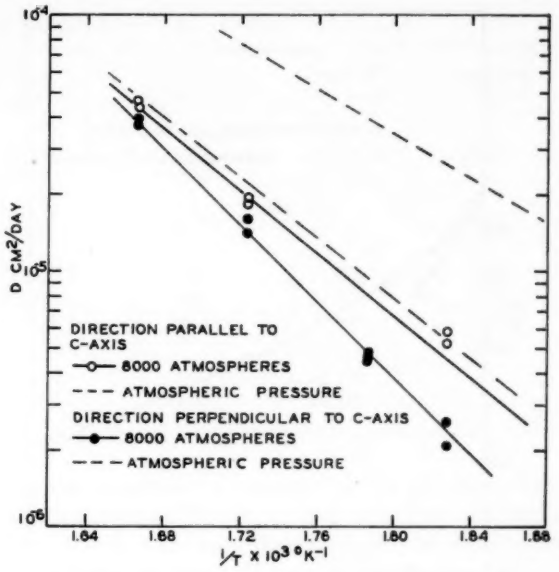

FIG. 7. Self-diffusion in zinc under 8000 atmospheres pressure.

diffusion coefficients with the applied force parallel to the direction of diffusion, one can readily see that the direction of compression with respect to the direction of diffusion has little, if any, effect on the rate of diffusion. Figure 5 also shows the effect of compression on diffusion to be larger in the direction parallel to the C axis; this is reasonable as the Young's modulus along this direction is only about one-fourth of that along the perpendicular direction. Hence, one may expect a larger change of lattice structure in the direction parallel to the C axis with the same applied force.

The enthalpy of activation in the direction parallel to the C axis decreases from 19 600 to 17 700 cal/g-atom, with an applied stress of approximately 500 psi. The strain introduced by the applied force tends to ease the

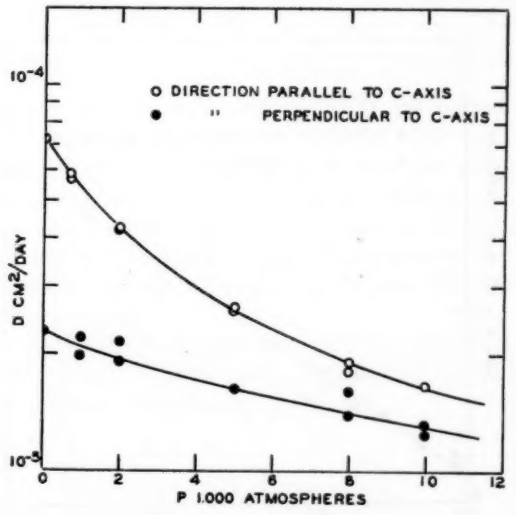

FIG. 8. The effect of pressure on self-diffusion in single crystals of zinc at 307°C.

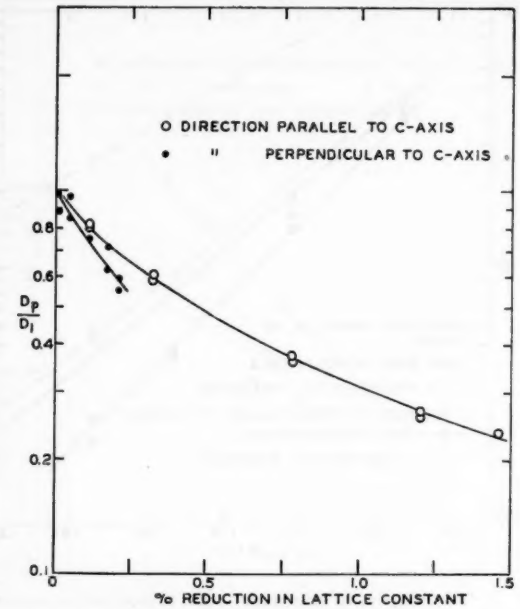

FIG. 9. $D_p/D_{1\text{ atm}}$ *versus* percent. Reduction in linear dimension at 307°C.

formation of vacancies and consequently decreases the enthalpy of activation. The change of cohesive force between the atoms due to applied force is apparently small, for otherwise the direction of the applied force should have a notable effect on the rate of diffusion.

The negative activation entropy obtained for diffusion in the direction parallel to the *C* axis is inconsistent with the theory of Zener.[6] Because of the difficulties involved in the interpretation of the entropy of activation in anisotropic solids, no discussion will be presented at this time.

THE EFFECT OF PRESSURE ON DIFFUSION

The experimental results (Figs. 7, 8) show a decrease of the rate of diffusion with pressure. A similar effect was found by Radavich and Smoluchowski[13] on Al-Cu alloy and by Nachtrieb, *et al.*,[3] on sodium. Figure 8 also shows that pressure has a larger effect on the diffusion parallel to the *C* axis. This is reasonable as the linear compressibility is larger in this direction and, consequently, pressure would cause a larger change in the lattice structure in the direction parallel to the *C* axis. A plot of D/D_{atm} at 307°C *versus* the percentage reduction in lattice constant due to the application of pressure is shown in Fig. 9. This indicates that for the same percentage reduction in linear dimension, perpendicular to the *C* axis, where the interatomic distance is smaller, the change of the rate of diffusion is greater percentagewise.

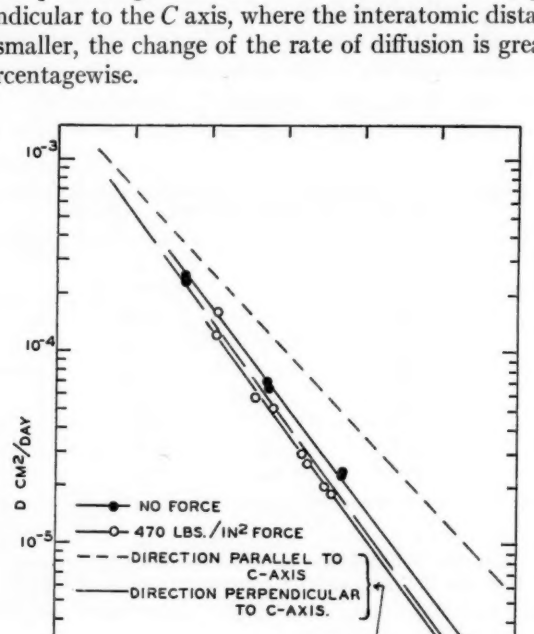

FIG. 11. Self-diffusion in polycrystalline zinc.

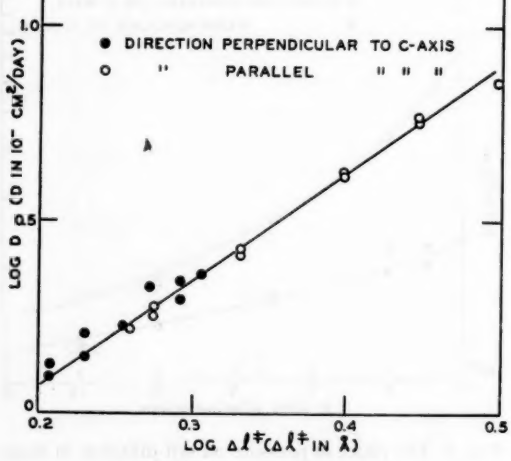

FIG. 10. Log*D* *versus* log$\Delta l^{\ddagger}$.

Under 8000 atmospheres it is found from Fig. 7 that $\Delta H_{\perp} = 32\,000$ cal/g-atom and $\Delta H_{\parallel} = 25\,000$ cal/g-atom. This indicates a 30-percent increase in the enthalpy of activation over the atmospheric-pressure value both parallel and perpendicular to the *C* axis. This increase is expected, as under pressure the enthalpy associated with the formation of vacancies must be increased. Possibly there is also a change in the cohesive energy. Since the change in the interatomic distance is small (Table XII), it is probable that the increase in the enthalpy associated with the formation of the vacancies predominates the increase in the enthalpy of activation with pressure.

The entropies of activation at 307°C under a pressure of 8000 atmospheres were found to be 8.30 and 20.1 cal/°K×g-atom for the directions parallel and perpen-

[13] F. J. Radavich and R. Smoluchowski, Phys. Rev. **65**, 62 (1944).

TABLE XI. Summary of quantities.

Description	D_0 cm²/day	D_0 cm²/sec	ΔH cal/g-atom	ΔS307°C cal/°K-g-atom	ΔF307°C cal/g-atom	$\Delta V^{\ddagger}$307°C cc/g-atom
Single crystal, diffusion parallel to the C axis						
Atmospheric pressure	1860	2.15×10^{-2}	19 600	1.88	18 500	16.8
475 psi stress	184	2.13×10^{-3}	17 700	−2.70	19 200	
920 psi stress	21.2	2.45×10^{-4}	15 800	...		
8000 atmospheres	4.8×10^{4}	0.56	25 000	8.30		4.04
Single crystal, diffusion perpendicular to the C axis						
Atmospheric pressure	1.38×10^{6}	1.60	25 900	10.5	19 800	4.95
515 psi stress	3.92×10^{4}	0.45	24 600	7.95	20 000	
8000 atmospheres	1.8×10^{7}	210	32 000	20.1	20 400	2.95
Polycrystalline zinc						
Atmospheric pressure	3.6×10^{4}	0.42	23 800	7.79	19 300	
470 psi stress	2.9×10^{4}	0.34	23 000	7.37	18 700	

dicular to the C axis, respectively. This compares with the atmospheric values of 1.88 and 10.5 cal/°K×g-atom for the directions parallel and perpendicular to the C axis, respectively.

The effect of pressure on the free energy of activation was found to be small, and the values under 8000 atmospheres at 307°C for the directions parallel and perpendicular to the C axis are very close (20 200 to 20 400 cal/g-atom, respectively).

The activation volume $\Delta V^{\ddagger}$ and the activation length, together with the interatomic distances of zinc at 307°C under different pressures, are tabulated in Table XII. It is interesting to note that under atmospheric pressure, $\Delta l_{\parallel}^{\ddagger}$ is of the order of $d_{\parallel}$ and $\Delta l_{\perp}^{\ddagger}$ is about 70 percent of $d_{\perp}$, whereas under an applied pressure of 8000 atmospheres both $\Delta l^{\ddagger}$'s become about 60 percent of the corresponding interatomic distance. Figure 10 is a plot of log$D$ *versus* log$\Delta l^{\ddagger}$ which indicates that the diffusion coefficient is proportional to the 2.8th power of the activation length regardless of direction in the crystal. The activation volume may be considered as the combination of the volume change associated with the formation of lattice dislocations, $\Delta V_v^{\ddagger}$, and the volume associated with the movement of the atoms $\Delta V_m^{\ddagger}$. $\Delta V_v^{\ddagger}$ must be positive for the vacancy mechanism and negative for an interstitial mechanism. In any case $\Delta V_m^{\ddagger}$ is always positive. It is difficult to decide which one of these volume changes is numerically larger except in ionic crystals where $\Delta V_v^{\ddagger} > \Delta V_m^{\ddagger}$. If this is also true for zinc, a positive $\Delta V^{\ddagger}$ is evidently in favor of the vacancy mechanism.

DIFFUSION IN POLYCRYSTALLINE ZINC

Figure 11 shows that experimental results of the self-diffusion of polycrystalline zinc both under atmospheric pressure and an applied force of 470 psi. Also shown in Fig. 11 are the curves for diffusion in single crystals of zinc under atmospheric pressure in the directions both parallel and perpendicular to the C axis. One can readily see that the rate of self-diffusion of polycrystalline zinc is intermediate between the rate of the single crystals in the directions parallel and perpendicular to the C axis and is closer to that in the perpendicular direction. This is reasonable as the diffusing atoms might travel through many single crystals randomly oriented with the chances of diffusing in the directions parallel to the C axis being $\frac{1}{3}$ and perpendicular to the C axis $\frac{2}{3}$.

As in the case of single crystals the rate of self-diffusion of polycrystalline zinc is found to decrease with applied force. The decrease in the enthalpy of activation due to compression (800 cal/g-atom) is smaller than the single crystal values (1900 and 1300 cal/g-atom). This seems reasonable since the existence of the grain boundaries increases the strength of the crystal and hence reduces the degree of disturbance introduced by the applied force. This explains why the decrease in entropy of activation is also small (0.43 cal/°K×g-atom).

TABLE XII. The activation volume, the activation length and the interatomic distances of zinc at 307°C.

Pressure (atmospheres)	Activation volume cc/g-atom ∥ to C-axis	Activation volume cc/g-atom ⊥ to C-axis	Activation length A ∥ to C-aixs	Activation length A ⊥ to C-axis	Interatomic distances A $d_{\parallel}$	Interatomic distances A $d_{\perp}$	Atomic volume cc/g-atom
1	16.87	4.95	3.15	2.02	2.94	2.67	9.62
700	13.20	4.53	2.80	1.96	2.94	2.67	9.61
2000	9.36	3.93	2.50	1.87	2.93	2.67	9.59
5000	5.90	3.52	2.14	1.80	2.92	2.67	9.53
8000	4.04	2.97	1.88	1.70	2.91	2.66	9.49
10000	3.62	2.68	1.82	1.61	2.91	2.66	9.45

The authors wish to acknowledge the suggestions and advice of David Lazarus and L. F. Slifkin of the University of Illinois, Department of Physics.

THE JOURNAL OF CHEMICAL PHYSICS VOLUME 22, NUMBER 2 FEBRUARY, 1954

The Electronic Spectra of Cata-Condensed Hydrocarbons

WILLIAM MOFFITT
Department of Chemistry, Harvard University, Cambridge, Massachusetts
(Received August 20, 1953)

It is shown how the main features of the spectra of cata-condensed hydrocarbons may be explained on the basis of a very simple model. This, so-called perimeter model was used, in its free-electron variant, by Platt in order to classify the spectra. In this note, a more quantitative version is formulated which enables calculations to be made; it may be considered as an approximation either to an antisymmetrized molecular orbital treatment or to the method of atoms in molecules.

INTRODUCTION

THE electronic spectra of benzene, of its homologs, the polyacenes, and their isomers have been the subject of considerable experimental study. And this study has been rewarded by the appearance of remarkable similarities and regularities in the properties of the concomitant band systems. It is the purpose of this note to show how the more striking of these generic relationships may be understood.

The so-called cata-condensed hydrocarbons generally exhibit three main band systems in the near ultraviolet or visible region of the spectrum. The prototypes of all these systems are to be found in benzene, which absorbs strongly near 1750A, exhibits absorption of moderate intensity around 2000A, and shows a weak band system in the 2500A region. Clar demonstrated that band systems of a similar type also occur for the higher homologs of benzene.[1] He classified these as β, p, and α systems, respectively. This note will be concerned with the following aspects of the spectra:

I. The regular appearance of the three systems enumerated by Clar throughout the range from benzene to its very complex homologs containing fused rings.

II. The regular intensity relationships which they exhibit; very intense β bands, moderately intense p bands, and very weak α bands.

III. The relative insensitivity of the location of the α and β bands to isomerism, but the characteristic movement of the p bands, e.g., on going from anthracene to phenanthrene.

IV. The particular intensification of the α bands under inductive substitution, such as occurs on going from naphthalene to quinoline.

V. The relation between the spectra of naphthalene and azulene, in which analogous band systems may also be identified.

VI. The characteristic shifts exhibited by the α bands of azulene, to the red or to the violet, depending on the nature and position of different substituents in the aromatic system. Most of these topics have already been discussed by various authors, particularly during the last decade, and some reference to their work will be made later. The empirical characterization of these effects is particularly due to Clar,[1] and more recently to Jones[2] and to Klevens and Platt.[3] But no unified theoretical treatment has been put forward, for reasons which are not difficult to understand.

The potentialities of a given theory may be tested with reference to the account it gives of the benzene spectrum, and it is already here that calculations founder. The most appealing theory, on grounds of conceptual simplicity and predictive immediacy, namely the molecular orbital method, has been applied to benzene in stages of increasing sophistication. The first of these, which is based on purely qualitative considerations of simple orbital configurations, is undoubtedly the most successful. It correctly predicts the number and most probably also the symmetries of the low-lying singlet levels. However, the various attempts to locate these quantitatively, which mark succeeding stages, have met with indifferent results. The only formalism capable of ready generalization to more complicated systems without enormous increase in labor—the semi-empirical LCAO theory[4]—is incapable of distinguishing between the energies of the first three excited-singlet states (transitions to which account for the α, p, and β band systems). It is only by trying to assess the complicated electron repulsion terms that these states may be separated. And it appears that present computational techniques do not have sufficient accuracy to merit the attempt for all but the simplest systems. Moreover, the intricate methodology associated with such calculations would seem to mask rather than to reveal the generalizations that appear to underlie the spectra.

Platt has proposed a peculiarly simple approach to the classification of the spectra of these cata-condensed hydrocarbons.[5] It is based on what may be called the "perimeter" model of these systems, which is a simplification of the molecular orbital method. Essentially, he relates the electronic states of a given hydrocarbon to those of the corresponding cyclic polyene (e.g., of naphthalene to cyclodecapentaene). The first excited states of such cyclic polyenes, of general formula

[1] E. Clar, *Aromatische Kohlenwasserstoffe* (Julius Springer, Berlin), first edition 1941, second edition 1952.

[2] R. N. Jones, Chem. Rev. **32**, 1 (1943); **41**, 353 (1947).
[3] H. B. Klevens and J. R. Platt, J. Chem. Phys. **17**, 470 (1949).
[4] J. E. Lennard-Jones and C. A. Coulson, Trans. Faraday Soc. **35**, 811 (1939).
[5] J. R. Platt, J. Chem. Phys. **17**, 484 (1949).

TABLE I. The character table for the point group. $\mathbf{D}_{(4\nu+2)h}=\mathbf{C}_{(4\nu+2)v}\times\mathbf{C}_s$.

$\mathbf{C}_{(4\nu+2)v}$	I	$2C_{4\nu+2}$	$2C_{4\nu+2}^2$	...	$C_{4\nu+2}^{2\nu+1}=C_2$	$(2\nu+1)\sigma_v$	$(2\nu+1)\sigma_d$	
A_1	1	1	1	...	1	1	1	T_z
A_2	1	1	1	...	1	−1	−1	
B_1	1	−1	1	...	−1	1	−1	
B_2	1	−1	1	...	−1	−1	1	
E_1	2	$2Rl(\omega)$	$2Rl(\omega^2)$	...	−2	0	0	T_x, T_y
.	.	.	.		.	.	.	
.	.	.	.		.	.	.	
.	.	.	.		.	.	.	
E_ν	2	$2Rl(\omega^\nu)$	$2Rl(\omega^{2\nu})$	...	$(-1)^\nu 2$	0	0	
$E_{\nu+1}$	2	$2Rl(\omega^{\nu+1})$	$2Rl(\omega^{2\nu+2})$	...	$(-1)^{\nu+1}2$	0	0	
.	.	.	.		.	.	.	
.	.	.	.		.	.	.	
.	.	.	.		.	.	.	
$E_{2\nu}$	2	$2Rl(\omega^{2\nu})$	$2Rl(\omega^{4\nu})$	...	2	0	0	

I = identity operator; $C_{4\nu+2}$ = rotation by $2\pi/(4\nu+2)$ about the z axis; σ_v = reflection in a vertical plane of symmetry containing carbon atoms; σ_d = reflection in a vertical plane of symmetry bisecting carbon-carbon bonds. $\omega=\exp\{2\pi i/(4\nu+2)\}$.

$\mathbf{C}_s$ has only two elements, I and the reflection σ_h in the horizontal (xy-) plane of symmetry. Representations of the full group are therefore characterized first with respect to its $\mathbf{C}_{(4\nu+2)v}$ subgroup and then with respect to the inversion $i=C_2\cdot\sigma_h$ in the center of symmetry.

$C_{4\nu+2}H_{4\nu+2}(\nu=1, 2, \cdots)$, have certain symmetry properties which are preserved throughout the series of homologs. And these characteristics are empirically parallelled by the permanence of certain band types in the cata-condensed molecules, of general formula $C_{4\nu+2}H_{2\nu+4}$. This leads to an exceedingly fruitful classification of the spectra. There is, however, a variety of questions which Platt's treatment throws into relief—particularly those related to features II–VI above.

In the present note, a preliminary solution to these questions is outlined. To this end, simple LCAO theory will be used in conjunction with perturbation theory. Adopting the perimeter model, a description of the (hypothetical, planar) cyclic polyenes is first put forward and some plausible assumptions are made regarding their spectra—essentially an extrapolation from diatomic molecules and benzene to cyclic homologs of the latter. These are then regarded as unperturbed states, from which the cata-condensed systems are formed by perturbation. In this way, there is a direct correspondence between the two types of molecule and the essential properties of the perimeter model may be handled simply and semiquantitatively.

There is one important respect in which the treatment will differ from that of conventional LCAO theory. It is in the recognition that configurational interaction may be of two types. This classification is only rigid for the cyclic polyenes, but it is also important in other cases. The first type is due to the degeneracy of a particular configuration and may be considered as a first-order effect. The second is of little account in the cyclic polyenes, involving the "high-frequency" terms of second-order perturbation theory.[6] When the high symmetry of the cyclic polyenes is broken down, the distinction between these different types is obscured. By adopting the perimeter model, however, it remains a fairly real distinction and it is possible to refer the first-order assessment of configurational interaction in the cata-condensed molecules to that in the cyclic polyenes.

[6] W. Moffitt and J. Scanlan, Proc. Roy. Soc. (London) (to be published).

1. THE CYCLIC POLYENES

(a) Molecular Orbitals and Electronic Configurations

Consider a cyclic polyene of general formula $C_{4\nu+2}H_{4\nu+2}$ in which the carbon atoms are regularly spaced on the circumference of a circle. For convenience, let the $(4\nu+2)$-fold axis of symmetry be called the z axis. As origin of coordinates take the center of the circle and number the carbon atoms serially from 0 to $(4\nu+1)$ on going around the ring. The x axis is taken as passing through the carbon atom labeled 0, and therefore also through atom $(2\nu+1)$; the y axis then bisects the bonds linking atoms ν, $(3\nu+1)$ with atoms $(\nu+1)$, $(3\nu+2)$, respectively. Except in the simplest case of benzene $(\nu=1)$, these cyclic polyenes are hypothetical, planar molecules defined for convenience in handling only the unsaturation electrons; the associated σ-bond strain energies and so forth are of no concern.

Owing to the high symmetry of the cyclic polyenes, the appropriate molecular orbitals ψ_ξ may be prescribed as linear combinations of $2p\pi$ atomic orbitals ϕ_m straight away,

$$\psi_\xi=\sigma_\xi\sum_{m=0}^{4\nu+1}\omega^{m\xi}\phi_m,\quad(\xi=0,\pm1,\cdots,\pm2\nu,2\nu+1),\qquad(1.1)$$

where

$$\omega=e^{i\theta}=\exp\{2\pi i/(4\nu+2)\},$$

and σ_ξ is a normalizing factor which we shall take to be real and positive. It is easily verified that $\psi_{-\xi}=\psi_\xi^*$. By considering their transformation properties (see the following), we may set these orbitals in correspondence with Platt's free-electron orbitals: ψ_ξ is then the LCAO equivalent of his orbital of angular momentum $\xi h/2\pi$ about the z axis. The one-electron energy ϵ_ξ associated

TABLE II. The transformation properties of the molecular orbitals.

	ψ_ν	$\psi_{-\nu}$	$\psi_{\nu+1}$	$\psi_{-\nu-1}$
$C_{4\nu+2}$	$\omega^\nu\psi_\nu$	$\omega^{-\nu}\psi_{-\nu}$	$\omega^{\nu+1}\psi_{\nu+1}$	$\omega^{-\nu-1}\psi_{-\nu-1}$
σ_v	$\psi_{-\nu}$	ψ_ν	$\psi_{-\nu-1}$	$\psi_{\nu+1}$
σ_d	$(-1)^\nu\psi_{-\nu}$	$(-1)^\nu\psi_\nu$	$(-1)^{\nu+1}\psi_{-\nu-1}$	$(-1)^{\nu+1}\psi_{\nu+1}$
σ_h	$-\psi_\nu$	$-\psi_{-\nu}$	$-\psi_{\nu+1}$	$-\psi_{-\nu-1}$

with ψ_ξ will be a monotonically increasing function of $|\xi|$, with the identity $\epsilon_{-\xi}=\epsilon_\xi$. Thus all orbitals apart from the most stable (ψ_0) and the most highly excited ($\psi_{2\nu+1}$) are doubly-degenerate. (The precise definition of the Hartree-Fock energy parameter ϵ_ξ will, of course, be a function not only of ν and ξ, but also of the particular molecular state with which it is associated; it is not, however, necessary to pursue this subject here.)

The molecular orbitals ψ_ξ span an irreducible representation of the molecule's spatial symmetry group, namely, $\mathbf{D}_{(4\nu+2)h}=\mathbf{C}_{(4\nu+2)v}\times\mathbf{C}_s$, whose characters are assembled in Table I. $\mathbf{C}_{(4\nu+2)v}$ is a group of order $(8\nu+4)$ whose elements fall into $(2\nu+4)$ classes, so that it has four one-dimensional and 2ν two-dimensional irreducible representations. $\mathbf{C}_s$ consists of only two elements, the identity I and the reflection σ_h in the horizontal plane of symmetry. The full group therefore has twice as many representations as $\mathbf{C}_{(4\nu+2)v}$, which are described by symbols characteristic of representations of this invariant subgroup, together with subscripts g or u according as these are even or odd with respect to the inversion $i=C_2\cdot\sigma_h$. In Table II, it is shown how the ψ_ξ transform; the particular reflections σ_v, σ_d which are chosen here and in Table III refer to the zx and yz planes, respectively. It should be noticed that, as is customary for benzene, the σ_v planes contain carbon atoms, whereas the σ_d planes bisect bonds. By inspection, it is clear that the molecular orbitals may be labeled according to their symmetry properties as follows:

$$\begin{aligned}&\psi_0=a_{1u}=a_1,\quad \psi_{2\nu+1}=b_{1g}=b_1,\\ &\psi_{\pm|\xi|}=e_{|\xi|s}{}^{\pm}=e_{|\xi|}{}^{\pm},\quad (|\xi|=1,2,\cdots,2\nu),\end{aligned}\tag{1.2}$$

where $s=g$ when $|\xi|$ is odd and $s=u$ when $|\xi|$ is even. The last form of writing is that which we shall use in the sequel; it will always be used in conjunction with (1.1) rather than with Table II, so that this analytical form for the molecular orbitals is preserved even when the molecule is distorted in such a way that the symmetry is partially or completely lost.

Molecular states are now built up in the usual way by constructing orbital configurations, or making electron assignments. The ground configuration will be

$$\mathfrak{N}\colon\ (a_1)^2(e_1)^4\cdots(e_\nu)^4,$$

and the first-excited configuration is

$$\mathfrak{A}\colon\ (a_1)^2(e_1)^4\cdots(e_\nu)^3(e_{\nu+1}).$$

In prescribing these configurations, we do not at first distinguish, for example, $e_\nu{}^+$ from its complex conjugate $e_\nu{}^-$. This is of no consequence to the specification of $\mathfrak{N}$, for which there is only one permissible electron assignment, corresponding to the antisymmetric function

$$\begin{aligned}\Theta_N&=\{(4\nu+2)!\}^{-\frac{1}{2}}\det\{a_1(1)\alpha(1),\ a_1(2)\beta(2),\\ &\qquad\cdots,\ e_\nu{}^-(4\nu+2)\beta(4\nu+2)\}\\ &=|a_1\bar{a}_1e_1{}^+\bar{e}_1{}^+\cdots e_\nu{}^+\bar{e}_\nu{}^+e_\nu{}^-\bar{e}_\nu{}^-|,\quad\text{say.}\end{aligned}\tag{1.3}$$

On the other hand, there are several linearly independent functions of this type which may be constructured from configuration $\mathfrak{A}$, which is therefore said to be degenerate; all are associated with the same zeroth-order energy. Confining our attention to the singlets, although the subsequent development is in no way restricted to these, we may specify only four independent functions:

$$\begin{aligned}\Theta_1&=1/\sqrt{2}\{|\cdots e_\nu{}^+\bar{e}_\nu{}^+e_\nu{}^-\bar{e}_{\nu+1}{}^-|\\ &\qquad+|\cdots e_\nu{}^+\bar{e}_\nu{}^+e_{\nu+1}{}^-\bar{e}_\nu{}^-|\},\\ \Theta_2&=1/\sqrt{2}\{|\cdots e_\nu{}^-\bar{e}_\nu{}^-e_\nu{}^+\bar{e}_{\nu+1}{}^+|\\ &\qquad+|\cdots e_\nu{}^-\bar{e}_\nu{}^-e_{\nu+1}{}^+\bar{e}_\nu{}^+|\},\\ \Theta_3&=1/\sqrt{2}\{|\cdots e_\nu{}^+\bar{e}_\nu{}^+e_\nu{}^-\bar{e}_{\nu+1}{}^+|\\ &\qquad+|\cdots e_\nu{}^+\bar{e}_\nu{}^+e_{\nu+1}{}^+\bar{e}_\nu{}^-|\},\\ \Theta_4&=1/\sqrt{2}\{|\cdots e_\nu{}^-\bar{e}_\nu{}^-e_\nu{}^+\bar{e}_{\nu+1}{}^-|\\ &\qquad+|\cdots e_\nu{}^-\bar{e}_\nu{}^-e_{\nu+1}{}^-\bar{e}_\nu{}^+|\}.\end{aligned}\tag{1.4}$$

Their transformation properties are gathered together in Table III, as are those of the linear combinations

$$\begin{aligned}&\Theta_X=1/\sqrt{2}(\Theta_1+\Theta_2),\quad \Theta_Y=1/i\sqrt{2}(\Theta_1-\Theta_2),\\ &\Theta_U=1/\sqrt{2}(\Theta_3+\Theta_4),\quad \Theta_V=1/i\sqrt{2}(\Theta_3-\Theta_4).\end{aligned}\tag{1.5}$$

It will be noticed that whereas Θ_1, Θ_2 (or Θ_X, Θ_Y) together span the irreducible representation ${}^1E_{1u}$ of the molecular symmetry group, Θ_3 and Θ_4 span a reducible representation. The linear combinations Θ_U, Θ_V are appropriate in this case and are of species ${}^1B_{1u}$, ${}^1B_{2u}$, respectively. Since $\Theta_2=\Theta_1{}^*$, $\Theta_4=\Theta_3{}^*$, it will be noticed

TABLE III. The transformation properties of the configurational functions.

	Θ_1	Θ_2	Θ_3	Θ_4	Θ_X	Θ_Y	Θ_U	Θ_V
$C_{4\nu+2}$	$\omega^{-1}\Theta_1$	$\omega\Theta_2$	$-\Theta_3$	$-\Theta_4$	$Rl(\omega)\Theta_X+Im(\omega)\Theta_Y$	$Rl(\omega)\Theta_Y-Im(\omega)\Theta_X$	$-\Theta_U$	$-\Theta_V$
σ_v	Θ_2	Θ_1	Θ_4	Θ_3	Θ_X	$-\Theta_Y$	Θ_U	$-\Theta_V$
σ_d	$-\Theta_2$	$-\Theta_1$	$-\Theta_4$	$-\Theta_3$	$-\Theta_X$	Θ_Y	$-\Theta_U$	Θ_V
σ_h	Θ_1	Θ_2	Θ_3	Θ_4	Θ_X	Θ_Y	Θ_U	Θ_V

that all the functions Θ_S, (S=X, Y, U, V) are real. Moreover, Θ_X, Θ_Y transform like translations along $0x$, $0y$, respectively; this is useful to remember when the symmetry is partially destroyed, since a suitable numbering of the carbon atoms will ensure that Θ_X, Θ_Y, as also Θ_U, Θ_V, conform to primitive symmetry species of the lower group.

Thus in every case (i.e., for all $\nu \geq 1$), the first excited configuration gives rise to three singlet functions, $^1B_{1u}$, $^1B_{2u}$ and doubly-degenerate $^1E_{1u}$, which Platt calls ^1L_a, ^1L_b, and ^1B, respectively (see Table IV). That these states differ in energy may be attributed to "intra-configurational" interaction or, as we shall prefer to call it, first-order *CI*. Now states of the same symmetry are obtained from more highly excited configurations as well: there is, formally at least, another type of interaction which is "inter-configurational" in origin; this we call second-order *CI*. For the purposes of this note, we shall neglect second-order *CI* altogether, justifying this by a reference to recent work on simple hydrocarbons.[6,7]

In what follows we shall reserve the symbols Θ_S, (S=X, Y, U, V) for the singlet functions (1.5). When second-order *CI* is ignored, these represent the associated singlet states arising from $\mathfrak{A}$, and in this specific sense, we may call them $\Omega_S{}^0$, $(S=X, Y, U, V)$. The distinction, though real, is not important for the cyclic polyenes themselves, but is introduced for the purposes of later perturbation theory, when the Θ_S are used as the basis of representation for perturbed states Ω_S of the cyclic polyenes.

The pictorial representation and qualitative description of transitions between the states of $\mathfrak{N}$ and $\mathfrak{A}$ have been discussed by Platt in some detail. Having formalized his perimeter model in LCAO terms, we shall not trouble to repeat such descriptions here. It may be noticed, however, that Θ_U has 2ν nodal planes (σ_d) normal to the polyene ring which bisect carbon-carbon bonds, whereas Θ_V has 2ν nodal planes (σ_v) which pass through carbon atoms.

(b) Orbital Energies

We shall now give an outline of the simplest LCAO calculations which can be made.[4] For this purpose, we neglect overlap and interactions between all but nearest neighbors. Energies are then expressed in terms of the usual Coulomb integral α and the resonance integral β.

Firstly, the orbital energy of an electron in ψ_ξ is easily seen to be

$$\epsilon_\xi = \alpha + 2\beta \cos(\xi\theta), \quad \theta = \pi/(2\nu+1). \tag{1.6}$$

The energy of the unsaturation electrons in their ground state $\mathfrak{N}$ is therefore

$$2\{\epsilon_0 + \sum_{\xi=1}^{\nu} (\epsilon_\xi + \epsilon_{-\xi})\} = (4\nu+2)\alpha + 4\beta \operatorname{cosec}(\theta/2), \tag{1.7}$$

[7] W. Moffitt and J. Scanlan, Proc. Roy. Soc. (London) **A218**, 464 (1953); W. Moffitt, Proc. Roy. Soc. (London) **A218**, 486 (1953).

TABLE IV. Different nomenclatures for states of cyclic polyenes and polyacenes.

This paper	Platt (reference 5)	Group theory
X, Y	^1B	$^1E_{1u}$
U	^1L_a	$^1B_{1u}$
V	^1L_b	$^1B_{2u}$

(a) Cyclic polyenes.

This paper	Platt (reference 5)	Group theory (reference 11)	Upper state of Clar's (reference 1)
Y	^1B_b	$^1B_{1u}$	β bands
U	^1L_a	$^1B_{2u}$	p bands
V	^1L_b	$^1B_{1u}$	α bands

(b) Polyacenes.

which corresponds to a resonance energy of

$$2|\beta|\{2 \operatorname{cosec}(\theta/2) - (2\nu+1)\} \tag{1.8}$$

and a mobile bond order of

$$(2\nu+1)^{-1} \operatorname{cosec}(\theta/2). \tag{1.9}$$

As the number of carbon atoms, and thus ν, increases, so the mobile bond order approaches the value $(2/\pi)$.

Secondly, we may give an estimate for the lowest excitation energy, which corresponds to the process $(e_\nu)^{-1}(e_{\nu+1})$. This is then simply

$$\epsilon_{\nu+1} - \epsilon_\nu = 4|\beta| \sin(\theta/2), \tag{1.10}$$

which vanishes as ν increases indefinitely. Now, this prediction gives, at best, only some mean excitation energy of the totality of states ($^{1,3}B_{1u}$, $^{1,3}B_{2u}$, $^{1,3}E_{1u}$) arising from $\mathfrak{A}$, with respect to the ground state. The method is insufficiently sensitive to separate these states energetically.

The methods of antisymmetrized molecular orbitals and of atoms in molecules are sufficiently discerning in this respect, but not sufficiently accurate for us to apply them with any confidence.[6] For this reason, we make the assumption that (1.10) may be used to compute the mean excitation energies of the higher cyclic polyenes, taking for β that value which is appropriate for benzene. In order to locate the particular states of $\mathfrak{A}$ relative to this mean, we shall also adopt an extrapolation method from benzene, which will now be described.

(c) Excitation Energies

As Göppert-Mayer and Sklar first pointed out, the molecular orbital theory correctly predicts the number of low-lying singlet states of benzene as three.[8] The first, very weak absorption system, with an excitation energy of ~4.9 ev, they identified as the $^1A_{1g} \rightarrow {}^1B_{2u}$ transition (Clar's α bands), which is electronically forbidden. The second, stronger system around 6.2 ev they attributed to the forbidden process $^1A_{1g} \rightarrow {}^1B_{1u}$ (p bands), whereas the intense 7.0 ev absorption is clearly due to

[8] M. Göppert-Mayer and A. L. Sklar, J. Chem. Phys. **6**, 645 (1938).

the allowed transition ${}^1A_{1g} \rightarrow {}^1E_{1u}$ (β bands). We shall accept their assignments in this note, as did Platt.

Now it is easily shown that as ν increases, so the separation of the different electronic states arising from configuration $\mathfrak{A}$ decreases, vanishing asymptotically. Since in the higher cyclic polyenes ($\nu > 1$), the transformation properties of the associated eigenfunctions remain identical, we may expect the relative separations of these states to be roughly proportional: $({}^1E_{1u} - {}^1B_{1u})/({}^1B_{1u} - {}^1B_{2u})$ for benzene will be the same as $({}^1E_{1u} - {}^1B_{1u})/({}^1B_{1u} - {}^1B_{2u})$ for cyclodecapentaene, and so on. And we shall further suppose that this similarity extends to the separation of these states from the corresponding ground states. On the basis of these qualitative arguments, we may now make (admittedly rather approximate) estimates of the relevant excitation energies in the higher cyclic polyenes:

Using (1.10) to furnish the mean excitation energies and exploiting our proportionality assumptions it is easily seen that the excitation energy of a particular state $\Xi (= {}^1E_{1u}, {}^1B_{1u}, {}^1B_{2u})$ is given by

$$4 |\beta(\Xi)| \sin(\theta/2), \tag{1.11}$$

where $\beta(\Xi)$ is chosen separately for each symmetry species from the known benzene spectrum. For example, since $\nu = 1$ and therefore $\theta = \pi/3$ for benzene, $|\beta({}^1B_{1u})| = \frac{1}{4}(6.2)\ \mathrm{cosec}(\pi/6) = 3.1$ ev; and, accordingly, the ${}^1B_{1u} - {}^1A_{1g}$ interval for cyclodecapentaene is predicted to be of the order $4(3.1) \sin(\pi/10)$ ev.

There seems to be little doubt that these very approximate calculations are qualitatively correct. And, in the absence of a more reliable method, it seems rather pointless to use more elaborate techniques to attain results which are bound to be qualitatively similar and no more accurate. Essentially, we use the simplest LCAO theory as a means of extrapolating the spectra of the higher cyclic polyenes from the known benzene spectrum.

(d) Perturbation Theory

We have now constructed a semi-empirical description of our cyclic polyenes (the "perimeters") in both their ground and lower excited states. Their spectroscopic properties can be assessed roughly by means of (1.11) and their approximate eigenfunctions are given by (1.3) and (1.5). In these paragraphs, we shall outline the way in which the lower states of the cyclic polyenes are modified by perturbations of a particular type.

Of these perturbations, we shall require: (i) that they are small with respect to the separation of different electronic configurations giving rise to states of the same symmetry, if comparable to the separation of different electronic levels within the same configuration; (ii) that they may be expressed as the sum of one-electron Hermitian operators

$$\mathcal{P} = \sum_{i=1}^{4\nu+2} \mathfrak{p}_i.$$

With respect to the molecular orbitals ψ_ξ as basis, a typical perturbation $\mathcal{P}$ is represented by a matrix $[P_{\xi\eta}]$, where

$$P_{\xi\eta} = \int \psi_\xi^* \mathfrak{p} \psi_\eta dv = P_{\eta\xi}^*$$
$$= \sigma_\xi \sigma_\eta \{ \sum_m \omega^{(\eta-\xi)m} A_m + \sum_m \sum_{n>m} (\omega^{n\eta - m\xi} + \omega^{m\eta - n\xi}) B_{mn} \} \tag{1.12}$$

and

$$A_m = \int \phi_m^* \mathfrak{p} \phi_m dv, \quad B_{mn} = \int \phi_m^* \mathfrak{p} \phi_n dv \tag{1.13}$$

are the elements of the matrix representing the separate one-electron operators in a basis of AO functions. However, it is not in the molecular orbitals, but rather in the molecular states themselves that we shall be interested. In particular, referred to the four singlet functions Θ_S, which we regard as the approximate unperturbed eigenfunctions of the states arising from $\mathfrak{A}$, the perturbation operator is represented by the matrix

$$\begin{array}{cccccc} \mathrm{X} & \kappa & 0 & Rl(\lambda) & Im(\mu) \\ \mathrm{Y} & 0 & \kappa & -Im(\lambda) & Rl(\mu) \\ \mathrm{U} & Rl(\lambda) & -Im(\lambda) & \kappa & 0 \\ \mathrm{V} & Im(\mu) & Rl(\mu) & 0 & \kappa \end{array}, \tag{1.14}$$

where κ is a constant, and

$$\lambda = P_{-\nu-1,\nu+1} - P_{\nu,-\nu},$$
$$\mu = P_{-\nu-1,\nu+1} + P_{\nu,-\nu}. \tag{1.15}$$

Here the element of the Sth row and Tth column gives the value of the integral

$$P_{ST} = \int \Theta_S^* \mathcal{P} \Theta_T dV. \tag{1.16}$$

The common diagonal term, namely κ, is related to the diagonal element corresponding to the ground state by the formula

$$\int \Theta_N^* \mathcal{P} \Theta_N dV = \kappa + P_{\nu,\nu} - P_{\nu+1,\nu+1} = \chi, \quad \text{say.} \tag{1.17}$$

Since it is supposed at the outset that the perturbation is small with respect to the energetic intervals separating Θ_N from the Θ_S, the matrix elements of $\mathcal{P}$ connecting Θ_N with the Θ_S are of no interest.

Now, apart from the obvious appearance of zeros in (1.14), this matrix has certain other most illuminating properties. Suppose we neglect overlap, when $\sigma_\xi = (4\nu+2)^{-\frac{1}{2}}$ for all ξ. It is then easily shown that

$$\lambda = (2\nu+1)^{-1} \sum_m \sum_{n>m}{}^{\S} 2\omega^{(\nu+1)(m+n)} B_{mn},$$
$$\mu = (2\nu+1)^{-1} \{ \sum_m \omega^{2(\nu+1)m} A_m + 2 \sum_m \sum_{n>m}{}^{\dagger} \omega^{(\nu+1)(m+n)} B_{mn} \}, \tag{1.18}$$

where the first double summation (§) is taken over only those pairs of atoms for which $(m+n)$ is odd, and the second (†) is taken over only those pairs for which $(m+n)$ is even. Moreover, Θ_U is connected with the degenerate Θ_X, Θ_Y pair only through λ, and Θ_V is connected with Θ_X, Θ_Y only through μ, the matrix elements between Θ_U and Θ_V vanishing. This means that the $^1B_{1u}$ and $^1B_{2u}$ states will in general behave differently, and characteristically so, under the influence of a particular perturbation $\mathcal{P}$.

For example, suppose $\mathcal{P}$ to be such that $A_m=0$ for all m and $B_{mn}=0$ whenever $(m+n)$ is even. Then $\mu=0$, and that part of the energy matrix referring to configuration $\mathfrak{A}$ has the form

$$\begin{matrix} W_X+\kappa & 0 & Rl(\lambda) & 0 \\ 0 & W_Y+\kappa & -Im(\lambda) & 0 \\ Rl(\lambda) & -Im(\lambda) & W_U+\kappa & 0 \\ 0 & 0 & 0 & W_V+\kappa \end{matrix}, \quad (1.19)$$

$W_X=W_Y$ being the energy of the cyclic polyene in its unperturbed $^1E_{1u}$ state and W_U, W_V being the energies of its unperturbed $^1B_{1u}$, $^1B_{2u}$ states, respectively. The eigenfunctions of the perturbed states then have the form

$$\begin{aligned} &\Omega_V=\Theta_V, \quad \Omega_Y=\cos\tau\Theta_Y-\sin\tau\Theta_X, \\ &\Omega_X=\cos\rho\{\cos\tau\Theta_X+\sin\tau\Theta_Y\}-\sin\rho\Theta_U, \quad (1.20) \\ &\Omega_U=\cos\rho\Theta_U+\sin\rho\{\cos\tau\Theta_X+\sin\tau\Theta_Y\}, \end{aligned}$$

where the parameters τ, ρ are easily determined when the latent roots of (1.19) are obtained. Under such a perturbation we see that apart from the common additive term κ, the state V and one of the components Y of the degenerate Θ_X, Θ_Y pair are left unchanged, whereas the Θ_U state and the remaining component of this pair interact, to form states X and U. Such a perturbation is illustrated graphically in Fig. 1(a).

Similarly, if $\mathcal{P}$ is such that $B_{mn}=0$ whenever $(m+n)$ is odd, it is seen that one component X of the Θ_X, Θ_Y pair, and U remain pure, whereas its remaining component mixes with Θ_V to form states Y and V. This type of interaction is illustrated in Fig. 1(b).

For convenience, we shall refer to these two different types of perturbation as "odd" and "even," respectively. The selectivity which they show is very important for the ensuing discussion.

2. BENZENE PERTURBATIONS

(a) "Even" Perturbations

As a first example of the perturbation technique outlined in the last section, we shall consider the effect of inductive substituents on the intensity of the forbidden electronic transitions in benzene. The appropriate perturbation operator in LCAO theory may be defined with respect to its representatives referred to a basis of atomic orbitals. If atoms r, s, $\cdots$, t have a common inductive substituent, then the relations

$$B_{mn}=0, \quad A_m=A(\delta_{mr}+\delta_{ms}+\cdots+\delta_{mt}) \quad (2.1)$$

define the perturbation. The constant A is the difference between the substituted and unsubstituted Coulomb integral α associated with a particular carbon atom. Clearly this substitution is "even" in the sense of Fig. 1. It follows immediately that only the $^1B_{2u}$ state is affected by the perturbation—at least to a first approximation. This means that the $^1A_{1g}\rightarrow{}^1B_{2u}$ band system should be more strongly affected by purely inductive substituents than the $^1A_{1g}\rightarrow{}^1B_{1u}$ system, other things being equal.

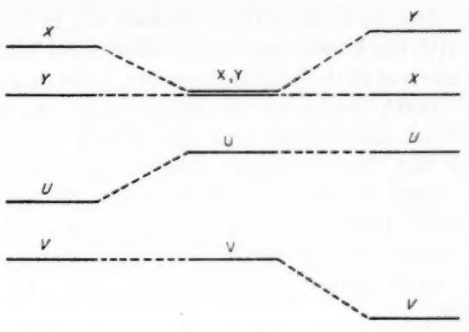

FIG. 1. The behavior of the lower-excited singlet states of the cyclic polyenes under perturbations. (Shifts K common to all levels have not been indicated.)

Putting these arguments on a more quantitative basis, we may suppose $|\mu|\ll(W_X-W_V)$ and therefore write

$$\Omega_V=\Theta_V+R(\cos\tau\Theta_Y+\sin\tau\Theta_X), \quad (2.2)$$

where

$$R=-|\mu|/(W_X-W_V), \quad \tau=\arg\mu, \quad (2.3)$$

for the perturbed $^1B_{2u}$ state. Since Ω_V now contains a small contribution from the $^1E_{1u}$ state, to which transitions from the ground state are allowed, we see that the intensity of the $^1A_{1g}\rightarrow{}^1B_{2u}$ absorption should be enhanced. For different types of inductive substitution, this enhancement will be roughly proportional to $|R|^2$ and therefore to $|\mu|^2$.

In Table V we give values of $|3\mu/A|^2$ for mono-, di-, and tri-substitution by a common substituent type (constant value of A). These rules agree perfectly with those derived on different grounds by Sklar[9] and by

TABLE V. The effect of substitution on the intensities of the α bands in the benzene spectrum.

Type of di-substitution	Enhancement factor	Type of tri-substitution	Enhancement factor[a]
ortho-	1	1, 2, 3	0
meta-	1	1, 2, 4	3
para-	4	1, 3, 5	0

[a] The enhancement factor is taken relative to the effect $|3\mu/A|^2$ of mono-substitution.

[9] A. L. Sklar, J. Chem. Phys. **10**, 135 (1942).

Förster[10] and, as these authors showed, are in excellent accord with the known spectra of substituted benzenes. By our method of derivation, however, it becomes clear why the 2600A band system in benzene is more sensitive to inductive substitution than the 2000A system, despite the fact that the upper state of the latter transition is nearer to the state from which the intensity is borrowed. This result may be considered as confirming, if somewhat indirectly, the assignment of the longest wave length absorption to the $^1A_{1g}\rightarrow{}^1B_{2u}$ transition.

(b) "Odd" Perturbations

As an example of an "odd" perturbation in benzene, let us take the case where $A_m=0$ for all m, and B_{mn} also vanishes unless m and n are neighbors ($m+n$ odd). Under these conditions, it is seen from (1.18) that μ vanishes identically and of the lower states $^1B_{1u}$, $^1B_{2u}$ only the former interacts with the degenerate $^1E_{1u}$ state. Now this is exactly the type of perturbation associated with a distortion of the benzene ring in LCAO terms. The nonvanishing B_{mn} correspond to the changes in the values of the resonance integrals β_{mn} associated with the distortion. Clearly it is just such an operator which must be used to describe vibrational perturbations of the benzene system. Rather naively, we may say that vibrations will allow the $^1E_{1u}$ state to contribute only to the $^1B_{1u}$ state and not to the $^1B_{2u}$ state. That is, the borrowed intensity which permits the observation of the forbidden $^1A_{1g}\rightarrow{}^1B_{1u}$, $^1B_{2u}$ transitions should be greater for the former, 2000A system than for the latter, longer wavelength system, other things being equal.

Now, it has been verified that both ^1B_u states may formally interact with the $^1E_{1u}$ state on symmetry grounds, suitable vibrational species being present for both. On the other hand, the closer proximity of the $^1B_{1u}$ to the $^1E_{1u}$ state, should lead to a greater intensity for the $^1A_{1g}\rightarrow{}^1B_{1u}$ transition than for the $^1A_{1g}\rightarrow{}^1B_{2u}$ system by the factor $\{(W_X-W_V)/(W_X-W_U)\}^2\approx 6$. That the $^1A_{1g}\rightarrow{}^1B_{1u}$ system is in fact between six and eight times as strong again in absorption than this proximity reasoning would suggest, or rather that the $^1A_{1g}\rightarrow{}^1B_{2u}$ system is between six and eight times as weak, we may tentatively attribute to the insensitivity of the $^1B_{2u}$ state to "odd" perturbations. More thoroughgoing calculations are in progress to amplify this reasoning.

3. THE POLYACENES

(a) Excitation Energies

We now apply the perimeter model to the polyacenes. To this end, we take a typical cyclic polyene $C_{4\nu+2}H_{4\nu+2}$ and perturb it in such a way that its unsaturation electrons simulate those of the corresponding polyacene $C_{4\nu+2}H_{2\nu+4}$. For example, by introducing a perturbation whose nonvanishing elements in a representation referred to the AO's are $B_{05}=B_{50}=B$, say, we form a "bond" between atoms 0 and 5 of cyclodecapentaene, which then becomes, to all intents and purposes, naphthalene. Similarly, we form π-electron systems analogous to anthracene, naphthacene, and pentacene by introducing suitable cross-linking perturbations to the cyclic polyenes with the same number of carbon atoms. At the same time we complete the distortion of our cyclic polyenes in such a way that its unsaturation electrons become isosteric with the corresponding polyacene; this is of no importance for the prediction of excitation energies, since we employ an approximation which neglects interactions between nonnearest neighbors, but is vital when we come to compute oscillator strengths.

For convenience, we number the carbon atoms in such a way that the x axis, which contains atoms 0 and $(2\nu+1)$, is the transverse (shorter) axis of twofold symmetry. The origin then lies at the center of symmetry of the polyacene, and the y axis is the molecule's longitudinal axis. The polyacene-forming perturbations are symmetrical (under their action, only states of the same symmetry interact) and the unperturbed functions Θ_X, Θ_U transform like translations along $0x$, and Θ_Y, Θ_V like translations along $0y$. In the notation appropriate to the point group $\mathbf{D}_{2h}$, Θ_X, Θ_U are of species $^1B_{2u}$, whereas Θ_Y, Θ_V are of species $^1B_{1u}$.[11] On grounds of symmetry alone, all four unperturbed states are now accessible by dipole transitions from the ground state, owing to the distortion of the π-electron system.

Before proceeding with the calculations, our attitude to these might be clarified. In the first place, we assume that the perturbations may be handled in terms of the simplest LCAO theory. This is certainly only true as a first approximation, but it is not intended to aspire to greater quantitative accuracy. It is rather in the qualitative behavior of the resultant states that we shall be interested, and in the more important sources of this behavior. Secondly, we shall suppose that the relevant perturbations may be handled in the manner of Sec. 1(d): that only states arising from the same configuration of the cyclic polyene will interact under their influence. This will not be a good approximation for the more highly excited states, but should be adequate, within our prescribed limits of accuracy, for the lower states.

In order to illustrate the nature of the perturbations, we shall first compute the diagonal terms of the perturbed energy matrix. For the states arising from $\mathfrak{C}$, these are simply the $(W_S+\kappa)$ and for the ground state $(W_N+\chi)$. We shall plot our results with respect to $(W_N+\chi)$ as the origin of energy units, so that they are

[10] T. Förster, Z. Naturforsch. **2A**, 149 (1947).

[11] C. A. Coulson, Proc. Phys. Soc. (London) **60**, 257 (1948). We use the same group notation for the transverse and longitudinal polarizations as Coulson, although we have had to use a different choice of x, y, and z axes; this is due to the fact that the principal axis of symmetry for the cyclic polyenes is, by convention, the z axis.

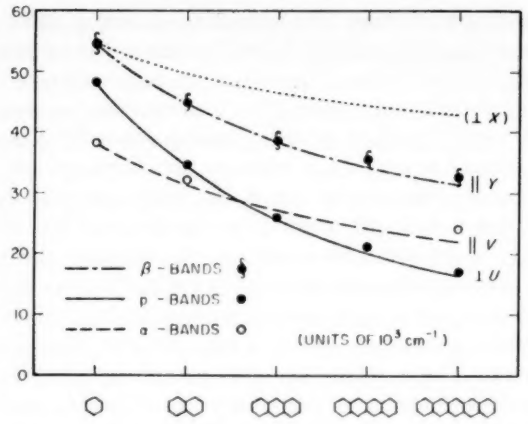

FIG. 2. A preliminary stage in the calculation of the excitation energies of the polyacenes.

expressed as "excitation" energies in Fig. 2. For a particular state, Θ_U say, we use (1.11), (1.12), and (1.17), setting the perturbation parameter $B=\beta(^1B_{1u})$, the resonance integral used in (1.11) for this particular symmetry species. And similarly for Θ_X, Θ_Y, and Θ_V. The behavior of these curves, as functions of ν, is determined very largely by the form of the excitation energies of the cyclic polyenes; they do not, however, fall off as rapidly with increasing ν as do the latter. The degeneracy of the Θ_X, Θ_Y pair has not yet been lifted.

The second, and final stage of the calculations is concerned with the scrambling of the unperturbed states arising from configuration $\mathfrak{A}$ under the influence of the perturbations. By symmetry, Θ_X may interact with Θ_U, and so may Θ_Y with Θ_V. However, it is easily seen that the sum of the indices of the atoms linked by the newly-formed bonds is always odd. The perturbation is therefore also "odd" and the possibility of mixing Θ_Y with Θ_V is never realized: the perturbed states are represented by the unperturbed functions

$$\Omega_V=\Theta_V, \quad \Omega_Y=\Theta_Y. \tag{3.1}$$

These correspond to the upper states of Clar's α and β bands, respectively (see the following). However, under an "odd" perturbation of this type, Θ_U and Θ_X interact to form the perturbed states

$$\begin{aligned}\Omega_X&=\cos\rho\Theta_X-\sin\rho\Theta_U,\\ \Omega_U&=\cos\rho\Theta_U+\sin\rho\Theta_X,\end{aligned} \tag{3.2}$$

where

$$\rho=\tfrac{1}{2}\tan^{-1}\{2\lambda/(W_U-W_X)\}. \tag{3.3}$$

As a result, the curves representing Θ_X and Θ_U in Fig. 2 repel each other and the complete excitation diagram follows Fig. 3. The rapid movement downwards of the p bands is ascribed to the resulting stabilization of its upper state, namely Ω_U.

It is easily seen that λ of (1.18) is real in all these cases, and a multiple of the perturbation parameter B. More specifically, it is found that

$$\lambda=2B(-1)^{\nu+1}(\nu-1)/(2\nu+1). \tag{3.4}$$

For the excitation energies shown in Fig. 2, we set B equal to the "resonance integrals" β, appropriately chosen for the different states using the observed benzene levels, and therefore consistently with the extrapolations from benzene we had used to determine the spectra of the cyclic polyenes. The off-diagonal parameter B cannot be chosen in this way, except in so far as it must obviously be of the same order of magnitude as the three $\beta(\Xi)$'s. We choose it semiempirically as $\sim$2.5 ev. It should be remembered that we are not aiming at quantitative results, and fortunately the accuracy we do obtain owes little to the particular values assigned to the perturbation parameters, always provided that these are in the neighborhood of 3 ev.

In addition to the predicted curves of Fig. 3, we show the observed spectroscopic intervals as points. We have only included data for the three lowest states Y, U, and V (or ^1B_b, ^1L_a and ^1L_b in Platt's notation), since the X state probably begins to interact with states from higher configurations on the one hand, and because the empirical identification of the higher states is neither complete, nor does it appear so reliable. The quantitatative agreement is remarkably good but probably fortuitous in part. It is "stable" with respect to the parameters B and derives almost entirely from the qualitative properties of the "perimeters," the cyclic polyenes. The lowest states of the polyacenes may be described as arising from states of the corresponding cyclic polyenes under the appropriate cross-linking perturbations. Of these states, only Θ_X and Θ_U may interact with the result that the simple behavior in Fig. 2 is modified only by the more rapid descent of the curve representing state U, as in Fig. 3.

(b) Isomerism

In order to confirm and to extend our description of the lower excited states of the polyacenes, we may apply

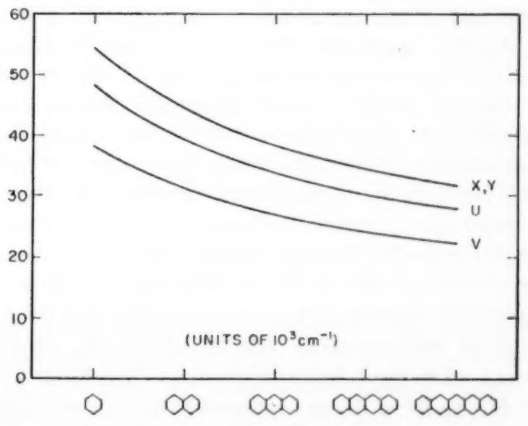

FIG. 3. The predicted and observed excitation energies in the polyacene spectra.

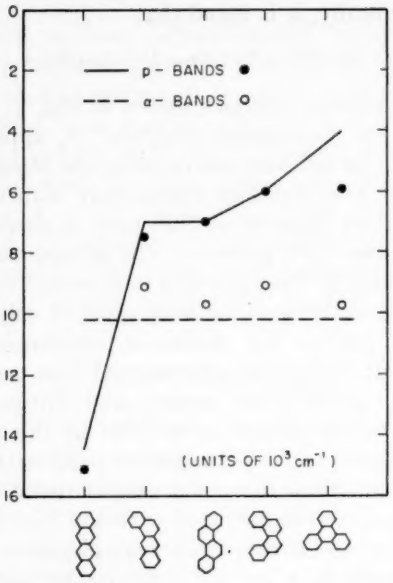

FIG. 4. The movement of the $\alpha+$ and $p+$ bands of napthacene and its isomers, relative to their $\beta+$ bands.

the same considerations to their isomers. Two distinct cases arise. If we suppose the new cata-condensed systems to be built up from fused benzene rings, e.g., phenanthrene, then the cross-linking perturbations remain "odd." However, if the isomeric molecules contain odd-membered rings, e.g., azulene, we shall discover a different type of behavior. In these paragraphs, we shall confine our attention to the cases where the ring systems all contain six carbon atoms; the case of azulene will be taken up again in the next section.

The positions at which cross linking is effected to produce cata-condensed systems from cyclic polyenes are important not only in deciding whether the appropriate perturbations are "even," "odd" or have some more complicated form, but also in determining their more quantitative aspects. Thus, for any "odd" perturbations, the behavior symbolized in (1.20) is obeyed. But the extent to which the Θ_U state is stabilized by interaction with the Θ_X, Θ_Y pair is determined by the magnitude of the parameter λ of (1.18). It is in this way that phenanthrene differs from isomeric anthracene.

Let us number our cyclic polyene ($\nu=3$) in such a way that its atoms 3 and 4 occupy the meso-positions of phenanthrene, and atoms 0 and 7 the meso-positions of anthracene. Then it is easily seen that $\lambda=(4B/7)\times\cos(4\pi/7)$ in the former case, whereas $\lambda=(4B/7)$ in the latter, $(\kappa-\chi)$ being the same in both. (The magnitude of the perturbation is determined by $|\lambda|$, which is independent of the origin of indexing, of course, but by adopting this specific form, we ensure that Θ_X, Θ_Y transform independently and that only Θ_X can then interact with Θ_U.) Accordingly it is clear from (1.19) that Θ_U and Θ_X do not interact nearly as strongly in phenanthrene as they do in anthracene. As a consequence, we should expect that of the three lower excited states of these two molecules, Y and V have the same excitation energies in both whereas the excitation energy of the state U is 4.0 ev in phenanthrene and only 3.2 ev in anthracene. This is in excellent agreement with the comparison of their spectra made by Klevens and Platt,[3] who call the relevant transition ${}^1A\rightarrow{}^1L_a$.

Similar comparisons may be made for the cata-condensed systems with four or five nuclei. Since $(\kappa-\chi)$ is the same for nearly all the isomers, and does not vary significantly for the few exceptions, we should expect, to a first approximation, that the location of the V and Y states of (1.20) is the same in all isomeric spectra. These states are not mixed by the "odd" cross-linked perturbations. They are called ${}^1L_b$ and ${}^1B_b$ respectively by Klevens and Platt, and the data assembled by these authors confirm our conclusion. On the other hand, the behavior of the U state depends on λ and this quantity is the only one which distinguishes different isomers in our work. Accordingly we show the predicted movement of this band, and of the V band (which should remain inactive) relative to the Y band in Figs. 4 and 5. It will be seen that the characterization of the isomers is very satisfactory, especially when the relative crudity of our method is taken into account. The specificity of Clar's p bands (our $N\rightarrow U$) to isomerization and the concomitant insensitivity of his α and β bands ($N\rightarrow V$, Y respectively) is easily understood.

(c) Intensities

So far, we have been able to see how the α, p, and β bands persist in the spectra of the cata-condensed hydrocarbons. We have shown how their locations may be explained and, in particular, we have followed the characteristic movement of the p bands. Before going

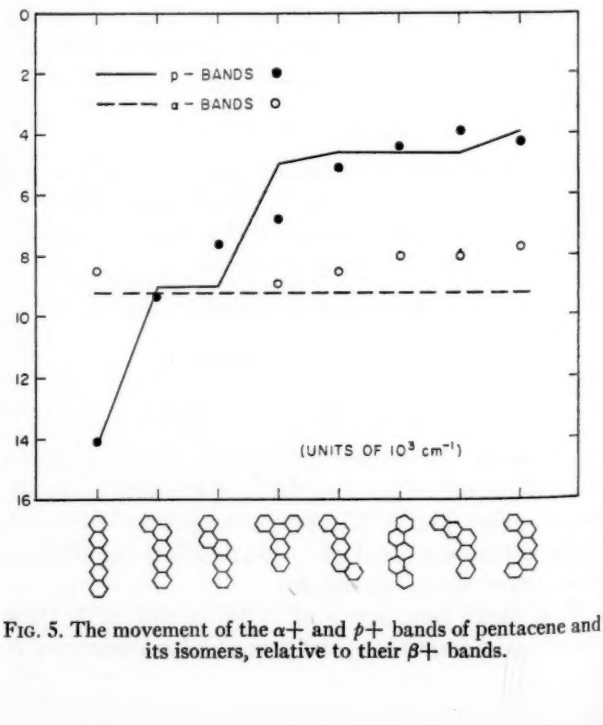

FIG. 5. The movement of the $\alpha+$ and $p+$ bands of pentacene and its isomers, relative to their $\beta+$ bands.

on to discuss azulene (features V and VI of the introduction), we must attend to the intensity relationships (II) and the effects of substitution (IV). For benzene, these have already been considered in Sec. 2.

Let us first assess the intensities of transitions from the ground state Θ_N to the unperturbed states Θ_S of some cyclic polyene, which has been distorted so as to have the same shape as a particular cata-condensed hydrocarbon. (For the undistorted rings, of course, transitions $N\rightarrow X$, Y are electronically allowed, whereas $N\rightarrow U$, V are electronically forbidden; vibrational perturbations enable the latter to "borrow" intensity from the former, but the $N\rightarrow U$ transition is more susceptible to this than the $N\rightarrow V$ transition.) As a first step in this calculation, we follow Mulliken[12] and evaluate the effective dipole vectors

$$\mathbf{Q}_{NS}{}^0=\int\Theta_N{}^*(\sum_i\mathbf{r}_i)\Theta_S dV,\quad (S=X,Y,U,V),\tag{3.5}$$

where $\mathbf{r}_i$ is the position vector of the ith unsaturation electron, referred to the centroid of charge as origin. If the molecular orbitals are considered to remain orthogonal, despite the distortion, it is easily seen that

$$\begin{aligned}&\mathbf{Q}_{NX}{}^0=2R\mathbf{i}\mathbf{q}_{-\nu,-\nu-1},\quad &&\mathbf{Q}_{NY}{}^0=2Im\mathbf{q}_{-\nu,-\nu-1},\\ &\mathbf{Q}_{NU}{}^0=2R\mathbf{i}\mathbf{q}_{-\nu,\nu+1},\quad &&\mathbf{Q}_{NV}{}^0=2Im\mathbf{q}_{-\nu,\nu+1},\end{aligned}\tag{3.6}$$

where

$$\mathbf{q}_{\xi\eta}=\int\psi_\xi{}^*\mathbf{r}\psi_\eta dv.\tag{3.7}$$

So that, neglecting overlap between all but adjacent carbon atoms,

$$\begin{aligned}\mathbf{Q}_{NX}{}^0&=2\sigma_\nu\sigma_{\nu+1}\sum_m\cos\{m\pi/(2\nu+1)\}\mathbf{a}_m,\\ \mathbf{Q}_{NY}{}^0&=2\sigma_\nu\sigma_{\nu+1}\sum_m\sin\{-m\pi/(2\nu+1)\}\mathbf{a}_m,\\ \mathbf{Q}_{NU}{}^0&=2\sigma_\nu\sigma_{\nu+1}\sum_m\cos(m\pi)\mathbf{a}_m,\\ \mathbf{Q}_{NV}{}^0&=4\sigma_\nu\sigma_{\nu+1}\sum_m\sum_{n>m}\sin\{(m+n)\pi/2\}\\ &\qquad\times\cos\{(m-n)\pi/(4\nu+2)\}\mathbf{b}_{mn},\end{aligned}\tag{3.8}$$

where

$$\begin{aligned}\mathbf{a}_m&=\int\phi_m{}^*\mathbf{r}\phi_m dv=\mathbf{r}_m,\\ \mathbf{b}_{mn}&=\int\phi_m{}^*\mathbf{r}\phi_n dv=\tfrac{1}{2}(\mathbf{r}_m+\mathbf{r}_n)S_{mn},\end{aligned}\tag{3.9}$$

$\mathbf{r}_m$, $\mathbf{r}_n$ being the position vectors of the m, nth carbon atoms and S_{mn} being the overlap integral between ϕ_m and ϕ_n. We have used the fact that, under the distortion, the cyclic polyene assumes the geometry of some cata-condensed hydrocarbon containing only even-membered rings, so that all adjacent carbon atoms differ in their indices by an odd number. It will be noticed, immediately, that contributions to the effective dipole vectors $\mathbf{Q}^0$ arise only from atoms for "transitions" N→X, Y, U, whereas $\mathbf{Q}_{NV}{}^0$ consists of contributions from bonds only, and therefore contains the overlap integral as a factor.

Even though these formulas are only approximate—we have assumed the MO's to remain orthogonal under the distortion—it is very instructive to evaluate the $\mathbf{Q}^0$'s. For this purpose, we choose the polyacenes themselves, which serve to illustrate the essential factors determining intensities. Similar results are easily obtained for their isomers, whose condensation is not linear. For simplicity, we suppose the molecules to consist of fused regular hexagons with sides of length $R=1.4$A. Using the approximation $\sigma_\nu\approx(4\nu+2)^{-\frac{1}{2}}\approx\sigma_{\nu+1}$, it is found that

$$\begin{aligned}\mathbf{Q}_{NX}{}^0&=R\mathbf{i}\{3/(4\nu+2)\}\operatorname{cosec}(\theta/2),\\ \mathbf{Q}_{NY}{}^0&=-R\mathbf{j}\{\sqrt{3}/(4\nu+2)\}\operatorname{cosec}(\theta/2)\cot(\theta/2),\\ \mathbf{Q}_{NU}{}^0&=R\mathbf{i}(-1)^{\nu+1}\{(\nu-1)/(2\nu+1)\},\\ \mathbf{Q}_{NV}{}^0&=SR\mathbf{j}(-1)^\nu\{\sqrt{3}/(4\nu+2)\}\operatorname{cosec}\theta\{\operatorname{cosec}(\theta/2)\\ &\qquad-2\nu\sin(3\theta/2)\},\quad(\theta=\pi/(2\nu+1))\end{aligned}\tag{3.10}$$

where $\mathbf{i}$, $\mathbf{j}$ are unit vectors along $0x$, $0y$ respectively and we have put $S_{mn}=S$ whenever m, n are adjacent. Certain results are apparent at once.

For example, $|Q_{NX}{}^0|$ never becomes large; its magnitude for benzene is R and for a very long polyacene, it approaches $(3/\pi)R$ monotonically. $|Q_{NY}{}^0|$, on the other hand, increases almost linearly on increasing the number of fused rings. $|Q_{NU}{}^0|$ is again bounded, and never exceeds $\frac{1}{2}R$. $|Q_{NV}{}^0|$ vanishes identically for distorted cyclodecapentaene, which is the perimeter of naphthalene, and remains small even as far as pentacene; it contains the overlap integral. For benzene itself, of course, we have $|Q_{NX}{}^0|=|Q_{NY}{}^0|=R$ and $|Q_{NU}{}^0|=|Q_{NV}{}^0|=0$.

We are now in a position to make estimates of the intensities of the various bands which arise in the spectra of the polyacenes. These are best compared on the basis of their oscillator strengths f, which are proportional to the excitation energy of the upper state and to the square of the effective dipole lengths associated with the transitions.[12] When Ω_N is the ground-state function, and Ω_S the eigenfunction of the upper state, the effective dipole length is defined as

$$\mathbf{Q}_{NS}=\int\Omega_N{}^*(\sum_i\mathbf{r}_i)\Omega_S dV.\tag{3.11}$$

Thus $|Q_{NS}|^2$ is the main criterion for the purely electronic contribution to the intensity of the $N\rightarrow S$ bands. We shall discuss the three different band systems in turn.

The very intense bands which Clar calls β bands are those due to the transitions $N\rightarrow Y$ in our notation

[12] R. S. Mulliken, J. Chem. Phys. **7**, 14 (1939).

(Platt's $^1A \rightarrow {}^1B_b$). They are longitudinally polarized. Now, in our approximation, we have, according to (3.1), $\Omega_N = \Theta_N$, $\Omega_Y = \Theta_Y$, so that the effective dipole lengths are given by the $\mathbf{Q}_{NY}{}^0$ of Eq. (3.10). Thus we should expect the intensities of these transitions to increase as we go to the higher polyacenes. They correspond to the allowed transition ($^1A_{1g} \rightarrow {}^1E_{1u}$) in benzene, and therefore absorb very strongly.

The very weak α bands, which are obscured by the stronger p bands in anthracene and naphthacene, correspond to our transition $N \rightarrow V$. Just as for the β bands, we may use Eq. (3.10) to calculate the effective dipole lengths, since $\Omega_V = \Theta_V$ in our approximation. Now the $N \rightarrow V$ transitions are formally allowed electronically, since they too are polarized longitudinally. However, we have seen that $|Q_{NV}{}^0|$ vanishes identically for naphthalene and is still very small for pentacene. The absorptions associated with these transitions are therefore exceedingly weak. It is, moreover, easily shown, by arguments analogous to those used for benzene, that the upper states of these bands are insensitive to vibrational ("odd") perturbations. So that, although they are often not far from more intense systems, they do not "borrow" intensity at all effectively. (The f value for benzene is only 0.002.)

Lastly, we consider the p bands, whose moderate to strong intensity is attributed to the transition $N \rightarrow U$. The situation is slightly more complicated, since the U state is represented as the linear combination

$$\Omega_U = \cos\rho\Theta_U + \sin\rho\Theta_X. \tag{3.12}$$

Accordingly, the effective dipole length is given by

$$\mathbf{Q}_{NU} = \cos\rho\mathbf{Q}_{NU}{}^0 + \sin\rho\mathbf{Q}_{NX}{}^0. \tag{3.13}$$

Now, we have seen that $|Q_{NU}{}^0|$ is small for small ν and approaches $\frac{1}{2}R$ for very long polyacenes; $|Q_{NX}{}^0|$ is always very close to R. Thus $|Q_{NU}|$ begins by being rather small and never exceeds $1/\sqrt{2}[\frac{1}{2}+(3/\pi)]R$. The intensity of these bands is markedly affected by the vibrational couplings ("odd" perturbations), which we have considered qualitatively for benzene. As we shall see more specifically below, this accounts for the moderate intensity of the p bands quite nicely.

TABLE VI. The calculated and observed oscillator strengths of band systems in the polyacene spectra.

Method	Transition	Benzene	Naphthalene	Anthracene	Naphthacene	Pentacene
calc. I	$N \rightarrow V$	0	0	0.0016	0.008	0.019
calc. II	(α bands)	0	0	0.0005	0.002	0.006
obs.		0.002	0.002	?	?	~0.006
calc. I	$N \rightarrow U$	0	0.38	0.37	0.32	0.29
calc. II	(p bands)	0	0.11	0.11	0.10	0.09
obs.		0.10	0.18?	0.10	0.08	0.08
calc. I	$N \rightarrow Y$	1.2	2.8	4.8	7.2	9.9
calc. II	(β bands)	(0.35)	0.85	1.45	2.16	2.97
obs.		0.35	1.70	2.28	1.85	2.2

The important contributions of vibrational coupling to the observed oscillator strengths, particularly for the α and p bands are discussed in the text.

To illustrate the more quantitative aspects of these arguments, we shall estimate the oscillator strengths f of the three band systems using the formula[12]

$$f_{N \rightarrow S} = 1.085 \times 10^{11} \times |Q_{NS}|^2 \times E_{NS}, \quad (S = V, U, Y), \tag{3.14}$$

where $\mathbf{Q}_{NS}$ is expressed in cm and E_{NS}, the excitation energy of the relevant upper state, is expressed in cm^{-1}. Then, using (1.19), (3.10), and (3.13) in conjunction with (3.14), we prepare Table VI. In the first row, we use (3.14) directly. But, as Mulliken has shown, calculations of oscillator strengths by means of this equation always lead to results whose values are too high. Accordingly he used correction factors in the range from 0.4 to 0.25. To obtain a better comparison with the experimental results, we therefore multiply all oscillator strengths in the first row by 0.3, thereby "normalizing" with respect to benzene, whose oscillator strength then comes out correctly. (Only $N \rightarrow Y$ is shown for benzene, since we do not include $N \rightarrow X$ for the polyacenes.) These modified values are given in the second row. The third row lists the observed values, which are taken from Klevens and Platt's compilation.

The agreement is strikingly good. For example, the calculated range of intensities falls sharply into the three observed domains. Those band systems of exceedingly low oscillator strengths ($N \rightarrow V$) cannot be compared at all closely with the empirical values, since the predicted intensities for the electronic processes are lower than those due to the vibrational coupling ($\Delta f \sim 0.002$). The bands of moderate intensity ($N \rightarrow U$) are more strongly affected by vibrational perturbations ($\Delta f \sim 0.1$) but presumably also have electronic contributions to their intensity. Our estimates of the latter show these to be of the right order of magnitude. Finally, the strong $N \rightarrow Y$ bands are predicted to be in just the right intensity range. A more detailed comparison of the numerical results does not seem very profitable. In the first place, our theoretical method was not aimed at great accuracy, and in the second, the oscillator strengths in the shorter wavelength region are not easy to measure exactly. The uniform increase of f with ν predicted for the β bands may well occur, but its observation may be obscured by possible interference from neighboring, more highly excited levels; the experimental behavior of ϵ_{max} certainly confirms the regular intensification which we have calculated.

As a last feature of the intensities of these three band systems, we may consider the effect of inductive substituents. The most striking change that is observed on going from a cata-condensed hydrocarbon to its aza-derivative, by the replacement of $-CH=$ by $-N=$, is the sharp intensification of the α bands.[13] And similar changes occur on replacing hydrogen atoms by more or

[13] Badger, Pearce, and Pettit, J. Chem. Soc. **1951**, 3199.

less electronegative groups. Now the upper state of these bands is our V state which is sensitive only to the "even" perturbations analyzed in Sec. 1(d). As an example of these, variations (A_m) of the Coulomb integrals at particular atomic centers constitute an "even" perturbation. And such inductive changes at a carbon atom are of just this type. Accordingly, the effect of these perturbations is to mix the unperturbed V states, to which transitions from the ground state are virtually "forbidden," with contributions from X and Y, to which transitions are strongly allowed. The observed intensification of the ensuing bands is easily explained on this basis.

4. AZULENE

(a) Excitation Energies

In the preceding section, we have dealt with the "formation" of cata-condensed hydrocarbons containing fused benzene rings, from their perimeters. It was always found that the cross-linking perturbations were "odd." However, stable aromatic systems may also be formed in which the fused rings contain odd numbers of carbon atoms. The most simple of these is azulene which, like naphthalene, we relate to cyclodecapentaene. In this case, the relevant perturbation, when referred to an AO representation, has only two nonvanishing elements, namely, $B_{28}=B_{82}=B$, say. This will link together atoms 2 and 8, so that the new aromatic system contains fused five- and seven-membered rings. Since the sum of the atomic indices is now even, we are dealing with an "even" perturbation.

The atoms have been labeled in such a way that 0 and 5 lie on the twofold (x) axis of symmetry, with the former belonging to the five-membered ring. It is then easily verified that Θ_Y, Θ_V transform like translations along the shorter, transverse (y) axis of the molecule, whereas Θ_X, Θ_U are longitudinally polarized. Once again, it is formally possible for Θ_X and Θ_U to interact under the perturbation, and similarly for Θ_Y and Θ_V. In contrast to the behavior found for naphthalene, however, it is Θ_Y and Θ_V which interact under the "even" perturbation, whereas the possibility of mixing Θ_X with Θ_U is not realized.

A comparison of the predicted properties of naphthalene and azulene is made in Fig. 6. At the sides of this figure, we show the location of the diagonal terms of the energy matrix (1.14), referred to their respective ground states, for both cases. It will be noticed that $(\kappa-\chi)$ is greater for naphthalene than for azulene. In the middle, the results of the full perturbation calculations are illustrated. For azulene, we see that the interaction of Θ_Y and Θ_V accounts for the low level of the V state, whereas the remaining states are unaffected. For naphthalene, on the other hand, it is the location of the U state which is affected by the appropriate cross-linking perturbation. We also indicate the observed energies of the three lowest-excited singlet states by

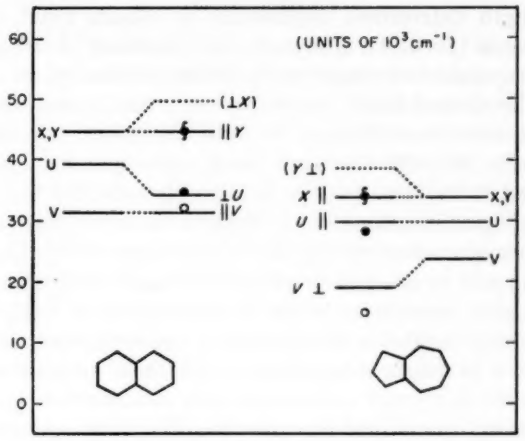

FIG. 6. A comparison of the spectra of azulene and naphthalene.

circles on this diagram.[14] It will be seen that the qualitative behavior we predict is perfectly correct. The quantitative results are also quite good. Least accurate is the location of the lowest state in azulene. Considering the relative crudity of our method, it does not seem profitable at present to speculate on the reason for the greater disparity in this particular case.

(b) Intensities

In the case of the polyacenes, it was possible to confirm the assignment of the observed band systems, to the theoretically located transitions, on grounds other than those of excitation energies alone. Similar considerations must now be applied to the azulene levels. As before, we shall use the intensity of the bands for this purpose. (For the polyacenes, it was also possible to use isomerism and sensitivity to inductive substitution; the application of an additional criterion will also be discussed for azulene below.)

Calculations of the oscillator strengths associated with the three azulene transitions $N\rightarrow V$, U, X may be made in the same manner that similar computations were undertaken in Sec. 3(c) for the polyacenes. We assume that the geometry of the molecule is not far from that of a system which fuses a regular pentagon together with a regular heptagon of side $R=1.4$A. The calculations are then straightforward and it is unnecessary to comment further on them, except to state that the same correction factor of 0.3 is applied to these cases, as was applied to benzene and the polyacenes.

For the lowest $N\rightarrow V$ transition, the electronic contribution to the intensity is almost entirely due to the admixture of Θ_Y contained in Ω_V. This is predicted to lead to an oscillator strength which is rather less than 0.02. Skeletal vibrations will not affect the intensity of these bands very much, since variations in the lengths of the ten perimetric bonds constitute "odd" perturbations, to which the upper and lower states are relatively insensitive. This is in good agreement with the oscillator

[14] Mann, Platt, and Klevens, J. Chem. Phys. 17, 481 (1949).

strength determined empirically by Mann, Platt, and Klevens ($f \approx 0.01$), who call this transition ${}^1A \rightarrow {}^1L_b$. It corresponds to a transversely polarized absorption.

The second band system, $N \rightarrow U$, has a very small electronic contribution to the oscillator strength, namely, 0.01. On the other hand, the upper state associated with this system is strongly affected by the "odd" perturbations which describe the more important effects of nuclear vibrations. By analogy with benzene, we should expect this coupling to enhance electronically negligible intensities by an amount $\Delta f \approx 0.1$. That the observed oscillator strength is in the neighborhood of 0.08, is in excellent agreement with these expectations. The $N \rightarrow U$ system is longitudinally polarized.

Lastly, we consider the longitudinally polarized $N \rightarrow X$ bands. Here the transition is very strongly allowed, electronically, and we compute an oscillator strength $f \approx 0.6$. This also agrees quite nicely with the empirical value of $f \approx 1.1$. (Mann, Platt, and Klevens call this transition ${}^1A \rightarrow {}^1B_b$. It would seem, however, that the upper state of this system could profitably be renamed ${}^1B_a$. For both ${}^1L_a$ and ${}^1B_a$ would then be polarized along the same twofold axis of symmetry, and the subscripts a and b for Platt's ${}^1B$ states would have an enhanced significance. It would also appear to be more consistent with his usage for the polyacenes, where ${}^1L_b$ and ${}^1B_b$ have the same axis of polarization.)

It will be noticed in these cases, as for the polyacenes, that the intensity criterion is particularly good since the observed, as well as the calculated oscillator strengths differ sharply for the three lowest band systems. But it is most important in this connection to assess, however approximately, the vibrational contributions to those band systems whose purely electronic dipole lengths are small. In this note, we have used the criterion $\Delta f \approx 0.1$ for those transitions whose upper states are vulnerable to "odd" perturbations, whereas $\Delta f \approx 0.002$ for the remainder—using the known benzene spectrum as the basis for these estimates. A more fundamental treatment of this topic is being carried out and will be published at a later date.

(c) The Effect of Inductive Substituents

One of the most striking features of the azulene spectrum is the sensitivity exhibited by the lowest $N \rightarrow V$ band system. On effecting substitutions for hydrogen atoms by more or less electronegative groups at different positions in either or both of the fused rings, characteristic and quite appreciable shifts to greater or to lower wavelengths are observed. But concomitant shifts in the other two band systems are much smaller and of the usual bathochromic type. Coulson and others have discussed this phenomenon but, as he remarked,[15] it has remained a mystery why the $N \rightarrow V$ system should be unique in this respect. The present approach offers a very natural explanation of these effects.

[15] C. A. Coulson, Proc. Phys. Soc. (London) **A65**, 933 (1952).

Consider first the cyclic polyenes of $(4\nu+2)$ carbon atoms. It is easily verified that the description of these molecules given in Sec. 1 assigns the electronic charges uniformly among the equivalent carbon atoms in all their states $\Omega_T{}^0$, $(T=N, X, Y, U, V)$. Under an "odd" perturbation, these charge distributions remain unaltered. However, under an "even" perturbation, the situation is different. The separate, unperturbed functions Θ_T, (T = N, X, Y, U, V) describe states of the molecules in which no atom has a net charge. And therefore the N, U, and X states are unaffected by the perturbation in this respect. But the linear combination of Θ_V and, in our case, Θ_Y—which is needed to describe the perturbed V state (of azulene, say)—is such that the charge distribution is no longer uniform: fractional positive and negative charges appear on the various carbon atoms in this particular state, and in this state only.

More specifically, we may write for the eigenfunction of the V state in azulene

$$\Omega_V = \cos\rho\Theta_V + \sin\rho\Theta_Y,$$

where the parameter ρ is determined by the usual methods of Sec. 1; it turns out to be in the neighborhood of $27\frac{1}{2}°$. Then, although the separate distributions Θ_V, Θ_Y are uniform, it is readily shown that their interference induces a net charge of

$$-(1/5)\sin 2\rho \cos(6m\pi/5)$$

at the carbon atom which we have labeled m. It may be noticed that the ratios of these charge increments are independent of the specific value calculated for ρ. Up to the present, we have found it convenient analytically to index carbons serially on going around the ring of the parent cyclic polyene. Since this is at variance with chemical nomenclature, we shall adopt the latter from now on and abandon our original designation. The net charges are therefore given numerically, together with the conventional labelling, in Fig. 7.

That such charge separation should occur for the V state of azulene, which arises from an "even" perturbation of cyclodecapentaene, is not in any way surprising. It will be recalled that electrostatic perturbations of benzene induced a mixing of its ${}^1B_{2u}(V)$ and ${}^1E_{1u}(X, Y)$ states in Sec. 2(a). The cyclic polyene in this case $(\nu=1)$ rearranged its electronic densities in such a way as best to accommodate itself to the different conditions defined by its substituents; some charge separation

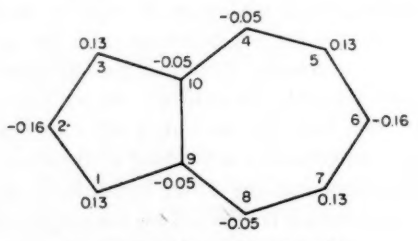

(in units of the protonic charge)

FIG. 7. The charge distribution in the first excited state of azulene.

occurred. This effect was also due to an "even" perturbation.

The changes to be observed in the azulene spectrum on replacing hydrogen atoms by electron donors or acceptors may now be worked out quite simply—to a first approximation, at least. The charge distribution being uniform in states N, U, and X, we should anticipate only second-order shifts in the band systems $N \rightarrow U$ and $N \rightarrow X$. However, an inspection of Fig. 7 shows that if electron donors (e.g., methyl groups) replace hydrogen atoms at positions 1, 3, 5, and 7, the V state is stabilized and we should expect corresponding first-order shifts in the $N \rightarrow V$ bands to longer wavelengths (bathochromically). Conversely, similar substitutions at positions 2, 4, 6, and 8 should lead to hypsochromic shifts. Moreover, within the limits of accuracy set by our first-order treatment, the effect of successive replacements should be additive. Substitution by electron acceptors (more electronegative atoms or groups, like $-$COOH), on the other hand, should follow exactly the opposite laws: at positions 1, 3, 5, and 7 hypsochromic shifts are expected, whereas at 2, 4, 6, and 8 the $N \rightarrow V$ bands should be moved to longer wavelengths.

These qualitative rules reproduce precisely the empirical behavior of the $N \rightarrow V$ band system.[16] Moreover, the shifts observed are much larger than those obtained for the $N \rightarrow U, X$ systems, which is again what we should have expected. Using the magnitudes of the charge increments of Fig. 7 as a quantitative guide, it appears that the numerical value of the methyl shifts at positions 1 and 4 is rather larger than would have been anticipated. No importance is attached to this, however, since neither the second-order effects of the substitutions nor their hyperconjugative propensities—which are probably also subsidiary factors—have been considered. We should be content that a treatment as simple as that described is qualitatively so successful. It lends powerful support to the identification of the band systems.

[16] P. A. Plattner, Helv. Chim. Acta **24**, 283 (1941); **34**, 971 (1951); P. A. Plattner and E. Heilbronner, Helv. Chim. Acta **31**, 804 (1948).

DISCUSSION

It has been shown how the perimeter model accounts for the more prominent features of the electronic spectra of cata-condensed hydrocarbons. These include the location of the three lowest band systems, their intensities and particularly the way in which these are affected by vibrational coupling and substitution, the effects of isomerism and the characteristic shifts accompanying substitution in azulene. Starting with the supposedly known benzene spectrum, the properties of the cyclic polyenes were estimated. These hypothetical molecules were then subjected to perturbations under which their unsaturation electrons simulated the behavior of the cata-condensed systems of interest. The most interesting properties which emerged were due to the very specific, almost geometrical nature of these perturbations.

The method which was used has several advantages. More particularly, it is sufficiently simple for its general results to become apparent almost immediately on qualitative grounds. The calculations never require the solution of difficult secular equations, but may be carried out directly using trigonometric tables. Another of its more important aspects concerns the sense in which perturbation theory is employed: the zeroth-order levels in the treatment refer to states, and not to orbitals. It is in this way that many of the complications (particularly those connected with configurational interaction) of previous theoretical work are avoided. There are many points of interest which arise relating the perimeter theory to the conventional methods of approach. In view of the very limited ability of the latter to rationalize the spectral features, it would be desirable in many ways to pursue this topic here. It seems, however, that this could more profitably be discussed in a later and quite separate communication.

The work reported in this note was largely stimulated by the publications of Clar, Jones, and particularly of Platt, references to which have been made above.

Diffusion Effects in the Photochemistry of Solid Films

JOSEPH E. WILSON
Bakelite Company, A Division of Union Carbide and Carbon Corporation, Bound Brook, New Jersey
(Received August 7, 1953)

Little work has been done, either experimentally or theoretically, on the problem of photochemical reaction kinetics in the solid phase, although this field is of practical importance in connection with the weathering of polymeric films and sheets. Reaction kinetics in solid films are greatly influenced by diffusion phenomena. The Laplace transformation technique offers a convenient method of solving many problems concerning the interaction of diffusion behavior with reaction kinetics. The method is illustrated for the diffusion of a gaseous product from an irradiated film, with and without reaction rate dependence on product concentration, and for the diffusion of a gaseous reactant into an irradiated film, with and without reaction rate dependence on reactant concentration. In each case the expression for dissolved gas concentration across the thickness of the film is computed, and the quantum yield for the reaction involved is expressed as a function of film thickness, diffusion coefficient, rate of light absorption, and initial conditions. Equations for the effect of temperature variation and of intermittent light are derived in a few instances.

INTRODUCTION

THE production of high-polymeric materials of improved weathering properties has been a long-standing objective of industrial research. Perhaps the major cause of failure in weathering is the catalytic effect of the sun's rays on the various degradation reactions. The spectrum of sunlight extends down to 2950A, and on a clear day the energy flux between 3000 and 4000A has been estimated[1] as about one hundred times that from a 500-watt mercury vapor arc at a distance of ten centimeters. Considerable success in combating the degradative action of this powerful light source has been attained by empirical approaches, but a more fundamental understanding of the principles of photochemical reaction kinetics in the solid phase is needed.

While a large body of quantitative information has grown up on the subject of photochemistry in the gas phase, most of the publications dealing with the solid phase merely present data on changes in color or physical properties with no information on the amount of light absorbed in the process. Recently a few papers have appeared that give a discussion of the relationship between the quantity of light absorbed by solid films and the amount of chemical change resulting. Bateman[2] measured the quantum yield of hydrogen diffusing from a rubber film irradiated in vacuum with ultraviolet light. Wilson[3] irradiated a thin film prepared from the copolymer of vinylidene and vinyl chloride with monochromatic 2537A radiation and determined the quantum yields of hydrogen chloride and water vapor diffusing from the film. Hart and Matheson[4] measured the quantum yields of oxygen uptake for GR−S and natural rubber films irradiated with monochromatic light of various wavelengths. In the work of Hart and Matheson, especially, rate effects were observed that appeared to result from the slowness of gaseous diffusion in the solid film.

The principal differences between the reaction kinetics of the gaseous and the solid phase can be attributed to the much closer packing of the molecules in the solid phase. All effects due to the interaction of molecular fields will be enhanced, and the frequency of intermolecular contacts and collisions will be greatly increased in the solid. Phenomena such as the collisional deactivation of excited molecules and the Franck-Rabinowitsch type of recombination might be expected to proceed with high efficiency. The diffusion of gaseous molecules and radicals through the close-packed solid molecules will be quite slow as compared to the same process in the gas phase, and this latter property can be directly responsible for a number of peculiarities in the observed reaction kinetics.

When a gaseous product of photodegradation is formed in a solid film the close packing of the molecules will prevent the immediate diffusion of the product from the film and cause a concentration buildup within the film. If the reaction rate within an infinitesimal volume is independent of product concentration, the accumulation of product within the film will have no effect on the observed rate of product diffusion from the film in the steady state. But if the reaction rate is some function of product concentration, the observed rate of product diffusion from the film will be altered in a complex way.

When the irradiation of a solid material is discontinued, the gaseous product accumulated in the interior of the solid will continue to diffuse out. This phenomenon was observed by Noyes and Kouperman[5] in the photochemical decomposition of anhydrous oxalic acid crystals. Thus when intermittent light is employed, such as sunlight, for example, a plot of the product concentration in a solid film *versus* the time will exhibit a cyclic nature, with the concentration function alternately

[1] A. R. Burgess, Chemistry & Industry **71**, 78 (1952).
[2] L. Bateman, J. Polymer Sci. **2**, 1 (1947).
[3] J. E. Wilson, J. Am. Chem. Soc. **72**, 2905 (1950).
[4] E. J. Hart and M. S. Matheson, J. Am. Chem. Soc. **70**, 784 (1948).
[5] W. A. Noyes, Jr., and A. B. Kouperman, J. Am. Chem. Soc. **45**, 1398 (1923).

increasing in the light periods and decreasing in the dark periods.

When the reaction rate is a function of product concentration, the interaction of the diffusion behavior with the reaction kinetics can lead to anomalous temperature effects. This arises from the fact that the diffusion coefficient is greater at higher temperature and the rate of product diffusion from the film is correspondingly increased. Other things being equal the resultant lowering of the product concentration within the film may cause a decrease in the over-all rate of product formation in some cases, thus presenting the superficial appearance of a reaction having a negative energy of activation.

In the case of an external gas diffusing into, and reacting with an irradiated film, the dissolved gas in the center of the film may react so rapidly that it becomes completely exhausted before more gas can diffuse in from the outside. When such a situation holds true after a steady state has been reached the center portion of the film will continue to absorb light while reaction occurs at the surface layers only. This condition causes a substantial reduction in the measured quantum yield below the theoretical value for an infinitely thin film. For certain types of reaction kinetics, however, it can be shown that it is impossible to exhaust the supply of dissolved gas in the center of the film, no matter how rapidly the reaction may proceed.

In gas phase photochemical reactions it is ordinarily taken for granted that the reactants and reaction intermediates are uniformly distributed throughout the reaction vessel. In the rare cases when this condition does not hold true it is necessary to derive the local rate equations for an infinitesimal volume, dV, and then obtain the over-all or observed reaction rates by integrating over the total volume of the vessel.[6] In solid phase reactions, on the other hand, the relatively slow diffusion always prevents the uniform distribution of the reaction intermediates, and in most cases it is necessary to employ an integration over the irradiated volume to derive the expression for the observed reaction rate.

The interaction between photochemical reaction kinetics and diffusion effects can generally be expressed by a partial differential equation. It has been found that the application of the Laplace transformation to the equation and its boundary conditions often makes it possible to obtain the solution in a straightforward way. It is the purpose here to demonstrate the use of this technique and to show the types of quantum yield and rate functions obtained from certain combinations of reaction kinetics and diffusion behavior. There is no limit to the number of such combinations, but the discussion here will be confined to a few simple examples chosen to illustrate the principles involved. The diffusion of a gaseous product from a film will be investigated first, followed by a study of the relationships obtained when an external reactive gas diffuses into and reacts with a solid film. Each of these broad classifications will be further subdivided into the following types: (a) the rate of reaction independent of the concentration of the diffusing material, and (b) the rate of reaction directly proportional to the concentration of the diffusing material.

CASE I. RATE INDEPENDENT OF GASEOUS PRODUCT CONCENTRATION

Consider the case of gaseous product formation within an irradiated film, the rate of product formation in any infinitesimal volume being independent of product concentration. Let the film be of planar surface and of uniform thickness, and suppose that the beam from a monochromatic light source passes through the film in a direction perpendicular to the surface. If the thickness of the film is taken to be small as compared to the irradiated area the product diffusion is essentially one dimensional. The present treatment excludes situations where strong forces of mutual attraction between the gaseous product and the solid phase cause the diffusion process to deviate from Fick's law.[7] Under the limiting conditions defined here the product concentration function θ will satisfy the equation

$$\theta_t(X,t)=D\theta_{XX}(X,t)+k_1, \quad (0<X<l,\ t>0), \qquad (1)$$

where the X coordinate is taken perpendicular to the film surface, D represents the diffusion coefficient, and k_1 the local rate of product formation due to the photochemical reaction. It is convenient to consider k_1 proportional to the rate of light absorption I_a. For this discussion I_a is taken as constant along the X coordinate within the film, a condition that is approximated in practice for low absorption coefficients or thin films.

The origin of the X axis is placed at one surface of the film while the other surface intersects the axis at a distance l in the positive direction. Before the start of the irradiation the concentration θ_0 of the gaseous product within the film is proportional to its external pressure in the space surrounding the film (Henry's law). The treatment here will omit any reference to surface adsorption effects, thus restricting the applicability of the results to cases where adsorption effects are of minor importance. The external pressure of the product will be held substantially constant throughout the irradiation so that the concentration at the surface does not change from the θ_0 value. With these restrictions the boundary conditions can be written

$$\theta(X,0)=\theta_0, \quad (0<X<l); \qquad (2)$$

$$\theta(0,t)=\theta_0, \quad \theta(l,t)=\theta_0, \quad (t>0). \qquad (3)$$

[6] W. A. Noyes, Jr., and P. A. Leighton, *The Photochemistry of Gases* (Reinhold Publishing Corporation, New York, 1941), p. 200.

[7] R. M. Barrer, *Diffusion In and Through Solids* (Cambridge University Press, Cambridge, 1941), p. 451.

Letting $L\{\theta(X,t)\}=u(X,s)$, the problem in the transform of $\theta(X,t)$ is then

$$s^2u(X,s)-s\theta_0=sDu_{XX}(X,s)+k_1, \tag{4}$$

$$su(0,s)=\theta_0, \quad su(l,s)=\theta_0. \tag{5}$$

The solution is

$$u(X,s)=\frac{[(k_1+\theta_{0s})\sinh l(s/D)^{\frac{1}{2}}-k_1\sinh X(s/D)^{\frac{1}{2}} -k_1\sinh(l-X)(s/D)^{\frac{1}{2}}]}{s^2\sinh l(s/D)^{\frac{1}{2}}}. \tag{6}$$

It follows from the inversion theorem that

$$\theta(X,t)=\frac{1}{2i\pi}\int_{\gamma-i\infty}^{\gamma+i\infty}e^{\lambda t} \times\left[\frac{(k_1+\theta_0\lambda)\sinh(\lambda/D)^{\frac{1}{2}}-k_1\sinh X(\lambda/D)^{\frac{1}{2}} -k_1\sinh(l-X)(\lambda/D)^{\frac{1}{2}}}{\lambda^2\sinh l(\lambda/D)^{\frac{1}{2}}}\right]d\lambda, \tag{7}$$

where $\gamma>0$.

Let the multiplier of $e^{\lambda t}$ in the integrand of (7) be denoted by $f(\lambda)$. The integral can be evaluated readily provided $f(\lambda)$ satisfies certain order requirements. The poles of $f(\lambda)$ lie at

$$\lambda=0; \quad \lambda=-Dn^2\pi^2/l^2, \quad (n=1,2,\cdots). \tag{8}$$

In Fig. 1, AB is at a distance γ from the imaginary axis. If the circle Γ has a radius equal to $D(n+\frac{1}{2})^2(\pi^2/l^2)$ it will not pass through any pole of the integrand. On the arc of the circle BCA let $\lambda=Re^{i\beta}$, $-\pi\leqq\beta\leqq\pi$. It can be shown, for the domain $0\leqq X\leqq l$ and $-\pi\leqq\beta\leqq\pi$, that

$$\left|\frac{\sinh X(\lambda/D)^{\frac{1}{2}}}{\sinh l(\lambda/D)^{\frac{1}{2}}}\right|<M'$$

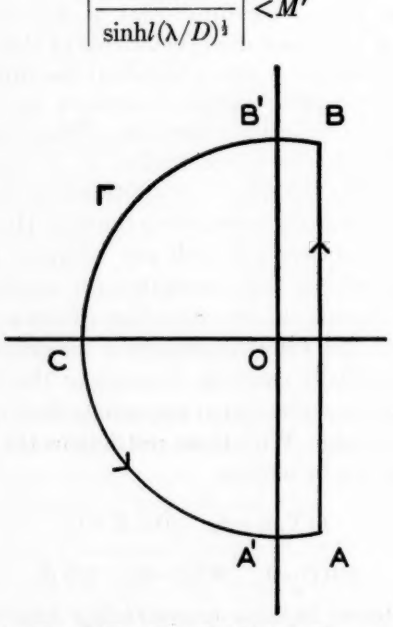

FIG. 1. Case I, path of integration.

and

$$\left|\frac{\sinh(l-X)(\lambda/D)^{\frac{1}{2}}}{\sinh l(\lambda/D)^{\frac{1}{2}}}\right|<M'', \tag{9}$$

where M' and M'' are constants independent of n, and hence

$$|f(\lambda)|<\frac{M}{R^q}, \tag{10}$$

where M is a constant independent of n, and $q>0$.

Because of this order property of $f(\lambda)$ it is known[8] that $\int e^{\lambda t}f(\lambda)d\lambda$ taken over the arcs $BB'C$ and $CA'A$ of Fig. 1 tends to zero as $R\to\infty$, provided $t>0$. The line integral of Eq. (7) can therefore be replaced by the integral around the contour of Fig. 1, and this in turn by the integral around any circle centered at the origin and enclosing the singularities at zero and $-Dn^2\pi^2/l^2$ of the integrand. By Cauchy's theorem this is equal to $2i\pi$ times the sum of the residues of the integrand at its poles.

The residue at the pole $\lambda=0$ is

$$\theta_0+\frac{k_1(Xl-X^2)}{2D}.$$

The sum of the residues at the poles $\lambda=-Dn^2\pi^2/l^2$ is

$$-\frac{4k_1l^2}{D\pi^3}\sum_{n=1,3,5}^{\infty}\frac{1}{n^3}\exp\left\{-\frac{Dn^2\pi^2}{l^2}t\right\}\sin\frac{n\pi X}{l},$$

where n takes odd integral values only. Using these results in (7) gives the complete solution,

$$\theta(X,t)=\theta_0+\frac{k_1(Xl-X^2|}{2D}-\frac{4k_1l^2}{\pi^3D} \times\sum_{n=1,3,5}^{\infty}\frac{1}{n^3}\exp\left\{-\frac{Dn^2\pi^2}{l^2}t\right\}\sin\frac{n\pi X}{l}. \tag{11}$$

By direct substitution it can be shown that this solution satisfies the statement of the problem in Eqs. (1), (2), and (3). By a more rigorous consideration of the continuity and order conditions of the required concentration function, it is possible to prove the uniqueness of the solution, but this is omitted for the sake of brevity. Furthermore, the physical problem of the concentration through a film with prescribed initial concentration function and prescribed concentration conditions at the surfaces must have just one solution.

Figure 2 presents a plot of θ *versus* X according to Eq. (11), using arbitrary values for the other quantities. The diffusion coefficient D and the initial concentration θ_0 were chosen of an order of magnitude in conformity with the data of Barrer[9] on gaseous diffusion in polymers at room temperature. The rate constant k_1 was selected

[8] H. S. Carslaw and J. C. Jaeger, *Operational Methods in Applied Mathematics* (Oxford University Press, London, 1941), second edition, p. 76.

[9] See reference 7, p. 420.

to give a rate of product formation of the order of that reported by Bateman.[2] The several curves shown present the concentration function for different values of t, with the top curve indicating the form of the function in the steady state.

Each square centimeter of film contains $\theta_0 l$ moles of gaseous product at the start of the irradiation. The total amount of gas formed by decomposition after time t is $k_1 l t$ mole cm^{-2}. By integrating $\theta(X,t)$ from 0 to l the total amount of product gas within one square centimeter of film at any time is shown to be

$$\theta_0 l+\frac{k_1 l^3}{12D}-\frac{8k_1 l^3}{\pi^4 D}\sum_{n=1,3,5}^{\infty}\frac{1}{n^4}\exp\left\{-\frac{Dn^2\pi^2 t}{l^2}\right\}.$$

The total amount W of gaseous product diffused from each square centimeter of film after time t is obtained by subtracting the amount present in the film at time t from the sum of the total amount of gas formed after time t and the amount of gas originally present in the film:

$$W=k_1 l t-\frac{k_1 l^3}{12D}+\frac{8k_1 l^3}{\pi^4 D}\sum_{n=1,3,5}^{\infty}\frac{1}{n^4}\exp\left\{-\frac{Dn^2\pi^2 t}{l^2}\right\}. \quad (12)$$

As t increases the W function approaches asymptotically to the line

$$W=k_1 l t-\frac{k_1 l^3}{12D}, \quad (13)$$

having an intercept on the t axis at

$$t=\frac{l^2}{12D}. \quad (14)$$

This length of time may be defined as the induction period due to diffusion. It is caused only by the slowness of the gaseous product in escaping from the solid film. If there is in addition the usual sort of induction period resulting from the mechanism of the chemical reaction, the total observed induction period will be increased by some undetermined amount.

Differentiating (13) with respect to t and dividing by the rate of light absorption, $I_a l$, gives the quantum yield in the steady state:

$$\Phi=\frac{k_1}{I_a}. \quad (15)$$

In this case the quantum yield is unaffected by variations in θ_0, D, or l. As stated in the foregoing, k_1 has been taken proportional to I_a, so Φ is also independent of I_a.

When intermittent light is used the concentration function becomes periodic. If there are alternate periods of light and darkness of equal length a the equation for the problem of Case I becomes

$$\theta_t(X,t)=D\theta_{XX}(X,t)+k_1\sum_{n=0}^{\infty}(-1)^n H(t-na), \quad (0<X<l,\ t>0), \quad (16)$$

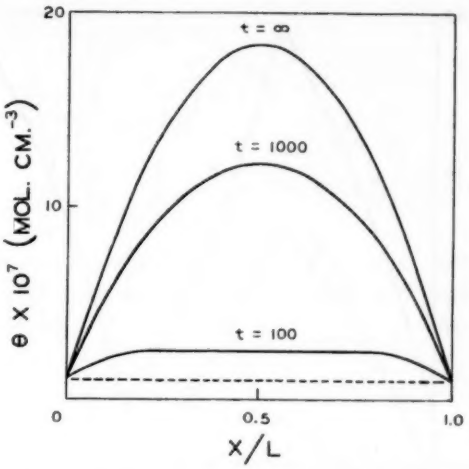

FIG. 2. Case I, θ *versus* X/l; with $k_1=1.5\times10^{-9}$ mole cm^{-3} sec^{-1}, $D=1.0\times10^{-6}$ cm^2 sec^{-1}, $l=9.6\times10^{-2}$ cm, $\theta_0=1.0\times10^{-7}$ mole cm^{-3}, and values of t indicated in sec.

with the arrangement of the film and the boundary conditions the same as described above. Here $H(t-\alpha)$ is defined as:

$$\left.\begin{aligned}H(t-\alpha)&=1\\&=0\end{aligned}\right\}\begin{aligned}&t>\alpha,\\&t<\alpha.\end{aligned} \quad (17)$$

The problem in the transform is

$$su(X,s)-\theta_0=Du_{XX}(X,s)+\frac{k_1}{s(1+e^{-as})}, \quad (18)$$

$$su(0,s)=\theta_0, \quad su(l,s)=\theta_0. \quad (19)$$

The solution of the transformed problem is

$$u(X,s)=\frac{\theta_0}{s}+\frac{k_1}{s^2(1+e^{-as})}-\frac{k_1}{s^2(1+e^{-as})}\times\left[\frac{\sinh X(s/D)^{\frac{1}{2}}+\sinh(l-X)(s/D)^{\frac{1}{2}}}{\sinh l(s/D)^{\frac{1}{2}}}\right]. \quad (20)$$

The justification for the use of the inversion theorem can be carried out as in the preceding problem, but will be omitted for brevity. The application of the inversion theorem to (20) yields the following series expansion of the inverse transform:

$$\theta(X,t)=\theta_0-k_1\left(\frac{X^2-Xl}{2D}+\frac{4l^2}{\pi^3 D}\times\sum_{n=1,3,5}^{\infty}\frac{1}{n^3}\sin\left(\frac{n\pi X}{l}\right)\exp\left\{-\frac{Dn^2\pi^2 t}{l^2}\right\}+\sum_{n=0}^{\infty}(-1)^n\left[\frac{X^2-Xl}{2D}+\frac{4l^2}{\pi^3 D}\sum_{m=1,3,5}^{\infty}\frac{1}{m^3}\sin\left(\frac{m\pi X}{l}\right)\times\exp\left\{-\frac{Dm^2\pi^2(t-na)}{l^2}\right\}\right]H(t-na)\right). \quad (21)$$

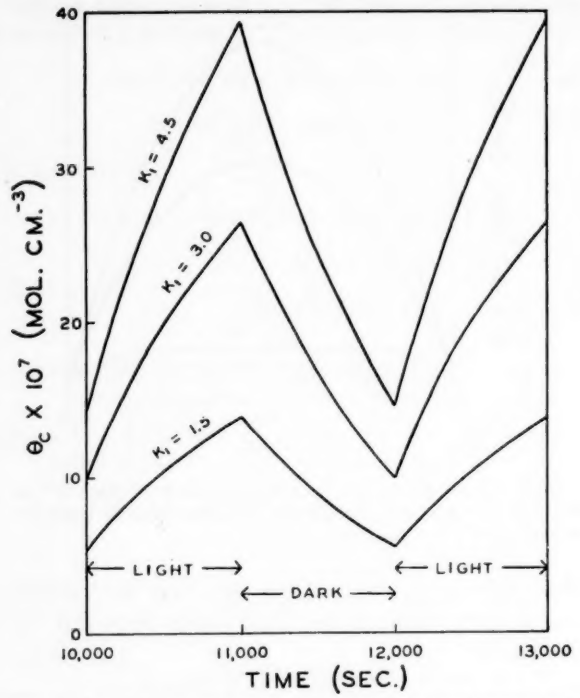

FIG. 3. Case I, θ_c *versus* t; with $D=1.0\times10^{-6}$ cm^2 sec^{-1}, $l=9.6\times10^{-2}$ cm, $\theta_0=1.0\times10^{-7}$ mole cm^{-3}, $a=1000$ sec, and values of $k_1\times10^9$ indicated in mole cm^{-3} sec^{-1}.

This is the complete solution of Eq. (16). Substitution shows that it satisfies the statement of the problem and the boundary conditions.

The concentration function at the center of the film for large values of t reduces to

$$\theta_c=\theta_0+k_1\left(\frac{l^2}{8D}+\sum_{n=0}^{\infty}(-1)^nH(t-na)\times\left[\frac{l^2}{8D}-\frac{4l^2}{\pi^3D}\sum_{m=1,3,5}^{\infty}\frac{1}{m^3}(-1)^{(m-1)/2}\times\exp\left\{-\frac{Dm^2\pi^2(t-na)}{l^2}\right\}\right]\right). \quad (22)$$

A plot of θ_c *versus* t for $a=1000$ sec is shown in Fig. 3.

Over long periods of time the amount of product formed is halved, but the amount of light absorbed is also halved so the average value of the observed quantum yield remains unchanged. If the length of the light and dark periods is reduced to the order of the mean life of the reaction intermediates, by the use of a rotating sector, for example, there may be a pronounced alteration in the quantum yield for certain special types of reaction kinetics.[6] In the present discussion this effect is eliminated by considering only light and dark periods of relatively long duration.

CASE II. RATE PROPORTIONAL TO GASEOUS PRODUCT CONCENTRATION

Consider the irradiation of a film under the same conditions as in Case I, but now suppose that the rate of gaseous product formation within any infinitesimal volume is proportional to the product concentration within that volume. The local rate of product formation is therefore $k_2\theta(X,t)$, where the rate constant k_2 is taken proportional to I_a. The boundary value problem in $\theta(X,t)$ now becomes

$$\theta_t(X,t)=D\theta_{XX}(X,t)+k_2\theta(X,t), \quad (0<X<l,\ t>0), \quad (23)$$

$$\theta(X,0)=\theta_0, \quad (0<X<l), \quad (24)$$

$$\theta(0,t)=\theta_0, \quad \theta(l,t)=\theta_0, \quad (t>0). \quad (25)$$

The problem in the transform is

$$(s-k_2)u(X,s)-\theta_0=Du_{XX}(X,s), \quad (26)$$

$$su(0,s)=\theta_0, \quad su(l,s)=\theta_0. \quad (27)$$

The solution is

$$u(X,s)=\frac{\theta_0}{s-k_2}-\frac{\theta_0k_2}{s(s-k_2)}\times\left[\frac{\sinh X\left(\frac{s-k_2}{D}\right)^{\frac{1}{2}}+\sinh(l-X)\left(\frac{s-k_2}{D}\right)^{\frac{1}{2}}}{\sinh l\left(\frac{s-k_2}{D}\right)^{\frac{1}{2}}}\right]. \quad (28)$$

This function has simple poles at $s=0$ and $s=k_2-Dn^2\pi^2/l^2$, with n taking integral values from one to infinity. The residue of $u(X,s)e^{st}$ at $s=0$ is

$$\theta_0\left[\frac{\sinh X\left(-\frac{k_2}{D}\right)^{\frac{1}{2}}+\sinh(l-X)\left(-\frac{k_2}{D}\right)^{\frac{1}{2}}}{\sinh l\left(-\frac{k_2}{D}\right)^{\frac{1}{2}}}\right].$$

The residue of $u(X,s)e^{st}$ at $s=k_2-Dn^2\pi^2/l^2$ is

$$\sum_{n=1,3,5}^{\infty}\exp\left\{k_2t-\frac{Dn^2\pi^2t}{l^2}\right\}\left[\frac{4k_2\theta_0\sin\frac{n\pi X}{l}}{n\pi\left(k_2-\frac{Dn^2\pi^2}{l^2}\right)}\right].$$

The inversion theorem now gives the complete solution to the original problem, namely,

$$\theta(X,t)=\theta_0\left[\frac{\sinh(X)\left(-\frac{k_2}{D}\right)^{\frac{1}{2}}+\sinh(l-X)\left(-\frac{k_2}{D}\right)^{\frac{1}{2}}}{\sinh l\left(-\frac{k_2}{D}\right)^{\frac{1}{2}}}\right]+\sum_{n=1,3,5}^{\infty}\exp\left\{k_2t-\frac{Dn^2\pi^2t}{l^2}\right\}\left[\frac{4k_2\theta_0\sin\frac{n\pi X}{l}}{n\pi\left(k_2-\frac{Dn^2\pi^2}{l^2}\right)}\right]. \quad (29)$$

The solution may also be written

$$\theta(X,t)=\frac{4\theta_0}{\pi}\sum_{n=1,3,5}^{\infty}\frac{1}{n}\left[\frac{a_n}{a_n-k_2}-\left(\frac{k_2}{a_n-k_2}\right)\times\exp\{-(a_n-k_2)t\}\right]\sin\frac{n\pi X}{l}, \quad (30)$$

where n takes odd values only and $a_n=Dn^2\pi^2/l^2$. It can easily be shown that the solution satisfies the statement of the problem and boundary conditions. Carslaw[10,11] obtained the corresponding solution for a similar problem in heat conduction by a different method.

Figure 4 presents a plot of θ *versus* X computed from Eq. (30). The values for D, l, and θ_0 are the same as in Case I, while k_2 has been chosen so that the amount of gaseous product present in the film after the steady state has been reached is approximately the same as for Case I. A comparison of Fig. 4 with Fig. 2 shows that more product is present in the film after 1000 seconds in Case I than after 10 000 seconds in Case II. The exponential term in Eq. (30) becomes infinite as $t\to\infty$ when $k_2>D\pi^2/l^2$, preventing a steady state from being reached under these conditions. This is in contrast to Case I, where a steady state occurs regardless of the relative values of k_1, D, and l.

Integration of $k_2\theta(X,t)$ over X from 0 to l and over t from 0 to t gives the total amount of gas formed after time t as

$$\frac{8k_2\theta_0 lt}{\pi^2}\sum_{n=1,3,5}^{\infty}\frac{1}{n^2}\left(\frac{a_n}{a_n-k_2}\right)+\frac{8k_2\theta_0 l}{\pi^2}\times\sum_{n=1,3,5}^{\infty}\frac{1}{n^2}\left[\frac{k_2}{(a_n-k_2)^2}\right][\exp\{-(a_n-k_2)t\}-1].$$

By integrating $\theta(X,t)$ from $X=0$ to $X=l$ the total amount of gas present in the film at any instant is shown to be

$$\frac{8\theta_0 l}{\pi^2}\sum_{n=1,3,5}^{\infty}\frac{1}{n^2}\left[\frac{a_n}{a_n-k_2}-\left(\frac{k_2}{a_n-k_2}\right)\exp\{-(a_n-k_2)t\}\right].$$

The total amount of gas W diffused from the film after time t is obtained by subtracting the amount present in the film from the sum of the total amount formed and the amount originally present:

$$W=\frac{8\theta_0 l(k_2t-1)}{\pi^2}\sum_{n=1,3,5}^{\infty}\frac{1}{n^2}\left(\frac{a_n}{a_n-k_2}\right)+\frac{8\theta_0 l}{\pi^2}\times\sum_{n=1,3,5}^{\infty}\frac{1}{n^2}\left(\frac{k_2}{a_n-k_2}\right)\exp\{-(a_n-k_2)t\}+\frac{8k_2\theta_0 l}{\pi^2}\sum_{n=1,3,5}^{\infty}\frac{1}{n^2}\left[\frac{k_2}{(a_n-k_2)^2}\right]\times[\exp\{-(a_n-k_2)t\}-1]+\theta_0 l. \quad (31)$$

As t approaches infinity the W function approaches asymptotically to the line,

$$W=\frac{8\theta_0 l(k_2t-1)}{\pi^2}\sum_{n=1,3,5}^{\infty}\frac{1}{n^2}\left(\frac{a_n}{a_n-k_2}\right)-\frac{8k_2\theta_0 l}{\pi^2}\sum_{n=1,3,5}^{\infty}\frac{1}{n^2}\left[\frac{k_2}{(a_n-k_2)^2}\right]+\theta_0 l. \quad (32)$$

Dividing the slope of this line by the rate of light absorption gives an expression for the quantum yield of product diffusion from the film in the steady state:

$$\Phi=\frac{8k_2\theta_0}{\pi^2 I_a}\sum_{n=1,3,5}^{\infty}\frac{1}{n^2}\left[\frac{1}{1-\dfrac{k_2l^2}{Dn^2\pi^2}}\right]. \quad (33)$$

Here Φ is an increasing function of θ_0, I_a, and l, and a decreasing function of D. This behavior contrasts with Case I above where Φ was independent of all of these quantities.

The diffusion coefficient is a function of the temperature, in general obeying a relationship[9] of the type

$$D=D_0\exp\left\{-\frac{E}{RT}\right\}, \quad (34)$$

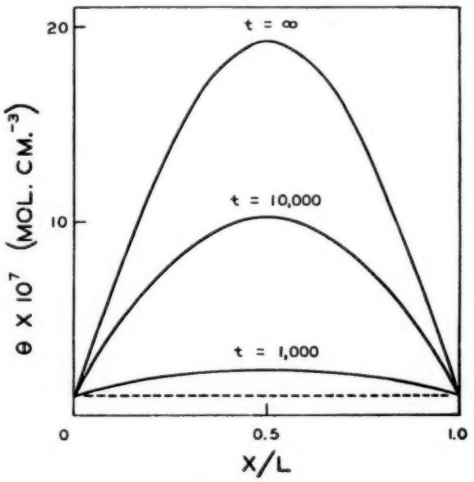

FIG. 4. Case II, θ *versus* X/l; with $k_2=1.0\times10^{-3}$ sec^{-1}, $D=1.0\times10^{-6}$ cm^2 sec^{-1}, $l=9.6\times10^{-2}$ cm, $\theta_0=1.0\times10^{-7}$ mole cm^{-3}, and values of t indicated in sec.

[10] H. S. Carslaw, *Mathematical Theory of the Conduction of Heat in Solids* (Macmillan and Company, London, 1921), second edition, p. 69.

[11] Goodlet, Edwards, and Perry, J. Inst. Elec. Engrs. **69**, 695 (1930).

where E is the energy of activation of diffusion, R the gas constant, T the absolute temperature, and D_0 the proportionality constant. As an illustration of the effect of temperature variation suppose D is known to be 8.0×10^{-6} cm^2 sec^{-1} at 50°C, E is 10 kcal, and the other quantities have the values assigned to them in Fig. 4. Then the quantum yield will approach infinity at about 10°C as shown in Fig. 5, provided that the energy of activation of the fundamental photochemical reaction is zero as usual. Under such conditions the reaction will present the superficial appearance of having a negative energy of activation. Figure 5 also illustrates the effect of a variation in k_2.

CASE III. RATE INDEPENDENT OF GASEOUS REACTANT CONCENTRATION

Consider now a reactive external gas that diffuses into the film and is consumed by a photochemical reaction with the film when irradiation starts. The arrangement of the film and other conditions are the same as described above in Case I. The reactive gas is present in the film initially at a certain concentration θ_1 in equilibrium with its pressure external to the film. As in Case I the external pressure and hence the surface concentration is maintained constant throughout the irradiation.

The equation for the problem is

$$\theta_t(X,t)=D\theta_{XX}(X,t)-k_3, \quad (0<X<l, t>0), \quad (35)$$

where k_3 is the rate of reactive gas consumption by reaction with the film in any infinitesimal volume. By analogy with the previous cases k_3 is taken proportional to I_a. The boundary conditions are

$$\theta(X,0)=\theta_1, \quad (t=0, 0<X<l), \quad (36)$$

$$\theta(0,t)=\theta_1, \quad \theta(l,t)=\theta_1, \quad (t>0). \quad (37)$$

The problem in the transform is

$$s^2u(X,s)-s\theta_1=sDu_{XX}(X,s)-k_3, \quad (38)$$

$$su(0,s)=\theta_1, \quad su(l,s)=\theta_1. \quad (39)$$

The general solution that satisfies (38) and (39) is

$$u(X,s)=\frac{\theta_1}{s}-\frac{k_3}{s^2}+\left(\frac{k_3}{s^2}\right)\times\left[\frac{\sinh X(s/D)^{\frac{1}{2}}+\sinh(l-X)(s/D)^{\frac{1}{2}}}{\sinh l(s/D)^{\frac{1}{2}}}\right]. \quad (40)$$

This function has poles at $s=0$ and at $s=-Dn^2\pi^2/l^2$, with n taking integral values from one to infinity. Computation of the residues at the poles followed by application of the inversion theorem yields the solution of the original problem,

$$\theta(X,t)=\theta_1+\frac{k_3(X^2-Xl)}{2D}+\frac{4k_3l^2}{\pi^3D}\times\sum_{n=1,3,5}^{\infty}\frac{1}{n^3}\sin\left(\frac{n\pi X}{l}\right)\exp\left\{-\frac{Dn^2\pi^2t}{l^2}\right\}, \quad (41)$$

where n takes odd integral values only. The application of the inversion theorem can be justified as in Case I above. The correctness of the solution can be verified by substitution in the statement of the problem and boundary conditions.

Figure 6 shows a plot of θ *versus* X according to Eq. (41) for selected values of t. For the particular values of the constants used in Fig. 6 it can be seen that complete exhaustion of the reactive gas occurs in the center portion of the film when the steady state is reached. Figure 6 demonstrates that the concentration gradient at the surface of the film can become quite steep in the steady state. Hart and Matheson[4] concluded that the oxygen concentration gradient was probably high at the surface of GR−S or rubber films irradiated in oxygen.

Provided exhaustion does not occur in the center of the film the total amount of gas diffused into the film can be readily calculated. The total amount Q of gas taken up by the film after time t is equal to the sum of the total amount reacted and the amount present in the film at time t less the amount originally present in the film:

$$Q=k_3lt-\frac{k_3l^3}{12D}+\frac{8k_3l^3}{\pi^4D}\sum_{n=1,3,5}^{\infty}\frac{1}{n^4}\exp\left\{-\frac{Dn^2\pi^2t}{l^2}\right\}. \quad (42)$$

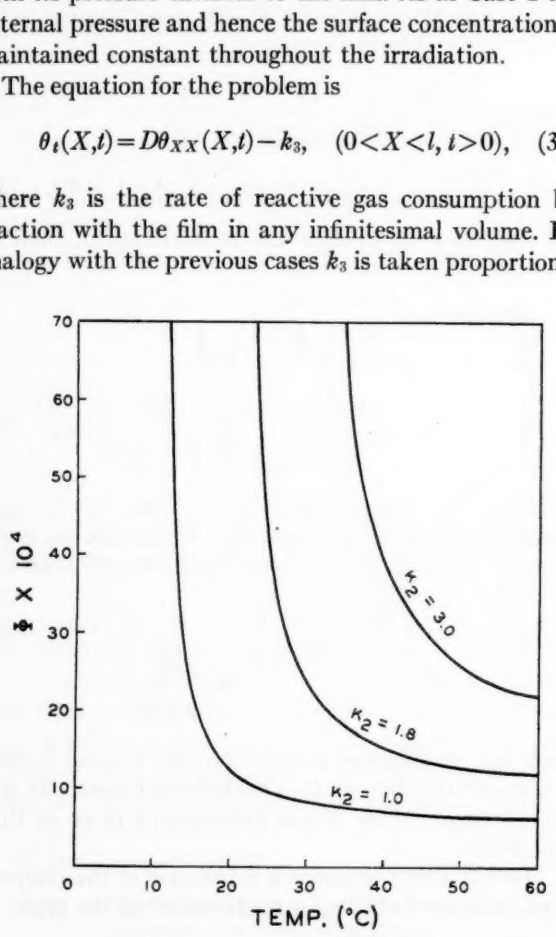

FIG. 5. Case II, Φ *versus* temperature; with $D=8.0\times10^{-6}$ cm^2 sec^{-1} at 50°C, $E=10$ kcal, $l=9.6\times10^{-2}$ cm, $\theta_0=1.0\times10^{-7}$ mole cm^{-3}, and values of $k_2\times10^3$ indicated in sec^{-1}.

For large values of t a steady state is reached and the last term of Eq. (42) becomes neglible. Differentiation with respect to t and division by the rate of light absorption then gives an expression for the quantum yield in the steady state:

$$\Phi=\frac{k_3}{I_a}. \tag{43}$$

The situation is somewhat different when exhaustion of dissolved gas occurs in the center of the film. Under these conditions the θ function intersects the X axis at two points. By setting $\theta=0$ and allowing t to approach infinity in Eq. (41) the values of X at the intersections are found to be

$$X=\frac{k_3l\pm(k_3^2l^2-8k_3D\theta_1)^{\frac{1}{2}}}{2k_3}, \tag{44}$$

while the quantum yield in the steady state becomes

$$\Phi=\frac{k_3l-(k_3^2l^2-8k_3D\theta_1)^{\frac{1}{2}}}{I_al}. \tag{45}$$

An inspection of Eq. (45) shows that an abrupt drop-off in the value of the quantum yield occurs when l becomes greater than $(8D\theta_1/k_3)^{\frac{1}{2}}$. This behavior is illustrated in Fig. 7 for selected values of θ_1. In this connection, Hart and Matheson[4] found that an increase in the film thickness was paralleled by a decrease in the quantum yield of oxygen uptake by rubber films. In their work, however, the decrease in Φ was not definitely assigned to the increase in thickness because a change in the molecular weight distribution of the rubber occurred simultaneously with the thickness increase.

When an intermittent light source is used, with light and dark periods of equal length a, the statement of the problem for Case III becomes

$$\theta_t(X,t)=D\theta_{XX}(X,t)-k_3\sum_{n=0}^{\infty}(-1)^nH(t-na),$$
$$(0<X<l,\ t>0), \tag{46}$$

where $H(t-\alpha)$ is defined as in Case I. The boundary conditions remain the same as in Eqs. (36) and (37). The problem in the transform is

$$su(X,s)-\theta_1=Du_{XX}(X,s)-\frac{k_3}{s(1+e^{-as})}, \tag{47}$$

$$su(0,s)=\theta_1,\quad su(l,s)=\theta_1. \tag{48}$$

Solving the problem in the transform yields

$$u(X,s)=\frac{\theta_1}{s}-\frac{k_3}{s^2(1+e^{-as})}+\frac{k_3}{s^2(1+e^{-as})}$$
$$\times\left[\frac{\sinh X(s/D)^{\frac{1}{2}}+\sinh(l-X)(s/D)^{\frac{1}{2}}}{\sinh l(s/D)^{\frac{1}{2}}}\right]. \tag{49}$$

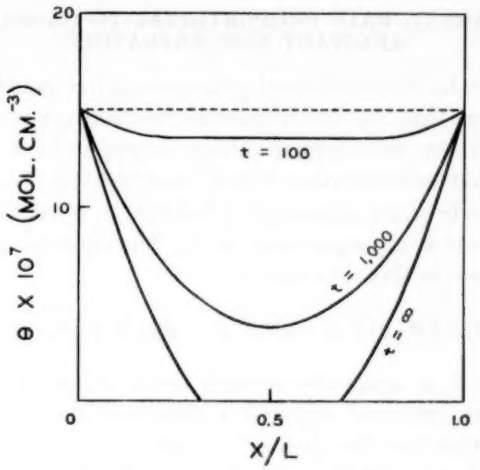

FIG. 6. Case III, θ *versus* X/l; with $k_3=1.5\times10^{-9}$ mole cm^{-3} sec^{-1}, $D=1.0\times10^{-6}$ cm^2 sec^{-1}, $l=9.6\times10^{-2}$ cm, $\theta_1=15\times10^{-7}$ mole cm^{-3}, and values of t indicated in sec.

Application of the inversion theorem to (49) gives the inverse transform:

$$\theta(X,t)=\theta_1+k_3\left[\frac{X^2-Xl}{2D}+\frac{4l^2}{\pi^3D}\right.$$
$$\times\sum_{n=1,3,5}^{\infty}\frac{1}{n^3}\sin\frac{n\pi X}{l}\exp\left\{-\frac{Dn^2\pi^2t}{l^2}\right\}$$
$$+\sum_{n=0}^{\infty}(-1)^n\left(\frac{X^2-Xl}{2D}+\frac{4l^2}{\pi^3D}\sum_{m=1,3,5}^{\infty}\frac{1}{m^3}\sin\frac{m\pi X}{l}\right.$$
$$\left.\left.\times\exp\left\{-\frac{Dm^2\pi^2(t-na)}{l^2}\right\}\right)H(t-na)\right]. \tag{50}$$

This is the solution of Eq. (46) that satisfies the boundary conditions.

At the center of the film for large values of t the concentration function closely approximates

$$\theta_c=\theta_1-k_3\left[\frac{l^2}{8D}+\sum_{n=0}^{\infty}(-1)^nH(t-na)\left(\frac{l^2}{8D}-\frac{4l^2}{\pi^3D}\right.\right.$$
$$\times\sum_{m=1,3,5}^{\infty}\frac{1}{m^3}(-1)^{(m-1)/2}$$
$$\left.\left.\times\exp\left\{-\frac{Dm^2\pi^2(t-na)}{l^2}\right\}\right)\right]. \tag{51}$$

A plot of this function would be similar to that of Fig. 3, but inverted. This would hold true provided the initial concentration θ_1 was large enough to prevent exhaustion from occurring in the center of the film. Under the same conditions the quantum yield of gas uptake would average (k_3/I_a) mole quantum^{-1} over an equal number of light and dark periods, while the rate would average $(k_3l/2)$ mole cm^{-2} sec^{-1}.

CASE IV. RATE PROPORTIONAL TO GASEOUS REACTANT CONCENTRATION

Now let the conditions be the same as in Case III, but suppose that the rate of gaseous reactant consumption within any infinitesimal volume is proportional to the reactant concentration within that volume. Thus the local rate of gas consumption is $k_4\theta(X,t)$, where the rate constant k_4 is proportional to I_a. The equation for the problem in this situation is

$$\theta_t(X,t)=D\theta_{XX}(X,t)-k_4\theta(X,t), \quad (0<X<l,\ t>0), \quad (52)$$

where θ_1 is again the uniform initial concentration of gaseous reactant within the film and the boundary conditions are the same as in Case III.

In terms of the transform the problem is

$$(s+k_4)u(X,s)-\theta_1=Du_{XX}(X,s), \quad (53)$$

$$su(0,s)=\theta_1, \quad su(l,s)=\theta_1. \quad (54)$$

Solving for $u(X,s)$,

$$u(X,s)=\frac{\theta_1}{s+k_4}+\frac{\theta_1 k_4}{s(s+k_4)} \times\left[\frac{\sinh X\left(\frac{s+k_4}{D}\right)^{\frac{1}{2}}+\sinh(l-X)\left(\frac{s+k_4}{D}\right)^{\frac{1}{2}}}{\sinh l\left(\frac{s+k_4}{D}\right)^{\frac{1}{2}}}\right]. \quad (55)$$

The solution to the original problem is readily obtained by computation of the residues of (55) followed by the application of the inversion theorem:

$$\theta(X,t)=\theta_1\left[\frac{\sinh X\left(\frac{k_4}{D}\right)^{\frac{1}{2}}+\sinh(l-X)\left(\frac{k_4}{D}\right)^{\frac{1}{2}}}{\sinh l\left(\frac{k_4}{D}\right)^{\frac{1}{2}}}\right] + \sum_{n=1,3,5}^{\infty}\frac{4\theta_1 k_4 \sin\frac{n\pi X}{l}}{\frac{Dn^3\pi^3}{l^2}-n\pi k_4}\exp\left\{-k_4 t-\frac{Dn^2\pi^2 t}{l^2}\right\}. \quad (56)$$

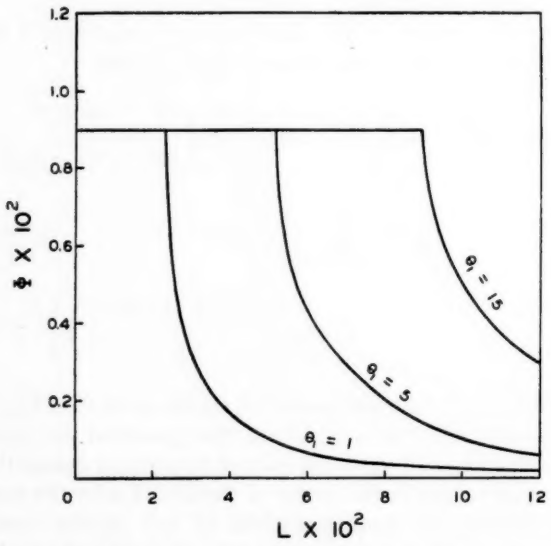

FIG. 7. Case III, Φ *versus* l; with $k_3=1.5\times10^{-9}$ mole cm^{-3} sec^{-1}, $I_a=1.0\times10^{-17}$ quanta sec^{-1} cm^{-3}, $D=1.0\times10^{-6}$ cm^2 sec^{-1}, and values of $\theta_1\times10^7$ indicated in mole cm^{-3}.

The solution can also be written in the form,

$$\theta(X,t)=\frac{4\theta_1}{\pi}\sum_{n=1,3,5}^{\infty}\frac{1}{n}\left[\left(\frac{a_n}{a_n+k_4}\right)+\left(\frac{k_4}{a_n+k_4}\right)\times\exp\{-(a_n+k_4)t\}\right]\sin\frac{n\pi X}{l}, \quad (57)$$

where $a_n=(Dn^2\pi^2)/l^2$ as before. This solution can be verified by substitution in Eq. (52) and the boundary conditions.

Because the exponent in (57) is negative, a steady state is always reached, regardless of the relative values of k_4, D, and l. It is also seen that for large values of t the second term vanishes and the first term remains greater than zero for all values of X. Thus the concentration of dissolved gas at the center of the film cannot fall to zero in the steady state.

The total amount of gas reacted with the film after time t can be calculated by integrating $k_4\theta(X,t)$ over X from 0 to l and then over t from 0 to t, and is equal to

$$\frac{8k_4\theta_1 lt}{\pi^2}\sum_{n=1,3,5}^{\infty}\frac{1}{n^2}\left(\frac{a_n}{a_n+k_4}\right)-\frac{8k_4\theta_1 l}{\pi^2} \times\sum_{n=1,3,5}^{\infty}\frac{1}{n^2}\left[\frac{k_4}{(a_n+k_4)^2}\right]\left[\exp\{-(a_n+k_4)t\}-1\right].$$

By integrating $\theta(X,t)$ from $X=0$ to $X=l$ the total amount of gas present in the film at any instant is shown to be

$$\frac{8\theta_1 l}{\pi^2}\sum_{n=1,3,5}^{\infty}\frac{1}{n^2}\left[\frac{a_n}{a_n+k_4}+\left(\frac{k_4}{a_n+k_4}\right)\exp\{-(a_n+k_4)t\}\right].$$

Now the total amount of reactive gas Q taken up by one square centimeter of film after time t is equal to the sum of the total amount reacted and the amount present in the film at time t less the amount originally present in

the film:

$$Q=\frac{8k_4\theta_1 lt}{\pi^2}\sum_{n=1,3,5}^{\infty}\frac{1}{n^2}\left(\frac{a_n}{a_n+k_4}\right)-\frac{8k_4\theta_1 l}{\pi^2}$$
$$\times\sum_{n=1,3,5}^{\infty}\frac{1}{n^2}\left[\frac{k_4}{(a_n+k_4)^2}\right]\left[\exp\{-(a_n+k_4)t\}-1\right]$$
$$+\frac{8\theta_1 l}{\pi^2}\sum_{n=1,3,5}^{\infty}\frac{1}{n^2}\left[\left(\frac{a_n}{a_n+k_4}\right)+\left(\frac{k_4}{a_n+k_4}\right)\right.$$
$$\left.\times\exp\{-(a_n+k_4)t\}\right]-\theta_1 l. \quad (58)$$

As t approaches infinity the curve of Q *versus* t approaches asymptotically to the line

$$Q=(k_4t+1)\frac{8\theta_1 l}{\pi^2}\sum_{n=1,3,5}^{\infty}\frac{1}{n^2}\left(\frac{a_n}{a_n+k_4}\right)$$
$$+\frac{8k_4\theta_1 l}{\pi^2}\sum_{n=1,3,5}^{\infty}\frac{1}{n^2}\left[\frac{k_4}{(a_n+k_4)^2}\right]-\theta_1 l. \quad (59)$$

The quantum yield in the steady state can be computed by differentiating Eq. (59) with respect to t and dividing by the rate of light absorption:

$$\Phi=\frac{8k_4\theta_1}{\pi^2 I_a}\sum_{n=1,3,5}^{\infty}\frac{1}{n^2}\left[\frac{1}{1+\dfrac{k_4 l^2}{Dn^2\pi^2}}\right]. \quad (60)$$

As $I_a l$ approaches zero, or as D approaches infinity, the quantum yield approaches an upper limiting value of $(k_4\theta_1)/I_a$.

If intermittent light is used the statement of the problem corresponding to Eq. (52) contains the term $k_4(t)\theta(X,t)$, denoting that k_4 is a function of t. In this case the application of the Laplace transformation does not lead to the solution of the problem. In general the present technique is not applicable when the partial differential equation of the problem is nonlinear, or when the coefficients appearing in the equation are functions of t.

Letters to the Editor

THIS section will accept reports of new work, provided these are terse and contain few figures, and especially few half-tone cuts. The Editorial Board will not hold itself responsible for opinions expressed by the correspondents. Contributions to this section should not exceed 600 words in length and must reach the office of the Editor not later than the 15th of the second month preceding that of the issue in which the Letter is to appear. No proof will be sent to the authors. A publication charge of $10.00 per Letter is made which, when honored, will entitle the Institution to 100 free reprints.

Residual Entropy of the Polar Structure of Ice

WILLIAM N. LIPSCOMB
School of Chemistry, University of Minnesota, Minneapolis 14, Minnesota
(Received August 14, 1953)

RUNDLE[1] has proposed two types of disorder in a treatment of the residual entropy of polar ice. The number of configurations that yield H_2O molecules contributes $S_1=(R/2)\ln(9/8)=0.11$ eu, while the "rocking" disorder associated with the two ways of placing one H_2O, with bond angle $104\frac{1}{2}°$, into a tetrahedral angle contributes $S_2=R/2\ln 2$. Correction of his value of S_1 and a discussion of S_2 are presented here.

Let us consider first the "configurational" term S_1. Assume that one-fourth of the hydrogens have been placed along the c axis of the hexagonal unit, so that we now have equal numbers of OH^- and O^{-2} and that the only disorder which remains is confined to the infinite puckered sheets perpendicular to c. Now placement of an additional H^+ on the OH^- and the $2H^+$ on the O^{-2} to which this H^+ points is exactly the problem of placement of a double bond in an infinite layer of graphite. Hence, the number of configurations is the same as the number of resonance structures for graphite. Now choose a hexagonal cell (Fig. 1) in a layer. There

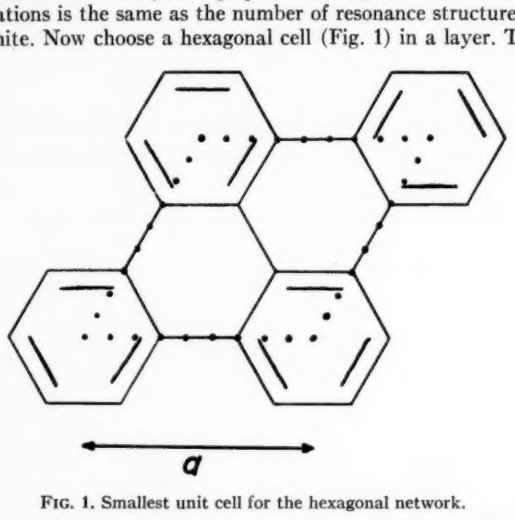

FIG. 1. Smallest unit cell for the hexagonal network.

are two possible configurations, all mutually independent for each ring at each origin. Thus, $W_1=2^{N/6}$, and $S_1=(1/6)R\ln 2=0.23$ eu for this choice. A better approximation is obtained by placement of coronene-type of units (20 configurations) at each origin of a correspondingly larger hexagonal unit cell containing 24 atoms. Then, $S_1=(1/24)R\ln 20=0.25$ eu. Continuation of this procedure to still larger unit cells, with the help of a formula established by Woodger[2] leads to rapid convergence to $S_1=0.26$ eu for very large units.

A different argument leads to very nearly this same result. Locate "independent" atoms, such that the choice of one of the three configurations about each is independent of all others, and yet any randomness which remains contributes little to the residual entropy. A suitable choice is atoms at the points of a hexagonal lattice with $a'=2a/\sqrt{3}$, at 30° with respect to a in Fig. 1. The resulting value of $S=(1/8)R\ln 3=0.27$ eu is close to the correct result.

Now if we assume the additional "rocking" disorder, the residual entropies of both polar ice and nonpolar ice are significantly greater than the observed value[3] of 0.82 eu. There are thus thermodynamic reasons for not requiring this additional disorder. In addition, the difference of energy between that of the two disordered positions and that of the intermediate position seems likely, on simple electrostatic grounds, to be smaller than that of an expected zero-point torsional oscillation. Finally, these electrostatic calculations, based on central forces, indicate that the intermediate position is the more stable one.

Thus, the measured residual entropy is in agreement with that of the nonpolar form of ice, and in disagreement with the polar form. However, other physical properties than the entropy may be much more sensitive to the occurrence of an intermediate form of ice, and the suggestion of the polar structure remains interesting.

Support of this work by the U. S. Office of Naval Research is gratefully acknowledged.

[1] R. E. Rundle, J. Chem. Phys. **21**, 1311 (1953).
[2] M. Gordon and W. H. T. Davison, J. Chem. Phys. **24**, 428 (1952).
[3] W. F. Giauque and J. W. Stout, J. Am. Chem. Soc. **58**, 1144 (1936).

Polar *Versus* Nonpolar Ice

R. E. RUNDLE
Institute for Atomic Research and Department of Physics, Iowa State College, Ames, Iowa
(Received September 18, 1953)

LIPSCOMB has kindly informed me, prior to publication,[1] of his discovery of my mistake in calculating the configurational part of the entropy for polar ice.[2] With corrected values polar ice has an entropy of 0.95 eu *versus* 0.82 eu observed. It would seem hard to maintain that this lack of agreement eliminates the polar structure, since it is often found that possible disorders are not completely frozen in.

Indeed, since the configurational contribution to the residual entropy of polar ice is now somewhat too high, it seems well to point out that in my previous paper I ignored restrictions due to dipole interactions, as Bjerrum would insist upon,[3] except where these led to a net crystal dipole. Strict application of these restrictions would tie layers together along C_0 by Bjerrum's "inverse mirror symmetric" configuration, eliminating all configurational contribution to the entropy. Hence, if Bjerrum's arguments are important but not fully realized, the residual entropy of this model for polar ice will lie between 0.69 and 0.95 eu.

The serious objection to the nonpolar ice structure is the weight of crystallographic evidence that ice is polar.[4] If this evidence is accepted, there is a pressing reason for attempting to find a new source of residual entropy in ice.

A serious objection to the "rocking" disorder which I suggested has been rasied by Lawrence Bartell, who noted that a large barrier would be required to restrict water molecules to one of the two extreme positions in the rocking motion. This is impossible, but a similar residual entropy would be found if the lowest-energy state for torsional vibration were substantially doubly degenerate. It appears that a barrier of reasonable height will suffice to produce degeneracy, but only if it is an extremely sharp barrier in a broad potential well. This is physically unreasonable. Variations can be suggested to try to save the model, but it seems best to say that if ice is polar the entropy is not yet understood.

Certain aspects of the proposed polar model seem worth saving, nonetheless, particularly the preferred orientation of one-fourth the O—H bonds directly along the c axis (and O—O direction), *versus* O—H bonds slightly off O—O directions in other cases. This is attractive in explaining the c/a ratio, its change with temperature, and the doublet in the O—H stretching frequency of ice.

In addition to Dr. Bartell I am indebted to Dr. Robert S. Hansen and Mr. James Richardson for lengthy discussions concerning this problem.

[1] W. N. Lipscomb, J. Chem. Phys. **21**, 344 (1954).
[2] R. E. Rundle, J. Chem. Phys. **21**, 1311 (1953).
[3] N. Bjerrum, Science **115**, 385 (1952).
[4] See, especially, F. Rossmann, Experientia **6**, 182 (1950).

Intensities of the Infrared Bands of Carbon Suboxide

R. L. WILLIAMS*
Department of Chemistry and Chemical Engineering, University of California, Berkeley, California
(Received November 30, 1953)

DURING a recent investigation of the infrared and Raman spectra of carbon suboxide,[1] it was found that the ν_3 fundamental band was extremely strong in absorption. The intensities of both the Σ_u^+ fundamentals have, therefore, now been measured in order to determine the values of $\partial\mu/\partial r_{CO}$ and $\partial\mu/\partial r_{CC}$, the variation of the bond dipole moments with bond length, for the CO and CC bonds, respectively.

The sample of carbon suboxide, prepared by dehydration of malonic acid with phosphorous pentoxide, was the same as was used for the earlier infrared and Raman measurements and was better than 98 percent pure by mass spectrometric analysis. The absolute band intensity was determined on a Perkin-Elmer 12C spectrometer by the extrapolation method of Wilson and Wells,[2] dry air, free from carbon dioxide, being admitted up to one atmosphere to broaden any fine structure.

The extrapolated integrated absorption area B_0, for the ν_3 fundamental, lying at 2264 cm^{-1}, was found to be $29\,300\times10^{10}$ cy/cm atmos at NTP, while the area for the ν_4 fundamental, which absorbs at 1575 cm^{-1}, was 442×10^{10} cy/cm atmos. From these values and the equation $\partial\mu/\partial Q_i=\pm(3cB_0^{\frac{1}{2}}/N\pi)^{\frac{1}{2}}$, where N is the number of molecules per cc, c is the velocity of light, and Q_i the normal coordinate of the ith vibration, it follows that $\partial\mu/\partial Q_3=\pm558.4$ and $\partial\mu/\partial Q_4=\pm68.6$ cgs units. If, however, there is Fermi resonance between ν_4 and the neighboring level at 1665 cm^{-1}, which is assigned tentatively as $\nu_2+\nu_5+\nu_7$ (calculated = 1610 cm^{-1}), the whole of the intensity of this latter band, $B_0=110\times10^{10}$ cy/cm atmos, should be added to that of ν_4. In this case, $\partial\mu/\partial Q_4$ becomes ±76.7

The values of $\partial\mu/\partial R_k$ can now be found from the equation $\partial\mu/\partial R_k=\Sigma_i L_{ik}^{-1}(\partial\mu/\partial Q_i)$, where L_{ik}^{-1} are the matrix coefficients of the transformation $Q=L^{-1}R$, and R_k is the symmetry coordinate. Taking the following force constants: $f_{CO}=15.5$, $f_{CC}=12.15$, $f_{CO,CC}=1.3$, and $f_{CC,CC}=2.4\times10^5$ dynes/cm, respectively, and the interatomic distances suggested by Mackle and Sutton,[3] *viz.*, $r_{CO}=1.19$A, $r_{CC}=1.28$A, the coefficients L_{33}^{-1}, L_{34}^{-1}, L_{43}^{-1}, and L_{44}^{-1} are found to be -1.827, 1.643, 3.276, and 2.348×10^{-12}. Substitution for these values gives

$$\partial\mu/\partial R_3=\pm12.45\times10^{-10},\quad \partial\mu/\partial R_4=\mp7.56\times10^{-10},$$

or

$$\partial\mu/\partial R_3=\pm7.95\times10^{-10},\quad \partial\mu/\partial R_4=\mp10.78\times10^{-10}.$$

Since $R_3=2^{-\frac{1}{2}}(\Delta r'_{CO}-\Delta r''_{CO})$ and $R_4=2^{-\frac{1}{2}}(\Delta r'_{CC}-\Delta r''_{CC})$, it follows that $\partial\mu_{CO}/\partial r_{CO}=2^{-\frac{1}{2}}\cdot\partial\mu/\partial R_3$ and $\partial\mu_{CC}/\partial r_{CC}=2^{-\frac{1}{2}}\cdot\partial\mu/\partial R_4$, so that $\partial\mu_{CO}/\partial r_{CO}=\pm8.80\times10^{-10}$ and $\partial\mu_{CC}/\partial r_{CC}=\mp5.34\times10^{-10}$, or $\partial\mu_{CO}/\partial r_{CO}=\pm5.62\times10^{-10}$ and $\partial\mu_{CC}/\partial r_{CC}=\mp7.62\times10^{-10}$ cgs units. Changes in magnitude of about 3 percent occur, if the effect of $\nu_2+\nu_5+\nu_7$ is taken into account. Comparison of these values with those for other carbonyl linkages[4] suggests that either value is possible, but that the first set is preferable, since it is unlikely that the value for the carbonyl link would be smaller than that for the ethylenic link. Measurements are now in progress on the intensity of the π_u vibrations.

I should like to thank the committee for Pressed Steel Company (Oxford) Fellowships for an award, during the tenure of which this work was partly carried out, and also Dr. H. W. Thompson for facilities in the Physical Chemistry Laboratory, Oxford. I acknowledge also several helpful discussions with Dr. D. C. McKean.

* Commonwealth Fund Fellow, 1953
[1] Long, Williams, and Murfin, Proc. Roy. Soc. (London) (to be published).
[2] E. B. Wilson and A. J. Wells, J. Chem. Phys. **14**, 578 (1946).
[3] H. Mackle and L. E. Sutton, Trans. Faraday Soc. **47**, 937 (1951).
[4] Callomon, McKean, and Thompson, Proc. Roy. Soc. (London) **A208**, 341 (1951).

The Dissociation Energy of Fluorine

R. T. SANDERSON
Department of Chemistry, State University of Iowa, Iowa City, Iowa
(Received December 8, 1953)

RECENT studies seem to favor a value of about 37 kcal/mole for the heat of the reaction,

$$F_2(g)\rightleftharpoons 2F(g).$$

This order of magnitude is indicated by a variety of experimental approaches,[1–11] both indirect and direct, some of which have been very carefully executed. However, the value seems chemically anomalous and deserves very critical study. In particular, the intense reactivity of fluorine, especially at high temperatures, makes experimental work of adequate precision extremely difficult. It is imperative that the nature of the reaction and of the possible products of apparatus corrosion be taken very thoroughly into account. For example, the use of nickel must involve not only a knowledge of the rate of fluorination of the nickel but also of the nature of the product. No exact vapor tension data on NiF_2 appear to be available, but it has been reported[12] that NiF_2 sublimes, without melting, at about 1000°. This sublimation was observed not in a vacuum but in an atmosphere of HF. This could easily mean that NiF_2 has an appreciable vapor tension at temperatures where increase in pressure or thermal conductivity or other change has appeared to indicate dissociation of fluorine. Other complications may also exist. This may not be the case, but unless contrary experimental evidence is obtained, no measurements of fluorine at high temperatures in nickel can be unambiguously interpreted. The same is probably true of all other possible materials of apparatus construction.

The dissociation energies of diatomic gas molecules of elements of the different groups appear to be related in a similar way to the principal quantum number of the valence level, as shown in Fig. 1.

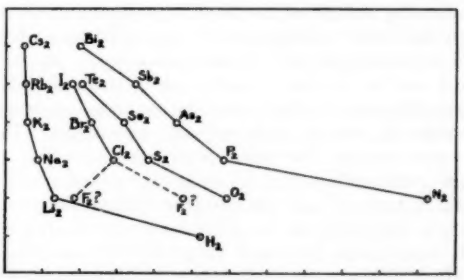

FIG. 1. Relation of dissociation energy to principal quantum level of valence electrons.

The anomalous position of the low value for F_2 is striking. In general, one would expect the dissociation energies of molecules of similar elements to be similarly related to such fundamental properties as internuclear distance, polarizability, ionization energy, and electronegativity. This is true of I_2, Br_2, and Cl_2, but the low value of F_2 is wholly out of line. In fact, no hitherto proposed value for F_2 fits smoothly with the values for the other halogens. Extrapolation is not necessarily justifiable, and in the halogens must be too far extended to be precise, but it is very interesting that a value of about 95 kcal/mole seems very satisfactory. This holds for graphical plots of the dissociation energies of the halogens *versus* many other fundamental properties, as illustrated in Fig. 2. Furthermore, a value of 95 leads to 165 kcal/

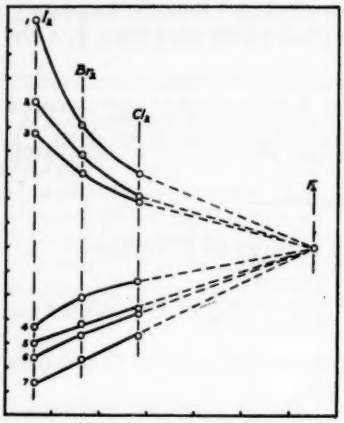

FIG. 2. Dissociation energies *versus* other properties of halogens. [(1) polarizability, (2) melting point, (3) critical temperature, (4) electronegativity, (5) ionization potential, (6) reciprocal of internuclear distance, (7) dissociation energy of HX.]

mole for the heat of dissociation of gaseous HF. This value is found similarly to fit smoothly in plots of the dissociation energies of the hydrogen halides *versus* other properties.

Proponents of the low value for the dissociation energy of fluorine will therefore not be wholly convincing until they can (1) produce completely certain experimental evidence, and (2) explain why this alone of the properties of fluorine seems wholly inconsistent with those of the other halogens.

[1] R. L. Potter, J. Chem. Phys. **17**, 957 (1949).
[2] A. D. Caunt and R. F. Barrow, Trans. Faraday Soc. **46**, 154 (1950).
[3] A. Eucken and E. Wicke, Naturwiss. **37**, 233 (1950).
[4] Evans, Warhurst, and Whittle, J. Chem. Soc., 1524 (1950).
[5] M. W. Nathans, J. Chem. Phys. **18**, 1122 (1950).
[6] H. J. Schumacher, Anales asoc. quím. argentina **38**, 113 (1950).
[7] R. N. Doescher, J. Chem. Phys. **20**, 330 (1952).
[8] E. Wicke, J. Phys. Chem. **56**, 358 (1952).
[9] H. Wise, J. Chem. Phys. **20**, 927 (1952).
[10] Natl. Bur. Standards (U.S.), Cir. 500 (1952).
[11] P. W. Gilles and J. L. Margrave, J. Chem. Phys. **21**, 381 (1953).
[12] C. Poulenc, Ann. chim. et phys. **2**, 41 (1894).

A Quantum-Mechanical Study of the Fluorine Molecule

HANS DINGER AND INGA FISCHER-HJALMARS
Institute of Theoretical Physics, University of Stockholm, Stockholm, Sweden

(Received November 23, 1953)

THE binding energy of the fluorine molecule in the ground state has been computed in an approximation where only two electrons are considered. In order to simplify the computational work and to be able to make use of the available tables of molecular integrals, we have used the common, analytical form of the atomic $2p$ orbitals with only one exponential. The two-electron wave function has been constructed according to both the valence bond method and the molecular orbital method. The interatomic distance R and the effective nuclear charge 2μ have been chosen as parameters to be determined by a variation method. μ has only been varied for one R value, $R=2.68$ au (the experimental value). The μ value appropriate to this distance has been used throughout the computation of the potential energy curve. The numerical results are collected in Table I.

TABLE I. Effective nuclear charge 2μ, equilibrium distance R, and binding energy D for F_2 as a two-electron problem.

Method	2μ	R au	D au	D kcal/mole
Valence bond	1.98	2.46	0.097	60
Molecular orbital	1.56	2.68	0.043	26
Experimental	···	2.68[a]	0.064–0.072	40–45[b]

[a] D. Andrychuk, Can. J. Phys. **29**, 151 (1951).
[b] E. Wicke, J. Phys. Chem. **56**, 358 (1952).

It is remarkable that the computed values of the effective nuclear charge are less than 2. According to Slater's rules the charge should be 5.2. However, our results are in good agreement with the results obtained by Kopineck[1] in his treatment of the nitrogen molecule as a six-electron problem. These results indicate that screening constants, which have been calculated with explicit allowance for all the electrons of the atom, should not be adopted in less accurate treatments were part of the electrons are considered as point charges coinciding with the nucleus. This conclusion does not seem to be generally recognized, although it can also be justified by general arguments.

A treatment of the fluorine molecule as a ten-electron problem according to the linear combination of atomic orbitals approximation of the molecular orbital method is going on at this institute.

During the course of the present study other calculations of the energy levels of the fluorine molecule have been published.[2,3] As both our treatment of the problem and our results are somewhat different from those of the other authors, a comparison cannot be made without more details of the computational methods. Therefore, the comparison will be postponed to the publication of all details of the present treatment, which will appear elsewhere.

[1] H. J. Kopineck, Z. Naturforsch. **7a**, 22 (1952).
[2] F. Schlögl, Z. Physik **131**, 505 (1952).
[3] C. R. Mueller, J. Chem. Phys. **21**, 1013 (1953).

Nonequivalent Zinc Bonds in Chalcophanite

D. P. CRAIG, *University of Sydney, Sydney, Australia*
AND
A. D. WADSLEY, *Division of Industrial Chemistry, Commonwealth Scientific and Industrial Research Organisation, Melbourne, Australia*

(Received December 11, 1953)

THE crystal structure of the mineral chalcophanite, $ZnMn_3O_7\cdot 3H_2O$, has been described elsewhere by one of us.[1] The properties of the six bonds formed by zinc is the subject of this note. Around each zinc atom are three oxygen ions and three water molecules in a distorted octahedral grouping. The three equal bonds to water are 2.15 ± 0.05A like the Zn−O or Zn−H_2O bonds in the octahedrally coordinated $ZnCO_3$ and $Zn(BrO_3)_2 6H_2O$[2] but make angles of only $83°\pm2°$ with one another. The bonds to oxygen have a mean value of 1.95 ± 0.05A, like those in tetrahedrally coordinated ZnO[3] and make angles of $90°\pm2°$. Other constraints on the oxygen ions (*viz.*, their attachments to Mn), help to fix the angles they subtend at the zinc. One of the more probable hydrogen bond schemes would tend to reduce the H_2O−Zn−H_2O angle, but in this case the O−H−O distance is 2.95A, and the bonds thereby are probably too weak to have caused much reduction in this angle. We consider that the small angles subtended by water, and the differences in Zn−O distances, are properties of the zinc and its immediate neighbors and are not forced on it by other lattice constraints. An interpretation of these features maybe given in the covalent bond model of the sixfold coordination complexes in which the bonds are formed using sp^3d^2 hybrid orbitals of the metal directed to the attached oxygens. Now in general isovalent d hybridization, using, in this case, $4d$ orbits, is more readily evoked by the more electronegative atoms[4] (as in SF_6, PCl_5, SO_2Cl_2, etc.), so that we might expect the d orbitals in the present case to concentrate in the water-directed hybrids at the expense of those directed at the negatively charged and therefore less electronegative oxygen ions. The novel features of the structure may be understood on this basis. The bonds formed by orbitals with more d character are expected to be longer than those with less (compare the differences in the metal −O distances of tetrahedral and octahedral zinc compounds) and they form at angles to one another of less than 90°.[5]

Some years ago Hultgren showed that, according to Pauling's strength criterion, the strongest three spd equivalent bond orbitals may form at angles of 73° with one another and that they use one and two thirds d orbitals, instead of one only as do three right-angled regular octahedral bond hybrids. The bonds to water in chalcophanite fall between these two limits. The remaining three

bond orbitals are left with less than the regular octahedral proportion of d character and so tend to be shorter and to make angles greater than 90°. This latter feature is not manifest in chalcophanite because the disposition of the oxygen ions is governed by other forces as well as those exerted by the zinc.

We believe that this phenomenon of the unequal partition of d orbitals in hybrids directed to nonequivalent atoms, in which the d character is "stolen" by the more electronegative atoms, is fairly common and might occur for example in PF_3Cl_2. The evidence, however, is clearest in cases where all bonds are to be the same kind of atom as in chalcophanite. A theoretical discussion of the effect is to be published elsewhere.

[1] A. D. Wadsley, Acta Cryst. (to be published).
[2] A. F. Wells, *Structural Inorganic Chemistry* (Oxford University Press, London, 1950), p. 388.
[3] W. L. Bragg, Phil. Mag. **39**, 647 (1920).
[4] Craig, Maccoll, Nyholm, Orgel, and Sutton, J. Chem. Soc. (to be published).
[5] R. Hultgren, Phys. Rev. **40**, 891 (1932).

A Structure for Collagen

F. H. C. Crick
Polytechnic Institute of Brooklyn, The Protein Structure Project, Brooklyn 1, New York
(Received December 7, 1953)

THE structure of collagen has recently been reviewed by Bear.[1] Since then Cowan, North, and Randall[2] have presented an improved wide-angle x-ray diffraction photograph,[3] which strongly suggests that the structure is helical. Cohen and Bear[4] have pointed out that the spacings of the higher layer lines also suggest a helix. In spite of these important advances, no satisfactory structure has yet been proposed.

Bear[1] has argued that the bands and interbands of collagen seen in the electron microscope may have different amino acid compositions, and in particular that the more ordered interbands may contain predominantly the shorter amino acids. If this were so, then it would be possible in the interbands to accommodate four residues in every stretch of 2.9A in the fiber direction, instead of the three normally assumed. The model proposed here has been constructed on this basis, and therefore applies only to part of the collagen molecule.

The model consists of two polypeptide chains wound helically round a common axis. The backbones of these chains are related by a diad coinciding with the fiber axis. The asymmetric unit consists of two residues, which will be called A and B.

All the peptide links have the *cis*-configuration. The planes of successive peptide links on either chain are alternately perpendicular and parallel (approximately) to the fiber axis, as shown in Figs. 1 and 2, respectively. The two chains are held together

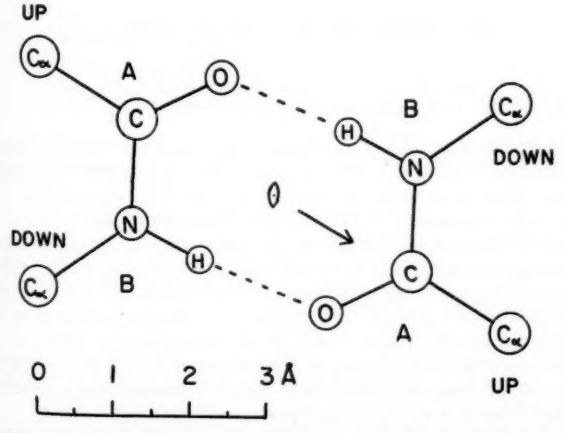

FIG. 1. A *section* of the structure perpendicular to the fiber axis at the plane $z=0$. A and B denote the two types of residue. Hydrogen bonds are shown dotted. DOWN and UP show the general run of the polypeptide chains. The arrow represents the direction of the projection shown in Fig. 2.

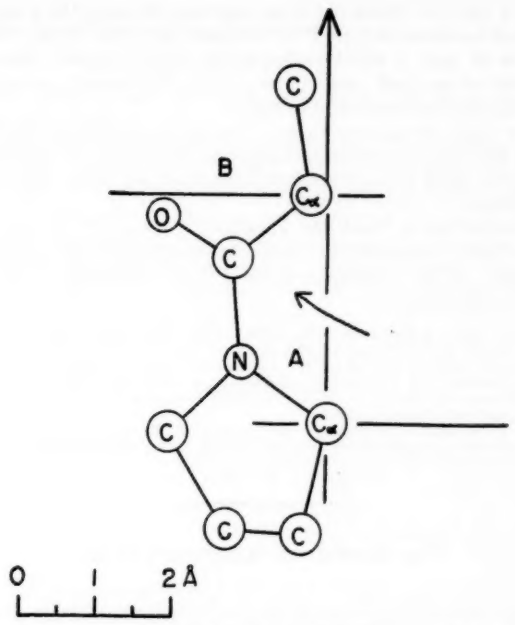

FIG. 2. A *projection* of part of one chain of the structure in the direction shown by the arrow in Fig. 1. The vertical arrow is the fiber axis. The small arrow represents the general run of the helix. The two horizontal lines represent two of the planes of atoms, separated by 2.95A, of the type shown in Fig. 1. The residue of type A has been shown as proline; that of type B as alanine.

by hydrogen bonds perpendicular to the fiber axis, and passing quite close to it (Fig. 1). The pairs of peptide groups thus linked together form sheets of atoms perpendicular to the fiber axis and 2.95A apart, and they therefore contribute strongly to the meridional reflections. These sheets are linked by the other, alternate, peptide groups of the polypeptide chains, as shown in Fig. 2.

There are two distinct structures of this general type.[5] One has a right-handed helix, and has a close van der Waals contact between Cα(B) and N(A). The other has a left-handed helix, and has a close contact between Cα(A) and O(B). The latter accommodates proline more easily, and is the one for which details are given here. The left-handed screw axis of the helix has been given a translation of 2.95A and a rotation of 55°. This represents a slightly extended form of the molecule. The wide-angle x-ray diagram normally observed[1] probably corresponds to a somewhat distorted helix.

Approximate cylindrical coordinates for the structure are given in Table I. They should not be regarded as final. Because of the

TABLE I. Approximate cylindrical coordinates.

Atom	Residue (A)	θ	z (A)
	Residue A		
Cα	3.55	0°	0.0
C	2.05	+ 1.5°	0.0
O	1.65	−36°	0.0
N	4.3	−15°	+0.8
(Cβ)	4.1	− 4.5°	−1.4
(Cγ)	5.4	−14°	−1.35
(Cδ)	5.25	−23°	−0.1
	Residue B		
Cα	3.3	− 4°	+2.95
C	4.3	−17°	+2.15
O	5.2	−24°	+2.7
N	1.9	−14°	+2.95
(Cβ)	3.9	− 6.5°	+4.35

very short van der Waals contacts, several of the angles have been distorted by a few degrees from their most likely values.

The model imposes certain restrictions on the side chains. Residues of type B cannot be proline or hydroxyproline; those of

type *A* may be. There is a close approach between the β carbon atom of a residue of type *B* on one chain and that of the nearest residue of type *A* on the other chain, which suggests that one member of any such pair will be glycine. This would account for the high glycine content of collagen.

The structure appears to be in qualitative agreement with the x-ray data, but in view of its usual features it must be considered tentative until a more careful comparison has been made with experiment.

I should like to thank Dr. Thomas C. Furnas, Jr., for allowing me to study his unpublished monochromatic x-ray photographs of collagen, and my colleagues at the Protein Structure Project for helpful discussion.

[1] R. S. Bear, *Advances in Protein Chemistry* (Academic Press, Inc., New York, 1952), Vol. VII, pp. 69–160.
[2] Cowan, North, and Randall, *The Nature and Structure of Collagen*, editor, Professor J. T. Randall. (Butterworth, London, 1953), p. 241–9.
[3] Obtained by Mr. A. C. T. North under Professor J. T. Randall's direction (personal communication).
[4] C. Cohen and R. S. Bear, J. Am. Chem.Soc. **75**, 2783 (1953).
[5] If the peptide bond of Fig. 2 is twisted far from the planar configuration a third, intermediate type of structure is possible.

Flat Flames of Ammonia in Air

N. W. Luft and L. Cohen
Research Department, Simon-Carves Ltd., Cheadle Heath, Stockport, England
(Received November 30, 1953)

It has been shown[1] that the combustion of lean butane-air mixtures near the lower limit of inflammability can be stabilised sufficiently to produce a flat flame. These flames are luminous surfaces of low curvature the edges of which are bent sharply. With tube burners the edges are turned upwards, in a meniscus-like way. Nozzle burners give "meniscus flames" for very lean mixtures or "button flames" with edges bent downwards. Small changes of the gas flow will cause either blowoff or flashback.

Similar flat flames, and also a whole range of polyhedral flames, have been obtained by burning mixtures of ammonia and oxygen in tube and nozzle burners. The most interesting results, however, are probably those on the combustion of slightly preheated mixtures of ammonia with excess air in tube burners. Homogeneous flame reactions have never been previously observed with ammonia-air mixtures and, indeed, flame propagation in these mixtures has been thought impossible.[2] It is also worth mentioning that these flat flames occur for ammonia-air mixture ratios which are close to stoichiometric. The appearance of the ammonia-air flames differs only slightly from that of butane[1] in that there is a very small peak in the center and the edges are not so sharply upturned.

Fig. 1. Flat ammonia-air flame.

With the flame reproduced in Fig. 1, a tube burner of 1.25 cm internal diameter was used and the mixture containing 19.4 volume percent of ammonia was preheated to 150°C. From the gas-flow rate, 18.6 cm³/sec at N.P.T., and the nearly planar flame area, the burning velocity is calculated as $v_b = 21.3$ cm/sec. Making allowance for large thermocouple radiation losses, the measured temperature is very roughly 1600°C. The calculated flame temperature is about 1810°C, for complete combustion to H_2O, N_2, and excess oxygen, or ~1590°C, with the assumption that all excess oxygen appears as NO, or ~1540°C if 33 percent of the ammonia remains unreacted. Analytically only traces of ammonia could be detected in the combustion products together with about 0.2 percent NO which is approximately equal to the equilibrium concentration of NO for the given conditions.

The observation, that the burning velocities of mixtures of ammonia with excess air are higher than for mixtures with excess ammonia having the same flame temperature, and other results seem to indicate that apart from oxygen atoms[3] and hydrogen atoms, *viz.*, the self-decomposition chain

$$\begin{aligned} NH_3 &\rightarrow NH_2+H, \\ NH_3+H &\rightarrow NH_2+H_2, \\ NH_2+NH_3 &\rightarrow N_2+2H_2+H, \text{ etc.} \end{aligned}$$

OH radicals are especially important for flame propagation, e.g., by

$$\begin{aligned} NH_3+O_2 &\rightarrow NH_2+HO_2, \\ NH_2+O_2 &\rightarrow HNO+OH, \\ OH+NH_3 &\rightarrow H_2O+NH_2, \end{aligned}$$

and

$$\begin{aligned} H_2O &\rightarrow H+OH, \\ NH_3+OH &\rightarrow NH_2+H_2O, \\ NH_2+O_2 &\rightarrow HNO+OH. \end{aligned}$$

This is also in agreement with spectroscopic evidence[4] and supported by recent views[5] on the role of OH radicals in catalytic NH_3 oxidation.

In a plot of log v_b against the inverse of the (calculated) absolute combustion temperature, the foregoing value lies on a fairly smooth curve between the earlier data for ammonia-oxygen flames[2,6] and on catalytic combustion of ammonia-air mixtures[7,8] if in the latter case the poor NO yields (~50 to 10 percent NO between 1000 and 1300°K), obtained at low gas velocities, are attributed mainly to homogeneous combustion of ammonia.

The authors are indebted to the Director of Research and the Management Board, Simon-Carves Ltd., for permission to publish, and to Mr. J. Swindells for assistance with the experimental work. A detailed account of these investigations will be published shortly.

[1] Wohl, Kapp, and Garley, *Third Symposium on Combustion, Flame and Explosion Phenomena* (Williams and Wilkins, Baltimore, 1949), p. 3.
[2] P. Ausloos and A. v. Tiggelen, Bull. soc. chim. Belges. **60**, 433 (1951).
[3] N. Semenoff, Acta Physiochim. U.R.S.S. **9**, 453 (1938).
[4] A. G. Gaydon and H. G. Wolfhard, *Flames* (Chapman and Hall, Ltd., London, 1953).
[5] N. W. Luft, Discussions Faraday Soc. **8**, 302 (1950).
[6] R. C. Murray and A. R. Hall, Trans. Faraday Soc. **47**, 743 (1951).
[7] L. Andrussow, Angew. Chem. **63**, 21, 350 (1951).
[8] L. Andrussow, Bull. soc. chim. France 50 (1951).

The Decomposition of CF_4 in Flames

D. E. Mann, H. P. Broida, and B. E. Squires
National Bureau of Standards, Washington, D. C.
(Received December 9, 1953)

Recent studies of discharges through fluorocarbon vapors have led to the discovery and partial analysis of several band systems ascribed to emission by electronically excited CF and CF_2 molecules.[1–3] The thermal decomposition of CF_4 in a graphite furnace has permitted the observation of the same band systems in absorption.[4] It seemed of interest to us to explore other convenient means for studying the breakdown of CF_4. The admixture of the stream of the vapor of this fluorocarbon in an acetylene-oxygen flame results in a many-banded spectrum in which new bands belonging to the previously found $^2\Sigma-^2\pi$ transition of CF have been identified. The CF_2 bands found in earlier work[1,2,5] do not seem to be present.

Introduction of CF_4 deepens the color of the blue outer cone of the acetylene-oxygen flame and seems to reduce carbon formation. In the inner cone the 1−0, 0−0, 1−1, 0−1, 0−2, and 0−3 bands

of the CF system $A-X$ were observed. The 0−2 and 0−3 bands with heads at 2479 and 2559A were not reported by Andrews and Barrow[1,3] and may have been missed because of overlapping by the CF_2 bands found in the discharge.

The 0−4 and possibly the 0−5 bands also were present in the flame but were obscured by overlapping bands of CS, which were strong in the region between 2494 and 2715A. No evidence was found of the $B-X^2\pi$ system attributed to CF; this is most probably due to the greater intensity of the CO fourth positive system in this region. CCl bands between 2777 and 2790A also were prominent.

The appearance of hydrogen-oxygen flames is markedly changed by the addition of CF_4. The nearly colorless flame becomes blue in appearance with a tinge of red. The spectrum contains several bands due to impurities between 4000 and 9000A. Other than the usual OH bands, no radiation was observed below 3000A with exposures as long as 1½ hours. The spectrum contains several band systems of compounds of copper—CuO, CuCl, and CuF. These bands were fairly intense, showing several vibrational transitions not listed in the compilation of Pearse and Gaydon.[6] The copper as an impurity in the spectra comes from the tip of the brass burner which showed definite signs of erosion after several hours of use with these flames, particularly hydrogen. These spectra were obtained with a medium Hilger (E-2) spectrograph with interchangeable glass and quartz optics. Eastman plates were used of emulsions 103 and I variously sensitized from 2100A to 9000A.

This preliminary study of these spectra has encouraged us to investigate such "mixed" flames, partly in order to search for new bands or spectra, and partly to obtain spectra under higher resolution so that detailed analyses may be made.

[1] Andrews and Barrow, Nature **165**, 890 (1950).
[2] P. Venkateswarlu, Phys. Rev. **77**, 676 (1950).
[3] Andrews and Barrow, Proc. Phys. Soc. (London) **64**, 481 (1951).
[4] J. L. Margrave and K. Wieland, J. Chem. Phys. **21**, 1552 (1953).
[5] Laird, Andrews, and Barrow, Trans. Faraday Soc. **46**, 803 (1950).
[6] Pearse and Gaydon, *The Identification of Molecular Spectra* (Chapman and Hall, Ltd., London, 1950), second edition.

Critical Temperatures of Normal Paraffins

Y. P. Varshni and S. N. Srivastava
Department of Physics, Allahabad University, Allahabad, India
(Received November 30, 1953)

Egloff, Sherman, and Dull[1] have proposed the following formula for the boiling points at 1 atmos of the normal paraffins:

$$T_n = 745.42 \log(n+4.4) - 416.31,$$

where n is the number of carbon atoms. The error in case of methane is rather large (18°), for others it is quite satisfactory.

It is found that the same formula, with different values of the constants can also represent the critical temperatures of the normal paraffins. It can be represented as

$$T\eta = 644.5 \log(n+2) - 75.$$

The observed and the calculated values and the errors are recorded in Table I.

Table I.

No. of C atoms	Paraffin	T_c obs in °K	T_c calc in °K	Errors
1	methane	190.7	232.5	−41.8
2	ethane	305.3	313.1	−7.8
3	propane	368.8	375.5	−6.7
4	butane	426.2	426.6	−0.4
5	pentane	470.4	469.8	+0.6
6	hexane	508	507	+1
7	heptane	540	539.9	+0.1
8	octane	569.4	569.7	−0.3
9	nonane	595.4	596.1	−0.7
10	decane	619.3	620.5	−1.2
11	undecane	642.6	642.8	−0.2
12	dodecane	663.8	663.6	+0.2
13	tridecane	683.2	682.8	+0.4
14	tetradecane	701	699.9	+1.1
15	pentadecane	717.6	717.9	−0.3
16	hexadecane	734.3	733.9	+0.4
17	heptadecane	749.3	749.1	+0.2
18	octadecane	763.2	763.3	−0.1
19	nonadecane	776	776.5	−0.5

The observed and the calculated values and the errors are recorded in Table I.

It will be observed that excepting the first three members, the agreement between the observed and the calculated values is quite good. It is a well-known fact that usually the earlier members of the organic series do not show the regular behavior of the higher members. The error in case of methane is very large, as has been mentioned; similar is the case with Ebloff's boiling point equation.

The authors express their thanks to Dr. K. Banerji and Dr. K. Majumdar for their interest in the work.

[1] Egloff, Sherman, and Dull, J. Phys. Chem. **44**, 730 (1940).

Relation between Vapor Pressure and Viscosity of Liquids

Shashanka Shekhar Mitra
Department of Physics, Allahabad University, Allahabad, India
(Received December 7, 1953)

Both vapor pressure and viscosity of liquids vary considerably with temperature, one increasing and the other decreasing. In the present note a temperature-independent relation between them has been proposed.

If we plot $\log P$ against $\log\eta$, symbols having their usual meanings, roughly a straight line is obtained. The exact relation is, of course, a quadratic equation in $\log\eta$,

$$\log P + n\log\eta = n'(\log\eta)^2 = C, \quad (1)$$

where n, n', and C are characteristic constants for a particular liquid. The validity of the formula is shown by the constancy of C. In its calculation sizable values of P and η were taken, namely, P in mm and $10^3\eta$. For certain nonassociative organic liquids a linear relation exists between $\log P$ and $\log\eta$, *viz.*,

$$\log P + n\log\eta = C. \quad (2)$$

Table I.

Liquids	n	n'
Water	4.142	0.8030
o-toluidine	4.999	0.8720
Chloroform	4.335	0

Table II. Water.

t°C	P mm	$10^3\eta$ (cgs)	10^3 C
0	4.579	17.93	459.38
10	9.209	13.11	458.92
20	17.54	10.06	458.93
30	31.82	8.00	458.89
40	55.32	6.57	459.20
50	92.51	5.50	459.38
60	149.38	4.69	459.27
70	233.7	4.06	459.23
80	355.1	3.56	459.01
90	525.8	3.16	458.95
100	760.0	2.84	459.38

Table III. *o*-toluidine.

t°C	P mm	$10^3\eta$ (cgs)	10^3 C
40	1.1	24.36	529.41
50	2.1	19.19	530.02
60	3.7	15.78	530.62
70	6.4	13.02	529.41
80	10.5	11.09	529.25
90	17.3	9.52	529.59
100	27.2	8.31	529.41

TABLE IV. Chloroform.

t°C	P mm	$10^3\eta$ (cgs)	10^3 C
−10	34.75	7.86	542.3
0	61.0	6.99	544.6
+10	100.5	6.25	544.9
20	159.6	5.63	545.7
30	246.0	5.10	545.8
40	366.4	4.64	545.3
50	526.0	4.24	544.1
60	739.6	3.89	542.7

Table I gives the values of n and n' for different liquids. Tables II, III, and IV show the constancy of C for water, *o*-toluidine, and chloroform.

A theoretical justification of the above formulas can be furnished as follows. The variation of vapor pressure with temperature can be expressed very roughly (excepting for certain organic liquids, for which the formula is very accurate) as[1]

$$\log P = A - (B/T), \tag{3}$$

and the variation of viscosity of liquids with T is given by Andrade's[2] formula

$$\log\eta = A' + (B'/T), \tag{4}$$

where A, B, A', and B' are constants, and T is temperature in °K. Eliminating T between (3) and (4) we get

$$\frac{\log P - A}{\log\eta - A'} = -\frac{B}{B'} = -n \text{ (say)}$$

or

$$\log P + n \log\eta = C,$$

where C is another constant. We thus get (2), a temperature-independent relation between P and η.

Since the vapor-pressure formula is roughly approximate and Andrade's formula is also not very accurate, (2) cannot be successfully applied to all liquids and hence the inclusion of a quadratic term in $\log\eta$ is necessary.

The author is grateful to Dr. K. Mazumdar for his guidance.

[1] Glasstone, *Physical Chemistry* (D. Van Nostrand Company, Inc., New York, 1947), p. 453.
[2] Andrade, Phil. Mag. **17**, 497, 698 (1934).

Pure Quadrupole Spectra of Solid Bromine and Iodine Compounds

KENJI SHIMOMURA, TOSHIMOTO KUSHIDA, AND NORIYOSHI INOUE,
Department of Physics, Hiroshima University, Hiroshima, Japan
AND
YOSHIRO IMAEDA, *Faculty of Technology, Tokushima University, Tokushima, Japan*
(Received November 2, 1953)

THE resonance frequency absorption resulting from transitions between levels of the nuclear electric quadrupole splitting in Br^{79}, Br^{81}, and I^{127} has been studied in several compounds. A frequency modulated regenerative oscillator was used, and the absorption lines were viewed on an oscilloscope.

TABLE I.

Compound		Frequency Mc/sec	Temperature	Multiplicity	Intensity
$CH_2BrCOOH$	Br^{79}	279.3	Room temperature	Doublet	Strong
	Br^{81}	234.0			
CH_2BrCH_2Br	Br^{79}	261.97	Liquid air	Doublet	Strong[a]
	Br^{81}	259.09			
		218.85	Liquid air		
		216.45			
I_2O_5	I^{127}	179.3	Room temperature	Several lines	Weak

[a] H. Zeldes and R. Livingston, J. Chem. Phys. **21**, 1418 (1953). We found that this line had been measured independently by these authors.

TABLE II. Resonance frequencies for Br^{79} in some bromates[a] at 20°C.

Compound	$LiBrO_3$	$NaBrO_3$	$KBrO_3$	$AgBrO_3$
Resonance frequency, Mc/sec	184.12	178.95	173.11	168.19
Compound	$Ca(BrO_3)_2H_2O$	$Sr(BrO_3)_2H_2O$		$Ba(BrO_3)_2H_2O$
Resonance frequency, Mc/sec	176.85	173.76		173.69

[a] A. L. Schawlow, Phys. Rev. **90**, 348 (1935).

The results obtained are listed in Tables I and II.

In CH_2BrCH_2Br the resonance lines are observed at liquid air temperature showing doublet lines, while at higher temperature no line is observed. The coupling in this substance is slightly lower than that in CH_3Br.[1] This fact indicates that replacing an H by a CH_2Br group produces very little change in coupling and, accordingly, that this group has an electronegativity nearly equal to or slightly smaller than that of H.

The resonance line of $CH_2BrCOOH$ vanishes when it is cooled below room temperature. By comparing its frequency observed by us with that of CH_2Br_2 reported by Zeldes and Livingston, the electronegativity of COOH group seems to be nearly equal to that of Br, if the temperature effect is neglected.

The resonance frequency in alkali metal bromates increases monotonically with the electronegativity of alkali metals.

[1] H. G. Dehmelt and H. Krüger, Z. Physik **129**, 401 (1951).

Erratum: Absorption of 3.3-cm Microwaves in Chloroform and Ethylene Dichloride in the Liquid State

[J. Chem. Phys. **21**, 1614 (1953)]

S. C. SIRKAR AND D. K. GHOSH
Optics Department, Indian Association for the Cultivation of Science, Jadavpur, Calcutta, India

THE address of the second author should be read as Optics Department, Indian Association for the Cultivation of Science, Jadavpur, Calcutta, India.